NASA CR-132687

ANALYTICAL EVALUATION OF ILM SENSORS

By Raymond J. Kirk

SEPTEMBER 1975

VOLUME I

FINAL REPORT

Prepared under Contract No. NAS1-13489 by
HONEYWELL INC.
Systems and Research Center
Minneapolis, Minnesota

for

NATIONAL AERONAUTICS AND SPACE ADMINISTRATION

Analytical Evaluation of ILM Sensors

Volume I

Final Report

Contract No. NA51-13489

Systems and Research Center
Honeywell Inc.

1. Report No.	2. Government Accession No.	3. Recipient's Catalog No.
NASA CR-132687		

4. Title and Subtitle	5. Report Date
Analytical Evaluation of ILM Sensors	September 1975
	6. Performing Organization Code

7. Author(s)	8. Performing Organization Report No.
Raymond J. Kirk	F-2132
	10. Work Unit No.

9. Performing Organization Name and Address	11. Contract or Grant No.
Honeywell Inc. Systems & Research Center Minneapolis, MN. 55413	NAS1-13489
	13. Type of Report and Period Covered

12. Sponsoring Agency Name and Address	
NASA Langley Research Center Hampton, VA 23665	Final Report
	14. Sponsoring Agency Code

15. Supplementary Notes

16. Abstract

Functional requirements and operating environment constraints for an Independent Landing Monitor for aircraft landings in Cat. II/III weather conditions are identified and translated into specific sensing requirements. State-of-the-art capabilities of radar, TV, FLIR, multilateration, microwave radiometry, interferometry, redundant MLS and nuclear sensing concepts are evaluated and compared to the requirements. Concepts showing the best ILM potential are identified.

17. Key Words (Suggested by Author(s))	18. Distribution Statement
Independent Landing Monitor Radar Landing Aids Multilateration Landing Aids Nuclear Landing Aids Microwave Radiometry Landing Aids Microwave Interferometry Landing Aids FLIR Landing Aids TV Landing Aids	Unclassified - Unlimited

19. Security Classif. (of this report)	20. Security Classif. (of this page)	21. No. of Pages	22. Price*
Unclassified	Unclassified	624 - 2 Vols.	

Foreword

This report documents the Analytical Evaluation of Various Potential Sensors for Use in an Independent Landing Monitor (ILM) for Conventional Take-off and Landing (CTOL) Aircraft study performed under National Aeronautics and Space Administration Contract NAS 1-13489 for Langley Research Center.

Honeywell Inc. Systems and Research Center performed this study program under the technical direction of Mr. R. J. Kirk. The program was conducted during the period of July, 1974 to June, 1975. Gratitude is extended to NASA/Langley Research Center for their technical guidance and direct assistance through our technical monitor, Mr. W. T. Bundick.

In addition to the author, Messrs. J. E. Luoma, C. E. Johnson, P. D. Mitchell, D. Doty, V. E. Edwards and N. R. Zagalsky of Honeywell made valuable contributions to the study.

TABLE OF CONTENTS

		Page
SECTION I	INTRODUCTION	2
SECTION II	SUMMARY OF RESULTS	7
	ILM Functions, Operational Environment and Requirements	8
	Sensor Capabilities	18
	Realizable System Descriptions	29
	Conclusions	37
	Recommendations	41
SECTION III	REQUIREMENTS	47
	ILM Functions	47
	Operational Environment	50
	Sensor Requirements	83
SECTION IV	ILM SENSOR CONCEPTS	103
SECTION V	SENSOR CAPABILITIES	133
	Radar Sensors	134
	Multilateration Sensors	227
	Nuclear Sensors	270
	Redundant MLS	277
	TV Sensors	287
	FLIR	346
	Microwave Radiometer ILM	379
	Microwave Interferometry	427
	Inertial Aiding	453
SECTION VI	FEASIBLE ILM CONCEPTS	464
SECTION VII	REFERENCES	504
SECTION VIII	BIBLIOGRAPHY	510
SECTION IX	APPENDICES	
	Appendix A Tentative MLS Accuracy Requirements	
	Appendix B MARSAM II Computer Program Summary	
	Appendix C Scattering of Electromagnetic Waves	
	Appendix D Atmospheric Attenuation of Microwaves	
	Appendix E Radiometry Computer Programs	
	Appendix F MLS Configuration K Airborne Equipment	

LIST OF FIGURES

No.	Title	Page
1	ILM Study Approach	5
2	Block Diagram of Imaging Radar	30
3	Block Diagram of Radar Triangulation	32
4	Ground Controlled Multilateration System	34
5	Nuclear Instrument Landing System	36
6	Typical Category III Landing Sequence	49
7	Possible Landing Approach Paths - Azimuth	56
8	Examples of Vertical Profiles	57
9	Calculated Soil Emissivities	62
10	ALSF-2 Approach Light Configuration	64
11	FAA Airspace Allocation 1982	70
12	Schematic of High Density Terminal Area Airspace	72
13	Upgraded Third Generation ATC System Functions	74
14	ILM Operational Range (Azimuth)	90
15	ILM Operational Range (Elevation)	91
16	Minimum Cross-Track Angle	93
17	Minimum Along-Track View Angle	94
18	Minimum Visibility Requirements, Transports (MIL-STD-850A)	101
19	Precision Approach Radar	105
20	Imaging Radar	106
21	Radar (Triangulation)	108
22	Multilateration (Air Control)	109
23	Multilateration (Ground Control)	111
24	Multilateration (Beacon Transponder)	112
25	FLIR (Imaging)	113
26	FLIR (Tracking)	115
27	Television (Imaging)	116
28	Television (Tracking)	117
29	Nuclear Instrument Landing System	119
30	Runway Centerline Radioactive Sources	120
31	Buried Magnetic Leader Cable	121
32	Monopulse/Ranging Radar	123
33	Monopulse/Ranging Radar (Ground Derived)	124
34	Microwave Imaging Radar	125
35	Microwave Interferometer	126
36	Microwave Interferometer Plus Range	128
37	Bistatic Radar	129
38	Redundant MLS	131
39	Inertial Aiding	132
40	Radar System Analytic Structure	137
41	Fluctuation Loss Vs Detection Probability	145
42	Effect of Detection Probability of Combined Losses Radar	146
43	Scan Distribution Loss, L_D	147
44	Scan Distribution Loss for Systems with Storage	147
45	Analysis Antenna Pattern	159
46	Standard Deviation of Clutter Component	187

LIST OF FIGURES (Continued)

No.	Title	Page
47	T_i, Time Between Samples	189
48	System Improvement Capability	190
49	Runway Geometry	193
50	Monopulse Edge Resolution Limitation	197
51	T/CP (Snow)	206
52	T/CP (Rain)	207
53	Capabilities for Target to Background Ratios	208
54	Maximum Range Variation	209
55	Minimum Range Variation	209
56	ILM Radar R1-K_a Band	210
57	ILM Radar R2-K_a Band	211
58	ILM R_t-K_a Band	212
59	ILM Radar R6-G Band	213
60	ILM Radar R2-K_a Band	214
61	Radar R5-X Band	215
62	The Trilateration Concept	228
63	Illustration of GDOP	229
64	Classical Adaptive Threshold Detection	232
65	Multipath Geometry	235
66	Threshold Crossing Time Error	238
67	Multipath Error Vs Phase	239
68	Transponder Block Diagram	241
69	Alternate Mechanism for Measuring Transponder Delay	242
70	Typical Amplitude Dependent Error	244
71	Horizontal Plane 6 DOF Near the Center of an Equilateral Triangle	248
72	Equilateral Triangle Altitude GDOP	249
73	Proposed Six Beacon System Layout	250
74	Horizontal Plane GDOP for Proposed Six Beacon System	251
75	Altitude GDOP Proposed Six Beacon Layout	252
76	PLRACTA Beacon Layout	257
77	PLRACTA Altitude GDOP	258
78	Effect of Kalman Filter	262
79	Effect of Optimum Filtering	263
80	Effect of Optimum Filtering (Continued)	264
81	ILM Multilateration Layout	268
82	Gamma Ray Source Strength Vs Range	276
83	System Block Diagram, Category III	279
84	Siting Diagram, Category III	280
85	Block Diagram of Airborne Equipment, Category III	281
86	Pictorial of Airborne Equipment Category III	282
87	Block Diagram of Interface Circuits	284
88	Block Diagram of Interface Circuits	285
89	Night Scene Illumination for Several Conditions	289
90	Percent of Month for which Illumination is Less Than a Given Level	290

LIST OF FIGURES (Continued)

No.	Title	Page
91	Atmospheric Transmission Vs Slant Range	293
92	Limiting Resolution Vs Apparent Angular Velocity	295
93	Camera Tubes	304
94	Comparison of MTF for an Image Identifier and SEC Vidicon	309
95	MTF of 9.87 Inch, T/1.5 Objective	312
96	Combined MTF for TV System	313
97	Spectral Response of Photosurfaces and Emission of Illuminator	315
98	Backscatter in an Active System	317
99	Backscatter Reduction	319
100	VIDl Output Current (I_o) Vs. Photocathode Illumination (E)	330
101	VIDl Limiting Resolution (R_{tv}) Vs Contrast (C_a) and Photocathode Illumination (E)	331
102	CRTl Brightness (B_d) Vs Grid Voltage (V)	334
103	TV Performance, Probability of Detection Vs Range	338
104	TV Performance, Probability of Recognition Vs Range	339
105	TV Performance, Against Runway Light	340
106	TV Performance, Against Approach Light	341
107	TV Performance, Detection of Obstacle	343
108	TV Performance, Recognition of ILM Box	344
109	Radiant Emittance Vs Wavelength 300°K Blackbody	348
110	Atmospheric Transmission Vs Wavelength	353
111	Atmospheric Transmission Vs Range 8-14 Microns	355
112	Photon Noise Limited D*	366
113	Improvement in Detectivity with Cooled Aperture Stops	368
114	CRTl Brightness (B_d) Vs Grid Voltage (V)	374
115	FLIR Performance, Probability of Detection Vs Range	376
116	FLIR Performance, Probability of Recognition Vs Range	377
117	Planck's Radiation Function	381
118	Sky Temperature Vs Grazing Angle - ILM Weather Case 1	384
119	Sky Temperature - ILM Weather Case 2	385
120	Sky Temperature - ILM Weather Case 3	386
121	Sky Temperature - ILM Weather Case 4	387
122	Radiometer Scene	388
123	Total Power Radiometer	393
124	DICKE Radiometer	395
125	Correlation Radiometer	396
126	Antenna Size Vs Beamwidth	400
127	Resolution Cell Size Vs Range for Various Antenna Bandwidths	402
128	Geometry for Field of View Computation	405
129	Scan Rate Vs Range	408
130	Phased Array Antenna	410
131	Beamwidth Vs Scan Angle	412

LIST OF FIGURES (Continued)

No.	Title	Page
132	Blass Array Radiometer System	414
133	Contrast of Concrete and Grass at 35 GHz	419
134	Contrast of Concrete and Snow at 35 GHz	420
135	Basic Interferometer	429
136	The Glistening Surface	433
137	Diffuse Multipath S/C Ratios	435
138	Elevation Channel Specular Multipath Scenario	437
139	Elevation Multipath	440
140	Multipath Phasor Diagram	445
141	Maximum Multipath Phase Error	446
142	Probability of Ambiguity Error	450
143	Inertial Reference Azimuth and Elevation Accuracy Requirements	456
144	Azimuth Fix Inertial Requirements	458
145	Azimuth Fix Inertial Requirements	459
146	ILS Inertial Integration Improvements	461
147	ILM Ranging Radar	466
148	ILM Triangulation Radar	473
149	Transponder Layout at Runway	474
150	Block Diagram for Radar Altimeter Concept	479
151	Block Diagram of MLS Elevation Antenna System	480
152	Multilateration Transponder Logic Block Diagram	485
153	Nuclear ILM Siting Configuration	493
154	NILS Shutter	495
155	Formation of Guidance Beams	495
156	Nuclear ILM Block Diagram	497

LIST OF TABLES

No.	Title	Page
1	ILM Operating Environment	9-11
2	Basic Sensor Requirements	13
3	Case I Requirements	14
4	Case II Requirements	15
5	Case III Requirements	16
6	Sensor System Evaluation Study	19
7	Key Factors of Feasible Concepts	26
8	Background Signature Data	58
9	Supplementary IR Emissivity Data	59
10	Microwave Emissivities for Two Angles of Incidence	60
11	Types of ILS Localizers	60
12	Airborne EMI Sources	65
13	Ground-Based EMI Sources	67
14	1982 Terminal Airspace	69
15	Initial Approach Gate Definition	72
16	Air Traffic Control -- Communication	75
17	Air Traffic Control -- Separation Assurance	77
18	Approach Separation Monitor Concepts, Potential Capabilities and Problem Areas	80
19	Air Traffic Control -- Navigation	81
20	Vertical Weather Profiles	84
21	Path Following Error Data	86
22	ILM System Specifications	135
23	5 mm/hr Rain at 1500 m (4920 ft) to 0 m Altitude	161
24	10 mm/hr Rain at 1500 m (4920 ft) to 0 m Altitude	161
25	16 mm/hr Rain at 1500 m (4920 ft) to 0 m Altitude	162
26	Radiation or Advection Fog, RVR = 213m	162
27	Radiation or Advection Fog, RVR = 46m	163
28	Radiation or Advection Fog, RVR = 0 m	163
29	Evaporation Fog, RVR = 213 m	164
30	Evaporation Fog, RVR = 46 m	164
31	Evaporation Fog, RVR = 0 m	165
32	3 mm/hr Snow at 3 Km (9850 ft) to 0 Km Altitude	165
33	6 mm/hr Snow at 3 Km (9850 ft) to 0 Km Altitude	166
34	9 mm/hr Snow at 3 Km (9850 ft) to 0 Km Altitude	166
35	Typical Airborne-Radome Performance Requirements	170
36	Conventional versus Lens Antenna Comparison	171
37	Target Radar Cross-Section	176
38	Terrain Cross-Section Factors	177
39	$\|K\|^2$	178
40	Precipitation Clutter Reduction Factor (dB)	179
41	Typical Radar System Parameters	199
42	Ground Differential Scattering Cross-Section	201
43	Summary of Loss and Gain Values for Typical Systems at 1 Km	217

LIST OF TABLES (Continued)

No.	Title	Page
44	Summary of Specific Radar Systems	222
45	ILM TV Weather Cases	328
46	VID1 Performance Characteristics	329
47	Three TV Lenses	332
48	CRT1 Performance Characteristics	333
49	TV Display Size	335
50	ILM Targets and Backgrounds (TV and FLIR)	337
51	Emissivity of Materials	349
52	ILM FLIR Weather Cases	371
53	FLIR Characteristics	372
54	FLIR Optics	372
55	CRT1 Performance Characteristics	373
56	Display Size	373
57	Bandwidth to Assure Recognition, Degrees	401
58	Radiometer Signal Strength, Concrete Against Grass (dB)	425
59	Summarized Path Losses (dB)	426
60	Accuracy Requirements, ft. (2σ)	455
61	Position Fix Rate Requirements	457
62	Imaging Radar System Physical Parameter Estimates	470
63	Triangulation Radar System	476
64	Airborne Component Estimates	501
65	Ground Component Estimates	501

SUMMARY

ANALYTICAL EVALUATION OF ILM SENSORS

Raymond J. Kirk
Honeywell Inc.

This report defines the requirements and operational environment for an independent landing monitor which will provide the flight crew with an independent assessment of the operation of the primary automatic landing system during Category II/III operations. The capabilities of radars, TV, FLIR, multilateration, microwave radiometers, interferometers and nuclear sensing concepts to meet the ILM conditions are analyzed.

The most critical need for the ILM appears in the landing sequence from 1000 to 2000 meters from threshold (middle marker) through rollout. Of the sensing concepts analyzed, six show potential of becoming feasible ILM's. These are: redundant MLS, precision approach radar, airborne perspective imaging radar, airborne triangulation radar, multilateration with radar altimetry and nuclear. Each has serious limitations in meeting all of the ILM functional requirements (goals) and will require significantly more development.

SECTION I
INTRODUCTION

The technology required for automatic landing of conventional fixed-wing aircraft using the VHF Instrument Landing System (ILS) and highly redundant flight control systems in Category III Conditions has been demonstrated many times. However, the introduction of this capability into general usage has been limited. One reason for the limited use of autoland systems has been the lack of a monitoring system operating independently from the primary guidance system. Independent operation would allow the pilot to assess the performance of the autoland system and the aircraft situation relative to the runway under conditions of low visibility and/or allow the pilot to manually land the aircraft in the event of failures in a fail-passive autoland system. This independent monitoring function should serve to build up the pilot's confidence in low visibility landings and permit the reduction of the flight control system from a fail-operational automatic unit to a fail-passive system with manual backup capability. The Independent Landing Monitor (ILM) is here defined to include the sensors, signal processors, and displays needed to provide the pilot with information to assess his situation and either make a missed approach or proceed in with the manual landing.

The primary objective of the ILM study is to evaluate analytically the capabilities of various generic sensor concepts to meet the functional requirements for an Independent Landing Monitor.

To evaluate the capabilities of the various sensing concepts over a range of ILM requirements, the functions required of the ILM were defined for a basic configuration and for three configurations of increasing complexity:

a. Basic - The ILM shall provide information to allow determination of aircraft position (elevation, azimuth, range) with respect to the runway down to a wheel altitude of 12 feet. The accuracy of the position information should be adequate to monitor the approach with a Category III Microwave Landing System (MLS) as the primary guidance system.

b. Case I - The requirements for the basic system configuration are extended to touchdown and through rollout to provide guidance to the aircraft through the full landing sequence. Heading with respect to end of runway should be provided with an accuracy of 0.1°.

c. Case II - Add the detection of obstacles, such as aircraft and ground vehicles on or near the runway to the Basic and Case I configuration functions. Detection of obstacles should be at a range sufficient to permit execution of a missed approach.

d. Case III - Meet the Basic, Case I, Case II requirements through the use of a real-world perspective image of the runway and its surroundings. The image should be of sufficient quality to provide position, rate of change of position, and attitude information to the pilot in a form analogous to the visual cues available during VFR approach and landing.

TECHNICAL APPROACH

The ILM Program was organized to carefully identify the usage of each potential sensor in its expected ILM system concept and then carry this concept along through the program. By so doing we could fully concentrate on critical sensor parameters and requirements and avoid being sidetracked collecting and evaluating sensor data of little value to the program. Sensors which could not meet

the critical parameters were then dropped from further consideration in the study.

Figure 1 shows a block diagram of the study approach used during the ILM Program. It also shows the planned outputs of the study.

The ILM study began with a concepts definition phase. This included defining the expected ILM operational environment covering the MLS baseline guidance system, expected airport constraints, aircraft considerations, weather constraints, etc. Tentative system concepts for a total of 20 sensor configurations were identified as possible ILM candidates.

The sensor evaluation phase of the program consisted of two parallel tasks. First, the unique sensor requirements for each of the four ILM functional cases were defined and sensor capability data was compiled for each of the generic sensors of interest. Second, a preliminary comparison of the sensor capabilities versus sensor requirements was undertaken to screen out those concepts which have little or no value to the ILM functions.

The concept refinement phase concentrated on those concepts which passed the first screening and appeared to be feasible ILM concepts. Estimates were made of physical parameters and key constraints of the hardware to implement the system for each ILM sensor concept. Data transfer requirements, interfacing the ILM sensors with the on-board information processor and displays, were identified together with external ground-link data interfaces.

A mutual interference analysis to determine compatibility with potential traffic

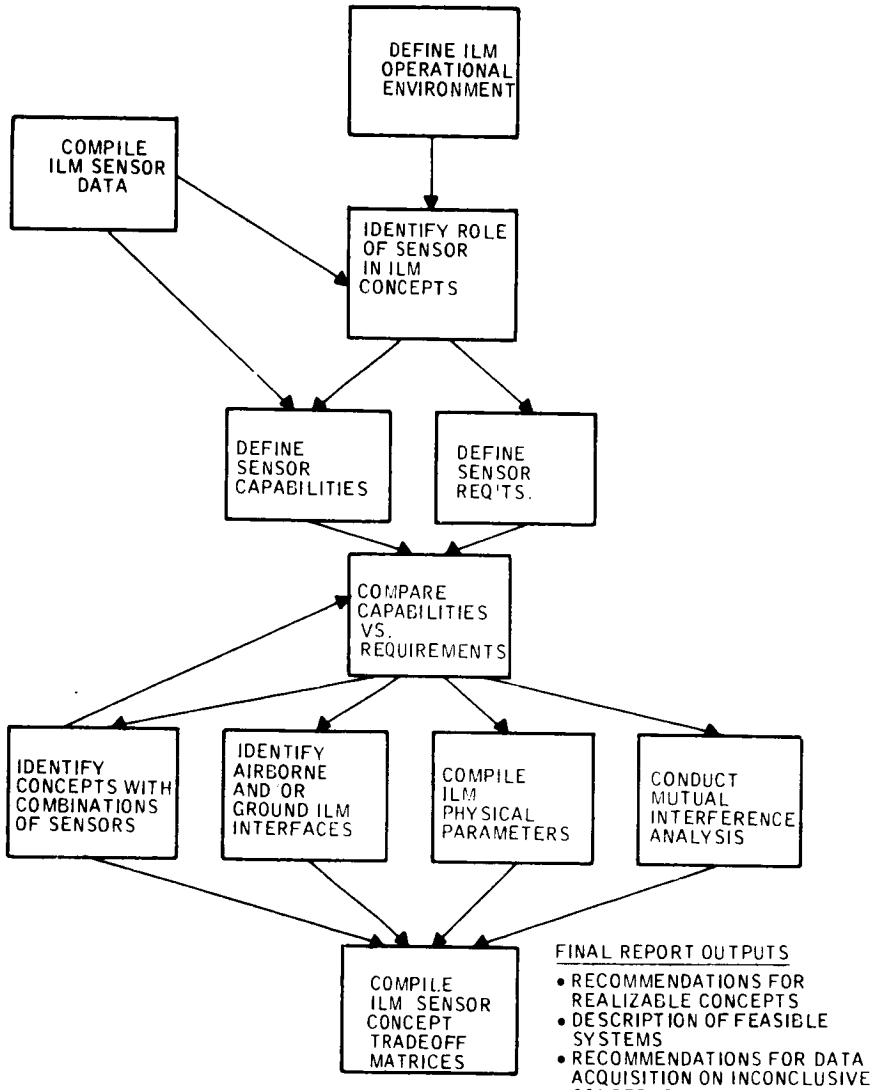

Figure 1 -- ILM Study Approach

and/or with other ATC system constraints, was made for each feasible ILM concept as an additional task of the concept refinement phase.

The results from these tasks were summarized in a form readily usable for comparison with other ILM studies. The ILM concepts were then ranked according to feasibility in each of the pertinent functional areas.

Section II of this report presents a summary of study results. It includes an overview of ILM functional and environmental requirements, a matrix of sensing concepts, a brief description of those ILM concepts that are considered realizable and the study conclusions and recommendations.

Section III presents the requirements established for the ILM. This section begins with a discussion of ILM functions, then continues with details on the ILM operational environment and sensor requirements.

Sections IV and V present discussions of the ILM Sensor Concepts and the capabilities of each generic sensor system. Section V contains the details of the analytical effort on each type of sensor including the results therefrom.

Section VI contains a discussion of the feasible ILM concepts that were considered for refined study.

See II

SECTION II
SUMMARY OF RESULTS

Landing safety and reliability, independent of terminal area weather conditions, is a goal towards which the air transport industry is striving. The benefits to passengers, the airlines, and the military are clear. To this end, fail-operational landing systems are minimum requirements for achieving all-weather landing capabilities. The systems, utilizing an accurate and reliable microwave landing system as the primary landing aid, form the basis for the FAA's and ICAO's plans to make Category III operations available at a limited number of high density airports in the 1980's.

To date, fail-operational systems for Category III conditions have required highly-redundant fail-operational flight control systems and high reliability landing aids in fully automatic configurations. An alternative approach to the fully automatic configurations is to utilize a fail-passive flight control system and primary landing aid with an independent back-up landing aid and manual flight control. The fail-passive primary landing system permits the use of dual redundancy rather than the more costly triple or quad redundancy of an automatic fail-operational system. The back-up independent landing monitor (ILM) with manual takeover capability upgrades the system from fail passive to fail operational.

The intent of this study was to survey potential sensors and sensing concepts to determine their utility as the independent landing aid and to identify the limits or conditions under which they would fulfill one or more of the required functions.

ILM FUNCTIONS, OPERATING ENVIRONMENT AND REQUIREMENTS

The required ILM functions were here defined as follows:

- The ILM must allow the pilot to assess the performance of the primary autoland system and the aircraft situation relative to the runway under conditions of low visibility prior to a commitment to land (decision height). Any indication of unsatisfactory conditions from the ILM at this point dictates a missed approach.

- The ILM must provide adequate information to the pilot to permit manual takeover to land on failure of the primary landing system after commitment to land.

- The ILM should warn the pilot of obstacles on the runway and turnoffs.

To provide a common baseline for evaluating each of the sensors, a typical operating environment for the ILM was developed. Detailed descriptions of the operating environment are provided in Section III of this report. A summary of the operating environment, including airport characteristics, aircraft parameters, approach paths, weather, and traffic density, is given in Table 1. The primary landing guidance system was assumed to be a configuration K MLS throughout the study.

To determine the capabilities of the various sensing concepts over the full range of potential ILM requirements, for purposes of the study, the functions required of the ILM were defined as follows for a basic system and for three optional systems of increasing complexity.

Table 1 -- ILM Operating Environment

Airport Characteristics	
Runway length	1520 to 3660 m (5000 to 12,000 ft)
Runway width	25 to 61 m (80 to 200 ft)
Runway material	concrete asphalt
Runway surroundings	grass weeds bare soil sand water snow ice
Approach terrain	level to hilly
Parallel runway spacing	820 m min. (2500 ft)
Aircraft Parameters	
Speed	Approach 165 to 270 km/hr (90 to 145 kts) Rollout 0 to 270 km/hr (0 to 145 kts) Turnoff and taxi 0 to 110 km/hr (0 to 60 kts)
Roll	Normal operation ±.175 rad (±10°) Automatic recovery ±.52 rad (±30°)
Pitch	-.052 to +.175 rad (-3 to +10°)
Crab	.35 rad (20°) maximum
Approach Path Coverage	
Glide paths	.0175 to .105 rad (1 to 6°)
Azimuth	±1.05 rad (±60°) about runway extension at threshold
ILM operating ranges	to 1.8, 5.6 and 15 km (1, 3, and 8 n mi.)

Table 1 -- ILM Operating Environment (Continued)

Approach Path Coverage (Continued)	
Curved paths	worst case - trombone path, turn radius of 2200 m (7200 ft), path length to touchdown of 9500 m (31,000 ft), straight-in path of 2700 m (9000 ft) with no deceleration.
Weather Conditions	
Rainfall rate	to 16 mm/hr
RVR in fog/smog	370, 210, 46, and 0 m (1200, 700, 150 and 0 ft)
Wet and dry falling snow	to 5 mm/hr (melted)
Wind velocity	60 km/hr (32 kts) maximum
Traffic Density	
Approach spacing	30 secs minimum
Taxiway spacing	30 secs minimum
Taxiing aircraft	50
Inflight A/C within 5 n mi. within 10 n mi.	8 33
MLS Configuration K	
Minimum guidance altitude	to touchdown
Coverage	
Elevation	20°
Azimuth	±60°
Mixed Approach	±40°
Range	20 n mi. minimum

Table 1 -- ILM Operating Environment (Continued)

MLS Configuration K (Continued)	
Accuracy	
Elevation (2σ)	0.1° bias error, 0.070° noise error (1.4 ft. noise error at threshold)
Azimuth (2σ)	0.072° bias error, 0.045° noise error (9 ft. noise error at threshold)
Range (σ)	20 ft. at touchdown
Runway length	to 14,000 ft.
Data rate	Azimuth 5 Hz Elevation 5 Hz above D.H., 10 Hz below D.H. Range 5 Hz

Basic

The ILM shall provide information to allow determination of aircraft position (elevation, azimuth, range) with respect to the runway down to wheel altitude of 12 feet. The accuracy of the position information should be adequate to monitor the approach with Category III microwave landing system as primary guidance.

Case I

The guidance requirements for the basic system configuration are extended to touchdown and through rollout of the aircraft. Heading with respect to end of runway should be provided during rollout to an accuracy of 0.1°.

Case II

Add a detection of obstacles, such as aircraft and ground vehicles on or near the runway, requirement to the Basic and Case I configuration requirements. Detection of obstacles should be at a range sufficient to permit execution of a missed approach.

Case III

Meet the Basic, Case I, Case II requirements through the use of a real-world perspective image of the runway and its surroundings. The image should be of sufficient quality to provide position, rate of change of position, and attitude information to the pilot analogous to the visual cues available during a VFR approach and landing.

Sensor requirements for each of the four configurations are summarized in Tables 2 through 5, respectively. These requirements were either derived directly from the operational environment constraints of Table 1 or from analysis of the functional requirements. Descriptions of this analysis are given in Section III.

Table 2 -- Basic Sensor Requirements

DATA TYPE

MINIMUM: azimuth, elevation deviations from centerline extension

MLS EQUIVALENT: azimuth, elevation angles relative to centerline and GPIP

ACCURACY: METERS 2σ (FT)

	ROLLOUT	GPIP	THRESHOLD	DISTANCE FROM THRESHOLD ON C.L. EXT. 1 N.M.	3 N.M.	8 N.M.
Azimuth	4.3 (14)	4.3 (14)	4.3 (14)	6.1 (20)	11.6 (38)	31.0 (103)
Elevation	--	--	.55 (1.8)	3.6 (11.8)	10.1 (33)	29.0 (95)
Range	12.2 (40	12.2 (40)	12.2 (40)	18.0 (58)	29.0 (94)	56.0 (184)
Flare (elev)	--	.55 (1.8)	.55 (1.8)	2.4 (7.7)	8.2 (27)	--

EFFECTIVE RANGE

MINIMUM: 1070 m (3500 ft)

PREFERRED: to 15 km (8 n.mi.)

FIELD OF VIEW / COVERAGE

RELATIVE TO A/C BORESIGHT

Azimuth: $\pm$ .415 rad (23.75°)

Elevation: + .052 rad to - .314 rad (3°to-18°)

RELATIVE TO RUNWAY

.14 rad azimuth, .14 rad elevation (8° azimuth, 8° elevation)

GROUND DERIVED

Azimuth: $\pm$ .07 rad (4°) on centerline measured from GPIP

Elevation: + .0175 to + .105 rad (+ 1° to + 6°) measured from GPIP

DATA RATE

MINIMUM

Azimuth: 5 samples / sec

Elevation: 5 samples / sec above D.H., 10 samples / sec below D.H.

Range: 40 interrogations / sec smoothed to 5 samples / sec

PREFERRED: 10 samples / sec

SPACIAL RESOLUTION

Equivalent to accuracy values

NOTES

1. Equivalent to ILS straight-in approach.
2. Equivalent to MLS, angle and range rates computed on aircraft for curved, segmented paths.
3. Accuracies derived from MLS path following requirements. Values estimated from combination of noise, bias errors for MLS.
4. 3-second decision time, 100 ft decision height, 2° glideslope.
5. Design goal.
6. Large angle due to $\pm$ 20° crab angle, could be reduced with lower crosswind requirement.
7. Needed to cover expected pitch angles, need larger f.o.v. if horizon must be near center of display.
8. May require separate crab, pitch angle symbolic display to pilot.
9. Minimum coverage for straight-in approaches.
10. Equivalent to MLS
11. Design goal.
12. Spatial resolutions should be approximately same as accuracy. That is, from threshold to touchdown, the pilot should be able to resolve 14 ft azimuth and 1.8 ft elevation errors in the touchdown point or aimpoint.

Table 3 -- Case I Requirements

B A S I C + :

NOTES

DATA TYPE

MINIMUM	Azimuth deviation from centerline.	Runway length remaining.	13. Equivalent to MLS.
PREFERRED	Azimuth deviation from centerline.	Runway length remaining.	14. Some ILM sensors may also have capability for turnoff. It is not considered as a requirement.

ACCURACY

15. Equivalent to MLS.

AZIMUTH DEVIATION	4.3 m (14 ft) (2 σ) from centerline 12.2 m (40 ft) (2 σ) to stop end of runway

DATA RATE

MINIMUM	5 samples / sec	16. Equivalent to MLS.
PREFERRED	10 samples / sec	17. ILM design goal.

COVERAGE

Full runway surface

SPACIAL RESOLUTION

Equivalent to accuracy values

Table 4 -- Case II Requirements

B A S I C + C A S E I + :

DATA TYPE

Discrete alert.
Relative position of object on runway to touchdown and centerline.

ACCURACY

Position relative to centerline -- 15 m (50 ft) 2σ
Position relative to touchdown -- 305 m (1000 ft) 2σ

EFFECTIVE RANGE

4300 m (14,000 ft) on objects:

Size: 3 m x 3 m x 3 m
Radar Cross Section: 1 square meter
Temperature: ambient
Emissivity: (0-15 microns) - 0.90

DATA RATE

1 sample / sec

SPATIAL RESOLUTION

0.35 mrad

NOTES

18. Pilot must know there is object on runway and its relative position on runway to permit him to continue his final approach.

19. Exact position of object is not critical. Pilot must detect it has left runway.

20. Pilot cannot touch down if object is on runway. He must be able to monitor full runway from decision height through rollout.

21. Pilot decision is go/no-go for land or missed approach. Data rate can be lower than for steering guidance.

22. Passive target detection requirement (minimum of two resolution elements on target) for imaging sensors.

Table 5 -- Case III Requirements

B A S I C + C A S E I + C A S E II + :

NOTES

DATA TYPE

Real world perspective image display

23. Design goal.

FIELD OF VIEW

RELATIVE TO BORESIGHT:

$\pm$ .415 rad (23.75°) az., +.052 rad to -.314 rad (+3° to -18°) el.

24. Minimum for straight-in approaches, $\pm$ 20° crab angle, -3° to +10° pitch angle.

RELATIVE TO RUNWAY:

.14 rad azimuth, .14 rad elevation (8° azimuth 8° elevation)

25. Minimum view angle of threshold area for pilot recognition of his position.

DATA RATES

DISPLAY REFRESH RATE:

20 / second

26. Actual value depends on data type and display characteristics

INFORMATION UPDATE RATE:

MINIMUM: 5 samples / second azimuth, range; 10 samples / second elevation

27. Equivalent to MLS.

PREFERRED: 10 samples / second

28. Design goal.

SPATIAL RESOLUTION

MINIMUM: 2 mrad azimuth; .8 mrad elevation

29. Angular resolution of ILS electromechanical flight director display.

PREFERRED: .3 mrad (1 min. of arc)

30. Typical human eye resolution.

SIGNAL TO NOISE RATIO

3 (4.8 dB) aim reticle sighting cues over background at minimum effective range of 1070 m (3500 ft)

31. Assumption based on target detection simulations for reconnaissance and weapon delivery and fact that target in this case is highly familiar form.

MAGNIFICATION

Unity

32. Pilot derives his orientation and position from shape and familiar size of objects. Deviations from unity magnification tend to reduce his capability.

It should be noted the parameters listed in Tables 2 through 5 are not necessarily requirements. In many cases, they could be considered design goals. By relaxing or reducing a number of the operating environment conditions, the sensor requirements could be relaxed. For example, changing the maximum wind conditions during landing directly impacts the field of view coverage requirements on the sensors through changes in required crab angle. Thus, this set of requirements corresponds to the typical set of operational environment conditions in Table 1 and can change for other environmental conditions.

A true real-world perspective image display meeting the minimum field-of-view requirements is not considered feasible for cockpit installation. To meet the ±23.75° azimuth and 21° elevation view angles at the nominal viewing distance of 71 cm (28 inches) requires a 62 cm (24.6 inches) by 26.4 cm (10.4 inches) display. A perspective image of the runway could be provided with crab and pitch angles displayed on separate scales or, alternatively, less than unity magnification could be used. Either of these alternatives must be analyzed and tested to determine pilot responses to the non-real imagery during stress periods.

During the course of this study a literature search of previous human factors work was conducted to determine the signal to noise ratio and resolution requirements on an imaging type of IIM system. The bulk of this work has been done in target detection with reconnaissance systems where signal to noise ratios of 3 db for detection and 5 db for recognition and resolutions of 2 elements for detection and 8 elements for recognition are commonly used. These numbers were also used in this study. We found no directly applicable analysis relating pilot performance with

imaging systems in detection, recognition and derivation of steering cues for large, very familiar targets such as runways. The numbers quoted in this case are probably conservative for detection and recognition, but not necessarily for derivation of steering cues. The capabilities of imaging sensors to fulfill the ILM functions cannot be fully determined until these requirements are defined.

SENSOR CAPABILITIES

Although this study was intended to be primarily an analysis of sensing techniques to meet the ILM requirements, it was necessary to consider the sensing techniques as part of total system concepts. For example, radar as a sensor can be used for several system concepts with the constraints and capability of the sensor occurring from the way it is used in the system. A total of 20 ILM system concepts, most of which have been suggested or partially developed at one time or another as potential landing monitors, were defined and considered during the course of this study. The concepts are described in more detail in Section IV of this report.

Each ILM system concept was evaluated in relation to the four sets of ILM requirements. Where the system concept would not meet a minimum requirement, it was dropped from further analysis. The results of this evaluation are summarized in Table 6. Potentially-feasible systems that meet a significant part or all of the ILM requirements are indicated in the table with key factors in the evaluation included under the notes.

Table 6 - - Sensor System Evaluation Study

CONCEPT	REQUIREMENTS				FEASIBLE	NOTES
	BASIC	CASE I	CASE II	CASE III		
1. Precision Approach Radar	X	No	No	No	x	Accuracy Question. Traffic Limited.
2a. Imaging Radar	X	X	X	X	xx	Accuracy Question. Low S/N for Unenhanced Image
2b. Radar (Triangulation)	X	X	No	No	xx	Accuracy Question
3a. Multilateration (air control)	Partial	X	No	No	x	Altitude Inadequate. Appears more Complex than 3c.
3b. Multilateration (hyberbolic)	Partial	X	No	No	x	Altitude Inadequate. Position Accuracy Poorer than 3a or 3c
3c. Multilateration (beacon xponder)	Partial	X	No	No	xx	Altitude Inadequate. Simplest Multilateration Concept
4a. FLIR (imaging)	No	No	No	No		Meets Minimum Range only in CAT. I Weather
4b. FLIR (tracking)	No	No	No	No		Meets Minimum Range only in CAT. I Weather
5a. Television (imaging)	No	No	No	No		Meets Minimum Range only in Good Weather
5b. Television (tracking)	No	No	No	No		Range Marginal Beyond CAT. I
6a. Nuclear Instrument Landing System	X	X	No	No	xx	Range Limited by Practical Size and Location of Sources, Near Independence of Weather.
6b. Runway Centerline Radioactive Sources	No	Partial	No	No		Gives Runway Position
7. Buried Magnetic Cable	No	Partial	No	No		Gives Deviation from Centerline. Pilot also needs distance along runway.
8. Monopulse Ranging Radar	X	X	No	No		Processing Concept Analyzed Under 1, 2a, 2b.
9. Microwave Imaging Radiometer	No	No	No	No		Resolution/Accuracy Inadequate. S/N poor in Degraded Weather.
10a. Microwave Interferometer	No	No	No	No		Angular Deviations only. Accuracy poor due to multipath.
10b. Microwave Interferometer Triad	No	No	No	No		Angular Deviations Plus Range. Accuracy Poor due to Multipath.
11. Bistatic Radar	No	No	X	No		S/N Levels too low for Runway Detection. Feasible but Complex for Obstacle Detection.
12. Redundant MLS	X	X	No	No	x	Full Fail-Operational System meets Basic and Case I. Not Totally Independent.
13. Inertial Aiding	Partial	Partial	No	No		Useful for Filtering Noisy Position Reference.

X Denotes potentially acceptable performance compared to requirements

x Denotes feasible sensor system: xx potentially feasible concepts defined

Precision approach radar is a feasible and operational system concept for ILM covering approach to touchdown (Basic requirements). It is limited to near straight-in approaches. The ground radar must maintain track on each incoming aircraft and is, thus, very traffic-limited with systems analyzed capable of tracking not more than 1 to 6 aircraft simultaneously.

The real-world perspective imaging radar appears feasible and could potentially meet all four sets of ILM requirements. The airborne K_a band radar will not provide accuracies equivalent to the MLS; however, these requirements may be more stringent than necessary. Adequate imagery for guidance under severe weather conditions may require enhancement of the runway outline through the use of passive or active reflectors. A literature search was conducted to determine measured radar backscatter characteristics of terrain and runway materials and radar backscatter and attenuation characteristics of precipitation. Variations in the measured data are too large to make radar performance predictions with high confidence in many cases. With the wide range of possible runway/background/weather conditions it appears the system performance will not in all cases meet the design goals.

The use of the airborne radar to triangulate on three or more active reflectors around the runway can potentially meet the Basic and Case I ILM requirements. The use of active reflectors on the ground to shift the frequency and re-transmit the received pulses extends the range of the radar system. Again, resolution capability of the radar limits the accuracy of the system.

Three multilateration concepts were considered during the study. The first concept consisted of a distance-measuring interrogator on each aircraft and three ground transponders around the airport. The second concept utilized three time

synchronized ground stations with an airborne receiver measuring time differences of the pulses received similar to a LORAN concept. The third concept, essentially an inverse of the first concept, utilizes a master interrogator on the ground with a transponder on the aircraft and two additional slave stations on the ground to measure ranges to the aircraft. It was shown in the analysis that all three of these concepts were potentially feasible for meeting the position requirements for approach to touchdown and through rollout. The third concept appeared least complex and also appeared to have the best accuracy; thus, it was the only one considered in further concept refinement. Altitude accuracy (up to 30 meters error) was inadequate with all three concepts. A radar altimeter with ground elevation mapped approach paths is required to provide adequate altitude accuracy along with the multilateration system for horizontal position accuracy. This combination can provide accuracies of 5 meters in horizontal position and 1 meter in altitude.

Forward looking infrared radiometers (FLIR) were examined in both boresighted wide angle imaging and platform mounted tracking modes in the study. The FLIRs meet minimum range requirements of 1,000 meters only in Category I or better weather conditions and, thus, are not considered feasible for the necessary ILM operational environments. The use of reasonable size IR sources or targets along the runway did not significantly improve the capability.

Fixed and platform-mounted television systems in tracking and boresighted imaging modes were reviewed. Like the FLIRs, they meet the minimum ILM requirements only in Category I or better weather conditions and are not considered feasible as ILM concepts. For TV, the approach lights and runway lights are

good targets, thus allowing the television to show approximately equivalent capability to that of the FLIR system, but still not adequate for ILM requirements.

Nuclear systems appear particularly attractive for ILM applications because of the near independence of gamma radiation to weather conditions. The range of the systems is limited to straight-in fixed approaches from middle marker through rollout by practical size and location constraints on the ground nuclear sources. A short-range nuclear ILM potentially meeting the Basic and Case I requirements using a combination of nuclear beacons and in-runway radioactive sources is further described in this document as a potentially feasible concept.

Buried cables along the sides of the runway carrying alternating currents will generate a magnetic field which, detected on the aircraft, will give deviation from the runway centerline guidance. This concept could partially fulfill requirements for Case I, but none of the other ILM requirements. The concept was carried along in the study to consider the possibility of using it in combination with one of the other concepts. We found no concepts where the addition of the buried cable technique would improve the characteristics and, therefore, dropped it from further consideration.

Monopulse ranging radar was initially included as a separate ILM system concept for analysis. Monopulse ranging is a technique which can be, and is, used on the other radars considered in these concepts to improve resolution. Thus, we included this technique in discussions of those concepts and did not analyze it further as a system concept of itself.

Microwave imaging radiometers are not feasible for ILM applications. Resolution/accuracy capabilities are inadequate, physical size of the required antenna is

not practical for aircraft installation, and the image signal/noise ratio at the low approach angles is not adequate in degraded weather. As an example, for a 3° glide slope, 2 km range, 35 GHz, 16 mm/hr rain and concrete runway against grass background, the signal/noise ratio is -3 db. Using a 1 meter antenna on the aircraft, 0.5 meters is the maximum practical resolution achievable.

Simple microwave interferometers in either single station or multiple ground station configurations were found to have severe accuracy problems due to multipath phase errors. Azimuth errors can become unbounded and elevation errors on the order of 60° phase angle are common. Using a 10 wavelength interferometer, this corresponds to 6° elevation error. Due to this accuracy constraint, they were classified as not feasible for ILM consideration. Complex interferometers using special filtering and processing techniques to minimize multipath errors were not analyzed in this study. Significant accuracy improvements may be achievable here since for a fixed site many of the multipath sources are predictable and can thus be filtered.

A bi-static radar concept, utilizing an airborne receiver and a ground transmitter to illuminate the runway area and the inverse approach of an airborne transmitter and ground receiver, was included in the ILM system concepts list for evaluation. Since the ground unit, transmitter or receiver, had to be mounted in the approach region to the runway, the grazing angles for reflected energy were much poorer than for the other radar cases considered. A concept could be feasible for the detection of obstacles on the runway ILM requirement; however, the low grazing angles should make signal-to-noise levels too low for adequate runway imaging against the background terrain unless the runway is outlined with reflectors. This is then effectively equivalent to a beacon system.

The configuration K MLS for Category III landings is, of course, a candidate ILM itself. It is essentially a fail-operational system with its extensive redundancy and monitoring features. It does meet the Basic/Case I ILM requirements. It is not designed for obstacle detection or generation of a real-world perspective image (Cases II and III). It also is not truly independent from the primary landing guidance system and, thus, as an ILM could suffer failures due to noise or non-redundant failed components such as antennas simultaneously with the primary system.

Inertial aiding was briefly considered for possible support or improvement to the other concepts investigated for ILM. Inertial platforms alone do not provide sufficient accuracy for the landing function, but are useful for filtering and smoothing noisy position reference data from other landing aids. Because inertial platforms are relatively costly and most commercial transports are not outfitted with them, we did not include inertial aiding in our recommended feasible concepts.

As can be noted from Table 6, a total of 8 system concepts of the 20 analyzed are considered feasible. Three multilateration concepts were included in this list. The most promising concept, 3c, was selected for further analysis. Descriptions of potentially-feasible concepts were developed for 2a - imaging radar, 2b - radar (triangulation), 3c - multilateration with radar altimeter combination, and 6a - nuclear instrument landing system in combination with 6b - runway centerline radioactive sources. Several types of precision approach radars have been in operation for years and their capabilities are well known. The design goals of the MLS are well documented and are apparently being met in the continuing MLS development.

Key factors of the feasible concepts are given in Table 7. The numbers shown should be considered approximate and are provided in this chart purely to comparatively summarize the capabilities and constraints of the feasible ILM concepts.

Redundant MLS and multilateration are the only concepts capable of providing monitoring of the primary landing system (MLS) over the full guidance coverage. The precision approach radar and nuclear concepts are constrained to essentially straight-in approaches at selected glide paths. The triangulation radar using 3 active reflectors on the ground has its best accuracy on straight-in approaches and degrades as it moves off in azimuth. The imaging radar will continually provide a perspective image to the pilot; however, until at least segments of the runway are in the image, it is of doubtful value for guidance. It should be noted from our definition of ILM functional requirements that the primary need for ILM guidance occurs from approximately the middle marker through rollout. All approaches are straight-in to touchdown through this region.

The effective range for the MLS is approximately 50 kilometers. The multilateration concept could be extended to the 50 kilometer range if a demonstrated need exists. However, for our multilateration concept, using a radar altimeter for elevation inputs with ground mapping of approach paths, a more practical limit of 20 km was assumed. At the longer ranges from threshold where high accuracy in elevation is not required, the use of baro altimeters for altitude input may be adequate. The effective ranges of the three radars shown are limits imposed by the 16 mm/hr rainfall capability requirement. The precision approach radar, being ground-based, uses very high transmitted power to penetrate the weather. The triangulation radar achieves greater range than the imaging radar through

Table 7 -- Key Factors of Feasible Concepts

FACTORS / CONCEPTS	GUIDANCE COVERAGE	EFFECTIVE RANGE TO THRESHOLD	TRAFFIC CAPACITY	ADDED WEIGHT IN AIRCRAFT	COMPARATIVE COSTS AIRCRAFT/AIRPORT		INSTALLATION PROBLEMS	PILOT DISPLAY
Redundant MLS	±60° azimuth, 1° to 20° elevation, rollout (relative to runway)	50 km	Hundred's	16 kgms	$14K	$122K	Complex Monitoring	Steering Cues Range-to-go
Multilateration & Radar Altimeter	Full azimuth, Mapped approach paths in elevation, rollout (relative to runway)	20 km	Hundred's	9 kgms	$7.5K	$200K	Gnd Sites remote from airport, need line-of sight to runway surface	Steering Cues Range-to-Go
Precision Approach Radar	±7.5° azimuth, 1° to 20° elevation to touchdown (relative to runway)	20 km	1 to 6	5 kgms	$5K	$400K to $800K	Complex, large ground antennas	Steering Cues Range-to-go
RADAR (Triangulation)	±15° azimuth, 1° to 6° elevation, rollout (relative to runway)	10 km	No Practical Limit	87 kgms	$77K	$75K	A/B scanning antenna	Steering Cues Range-to-go
Imaging RADAR	±15° azimuth, 15° elevation, rollout, obstacles (relative to A/C boresight)	1 km	No Practical Limit	75 kgms	$62K	---	A/B scanning antenna, CRT Display	Perspective Image
Nuclear	Fixed Az-El to touchdown, rollout (relative to runway)	1 km	Not limited	7.3 kgms	$1.8K	$26K	Radiation hazard to ground personnel	Steering Cues Range-to-go

the use of active repeating reflectors on the ground. At 5 mm/hr rainfall, the imaging radar range is approximately 5 km. The nuclear system is constrained to approximately one kilometer effective range due to practical location of the ground nuclear sources.

The traffic capacity of both MLS and multilateration concepts are limited by the response capabilities of the ranging interrogators/transponders. These can be designed to handle several hundred aircraft simultaneously. Angle information of the MLS is air derived and is not traffic limited. The precision approach radar must track each incoming aircraft to generate guidance commands with present configurations capable of tracking from 1 to 6 aircraft simultaneously. The triangulation and imaging radars will experience interference from the other aircraft ILM radars in close proximity to them unless frequency shifting techniques can be incorporated for high-density traffic situations. Frequency shifting and operational procedures should reduce this problem to satisfactory use for any practical traffic levels. The nuclear system is an air-derived guidance concept and is not limited in traffic capacity.

The added weight of equipment on the aircraft is relatively small for all of the concepts except for the triangulation and imaging radars. The weight factor and antenna size constraints could limit use of the airborne radar ILM concepts to the larger classes of CTOL transports.

The comparative costs of the redundant MLS are those costs estimated for increasing the MLS system from a fail-passive configuration to fail-operational. The costs quoted here were derived from literature sources, discussions with developers and from comparisons to equivalent equipments. Since the costs vary

drastically with quantity, redundancy, state of development, etc., these numbers should only be used for comparative purposes. It should be noted, the airport equipment costs for redundant MLS, multilateration, precision approach radar and nuclear are relatively high in comparison to aircraft equipment costs. For the triangulation radar equipment costs are significant for both airport and aircraft. All of the costs of the ILM are included in the aircraft equipment complement for the imaging radar concept.

Installation problems for adding redundancy to the MLS system should not be severe and consist primarily of adding redundant transmitters on the ground and redundant receivers on the aircraft with the associated switching and monitoring logic. For the multilateration concept to have a relatively large area of coverage, the ground sites may have to be remote from the airport. Line-of-sight clearance from the ground sites to the runway surface must be maintained to provide rollout coverage. The precision approach radars have complex large ground antennas which should be sited close to the runway surface. Both the triangulation and the imaging radars require large scanning antennas and radomes in the nose of the aircraft. An antenna of adequate size (1 meter horizontal dimension) may not be feasible for mounting in business jets and smaller transport aircraft. The imaging radar requires a CRT display to the pilot. In an operational configuration, this display would probably be superimposed on an EADI display. The primary installation problem with nuclear systems is the potential radiation hazard to ground personnel both for maintenance to the system and for general operational procedures in the vicinity of the nuclear sources.

The pilot display for the imaging radar will be a perspective image CRT display. Each of the other concepts provide steering cues or commands and range to go to touchdown or stop end of runway information. This information can be displayed on flight director types of displays as is currently done with ILS displays. More elaborate synthetic runway displays could be generated from the information and may be required for the pilot to adequately follow curved and segmented approach paths.

REALIZABLE SYSTEM DESCRIPTIONS

The four potential ILM sensor systems considered for refined study are:

- o imaging radar
- o radar triangulation
- o beacon transponder multilateration with radar altimetry
- o nuclear ILS

These sensor systems have been configured into four feasible ILM's which are briefly summarized in the following paragraphs. A functional description of each ILM is provided together with a discussion of special features and constraints. The details on each of these systems are presented in Section VI.

Imaging Radar

An imaging radar ILM is shown in the general block diagram of Figure 2. A phased array or slotted waveguide antenna is used for this concept to reduce size. It is physically slewable in azimuth to compensate for large aircraft crab angles but has electronic scanning for the generation of imagery. The antenna produces a fan beam with angular scanning only in azimuth.

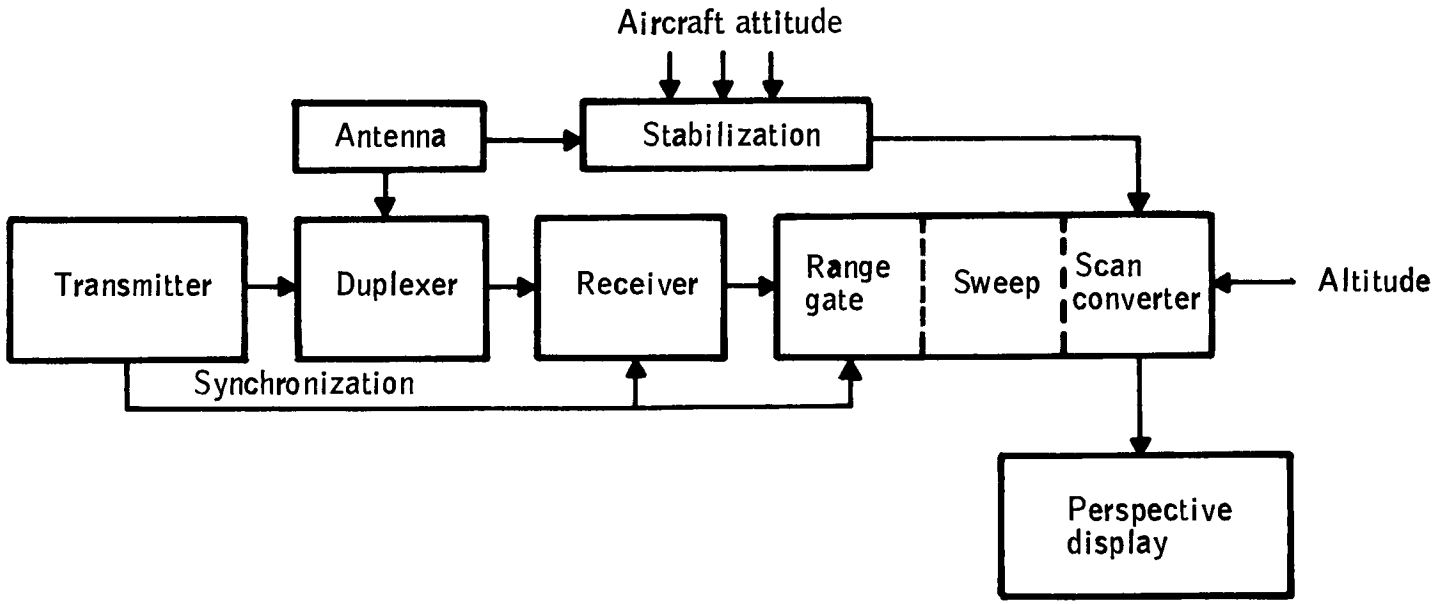

Figure 2 -- Block Diagram of Imaging Radar

The system will operate at K_a-Band in order to eliminate the need for monopulse resolution improvement (MRI). Receiver tuning and adjustment of transmitter power levels may be required to optimize the imagery as range to the runway decreases.

The system interfaces require an altitude input to the scan converter to convert the radar angle/range coordinates to angle/angle coordinates to display the proper real-world perspective image. Aircraft attitude inputs are required for stabilizing the real-world imagery as the aircraft maneuvers. The stabilization signals will come from the aircraft's inertial navigation system or from other instrumentation incorporating inertial sensors.

The imaging radar ILM does not require an interface or link with ground electronics and can be entirely an airborne system independent of airport equipment. However, passive reflectors at the edge of the runway at some air terminals with low runway-to-background contrast may be necessary to enhance the runway outline on the display.

Radar Triangulation

A general block diagram of the radar triangulation ILM is shown in Figure 3. The triangulation system decreases the problems of signal attenuation and precipitation backscatter by responding to a transmission through a ground transponder after a suitable frequency shift. Since detection is made on a transponder return which has ample strength, detection ranges can be extended beyond the capability of the imaging radar. Altitude data will not be required if three frequency translators and vertically-resolving beams are employed. Ambiguities

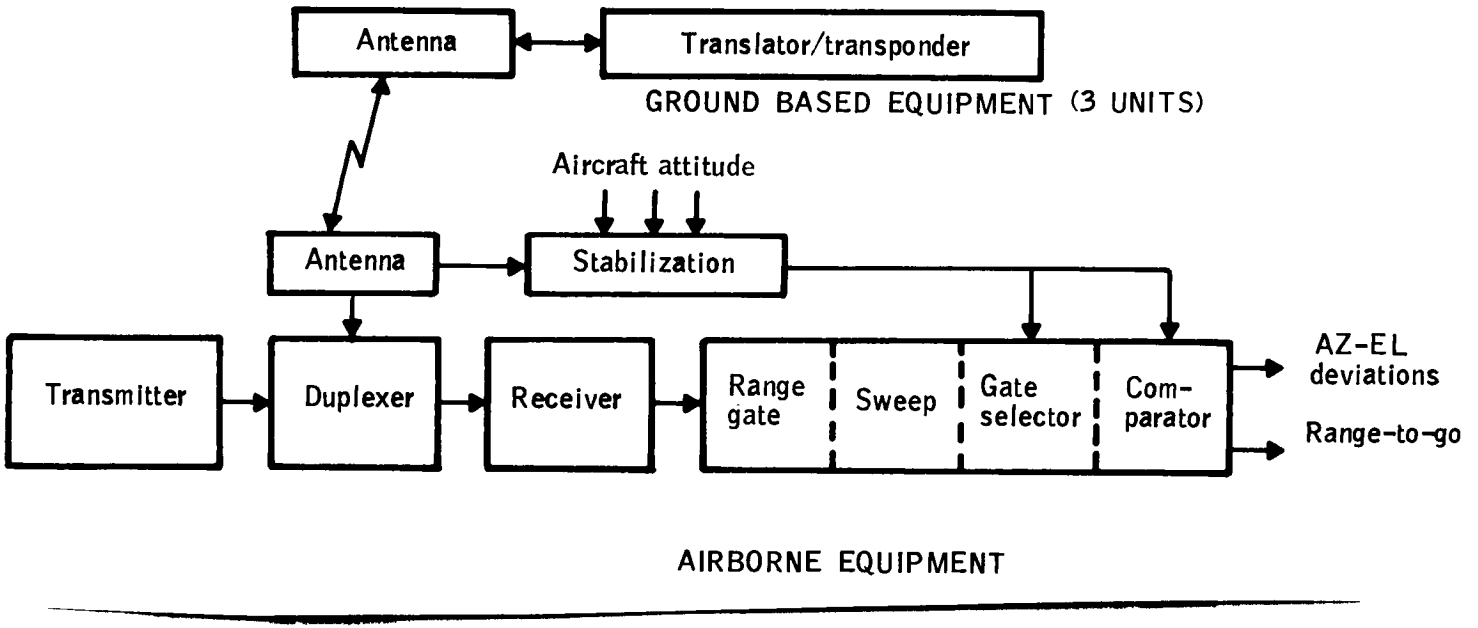

Figure 3 -- Block Diagram of Radar Triangulation

in angular position data can be removed by proper positioning of the transponders around the runway. Angles and range to each of the ground transponders are measured to compute aircraft position. Aircraft position is then compared to a pre-selected approach path to generate the steering commands.

This concept is capable of providing guidance over the desired ILM ranges. It, however, sacrifices the capability for obstacle detection and real-world imagery. The selected concept uses K_a-band to improve resolution. However, an X-band dual mode weather/landing aide radar is also feasible.

Ground Controlled Multilateration

A general block diagram of a ground controlled multilateration ILM with altitude enhancement is depicted in Figure 4 The equipment complements and basic system interfaces are shown. Altitude aiding is provided by a radar altimeter aboard the aircraft.

The multilateration ILM determines range from a ground station (either a command station or a remote slave station) to the aircraft by measuring transmission signal round-trip transit time. Each range measurement defines the radius of a sphere on which the aircraft is located. Solving for the intersection of spheres defines the target location.

Aircraft position is referenced to the approach path and deviations from the path are transmitted to the aircraft for display to the pilot. The path deviations are computed at the ground command station. For altitude enhancement provided by radar altimeter measurements, a map of the terrain under the approach

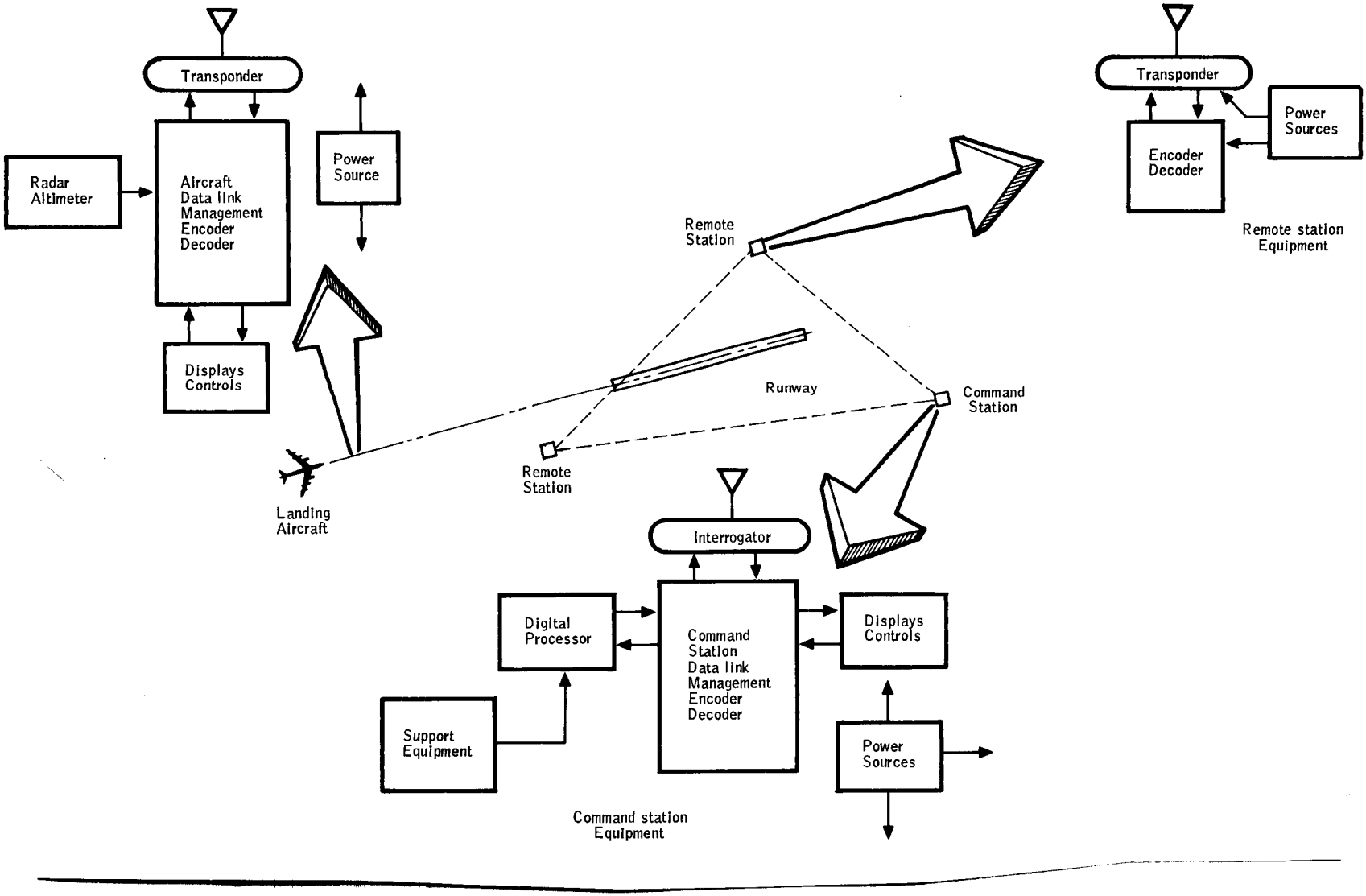

Figure 4 -- Ground-Controlled Multilateration System

path will be stored in the computer. This data is required in order to reference the radar altitude measurement to the runway surface.

Airborne equipment will process received DME pulses and respond with a reply. It will receive up-link commands for display to the pilot and will also down-link the radar altitude measurements to the command station.

The multilateration ILM will drive a non-imaging type of display to the pilot which shows deviations from the approach path and range-to-go to touchdown or stop end of runway. The ground antenna installations must maintain line-of-sight to each other and to the runway surface to provide continuous guidance through rollout. This requirement may require a unique siting configuration at each airport. In most cases, this concept should be capable of providing guidance to all runways at an airport.

Nuclear Sensor ILM

The nuclear instrument landing system (NILS) proposed for the ILM is primarily the one developed by TRW, Inc., with certain modifications to provide greater coverage. A general block diagram of this concept is shown in Figure 5.

The system consists of the radiation sources on the ground and the detection equipment aboard the aircraft. The radiation sources are sited to provide coverage from approximately the middle marker through rollout. The detection and processing equipment generate signals that indicate to the pilot where the aircraft is relative to the approach path.

The operation of the NILS is similar to that of a standard ILS in that it generates a fixed landing guidance beam. Four nuclear radiation beams, rather than

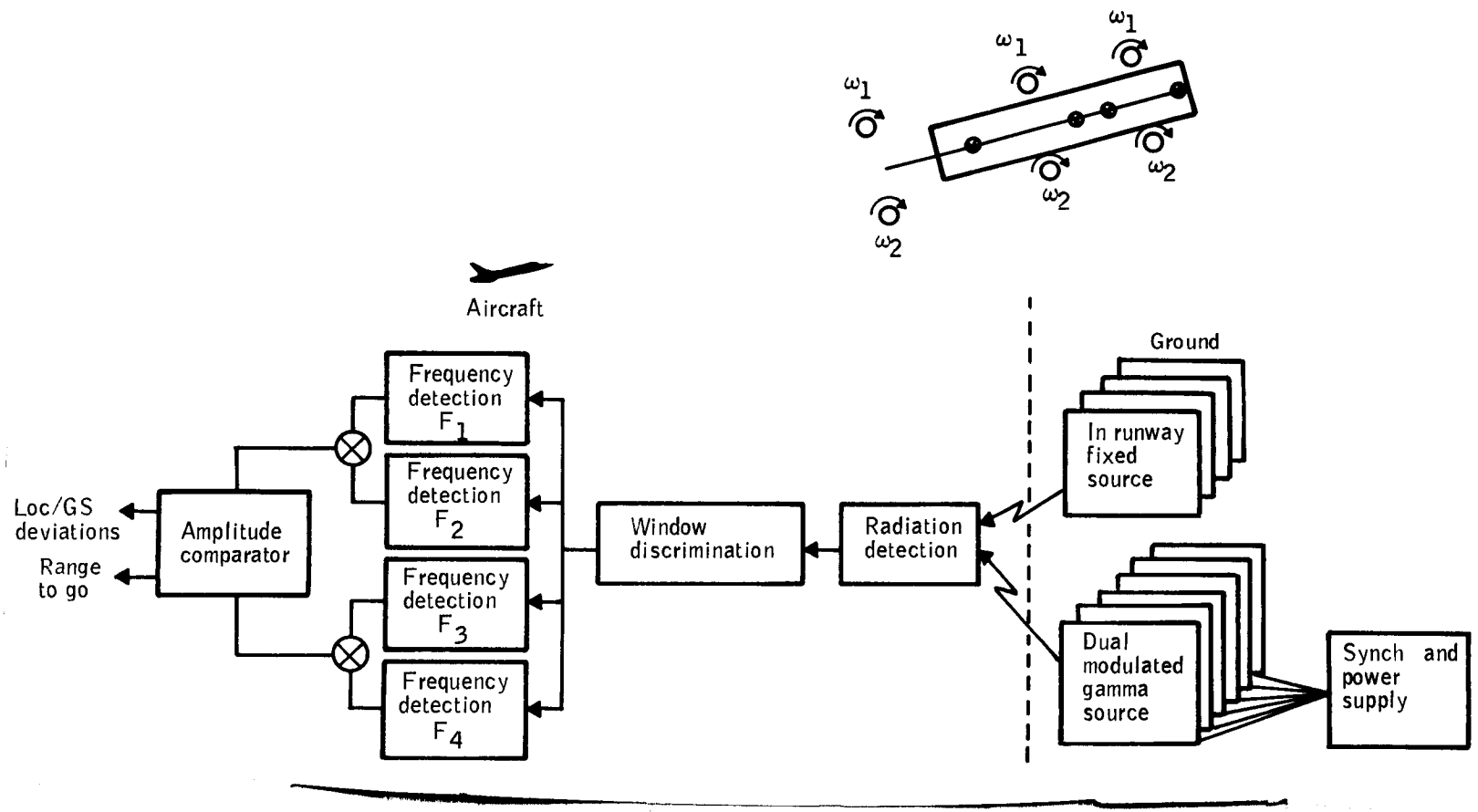

Figure 5 -- Nuclear Instrument Landing System

radio beams, are modulated at different frequencies; two are used for the localizer, two are for the glideslope. The nuclear beacons on the left side of the runway are mechanically modulated at 60 and 90 Hz; the right side beacons are modulated at 24 and 36 Hz. When the aircraft is on course, all four signals received have equal amplitudes.

The primary advantages of the NILS are its low cost and immunity to weather. Worst case weather degrades the signal by less than 2.5 db/Km.

This ILM concept is useable only for fixed straight-in approaches in the final steps of the landing sequence. It can be designed to meet the minimal requirements for an ILM at relatively low cost. The system cannot easily be expanded to provide greater coverage or more flexible approach paths.

CONCLUSIONS

1. From the baseline set of requirements used in this study for an Independent Landing Monitor (ILM), the most critical functional need for the ILM occurs in the approach range from middle marker through rollout. Failures of the primary landing guidance system outside this region in CAT II, CAT III weather will dictate a procedural missed approach (or break from the landing sequence). The guidance will revert to the VOR-DME, inertial or other terminal area/enroute guidance systems with the ILM being of little guidance value for this function.

   Inside of this region, time between events for decisions becomes compressed and maneuvering space for missed approach becomes limited. The best solution, in this case, may be to provide an ILM backup to the primary guidance

system to permit continuing the landing using manual steering in the event of failures in the primary system.

A cost payoff for addition of ILM capability to commercial transports may come from this feature, allowing the reduction of the primary guidance/flight control system from a fail-operational configuration to a fail-passive configuration with the ILM and the pilot providing manual landing capability in the event of failures to the primary system. To achieve this, the pilot must be able to manually land the aircraft using the ILM for guidance. No confidence building or monitoring capability can be derived from the ILM unless it is of adequate accuracy and reliability to allow the pilot to rely on the guidance presentation for this function.

Changes in the baseline requirements can change the critical region of operation for the ILM. For example, as a Category II landing aide it's functional need is limited to altitudes above decision height.

2. A total of six ILM concepts were considered feasible for meeting parts of, or all of, the ILM functional requirements. These are:

    - o Redundant MLS
    - o Precision approach radar
    - o Multilateration/radar altimetry combination
    - o Airborne radar (triangulation)
    - o Airborne perspective imaging radar
    - o Nuclear

Each of these sensors, except for precision approach radar, are in varying stages of development and will require significantly more development time and testing before they could be considered ready for operational usage. None of the configurations considered fully meet all of the desired ILM functional requirements or even show potential for fully meeting these goals.

3. Both FLIR and television sensing systems were ruled out as ILM candidates because of their very limited range capabilities in CAT II/III weather conditions. Microwave imaging radiometers were considered inadequate for resolution/accuracy requirements and for image quality in degraded weather. Microwave interferometer concepts reviewed exhibited very poor accuracy due to multipath problems and could not meet ILM requirements. Magnetic cable, bi-static radar, and inertial aiding concepts had very limited applications for meeting the ILM requirements and did not provide sufficient additional capability to warrant including their added complexity to recommended systems.

4. A true real-world perspective image of the runway should be a desirable display for the ILM since it would resemble the imagery of a VFR landing. When one considers the operational aspects of maximum expected pitch and azimuth (crab) angles and possibly close-in curved approaches for aircraft landings, the sensor field of view requirements and, thus, display size, become too large for aircraft mounting of the equipment to be practical. The question must then be asked, does the imaging display, which is not in a true size and perspective to ground, still provide adequate steering cues to the pilot, or does it become misleading at times of high stress or workload? If it is misleading, a synthesized display showing steering cues or commands only may

be a preferred concept. This question was not analyzed in this study; however, earlier studies with image magnification indicate pilots tended to land short for greater than unity magnification and long for less than unity magnification. Extending these results to this case, it would seem reasonable a non-true perspective image display could be misleading to the pilot for deriving steering cues.

5. Experimental data on radar differential cross sections for runway surfaces and background or surrounding surfaces of snow, grass, dirt, etc., for the very low grazing angles as are encountered on approaches, are extremely limited. Extrapolation of radar reflectance data experimentally measured at higher incidence angles was attempted, however, it is not satisfactory for a rigorous analysis. Thus, one can say under some conditions, the runway will be detectable on the imaging radar display against the surrounding background at adequate ranges. Calculation of a specific detection range is subject to great uncertainty with the limited data. It can be stated with certainty, however, that with the widely-varying possible runway surface conditions and surrounding background surface conditions, there will be cases when a runway is not distinguishable from the background in the imagery. For example, a snow-covered runway tends to appear as the snow-covered background.

6. An ILM concept which is totally contained on the aircraft, independent from ground equipment, is a desirable feature. It could permit so-equipped aircraft to make landings in more severe weather conditions than for which the airport is normally certified. The perspective image radar is the only

concept considered feasible which meets this objective. The same argument could be used for a ground-based ILM concept, however, in this case the aircraft must as a minimum be equipped to receive and use steering commands.

7. The signal to noise ratio and resolution requirement on imaging displays for target detection and recognition of "small" objects are well defined in the literature. We found no directly applicable studies defining these requirements for large familiar objects, such as runways, or defining the key runway/surrounding characteristics from which the pilot derives his steering cues. Definition of these parameters are necessary to adequately determine feasibility of imaging ILM sensors.

RECOMMENDATIONS

1. Radar sensors show a potential to meet all of the desired ILM functions. How well they will meet the functions is still a question which depends on many variables including:
    - o atmospheric conditions
    - o runway/surroundings type and characteristics
    - o aircraft flight parameters
    - o signal processing
    - o display characteristics
    - o sensor parameters

    Perspective imaging radars have been fabricated and put through flight tests. This work serves to demonstrate the potential of the concept, but cannot evaluate the system through all of the variables or to the extremes

of any of the variables. Hardware design optimization cannot be achieved when operating with a fixed set of flight test hardware.

A mathematical model should be developed to simulate the perspective imaging radar for the ILM functions. The model should permit variation of ground scene, atmospheric conditions, flight parameters and sensing/processing characteristics in generating realistic imagery outputs. Use of this simulation, varying the weather parameters and best estimates of terrain characteristics to their extremes, in a systematic analysis, should identify the range of environmental and operational conditions over which the imaging radar ILM will function and should aid in determining the optimum signal processing/display and sensor parameters for hardware design. With minor changes, the results should be applicable to all types of radar sensors. Much of this simulation and analysis can be done in non-real time with imagery at selected points in the approach path. Real-time operation of the model on a piloted simulator would provide a measure of the adequacy of the guidance information content of the display to the pilot.

2. The other potentially feasible concepts all generate aircraft position or deviation from desired position relative to the runway coordinates. Each concept differs, however, in the method of position generation, effects of weather, areas of coverage, siting constraints, etc.

Further analysis of these concepts should concentrate in two areas at this time. A more detailed definition of expected performance and errors should be made for each potential concept over the full range of ILM operational and environmental conditions. The second area should define the ILM sensor/pilot interface. Display, display generation and installation are

major cost and weight factors which must be considered in selection of a preferred ILM system concept. Potential ILM displays range from simple localizer/glide slope deviation presentations on flight directors through CRT synthetic runway/aimpoint presentations to the real-world perspective image display.

Mathematical models of the MLS, multilateration, nuclear and triangulation radar concepts should be developed to analyze the two problem areas. Since the MLS is expected to be the primary guidance system, it's performance through curved, segmented and straight-in approaches should be used as a baseline comparison for the ILM concepts. The errors for each type of approach and environmental condition, and from this, the critical sensing requirements, can be identified for each ILM concept through comparison of the simulation outputs.

These ILM models can be incorporated in a real-time piloted landing simulator to drive potential ILM displays in realistic simulations. Through a systematic test program, the simplest display meeting the pilot's information needs for each ILM functional requirement could be identified for each potential concept.

3. The operational needs and the resulting functional requirements for an ILM must be better defined since these impact heavily on both ILM sensor requirements and displayed information requirements. For example, this study assumed the ILM will function as a monitor of, and backup to, a Configuration K MLS (Cat. III landing capability). With this assumed functional requirement, the critical ILM sensing requirements and pilot display requirements

(accuracy, weather degradation, field-of-view) occur in the final steps of the landing sequence from middle marker through rollout in Cat. III weather when the pilot must rely on the ILM for guidance in the event of MLS failure. This baseline function, however, is only one of several possible functions for an ILM.

An alternative baseline assumption, equally valid, could pose the primary ILM functional requirement of upgrading the aircraft landing capability beyond that for which the airport is normally equipped. For example, an ILM-equipped aircraft could land in Cat. II weather at an airport equipped with a Cat. I MLS or no MLS or in Cat. IIIa weather at a Cat. II MLS or ILS equipped airport. These assumptions change the range, coverage, weather attenuation, sensing requirements and also the pilot information requirements. Utilization for landings in Cat. II conditions moves the critical ILM sensing requirements to longer ranges (outer marker to decision height) with corresponding reduced accuracy requirements since the pilot can do final landing control with visual guidance.

The potential additional or alternate ILM functions with their unique sensing requirements should be compared with the sensing capabilities identified in this study. This comparison would permit more realistic value judgments to be made on each of the feasible ILM concepts. Some of the possible functions are:

- Permit Cat. II landings at airports equipped with Cat. I or no primary landing system.
- Permit Cat. IIIa landings at airports equipped with Cat. II MLS or ILS.

- o Permit curved and segmented approaches for Cat. II/IIIa at ILS equipped airports.
- o Add constraint ILM must be self-contained on aircraft independent of aircraft facilities.
- o Utilize ILM strictly as monitor of primary automatic landing system.

4. Heavy rain (signal attenuation) and high crosswinds (large viewing/scan angles) tended to be limiting factors on the feasibility of the ILM sensing concepts. However, these atmospheric conditions may be a very low percentage of the total weather conditions for which the ILM should function. For example, if fog is the predominant problem, it may be desirable to design the ILM to meet that condition and continue to use operational landing constraints for the low frequency occurrences.

   Statistical measures of the frequency of occurrence of the weather conditions of concern should be compiled (several analyses of this have been done and are available in the literature). From this, the relative value of including specific sensing requirements on the ILM selection and design can be identified. In addition, examination of the frequency of occurrence of Cat. II, Cat. III weather in conjunction with the alternate possible ILM functions discussed in Recommendation 3 for the projected 1980's operational conditions will permit relative value rankings to be placed on incorporation of the various ILM functions. Potential ILM users could convert these to true value rankings by incorporating the weather statistics and class of airports in their normal route structure.

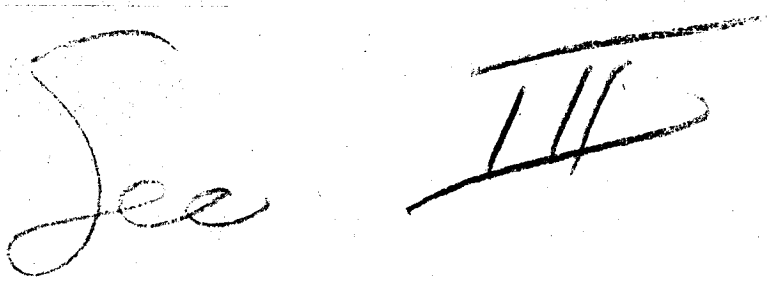

SECTION III
REQUIREMENTS

This section of the report discusses the requirements established or assumed for the ILM. The ILM functions are identified first, then the operational environment for the ILM is defined. Sensor requirements are discussed in relation to the four specified ILM functional configurations defined in the Introduction (Section I).

ILM FUNCTIONS

The Independent Landing Monitor can be used to serve one principal function and multiple secondary functions. As a minimum, its principal function must allow the pilot to assess the performance of the autoland system and aircraft situation relative to the runway under conditions of low visibility prior to a committment to land. This function is primarily a confidence giver to the pilot. If he receives any indication of unsatisfactory conditions from the Independent Landing Monitor, he makes a missed approach.

A secondary function, closely related to the primary function of the ILM, would allow manual take-over to land by the pilot on a failure of the autoland system after committment to land. This type of system would permit a fail-passive autoland system rather than the fail-operational type of system and allow a possible cost tradeoff justification for the ILM.

Another secondary function is warning the pilot of obstacles on the runway and turnoffs. This function is not presently performed by any equipment on the aircraft. It is partially performed by ground traffic control systems with warnings to the pilot.

Under Category III b and c conditions, the ILM should provide the pilot turnoff and taxi capability. This function is not provided by MLS or current landing aids.

For the ILM to function, it is clear the pilot must use the ILM as his eyes during Category III landings to make them appear as Category II types of landings. That is, at a specified decision height he must have adequate vision of the runway to make his decision on committing to land. If he does not have adequate vision he must make a missed approach. Below this decision height the pilot should be able to take over manual control of the aircraft on failures of the automatic landing system and manually land the aircraft.

A flow chart of a typical Category III Landing Sequence using ILM is shown in Figure 6. As shown the co-pilot monitors the automatic landing instruments and fault warning devices. The pilot monitors the Independent Landing Monitor and the normal visual approach. Landing is only completed if the pilot has the potential of taking over manual control using the Independent Landing Monitor or his own eyes for the approach. Decision height in this case would nominally be 30.5m (100 feet) altitude.

A detailed study (Reference 6) analyzed the extent of information the pilot needed to make his decision to land or make a missed approach prior to decision height. Four pertinent factors listed below were given in this report:

1. The pilot requires a minimum of 3 seconds of viewing the ground prior to decision height to assess the visual information and make his decision.
2. The pilot can manually adjust lateral offsets from the runway up to plus or minus 30.5m (100 feet) for a decision height of 30.5m (100 feet) altitude.

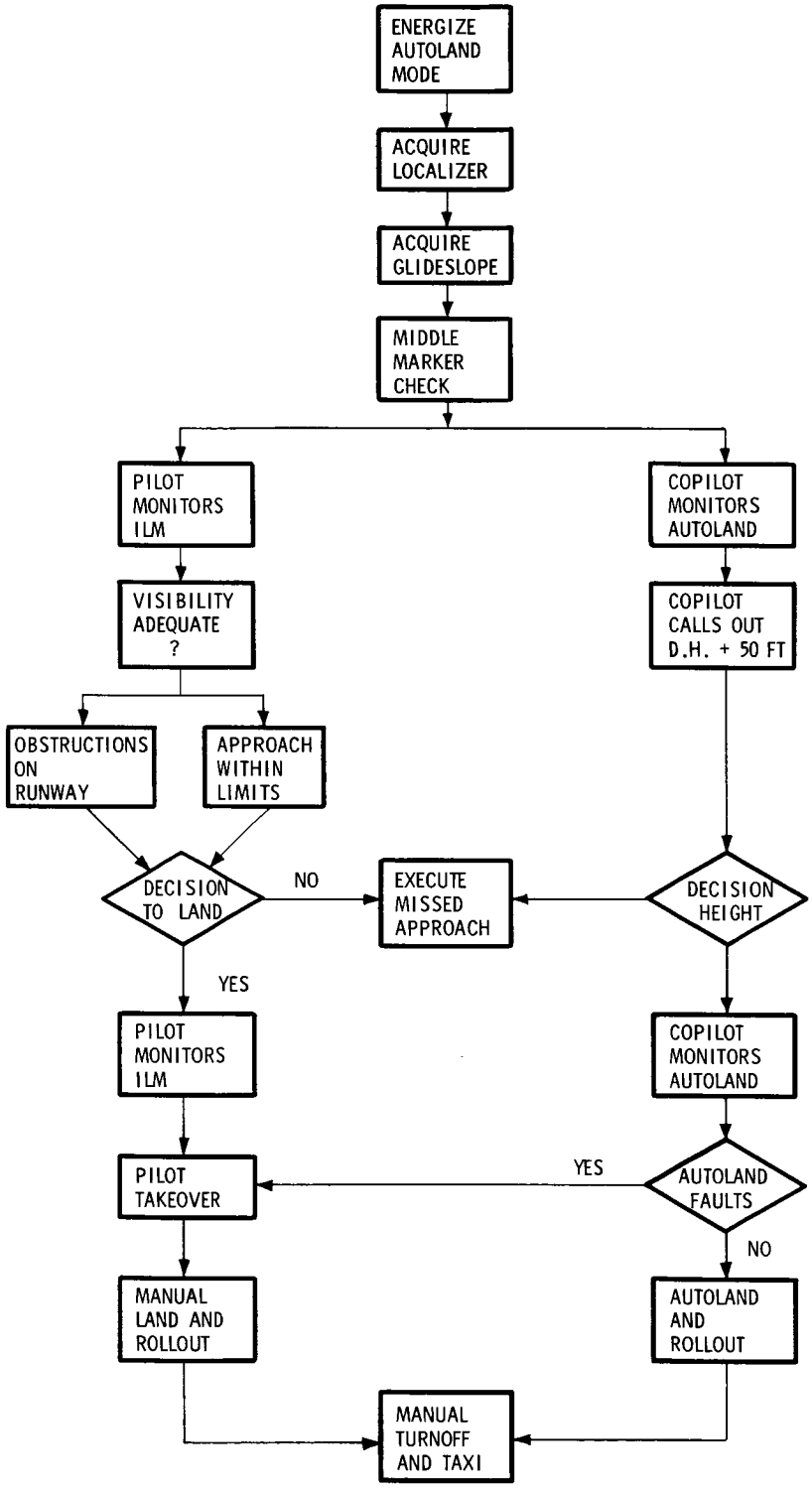

Figure 6 -- Typical Category III Landing Sequence

3. The visual segment of the ground approach path observed by the pilot should be greater than 304.8m (1000 feet) for the pilot to adequately assess his position in the approach. Overshoots or missed approaches increase to approximately 10% of the approaches for 182.9m (600 foot) segments.
4. It is not necessary for the pilot to initially see runway threshold to make his decision. He must be able from the visual segment he views to identify where he is on the approach.

These factors are used in the following sections to determine minimum sensing requirements for an Independent Landing Monitor.

OPERATIONAL ENVIRONMENT

An Independent Landing Monitor (ILM) is intended to provide the pilot/crew of an aircraft operating in a terminal area with a means of assessing the aircraft's approach state under adverse weather conditions (Category III). This means of assessment will be generated by a monitor system that is completely independent from the system generating autoland commands for the aircraft flight control system. Since ILM will be required to enhance the all-weather operation of the Microwave Landing System (MLS), it must operate within the same environment as the MLS. The following pages summarize the pertinent MLS operating environment data as it applies to the ILM functions.

Many of the environmental requirements presented here have been extracted directly from References 1 and 2 which explicitly present the requirements for the MLS. Some of the ILM sensing concepts will be located aboard the aircraft and others are co-located on the ground with the MLS equipment. Requirements

relating to both aircraft and ground installations are also presented (e.g., system accuracy requirements, and electromagnetic interference).

The data presented herein sets the framework within which the ILM must operate. The MLS baseline parameters are presented with emphasis on the airspace coverage and approach paths that MLS configuration K (and consequently the ILM) must be compatible with. In addition to data on required performance accuracies, the weather and other environmental considerations, a description is presented of the future ATC systems with which the ILM must interface.

MLS Baseline Parameters

Coverage -- The coverage volume identified for the operation of MLS is the volume of airspace in which the MLS can be used by the pilot/crew in the terminal area for precision approach path following, landing, and go-around. At long ranges and wide angles (azimuth and elevation), the coverage is defined to be that point when the data quality is adequate for the pilot to start following the automatic approach

The RTCA coverage goals for MLS configuration K are shown below:

ELEVATION:	Lateral	- ±1.047 rad (60°)
	Vertical	- 0.01745 rad (1°) to 0.349 rad (20°)
	Range	- 55.56 km (30 nm)
AZIMUTH:	Lateral	- ±1.047 rad (60°)
	Vertical	- 0 to 0.349 rad (20°)*
	Range	- 55.56 km (30 nm)

*The angle 0 applies to at least the length of the runway plus 0.926 km (0.5 nm) beyond the approach end of the runway.

DISTANCE:	Lateral	- ±1.047 rad
	Vertical	- 0 to 0.34 rad*
	Range	- Stop end to 37.04 km (20 nm)
BACK AZIMUTH:	Lateral	- ±0.698 rad (40°)
	Vertical	- 0 to 0.349 rad
	Range	- 0 to 9.26 km (5 nm)

Airport Characteristics and ILM Siting -- The ILM must not impose inherent limitations on the various operations of airports. It must be designed for adaptability to changes in patterns of operation and growth at various airports and to traffic handling capacities as great as any foreseeable acceptance rate of any airport runways.

ILM ground equipment (if used) must operate independent of the nature of runway surface material, adjacent surfaces, and other fixed airport equipment. Configurations of runways at present and future airports include single runways, crossed multiple runways, parallel runways (both adjacent and staggered), uncrossed multiple runways, special purpose runways, special purpose landing areas, and combinations of these configurations. The dimensions of runways or landing areas for which operational requirements for approach and landing service have been stated fall predominantly into the following ranges:

Runways ranging from 24.4m (80 feet) to 60.96m (200 feet) in width by 1524m (5000 feet) to 3657.6m (12,000) feet) in length for conventional aircraft.

*The angle 0 applies to at least the length of the runway plus 0.926 km (0.5 nm) beyond the approach end of the runway.

It is necessary that the primary approach and landing system serve airports and landing areas of this dimensional range. Thus, the ILM system should also meet these parameters. Future parallel runway spacings may be as low as 820 meters (2500 feet).

Equipment location must be no closer than 60.96m (200 feet) from any runway or crossing runway or taxiway. Where taxiing aircraft can potentially block the signal path, the system must be suitable for operation if it is sited within 152.4m (500 feet) (91.4m (300 feet) desired) of an active crossing runway or taxiway.

ILM equipment locations must conform to FAA Aviation Regulations, Part II, Objects Affecting Navigable Airspace, and FAA Handbook 8260.3A (TERPS). These regulations are summarized briefly below, as they affect equipment siting. Where compliance is not possible or would be too costly, request for waivers must be considered.

Any obstacles (terrain) or equipment along the approach paths to the runway are limited in elevation with respect to the runway. The approach surface increases at a slope of 50:1 from a point 61m (200 feet) from the end of the runway to a distance of 3048m (10,000 feet). The slope then decreases to 40:1 to a distance of 15,240m (40,000 feet).

System Capacity -- In order for the ILM to operate with and be totally independent from the MLS, it must have the capacity to service up to 200 aircraft simultaneously. At most airports, however, much lower capacities will be expected. In high air traffic densities, the ILM must be compatible with aircraft delivery to the runway at intervals as short as 30 seconds with an accuracy of ±5 seconds.

The traffic density within 18.52 Km (10 nm) considered to be a typical requirement for ILM will be up to 33 aircraft; within 9.26 Km (5 nm), up to 8 aircraft. The ILM must be functionally compatible with 50 taxiing aircraft.

Approach Paths

The MLS is required to provide guidance for a variety of approach paths, from a simple straight path to complex curved paths, in order to improve runway capacity and noise abatement procedures. In order to monitor such approaches, ideally the ILM should independently determine the position of an aircraft along such paths. The information provided to the pilot/crew should enable him to observe the aircraft's position and timing relative to the prescribed or computed curved path. It should be noted all of the paths converge to a straight in path to the runway at the shorter ranges from decision height to touchdown where the ILM functions are most critical.

The features of curved path capability that are possible by using MLS guidance are:

- o Approach or departure paths which facilitate minimizing the noise in sensitive areas with a minimum reduction in traffic capacity of the airport. This includes paths at higher altitudes and greater lateral distances than might otherwise be flown.
- o Approach paths which permit aircraft with different speed or descent capabilities to follow the minimum common path. The use of lateral and vertical separation will allow for increased runway capacity.
- o Precision following of prescribed routes with minimum path overshoot to allow high density operations into closely spaced parallel runways.

- Precision rate information in range and angle shall be available for accurate control of the aircraft "time of arrival" at the threshold. This will allow the potential for higher runway acceptance rates.

Azimuth Paths (Constant Elevation) -- The following paths will be possible using MLS guidance (the paths are illustrated in Figure 7):

1) A radial, constant heading flight path to the intercept point.
2) A dogleg or series of straight line segments at a succession of azimuth angles.
3) A curved transition path from any point within the MLS azimuth coverage volume to a zero-azimuth course.

Elevation Paths (Constant Azimuth) -- The following paths will be possible using MLS guidance (Figure 8):

1) A straight, constant-elevation angle flight path toward the Glide Path Intercept Point (GPIP) with the runway. The elevation angle will be either fixed or pilot-selectable in the aircraft over a range from 0.035 rad (2°) to 0.105 rad (6°) for CTOL aircraft and from 0.052 rad (3°) to 0.262 rad (15°) for V/STOL.
2) Same as paragraph 1) but with an offset GPIP. The offset may cover a range from -304.8 m (-1000 feet) to +609.6 m (+2000 feet) with respect to the actual GPIP.
3) A multi-segment flight path toward the actual or an offset GPIP. The initial segment may be steeper than the final segment, or vice versa for VTOL, as required for noise abatement purposes (see Figure 8).
4) A curved flight path to a specified touchdown point using precise range and

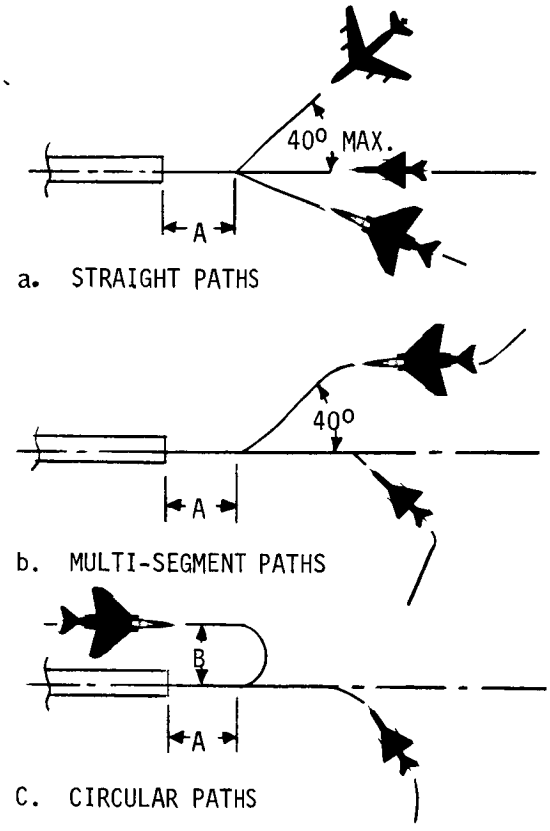

NOTES:

A. IF FLOWN AT CONSTANT ALTITUDE TO GLIDE SLOPE INTERCEPT, THIS DISTANCE WILL BE 2-8 MILES DEPENDING ON INTERCEPT ALTITUDE AND G.S. ANGLE. IF COMBINED WITH DESCENT, A MAY BE AS SHORT AS 1 NM.

B. THIS DISTANCE MAY BE 1/2 NM MIN FOR STOL, 2.4 NM FOR CTOL

Figure 7 -- Possible Landing Approach Paths -- Azimuth

altitude from the flare elevation system. A straight flare path may also be considered as a special case of the curved path.

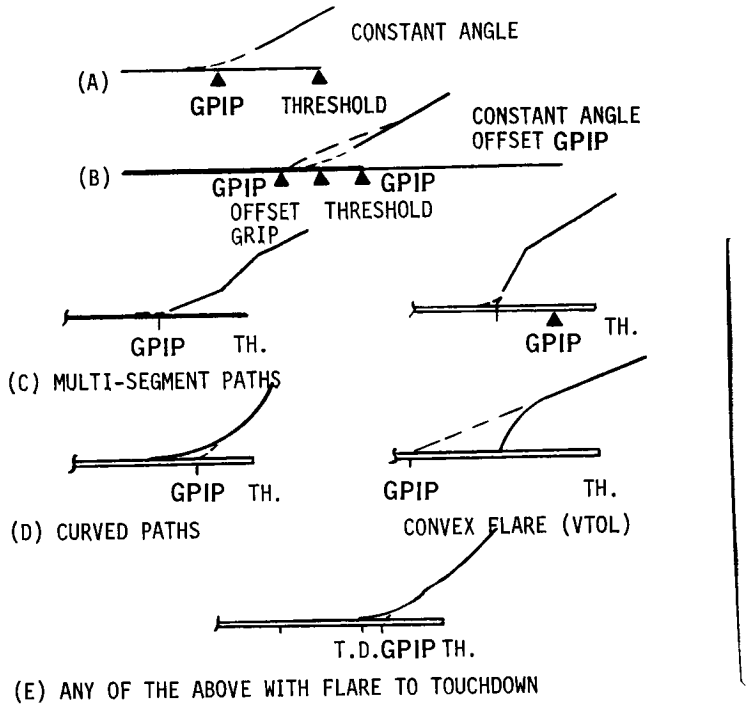

Figure 8 -- Examples of Vertical Profiles

Combined Variable Azimuth and Elevation Paths -- Flight paths which are combinations of the above shall be possible with the MLS guidance.

Airborne Flight Path Capability -- The ability of any aircraft to fly these paths will depend on its computing capability. Even to fly the simple segmented azimuth paths of (b) in Figure 5, a capability to offset the azimuth angle reference is required (except for the zero-azimuth straight-in approach).

Electromagnetic Signatures of Airports and Surroundings

Tables 8, 9 and 10 show electromagnetic signatures for background types and are

Table 8 -- Background Signature Data

ID Code No.	Computer Name	(a) Descriptive Comments	Photo/Visual Reflectivity r_b	Normalized Radar Cross-Section						IR Emissivity ε_b		
				X-Band		K_u-Band		K_a-Band				
				ϕ (deg)	Γ_b (db)	ϕ (deg)	Γ_b (db)	ϕ (deg)	Γ_b (db)	1-3μ	3-5μ	8-14μ
1A	ASPHALT ROAD	Dry	0.08	5	-43	5	-38	5	-23	0.75		
1B				40	-29	40	-25	40	-17		0.79	
1C				75	-25	75	-20	75	-10			0.91
2A	CONCRETE ROAD	Smooth, dry	0.35	5	-48	5	-44	5	-39	0.60		
2B				40	-26	40	-31	40	-29		0.88	
2C				75	-32	75	-22	75	-17			0.99
3A	DIRT ROAD		0.03	5	-37	5	-24	5	-22	0.54		
3B				40	-25	40	-17	40	-15		0.80	
3C				75	-18	75	-10	75	-10			0.98
4A	LOAM SOIL	Bare, black,	0.12	5	-27	5	-19	5	-14	0.58		
4B		rich		40	-20	40	-14	40	-14		0.85	
4C				75	-18	75	-12	75	-13			0.94
5A	SANDY SOIL	Bare	0.30	5	-31	5	-29	5	-25	0.56		
5B				40	-28	40	-25	40	-18		0.82	
5C				75	-22	75	-20	75	-14			0.94
6A	CLAY SOIL	Bare	0.15	5	-27	5	-19	5	-14	0.54		
6B				40	-21	40	-14	40	-14		0.88	
6C				75	-18	75	-12	75	-13			0.97
7A	CONIF FRST/SMR	Coniferous	0.03	5	-22	5	-23	5	-24	0.86		
7B		forest, summer		40	-27	40	-21	40	-14		0.96	
7C				75	-30	75	-22	75	-14			0.97
8A	CONIF FRST/WTR	Coniferous	0.07	5	-22	5	-23	5	-24	0.88		
8B		forest, winter		40	-27	40	-21	40	-14		0.97	
8C				75	-30	75	-22	75	-14			0.99
9A	DECID FRST/WTR	Deciduous	0.10	5	-22	5	-23	5	-24	0.62		
9B		forest, winter		40	-27	40	-21	40	-14		0.82	
9C				75	-30	75	-22	75	-14			0.88
10A	DECID FRST/SMR	Deciduous	0.15	5	-22	5	-23	5	-24	0.70		
10B		forest, summer		40	-27	40	-21	40	-14		0.89	
10C				75	-30	75	-22	75	-14			0.93
11A	GREEN GRASS	Short	0.08	5	-24	5	-22	5	-15	0.60		
11B				40	-21	40	-19	40	-14		0.75	
11C				75	-17	75	-16	75	-13			0.85
12A	BROWN GRASS	Short	0.05	5	-23	5	-22	5	-14	0.61		
12A				40	-21	40	-21	40	-14		0.80	
12C				75	-12	75	-15	75	-13			0.89
13A	SNOW		0.75	5	-25	5	-30	5	-37	0.15		
13B				40	-19	40	-23	40	-29		0.20	
13C				75	-13	75	-12	75	-25			0.25
14A	WATER STATE 0	Water, sea	0.05	5	-40	5	-39	5	-38	0.99		
14B		state 0		40	-39	40	-35	40	-33		0.99	
14C				75	-15	75	-14	75	-14			0.99
15A	WATER STATE 3	Water, sea	0.03	5	-39	5	-37	5	-35	0.99		
15B		state 3		40	-35	40	-33	40	-31		0.99	
15C				75	- 8	75	-10	75	-12			0.99

(a) This data is not stored in the library.

Table 9 -- Supplementary IR Emissivity Data[a]

Type of Material	Average Emissivity (Ref. 6)		
	1-3μ	3-5μ	8-10μ
Vegetation - Grass			
Bromegrass, Green	0.60		
Red Canary Grass, Green	0.60		
Orchard Grass, Green, Normal Healthy	0.60		
Orchard Grass, Full-rust infected	0.53		
Fescue, Meadow, Dry Grass	0.61	0.80	0.89
Tall Fescue, Green, Very Coarse	0.60		
Timothy, Green	0.60		
Alfalfa, Green, Healthy	0.68		
Alfalfa, Yellow	0.68		
Vegetation - Trees			
Beech Leaf, Top, Yellowing	0.48		
Beech Leaf, Top, Brown, Drying	0.54		
Oak Leaf, Winter Color, Top, Dry	0.66	0.89	0.91
Holly Leaf, Dry, Top	0.67	0.89	0.91
Holly Leaf, Bottom	0.66	0.87	0.94
Laurel, Mountain, Green	0.72	0.89	0.92
Maple Leaf, Pressed Dormant, Top, Dry	0.61	0.87	0.92
Needles - Pinus Resinosa (Red Pine)	0.77	0.97	0.98
Bark, Red Northern Oak	0.79	0.90	0.95
Bark, North American Jack Pine	0.68	0.88	0.97
Twigs, North American Jack Pine	0.88	0.96	0.97
Bark, Colorado Spruce	0.75	0.87	0.94
Water			
80-degree Angle of Incidence	0.68	0.66	0.68
60-degree Angle of Incidence	0.95	0.94	0.96
0-degree Angle of Incidence	0.99	0.98	0.99
Soil			
Vereeniging, Africa, Soil	0.58	0.82	0.94
Mesita Negro, Lower Test Site, Soil	0.71	0.75	0.92
Pullman Loam, New Mexico	0.65	0.78	0.93
Colts Neck Loam, New Jersey	0.70		
Hainanamu Silt Loam, Hawaii	0.84	0.84	0.94
Barnes Fine Silt Laom, South Dakota	0.64	0.78	0.93
Gooch Fine Silt Laom, Oregon	0.62	0.80	0.98
Maury Silt Loam, Tennessee	0.62	0.74	0.95
Grady Silt Loam, Georgia	0.65	0.85	0.94
Dublin Clay Loam	0.75	0.88	0.97
Sand, Atlantic City, N.J.	0.55	0.75	
Sand, Daytona Beach, Fla.	0.35	0.65	
Sand, Daytona Beach, Fla.	0.50	0.80	
Silica Sand	0.45	0.70	
Paint			
Pigment No. 6, Chrome Green I	0.65	0.85	0.99
Pigment No. 7, Chrome Green II	0.63	0.83	0.96
Galvanite, Zinc Coating - Galvanite Corp.	0.50	0.52	0.50
Aluminum Paint, Exterior and Interior, Chromaton	0.29	0.30	0.37
Aluminum Paint, Exterior and Interior, Steelcote	0.40	0.40	0.48
Krylon Aluminum Acrylic Spray, No. 1401, Krylon, Inc.	0.24	0.25	0.33
Aluminum, Asphalt Base, No. 3483, Sears Roebuck and Company	0.40	0.42	0.44
Aluminum Lacquer, No. S-2432-C, Stone-Hudge, Inc.	0.52	0.55	0.48
Kerpo No. 25, Aluminum, Protective Coatings Corp.	0.25	0.26	0.23
Construction Materials			
Cement	0.60	0.88	0.99
Asphaltic Road Material, SC-4, Standard Oil of California	0.75	0.79	0.91
Coal Tar Pitch (Melting Point 170-180° F.)	0.93	0.91	0.98
Metals			
Aluminum, Commercially Pure	0.21	0.12	0.07
Aluminum, Weathered, Aircraft	0.33	0.27	0.18
Chrome Plate on Stainless Steel	0.35	0.20	0.10
Stainless Steel, Bare, Clean	0.66	0.54	0.43

[a] This data is not stored in the library; it is for information only.

Table 10 -- Microwave Emissivities for Two Angles of Incidence

Material	30°	45°
Water	0.41	0.34
Concrete	0.88	0.80
Asphalt	0.89	0.82
Short Grass	0.94	0.94
Soybeans	0.96	0.96

Colocation With ILS -- The ILM must operate satisfactorily and without degradation when colocated with existing VHF/UHF instrument landing systems to serve the same or other runways. At the same time, the performance of the ILS should not be degraded by the presence of the ILM. Siting criteria are contained in FAA Handbook 6750.16.

ILS Localizers -- Various types of localizers currently in use are listed in Table 11. Consideration must be given to each of these in locating ILM equipment.

Table 11 -- Types of ILS Localizers

		Height (ft)	Length (ft)	Characteristic
1.	8 Loop	1.5m (5 ft)	12.2m (40 ft)	Transparent
2.	V-ring	2.1m (7 ft)	32.0m (105 ft)	Transparent
3.	Waveguide	1.8m (6 ft)	32.0m (105 ft)	Opaque
4.	AN/MRN-7	2.1m (7 ft)	25.9m (85 ft)	Opaque
5.	Alford Wave	1.8m (6 ft)	13.7m (45 ft) 25.9m (85 ft)	Transparent
6.	TI Parabola	4.0m (13 ft)	35.7m (117 ft)	Opaque
		5.5m (18 ft)	53.6m (176 ft)	
7.	2 frequency combinations of above			
8.	Tower installations of above			
9.	Future probably similar to above			

presented for consideration of sensor systems aboard the aircraft. The data was extracted from References 3 and 4 and presents coefficients for use in analysis of ILM sensors operating in the various regions of the electromagnetic spectrum.

The letter designation A, B, or C associated with each background type in the first two tables has significance only for the IR emissivity signatures. The letter "A" signifies the 1- to 3-micron region, "B" signifies the 3- to 5-micron region, and "C" signifies the 8- to 19-micron region.[1]

The signature data for each background type is:

- o Photo/visual reflectivity
- o Normalized radar cross-sections (db) as a function of radar frequency-band and depression angle
- o IR emissivity as a function of the spectral region of interest
- o Microwave Emissivity

Normalized radar cross-section is defined here in units of db as equal to ten times the logarithm (to the base 10) of the average value of cross-section per unit area at the given depression aspect angle.

The angular dependence of microwave emissivities for various background materials are shown in Figure 9 (taken from Reference 4).

[1]Thus, for example, background 2A, 2B, 2C all represent the same smooth dry, concrete road. However, if a 1-3 micron IR sensor is to be modeled, the user should input background 2A when considering a concrete road. If an 8-14 micron IR sensor is to be modeled, the user would input background 2C.

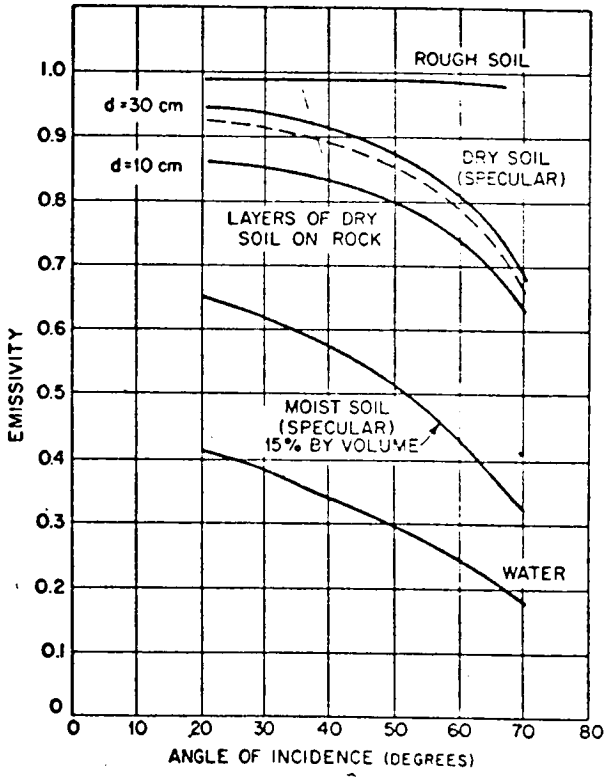

Figure 9 -- Calculated Soil Emissivities

Approach Lights -- ILM equipment may have to be located within the approach light lane of a runway instrumented for two-way service. FAA Handbook (6850.2) identifies four types of approach light configurations. ALSF-1 and 2 for Category I and II approaches respectively, represent the most stringent case. ALSF-2 is shown in Figure 10.

The lights are 30.5m (100 feet) apart and are aimed at a point 487.7m (1600 feet) ahead of the glide path. This affords about 2.4m (8 feet) of clearance above a light bar to avoid blocking the light ahead of it.

FAA Handbook 6850.2 also specifies that the approach light plane shall be even with the runway surface +2 percent, -1 percent. The +2 percent slope corresponds to the 50:1 obstacle clearance plane slope, and in these cases, a waiver may have to be obtained to penetrate the obstacle clearance plane with frangible antenna structures.

Electromagnetic Interference (EMI)

EMI from any potential source must not cause undetected guidance errors in the ILM which might endanger flight safety. This is defined to be angular errors not greater than four times the standard deviation of the specified accuracy limits during critical flight phases. Interfering signals which might cause greater errors must be detected and must activate flag alarms.

EMI Sources -- The radiating sources which may give rise to EMI may be located aboard the same aircraft as ILM, aboard other aircraft or on the ground as follows:

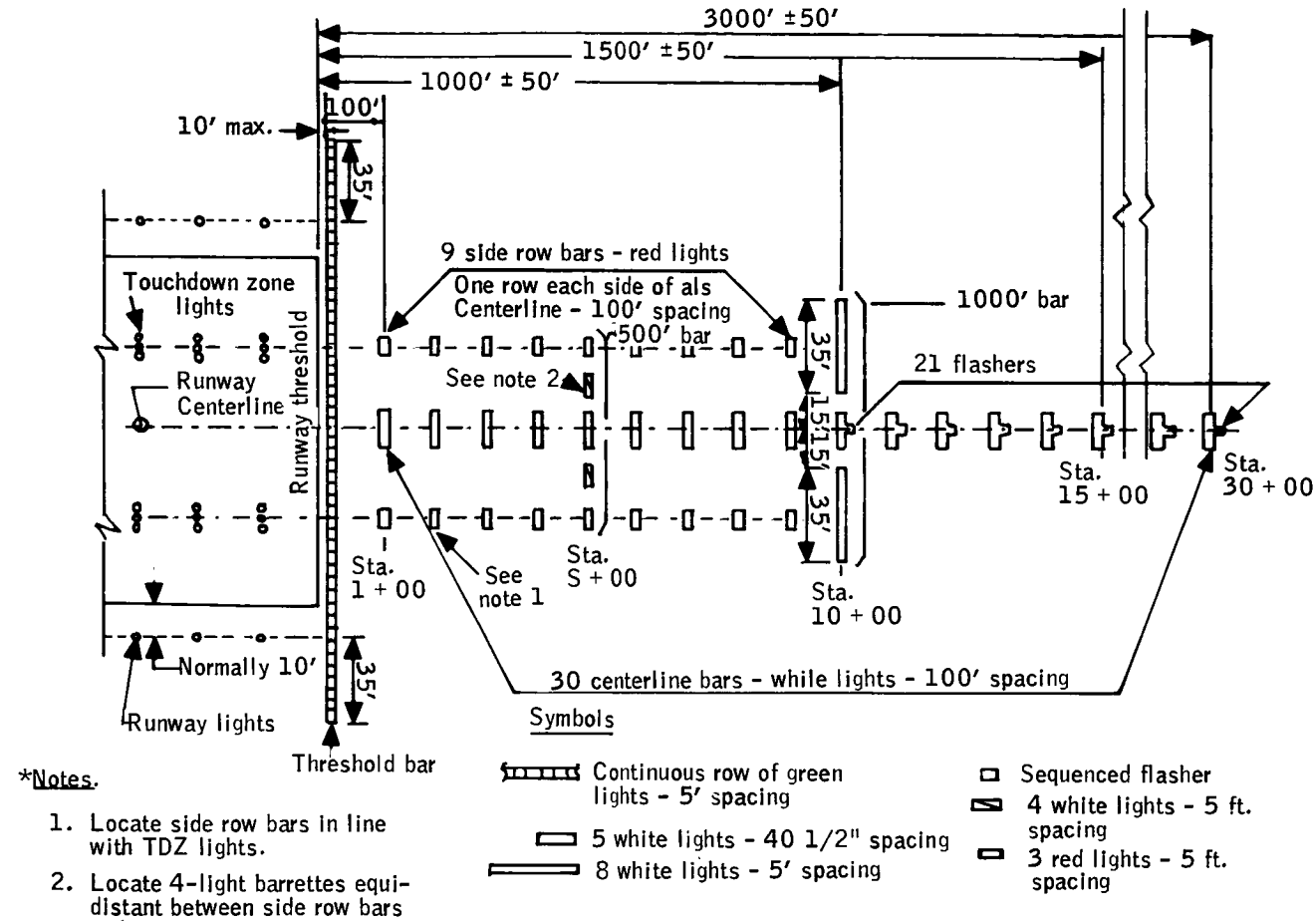

*Notes.

1. Locate side row bars in line with TDZ lights.
2. Locate 4-light barrettes equidistant between side row bars and centerline bars.

Figure 10 -- ALSF-2 Approach Light Configuration

Airborne Sources in the Same Aircraft

a. VHF, UHF and HF communications

b. Local oscillator radiation

c. Angle signal into C-band DME signal (MLS)

d. C-band DME signal into angle signal (MLS)

e. L-band DME and beaconry

f. Airborne radars (weather, doppler, surveillance)

Characteristics of these airborne sources are shown in Table 12.

Table 12 -- Airborne EMI Sources

Equipment	Frequency	Power Class
VHF Communications	118-136 MHz	10-50 watts
UHF Communications	225-400 MHz	10-50 watts
TACAN DME	960-1215 MHz	400 watts peak (3 watts avg)
Radio Altimeter	4200-4400 MHz	1.0-10 watts avg
Airborne Doppler	8800 MHz 13.25-13.40 GHz	0.5-10 avg 0.5-10 avg
MLS DME	5003-5060 MHz	400 peak (3 watts avg)
Weather Radar	C-band	No data
ATC Radar Beacon System	1025-1150 MHz	400 watts peak (3 watts avg)
Collision Avoidance	1592.5-1622.5 MHz	275 watts peak

Airborne Sources in Other Aircraft -- The same sources listed above apply here, but are further removed from onboard ILM equipment and, thus, should have lesser effect.

Radiating Sources on the Ground

a. Ground radars (L-, S-, X-band)
b. Communications VHF/UHF
c. Radio/TV broadcast

Most Probable Sources -- The most probable source of EMI will be closely spaced radiation sources in the same aircraft. Considerable reductions are possible using adequate antenna spacings and shadowing, as well as input filtering.

The second most probable sources will be high-power transmitters in the vicinity of landing sites: radars, VHF/UHF communications and other facilities. These may be in the 50-watt to 50-kilowatt range; or possibly in the megawatt peak power range in the case of military radar installations. The increased power levels of these sources can offset the greater distance separations, as compared with the airborne case. Characteristics of typical ground-based radiating sources are shown in Table 13.

EMI Standards -- MIL-STD-461A and 462 are intended to provide compatibility margins with any potential external environment. These standards should provide guidelines for the design of ILM equipment.

In particular, MIL-STD-461 and MIL-STD-462 will apply in the design stage, and MIL-E-6051 will apply to the system as installed in an aircraft.

Table 13 -- Ground-Based EMI Sources

Equipment	Frequency	Power Class
VHF Navigation	108-118 MHz	100 watts
VHF Communications	118-136 MHz	10-1000 watts
UHF Communications (Military)	225-400 MHz	10-1000 watts
TACAN	960-1215 MHz	100 watts
Approach Control Radar	S-band (3 GHz) X-band (10 GHz)	Megawatt class (Peak power)
ATC Radio Beacon	1030 MHz	
Airport Surveillance Radar	K-band	
MLS	5000-5250 MHz	

(Also TV at VHF and UHF, amateur, telephone relay, etc.)

The intent of the requirements covered in MIL-STD-461 is to ensure that interference control is considered and incorporated into the design of new equipment. To this end it sets forth acceptable limits of emission and susceptibility for interference control. MIL-STD-462 complements 461 by outlining test procedures to measure the pertinent emission or susceptibility. MIL-E-6051 is an installed equipment specification for airborne systems which is intended to ensure electromagnetic compatibility among all electronic systems on the aircraft. MIL-STD-469 presents EMC requirements for radar systems, and also is pertinent to this development.

Expected 1980's ATC Compatibility

The ILM must function within the confines of the ATC systems of today and those

planned for the future. Civil ATC environments can be characterized in several dimensions:

- o In terms of time it starts with the ATC complex of today involving the ARTS II and III systems. It will evolve into an upgraded third-generation ATC system during the 1980's, and potentially into a fourth generation ATC system in the 21st century.
- o In terms of needs, the ATC system will evolve to handle higher air traffic densities, and to provide higher runway acceptance rates.
- o There will continue to be a spectrum of different air traffic control system configurations depending on the level of service required in various geographical areas.

The different types of ATC air space considered for the 1982 time frame are characterized in Table 14. The high density air space will be characterized by the Intermittent Positive Control concepts presently being evolved for the upgraded third-generation ATC system. The low density air space will be quite similar to the current medium density general aviation airport environment.

The possible geographical interfaces between the ATC system and an ILM system are discussed in the following paragraphs. These areas of interface are identified as:

- o Control Zones
- o ATC Paths
- o ATC Gates

Table 14 -- 1982 Terminal Airspace

	Low Density	Medium Density	High Density
Type of Control	VFR	Mixed VFR and IFR	Positive Control
Data Acquisition	No surveillance	ATCRBS	ATCRBS+DABS
Communication	Voice Comm.	Voice comm + data link	Voice comm + data link
Aircraft Navigation	Heading, A/S, VORTAC	Precision VORTAC	Precision VORTAC + R-NAV
ATC System	Manual local control	ARTS-III	Upgraded ARTS-III
Separation Assurance	Collision avoidance - see and be seen	Manual on ground + IPC?	Automatic on ground + IPC Airborne CAS?
Landing Aid	MLS	MLS plus other Cat. II facilities	MLS plus other Cat. III facilities
ATC Concept	Manual flight plans	Computer flow control	Computer flow control

Control Zones -- The control zones for the different types of civil ATC have been moderately well planned by the FAA. Figure 11 shows the FAA air space allocation plan for 1982. The high density airports will have a special terminal control area with a radius that is likely to extend out to 27.78 km (15 nm) and ceilings that are likely to extend from 2133.6m (7000 ft) to 3048m (10,000 ft) altitude. Other airports are likely to have smaller control zones with a radius of 9.26 km (5 nm) and a ceiling of 914.4m (3000 ft). The significance of the terminal control areas is that this is where the highest precision of the MLS (and consequently the ILM) will be required. MLS may also be used for precision paths and gates outside of the control zones, but the requirements for precision are likely to be less.

For military operations such as the USAF, the radius of the terminal control areas are likely to be larger (i.e., out to 37.04 km (20 nm)). The minimum

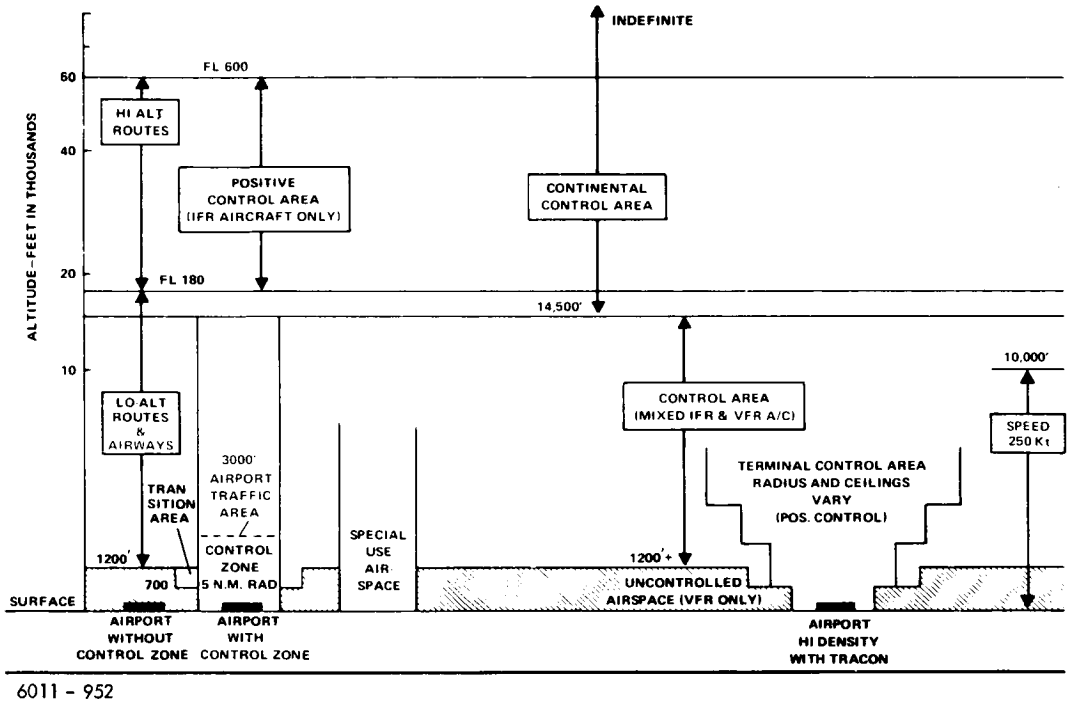

Figure 11 -- FAA Airspace Allocation 1982

controlled altitude for the USAF is likely to be higher to allow for Army controlled air space at low altitudes. In U.S. Army ATC, the maximum altitude of control is similarly likely to be limited to 914.4m (3000 ft) to 1219.2m (4000 ft) altitude.

ATC Paths -- In many types of ATC systems, a series of standardized approach paths will be established leading to an instrumented runway. Figure 12 illustrates a possible path arrangement presented by the ATC AC studies. There are a great variety of possible shapes, ranging from the presently used series of straight paths toward navigation facilities or intersections, through very complex corkscrew paths being considered for VTOL operations. In studies on ATC compatibility, several major types of paths have been considered:

- Multiple straight legs approaching the runway.
- Multiple straight legs approaching a closely spaced pair of parallel runways. Runway spacing is assumed to be 762m (2500 feet).
- Simple curved paths with a variable radius to achieve limited control of time arrival.
- Straight paths with trombone-shaped maneuvers for path stretching.
- Paths with spiral profiles for descent in confined areas.
- Elevation paths with multiple segments approaching the threshold.
- Pairs of multiple segment elevation paths to provide altitude separation as close to the runway as practicable.

Further work needs to be done to better define the range of paths that will be used for air traffic control in the future. It is assumed that a typical high density airport is likely to have a number of different standardized paths

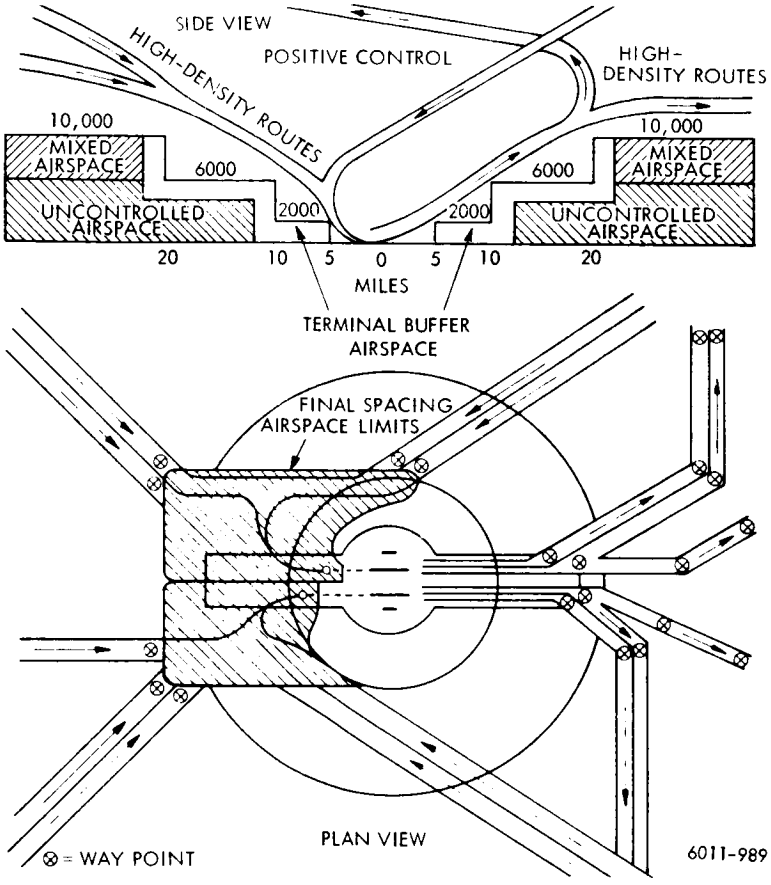

Figure 12 -- Schematic of High Density Terminal Area Airspace

Table 15 -- Initial Approach Gate Definition

Category	User	A/C Type	Gate Range (nmi)	Gate Altitude (ft)	Lateral Angle
III	FAA	CTOL	15	4-10,000	±45°
III	FAA/NASA	STOL	10	2- 8,000	±45°
III	USAF	CTOL	20	3-10,000	±30°
III	USN/USMC	CTOL	8	1- 8,000	±30°
II	FAA	CTOL	15	2-10,000	±10° to ±45°
II	USMC	V/STOL	8	1- 8,000	±10°
I	FAA	CTOL	6	1- 4,000	±10°
I	US Army	C/V/STOL	6	200- 8,000	±20° to Omnidirectional

approaching the runway or runways. Some of these paths will be relatively simple so that aircraft with a minimum complement of equipment can be integrated into the traffic pattern.

ATC Gates -- It is recognized that the ATC complex will not necessarily use a series of so called gates which are fixed in space. The initial approach gates are, however, a very useful tool to define the ATC interface with an ILM or the MLS. The rationale for establishing the gates is that the aircraft will enter the MLS and ILM covered zone under control of another navigation aid. At some point during the approach, the aircraft will become committed to a specific runway and a specific path to that runway. At an initial approach gate, the aircraft will be required to be on a precision flight path in order to assure separations. For this reason, the initial approach gates defined in Table 15 have been postulated.

ATC Communications Interface -- Communications from the air traffic control system on the ground to the aircraft are the key link in the overall process. In the future, there are a number of factors which will increase the demand for communications with the ATC system and/or with the MLS and ILM systems. The traffic densities are expected to be higher. The flight path and the timing precisions are expected to be tighter. In addition, the paths that the aircraft will follow in the high density air space will be more complex than presently used.

The various communication functions planned for the upgraded third-generation ATC system are shown graphically in Figure 13. The Communications which potentially are affected by the use of MLS and ILM include the Automatic Terminal

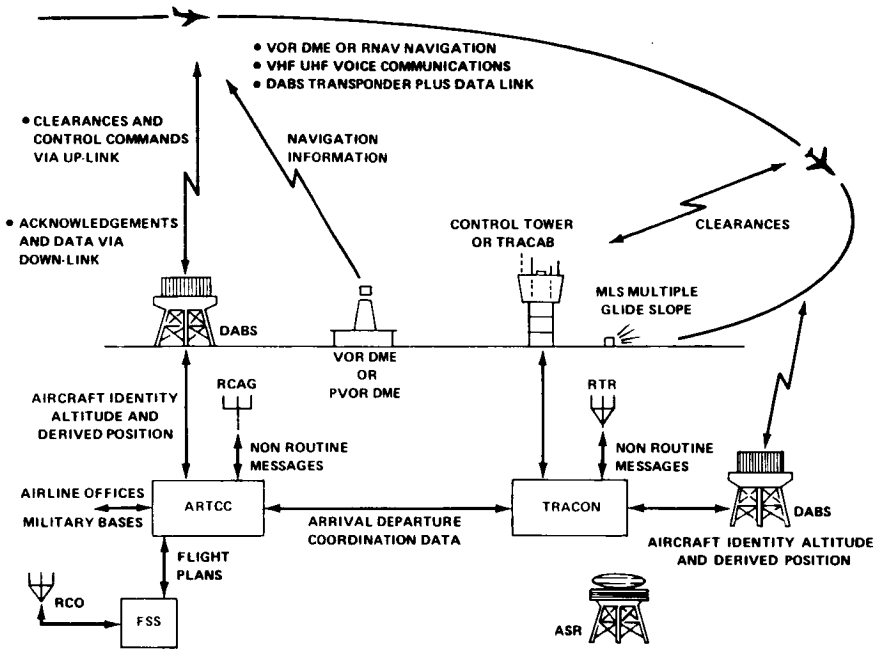

6011

Figure 13 -- Upgraded Third Generation ATC System Functions

Information Service nominally to be transmitted over the VOR signal, communications with the TRACON using either (1) voice or digital communication via the remote transmitter/receivers or (2) oral communication with the control tower. In addition to these, there will likely be a discrete address beacon system (DABS) as an upgrading of the ATCRBS. The MLS auxiliary data and the ILM may also play a part in the air traffic control communication process.

The factors associated with the ATC communication interface are summarized in Table 16. There seems to be a planned capability for all the information items needed for current ATC operations.

Table 16 -- Air Traffic Control - Communication

Channels	Aural (VHF comm, ATIS)
	Digital (data link, MLS aux. data, ATC)
	Charts (SID, STAR)
Information	Terminal area clearances
	Terminal area vectors
	ATIS field area data
	Runway clearances and data
	R-NAV and special path definition
Displays	Visual (alphanumeric and instruments)
	Aural
MLS Capability	Aux. data for runway clearance and data
	Does not provide field area data (ATIS)
	Does not provide terminal area ATC
	Displays are undefined and critical

In order to utilize the maximum potential of MLS and ILM for servicing closely spaced parallel runways and curved noise abatement paths, and to achieve higher delivery rates, there is a need for a substantial amount of additional information to be available in the aircraft. There are a number of optional solutions available to this extra communication requirement. They are:

- The data can be included in the charts and approach plates available to the pilot.
- The data may be standardized enough so that voice communication can be used.
- The data can be transmitted over a DABS data link.
- A separate data link can be introduced which communicates directly with the aircraft navigation computer and displays.
- There is potential to add a limited amount of additional ATC path information to the MLS auxiliary data and in an ILM.
- The ATC path data may be recorded in a form suitable for automatic insertion into the navigation computer and pilot displays. Magnetic tape cassettes or magnetic recorded cards appear quite reasonable for this application.

Another key item of the air traffic control communication interface involves the way the information is used in the aircraft. The data necessary for a flexible automatic landing capability is presently included in the MLS auxiliary data format, while the data used for the flexible curved path capability will have to be transmitted by another system. Much of this information must be automatically inserted into the electronic subsystems of the aircraft and should also be available for cross-checking by the crew. An important, unresolved question is the exact manner in which to display and/or insert this data. It appears that there are a number of potential ways to use much of the data with minimal additional pilot workload.

Separation Assurance -- The primary function of the air traffic control system is to provide assurance that safe aircraft separations are maintained. The factors associated with separation assurance are summarized in Table 17. This

table shows the needs for separation assurance in the future and the currently envisioned techniques to acquire the necessary position information for the air traffic control computer. The MLS system is considered to be compatible with air traffic control but does not provide a complete separation assurance to the degree considered necessary for flight safety. The MLS provides accuracy substantially higher than other systems; hence, there should be an inherently lower chance of midair collision. An ILM will add to this assurance.

Table 17 -- Air Traffic Control - Separation Assurance

Need	Independent monitor
	Data for ground directed control
	Possible future air-to-air data
Means	ASR (inadequate)
	PAR
	DABS
	MLS + down link
	CAS/PWI
MLS Capability	Accuracy better than monitors
	Does not provide direct ground data info
	Does not have down link
	No air-to-air capability

The level of integrity or confidence in the separation assurance function must be exceedingly high. The challenge is more demanding for Category III landings because the critical period starts when the air traffic routes' separation is reduced to 6.48 km (3.5 nm) or 3.70 km (2 nm). The separation assurance function must therefore account for not only single or multiple equipment failures, but also for blunders. A fully independent system is highly desirable for the primary separation assurance function. It is possible that MLS and ILM could be used for limited applications to separation assurance, but only for short

periods of time when the primary system has fully verified that no possible blunders could exist.

The function of separation assurance for the future closely spaced parallel runways is currently an unanswered question on the ATC interface. The concept of an approach separation monitor is based on a ground-based system which can be closely interfaced with the ARTS III or other air traffic control facility. The ASM would generally provide an additional source of precise position information. This concept is preferred because the ARTS facility is one place where the information on the "pilot's intentions" of all aircraft in the vicinity is available, together with the necessary aircraft identity information and an ATC data link to the aircraft. The functions of an approach separation monitor are typically as follows:

- o To accept identity flightpath and speed data from the basic ARTS memory.
- o Accept a handover of responsibility from the basic ARTS computation.
- o Determine course and cross-track velocities of each aircraft.
- o Detect hazardous overtake or cross track situations.
- o Provide visual and/or oral alarms to the controllers.
- o Provide course or speed warnings or advisories to the pilot.
- o Detect the need for a wave-off command and transmit it to the aircraft.
- o Perform a handover of wave-off or missed approach aircraft back to the ARTS.

Some of the characteristics desirable in an approach separation monitor equipment are as follows:

- o It should be desirable to have a capability to function with all currently equipped IFR aircraft.

- o It should be suitable to handle aircraft with mixed complements of equipment.
- o It would be somewhat desirable to have an independent capability to establish the aircraft identity. If this were not available the separation monitor would have to rely on receiving the identity at the handover process from ARTS and the continuity of position tracking information during the approach.

Detail consideration has been given to a number of potential options to provide this function. Table 18 illustrates six potential concepts which may be used for the approach separation monitor. Also shown are the potential capabilities and problem areas associated with equipped and unequipped aircraft. There may be other system concepts which are attractive but they have not been investigated in detail.

After consideration of the various system concepts and the system requirements, the following preliminary conclusions may be drawn:

- o The most promising concepts applicable to currently equipped aircraft appear to be the sector coverage ATCRBS with a precision monopulse measuring capability or an automatic pencil beam precision approach radar.
- o The concepts which appear promising to service presently planned new aircraft equipments would be the electronic scan ATCRBS system using the DABS feature or the MLS-DABS intertie. The period of time when these concepts may be available varies depending on the development period and the implementation of aircraft equipment.

Navigation Interface -- Another important interface that affects the air traffic control system involves the process that occurs when the aircraft changes from a terminal area navigation system to the MLS system guidance. This change of

Table 18 -- Approach Separation Monitor Concepts, Potential Capabilities and Problem Areas

	Beamwidth	Problems Equipped AC	Airborne Equipment	Problems Unequipped AC	Ident.	Data Link
ATCRBS/DABS	0.04 rad (2.3°)	Data Rate, Accuracy, Saturation, Resolution	XTG w/SEL Address	No capability	Yes	Yes
ATCRBS Sector Monopulse	0.03 rad (1.8°)	High PRF Interference	XTG	No capability	Yes	Yes
X-or C-band ASR Radar and Beacon	0.009 rad (0.5°)	Data Rate	New Beacon	Rain, Auto Track, Clutter	Potential	Limited
Pencil Peam PAR with Autotrack	.01 rad (0.6°)		None Required	Rain, Ident.	No	No
Multilateration (new)	Omni	Real Estate, Cost, Multipath	New Beacon	No capability	Yes	Yes
MLS-DABS Link	0.017 rad (1.0°)	Not Independent of NAV	Planned	No capability	Yes	Limited

navigation system will have to take place before the aircraft takes up the path which is unique to the specific runway. (Refer to Table 19.)

Table 19 -- Air Traffic Control - Navigation

Means	**Heading, altimeter, A/S**
	VORTAC + MLS
	Ground computation
	Airborne computation
Concepts	Central - Ground "tactical" control
	Dispersed - Air tactical control
MLS Capability	Accuracy better than VORTAC
	Some path computations simpler than VORTAC
	Origin at runway
	Range data important for reduced separation
	Displays are critical

Taxi System Interface -- It is presently envisioned that there will be a relatively separate ground traffic control system for the airport runways and ramp areas. There may also be a separate taxiway guidance system for operation in Category IIIc weather conditions.

For the purposes of compatibility analysis it is assumed that the surface control system would be similar to an airport surface detection radar sensor with automation of the identification and control features. It is also assumed that the taxiway guidance system would be independent of the taxi control system, probably taking the form of cables or loops installed in the runways. Although other system concepts are potentially feasible which include both the function of control and guidance, the above assumptions appear to represent a good compromise from the cost/benefit aspects.

Missed Approach Interface -- Consideration of the aircraft control compatibility includes the missed approach guidance function. From the standpoint of air traffic control the missed approach operation is essentially the same as the approach operation, but the functions and interfaces occur in the reverse sequence. There is a need to interface the communications, the separation assurance, and the navigation system.

Weather Environment

The primary function of the ILM is to provide backup guidance direction to the pilot for landings during degraded weather conditions. To evaluate the capabilities of the sensing concepts for weather dependence, a set of varied weather environment models were utilized. These models were incorporated in the computer programs to exercise the ILM concepts over the anticipated environments for Category II and III landing conditions. These expected environments are:

Rainfall Rate:	up to 16 mm/hour
Fog/Smog:	RVR of 365m (1200 ft), 213.4m (700 ft), 45.7m (150 ft) and 0m
Snow:	up to 5 mm/hour (melted)
Wind:	up to 33 knots

A total of four basic climatological conditions were set up to cover the environmental range. They are:

- o CASE 1: Summer Rain, Maritime Tropical Climate
- o CASE 2: Radiation or Advection Fog, Temperate Climate
- o CASE 3: Inland Evaporation - Fog, Temperate Climate
- o CASE 4: Winter Snow, Temperate Climate

Variations in RVR for Cases 2 and 3 will be accounted for by using subcases, where

- Subcase 2 (or 3) .1 is 365.8m (1200 ft) RVR
- Subcase 2.2 is 213.4m (700 ft) RVR
- Subcase 2.3 is 45.7m (150 ft) RVR
- Subcase 2.4 is 0 ft RVR

Case 1 is representative of a summer thunderstorm on the Gulf Coast, with cloud tops to 15240m (50,000 ft) and 16 mm/hour rainfall. Case 2 is representative of coastal fog, or fog associated with high pressure cells in the Midwest. Case 3 is frontal fog, usually experienced in the East and South during the spring. Case 4 is a typical winter snow storm caused by maritime polar air overrunning modified continental polar air. The vertical profiles for the various cases are shown in Table 20.

ILM SENSOR REQUIREMENTS

Minimum sensor requirements are defined from previous ILM operating environments/ requirements. The sensor requirements specify accuracy, range, data rates, field-of-view, coverage, etc. for each of the four ILM functional configurations (see the Introduction for a definition of these).

Some of the ILM sensor concepts evaluated were ruled out immediately because they did not meet the minimum sensor requirements discussed here. The elimination of these concepts early in the program has been justified by analysis and is discussed in detail in Section V of this report.

Table 20 -- Vertical Weather Profiles

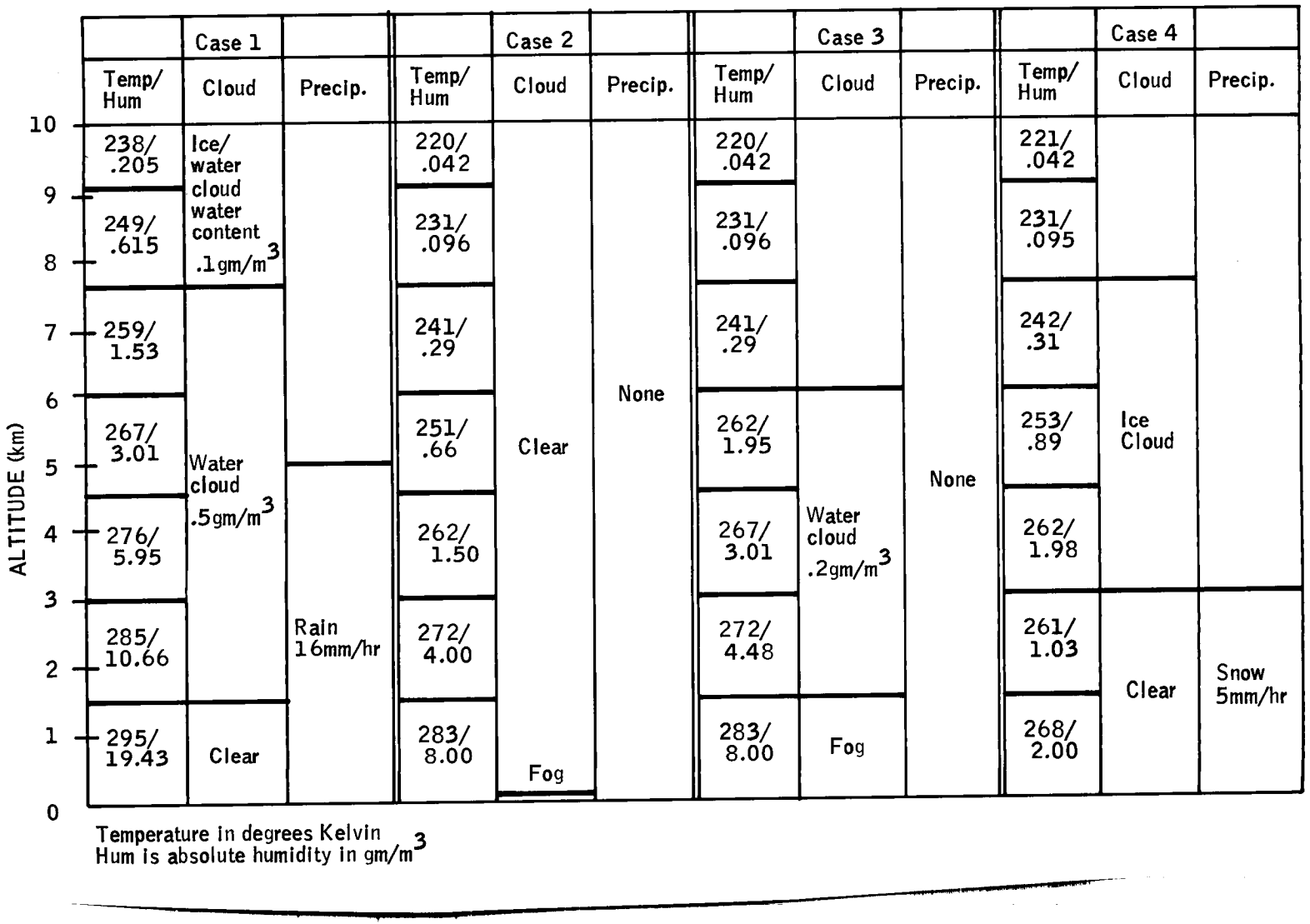

The minimum sensor requirements are discussed in the paragraphs below for each of the four ILM functional configurations.

Basic Configuration Sensor Requirements

Accuracies -- The Independent Landing Monitor's (ILM) principal function is to allow the pilot to manually land his aircraft safely when the primary automatic landing system fails. Thus, accuracies of the ILM must be equivalent to that of the primary landing system. A method for defining the accuracy requirements for MLS is given in Appendix A.

Using the path following error data from Table A-1 and Figure A-2 from Appendix A, the two sigma accuracy requirements in linear dimensions for ILM are given in Table 21.

The values given are for a .035 rad (2°) glide path. Appendix A also quotes angular errors as a function of position with respect to the various MLS antenna sites. The angular error, being a function of range to the target (signal source), may be different for the various ILM configurations.

With MLS, two elevation antennas are used to provide elevation guidance through flare to touchdown. Beyond threshold the accuracies differ slightly. For ILM requirements we can use the values quoted for elevation rather than flare where there are conflicting numbers.

The MLS system also provides a range rate output. Tolerable range rate error is 3.0m (10 ft) per second. This output is primarily used for curved and segmented path following and is not critical to the final straight in segment. The MLS is designed to provide great flexibility in the approaches for landing including curved and segmented flight paths. However, the region of most critical

Table 21 -- Path Following Error Data

	Rollout	GPIP	Threshold	Distance from Threshold on C.L. Extension		
				1.85km (1 nm)	5.56km (30 nm)	14.82km (8 nm)
Azimuth	4.3m (14 ft)	4.3m (14 ft)	4.3m (14 ft)	6.1 m (20 ft)	11.7 m (38 ft)	31.6 m (103 ft)
Elevation	-	-	0.5m (1.8 ft)	3.6 m (11.8 ft)	10.1 m (33 ft)	29.2 m (95 ft)
Range	12.2m (40 ft)	12.2m (40 ft)	12.2m (40 ft)	17.8 m (58 ft)	28.9 m (94 ft)	56.5 m (184 ft)
Flare (Elevation)	-	0.5m (1.8 ft)	0.5m (1.8 ft)	2.4 m (7.7 ft)	8.3 m (27 ft)	-

need for an independent landing monitor is the final 2.78 km (1.5 nm) to the threshold in a landing. In all cases the pilot will be attempting to line up with the runway centerline during this segment of the approach. Since the existing ILS instrument landing system provides guidance coverage in this region, one may examine the accuracies displayed to the pilot from that system. Reference 5 quotes a typical operational airborne concept for Category IIIa landing to an ILS equipped runway which may meet the requirements. It consists of "a single, monitored fail-passive automatic flight control system with flare computation and automatic flare and landing. It also includes an adequately failure-protected flight director system with dual displays with flare computation supplied to the command bars." The pilot must be capable of making a manual landing with the flight director display driven from ILS signals and a radar altimeter. The flight director displays localizer and glide slope deviation. The localizer deviation, representing 0.022 rad (1.25°) between dots, can be interpolated to approximately 1/10th of this spacing on the expanded flight director localizer scale, for an accuracy approaching .002 rad (0.125°). The glide slope deviation representing 0.004 rad (1/4°) between dots does not have an expanded scale. A pilot should be able to interpolate to approximately 1/5th of the spacing or 0.001 rad (.05°). Radar altimeters provide a separate altitude reading accurate to ±1.5m (±5 ft) or ±5% of altitude, whichever is greater. An ILS localizer antenna is normally located 304.8m (1000 ft) beyond the stop end of the runway, with angle measurements made from that point. The glide slope antenna is located at the glide path intercept point at approximately the touchdown area on the runway. For the final approach segment these accuracies roughly correspond with the accuracy requirements for MLS.

Data Frame Rates

The data frame rates for the MLS configuration are as follows:

1) Azimuth and primary elevation - 5 updates per second

2) Elevation number 2 for flare - 10 updates per second

3) DME-40 per second interrogation rate

These information rate requirements for MLS are based on the requirements for the autopilot and flight control systems of typical high performance jet transports. One may argue the information rate to the pilot for a manual landing should be approximately the same. Thus, a minimum data frame rate of 10 updates per second should be required from ranges of 1.85km (1 nm) through touchdown. For some sensing concepts, it may be feasible to reduce the data rate to 5 updates per second at ranges beyond 1.85 km (1 nm). The displayed information to the pilot should appear nearly smooth and continuous as it changes. At an update rate of 10 samples per second, the pilot may still see a flickering or stepping motion in the displayed parameters. This is a significant factor to consider in the type of display format selected for the ILM.

Effective Range

Ideally an ILM would cover the same range as the primary landing system. Recognizing that this would result in a very costly system, the ILM sensors should be evaluated at ranges 1.85 km (1 nm), 5.56 km (3 nm), and 14.82 km (8 nm) to runway threshold.

For the ILM to fulfill its function, the pilot or co-pilot must be able to scan the monitor prior to a decision height in the approach and make a decision whether it is safe to continue for the landing. This point defines a minimum

effective range for the ILM since a range capability less than this value makes the ILM useless.

Based on a minimum planned glide slope of .035 rad (2°), a 30.5m (100 ft) decision height and a minimum of 3 seconds decision time, the minimum effective range is approximately 1066.8m (3,500 ft). On an imaging type of display this would allow the pilot to see 304.8m (1,000 ft) of the approach area including the runway threshold. Night landing simulation studies detailed in Reference 6, indicate the pilot needs at least 3 seconds decision time and at least a 304.8m (1000 ft) visual segment of the runway approach area prior to reaching decision height for him to make a safe decision to continue his approach. For a flight director type of ILM display, the pilot would need a positive indication of solid guidance signals at the same effective range to make a landing decision.

Field of View/Coverage

The desired region of coverage for the ILM sensor is shown in Figures 14 and 15 for azimuth and elevation, respectively. This coverage is based on the expected MLS coverage and typical approach capabilities for CTOL aircraft. The ideal ILM sensor should provide steering cues to the pilot throughout this region to permit corrective action to be taken for failures in the primary landing system.

Recognizing that few feasible ILM concepts can meet the desired coverage, it is of interest to determine the minimum field of view/coverage requirements. All types of approaches converge to a standard straight in alignment to runway centerline at greater than 1.85km (1 nm) from the threshold as shown in Figure 14. This is well beyond the nominal 30.5m (100 ft) altitude decision height where

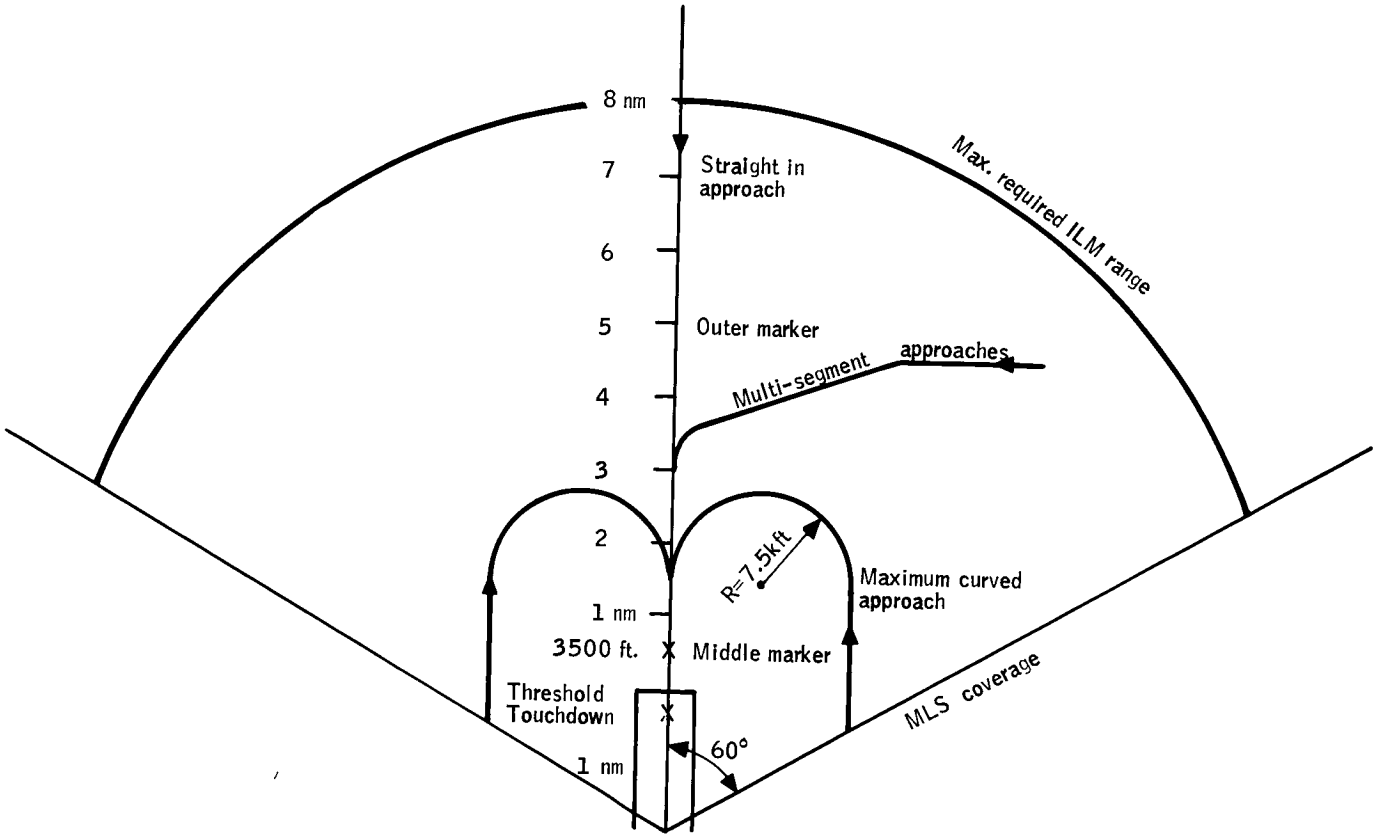

Figure 14 -- ILM Operational Range (Azimuth)

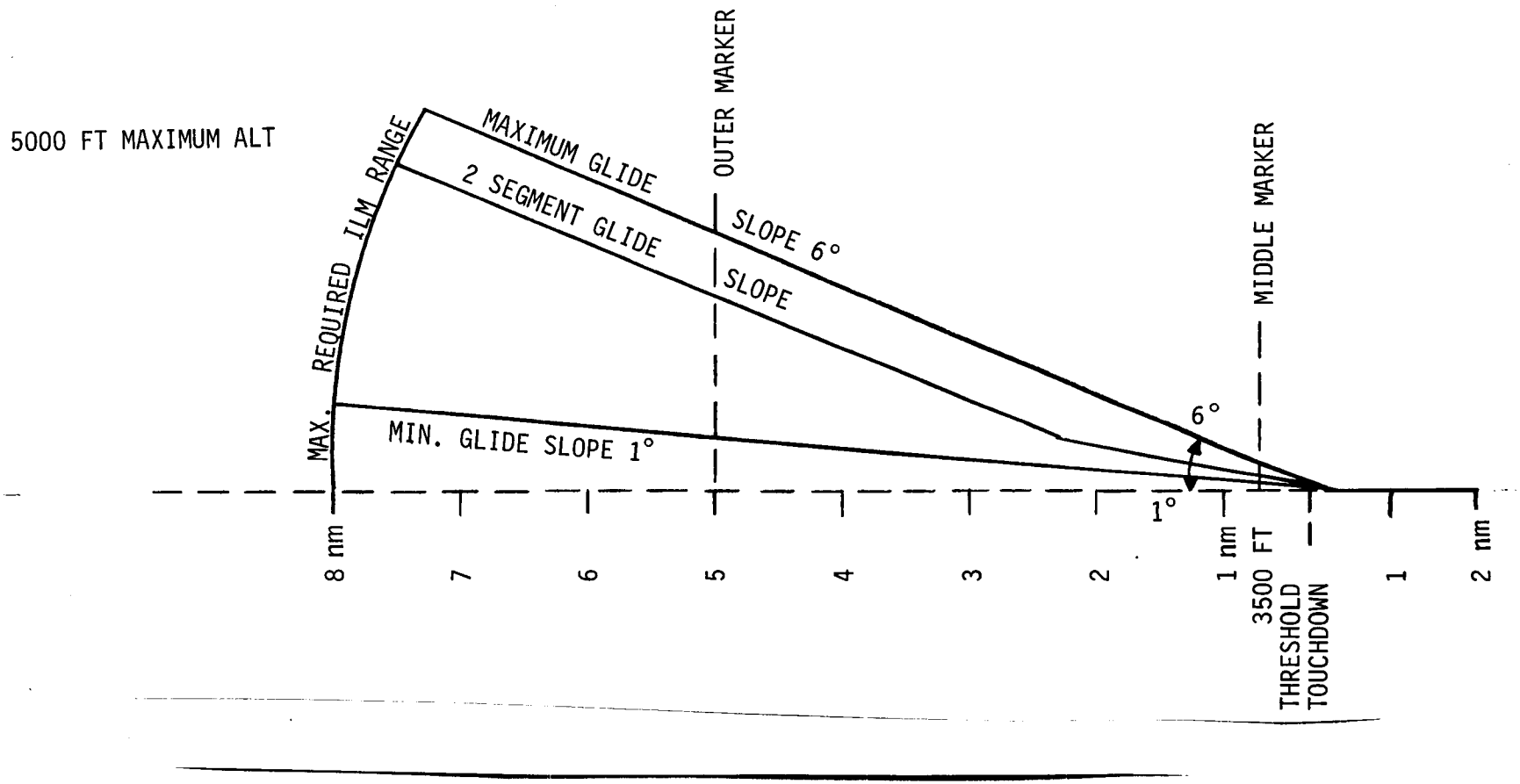

Figure 15 -- ILM Operational Range (Elevation)

the pilot must determine if he can continue or make a missed approach. Failures in the primary landing system prior to decision height in Category III weather conditions dictate a missed approach. From decision height to touchdown the ILM must provide both magnitude and direction of deviations from the desired approach to the pilot. Conclusions reached in Reference 6 pertinent to this requirement were:

1) The pilot needs at least 3 seconds prior to decision height to evaluate the situation.
2) For an imaging system he must see at least 304.8m (1000 ft) of the ground approach area to know his relative position.
3) Lateral deviations off centerline to 30.5m (100 ft) at decision height can be satisfactorily corrected.

The geometric constraints for minimum cross-track and along-track view angles are shown in Figures 16 and 17, respectively, using the above conclusions, a glide slope of .052 rad (3°), decision height of 30.5m (100 ft), maximum approach speed of 145 knots and maximum runway width of 61.0m (200 ft). Requiring that the pilot see at least the centerline lights and runway lights on one side of the runway at threshold for a 0.052 rad (3°) glideslope approach requires a cross-track view angle of 0.131 rad (7.5°). The minimum along-track view angle to see a 304.8m (1000 ft) segment of approach about the threshold is 0.07 rad (4°). The minimum view angle here will vary with glide slope approach angle, however, the decision height may also vary correspondingly to maintain range to threshold and, thus, view angle approximately constant. The angle, θ_2, in Figure 17 corresponds to the maximum depression viewing angle from horizontal for a sensor on the aircraft and is approximately 0.14 rad (8°). To provide the pilot a

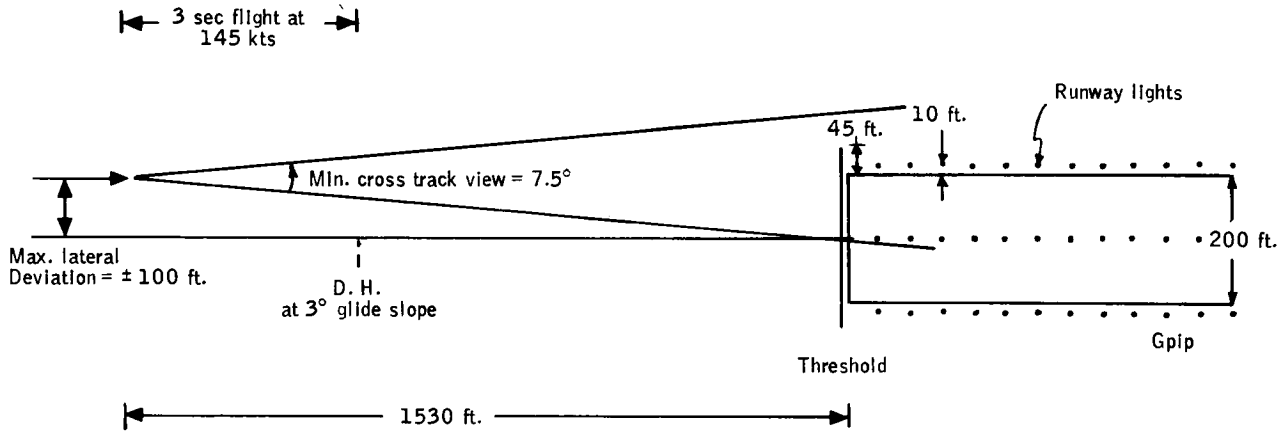

Figure 16 -- Minimum Cross-Track Angle

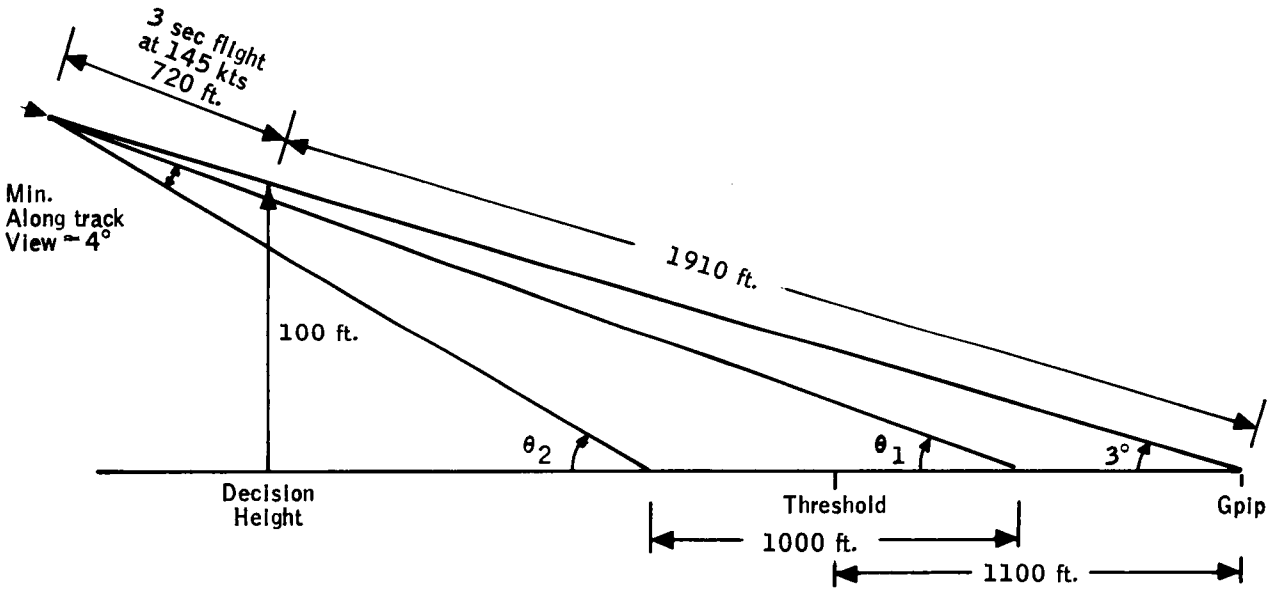

Figure 17 -- Minimum Along-Track View Angle

vertical reference in his approach, the horizon should also be displayed. This increases the minimum along-track view angle to 0.14 rad (8°).

For a boresighted or hard mounted sensor on the aircraft the expected pitch and yaw (crab angle) ranges of the aircraft must also be included in the minimum f.o.v. These ranges are: pitch = -0.052 rad (-3°),to +0.175 rad (+10°) and yaw = ±0.349 rad (±20°). The minimum f.o.v. for a fixed sensor becomes 0.367 rad (21°) along track over the angles of +0.052 rad (+3°) to -0.314 rad (-18°) relative to boresight and 0.829 rad (47.5°) in cross-track centered about boresight. It should be noted this is for the straight-in segment of the approach. In the curved path segments the f.o.v. requirements for maintaining the runway in the f.o.v. grows correspondingly.

A real world display to the pilot of this f.o.v. at a 28 inch CRT viewing distance and unity magnification would have minimum dimensions of 10.4 by 24.6 inches. This display may be feasible although certainly not practical to fit in a transport cockpit.

Reducing the maximum crab angle to ±0.175 rad (±10°) correspondingly reduces the display dimensions to 0.367 rad (21°) x 0.48 rad (27.5°) or 10.4 x 13.7 inches. Reduction of the viewing distance may be required to reduce these display dimensions to a practical size. A crab angle of ±0.175 rad (±10°) corresponds to crosswinds of 16 and 26 knots for approach speeds of 90 and 145 knots, respectively. Limiting landings in Category III weather to crosswinds less than this magnitude may not be a serious constraint since Reference 5 only considers crosswinds less than 15 knots. In some aircraft crosswinds are compensated for in landing by maintaining heading alignment with the runway centerline and introducing

a small roll component turning into the wind rather than completely correcting for wind with a heading (yaw) offset. Adoption of this procedure would also reduce the sensor field-of-view requirements.

Tracking types of sensors on the aircraft, such as a FLIR or radar on a slewable platform, must be capable of tracking over the 0.367 rad (21°) elevation and 0.829 rad (47.5°) azimuth angles. The actual f.o.v. requirement of the tracking sensor depends on the location of the ground objects being tracked relative to runway threshold. For most concepts, a f.o.v. near 0.14 rad (8°) x 0.14 rad (8°) appears adequate.

Ground derived ILM sensors must, as a minimum, be capable of providing proportional guidance commands over a +0.017 rad (1°) to +0.105 rad (6°) elevation angle and ±0.07 rad (±4°) azimuth angle measured from the runway GPIP. The pilot must have both magnitude and direction of approach deviations displayed. In this case, the minimum covers the straight in segment of the approach path. Preferred coverage should extend to ±60° in azimuth.

Case I Configuration Sensor Requirements

Case I extends the basic ILM function of providing pilot guidance through approach to touchdown to rollout and exit from the runway. This extension requires display to the pilot deviation from runway centerline, runway length remaining and, for Category IIIc conditions, turnoff point and direction.

The MLS as the primary landing aid is being designed to provide rollout guidance but does not cover turnoff. Over the region from touchdown to the stop end of the runway, MLS accuracies are ±4.3m (±14 ft) (2σ) or better for azimuth (deviation from runway centerline) and ±12.2m (±40 ft) (2σ) range to stop end of runway.

Data update rate is 5 per second for azimuth and 40 per second for range. Since the pilot must be capable of manually performing the same function with an ILM the same requirements should apply at least near touchdown. As aircraft velocity is reduced in the rollout accuracy and/or data rate could be reduced correspondingly, however, for most ILM concepts taking advantage of this fact would add complexity rather than reduce it.

Turnoffs from the runway lie at angles ranging from 0.524 rad (30°) to 1.571 rad (90°) with respect to the runway centerline. The low angle turnoffs are being incorporated at airports to accommodate turn-off velocities to 60 knots. Under Category III conditions turn-off velocities would probably be limited to much less than 60 knots. It should be noted that guidance during turnoff may be a desirable feature but not necessarily a critical function for the ILM to perform. Visibility of runway and centerline lights can be too restricted at the higher rollout velocities for the pilot to rapidly determine guidance and position information from them, but, except for the most extreme conditions, may not be at the low turnoff velocity. The guidance requirements for turnoff apply also to taxiing under Category III conditions. While some of the ILM sensing concepts may fulfill this function these should not be included as ILM requirements.

Case II Configuration Sensor Requirements

Case II extends the ILM function of providing pilot guidance through approach and rollout to include detection of potentially interfering obstacles in the vicinity of the runway at a range sufficient to permit execution of a missed approach. The obstacles can be landing aircraft, aircraft crossing the runway, airport vehicles, snowplows, etc.

For comparison of the sensor concepts the obstacle will be defined with the following minimum characteristics:

Size:	3 m x 3 m x 3 m
Radar Cross Section:	1 square meter
Temperature:	Ambient
Emissivity (0-15 microns):	0.90

It is highly likely the obstacle would be lighted or have IR temperatures (engines) significantly above background, however, from certain view angles on the object these signatures may not be observable.

Under high density traffic conditions the preceding aircraft will be making his rollout, braking and turnoff as the pilot comes in on his approach. The FAA rule is that a following aircraft may not touch down until the preceding aircraft clears the runway. From reference 7 the time required to clear the runway is roughly 60 seconds for CTOL aircraft and 30 seconds for STOL aircraft. This time is comprised of 1/2 for braking and 1/2 for taxiing to a turnoff. With high speed turnoffs the runway clearance times can be reduced to 30 seconds and 15 seconds for CTOL and STOL, respectively. Thus, under high density traffic for a desired landing spacing goal of 30 seconds there will often be an obstacle on the runway until just prior to touchdown.

The time of flight from a 30.5m (100 ft) decision height to touchdown is nominally 8 seconds or greater. For an obstacle avoidance system to function, the pilot must during this time determine he has a clear runway or is going to have a clear runway at touchdown. To assure a preceding aircraft is going to clear the runway requires a definite observation time by the pilot to determine it's

velocity toward an exit. Thus, a minimum effective range for the obstacle detection system should be the range from decision height to the stop end of the runway (nominally 4267.2m (14000 ft) for a .044 rad (2.5°) glideslope to a 3657.6m (12000 ft) runway). Since this is strictly a go/no go function (land or missed approach) the data rate can be much lower, on the order of one sample per second.

A common definition for minimum sensor spatial resolution for target detection calls for two resolution elements across the target. At the range of 4267.2m (14000 ft) on a 3 meter target this corresponds to a sensor angular resolution of 0.35 mrad. According to several studies cited in Reference 8, low to moderate contrast targets must subtend angles in the range of 1 to 3 m rad to the human eye for high probabilities of detection. Thus, the sensor requirement for 2 resolution elements on 3 meter targets at 4267.2m (1400 ft) range is conservatively equivalent to the human eye capability under good visibility. For an imaging type of sensor display with this resolution the magnification must be unity or greater to maintain this target angle on the display and achieve a high probability of detection.

Case III Configuration Sensor Requirements

Case III does not expand on the functional requirements for the ILM as do the three prior cases. For this case the ILM sensing concepts shall be evaluated for their ability to provide a real-world perspective image of the runway and surroundings to the pilot. The image must be of sufficient quality to provide relative position and rate of change of position of the aircraft with respect to the runway and aircraft attitude information to the pilot in a form analogous to the visual cues for a VFR approach and landing.

Field-of-View -- The real world visibility capability (Reference 9) for transport pilots under VFR conditions is shown in Figure 18. Although each specific aircraft may differ slightly from the profile shown, the angular area inside the dashed line approximately represents the view angles of the real world available to the pilot under visual approach and landing conditions. It is readily apparent no hardmounted sensor/display combinations can match this real-world field-of-view capability, yet for curved and segmented approaches the runway could appear at azimuth angles on the order of 1.571 rad (90°). If the runway view is displayed to the pilot in the real-world perspective at these angles he should be able to manually maneuver to approach and land as he could do under VFR conditions. Some military visually coupled systems, utilizing sensors slaved to the pilot's line of sight with a helmet (head) mounted sensor display, show potential of meeting an idealized requirement of this type, however, the complexity appears more than justified to meet a questionable requirement.

The sensor f.o.v. of 0.367 rad (21°) elevation by 0.829 rad (47.5°) azimuth derived earlier for a straight in approach is also shown in Figure 18. This can be considered the minimum f.o.v. for a real-world (runway appears on display to observer at it's normal size and location) perspective image ILM display meeting the expected aircraft dynamics. As noted, the display azimuth angles could be reduced by imposing limitations on Category III landings in high crosswinds. Thus, sensing with a smaller f.o.v. to approximately 0.367 rad (21°) x 0.48 rad (27.5°) could be utilized.

The large f.o.v. requirement occurs as a result of displaying the runway in it's real-world location. The necessary f.o.v. of the runway and surroundings is

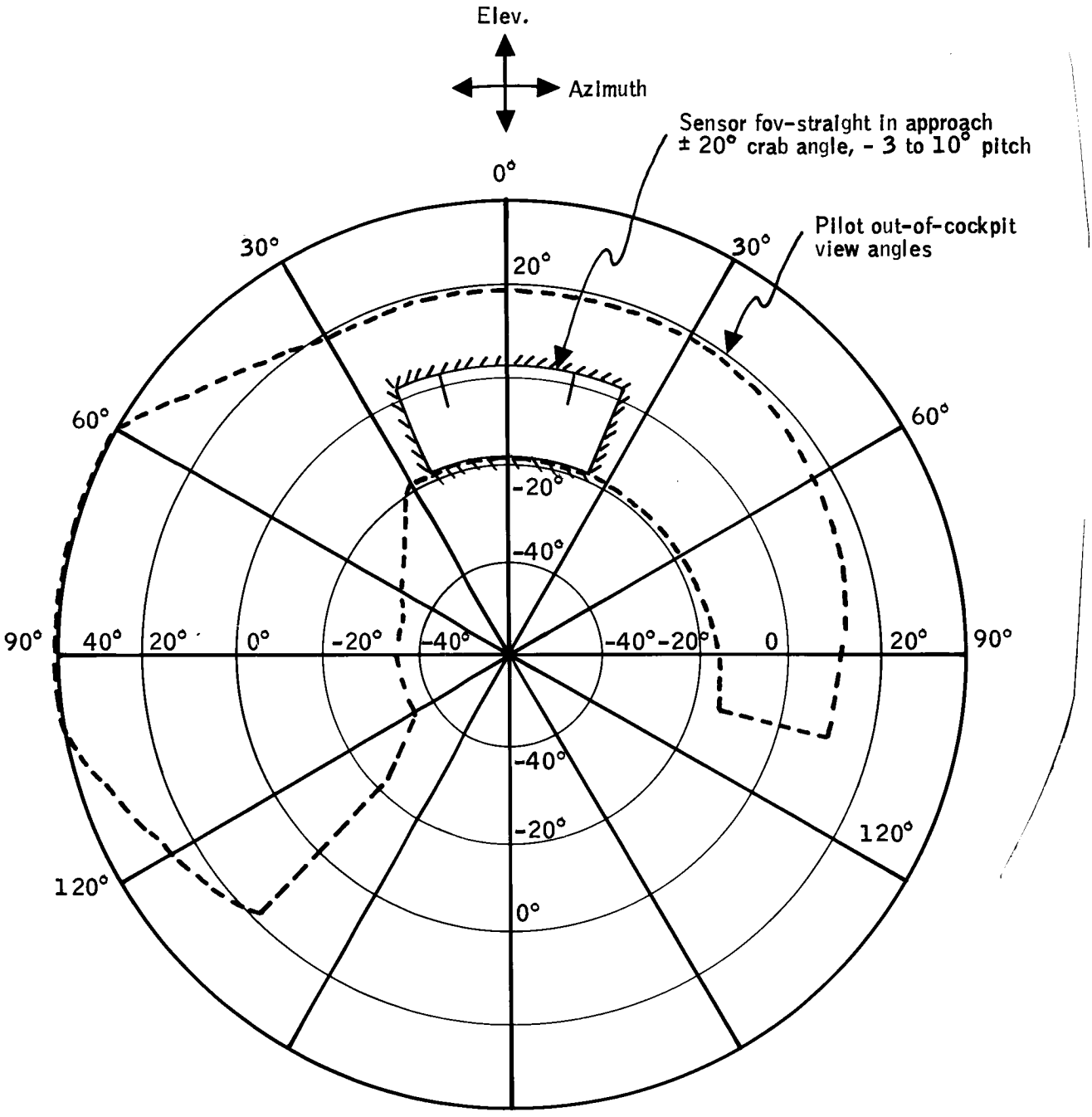

Figure 18 -- Minimum Visibility Requirements,
Transports (MIL-STD 850A)

nominally 0.14 rad (8°) x 0.14 rad (8°). It may be feasible to utilize a "semi-real-world" display showing the runway and surroundings at normal size allowing the pilot to rapidly identify localizer/glide slope deviations and symbolically show aircraft crab and pitch angles on separate scales on the display.

See IK

SECTION IV
INDEPENDENT LANDING MONITOR SYSTEM CONCEPTS

To adequately evaluate potential sensors for Independent Landing Monitors, it is necessary to identify the role of the sensor in the total ILM system concept. In many cases, the sensor requirements depend on its mode of operation in the concept. This section presents the multiple ILM system concepts which were reviewed and/or analyzed during the course of the study.

Each of the concepts shown are intended to include several possible variations. For example, many of the concepts will use passive or semiactive reflectors in various configurations as signal sources to outline the runway.

It was recognized that many of the concepts would not meet all of the sensing requirements for the Basic through Case III problems. However, they could have applicability to meet one or more of the functions involved in the total landing picture. Thus, an attempt was made to identify their potential ranges of operation.

The use of an inertial reference package standing alone as an ILM concept was not included here. It was considered for all sensor evaluations that an inertial reference package supporting an ILM sensor may be a feasible approach. For example, a concept providing periodic low rate fixes with inertial navigation between fixes may be a satisfactory concept and is included here as a general concept to be evaluated.

Some of the sensor concepts inherently provide real world imaging displays. Although not shown in the attached sketches, synthetic, symbolic runway displays

could feasibly be generated for any of the concepts measuring aircraft position w.r.t. the runway.

CONCEPT 1 - PRECISION APPROACH RADAR (PAR) - FIGURE 19

Precision Approach Radars have been in use and are installed at several airports around the country as secondary or backup landing aids. The approach radar locks on to the incoming aircraft and the ground controller then talks the pilot down on a straight in approach path. A similar concept is used for carrier landings with the AN/SPN-10 or 42 radars. In this case the precision approach radar measures range, azimuth, and elevation to the incoming aircraft with pitch and bank commands transmitted to the aircraft over a data link. This is a completely automated landing with the pilot only monitoring. The new USAF AN/TPN-19 PAR should be near state-of-the-art for this concept.

As an Independent Landing Monitor the PAR could monitor incoming aircraft and transmit via data link deviations from the nominal approach with these displayed on the aircraft. The precision approach radar is normally only used for near straight in approaches, and does not have coverage for curved approaches.

CONCEPT 2A - IMAGING RADAR - FIGURE 20

The imaging radar sensor concept is primarily an air derived system. Frequency ranges of interest are X through Ka band. The radar scans the approach path in front of the aircraft and generates a perspective display to the pilot. The display can either be a panel mount display or heads up projection. Altitude must be independently measured from the radar altimeter or other source to give a true perspective for the display. Image enhancement of various forms may be

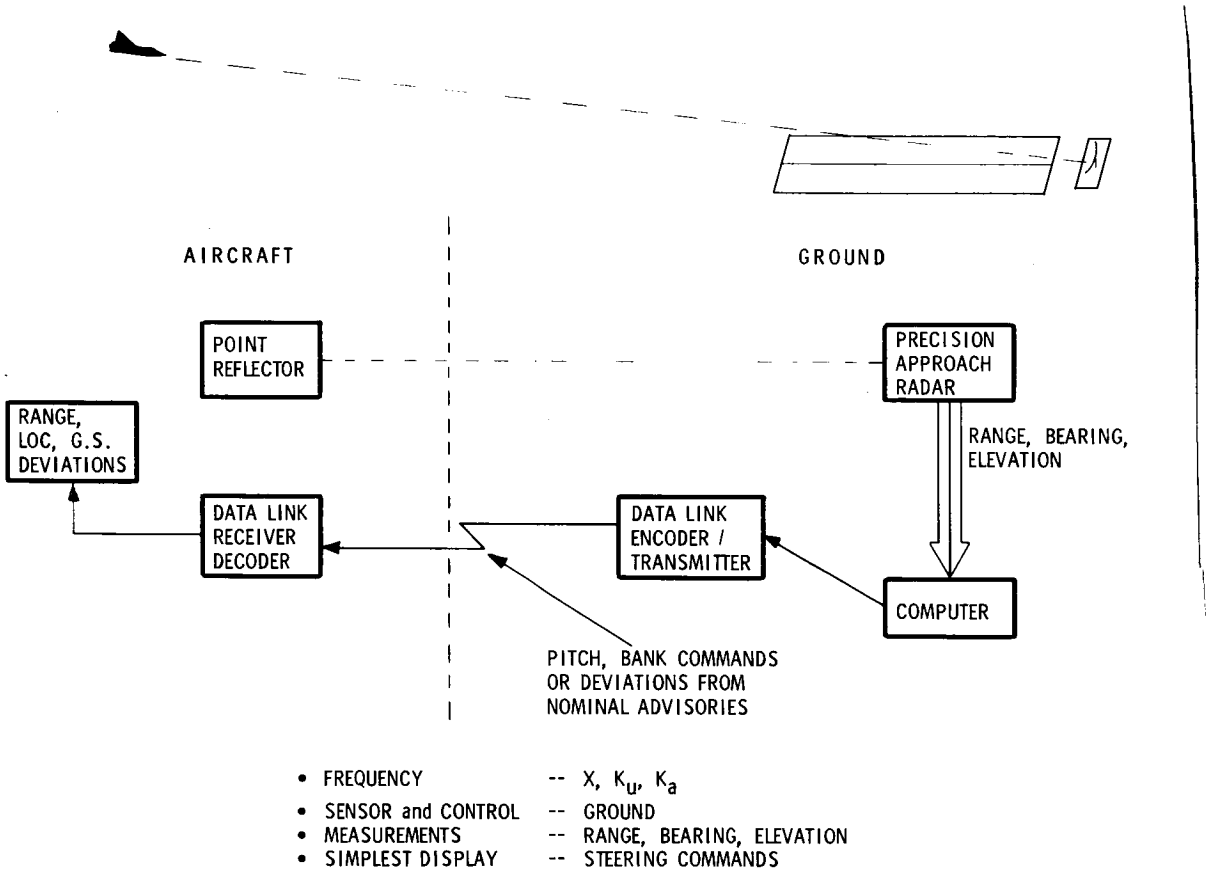

Figure 19 -- Precision Approach Radar

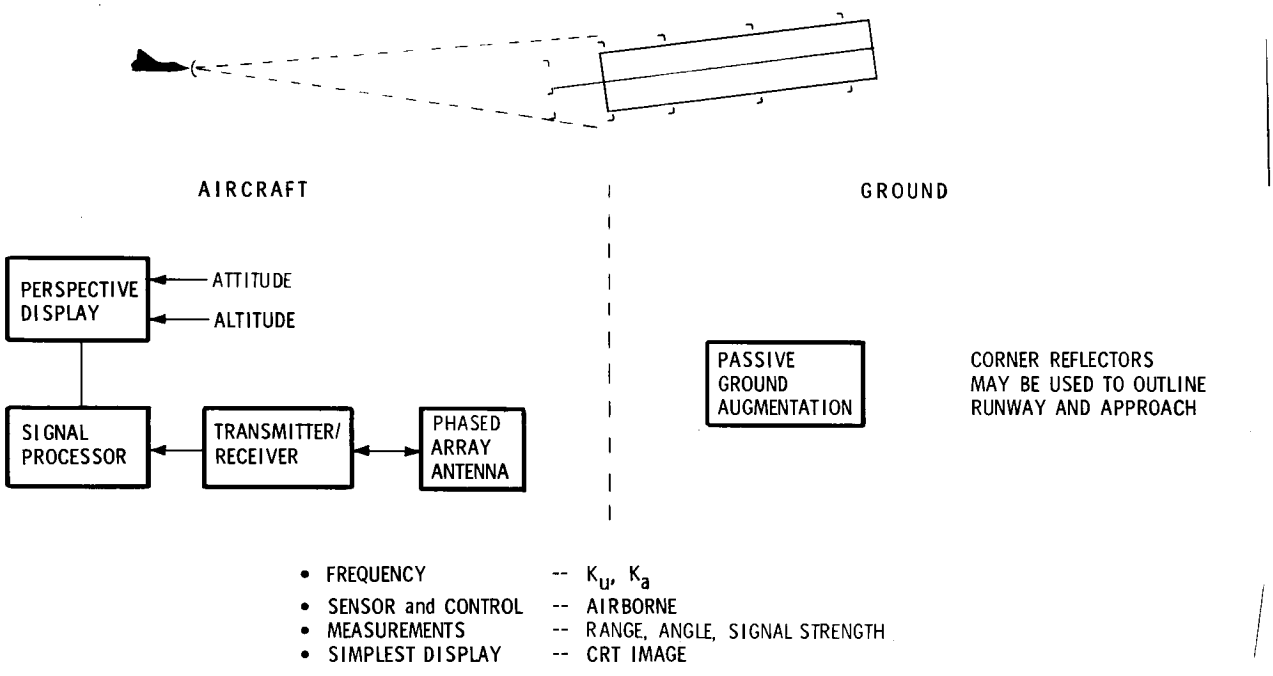

Figure 20 -- Imaging Radar

used to brighten the runway outline. Passive ground augmentation such as corner reflectors may be used to outline the runway and the approach path.

CONCEPT 2B - RADAR (TRIANGULATION) - FIGURE 21

The radar in this concept measures range and angles to 3 or more enhanced targets near the runway to generate a synthetic runway display and to measure range, localizer, and glide slope deviations from the approach path. In the case shown semi-active reflectors are used to frequency shift the transmitted radar pulse from the aircraft and reflect it back. The radar receiver on the aircraft is tuned to detect the shifted frequency and, thus, picks out the reflectors over heavy clutter background. Other types of targets, such as purely passive reflectors, should also be feasible with this concept.

CONCEPT 3A - MULTILATERATION (AIR CONTROL) - FIGURE 22

By measuring range or a function of range to 3 or more ground stations from the aircraft one can derive position of the aircraft relative to the ground stations and, thus, to a runway approach path.

This multilateration concept shows simple transponders on the ground with the interrogator and receiver on the aircraft. The aircraft position is computed on the aircraft, with an independent altitude measurement used to aid in the generation of range-to-touchdown and glide slope localizer deviations.

An inverse of this concept with transponder on the aircraft and multiple ground interrogators is also feasible. To give the pilot a monitor would require a data link capability to transmit position data to the aircraft.

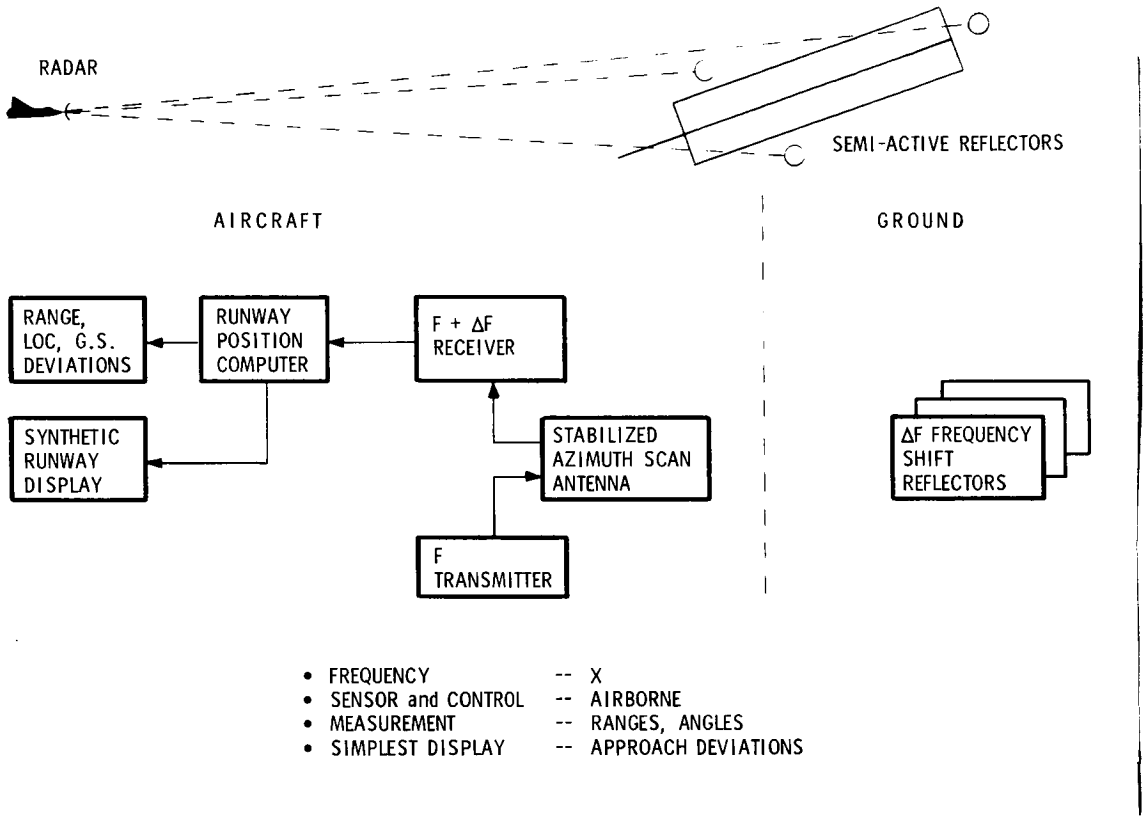

Figure 21-- Radar (Triangulation)

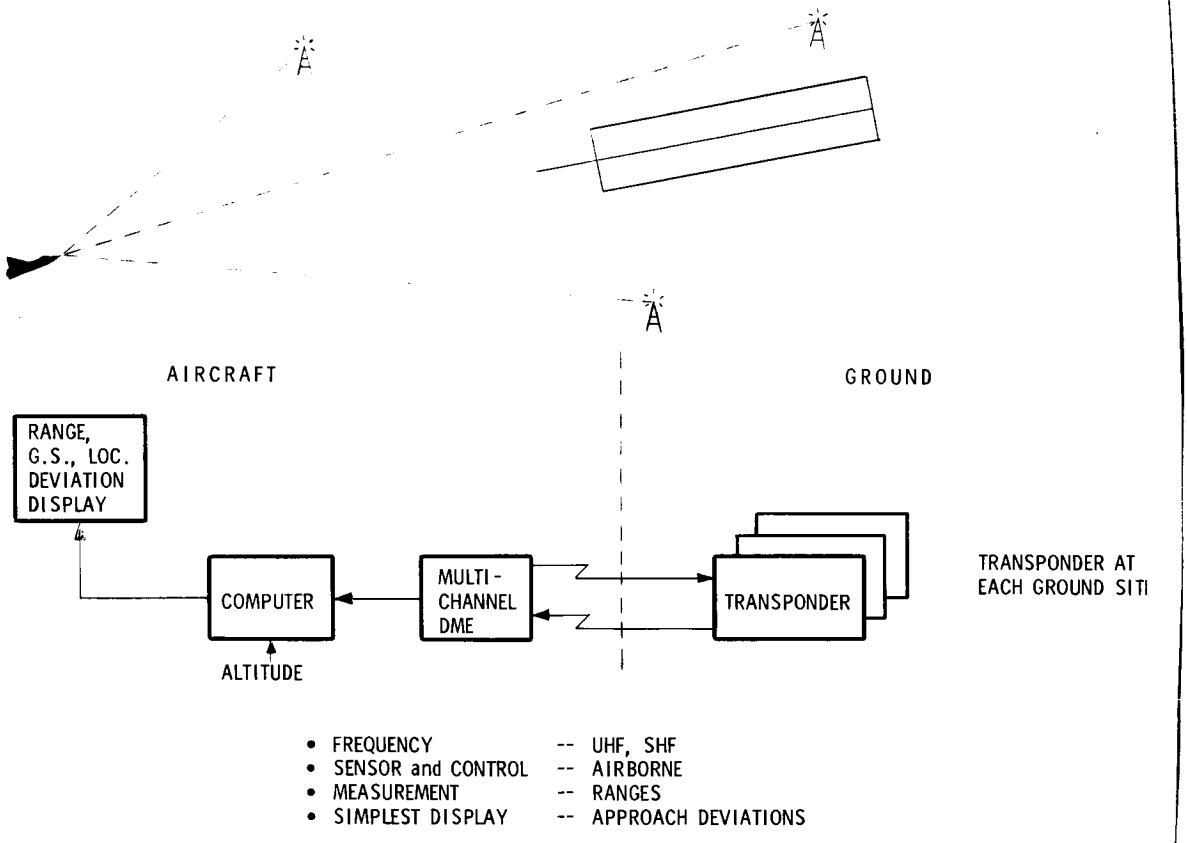

Figure 22 -- Multilateration (Air Control)

CONCEPT 3B - MULTILATERATION (GROUND CONTROL) - FIGURE 23

This concept, somewhat similar to 3A, utilizes precise synchronization to control the ground array of transmitters to transmit at fixed time intervals. The aircraft receiver, using the pulse arrival time differences, calculates its position with respect to the ground transmitters and, thus, the runway position. Range and glide slope localizer deviations can be calculated on the aircraft. An independent aircraft altitude measurement is normally required.

This concept includes among others the hyperbolic systems (LORAN).

CONCEPT 3C - MULTILATERATION (BEACON TRANSPONDER) - FIGURE 24

The current Air Traffic Control Radar Beacon System (ATCRBS) utilizes ground interrogators on a rotating antenna and altitude encoding transponder-equipped aircraft to determine aircraft position. Although ATCRBS is limited in accuracy and data rate (one sample per 4 seconds) an improved version of the beacon transponder concept could be of value as an ILM or check of the primary landing system.

CONCEPT 4A - FLIR (IMAGING) - FIGURE 25

A forward looking infrared radiometer could be mounted in the nose of the aircraft to scan the forward sector to provide a true perspective display to the pilot. Ground augmentation in the form of heated sources could be used to outline the runway and approach path. The normal runway and approach lights may adequately serve as heated sources. Slewing of the FLIR may be required to give adequate field of view coverage.

Several FLIR's are in existence for military reconnaissance and weapon delivery programs.

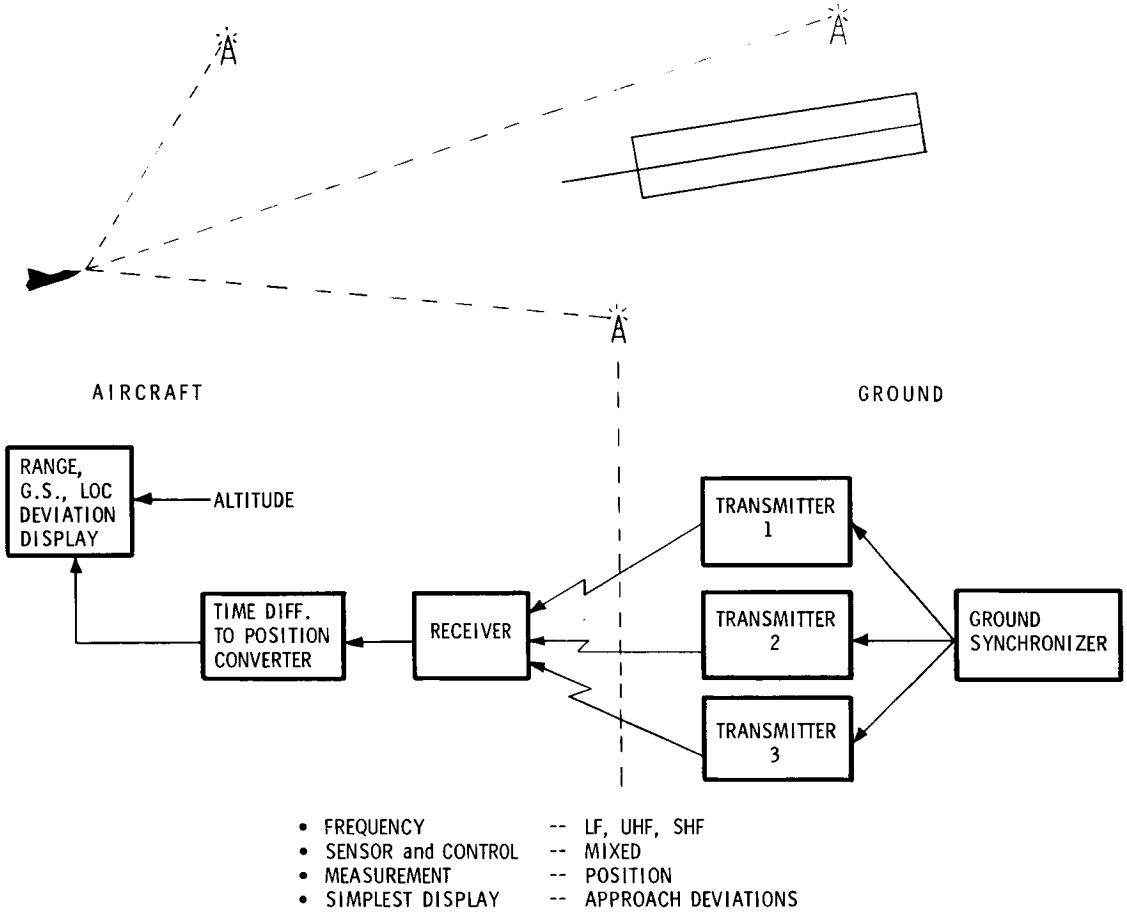

Figure 23 -- Multilateration (Ground Control)

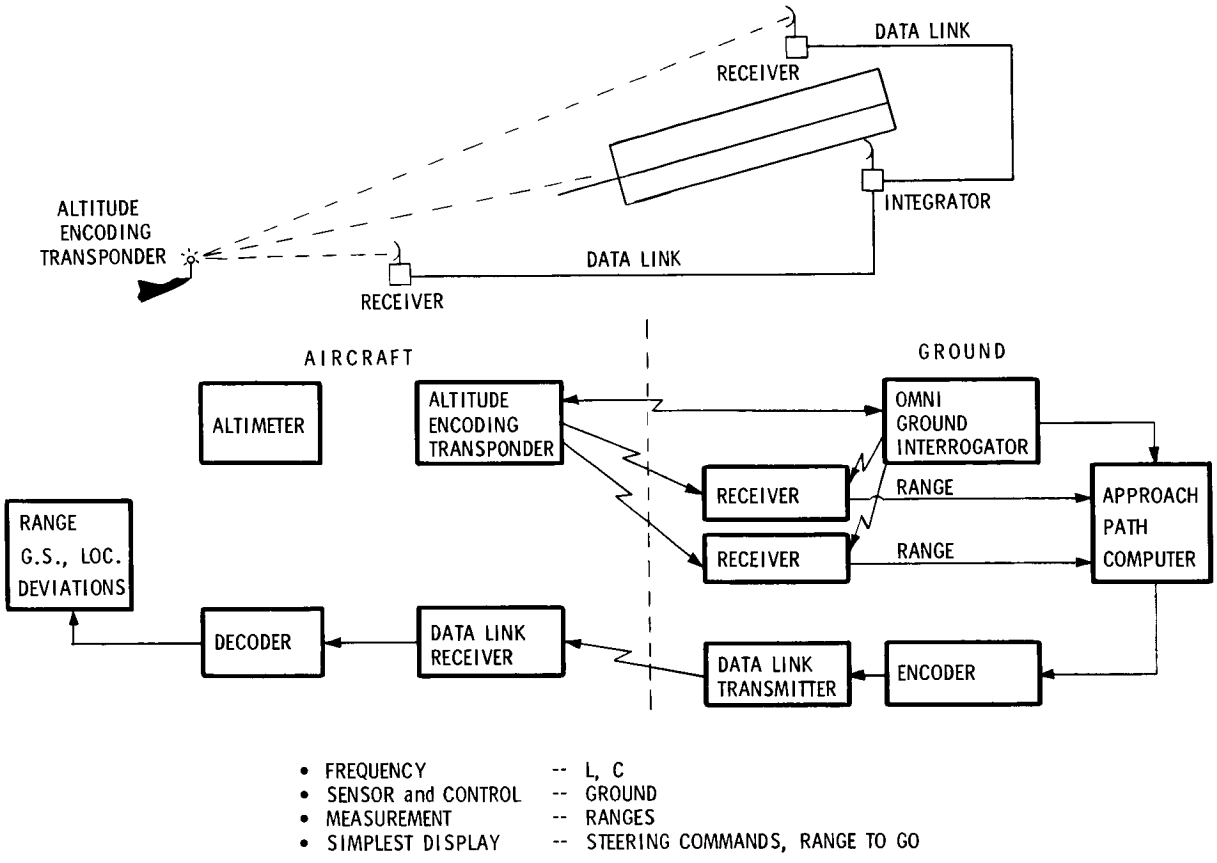

Figure 24 -- Multilateration (Beacon Transponder)

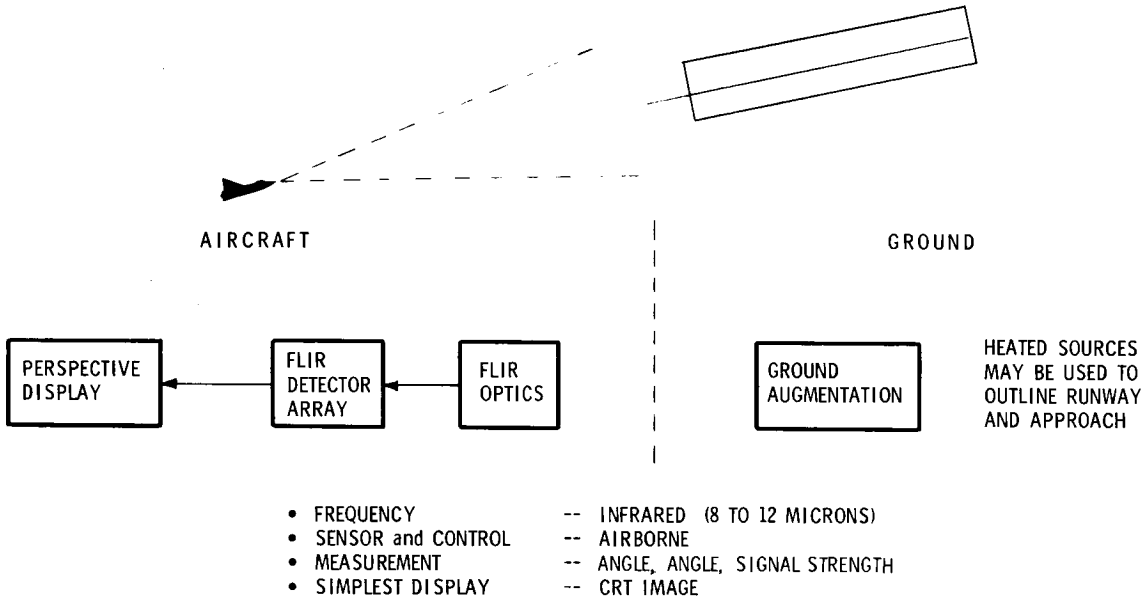

Figure 25 -- FLIR (Imaging)

CONCEPT 4B - FLIR (TRACKING) - FIGURE 26

A FLIR tracking concept similar to the visually augmented tracking system for weapon delivery may be feasible as an Independent Landing Monitor. In this case the FLIR would be mounted on a stabilized slewing platform on the aircraft and would track hot spots near the runway to generate glide slope and localizer deviation signals for display. The video image from the FLIR may also be displayed but it may not necessarily be in proper perspective if the FLIR is tracking off boresight.

Ranging to the runway can be achieved with another system such as a laser rangefinder or through tracking calculations on three or more known ground sources.

CONCEPT 5A - TELEVISION (IMAGING) - FIGURE 27

This concept utilizes a TV camera mounted on the aircraft to give a perspective display to the pilot of the runway and its surroundings. Ground augmentation would consist of the normal runway and approach lights at the airport. Consideration should be given to the use of an illuminator either mounted on the aircraft or near the runway on the ground.

CONCEPT 5B - TELEVISION (TRACKING) - FIGURE 28

In this case the TV camera is mounted on a stabilized platform with tracking electronics to track bright sources on the ground or such items as the approach light pattern. The output would be used to generate glide slope and localizer deviation signals for display. Range must be independently derived.

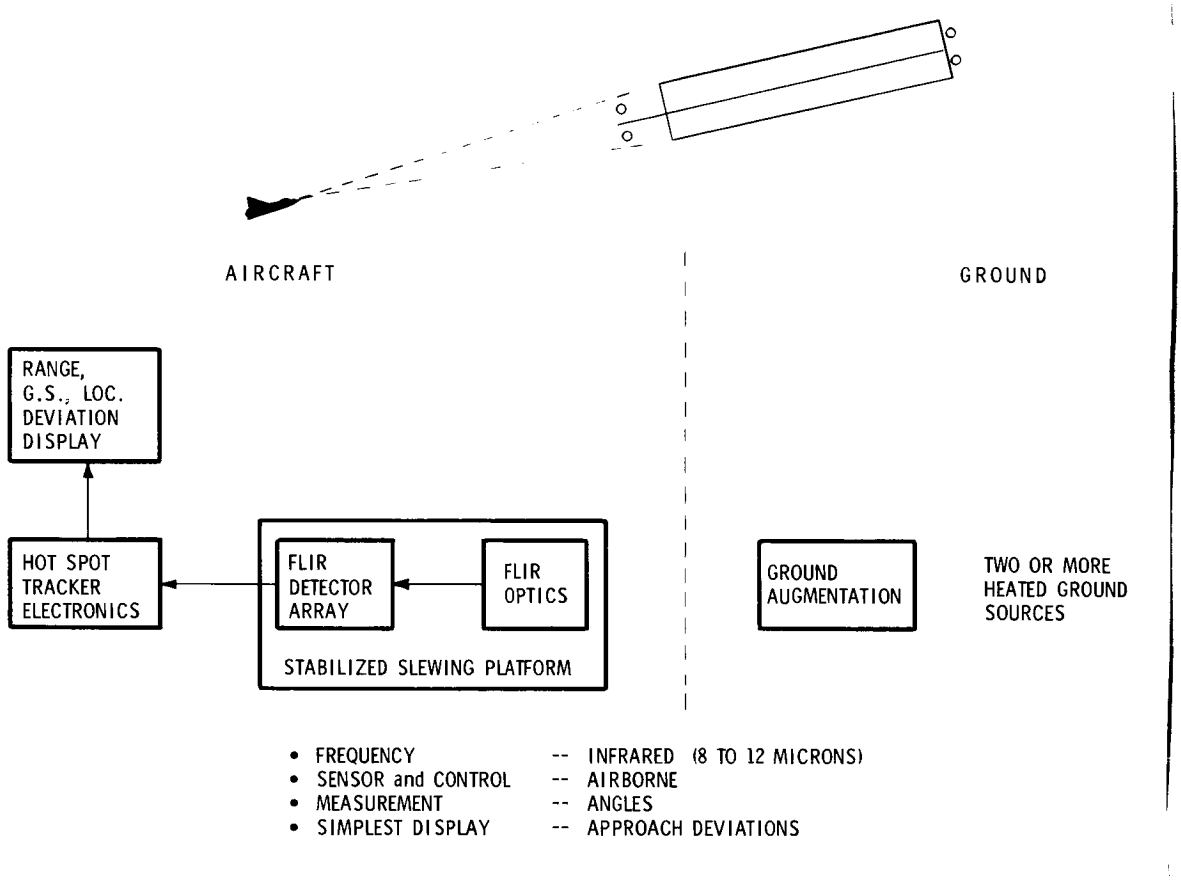

Figure 26 -- FLIR (Tracking)

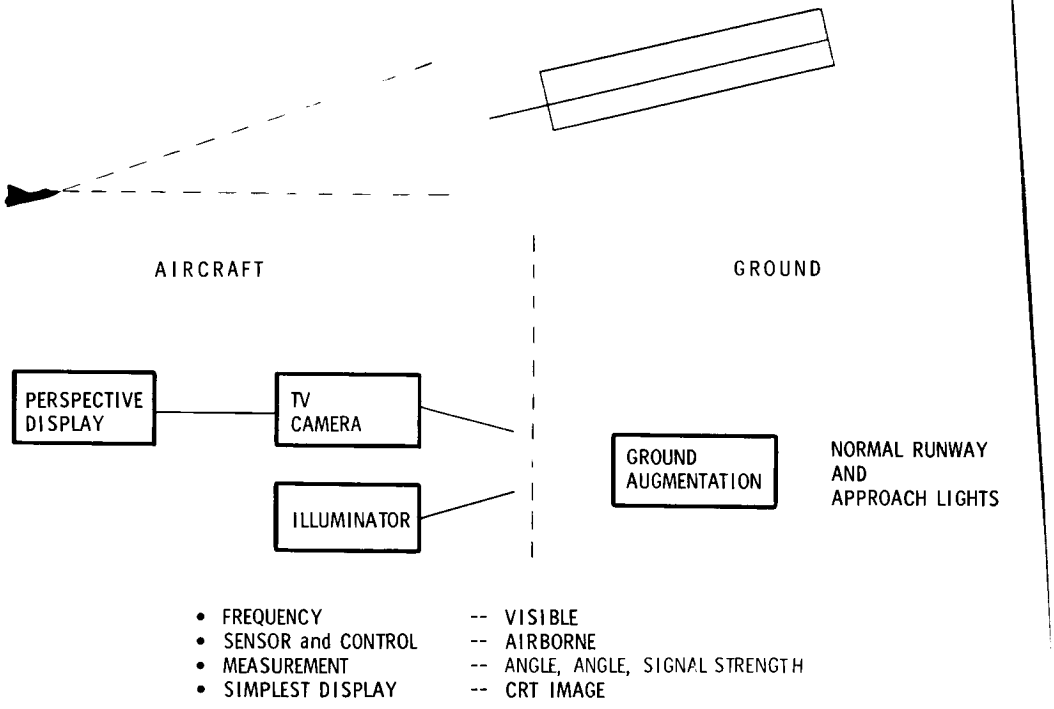

Figure 27- Television (Imaging)

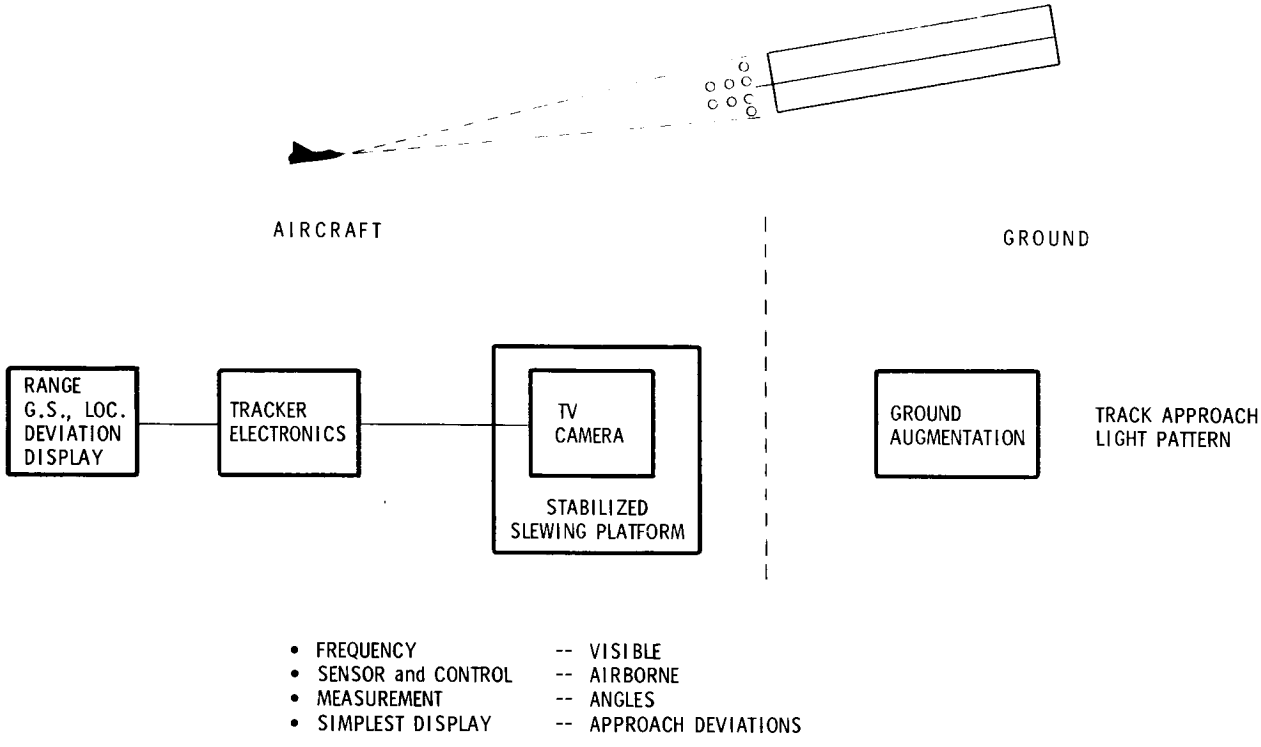

Figure 28-- Television (Tracking)

CONCEPT 6A - NUCLEAR INSTRUMENT LANDING SYSTEM - FIGURE 29

A number of instrument landing systems using gamma ray sources along the approach path and runway have been proposed or partially developed in the past. This concept uses multiple gamma sources whose radiation patterns can be modulated through various means (rotating shields, variable slit patterns in the shield). The aircraft carries a radiation detector (scintillation counter) to detect the gamma radiation and sort out the coding from the coded patterns. Localizer and glide slope deviation signals can be generated for display. Depending on the type of coding some indications of range can also be derived. Primary attraction of these systems are their relative independence of weather.

CONCEPT 6B - RUNWAY CENTERLINE RADIOACTIVE SOURCES - FIGURE 30

A similar nuclear landing monitor concept for touchdown and rollout guidance functions is a system studied by NASA Ames Research Center. It consists of a series of weak nuclear radiation sources embedded in the runway centerline and is used to provide a runway distance indication to the pilot during rollout under Category III conditions. It also should be feasible to use this concept for lateral deviation indications during rollout.

CONCEPT 7 - BURIED MAGNETIC LEADER CABLE - FIGURE 31

Generation of magnetic fields through the use of buried cable along the runway appears feasible to provide the pilot with rollout guidance. In the case shown the two cables are excited with slightly different low frequencies. The magnetic field sensor on the aircraft compares the amplitudes of the two fields to generate a runway centerline deviation indication.

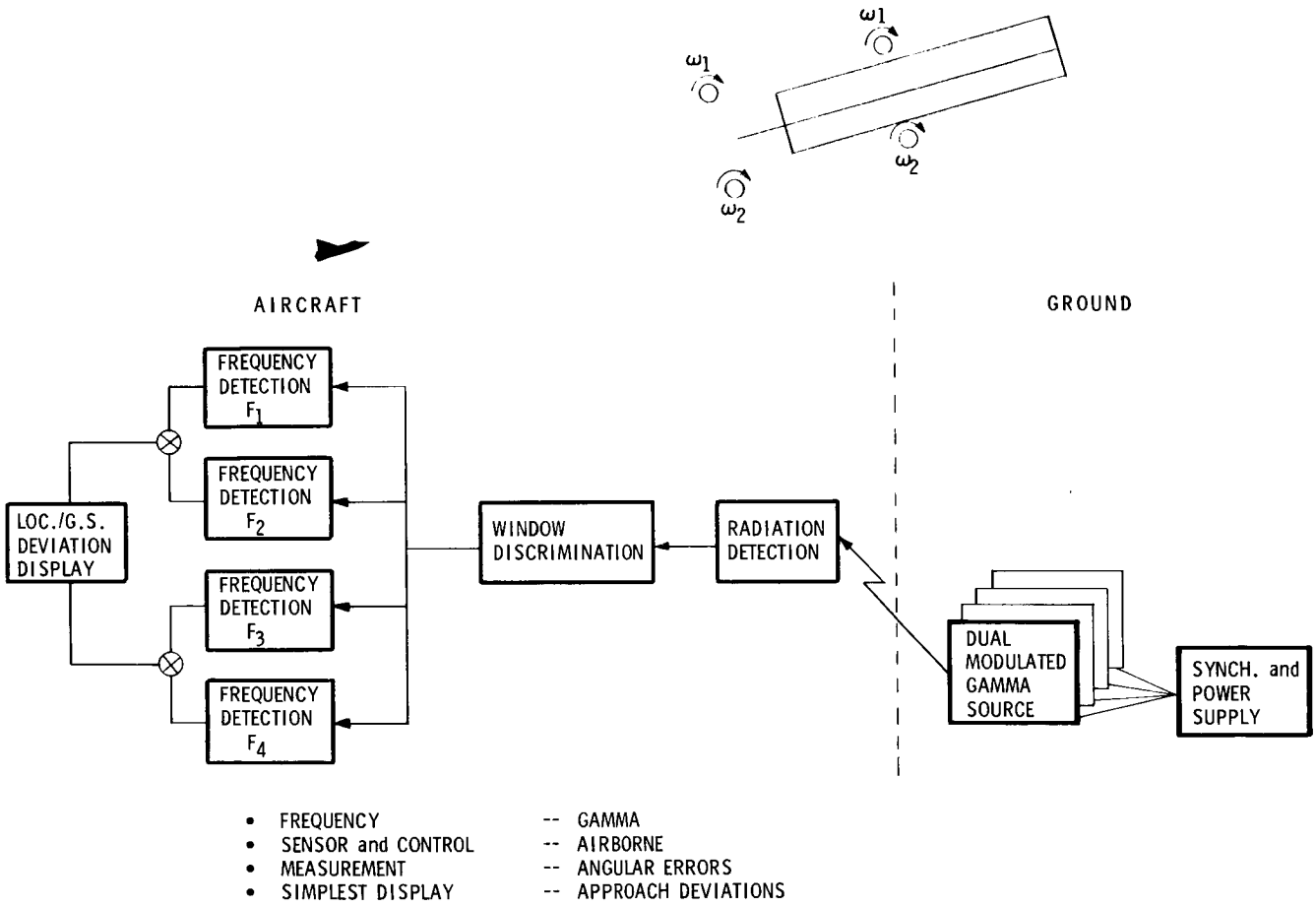

Figure 29 -- Nuclear Instrument Landing System

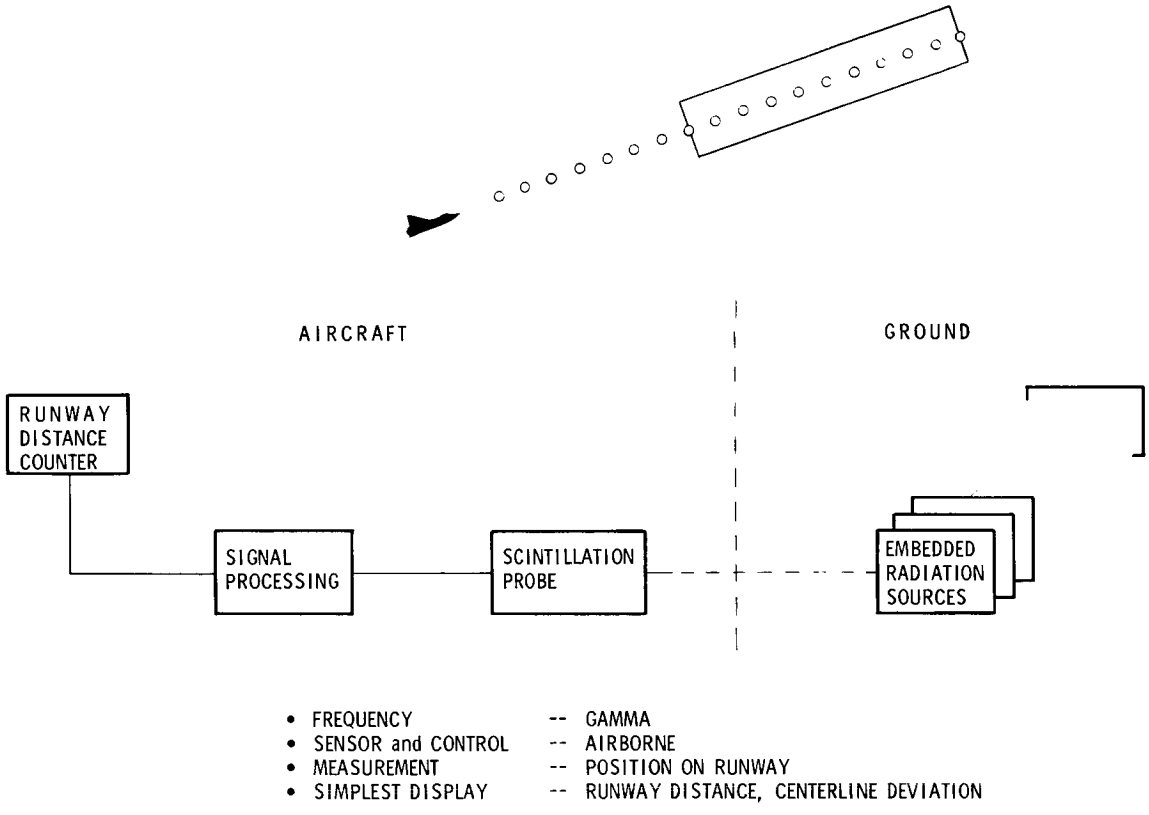

Figure 30 -- Runway Centerline Radioactive Sources

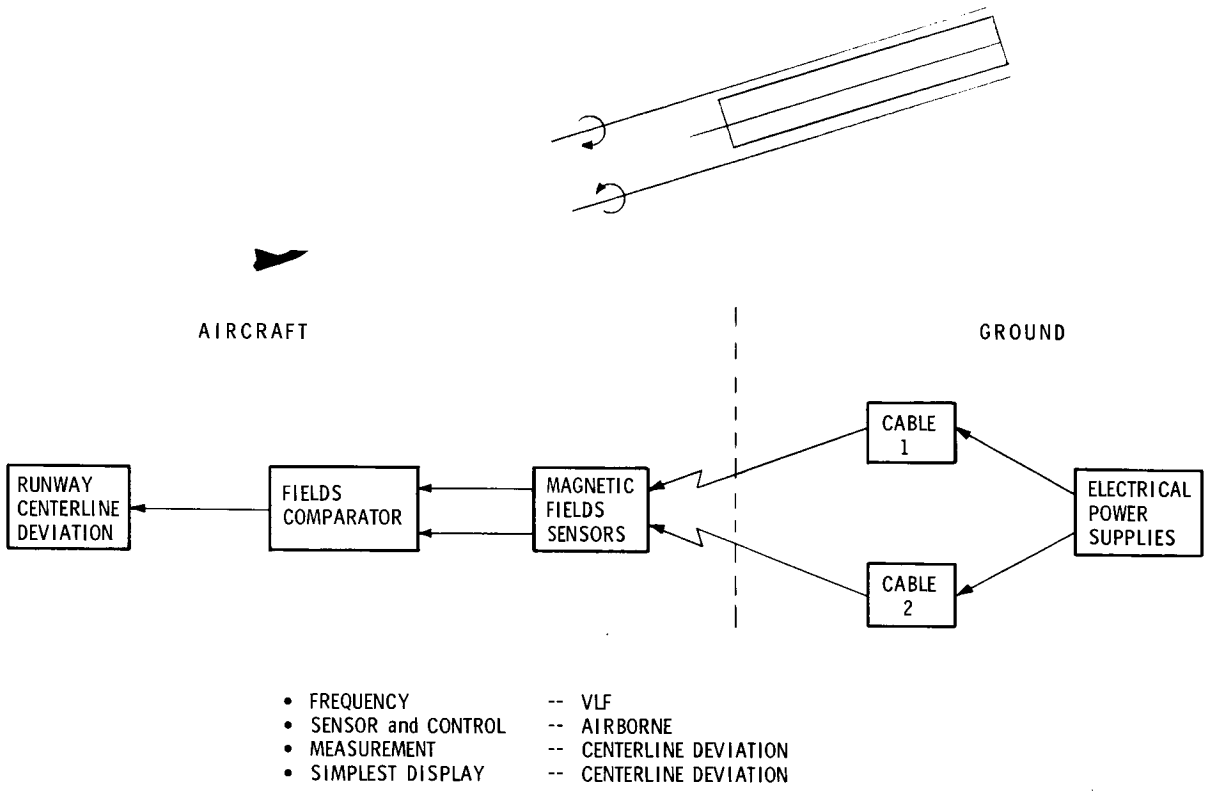

Figure 31 -- Buried Magnetic Leader Cable

CONCEPT 8A - MONOPULSE RANGING RADAR (AIR DERIVED) - FIGURE 32

This concept uses a quad antenna to measure phase differences of the radar signal reflected from a passive corner reflector on the far end of the runway. The phase difference measurements can be processed to provide localizer and glide slope deviation signals. The sum signals are used for range-to-target measurements.

CONCEPT 8B - MONOPULSE/RANGING RADAR (GROUND DERIVED) - FIGURE 33

This concept is a reverse of concept 8A with the quad antenna located on the ground. The steering commands or deviations from nominal advisories are encoded and transmitted to the aircraft by data link where they are decoded and displayed to the pilot.

CONCEPT 9 - MICROWAVE IMAGING RADIOMETER - FIGURE 34

This concept uses a microwave scanning antenna and receiver mounted on the aircraft to generate a perspective display of the runway and its surroundings. Discrete microwave emitters may be used along the runway to enhance the outline. This concept should also consider the use of a microwave runway floodlight illuminator which may be mounted on the aircraft or on the ground ahead of the runway.

CONCEPT 10A - MICROWAVE INTERFEROMETER - FIGURE 35

An omni-directional microwave transmitter mounted on the aircraft transmits to an interferometric antenna array on the ground near the runway. By phase comparison measurements on the received signal, deviations of the aircraft from the

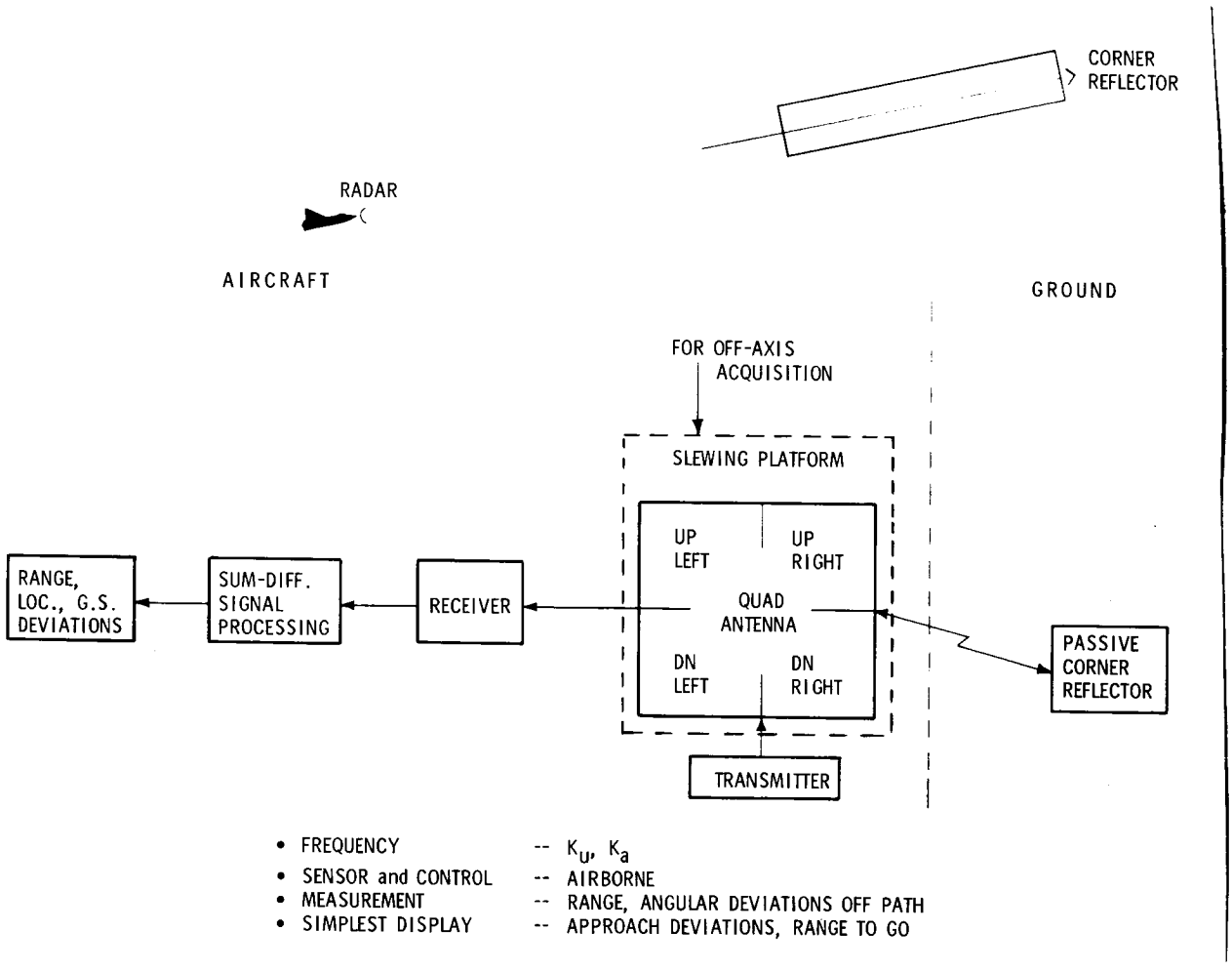

Figure 32 -- Monopulse/Ranging Radar

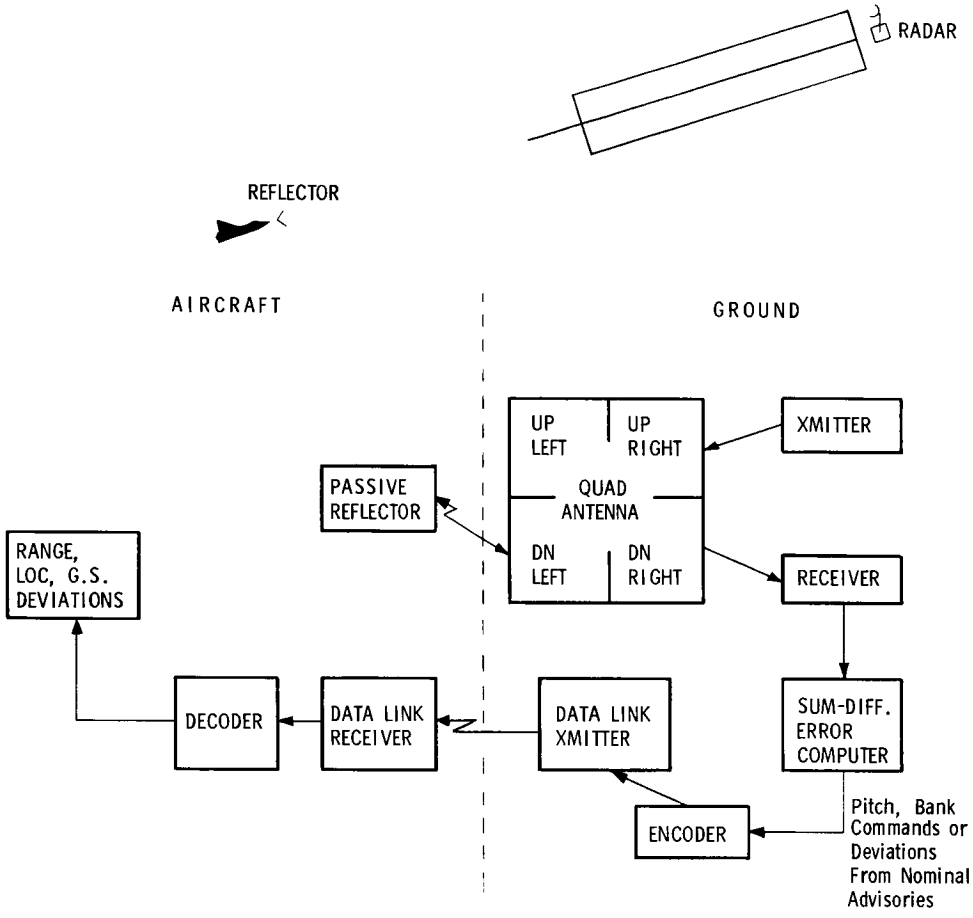

- FREQUENCY -- X, K_u, K_a
- SENSOR and CONTROL -- GROUND
- MEASUREMENT -- RANGE, ANGULAR DEVIATIONS
- SIMPLEST DISPLAY -- STEERING COMMANDS, RANGE TO GO

Figure 33 -- Monopulse/Ranging Radar (Ground Derived)

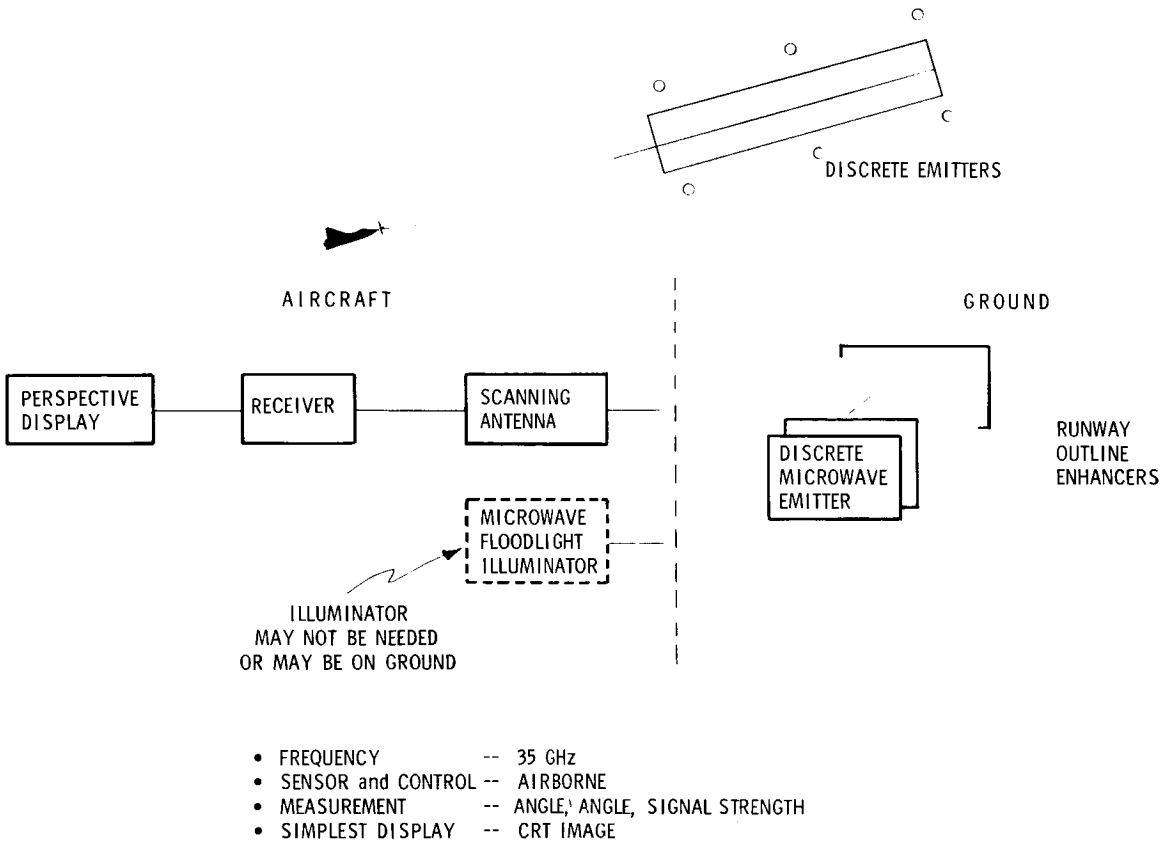

Figure 34 -- Microwave Imaging Radiometer

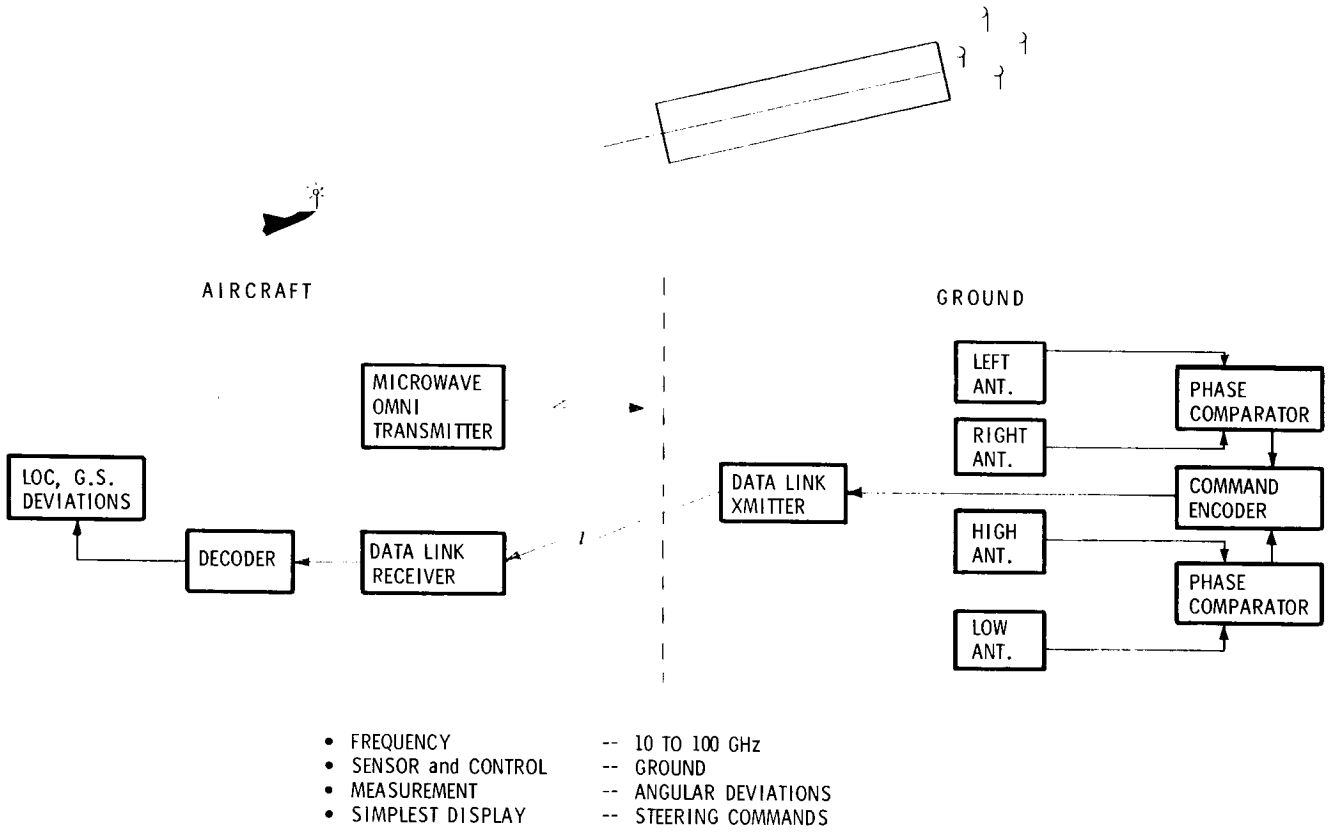

Figure 35 -- Microwave Interferometer

localizer and glide slope are measured. Advisories can be sent to the incoming aircraft by a data link for display to the pilot.

This concept would normally be designed for straight in approaches only.

CONCEPT 10B - MICROWAVE INTERFEROMETER WITH RANGE - FIGURE 36

A single interferometric antenna array provides angular data only for aircraft position. A concept using three or more arrays can be used to triangulate on the approaching aircraft and derive range also. Aircraft position would be computed on the ground and transmitted via data link to the aircraft for display. This concept should be feasible for limited curved approaches as well as straight in approaches.

CONCEPT 11 - BISTATIC RADAR - FIGURE 37

Bistatic radar is a concept where the radar transmitter is located in a different position than the radar receiver. The concept shown here has the transmitter located on the approach to the runway illuminating the runway area. The aircraft receives the reflected signal from the runway in addition to the primary transmitted signal from the transmitter. A signal processor then arranges the received data to generate a perspective display on the aircraft. This concept has the advantage of effectively shortening the radar signal path length and should, thus, increase the range of the system.

The inverse of this concept with the transmitter on the aircraft and receiver on the ground should also be possible. In this case the received signal would have to be processed to derive error commands or advisories and a data link to transfer these commands to the aircraft would be required.

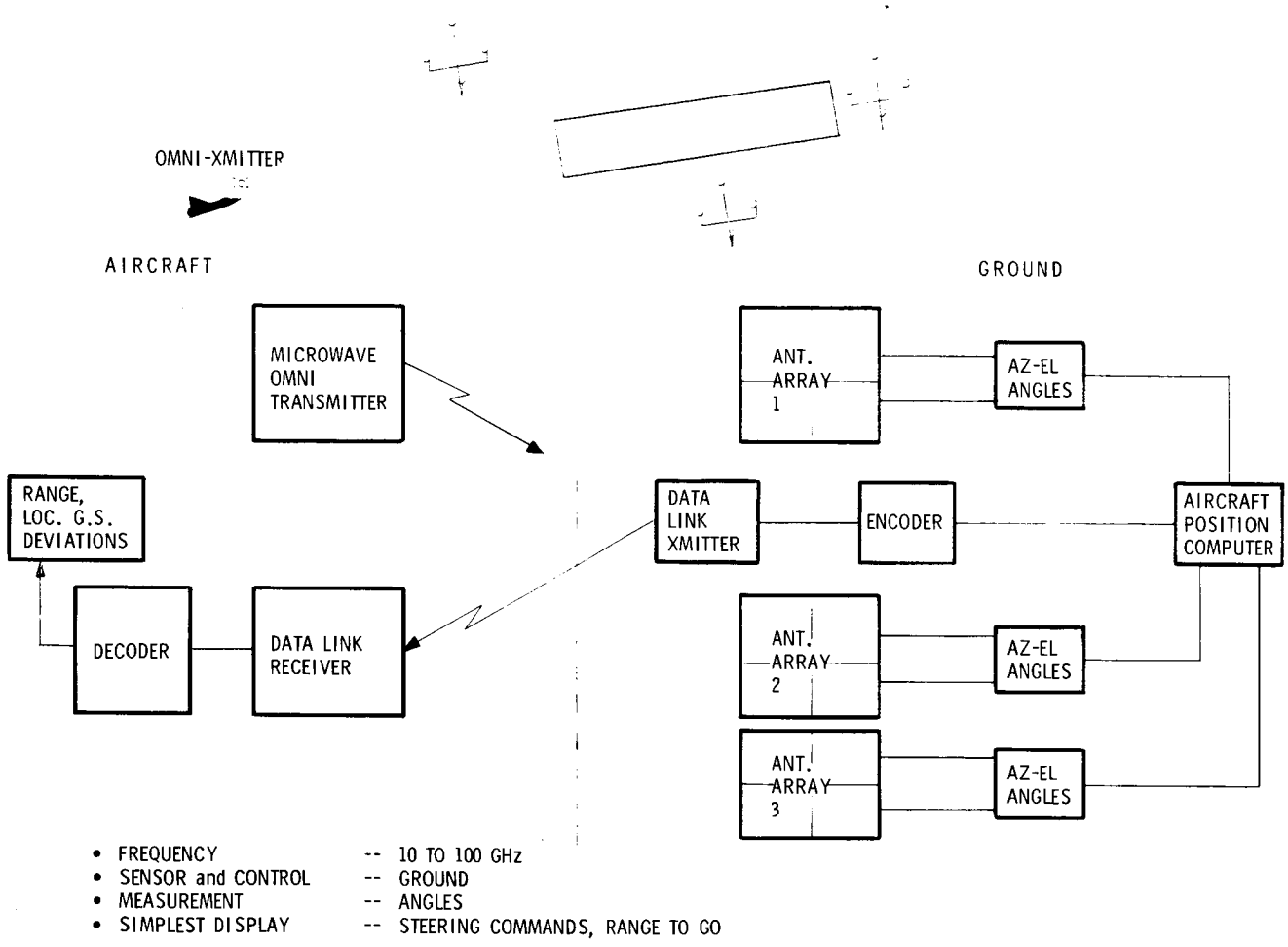

Figure 36 -- Microwave Interferometer Plus Range

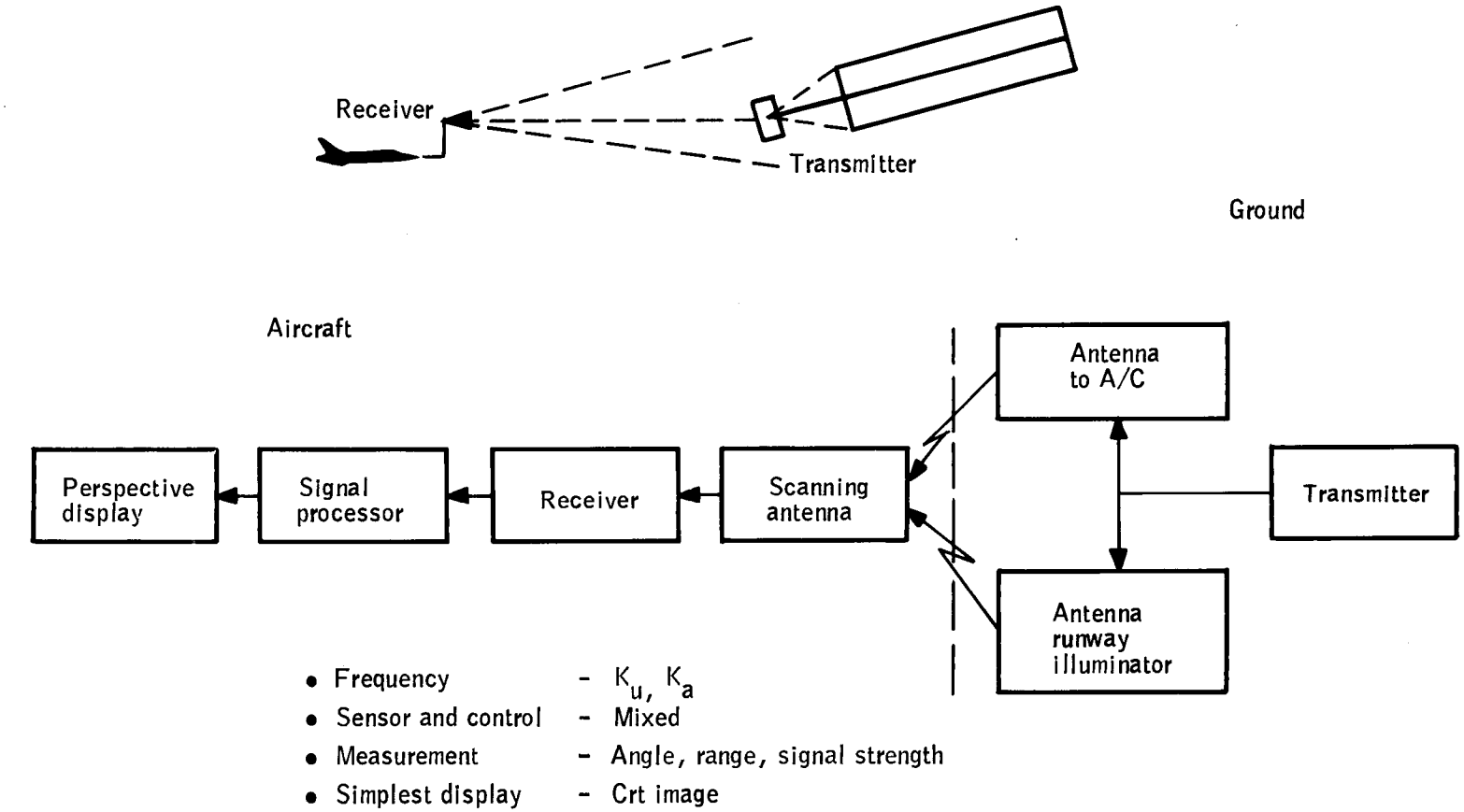

Figure 37 -- Bistatic Radar

CONCEPT 12 - REDUNDANT MLS - FIGURE 38

One of the primary requirements for the Independent Landing Monitor is that it serve as a backup and monitor of the baseline MLS system. Thus a feasible ILM is a redundant set of MLS equipment.

As presently conceived, the baseline Category III MLS system is already highly redundant. It has dual transmitters on the ground for each function, dual receiver front ends and quad signal processors on the aircraft along with detailed monitoring of each function. This configuration is to provide a fail operational capability in the event of a single failure in the MLS system. Since this is one of the functions of the ILM it can be argued that the redundant MLS capability is already included in the baseline Category III configuration. Pilot displays for MLS are not well defined at present. It may be desirable to add a separate display to fulfill the unique ILM display requirements.

CONCEPT 13 - INERTIAL AIDING - FIGURE 39

A stand alone inertial reference system as an ILM does not appear feasible due to cost/accuracy factors. However, for aircraft equipped with inertial platforms for enroute navigation and other functions it should be feasible to incorporate the inertial system with a low data rate position fixing system (small number of nuclear sources, ATCRBS, etc.) as an ILM concept. The inertial system would provide error signals for display about the selected approach path with periodic position updates from the position fixing system before inertial drift errors become significant.

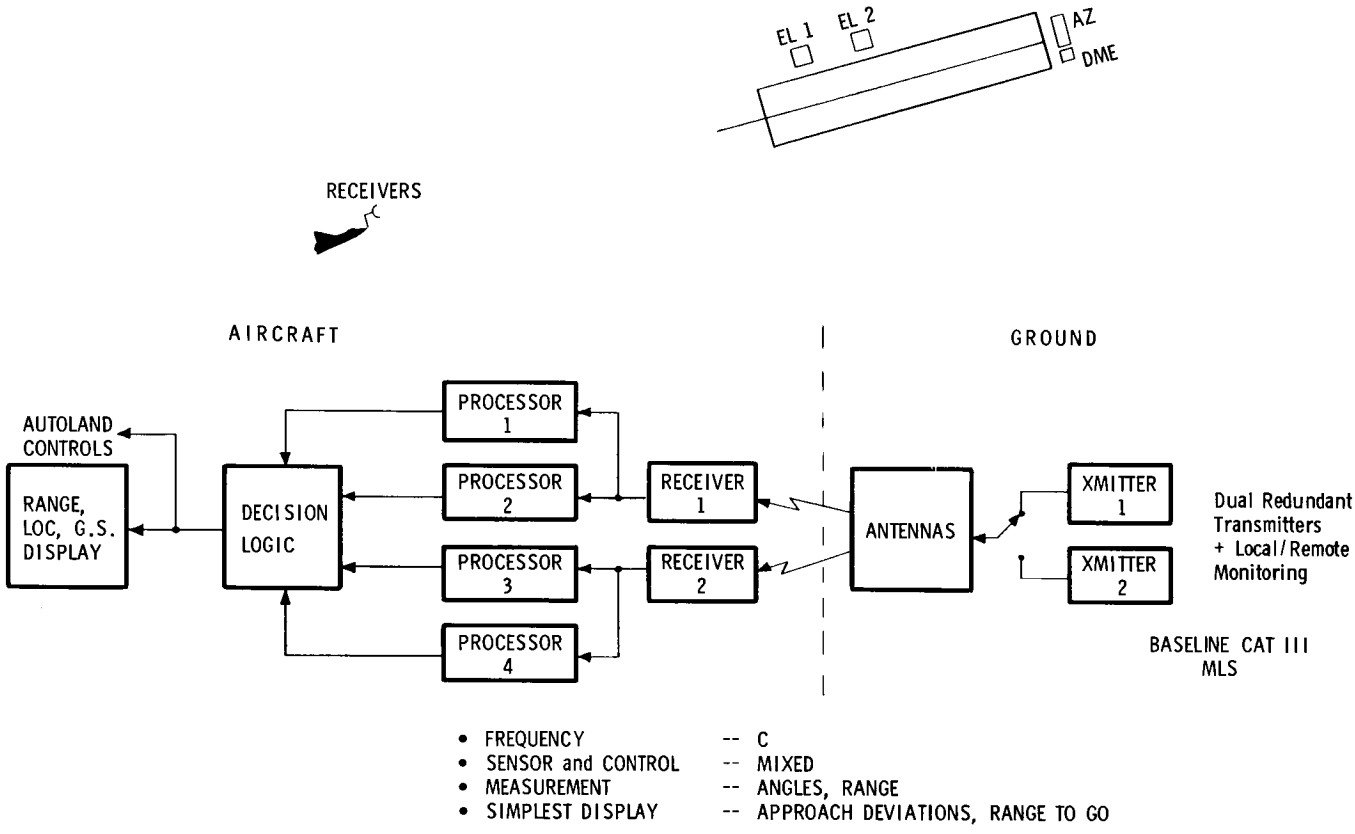

Figure 38 - Redundant MLS

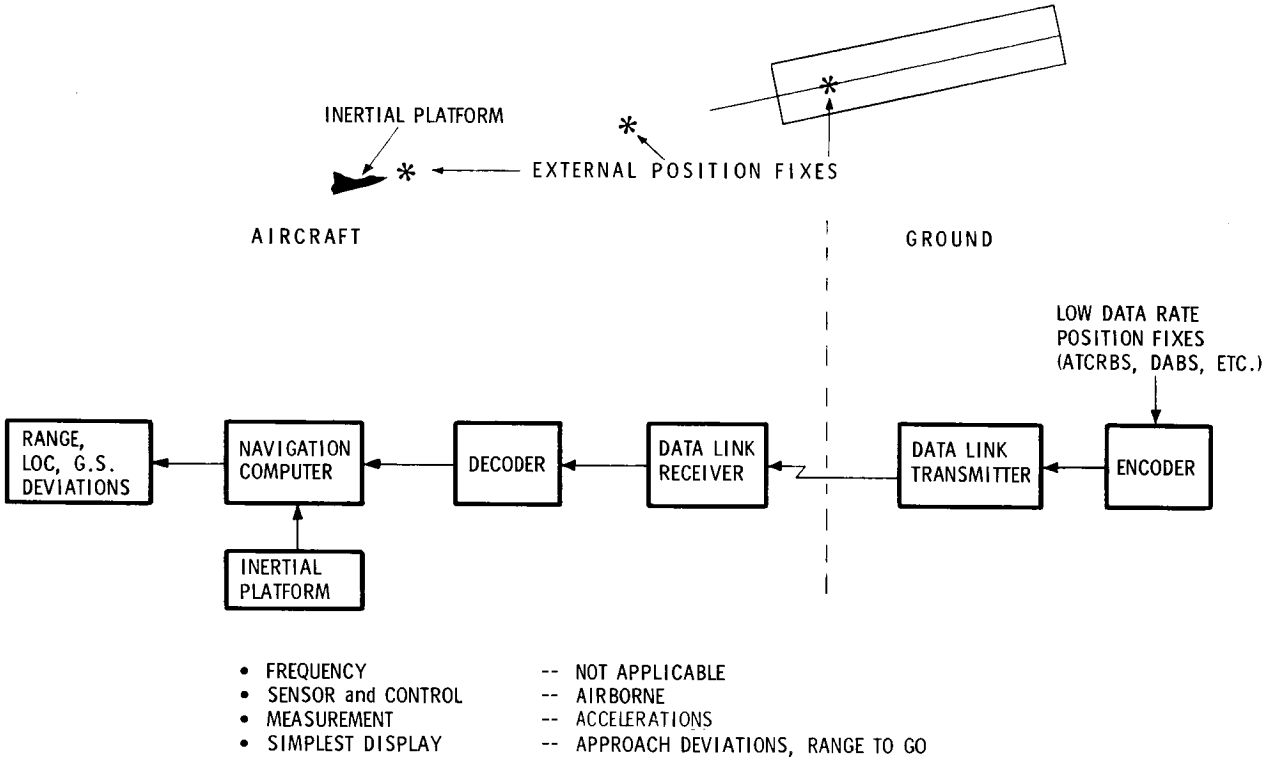

Figure 39 -- Inertial Aiding

Sec. II

SECTION V
SENSOR CAPABILITIES

This section of the report presents a detailed discussion of capabilities of the various generic sensor types that were analyzed during the program in relation to the ILM sensing requirements. The sensors discussed are:

- o Radar
- o Multilateration
- o Nuclear
- o Redundant MLS
- o Television
- o FLIR
- o Microwave Radiometry
- o Interferometry
- o Inertial Aiding

It should be pointed out that some sensor systems are used in more than one concept for the ILM. For example, radar and multilateration have been configured into several different concepts as described in Section IV. The sensor as a feasible mechanism for meeting the overall needs of an ILM were evaluated. If the sensor failed to meet minimum requirements, it was no longer considered in the analysis.

RADAR SENSORS

The theoretical radar analysis presented here is based on basic radar equations with a discussion of parameter dependencies and sensitivities. The radar equations necessary for a generalized radar system analysis were inserted into an existing airborne forward-looking radar computer subroutine under the Honeywell Multiple Airborne Reconnaissance Sensor Assessment Model (MARSAM) software system. The following pages present a derivation and discussion of the technical considerations that were either included in the subroutine modification or considered in the analysis of the results.

The analysis and predictive modeling of radar systems has generated volumes of scientific literature which have probed the disciplines of RF, microwave, communications, information, statistical, and psychological theories to analyze the many aspects of the complex radar system. It becomes immediately necessary to constrain the analysis, in this case, to considerations appropriate for an Independent Landing Monitor (ILM).

The requirements for an aircraft instrument landing system under low or zero visibility weather conditions have been presented previously. These specifications, which summarize the positional accuracy requirements necessary for instrument landings, will form the accuracy goal for a radar ILM and provide information on what system limits are required for instrument landings without entering into a detailed analysis of aircraft flight dynamics. The accuracy goals and system parameters are repeated in Table 22 for the basic approach/touchdown.

Table 22 -- ILM System Specifications

Basic Positional Accuracy (2σ)

	AIRCRAFT POSITION					
	ROLLOUT	GPIP	THRESHOLD	1.85 Km (1 nm)	5.56 Km (3 nm)	14.83 Km (8 nm)
Azimuth	4.27m (14ft)	4.27m (14ft)	4.27m (14ft)	6.1m (20ft)	11.6m (38ft)	31.4m (103ft)
Elevation	-	-	.55m (1.8ft)	3.6m (11.8ft)	10m (33ft)	29m (95ft)
Range	12.2m (40ft)	12.2m (40ft)	12.2m (40ft)	17.68m (58ft)	28.7m (94ft)	56m (184ft)

SLEW/SCAN ANGULAR LIMITS

Elevation: .052 rad (+3°) to -.314 rad (-18°)

Azimuth: .838 rad (±24°)

Minimum FOV: .14 rad x .14 rad (8° x 8°)

DATA RATES (INDEPENDENT SAMPLE UPDATE RATES)	RATE
All angle functions except during flare	5/sec
Angle functions during flare	10/sec
DME Interrogation	
Normal	40/sec
On Ground	5/sec

Analytical Approach

The basic radar equations for software implementation have been derived from many approaches available. The one used here was to incorporate as many characteristics as possible into a set of variables to be defined in the following pages.

Radar System Assumptions --

1. Radar operational frequencies considered are C-band (3 GHz) to K_a-band (36 GHz) as these frequencies have been shown in previous studies to be the trade-off range for resolution versus weather-penetration capabilities.

2. Ranging information is essential for ILM reporting so all radars considered are pulsed radars with range gating of received signals.

3. Adverse weather conditions associated with the requirement for ILM's impose precipitation - clutter limited operation. Radar processing techniques for this analysis will be directed at those techniques that provide, or enhance, clutter rejection.

4. The short ranges considered for ILM aiding allow the use of flat earth approximations for geometrical representation of aircraft approaches and aspects.

5. Approach paths are assumed smooth such that radial and transverse accelerations are assumed negligible and velocities are constant. Radial aircraft velocity is assumed 145 kts unless otherwise noted.

Analytical Structure -- The mathematical approach used in the analysis is represented in Figure 40. The description of each block shown and definition of the equation variables are presented below.

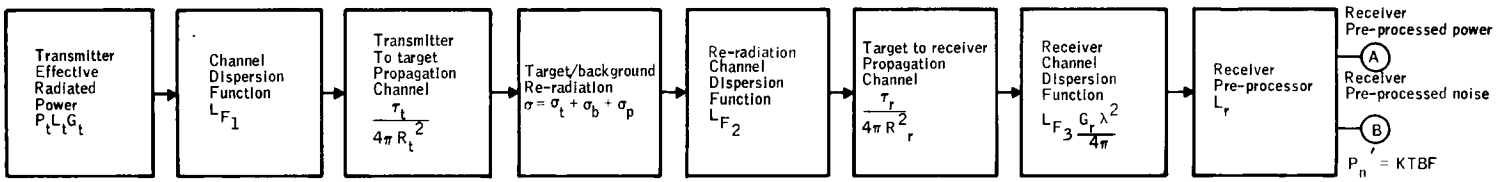

Generalized radar equation

$$P_r = \frac{P_t G_t G_r \tau_t \tau_r L_t L_r \lambda^2 (\sigma_t + \sigma_b + \sigma_p)}{(4\pi)^3 R_t^2 R_r^2} L_{F_1} L_{F_2} L_{F_3} L_p$$

$$P_n = \frac{L_n}{F} P_n' = KTB L_n$$

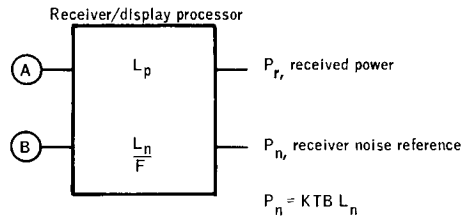

Figure 40 -- Radar System Analytic Structure

The basic radar equation is:

$$\text{Received Power, } P_r = P_t L_t G_t \cdot \frac{\tau_t}{4\pi R_t^2} \cdot \sigma \cdot \frac{\tau_r}{4\pi R_r^2} \cdot \frac{G_r \lambda^2}{4\pi} \cdot L_r \cdot L_p \cdot L_{F_1} \cdot L_{F_2} \cdot L_{F_3} \quad (1)$$

where,

P_t = Peak Transmitter Pulse Power

L_t, L_r = Transmitter/Antenna and Receiver/Antenna plumbing losses

G_t, G_r = Peak Antenna gain referenced to an omnidirectional radiator

τ_t, τ_r = Propagation Channel Attenuation as a function of path atmosphere conditions

R_t, R_r = Transmitter/Target, Target/Receiver propagation path length

σ = Re-radiation or scattering cross-section which relates the ratio of reflected or re-radiated power directed at the receiving aperture to the incident power from the transmitter channel.

λ = Signal Wavelength

L_p = Loss (and gain) values attributed to Receiver processing techniques

L_{F_1} = Transmitter channel dispersion function relates the effects of a scanning beam antenna function with a spatially distributed antenna pattern (i.e.: $\frac{\sin x}{x}$ pattern).

L_{F_2} = Re-radiation channel distribution function relates the effects of scattering that cannot be included under the definition of σ.

L_{F_3} = Receiver channel dispersion function includes the effects of relative scan differences between transmitter and receiving antenna, the effective receiving aperture efficiency, and the receiving antenna spatial distribution function.

The pre-processed noise power equation is $P_n' = KTBF$ and the processed receiver noise power equation is $P_n = KTBL_n$.

K = Boltzmann's Constant

T = Receiver Noise Temperature

B = Receiver Bandwidth

F = Receiver Noise Figure which references the thermal noise generated by the receiver to the receiver bandwidth.

L_n = Loss term that compensates for the definitions of T and B above (i.e., whether or not the values used are "equivalent noise" values), inputs additional noise due to receiver noise Figure F measurements; incorporates the receiver and display noise processing mechanisms (e.g., uncorrelated noise integration gain); and considers collapsing losses due to multiple noise sources such as multiple channels.

The above equations were programmed, in part, on the Honeywell H6080 Computer for computational parameter analysis. The additional factors in the radar analysis that were not included in the computer analysis include parts of the variables L_{F_1}, L_{F_2}, L_{F_3}, L_p and L_n. The factors and loss terms included in these variables are defined below. The derivation of values for the variables will follow.

- $L_{F_1} = f(L_d, L_j, L_c, L_a, L_b)$ (2)

  L_d - Scan distribution loss which considers the probability of detection variation as a function of varying scan rates.

  L_j - Scanning loss which relates the relative motion of antenna patterns between transmission and reception of a pulse due to propagation time.

  L_c - Sensor cueing loss due to the radar system dependence on other systems providing pointing or direction.

  L_a - Sensor losses due to aircraft motion.

  L_b - Antenna beamshape losses due to variations in pattern shape or aperture illumination due to scanning angle, pulsewidth variation (very narrow pulses), or radome distortions.

- $L_{F2} = f(L_\sigma, L_s, L_g, L_{pol})$ (3)

  L_σ - Losses or variations due to cross-section measurement accuracy.

  L_s - Consideration of radar cross-section scintillation (time varying amplitude fluctuations).

  L_g - Consideration of radar cross-section "glint" (time varying angle fluctuations).

  L_{pol} - Consideration of σ variation due to signal polarization.

- $L_{F3} = F(L_e, L_j, L_n)$ (4)

  L_e - Effective aperture efficiency variations due to angle or scanning rates.

L_j - (previously defined for L_{F_1}) considers the relative scanning motions of transmitting and receiving antennas.

L_{nf} - Loss or resolution degradation due to near-field phase considerations.

- $L_p = F(L_i, L_{nl}, L_{di}, L_{rd}, L_f)$ (5)

L_i - Integration gain based on the temporal correlation function of the respective signal (target, background clutter, precipitation clutter)

$L_i = n^{\gamma}$, $0.5 < \gamma < 1$, for n pulse returns (6)

L_{nl} - non-linear gain and variable threshold consideration.

L_{di} - Consideration for display efficiency not included in L_i and L_{nl} (e.g., non-linear resolution cell mapping to resolution (line) limited CRT perspective display).

L_{rd} - Range gate and doppler filter considerations.

L_f - Fluctuating signal losses in processing.

- $L_n = f(F, L_i, L_{bw}, L_{cl})$ (7)

F - Receiver noise figure

L_i - Integration gain (see above).

L_{bw} - Bandwidth factor for filter type and shape.

L_{cl} - Collapsing loss due to consideration of multiple noise sources or channels.

Terms not significant or considered beyond the scope of this analysis are:

- L_j, scanning loss is not significant for typical systems at short ranges.

- L_c, sensor cueing loss is not predictable without an overview of other systems and specific configurations, and is assumed negligible.

- L_a, sensor losses due to aircraft motion or instabilities is assumed small on the assumption that signal, or image, stability is achieved with stabilization techniques such as inertial platform components or a high signal return ground reference such as a beacon or reflector.

- L_b, antenna beamshape losses due to variations in antenna pattern under radome distortion are assumed reduced by calibration. Variations due to other beamshapes or aperture illumination functions will affect off-boresight values (scan profiles) but will not significantly alter boresight or maximum return values. Since the radar equation powers of a scanning beam are average values in a Rayleigh statistic, the (standard deviation) variation is greater than the variation between antenna pattern shapes and aperture distributions (Reference 4). Variations due to scan angle (such as with electronically scanned phased arrays) is assumed small on the assumption the antenna is mechanically slewable to center the array near the runway.

- L_σ, the loss or variation due to cross-section measurement accuracy or reliability is not quantitatively predictable. This is because variations in individual measurements (e.g., 1.5 dB for γ is from Reference 22) are more accurate than the predictability of the terrain type that would be encountered in an operational environment. This, compounded with the uncertainty of the extrapolation of results to 3° glideslope, dictates that

the uncertainty lies between the expected values of Table 38. The analytic results, to be presented in a later section, will assume a range of scattering to smooth earth values from 15 cm to 25 cm vegetation (6 inches to 10 inches) as an estimate for the expected range of returns. For this reason, the losses will be assumed negligible with variation of results left to the later discussion of results.

- L_s and L_g, scintillation and glint fluctuations will be discussed in integration, L_i, and fluctuating signal loss, L_f.

- L_{pol}, the uncertainty of the clutter reduction assumption (Table 40) is unpredictable with the limited information available over the extended frequency bands. This uncertainty is negligible under the assumption the system ellipticity of polarization is optimized to the Table 40 values for the required ILM weather conditions.

- L_e, effective aperture efficiency variations due to angle or scanning rates is related to the L_b losses previously discussed. The simulation assumed transmitting and receiving efficiencies as similar such that:

$$\text{Effective Receiving Aperture} \cong \frac{G_t \lambda^2}{4\pi} \tag{8}$$

This assumption is maintained for lack of specific system information to the contrary.

- L_{nf}, the loss due to near-field phase variations will be considered, as previously discussed, in the discussion section, but is not quantitatively definable for specific systems.

- L_{nl} and L_{di}, the functions for non-linear gain, variable threshold, and display parameters are system and human factors considerations to be analyzed in specific applications. The effects will not be addressed quantitatively.

- F and L_{bw}, receiver noise figure and bandwidth factor are used as reported or calculated as described in later analyses using the reported bandwidths. The thermal noise variations due to F and L_{bw} inaccuracy in measurement are small compared to integration L_i, and collapsing loss, L_{cl}, effects and may be assumed small for these applications.

The remaining terms which are significant to ILM radar systems are L_d, L_f, L_{cl}, L_s, L_g, and L_i.

- L_d, scan distribution loss, is proportional to scan frequency as shown in Figure 43. Assuming the same high probability of detection (90%) as Barton (Reference 12), a value of scan distribution loss may be approximated by making some assumptions. Assume the 90% probability of detection refers to one time interval that the ILM is referenced during an approach sequence. Since it is not a primary landing instrument, the time for a crew member to check its indicator (e.g., CRT video display) would probably not exceed a couple of seconds. For typical scan rates of 5 images per second (2.5 scan cycles), the number of individual scene images would be of the order of 10 for a loss of approximately 8 dB. (From P_d - probability of detection on one scan, $P_c = 1 - (1 - P_d)^j$ = probability of detection on j scans).

o The fluctuating signal loss, L_f, due to Rayleigh statistical variations in signal voltages has been characterized by Swerling and Schwarts (References 4, 12, 14, 15, and 17). Results from Reference 12 are shown in Figure 41.

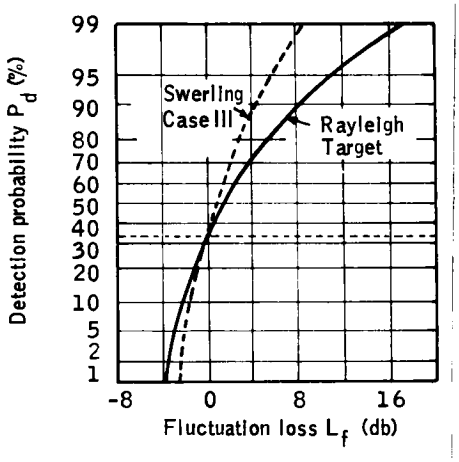

Figure 41 -- Fluctuation Loss Vs Detection Probability

The example for probability of detection of 90% is shown in Figure 43 as a function of scanning.

Figure 43 shows the composite of L_d, L_f, and a relative L_i, proportional to the decreased number of pulses per scan integrated. Figure 42 from Reference 12 shows the effect of varying probability of detection on the combined losses for the steady target case ($L_i + L_d$) and the Rayleigh fluctuating target ($L_i + L_d + L_f$).

o L_s and L_g, scintillation and glint terms will be approximated by the fluctuating signal case described above since target angular velocities are not predictable under the previous assumptions. Uncertainties in return level will be assumed to lay between the curves for steady and fluctuating targets.

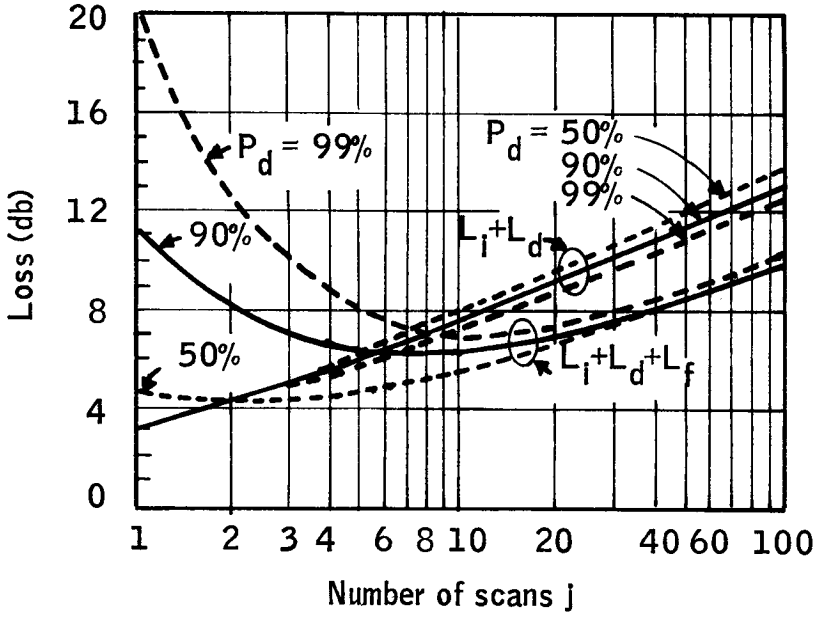

Figure 42 -- Effect of Detection Probability on Combined Losses Radar

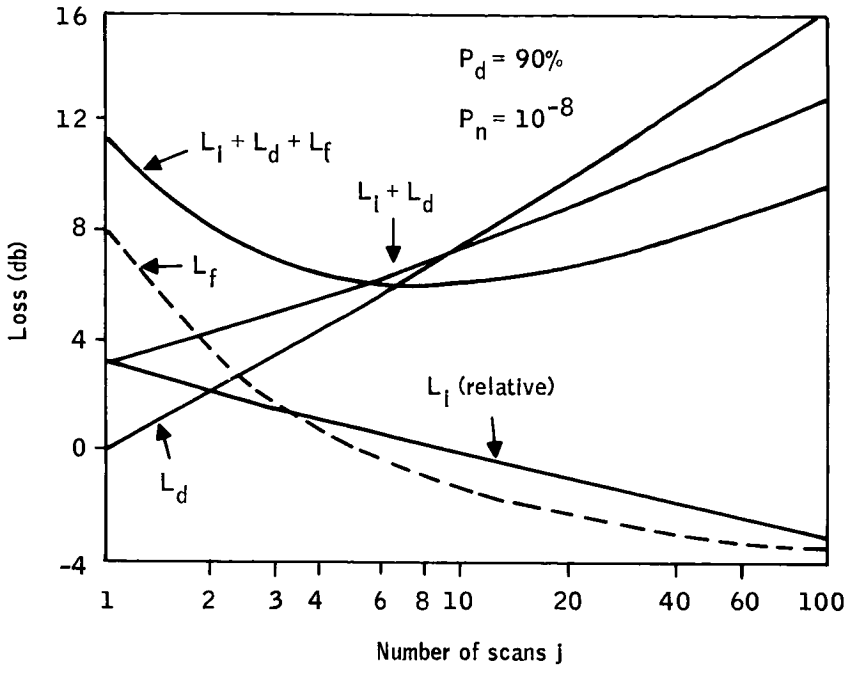

Figure 43 -- Scan Distribution Loss, L_d

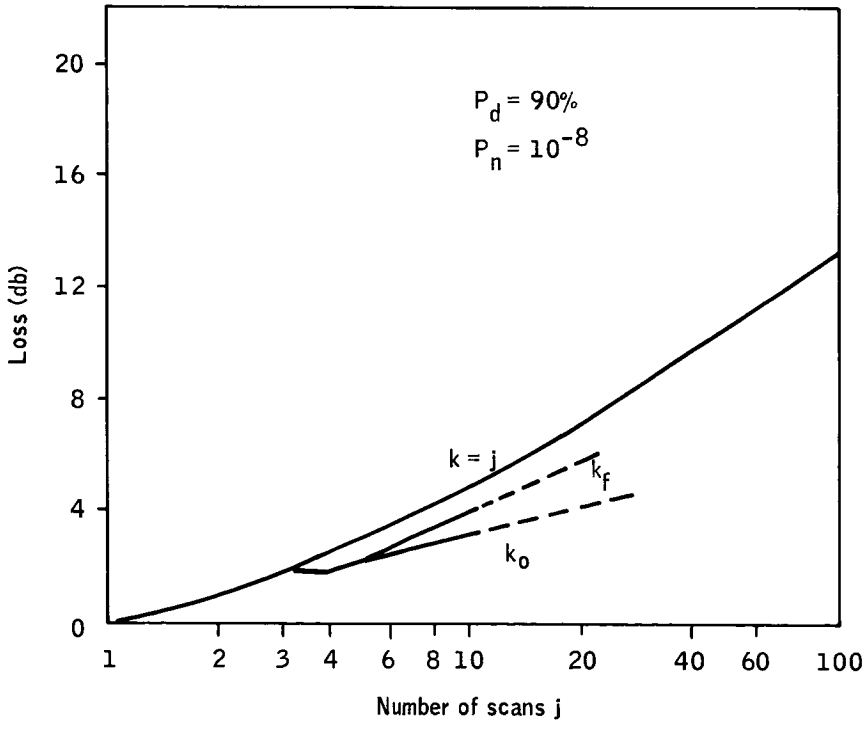

Figure 44 -- Scan Distribution Loss for Systems with Storage

- L_{cl}, collapsing loss can be considered as being from three sources: noise, beam, and range. Noise considerations due to mixing of multiple receiver input channels (such as monopulse) may increase the noise level up to 3 dB (typically 1.5 dB) for two receiver channels of bandwidth B each as compared to a single channel of bandwidth B. Beam collapsing loss was considered in the beam and sidelobe pattern function. Range collapsing loss is the addition of ambiguous range clutter when ambiguity resolution is not incorporated. Worst case collapsing could add in features or targets approximately 6 dB to 12 dB below what the area or target would reflect if at the unambiguous range for reflection coefficients of nearly 1.0.

- L_{rd}, losses due to range gate and doppler gate filtering are reducable by state-of-the-art filter design techniques to "straddling" loss occurring when a target is between two non-overlapping gates. The airborne radars with high resolution (6.7 m or 20 feet) will require many range bins (greater than 700 for a 14,000 foot runway) so the use of overlapping range bins is very unlikely. Adjacent continuous, but non-overlapping, bins could provide up to 3 dB loss for discrete targets. Area targets will be considered under correlation effects in the discussion of integration below so L_{rd} would apply only for discrete targets. (Doppler filtering is not considered as a clutter reduction technique due to the small differences in doppler discussed previously for area and volumetric clutter.)

- L_i, integration loss (referenced to N, the maximum integration gain possible from integration of N samples) was discussed for some typical systems. It is generally accepted (References 4, 12) that video (post detection) integrators

can integrate N returns with an efficiency N^{γ} where γ varies from approximately 0.9 to 0.7 as N increases from a few (2 to 4) returns to many (100's) returns. Private correspondence with C. M. Whitaker of Texas Instruments provides a γ of 0.7 as the integration factor for a specific DVST application on an ILM display. This was used previously to anticipate background to precipitation clutter enhancement. At longer ranges, it was shown that some improvement may be realized (a few dB) due to different correlation times from doppler frequency spreads of the returns. Thermal noise considerations will be assumed uncorrelated for $\gamma = 0.5$.

The following paragraphs discuss the steps of the analytical approach to the radar system capability as shown by each block of Figure 40.

Transmitter effective radiated power (ERP) -- The peak power radiated from the antenna may be represented as:

$$\text{Peak ERP} = P_t L_t G_t \tag{9}$$

P_t - peak transmitter RF pulse power

L_t - transmitter, antenna, and waveguide plumbing losses

G_t - transmitting antenna maximum or boresight referenced to the power that would be radiated by an omnidirection lossless radiator

This power is radiated as a short pulse of effective pulsewidth, τ_p, and effective energy $\tau_p P_t L_t G_t$.

Channel Dispersion (CD) Functions (L_F, L_{F_1}, L_{F_2}, L_{F_3}) -- The channel dispersion function defines the temporal and spatial distributions of the ERP into the propagation channels. The CD function is defined to provide information on:

- o Time dependency effects of a scanning beam
- o Antenna beam pattern and Aperture Illumination
- o Collapsing losses from beam pattern compression of clutter, other targets, and interfering emitters to the boresight reference.

The system operational parameters that influence the channel distribution function are:

- o System Resolution
- o Scan Rate
- o Scan Limits and Field-of-View

These parameters are defined, by the accuracy specification and physical constraints imposed on the ILM application by the airborne configuration.

- Resolution -- The resolution requirements of an ILM system are necessarily high due to the high accuracy requirements presented in the ILM functional specifications. The considerations for resolution are related to the constraints of power ratios and the antenna physical size.

  Resolution, or the ability to resolve two distinct targets, is proportional to the beamwidth, θ (i.e., two targets may be resolved if they are spatially separated by one half beamwidth). The beamwidth is proportional to $\frac{\lambda}{\ell}$, where λ is the wavelength and ℓ is the antenna physical dimension in the plane in which the beamwidth is referenced. Background clutter power returns

are proportional to the area resolution cell (the azimuth beamwidth times the range resolution, $\frac{C\,\tau_p}{2}$, with C, the speed of light and τ_p, the effective pulsewidth). Volumetric or Precipitation clutter power is proportional to the volumetric resolution cell (product of the azimuthal and elevation beamwidths (resolutions) and the range resolution, $\frac{C\,\tau_p}{2}$.

Later discussion of channel attenuation will show that the maximum resolution (highest clutter rejection) capable from a radar will be obtained by a trade-off among the system parameters. The trade-off will be made by maximizing the antenna size in a limited space aircraft, using as high a frequency as possible to achieve resolution at the expense of decreased return signal power due to decreased resolution cell cross-section, and by increasing channel attenuation as the frequency is increased.

- Scanning -- The specification for high independent update rates (5 to 10 updates/sec) for angular information requires that independent information from each resolution cell be received at that rate (as a minimum). For imaging systems the angular information is derived from the imaged perspective scene so the scene must be "imaged" or scanned at that rate. Aircraft velocity of 75 m/sec (145 kts) will have spatially independent range "bins" on successive boresight passes of a 2.5 Hz azimuthal scanning fan beam for range bins less than 15 m (i.e., a 2.5 Hz scanning fan-beam antenna images a target directly ahead every 0.2 sec. Each range bin of 15 m or less sees a different area on each scan (75 m/sec . 0.2 sec = 15 m) so the samples of each range bin are spatially uncorrelated between scans neglecting overlap effects.) The high independent data rates are required due to the dynamics

of aircraft approach and the high accuracy requirements (position/range variation is approximately 15 m between samples and the altitude variation or aircraft sink rate is 0.8 m between samples at .05 rad (3°) glideslope).

- Field-of-View (FOV) and Scan Limits -- The system specifications have large scan limits required to compensate for large "crab" angles due to excessive winds in adverse weather conditions. With narrow beamwidths, the PRF must be very high to return multiple correlated pulses from a resolution cell. The number of pulses received from a resolution cell of effective beamwidth, θ_{eff}, in the direction of scan is:

$$\text{Number of Pulses, } N = \frac{PRF \cdot \theta_{eff}}{f_a \cdot \theta_{scan}} \tag{10}$$

where:

PRF	-	pulse repetition frequency
θ_{Scan}	-	total scan angle in one sweep angle*
f_a	-	sweep or scan cycle frequency defined as $\frac{1}{\text{time per } \theta_{scan}}$

*Sweep angle is defined as total angular extent traced by the beam boresight in one scan. Depending on the scan definition, a scene point may be imaged once or twice per scan (e.g. a circular scan would see each point at most once per scan cycle, whereas, a back and forth scanning fan beam could see a point twice).

The effects of the previously described scan specifications on the radar system may be considered as loss terms in the radar equation (Reference 12). The losses may be described as originating from several phenomena characteristic of scanning radars.

- Scan Distribution Loss, L_d
- Scanning Loss, L_j
- Sensor Cueing Loss, L_c
- Aircraft/Display Stability Loss, L_a

- Scan distribution loss -- Scan distribution loss is derived by considering the relative probabilities of target detection in a single scan or over several scans. Consider a fixed PRF radar with a variable scan rate. Slowing the scan rate increases the number of pulses considered in making a detection decision on a pulse-to-pulse basis at the expense of decreasing the number of scans used to make a target decision on a scan-to-scan basis. Conversely, increasing the scan rate decreases the pulse-to-pulse detection probability and increases the scan-to-scan detection probability. D. K. Barton (Reference 12) has derived a representation of the scan distribution loss, L_d; integration loss, L_i; and fluctuating target loss, L_f, for a Rayleigh distributed fluctuation signal shown in Figures 43 and 44. The single scan integration loss, L_i, refers to the idealized post-detection integration of N $(0.5 \leq \gamma \leq 1.0)$ relative to ideal integration of N pulses. The fluctuating signal loss, L_f, will be considered in more detail in the section on scattering cross-section. The scan distribution loss, L_d, is essentially independent of detection probability. P_c, the probability of detection on j scans is related to the single scan probability of detection, P_d, from Figure 43 by:

$$P_c = 1 - (1 - P_d)^j \qquad (11)$$

The integration loss shown in Figure 43 refers to the loss due to decreased number of pulses per scan as the scan rate is increased. If signal information

is stored from scan to scan, the scan distribution loss may be decreased.

Detection decisions based on single scan detection in k of j successive scans is shown in Figure 44 depicting scan distribution loss for k = j, k = k_p (optimized for Rayleigh fluctuating targets), and k = k_o for optimum coincidence detection (References 12 and 15). The curves of Figures 43 and 44 represent uncorrelated pulse returns so the results are optimistic for integration gains. The results will be discussed in the analysis results following the discussion of correlation in the section on re-radiation and scattering cross-section.

- Scanning loss (L_j) -- Scanning loss (Reference 12) occurs because of the beam displacement between pulse transmission and reception of the echo. The time delay between transmission and reception of the return signal is the propagation time, Δt:

$$\Delta t = \frac{R_t + R_r}{C} \tag{12}$$

C = propagation velocity (speed of light)

Relating this propagation delay to tbe beam scanning for a dual transmitting/receiving (monostatic) azimuth-scanned fan-beam antenna,

$$\text{scan rate, } w = f_a \, \theta_{scan} \tag{13}$$

$$\text{Displacement, } \theta_D = W t = \frac{2Rf_a \theta_{scan}}{C} \tag{14}$$

An ILM application has typical parameters of:

$R < 20$ km

$\theta_{scan} \cong 1.67$ rad (96°) (± 24° scan limits)

$f_a \tilde{=} 2.5$ Hz

$C = 3 \times 10^8$ m/sec

Thus θ_d 0.0005 rad (0.03°), which may be related to the antenna beam pattern. Typical beamwidths of greater than 0.002 rad (0.1°) would have negligible scan loss at near ranges. Higher scan rates and/or long ranges must consider this scan loss unless the specific displaced antenna patterns of G_t and G_r are considered as a function of range and scan parameters.

- Sensor cueing loss (L_c) -- This loss considers the system loss incurred due to another sensor directing the aperture or antenna pointing. An example of this would be a minimized scanning antenna that scans only the minimum field-of-view limits of .14 rad by .14 rad (8° by 8°). In order to compensate for crab angle on approach other sensors are required for providing a cue to the .14 rad (8°) azimuth scan as crab angles of .349 rad (20°) may be required. This loss will be a function of the parameters of acquisition by other systems so this loss will be considered, at least qualitatively, in the analysis of composite ILM systems composed of several sensor types.

- Aircraft/Display stability loss (L_a) -- This loss is due to image or return signal de-correlation due to relative movement between the sensor and the "stationary" scene or targets being detected or imaged. A later section on target re-radiation and scattering cross-section will consider the effects of different relative velocities due to the scene or target geometry causing doppler frequency spectral spreading. This loss, L_a, considers the aircraft, antenna, or display movement and instabilities in the aircraft reference frame of pitch, roll, and yaw. Skolnik (Reference 4) provides some

information on rms angular yaw error rates for a Boeing 707. The random motions for this aircraft create a spectral spread due to a 0.8°/sec rms rate. For a 2.5 Hz scan rate and 0.002 rad (0.1°) azimuth resolution cell 0.003 rad (0.2° beamwidth) this motion creates an error of:

$$\text{rms error in resolution cells per second} = \frac{(\text{rms angle rate in deg/sec})}{(.01°/\text{resolution cell})(96°/\text{scan})(2.5\ \text{scans/sec})} \quad (15)$$

$$= .03 \text{ resolution cells}$$

This is a small error between cells, however, the error from scan to scan (1.8 resolution cells) would prohibit scan-to-scan integration unless external stabilization is provided. This loss may be related to pulse-to-pulse or scan-to-scan decorrelation under compensated (stabilized) or uncompensated displays. The effects of stabilization (e.g., with INS's (inertial navigation systems) sensors) is beyond the scope of the radar sensor analysis and is included in this analysis only to indicate that systems with storage or integration beyond the pulse-to-pulse level will require compensation considerations for high resolution (fractional degree beamwidth) systems.

The antenna pattern and aperture illumination were considered in the analysis by providing the weighted antenna spatial distribution functions that describe the beam shape in both the horizontal (azimuthal) and vertical (elevation) directions. This procedure considers the effects of transmitting versus receiving aperture efficiencies by requiring separate receiving and transmitting spatial distribution functions.

The solution of the Fresnel-Kirchoff diffraction interval (References 4 and 19) provides the far-field radiation pattern, $E(\theta)$, of linear array antennas as:

$$E(\theta) = E_e(\theta)E_a(\theta) \tag{16}$$

$E_a(\theta)$ - Array Factor

$E_e(\theta)$ - Element Factor

The array factor may be approximated for both phased array and parabolic reflector antennas by

$$E_a(\theta) = \frac{\text{Sin } u}{u} \tag{17}$$

where u is a function of physical aperture a, sin θ, and the aperture phase distribution, sin θ_o, across the aperture.

For mechanically scanned arrays, or small angles off boresight, the field may be approximated by:

$$E(\theta) = \frac{\text{Sin } u}{u} \tag{18}$$

$$u = \pi \frac{a}{\lambda} \sin \theta \tag{19}$$

with half-power beamwidth, θ_B

$$\theta_B \cong \frac{50.8\lambda}{a} \text{ degrees} \tag{20}$$

a = array length in same units as λ

$$E_e(\theta) \cong 1/2(1+\cos \theta) \cong 1 \tag{21}$$

The normalized beam patterns for an array (power) is approximately:

$$\frac{P(\theta)}{P_{max}} = |E(\theta)|^2 = \frac{\text{Sin}^2 u}{u^2} \quad \text{(Reference 4)} \tag{22}$$

$P_{max} = P_t G_t$ = boresight maximum power

This expression for the gain pattern may be extended to an electrically scanned phase array which is approximated for small scanned angles, θ_o, and small beamwidth by:

$$\frac{P(\theta)}{P_{max}} = \left| \frac{\mathrm{Sin}\left[\frac{(\pi\, a\, \theta - \theta_o)}{\lambda}\right]\cos\theta}{\left[\frac{(\pi a\, \theta - \theta_o)}{\lambda}\right]\cos\theta} \right|^2 \qquad (23)$$

(Reference 4, corrected)

$$\theta_B = \frac{50.8}{(a/\lambda)} \cos\theta_o \text{ degrees}$$

The effect of scanning is small (less than 1 db increase in beamwidth for ±0.419 rad (±24°) scanning) for typical ILM applications. Additionally, the solution of the previously referenced diffraction integral provides solutions of the form $\left|\frac{\mathrm{Sin}\ u}{u}\right|$ for uniformly illuminated planar apertures. Extending the antenna pattern to parabolic reflector antennas, it has been shown that for narrow beamwidth antennas the assumption of $\left|\frac{\mathrm{Sin}\ u}{u}\right|^2$ antenna pattern shape and beamwidth $\theta_B = \frac{51}{a}\lambda$ degrees (for a, the antenna dimension in the plane of the beamwidth reference) provides a common antenna pattern. This pattern approximation is valid within 1 db for array or rectangular or circular apertures. The aperture illumination or the array element weighting functions will modify the $\left|\frac{\mathrm{Sin}\ u}{u}\right|^2$ function to provide sidelobe suppression and beam shaping of the $\left|\frac{\mathrm{Sin}\ u}{u}\right|^2$ pattern. These effects were considered in the analysis by attenuating the sidelobes of the $\left|\frac{\mathrm{Sin}\ u}{u}\right|^2$ function to typical system specification and matching the beamwidth to the $\left|\frac{\mathrm{Sin}\ u}{u}\right|^2$ value. Figure 45 shows the normalized general $\left|\frac{\mathrm{Sin}\ u}{u}\right|^2$ pattern used in the analysis which has input variables that allow modification of:

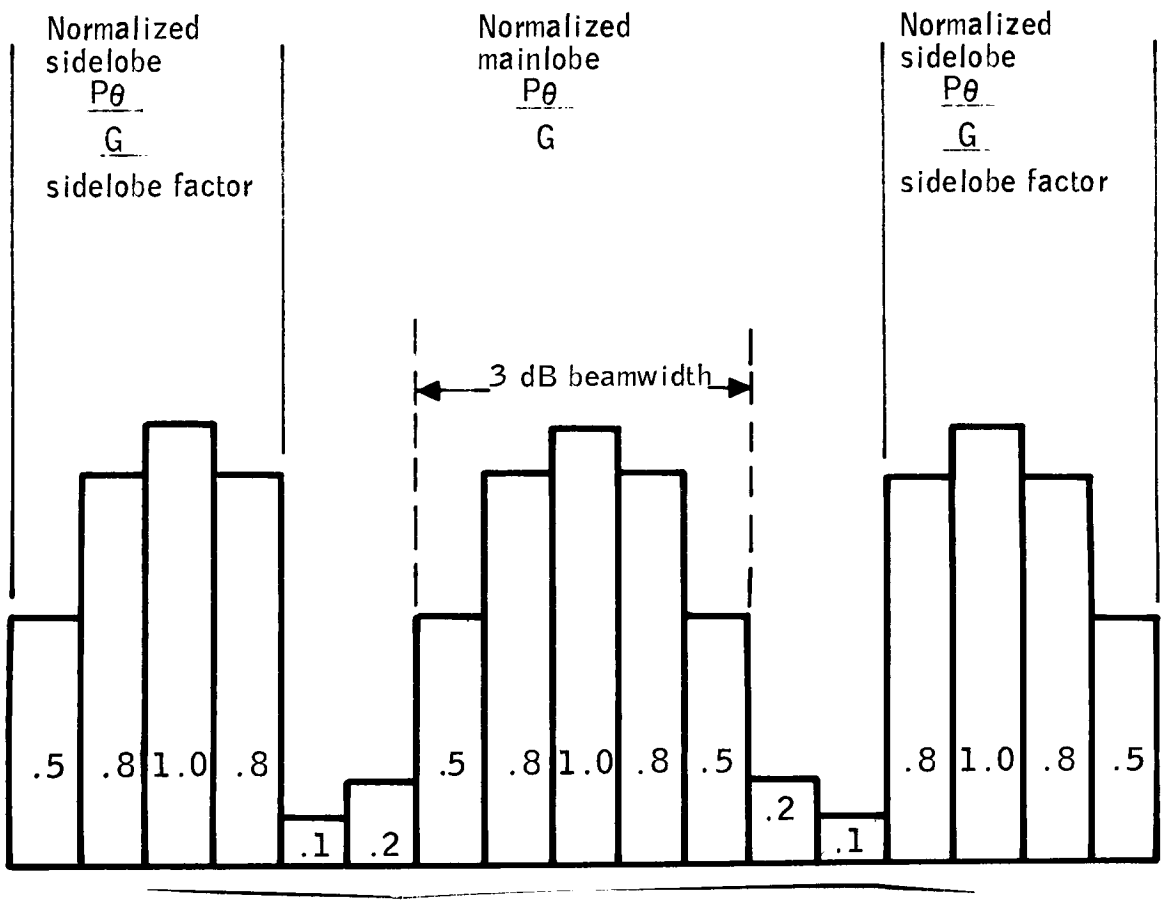

Figure 45 -- Analysis Antenna Pattern

- o Beamwidth
- o 1st null position
- o Sidelobe level relative to Mainlobe
- o Relative Gain Shape

Propagation Channel -- The propagation channel analysis considered three distinct areas: 1) atmospheric effects, 2) geometric effects, and 3) other effects, including radomes, lens, multipath, and lobing. Each area is discussed separately.

- o Atmospheric Effects -- Atmospheric refraction causes a downward bending of the radar beam due to atmospheric density gradient. The effect for short ranges and low altitudes is small creating a bias error of less than 3 ma at 10 Km (Reference 12), decreasing as range decreases. The uncertainty due to variations in gradient is much less than the range accuracy specification. Refractive effects under severe weather boundary effects are less predictable. The effects, however, are expected to be much less than the uncertainties due to reflection effects. Attenuation effects due to gaseous resonance and particulate scattering and absorption were analyzed (see Appendix D). The results of this analysis were expanded to consider additional weather cases.
  - Rain fall rates of 5, 10, and 16 mm/hr.
  - Snow fall rates (Equivalent water) of 3, 6, and 9 mm/hr.
  - Fog Densities of .14, 1.1, and 4.0 gm/m^3.

  The expanded data used in the analysis are presented in Tables 23 through 34. The values of cumulative attenuation are mathematically compatible with MARSAM expressions. This cumulative attenuation is used for extrapolation to path attenuation over the slant range path.

ONE-WAY PROPAGATION PATH ATTENUATION DATA

Table 23

Weather D1.1 5 mm/hr Rain at 1500 m (4920 ft) to 0m altitude

Altitude (Ft.)	ATTENUATION FACTORS (dB)			
	K_a λ = .009	K_u λ = .018	X λ = .032	C λ = .06
0	0	0	0	0
152.4m (500 ft)	.229	.033	.009	.003
304.8m (1000 ft)	.459	.066	.019	.006
457.2m (1500 ft)	.691	.099	.027	.010
609.6m (2000 ft)	.929	.134	.037	.013
762m (2500 ft)	1.17	.169	.049	.017
914.4m (3000 ft)	1.41	.191	.058	.020
1066.8m (3500 ft)	1.65	.226	.069	.024

Table 24

Weather D1.2 10 mm/hr Rain at 1500 m (4920 ft) to 0 m altitude

Altitude (Ft.)	ATTENUATION FACTORS (dB)			
	K_a λ = .009	K_u λ = .018	X λ = .032	C λ = .06
0	0	0	0	0
152.4m (500 ft)	.458	.073	.023	.008
304.8m (1000 ft)	.917	.147	.046	.015
457.2m (1500 ft)	1.38	.222	.061	.023
609.6m (2000 ft)	1.86	.300	.091	.031
762m (2550 ft)	2.34	.379	.116	.040
914.4m (3000 ft)	2.82	.428	.142	.048
1066.8m (3500 ft)	3.30	.506	.167	.056

Table 25

Weather D1.3 16 mm/hr Rain at 1500 m (4920 ft) to 0 m altitude

Altitude	ATTENUATION FACTORS (dB)			
	K_a	K_u	X	C
0	0	0	0	0
152.4m (500 ft)	.684	.126	.042	.014
304.8m (1000 ft)	1.37	.253	.084	.027
457.2m (1500 ft)	2.06	.382	.120	.041
609.6m (2000 ft)	2.79	.517	.165	.056
762m (2500 ft)	3.51	.653	.212	.071
914.4m (3000 ft)	4.23	.738	.258	.087
1066.8m (3500 ft)	4.95	.872	.304	.102

Table 26

Weather D2.2 Radiation or Advection Fog RVR = 213m (700 ft)(M = .14 gm/m^3)

Altitude	ATTENUATION FACTORS (dB)			
	K_a	K_u	X	C
0	0	0	0	0
152.4m (500 ft)	.530	.128	.042	.014
304.8m (1000 ft)	1.01	.297	.084	.027
457.2m (1500 ft)	1.50	.426	.127	.041
609.6m (2000 ft)	2.01	.562	.173	.056
762m (2500 ft)	2.53	.693	.219	.071
914.4m (3000 ft)	3.05	.828	.265	.086
1066.8m (3500 ft)	3.56	.962	.310	.101

Table 27

Weather D2.3 Radiation or Advection Fog RVR = 46m (150 ft)(M = 1.1 gm/m^3)

Altitude	ATTENUATION FACTORS (dB)			
	K_a	K_u	X	C
0	0	0	0	0
152.4m (500 ft)	.569	.138	.047	.015
304.8m (1000 ft)	1.05	.307	.089	.029
457.2m (1500 ft)	1.53	.437	.132	.043
609.6m (2000 ft)	2.06	.573	.177	.057
762m (2500 ft)	2.57	.704	.224	.073
914.4m (3000 ft)	3.09	.838	.269	.088
1066.8m (3500 ft)	3.60	.972	.315	.103

Table 28

Weather D2.4 Radiation or Advection Fog RVR = 0 m (M = 4.0 gm/m^3)

Altitude	ATTENUATION FACTORS (dB)			
	K_a	K_u	X	C
0	0	0	0	0
152.4m (500 ft)	.666	.164	.059	.018
304.8m (1000 ft)	1.15	.333	.100	.033
457.2m (1500 ft)	1.63	.463	.144	.047
609.6m (2000 ft)	2.16	.599	.190	.062
762m (2500 ft)	2.67	.730	.236	.077
914.4m (3000 ft)	3.19	.864	.282	.092
1066.8m (3500 ft)	3.70	.998	.327	.107

Table 29

Weather D3.2 Evaporation Fog RVR = 213 m (700 ft) (M = .14 gm/m^3)

Altitude	ATTENUATION FACTORS (dB)			
	K_a	K_u	X	C
0	0	0	0	0
152.4m (500 ft)	.023	.006	.003	.002
304.8m (1000 ft)	.046	.013	.006	.003
457.2m (1500 ft)	.069	.020	.009	.005
609.6m (2000 ft)	.097	.028	.013	.007
762m (2500 ft)	.126	.036	.017	.009
914.4m (3000 ft)	.156	.045	.022	.011
1066.8m (3500 ft)	.186	.054	.026	.012

Table 30

Weather dD3.3 Evaporation Fog RVR = 46 m (150 ft) (M = 1.1 gm/m^3)

Altitude	ATTENUATION FACTORS (dB)			
	K_a	K_u	X	C
0	0	0	0	0
152.4m (500 ft)	.111	.030	.014	.005
304.8m (1000 ft)	.224	.060	.028	.011
457.2m (1500 ft)	.330	.090	.041	.016
609.6m (2000 ft)	.378	.103	.047	.018
762m (2500 ft)	.408	.111	.051	.020
914.4m (3000 ft)	.437	.120	.055	.022
1066.8m (3500 ft)	.467	.128	.059	.024

Table 31

Weather D3.4 Evaporation Fog RVR = 0 m (M = 4.0 gm/m^3)

Altitude	ATTENUATION FACTORS (dB)			
	K_a	K_u	X	C
0	0	0	0	0
152.4m (500 ft)	.375	.205	.047	.010
304.8m (1000 ft)	.762	.310	.095	.032
457.2m (1500 ft)	1.05	.349	.143	.049
609.6m (2000 ft)	1.29	.357	.161	.055
762m (2500 ft)	1.32	.366	.165	.056
914.4m (3000 ft)	1.35	.374	.169	.058
1066.8m (3500 ft)	1.38	.374	.173	.060

Table 32

Weather D4.1 3 mm/hr Snow at 3 Km (9850 ft) to 0 Km altitude

Altitude	ATTENUATION FACTORS (dB)			
	K_a	K_u	X	C
0	0	0	0	0
152.4m (500 ft)	.007	.002	.002	.001
304.8m (1000 ft)	.013	.004	.003	.002
457.2m (1500 ft)	.019	.006	.004	.004
609.6m (2000 ft)	.025	.008	.006	.005
762m (2500 ft)	.031	.010	.007	.006
914.4m (3000 ft)	.036	.012	.008	.007
1066.8m (3500 ft)	.042	.014	.009	.008

Table 33

Weather D4.2 6 mm/hr Snow at 3 Km (9850 ft) to 0 Km altitude

Altitude	ATTENUATION FACTORS (dB)			
	K_a	K_u	X	C
0	0	0	0	0
152.4m (500 ft)	.007	.002	.002	.001
304.8m (1000 ft)	.013	.004	.003	.002
457.2m (1500 ft)	.019	.006	.004	.004
609.6m (2000 ft)	.025	.008	.006	.005
762m (2500 ft)	.031	.010	.007	.006
914.4m (3000 ft)	.036	.012	.008	.007
1066.8m (3500 ft)	.042	.014	.009	.008

Table 34

Weather D4.3 9 mm/hr Snow at 3 Km (9850 ft) to 0 Km altitude

Altitude	ATTENUATION FACTORS (dB)			
	K_a	K_u	X	C
0	0	0	0	0
152.4m (500 ft)	.007	.002	.002	.001
304.8m (1000 ft)	.013	.004	.003	.002
457.2m (1500 ft)	.019	.006	.004	.004
609.6m (2000 ft)	.025	.008	.006	.005
762m (2500 ft)	.031	.010	.007	.006
914.4m (3000 ft)	.036	.012	.008	.007
1066.8m (3500 ft)	.042	.014	.009	.008

Slant range path attenuation = Attenuation from point A to point B (point B on ground) = (cumulative attenuation from point A at altitude A to ground) x $\frac{\text{slant range from point A to point B}}{\text{Altitude A}}$.

Scattering of electromagnetic energy creating signal returns from atmospheric effects is considered in the discussion of radar cross-sections. A range-gated radar experiences signal attenuation due to scattering in the propagation path between the radar and the target. When the energy is scattered from within the target range bin, the back-scattered return appears in the radar in the form of clutter with the target return. Scattering of power between the target range bin and radar decreases the target illumination power density (and back-scattered power). This effect is included in the attenuation factors above. A localized highly-reflective cell within a precipitation weather case (e.g., "bright bands", References 18 and 24) can create multipath superposition of returns. These effects are time varying due to precipitation particle velocities so the multipath imagery would be highly distorted with short correlation times. This phenomena will be described in a later discussion of precipitation scattering effects.

- Geometric Effects -- The scanning narrow beam antenna defines the geometric path length and angular extent of the propagation channel. The path length geometry is important for radiated power because of the dependency of return signal power levels on the range parameters.

  The diffraction integral solutions for field $E(\theta)$ (and antenna power patterns) were based on simplifying range assumptions. Those assumptions and the effects are discussed below.

The $E(\theta) = \frac{\text{Sin } u}{u}$ is an approximation for far fields. The Fresnel Zone, or near field, is characterized by the radiated power being essentially confined to a channel with cross-sectional area of the effective area A_e of the antenna. Resolution is worse than the far-field angular beamwidth in this region due to phase effects across the physical antenna. This zone of approximately constant power density extends to a range of approximately $\frac{A_e}{\lambda}$. (50 - 100m for X-Band and 150 to 300 m for K_a-Band typical airborne antennas). The far-field Fraunhofer zone beyond $\frac{2A_e}{\lambda}$ follows the inverse square-law relationship (power density = $\frac{ERP}{4\pi R^2}$). The transition zone between these two zones is characterized by a power/range dependance transition from constant to inverse square-law.

The minimum range capability of a monostatic radar is a function of the antenna switching time from transmit to receive. Skolnik (Reference 4) presents several duplexer configurations that provide rapid switching. Short pulsewidths of the order of 10's of nanoseconds for high range resolution may be assumed so Transmit-Receive switching times of that order would be desirable. Switching times of less than 1 μsec (150 m minimum range) are possible for high power transmitters. Shorter switching times, especially at K_a-Band, for transmitters of 50 Kw - 100 Kw are questionable. Reduced power during rollout and taxiing would allow decreasing the switching time to the order of a few pulsewidths.

High data rates (5 independent samples per resolution to element per sec), narrow beamwidths 0.004 rad to 0.005 rad (.24° to .3°), and wide scan limits 0.838 rad (48°) require PRF's in excess of 1000 pps. Clutter correlation times and fluctuating signal returns, to be discussed later, will require

PRF's of 10,000 pps to 20,000 pps to allow pulse integration over a scan angle of one beamwidth. PRF's of this magnitude provide maximum unambiguous ranges of:

$$R_{max} = \frac{C}{2(PRF)} = \frac{3 \times 10^8}{2\ (2 \times 10^4)} \qquad (24)$$

$$= 15 \text{ Km to } 7.5 \text{ Km}$$

These short ranges will require consideration of ambiguous returns by using sensitivity time control (STC) or staggered PRF. (See Multipath and Lobing below).

The effect of first order range rates is to introduce a doppler shift in frequency. Higher order rates are negligible under the assumption of constant radial velocity.

The angular extent of the propagation channel is defined by the two dimensional antenna pattern function in azimuth and elevation. The effect of angular extent of the beam for propagation channel effects is minimal under the assumption that diffraction or bending effects of the beam are much less than the range resolution of the beam. For the purposes of this analysis, the line-of-sight path from antenna to target is sufficient for definition of the attenuation path length.

- Other Channel Effects -- Radomes distort antenna patterns causing boresight deviation (bias errors), beamwidth decreases, sidelobes increases, and attenuation. Some values of distortion for typical aircraft radomes are tabulated below:

Table 35 -- Typical Airborne-Radome Performance Requirements

Boresight Deviation	0.002 rad to 0.003 rad (0.1° to 0.2°)
Beamwidth Decreases (%)	10% (~ 1 dB)
Sidelobe Increase (At -20 dB)	3 dB
Sidelobe Increase (below -20 dB)	>3 dB
Attenuation	-45 dB to -.7 dB

(From Reference 4 for Normal incidence Radomes, incidence angle less than 0.524 rad (30°) (from normal)).

Beam shape effects are incorporated in the antenna gain pattern.

Boresight deviations are bias errors and may be partially calibrated out for high resolution radars. Monopulse antennas would be difficult since all distortions would have to be calibrated out to within the monopulse accuracy.

Lens elements may be used in conjunction with the antennas to provide:

- Beamshaping
- Sidelobe suppression
- Polarization changes

It is also conceivable to use a lens antenna instead of a conventional array or reflector system. The relative advantages of each are summarized in Table 36.

Table 36 -- Conventional Versus Lens Antenna Comparison

	Conventional Antenna	Lens Antenna
Design	Easier to Design	
Construction		Requires less mechanical precision
Size	Comparable	Comparable
Gain (for comparable sizes)	Comparable	Comparable
Weight	Lighter for same size/gain	
Beamshaping		Less spillover loss for lower sidelobes and back radiation
Cost	Less	

The lens antenna in a limited space application would provide better sidelobe suppression at increased cost.

Multipath reflection considerations due to specular reflection off the runway and surrounding terrain could create problems from ambiguous ranges (Ranges greater than the maximum unambiguous range, R_{max}) for high PRF's (greater than 10,000 pps imply R_{max} less than 15 Km). Specular reflection coefficients of greater than 0.8 were predicted from the scattering equations of analysis of other ILM sensors for runways and smooth terrains. An object at range $2R_{max}$, cross-section σ approximately 15 dB above a point target at R_{max}, could have approximately the same echo signal power at the receiver. Staggered PRF could decorrelate this return from pulse to pulse. Ranges closer than R_{max} would cause an additional required separation for ambiguous target images. As an example, consider the range bin at $\frac{R_{max}}{2}$. The ambiguous

range target (at $\frac{3\ R_{max}}{2}$) would require a cross-section approximately 22 dB greater. This neglects atmospheric attenuation and assumes a two-way 3 dB reflection loss. Area and volumetric (precipitation) clutter effects (see the section on Target Re-radiation Cross-Sections) would decrease these ratios since the projected image of the unambiguous range cell to the ambiguous ranges would correspondingly increase its respective clutter component.

Multipath lobing for the highly specular reflecting surfaces of the runway and smooth surrounding terrain does create detection problems. The expression for the lobing maximums and minimums are: (Reference 4)

$$\theta_{min} = \sin^{-1} \frac{(n-1)\ \lambda}{2h} \tag{25}$$

$$\theta_{max} = \sin^{-1} \frac{(2n-1)\ \lambda}{4h} \tag{26}$$

Using the concept of reciprocity (assuming the target is the transmitter) the value of h may be considered as the minimum height of the obstacle to be imaged. Assuming a value of h as 0.3 meters (1 ft) which assures taxiway light returns for sufficient S/N, the lobe maximums occur at approximately 0.007 rad (.39°), 0.02 rad (1.17°), 0.034 rad (1.95°), 0.048 rad (2.73°) at K_a-Band. The effect of these lobes relative to small glide slopes is to create amplitude variations, or scintillations, not entirely due to movement into and out of those lobes but, also, due to variations in incidence angle at the reflecting point of the runway or "smooth" surroundings due to variations in slope as the reflecting point moves in relation to the aircraft velocity. The additional mechanism of lobes created by the non-planar

surface of the obstacle itself and the finite null depth due to reflection coefficients of less than 1.0 compound the problem of analyzing lobing effects. Studies of these effects did not yield any conclusive approaches for estimating correlation times or scintillation frequencies. It must be assumed, due to lack of evidence otherwise, that the effect (scintillation) will be rapid and the effects will average to the nominal cross-section of the obstacles for integration intervals of sufficient length to satisfy other considerations.

Re-radiation Mechanisms -- Multipath specular reflection (two-way) causes the potential of ambiguous range representations as previously described. As radar cross-sections are reviewed in this section, it will become evident that the imaged scene may consist of returns with many 10's of dB variations in scattering cross-section. Highly specular backgrounds will have a high probability of imaging targets from an ambiguous range (greater than R_{max}) when such targets are positioned in the reflection geometry. Aircraft in holding patterns, as an example, may create momentary ambiguous returns for an approach aircraft by imaging as obstacles near a runway. Doppler considerations or other dynamics of the ambiguous image would allow the system some degree of ambiguity resolution to identify the image as a multipath signal.

Radar cross-section is defined as the ratio of power scattered to a receiving aperture to the incident power. Each scattering portion of an illuminated scene will have its return classified according to its return dependency on illuminating footprint size (or range for far-field constant beamwidths).

σ_t - target radar cross-section in area units or dB area units. Targets are usually assumed small with respect to footprint size (point targets) with a return signal power independent of footprint size and a one-way inverse square-law power dependency with range* ($\frac{1}{R^4}$ two-way dependency).

$\sigma_{background}$ - backgroundor area cross-sections have units of power ratio per area illuminated (e.g. dB/m^2). Scattering areas with extents greater than the illumination footprint will have a $\frac{1}{R^3}$ power dependency with range* for range-gated returns due to the footprint area being proportional to range.

$\sigma_{Precipitation}$ - precipitation or volumetric cross-sections have units of power ratio per volume illuminated. Scattering volumes with extents larger than the illuminated volume defined by vertical and horizontal beam patterns and range gating will show a $1/R^2$ range dependency.*

Radar Cross-Section has units of area such that the multiplication of the illuminating power density with σ provides a power radiated toward the receiving aperture. The point targets of interest such as aircraft or obstacles are large compared to the wavelength so the mechanisms for scattering are surface and edge scattering (Reference 15). The discrete values of radar cross-section vary rapidly (10's of dB) as a function of aspect angle so the values reported for radar cross-section are typically "median" values (values exceeded 50% of the time) or "average" values (statistical mean of measurement values) over a nominal

---

* These approximate dependencies do not consider attenuation, which is approximately proportional to range. Attenuation phenomena along the total propagation channel would decrease the power of R by one for each expression.

range of aspect angle (example from Skolnik are 0.175 rad (10°) intervals). When the return is composed of contributions from many reflecting points on a complex reflecting surface, much larger than λ, the Rayleigh distribution may be assumed for the return amplitudes with the mean and standard deviations equal. The Rayleigh distribution also is characterized by the median value equaling 0.69 times the mean value (Reference 12).

Large, smooth objects approach geometrical optical considerations at microwaves with approaching frequency independence. Measured cross-sectional values published in Skolnik support this consideration. Berkowitz shows the frequency dependence of some "standard" geometrical shapes. From these results, it can be expected that smaller targets, such as taxi-way lights or other lighting hardware, may vary from the reported (possibly assumed) value of -10 dBsm, sources (20, 23), at K_a-band to - 30 dBsm for flat normal reflecting surfaces to 0.0 dBsm for off-normal illuminated cylindrical reflecting surfaces at C-Band. This 30 dB theoretical range of values typifies the requirement for measurement studies of hardware of interest for particular radar situations. The large fluctuations in radar cross-section from measurements of large aircraft demonstrate more variation from individual aircraft measurements than between individual measurements of different aircraft. The detection of the targets becomes more qualitative since the returns must be considered in the receiver in a statistical sense. The Rayleigh statistical values of mean and standard deviation of "Classes" of targets are defined in Table 37. ($\text{dBsm} = 10 \log \frac{\text{Target area}}{1\ \text{m}^2}$).

Table 37 -- Target Radar Cross-Sections

Reference	Point Target Class	Mean Cross-Section (X-Band)	Frequency Dependence
1,2	Large Aircraft (nose or tail attitude)	8-20 dBsm	0
Assumed	Vehicles (trucks)	0-10 dBsm	$0 - \lambda^{-1}$
1	Small Aircraft (nose or tail attitude)	0-9 dBsm	$0 - \lambda^{-1}$
2	Man	-3-1 dBsm	$\lambda^{-1/2} - \lambda^{1/2}$
Assumed	Approach Lights	-10-0 dBsm	$\lambda^{-2} - \lambda^{1/2}$
12,15	Runway and Taxi Lights	-10 dBsm	$\lambda^{-2} - \lambda$

Runways and surrounding terrain and vegetation exhibit differential radar cross-sections that are measured and normalized per unit area of planar surface (σ_o) or per unit area of projected (normal to the beam) surface (γ_o). The two standard cross-sectional units are related by:

$$\gamma_o = \frac{\sigma_o}{\sin \theta} \tag{27}$$

where θ is the grazing angle

The variable γ_o was proposed for representing differential cross-section because of the "Semi-Lambertian" characteristic of γ_o being nearly independent of angle down to grazing angles of approximately 0.035 rad (2°) (21) for many dense vegetations. Experiments (4, 21, 22) have shown that as the vegetation becomes shorter or more sparse ("less rough") the value of γ_o changes progressively faster as very low grazing angles are approached. Most of the observations of de Loor (Reference 21) were made at X-Band; however, some measurements at K_a-Band were taken to verify the behavior. The multiple bands (X, K_u, K_a) of Peake (4, 22),

the results of de Loor (21), and the theoretical scattering expressions of Appendix 3 are used for interpolating and extrapolating the various measurement results to arrive at the results shown in Table 38 for 0.052 rad (3°) glide slope.

Table 38 -- Terrain Cross-Section Factors
γ_o, dBsm/unit area, 0.052 rad (3° grazing angle)

	FREQUENCY BAND			
Ground Features	C	X	K_u	K_a
6" to 10" Vegetation	-12 to -5	-11 to -5	-11 to -4	-11 to -4
Rough Tilled Ground and Stubble	-20 to -11	-20 to -11	-17 to -7	-13 to -4
2" Vegetation	-30 to -15	-24 to -15	-22 to -10	-19 to -7
Smooth Tilled Ground	-35 to -14	-31 to -14	-24 to -10	-16 to -6
Smooth Ground	-45 to -25	-40 to -20	-38 to -20	-35 to -15
Snow	-46 to -32	-43 to -29	-42 to -31	-42 to -32
Asphalt	-63 to -52	-56 to -45	-51 to -40	-46 to -35
Concrete	-68 to -43	-61 to -38	-57 to -34	-53 to -30

(Derived from Sources 10, 4, 21, 22)

The volumetric definition of a radar resolution cell bounded by azimuthal and elevation beamwidths and the range gate is used for defining the power returned by the precipitation scattering (σ_p) elements. The radar reflectivity per unit volume, η, of the precipitation is given as:

$$\eta = 2 \times 10^{-16} \frac{\pi^5 |K|^2 Z}{\lambda^4} \quad (m^{-3}) \tag{28}$$

$$|K|^2 = \left| \frac{(\varepsilon_c - 1)}{(\varepsilon_c + 1)} \right|^2$$

ε_c - dielectric constant of spheroid (precipitation)

Z - Reflectivity Factor $(\frac{m\ m^6}{m^3})$

Table 39 -- $|K|^2$

λ(m)	Rain	Snow
.0062	.83	.197
.0124	.91	.197
.0321	.93	.197
.1000	.93	.197

For Rain:

$$Z = r^{1.6} \tag{29}$$

r - rainfall rate in mm/hr

For Snow:

$$Z = 5\ r^{1.6} \tag{30}$$

r - equivalent rainfall rate in mm/hr

For Fog:

$$Z = 2.4 \times 10^{-10}\ M^{2.0} \tag{31}$$

M - liquid water content in mg/m^3

Expanded weather cases were used to study the effects of precipitation backscatter.

r (Rain) - 5, 10, 16 mm/hr

r (Snow) - 3, 6, 9 mm/hr

M (Fog) - 140, 1100, 4000 mg/m^3

The expressions for precipitation backscattering cross-section considered linear polarization. It has been demonstrated that a significant reduction in backscatter can be realized by using circular polarization (Sources 4, 14). Table 40 shows some typical values.

Table 40 -- Precipitation Clutter Reduction Factor (dB)

	C, X-Band	K_a-Band
Rain, Fog	25	17
Snow	16	14

Theoretically, the reduction can be made as large as possible depending on how closely the sphericity or ellipticity of the radar polarization may be matched to the corresponding shape of the precipitation spheroids. It cannot be absolute, naturally, due to the non-uniform shape of the spheroids. The values above have been measured, however.

An additional factor that should be considered is a backscattering phenomena known as "bright bands" (Source 24) that exist in weather conditions when a phase change is occurring between rain and snow. When these conditions are evident, returns from the bright band may be 3 to 5 dB greater than that predicted by the snow value of r and 10 to 17 dB above that predicted for rain. Additionally, degradation may also occur for circularly-polarized radars due to unusual particulate shape during the phase change degrading the clutter rejection ability of

circularly polarized waves on spheroidal particles.

The feasibility of using enhancement techniques to provide greater runway outline and orientation returns has been demonstrated (Source 25). The approach used a frequency translation on beacon retransmission of the airborne radar signal. This technique allows rejection of precipitation backscatter surrounding the beacon since the airborne receiver is tuned to a different frequency. The system requires antenna angular accuracies of approximately the accuracies required for glide slope and angular runway orientation. These accuracies are required in both azimuth and elevation since range gating and multilateration timing for elevation angle would have severe GDOP (geometrical dilution of precision) problems.

Passive enhancement elements such as radar reflectors may be used to outline the runway or provide threshold, touchdown, or extended centerline references.

Advantages are:

1. Passive - no power and minimal maintenance required.
2. Can decrease aircraft ERP requirements.
3. Enhanced returns will increase point target to clutter and noise ratios for more accurate referencing.
4. Real-world perspective and reference is maintained.

The disadvantage is:

1. Increased point target returns may mask obstacles.

Active enhancement of radar returns involve receiving the signal, possibly frequency translated or coded, and re-transmitted.

The advantages are:

1. Can more effectively minimize the onboard transmitter requirements of the airborne radar ERP.
2. Enhanced returns will increase point target to clutter and noise ratios for more accurate referencing. Clutter may be effectively eliminated.

The disadvantages are:

1. Obstacles are not detectable.
2. Real-world imaging is less likely due to costly, redundant repeaters required for runway edge, threshold, and extended centerline referencing.

Receiver Analysis -- Power Reception/Detection (Non-Discriminatory between signals and clutter).

- Antenna Aperture, A_e

  Effective Aperture $A_e \leq \frac{G_r \lambda^2}{4\pi}$ (32)

- Antenna Plumbing Losses, L_r

  antenna $i^2 R$ losses and incorporation of antenna efficiency to remove the inequality in expression for A_e above

Receiver Noise is expressed as $P_n = KTBL_n = \frac{KTL_n^1}{\text{pulse width}}$ (33)

$$L_n^1 = F \times L_{BW} \times L_{CL} \quad (34)$$

F - receiver noise figure

L_{BW} - loss incurred due to IF bandwidth differing from matched filter conventional bandwidth of $\frac{1}{\text{pulse width}}$ (usually less than 1 dB).

L_{CL} - collapsing loss due to additional receiver channels being combined to define a signal accounts for the uncorrelated noise in additional receiver channels when the signal (and clutter) powers are correlated.

Receiver/Display Processing (Discriminatory Enhancement or rejection or target and clutter signals) -- The sweep integrator is an idealized integrator that sums pulse returns in each range bin. The efficiency of the integrator is a function of:

1) Number of Pulses (PRF)
2) Antenna Scan Rate
3) Aircraft Velocity
4) Range
5) Spectral Distribution Function of:

   Beamwidth
   Velocities (Radial)
   Sampling

The efficiency of the integrator is a function of how well the processing function of the receiver performs the sampling and integration (summation) and, secondly, how independent the samples of the returns are. Ideally, the samples will be coherent returns and summations will provide an integration improvement proportional to N, the number of samples. The uncorrelated noise will sum proportional to $\sqrt{N}$ so the S/N enhancement capability is proportional to $\sqrt{N}$ ($= \frac{N}{\sqrt{N}}$) in the ideal case. N is necessarily limited to:

$$N \leq \frac{PRF^{*}\ \theta_B}{\omega} \tag{35}$$

θ_B - azimuthal beamwidth over which detectable returns may be summed

ω - azimuthal antenna scan rate

An example of expected efficiency was provided by C. M. Whitaker of Texas Instruments. For $\theta_B \simeq \frac{\theta_{3dB}}{2} = 0.005$ rad (0.3°), $N \cong 40$, the integration improvement of the referenced ILM system was:

$$\frac{\text{ILM System Signal Return Improvement}^{*}}{\text{ILM System Noise Improvement}}$$

$$= \frac{N^{0.667}}{N^{0.5}} \cong 2.6 \text{ dB for } N = 40 \tag{36}$$

*(The reported system integration gain of $N^{0.667}$ was given for a DVST display ILM).

This value of improvement is for point targets relative to uncorrelated noise. The improvement of point targets relative to clutter or background clutter relative to precipitation clutter would be less than this. The power spectral distribution (doppler bandwidth spread) of both clutter spectra are very similar since the spectral spread is created by two related phenomena. The first is the beamwidth geometry which intersects both clutter groups of point scatterers. This creates an almost-identical doppler spread due to the different radial velocities of the various scattering points due to different relative positions in the footprint (or volume).

The second phenomena is the wind-driven precipitation (and vegetation) which provide similar, and sometimes related, spectral spreads. Calculations and

measurements of the correlation function of background and precipitation clutter (References 10, 21, 18) have demonstrated Rayleigh distribution statistics for the detected clutter returns.

The spatial correlation function has been calculated and measured (References 10, 21, 18) and echos from background and precipitation may remain correlated for many milliseconds. The number of independent samples may be derived from the correlation time expression of References 4 and 21. For correlation of successive samples down to at least the correlation function value of 0.2, the time between samples must be at least:

$$T_i = \frac{0.65}{\Delta f_d} \quad \text{(Ref. 4, 21)} \tag{37}$$

Δf_d - (also called doppler resolution) is the doppler spread due to velocity variations.

The doppler spectrum is usually assumed uniform with several contributing sources of doppler deviations:

- o Finite Beamshape
- o Element Motion (wind effect)

The doppler spread, Δf_d, is derived in references 4 and 10 as:

$$\Delta f_d = \frac{v f_c \tau_p}{R} \text{ in Hz} \tag{38}$$

v - aircraft velocity (75 m/sec)

f_c - radar center frequency

τ_p - radar pulse width

R - slant range in meters

Expressing σ_v as the standard deviation of clutter velocity components, the clutter contributions from precipitation have been analyzed in References 4 and 18 and are expressed as having two principal components:

$$\sigma_{v_{Shear}} \cong 0.42\ K\ R\ \emptyset_2 \text{ m/sec} \tag{39}$$

$$\sigma_{v_{Turbulence}} \cong 1.0 \text{ m/sec for altitudes less than 3048 m (10,000 feet)}$$

K = 4 to 5.7 m/sec per nm

R - slant range (nm)

$\emptyset_2$ - elevation beamwidth in radians (2-way)

The clutter contributions from the ground return are analyzed by References 10, 4 and 21 and described as having two principal components.

$$\sigma_{v_{Geometry}} \cong \frac{V\ \rho_a}{2\ R\sqrt{3}} \text{ m/sec} \tag{40}$$

$$\sigma_{v_{Wind}} \cong 1 \text{ to } 5 \text{ m/sec}$$

V - aircraft velocity = 145 knots

R - slant range

ρ_a - along track resolution = $\frac{C\ \tau_p}{2}$

τ_p = pulsewidth

The smaller values of $\sigma_{v_{wind}}$ are to be expected since vegetation in the vicinity of a runway is expected to be groomed short. The velocity variations of interest are the precipitation contribution due to wind shear, $\sigma_{v_{shear}}$, and the background variation due to beam geometry, $\sigma_{v_{geometry}}$. $\sigma_{v_{wind}}$ and $\sigma_{v_{turbulence}}$ will be assumed very similar at approximately 1 m/sec. The factors $\sigma_{v_{shear}}$ and $\sigma_{v_{geometry}}$ are plotted in Figure 46 for typical ILM system parameters.

ILM imaging systems presently undergoing testing have pulse widths of 40 to 100 nanoseconds and vertical beamwidths of 0.262 rad to 0.349 rad (15° to 20°). This region of typical parameters is shown cross-hatched on Figure 46. T_i will be arbitrarily defined as the "de-correlation" time or the required time between samples for the samples to be sufficiently uncorrelated as to be considered independent. T_i as a function of frequency (or λ) and Δf_d (or v_{RMS} or σ_v) is plotted in Figure 47.

The doppler resolution may be expressed as the difference in doppler across the footprint of the beam resolution element (range gate). Assuming a uniform distribution of velocities, $\Delta v = \frac{\rho_a v}{R}$.

Then, $$\sigma_v = \frac{\Delta v}{2\sqrt{3}} = \frac{\rho_a v}{2\sqrt{3} R} = \frac{\lambda \Delta f_d}{4\sqrt{3}} . \qquad (41)$$

The value of T_i may be written in terms of σ_v as:

$$T_i = \frac{.65}{\Delta f_d} = \frac{.65 \lambda}{4\sqrt{3}\, \sigma_v} \qquad (42)$$

The significance of the curves is the clutter enhancement capability of the receiver processor. Typical systems (as shown by the cross-hatched areas on Figure 46) may provide background enhancement at ranges of greater than approximately 3 to 5 Km. This enhancement is progressively less as the range is decreased and the number of independent samples of the set of PRF-rate echo returns becomes greater.

If a technique is employed to provide scan-to-scan integration (such as a digital scan converter (DSC) or direct view storage tube (DVST) CRT) the integration improvement may be made much larger up to the limits of the dynamic requirements

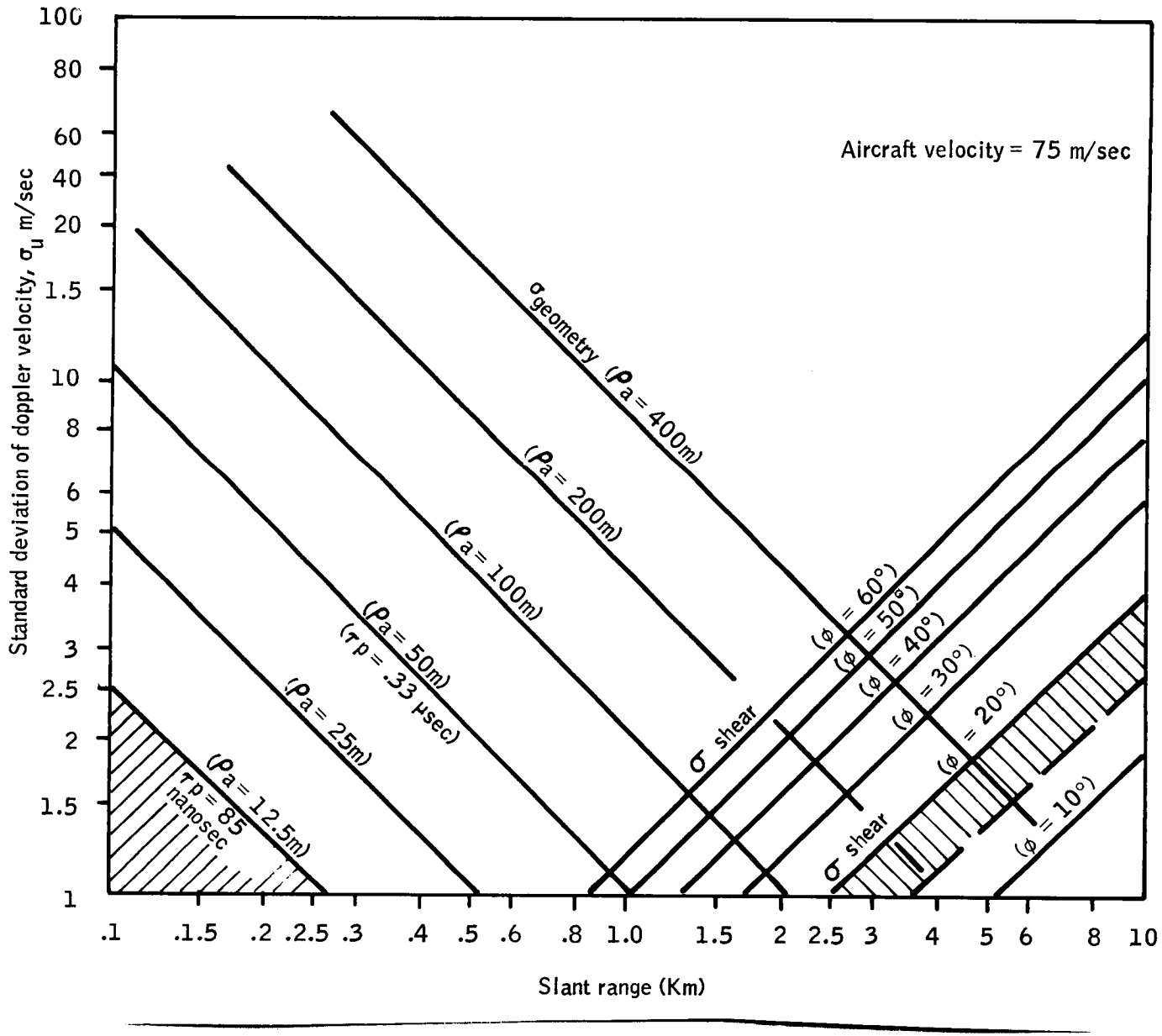

Figure 46 -- Standard Deviations of Clutter Component

of the real-world perspective display. At 75 m/sec (145 nm/hr) the maximum integration time could be extended to several milliseconds (several echo samples). Figure 48 illustrates the improvement capability of a system with 50 m or less range bin resolution as a function or range and beamwidth. The other assumed parameters are:

- o K_a-Band
- o Variable PRF optimized according to Figure 47
- o τ_p < 300 nsec
- o Aircraft velocity = 75 m/sec
- o DVST integration gain = $N^{.667}$

  where N number of independent samples of the background signals (correlated returns) = $N^{.5}$ for uncorrelated signals
- o Display Stabilization

The assumption of display stabilization was made to assure proper integration of returns over a relatively long time interval (see aircraft stability) to minimize turbulence effects to less than 1 m/sec. The graph is derived by optimizing the PRF to the maximum sample rate that correlated the background returns but decorrelates the precipitation returns. For example, at a given PRF, the correlated signals integrate as $N^{.667}$ and the uncorrelated as $N^{.500}$. The boundary is defined by setting the PRF high enough that the desired signal is correlated higher than 0.2 and the undesired signal is correlated less than 0.2. The PRF is set at the 0.2 correlation rate of the undesired signal such that it integrates as $N^{0.50}$. The desired signal integrates more efficiently up to $N^{0.667}$ over its correlated time interval. The integration interval is optimized to the correlation time (e.g., 1.6 msec).

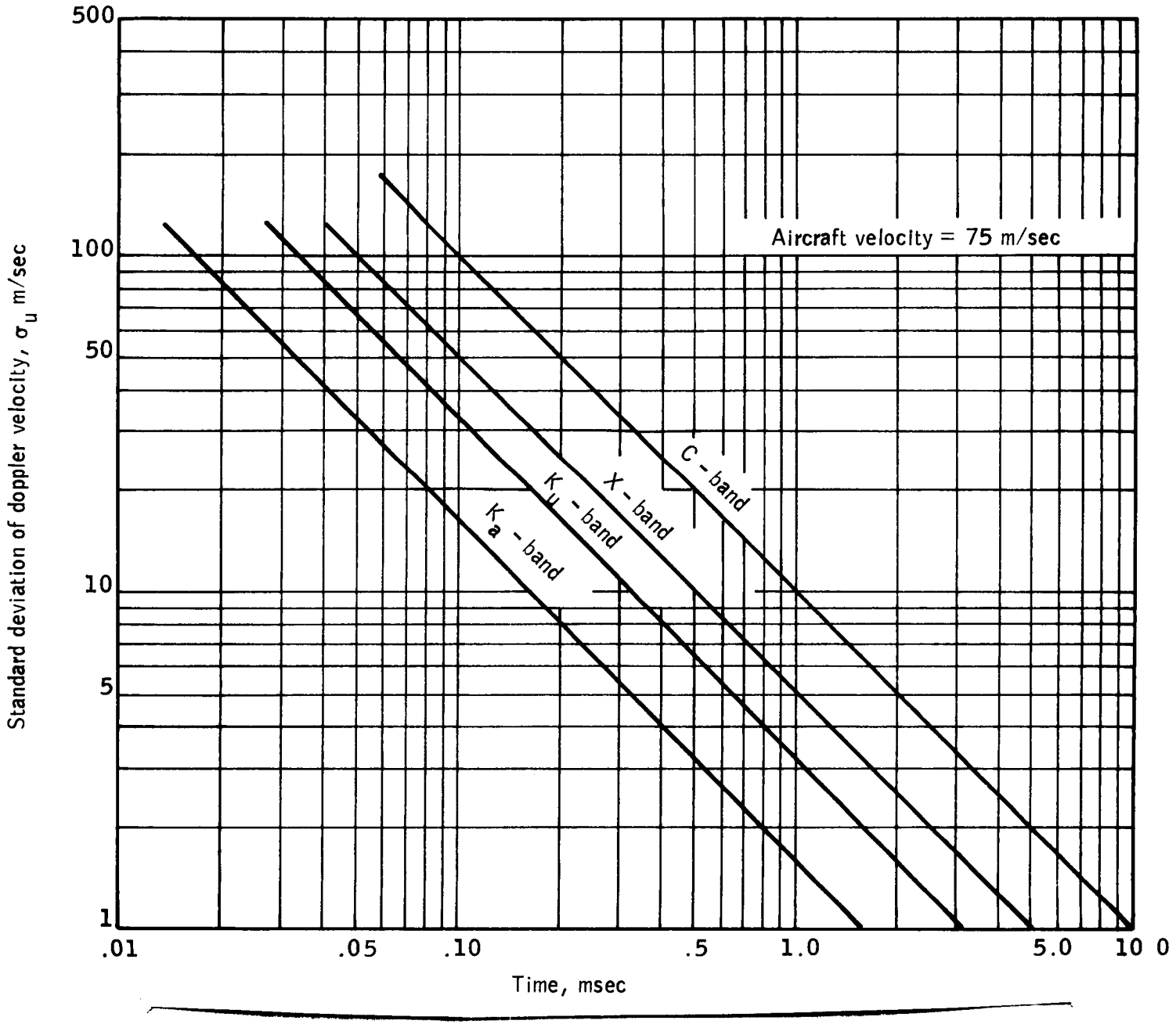

Figure 47 -- T_i, Time Between Samples

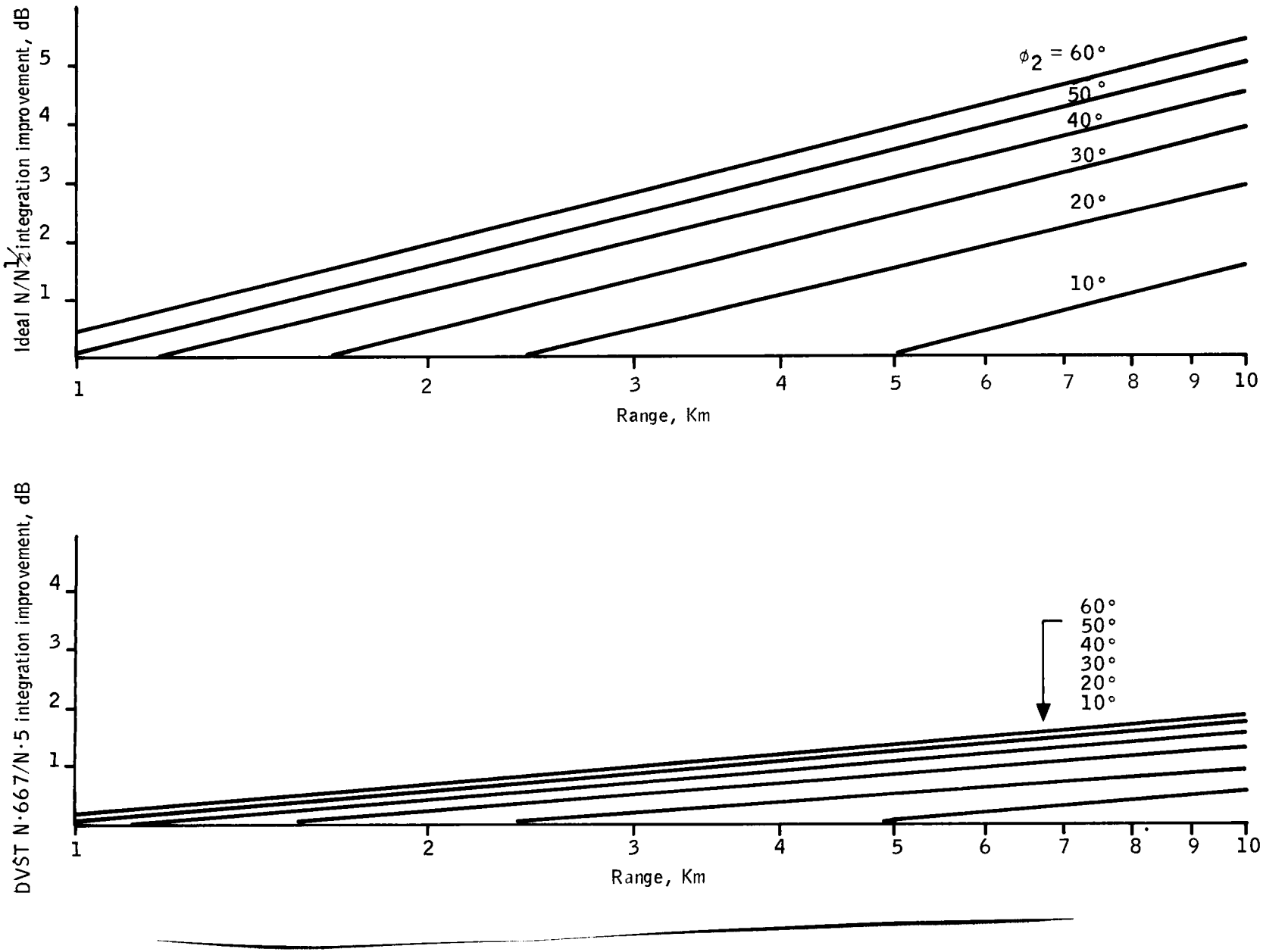

Figure 48 -- System Improvement Capability

The monopulse concept of sum and difference channel processing predicts that a very definitive interpolation of target position (of the order of .01 beamwidth) may be achieved at very high S/N. Theoretically, the monopulse sum and difference antenna patterns feed parallel sum and difference RF and IF channels which are ratio detected (the ratio being proportional to angular position within the beamwidth). The concept is directly applicable to tracking radars with isolated targets. Imaging radars may benefit from enhanced isolated target definition as previously described; however, the consideration for extended area clutter considerations (backgrounds, runway surfaces, and volumetric precipitation) are not as well defined. The assumption of uncorrelated clutter signals in the sum and difference channels due to the difference between the sum and difference antenna patterns would predict a decrease in point target to clutter power ratio of 1.5 dB. Since the clutter signals would not be totally uncorrelated, the decrease in power ratios for various image contributors would fall between 1.5 dB and 0 dB, depending on the degree of correlation between the sum and difference channel signals of each contributor. The point being emphasized here is that monopulse used for resolution improvement may be visualized as providing a decreased resolution beamwidth; however, the beamwidth considered for aperture detection of clutter is not decreased correspondingly. The consideration of clutter in a monopulsed system should consider an <u>increased</u> beamwidth over the non-monopulsed antenna to account for the collapsing loss associated with the multiple channels summing the uncorrelated clutter-signals. Monopulse systems are, thus, considered in this ILM analysis as providing resolution improvement at the expense of degraded S/N and S/C (signal to clutter).

Monopulse resolution enhancement processing provides a better definition of individual (point) target position or high contrast edge definition when sufficient contrast (or S/N) is available. Point targets such as beacons or reflectors may provide high signal returns which enable position interpolation within the normal 3 dB beamwidth definition by using sum and difference antenna pattern characteristics. A comparison, or ratio, of the sum and difference pattern phase or amplitude signals provide beam deviation information. The interpolation requires a signal return from an area smaller than the illuminated footprint; in fact, much smaller in lateral dimension compared to the corresponding lateral footprint extent than the expected improvement factor relative to the 3 dB beamwidth. For example, if a 10 dB improvement in horizontal resolution was desired, the horizontal extent of the reflecting area would have to be less than 1/10 of the horizontal footprint dimension. The desired improvement is limited by the physical extent of the target of interest. The ILM scenario consists of a high azimuthal resolution fan beam intercepting a runway. If enhanced resolution is desired on the runway to background grass edge, it must be assured that the dispersion of that edge in a minimum resolution footprint is sufficiently less than the azimuthal footprint extent. Figure 49 shows such a minimum resolution footprint bounded by the azimuthal beamwidth and one range bin. As ψ_r approaches large angles, the grass/runway contrast is distributed or dispersed over most of the footprint. For small angles of ψ_r, the contrast becomes sharper as a function of azimuthal angle. Thus, maximum resolution enhancement is possible for high contrast edges when the edge is viewed from an "end-on", or $\psi_r \cong 0$, aspect. The edge definition, or angular resolution, may approach the angular uncertainty, $\Delta\theta$, imposed by the interception of the runway edge and the resolution cell footprint (see Figure 49 below). The maximum edge resolution is bounded by the angle $\Delta\theta$ resulting from

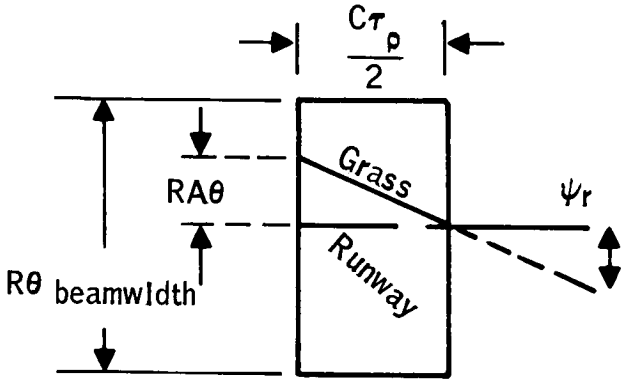

Figure 49-- Runway Geometry

the angular edge interception such that:

$$\text{maximum angular resolution} \geq \Delta\theta = \frac{C\,\tau_p}{2R} \tan \psi_r \tag{43}$$

When R, the aircraft to runway range, is much larger than the runway width, ψ_r is also the flight path to runway centerline deviation angle. For small angles of approach deviation:

$$\text{angular viewing uncertainty} \geq \Delta\theta = \frac{C\,\tau_p\,\psi_r}{2R} \tag{44}$$

The analysis of amplitude comparison monopulse systems (4, 12, 14, 15) derives expressions for angular deviation (or null degradation) as a function of system parameters and signal to uncorrelated "noise" ratio. Since clutter has varying degrees of decorrelation between channels, the extension of the expressions to the signal to clutter (and even clutter to clutter) ratios is acceptable in the sense of defining error limits. The most common expression for rms angular deviation is:

$$\Delta\phi_{rms} = \frac{\theta}{K\sqrt{2\ S/N\ B\ \tau_p}} \quad \text{(for } S/N > 4\text{)} \tag{45}$$

θ - angular beamwidth in same units as $\Delta\phi_{rms}$

k - error slope of antenna null beam pattern (typical K = 1.5)

S - correlated signal power

N - uncorrelated signal (clutter or noise) power

B - System Bandwidth

τ_p - Pulse width ($B\,\tau_p$ product is typically 1.2 as opposed to 1.0 for a matched filter system)

$\Delta\phi_{rms}$ is thus approximately:

$$\Delta\phi_{rms} = \frac{0.43\ \theta}{\sqrt{S/N}} \qquad S/N > 4 \tag{46}$$

This is the expression for point target enhanced resolution as limited by uncorrelated receiver channel signals. It is readily seen that angular enhancement on isolated point scatterers is very significant (e.g., $\Delta\phi_{rms} = \frac{\theta}{25}$ for 20 dB S/N). For clutter limited operation, the expression is range independent.

The angular uncertainty for edge definition previously defined angular uncertainty as proportional to range cell size and angular deviation from runway centerline and inversely proportional to range.

$$\Delta\theta \cong \frac{C\ \tau_p\ \psi_r}{2R} \quad \text{for } \Delta\theta,\ \psi_r \text{ small} \tag{47}$$

$$\Delta\theta = \sin^{-1}\left[\frac{C\ \tau_p}{2R}\ \sin\psi_r\right] \quad \text{for } \psi_r \text{ greater than a few degrees} \tag{48}$$

Equating the edge uncertainty to the angular deviation due to monopulse signal processing, it becomes possible to define the limits over which monopulse resolution edge improvements may be realized.

$$\frac{C\ \tau_p\ \psi_r}{2R} \leq \frac{0.43\ \theta}{\sqrt{S/N}} \tag{49}$$

$\frac{C\ \tau_p}{2}$ typically equals 10 m

$= .01$ Km

$$\frac{\psi_r\ .023\sqrt{S/N}}{\theta\ R(Km)} \leq 1 \qquad (S/N > 4) \tag{50}$$

The angles are normalized for presentation in Figure 50. The angular beamwidth is small (on the order of 0.007 rad - 0.07 rad (.4° - 4°). Rθ is necessarily constrained.

The limiting case of resolution for S/N = 4 is

$$\Delta\phi_{rms} = .215\ \theta \qquad (51)$$

$$\text{corresponding to } R(.215\ \theta) \geq \frac{C\ \tau_p\ \psi_r}{2}$$

which for $\frac{C\ \tau_p}{2}$ = 10 m yields

$$\frac{\psi_r}{\theta} \leq 21.5\ R\ (K_m) \qquad (52)$$

Figure 50 shows that for small angular deviations from runway centerline the edge enhancement is effectively noise limited for ranges beyond 1 Km. It is envisioned that guidance for large ratios of $\frac{\psi_r}{\theta}$ will be performed by other means (ILS provides accuracy within a few degrees). The ILS guidance limit (assumed at ±0.105 rad (±6°) is shown on the figure to illustrate the limits of external guidance at antenna beamwidths of 0.007 rad to 0.07 rad (.4° to 4°). The graph shows that by using ILS guidance to within ±0.105 rad (±6°) at the outer marker, (approximately 9 Km) the monopulse edge enhancement will not be geometry limited for S/N less than approximately 28 dB for 0.007 rad (0.4°) antennas or approximately 48 dB for 0.07 rad (4°) antennas.

It may be expected that monopulse resolutions will not approach the high theoretical values (.01 θ to .05 θ) due to external stability requirements (see aircraft stability). Systems with potential for improvements up to the limits of stability have been demonstrated (18 to 20) with fractional beamwidth resolution improvements of approximately .28 to .68 at high S/N ratios.

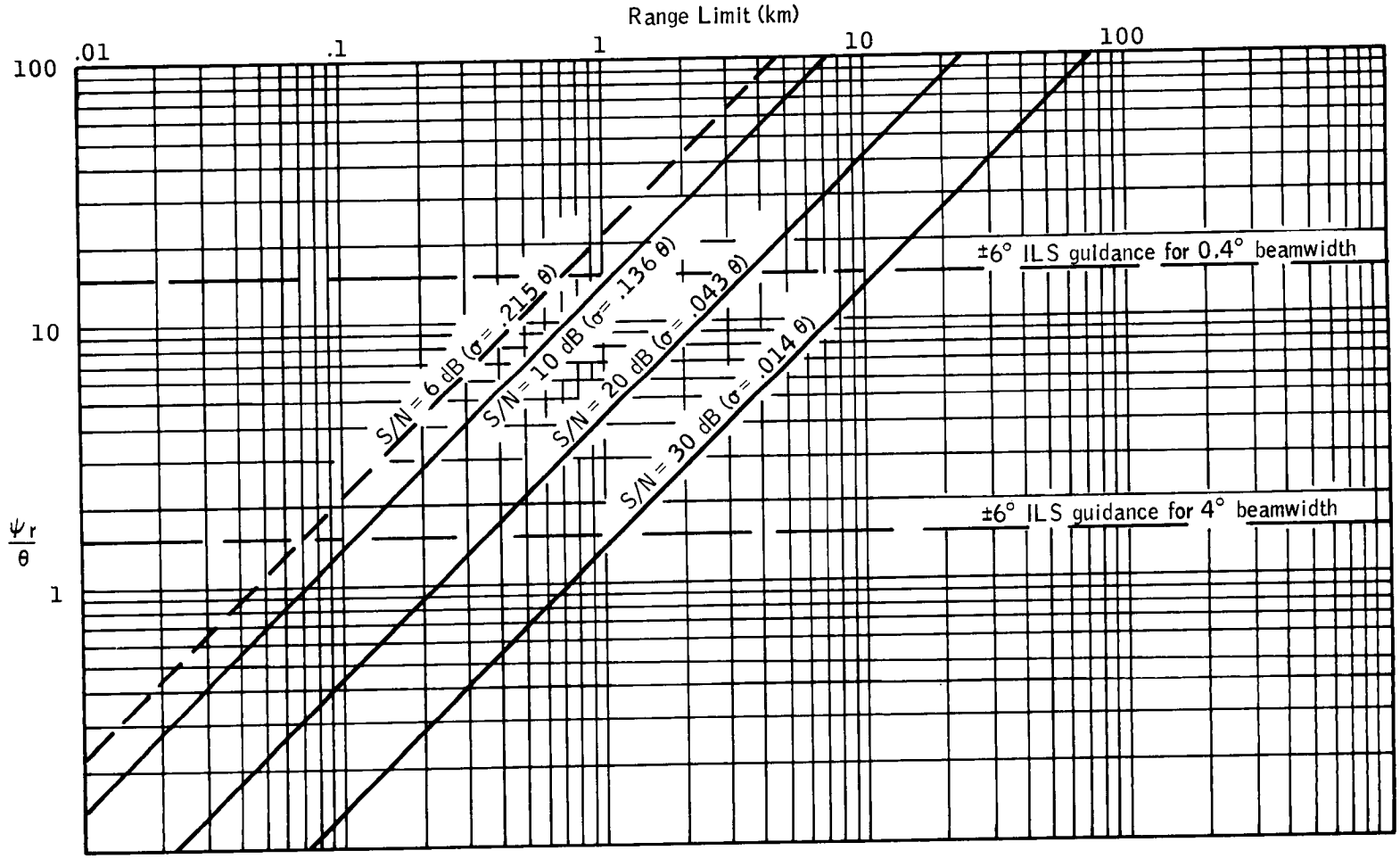

Figure 50 -- Monopulse Edge Resolution Limitation

Analysis Results

Several typical radar system parameters were inputs for the computer analysis. The results from the processing provide information on the use of particular radar systems as potential ILM sensors to verify analytical capabilities of the software. The results are then expanded to specify the potential of that type of radar system as an ILM with other system variables considered.

Computer Analysis of Radar Systems -- Radar System Parameters were compiled from several sources to describe the typical systems (References 23, 25, 26, 27, 28, and 29). The parameters, as they apply to the radar equation, are presented in Table 41 and are discussed in the following paragraphs.

Transmitter/Antenna Parameters -- P_t is the reported peak power output (pulse power maximum). G_t, L_t were used as reported to describe mainlobe maximum gain for a $\left|\frac{\sin u}{u}\right|^2$ beamshape. When L_t was not provided, it was assumed the measured value of G_t for the system included such losses. Other parameters, as reported, were used for the additional operational beam parameters and for considerations in the analysis following the software analysis results.

Receiver/Antenna Parameters -- G_r, L_r values were not reported so the gain and loss values of G_t, L_t were assumed with $L_r = L_t$ and effective receiving aperture $A_e = \frac{G_t \lambda^2}{4\pi}$. F, receiver noise figure was used when given to derive P_n.

Path Attenuation values, τ, were derived from equations presented in Appendix D and tabulated as Tables 23-34.

Radar Cross-Section values, γ=, were compiled in the Analysis section. Values used in the software routine were:

Table 41 -- Typical Radar System Parameters

Function	R1	R2	R3	R4	R5	R6
	ILM Imaging	ILM Imaging	PAR	PAR	Weather	Weather
Transmitter						
Band	Ka	Ka	X	X	X	C
Freq. (GHz)	34.9	33.0	9.1	9.1	9.4	5.4
Wavelength (cm)	0.86	0.91	3.30	3.30	3.2	5.6
Power (kw)	80	65	320	120	65	75
PRF (1000's)	10	15	3.5 (avg)	6,4.2	0.2	0.2
Pulse Width, T_p (nanoseconds)	50	40	500	250	5000	5000
Antenna						
Size						
Width (cm)	140 cm (56 in)	97 cm (39 in)	275 cm (110 in)	217 cm (87 in)	75 cm (30 in)	75 cm (30 in)
Height (cm)	23 cm (9 in)	Unknown	350 cm (140 in)	348 cm (139 in)	75 cm (30 in)	75 cm (30 in)
Mainlobe Gain (db)	27.5	33.5	42.5	39	35	30
1st Sidelobe (Horiz)	-30	-30	-23	-18	-30	-30
1st Sidelobe (Vert)	-13.2	-13.2	-23	-18	-30	-30
Az Beamwidth (°)	.45	.62	1.4	.98	2.9	5.2
El Beamwidth (°)	24	17	.75	.67	2.9	5.2
N_{AZ}****	.78	.87	.49	.89	.84	.82
N_{EL}****	.13	--	.72	.81	.84	.82
Receiver						
Noise Figure (db)	12	12*	3.3	3.3**	4***	4***

* Assumed from R1
** Assumed from R3
*** Computed from Bandwidth x T_p

**** $N = \frac{\lambda}{1 \times \text{beamwidth}}$

1 - reported physical dimension

- σ_t - OdBSM reference obstacle/target
- σ_B - 23m (75 ft.) and 91m (300 ft.) wide concrete and asphalt runways with extended backgrounds of grass or snow. Table 42 shows the range of differential scattering cross-sections used. $\left(\gamma = \frac{\sigma}{\sin \text{ (grazing angle)}}\right)$
- σ_p - Precipitation scattering cross-sections were derived for the weather cases of, and by the expressions presented in, the analytical approach section. Circular Polarization for reduced precipitation returns was used.

Expansion of Computer Analysis Results -- Parameter dependencies of the basic radar equation for return power, P_r, were analyzed to minimize processing time and avoid the volumes of data that sometimes result from parametric trade-off analysis. The power received, P_r, varies with range, precipitation rates, and frequency. Definition of the equation dependencies will be based on the following assumptions.

- Fixed physical aperture (antenna area). This assumes, for example, that the space available on an aircraft for mounting an antenna is fixed.
- τ_p, P_t, L_t, L_r, L_p, L_{F_1}, L_{F_2}, and L_{F_3} (except $\frac{G\lambda^2}{4\pi}$) are constants.

The expression for P_r then simplifies to:

$$P_r \propto \frac{G_t G_r \tau_t \tau_r \sigma \lambda^2}{R^4} \tag{53}$$

The following dependencies are derived from the theoretical radar analysis.

Table 42 -- Ground Differential Scattering Cross-Section, γ, dB/M^2 (3° Grazing Angle)

CULTURE	BAND C	BAND X	BAND Ku	BAND Ka
Asphalt	-63 to -52	-56 to -45	-51 to -40	-42 to -35
Concrete	-68 to -43	-61 to -38	-57 to -34	-53 to -30
Grass	-43 to - 5	-42 to - 5	-42 to - 4	-38 to - 4
Snow	-46 to -31	-43 to -29	-42 to -31	-42 to -32

- G, antenna gain $\propto \frac{1}{\lambda^2}$

$$G = \frac{4 \pi A_e}{\lambda^2} \tag{54}$$

effective aperture, A_e = efficiency X physical area, assume antenna efficiency is independent of Range, precipitation rates, and λ.

- σ - Radar Cross Sections

1. $\sigma_t \propto \frac{1}{\lambda^2}$ to λ, depending on shape of the target. (55)

2. $\sigma_b \propto R$ "Rough" surfaces (56)

$$\propto \frac{R}{\lambda} \text{ "Smooth" surfaces} \tag{57}$$

$\sigma_b \propto R \theta_B \gamma$

$\gamma \propto \frac{1}{\lambda}$ for "smooth" and nearly independent of frequency (or λ) for "Rough" surfaces ("smooth" surfaces have irregularities much smaller than λ (asphalt) and "rough" surfaces have variations much greater than λ(6" vegetation)).

$\theta_{beamwidth} \propto \lambda$(from $\theta_b = \frac{\lambda}{\ell}$)

3. $\sigma_{P_{snow}} \propto \frac{R^2 r^{1.6}}{\lambda^2}$ to $\frac{R^2 r^{1.6}}{\lambda^3}$ (58)

$$\sigma_{P_{rain}} \propto \frac{R^2 r^{1.6}}{\lambda^3} \text{ to } \frac{R^2 r^{1.6}}{\lambda^4} \tag{59}$$

$$\sigma_{P_{fog}} \propto \frac{R^2 M^2}{\lambda^3} \text{ to } \frac{R^2 M^2}{\lambda^4} \tag{60}$$

Derived from:

$$\sigma_p \propto R^2 \, \theta_{vertical} \, \theta_{horizontal} \, \eta$$

- $\eta \propto \frac{b^a}{\lambda^4}$ (61)

  Snow and Rain: b=r, fall rate a=1.6

  Fog: b=M, humidity a=2.0

- Circular Polarization Transmissivity for Rain, Fog: varies as approximately $\frac{1}{\lambda}$. Snow: approximately independent of λ.

- $\theta \propto \lambda$ (62)

- Path Attenuation, τ.

  1. Fog:

$$\tau \propto \frac{R(c(\lambda)+M)}{\lambda^{d(M)}} \quad * \qquad (63)$$

		BAND			
		C	X	Ku	Ka
C(λ)	weather case 2	9	10	13	15
	weather case 3	.30	.13	.12	.11

		M, humidity, Gm/m^3		
		.14	1.1	4.0
d(M)	weather case 2	2	2	2
	weather case 3	1.5	1.7	1.7

* Empirically derived from Tables 23 through 34.

2. Rain:

$$\tau \propto \frac{R\ r^{b(\lambda)}}{\lambda^{a(r)}} \tag{64}$$

BAND

	C	X	Ku	Ka
b(λ)	1.25	1.28	1.16	1.0

r, rain rate

	5mm/hr	10mm/hr	16mm/hr
a(r)	2.4	2.3	2.2

3. Snow:

$$\tau \propto \frac{R}{\lambda} \tag{65}$$

The expressions are complex when combined for P_r. The power ratio expressions are more straightforward and will be shown here for reference.

T - power returned by the reference 0 dBsm target.

C_B - minimum * average clutter power returned by grass terrain and an asphalt runway of 23m (75 ft.) width.

C_p - average clutter power returned by the precipitation.

$$\frac{T}{C_B} \propto \frac{1}{\lambda^{x_R}} \tag{66}$$

C_B Clutter

TARGET	"Rough"	"Smooth"
any size	$0 \leq X \leq 3$	$-1 \leq X \leq 2$
Typical large	$X = 1$	$X = 0$

$$\frac{T}{C_p} \propto \frac{\lambda^y}{R^2 r^{1.6}} \tag{67}$$

TARGET	WEATHER: RAIN	FOG	SNOW
Any	$1 \leq y \leq 5$	$1 \leq y \leq 5$	$0 \leq y \leq 4$
Typical large	y=3	y=3	y=2

$$\frac{C_B}{C_p} \propto \frac{\lambda^z}{Rr^{1.6}} \quad \text{for Rain, Snow} \tag{68}$$

$$\propto \frac{\lambda^z}{RM^2} \quad \text{for Fog} \tag{69}$$

	RAIN	FOG	SNOW
"Smooth"	Z=3 to 4	Z=3 to 4	Z=2 to 3
"Rough"	Z=4 to 5	Z=4 to 5	Z=3 to 4

Computer Results -- The six radars listed in Table 41 were analyzed by the software for the 12 weather cases (Tables 23-34). The results were expanded according to the power ratio dependencies derived above and summarized in Figures 51-55. The shaded regions show the effects of the scattering cross-section region of expected values as defined in Table 42. Clutter, C_B and C_p, values are average values with C_B being the smallest average value as the beam sweeps the runway/background composite image (i.e., the runway return).

Several representative scan profiles of average return values for the radars are shown in Figures 56-61. These scans are for the smaller values of scattering cross-section values for runway surfaces and grass. The scan profiles show the

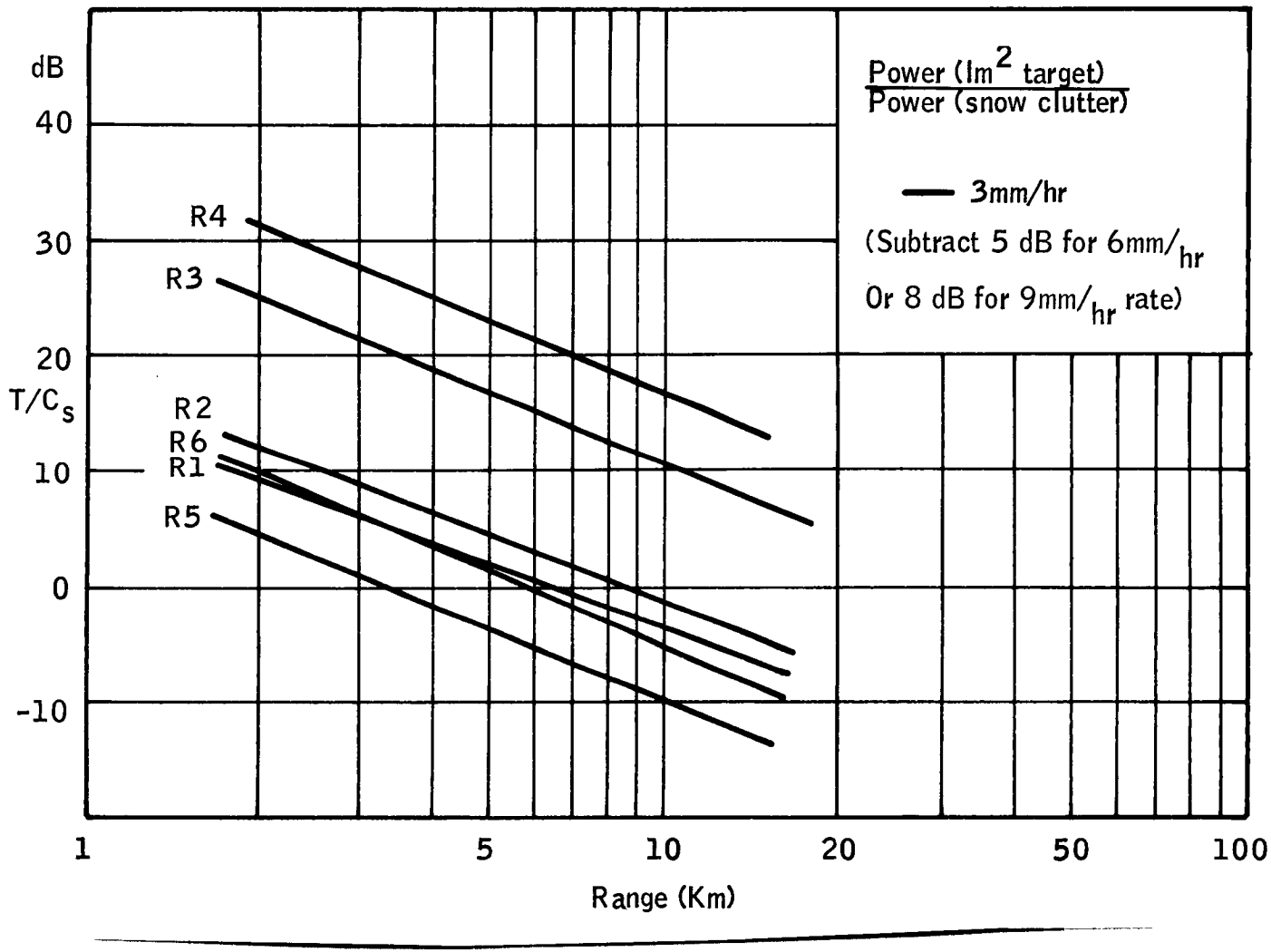

Figure 51 -- T/CP (Snow)

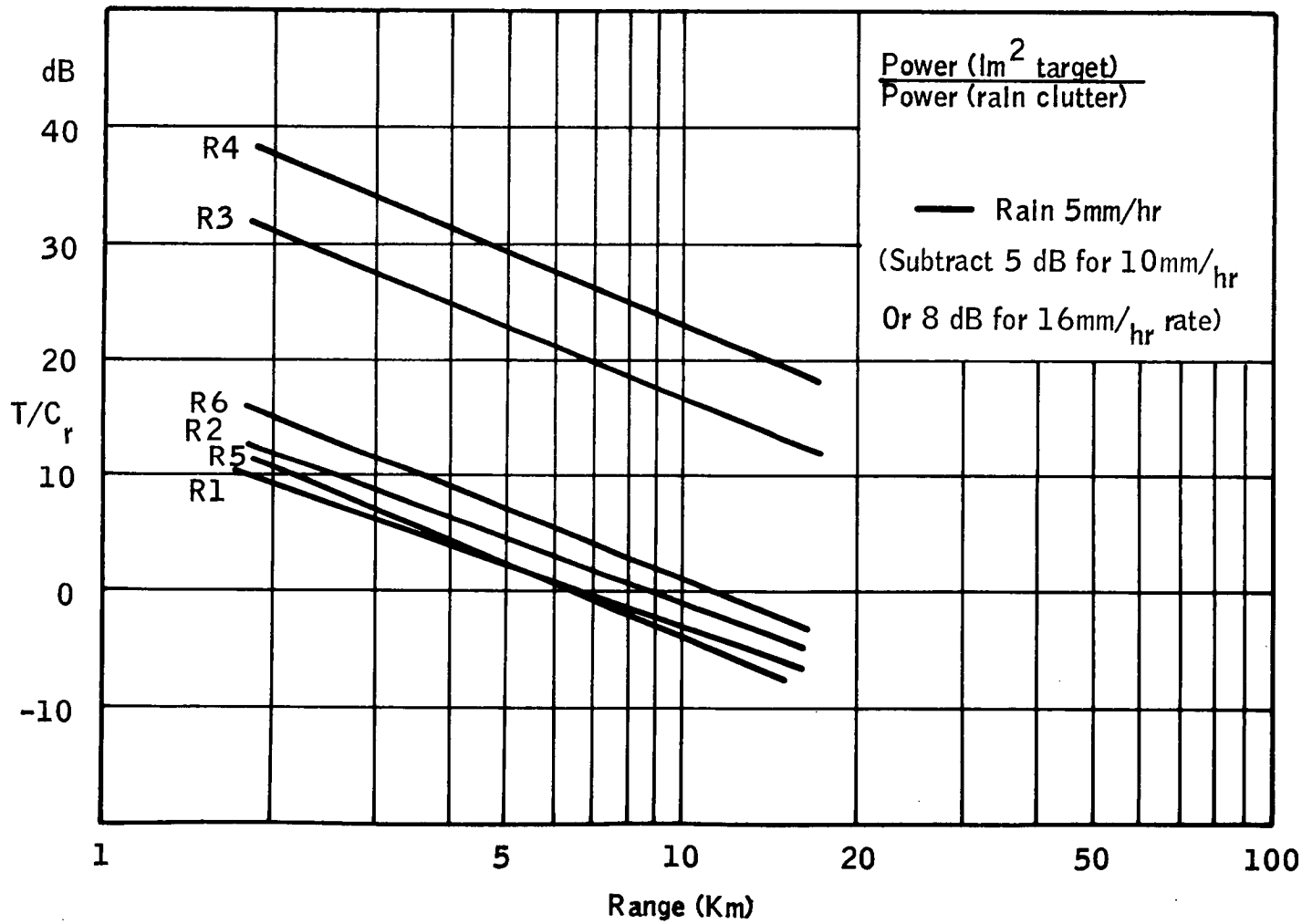

Figure 52 -- T/C_p (Rain)

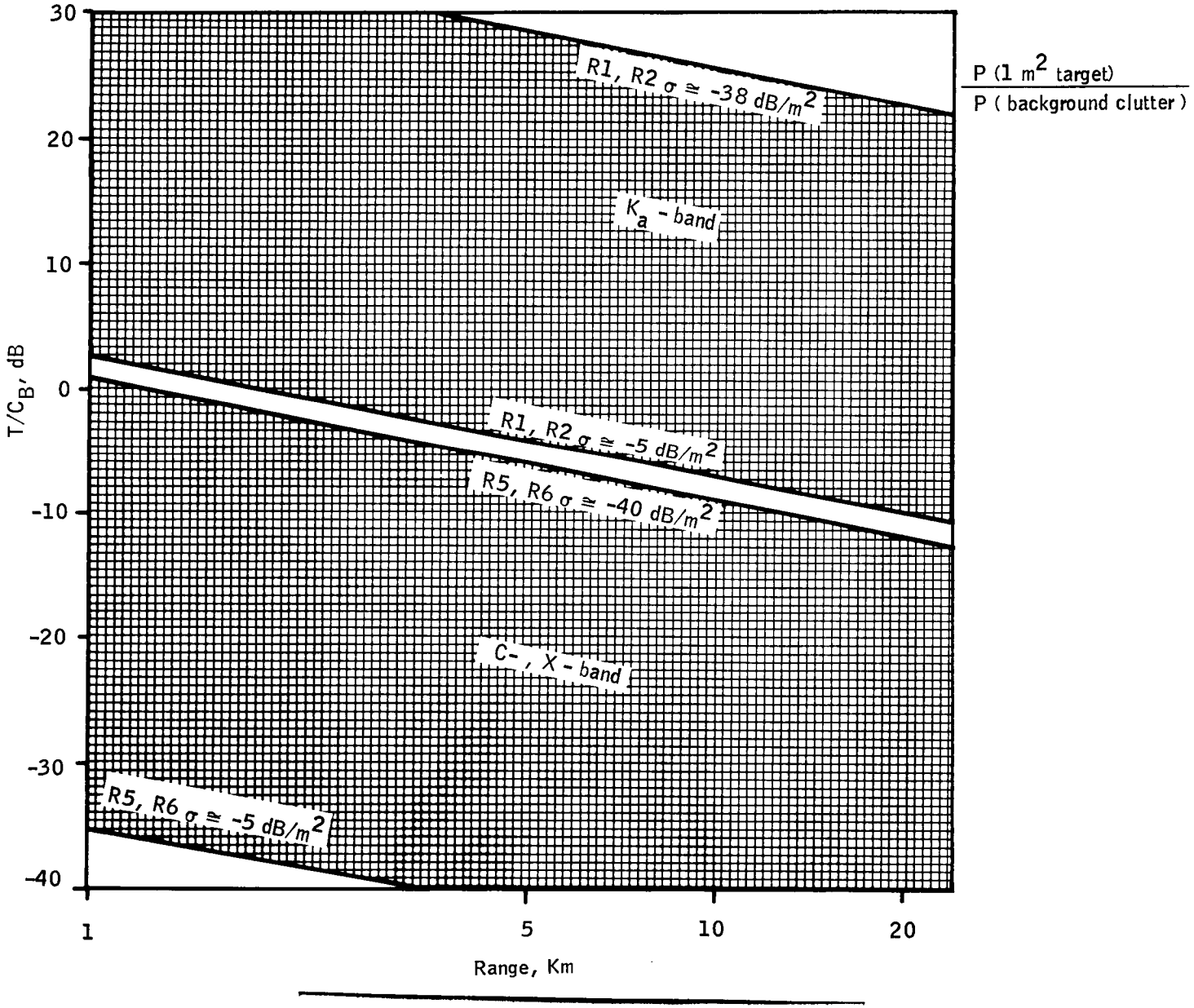

Figure 53 -- Capabilities for Target to Background Ratios

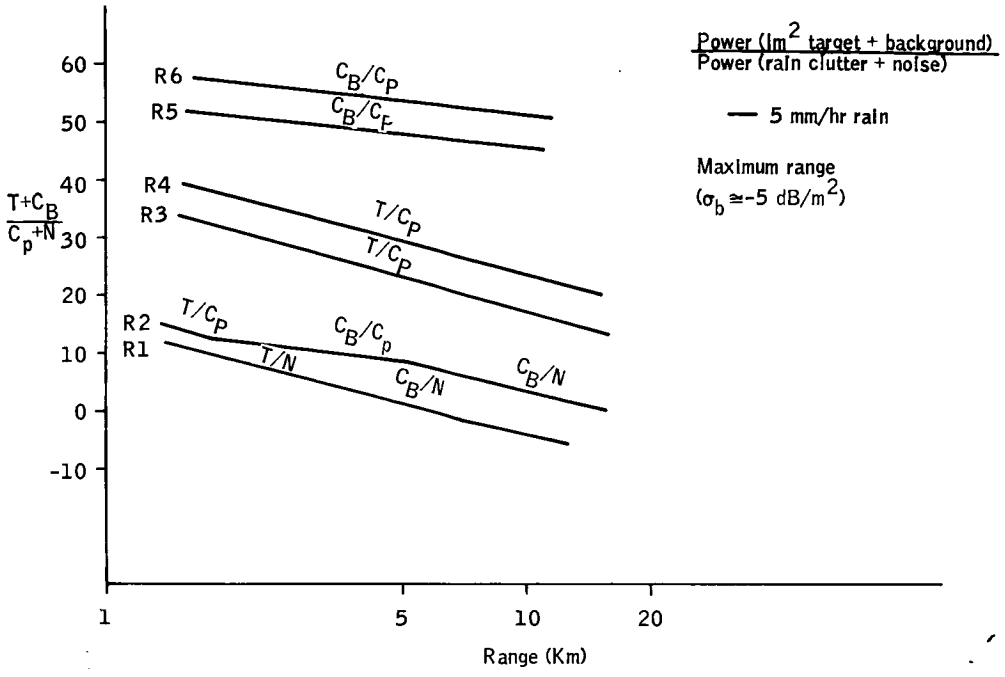

Figure 54 -- Maximum Range Variation

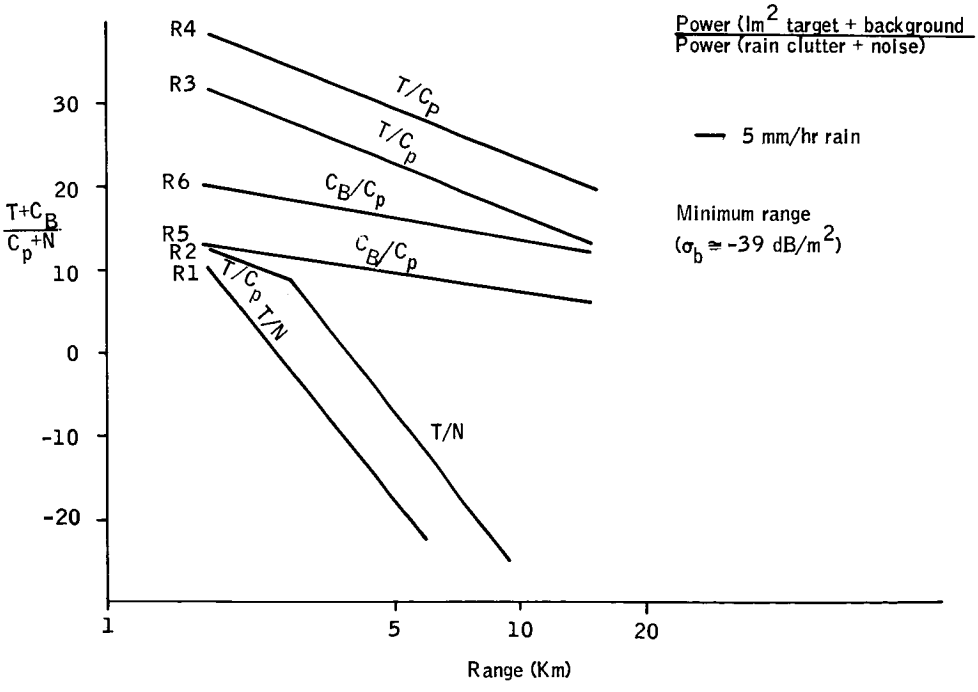

Figure 55 -- Minimum Range Variation

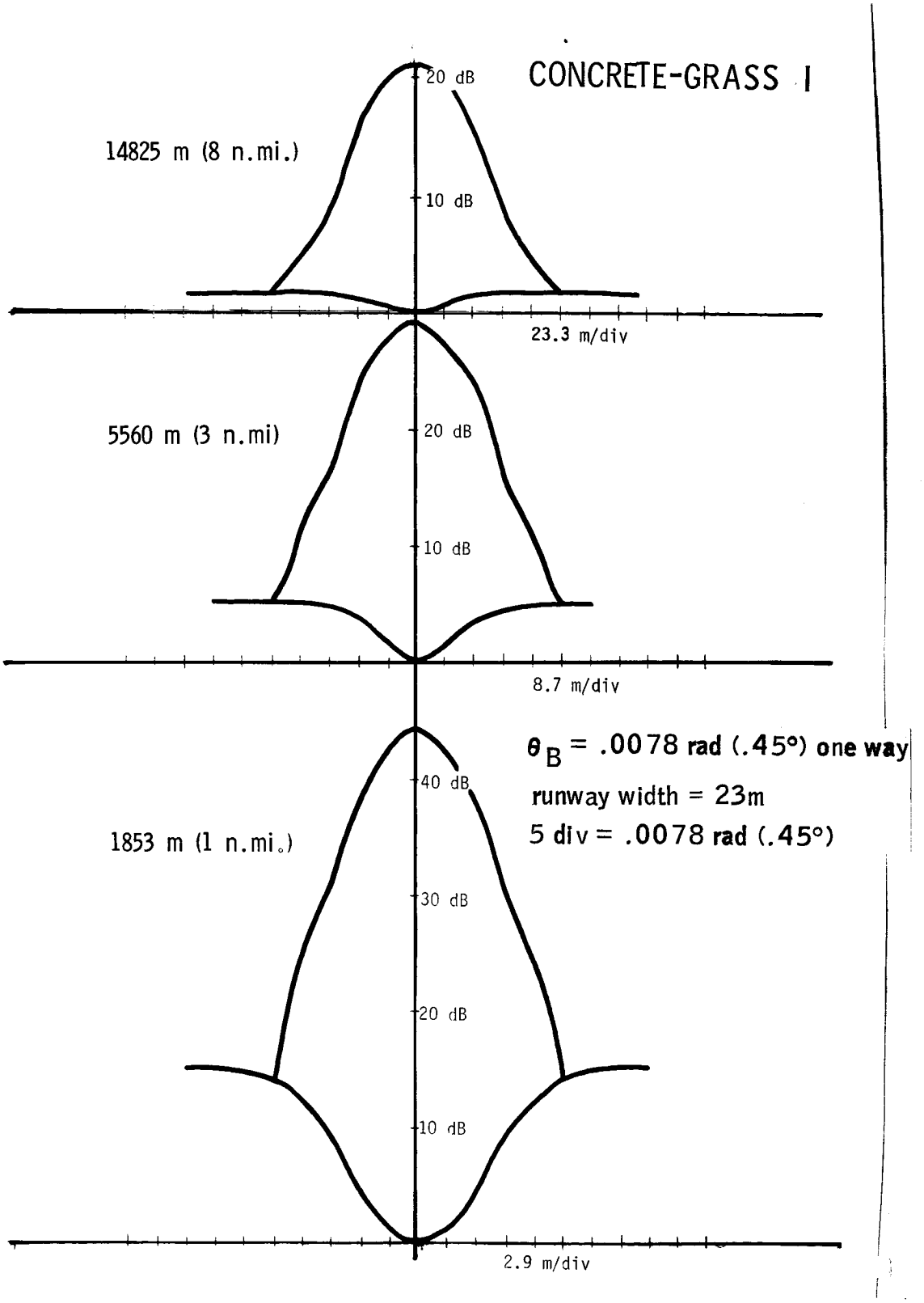

Figure 56 -- ILM Radar R1-K_a Band

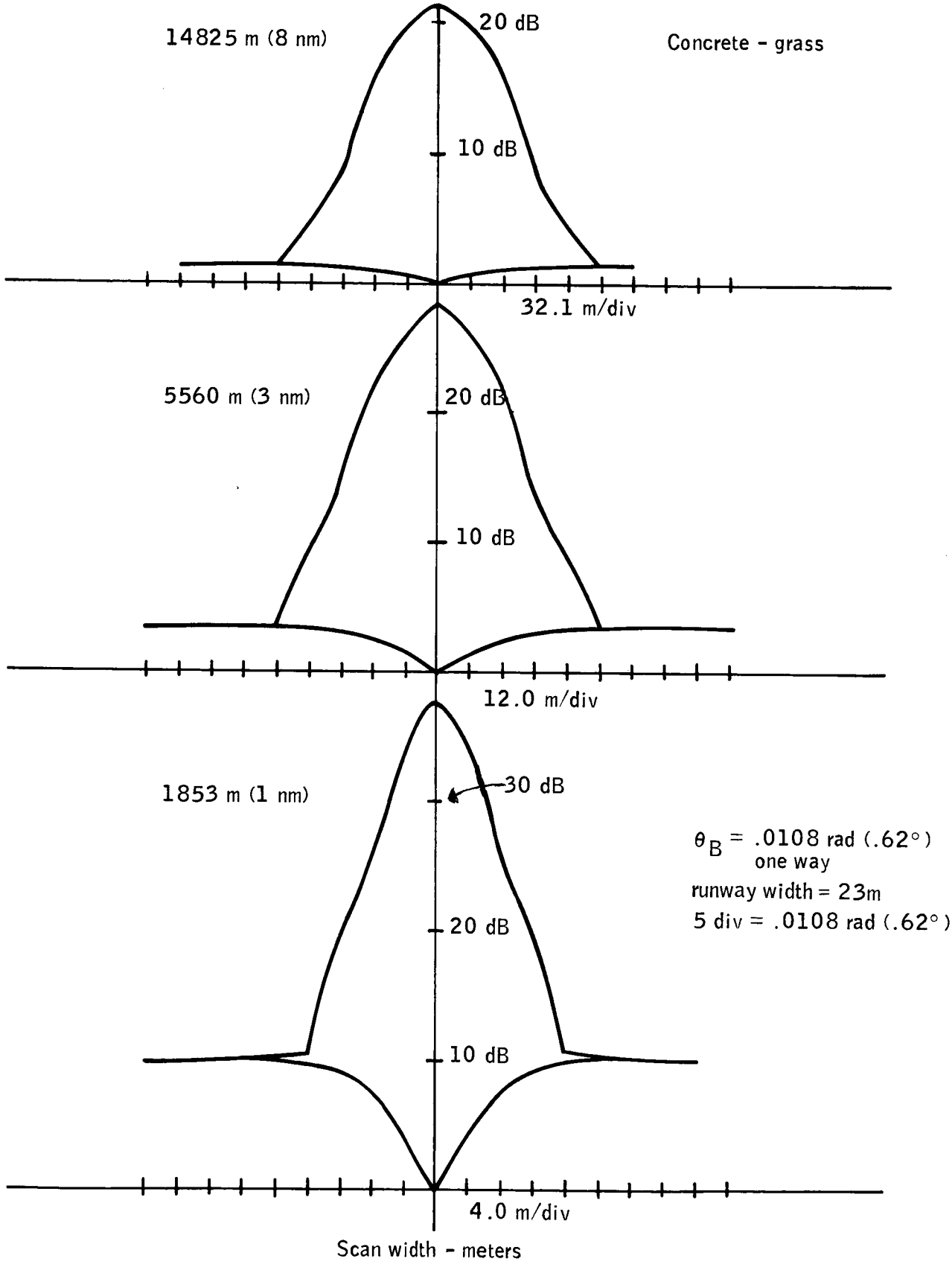

Figure 57-- ILM Radar -R_2-K_a Band

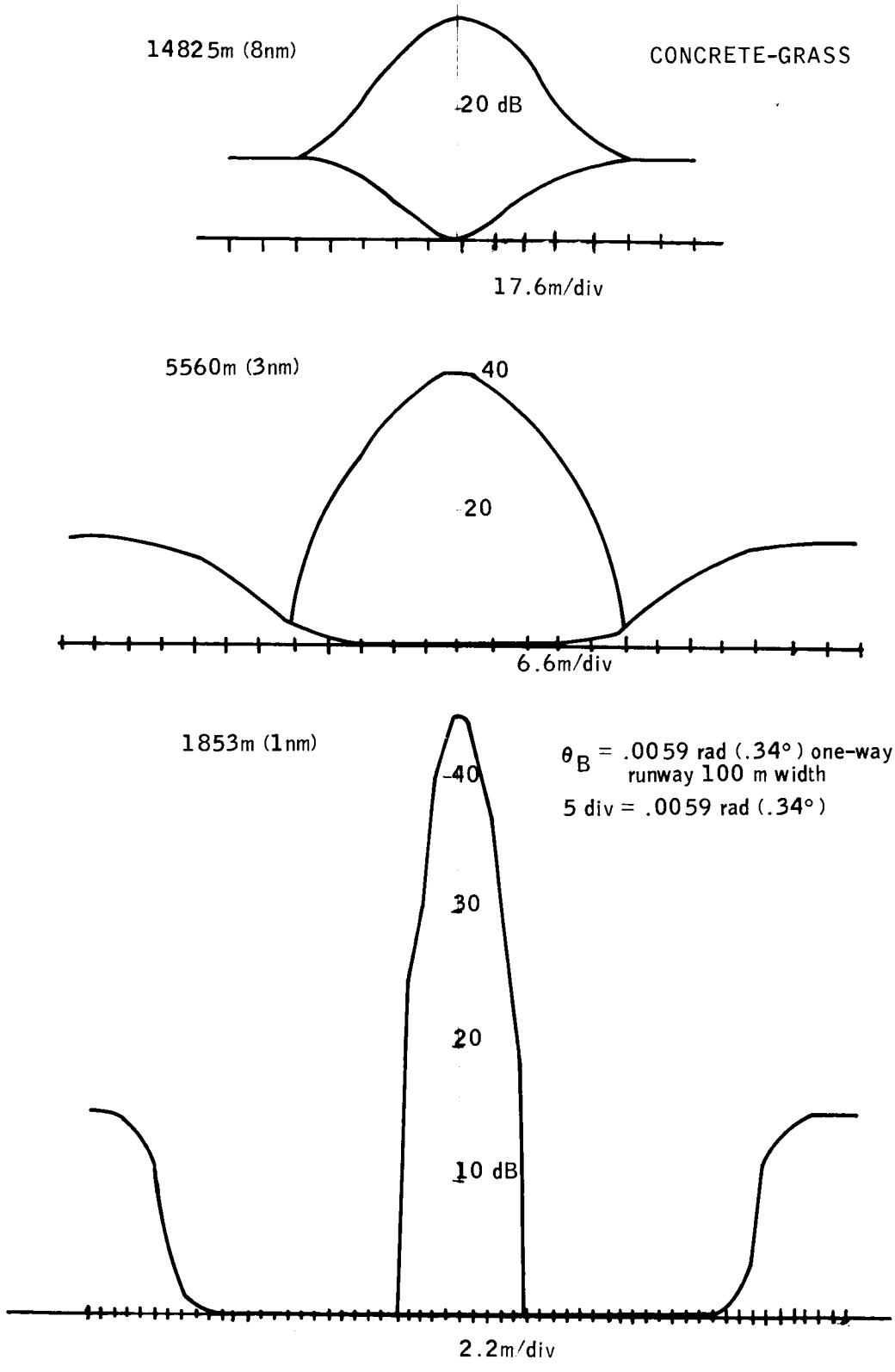

Figure 58 -- ILM Radar -R_t-K_a Band

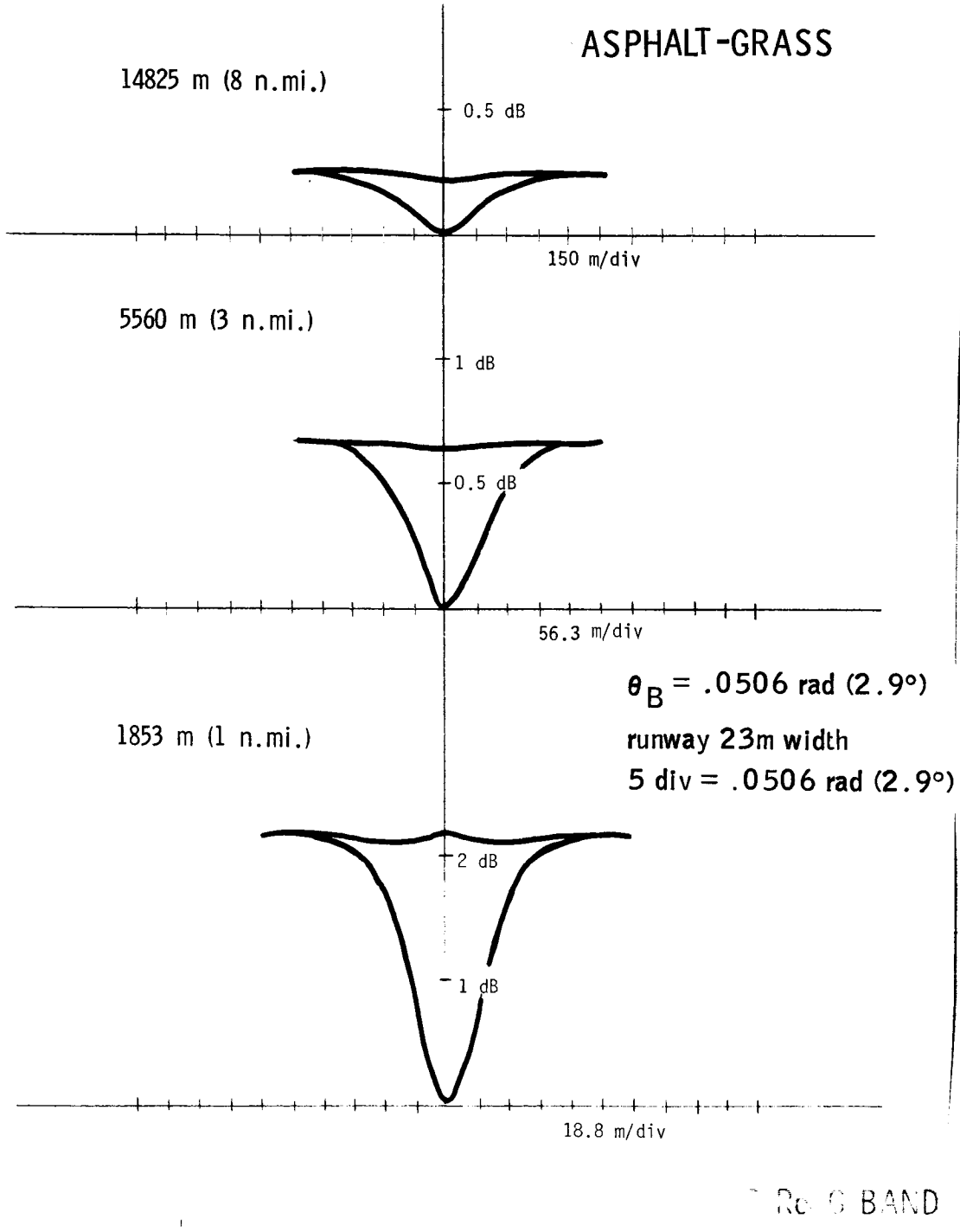

Figure 59 - ILM Radar R6-G Band

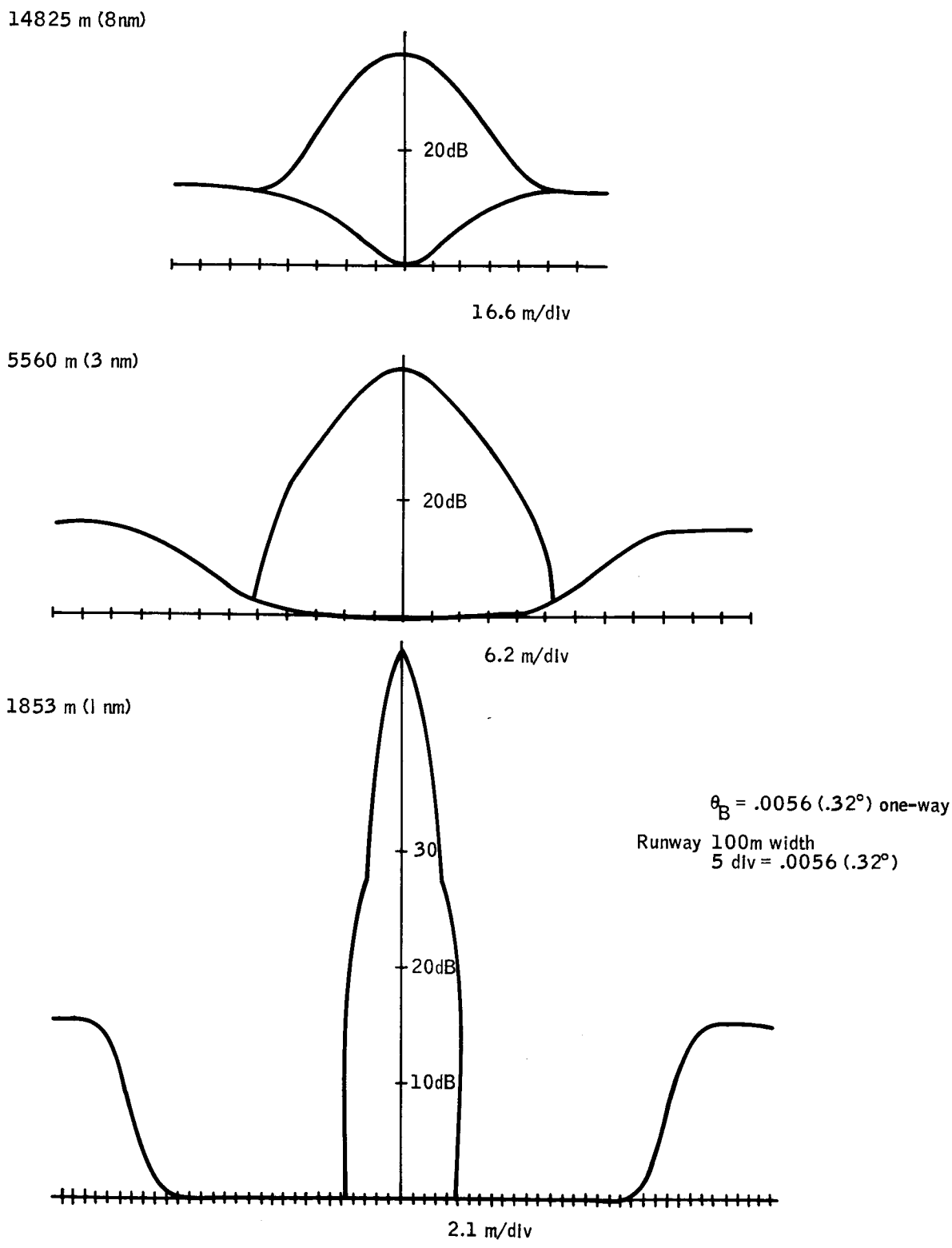

Figure 60 -- ILM Radar - R_2-K_a Band

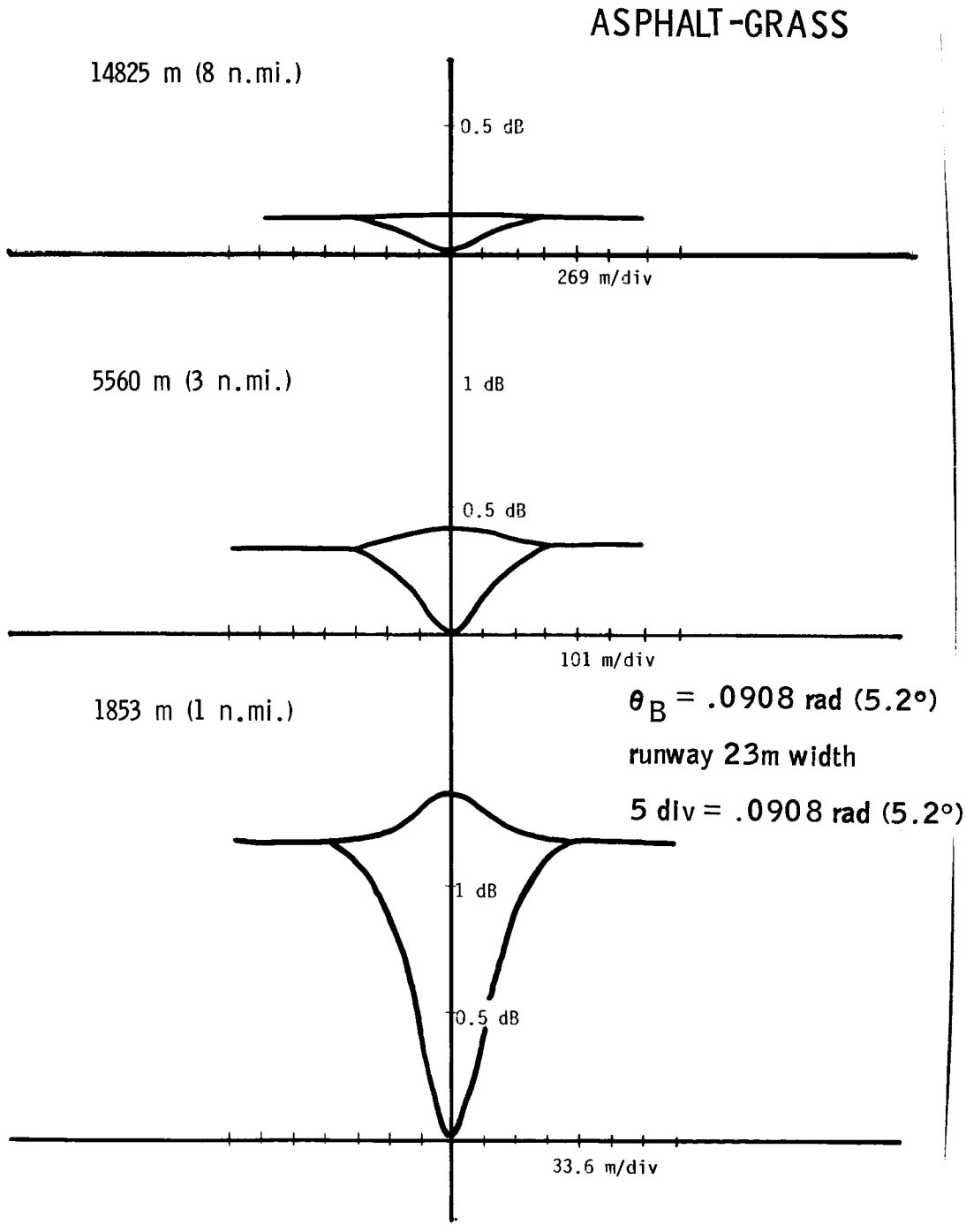

Figure 61 -- Radar R5-X-Band

normalized runway and background return power on the lower curve of each plot and the runway, background, and 1 m^2 reference target composite return on the upper curve.

The capabilities shown in Figure 53 for target to background ratios reference the target to background minimum (reference target in center of runway).

Table 43 summarizes the additional factors that may be added to the graphical results (Figures 51-55) to apply the other considerations of the technical analysis. The typical systems analyzed had little potential for processing enhancement other than to smooth fluctuating signal returns.

Summary of Capabilities of Typical Systems (e.g., R1, R2, R3, R4, R5) -- The following discussion summarizes, in general, the capabilities of the six individual radar systems as they apply to an ILM application. The six radars are:

- Ground-Based Precision Approach Radar (PAR)

  (Radars R3 and R4)

- Airborne Radar (Radars R1, R2, R5, R6)

  Imaging

  Imaging with Enhancement

The systems will be discussed for ability to meet the ILM specification. Specific items discussed are:

- Aircraft Positional Accuracy, Approach
- Aircraft Position Accuracy, Touchdown and rollout
- Obstacle Detection (4.2 Km visibility)
- Real-world perspective image to the pilot

Table 43 -- Summary of Loss and Gain Values for Typical Systems at 1 Km

L_d, scan distribution loss

Radar	Ti	Number of Scans	L_d
R1	0.2 msec.	<1	negligible
R2	0.25 msec.	<1	negligible
R5	.016 msec.	<1	negligible
R6	.016 msec.	<1	negligible

Radar	Ti	Nr. Pulses	L_i
R1	0.2 msec.	2	3 dB
R2	0.25 msec.	4	4-6 dB
R5	0.016 msec.	1	0 dB
R6	0.016 msec.	1	0 dB

$L_f + L_s + L_g$, fluctuating signal losses (P_d = 90%)

L_f = 4 - 8 dB for all radars for targets relative to clutter (reference Figure 9)

L_{cl}, collapsing loss approximately 1.5 dB if monopulse in azimuth or elevation is used.

L_{rd}, gate losses are assumed negligible under display configurations.

L_i, integration gains/losses.

Precision Approach Radar (X-band, R3 and R4) -- These high accuracy systems have the capability to meet the accuracy specifications for approach in moderate precipitation conditions. Multipath imposes limitations on accuracy near touchdown as the highly specular ground at X-band expands the effective vertical beamwidth, degrading the resolution. The high accuracy requirement would require the addition of monopulse resolution improvement in both azimuthal and vertical dimensions. The capability on a 10 dBsm aircraft at 8 nm would have the following limitations:

- Required accuracy = .0017 rad (0.1°) (2σ value)

  Beamwidth = .0244 rad (1.4°) (R3 radar typical)

For Gaussian distributed errors, the rms deviation for monopulse improvement is half the 2σ value above, or:

$$\Delta\phi_{rms} = \frac{2\sigma}{2} = .05° = \frac{.43\ (1.4°)}{\sqrt{S/N_r}} \tag{70}$$

$$\text{Thus, } S/N_r = \left(\frac{.6°}{.05°}\right)^2 = 100 = 20 \text{ dB} \tag{71}$$

Precipitation clutter is the limiting "noise" process so the resultant S/N at 8 nm = $\frac{T}{C_p}$ (dB) - S/N_r (dB) - L_f (dB) =

$$24 \text{ dB (Figure 47)} - 10 \text{ dB } (S/N_r) - (4 - 8 \text{ dB})(L_f) = 0\text{-}4 \text{ dB} \tag{72}$$

This result indicates .90 probability of tracking with the required accuracy for rainfall rates of 5 mm/hr to approximately 9 mm/hr (snow rates up to approximately 3 mm/hr equivalent rain). The 9 mm/hr was derived from:

$$4 \text{ dB} = 10 \log\ 2.5 = 10 \log \frac{r^{1.6}}{5^{1.6}} \tag{73}$$

The PAR system would have to transmit the guidance information to the approaching aircraft for instrument indication of position. The capability for real-world perspective display would not exist.

Imaging Radar (C-Band, R6; X-Band, R5; K-Band, R1 and R2) --

C-Band, R6 and X-Band, R5 -- Although the weather penetration capabilities of these radars are reasonable, the resolution for airborne imaging applications is not acceptable. Required signal to noise for the highest resolution system (R5) would be:

S/N_r = 28 dB for monopulse improvement to achieve 2σ of .0017 rad (0.1°)

Assuming the ideal situation exists for backgrounds with highly specular characteristics, it would take a reflector with cross-section, $\sigma_{reflector}$ dBsm to enhance the runway outline for imaging the entire runway at 1.6 km (1 nm).

$$\sigma_{Reflector} = +6 \text{ dB (Figure 3)} + 28 \text{ dB } (S/N_r) + (4\text{-}8 \text{ dB})(L_f) \quad (74)$$
$$= 38 - 42 \text{ dBsm}$$

This would require a trihedral corner reflector with a side dimension of approximately 3.3 m.

The X-band imaging system would have potential for providing imaging of an enhanced runway (large corner reflector or beacons) for ranges within approximately 1.6 Km (1 nm) for all weather conditions for smooth terrain such as deserts. Obstacle detection at decision height would not be possible for obstacles less than 6 dBsm. Obstacles with a radar cross section less than ~40 dBsm would have a low probability of detection due to masking by the strong returns of the

corner reflectors. The enhanced runway outline could be acceptable as a real-world perspective image.

K_a-Band, R1 and R2 -- The capabilities of R1 and R2 were sufficiently close that either system has potential as an ILM sensor. They both had insufficient vertical resolution for glide slope derivation because of antenna system limitations for vertical radome clearance. If sufficient room is made available for vertical arrays, the systems could be independent. The present configurations require external information on aircraft altitude and heading for display mapping of range bin to vertical perspective dimensions.

K_a-Band has precipitation attenuation limitations such that the range is borderline noise-limited at ranges of 2 to 5 km for rain rates as low as 5 mm/hr and highly specular culture.

The system would require monopulse resolution improvement to achieve the required accuracy specifications.

Background/Runway contrast ratios and $\frac{C_B}{N}$ ratios of S/N_r = 11 dB could provide the required accuracy of edge definition for ranges up to approximately 2 to 5 Km in 5 mm/hr rain. The range would rapidly degrade to less than 1 Km for rain rates of 16 mm/hr.

Obstacle detection for targets on the runway less than 0 dBsm is theoretically possible at the decision height for light rain (5 mm/hr). Rain at 16 mm/hr would obscure obstacles less than approximately 12 dBsm at the far end of the runway.

Real-world perspective images would be possible for high reflectivity culture for moderate precipitation levels.

Radar Systems as ILM Sensors

Radar systems have potential as Independent Landing Monitors to provide position and guidance information. The system potential is discussed in this section as it applies to the specifications listed in Table 22. The results are summarized in Table 44.

Accuracy during approach .0017 rad (0.1°) -- All radar systems (C- through K_a-Band) have theoretical accuracy potential using monopulse resolution improvement and integration to smooth fluctuating signals when the "signal-to-noise" ratio is sufficiently high and antenna pointing stabilization within 0.1° is provided. This accuracy during approach requires high values of background/obstacle cross-sections, and relatively low values of thermal noise and precipitation clutter return. Each band is discussed below as to ILM sensor potential.

C-Band radars with narrowed pulsewidths (relative to R6) and monopulse resolution improvement directed against large corner reflectors can theoretically achieve the required guidance accuracies for airborne radars. Since the demands of the monopulse resolution improvement are so large (approximately a factor of 100, beamwidth-improvement) it is doubtful that the capabilities can be achieved in the near future with current state-of-the-art in monopulse techniques.

X-Band Radars with narrowed pulsewidths have applications as both airborne and ground-based ILM's. Their successful application in PAR guidance has demonstrated ground capabilities. Airborne satisfaction of accuracy requirements would rely on monopulse resolution and ground corner reflectors or repeaters to provide high signal-to-noise ratios. Range accuracy of 13m (40 ft.) would require pulse-widths of approximately 40 nanoseconds (realizable) which would raise the T/C_B

Table 44 -- Summary of Specific Radar Systems

	Accuracy* (reference table 1)		Range** 0 dBsm target or background contrast	Obstacle detection***	Imaging
	Approach	Touchdown and rollout			
R1 with altimeter Ka-band ILM	Yes ($S/N_r \cong 11$dB for MRI) (Point target or edge)	Yes (Point targets only)	1 to 1.5 Km 2.5 to 3 Km (5mm/hr) (Target dominant within 2 Km, background beyond)	0 dBsm within 1 to 1.5 Km 10 dBsm within 5 Km	Real-world imaging for edge contrast of at least 6dB
R2 with altimeter Ka-band ILM	Yes ($S/N_r \cong 11$dB for MRI) (Point target or edge)	Yes (Point target only)	1 to 2 Km 4 to 6 Km (5mm/hr) (Target dominant within 2 Km, background beyond)	0 dBsm within 1 to 2 Km 10 DBsm within 6 Km	Real-world imaging for edge contrast of at least 6dB
R3 X-band PAR	Yes ($S/N_r \cong 20$ dB for MRI) (Point target)	Improbable (Multipath error)	14 to 18 Km for 0 dBsm target	0 dbSm 14 to 18 Km	Synthetic
R4 X-band PAR	Yes ($S/N_r \cong 18$ dB for MRI) (Point target)	Improbable (Multipath error)	25 to 30 Km for 0 dBsm target	0 dBsm 25 to 30 Km	Synthetic
R5 X-band Weather (modified)	Possible ($S/N_r \cong 28$ dB for MRI) (Point target or edge)	Possible (Point targets only)	>100 Km for background returns (1 to 1.5 Km for runway detection due to contrast)	No detection of 0 dBsm Beyond 1 to 1.t Km, target must be 6 dB larger than the background to runway contrast times the footprint area of the runway	Synthetic (Possible imaging at short ranges when edge contrast is sufficient)
R6 C-band Weather (modified)	Improbable ($S/N_r \cong 32$ dB for MRI) (Point target)	Improbable (Point targets only)	>100 Km for background returns (within 1 Km for runway detection due to contrast)	No detection of 0 dBsm Beyond 1 Km, target must be 6 dB larger than the background to runway contrast t'mes the footprint area of the runway	Synthetic (Possible imaging at very short ranges when edge contrast is sufficient)

LEGEND

* Monopulse resolution improvement (MRI) and reference stabilization required for all systems

** Maximum detection range of 0 dBsm target or rough (6" to 10") vegetation assuming:

a. 6 dB $\frac{T + C_B}{Cp + N}$ required for detection

b. Rain rate in excess of 16mm/hr unless otherwise noted

c. No clutter doppler enhancement

d. Integration smoothed fluctuating signals

*** Obstacle cross-section in dBsm referenced to $1m^2$ obstacles

a. 6 dB minimum $\frac{I}{C_B}$ and $\frac{T + C_B}{Cp + N}$

b. Rain rate in excess of 16mm/hr unless otherwise noted

c. Negligable target to clutter doppler enhancement

d. Integration smoothed fluctuating signals

e. Rough vegetation for the largest background cross-section

f. Frequency translation enhancement is not used

region of Figure 53 by approximately 20 dB. The effect would be a general lowering of the R5 curves of Figures 54 and 55. The lowering of the Figure 54 curve would not affect imagery as the background would still dominate. The Figure 55 curve for more specular surroundings would decrease such that point target returns (e.g., approach lights) would become evident and would probably create the dominant imagery in the presence of receiver noise and precipitation clutter. The airborne X-Band system, thus, has capability for accurately imaging the runway when highly diffuse scattering vegetation is present adjacent to a highly specular runway. For low contrast conditions ($\sigma_{background} - \sigma_{runway} \leq$ + 16 dB), the use of reflectors or repeaters would be necessary to achieve positional accuracies.

K-Band radars with parameters similar to R1 and R2 would have acceptable accuracy if monopulse resolution improvement is provided to achieve slightly higher azimuthal accuracy and either vertical beamshaping or high accuracy altimeters are used for vertical accuracy. Small signal-to-noise ratios of the order of 5 dB for point targets or runway edge contrast should be sufficient for achieving the required accuracy. K-band has problems with low scattering cross-section backgrounds due to precipitation clutter and attenuation for even moderate precipitation rates. It would be necessary to provide enhancement (reflectors or repeaters) for severe weather conditions to achieve the required accuracy. Also, higher transmitter pulse powers would be advisable if detection ranges beyond a few kilometers in moderate rain or evaporation fog were necessary.

Accuracy Near Touchdown and During Rollout -- Execution of aircraft flare and de-crab maneuvers will degrade accuracy, especially for high resolution "pencil beam" type systems, due to stabilization for aircraft and display reference. Runway edge definition during rollout would be limited by scan limits, near-field effects, and duplexer switching delay to beyond 50 m to 150 m and probably to within several hundred meters due to the very shallow grazing angle (i.e. less than .0349 rad (2°) at 300 m). Rollout guidance accuracy would, thus, be dependant on objects such as edge lights, reflectors, or approach lights at the ends of the runways. Ground radars such as PAR's experience multipath errors for targets near the ground so guidance near touchdown for vertical or height resolving is not reliable. Rollout guidance from PAR's would not be sufficiently accurate for the same reason.

Obstacle Detection -- Obstacle detection will be dependant on the relative fluctuating signal characteristics of the obstacle return and the competing returns. Assuming similar characteristics (comparable smoothing as a function of integration time), the detection ability is inversely proportional to resolution cell size and competing signal radar cross-section(s). K-band systems have potential for small obstacle detection (0 dBsm or less such as runway lights). Actual detection depends on the precipitation rate and absolute humidity (for attenuation). Figures 54 and 55 provide indications of potential X-band systems that have potential for detection of obstacles of larger than 0 dBsm (reference Figure 53). Obstacle detection would not be possible for systems with translating repeaters.

Real-World Imaging Capability -- Imaging capabilities exist for X- and K-band radars if adequate imaging display stabilization and runway edge contrast are evident in the system. Also, scene and ground returns must not be obscured by precipitation clutter or attenuation below acceptable thermal noise detection thresholds. C-band imaging is unreliable beyond a few kilometers due to insufficient resolution abilities, even with monopulse. X- and K-band systems both have theoretical capability although the X-band ability is of questionable application due to the dependance on monopulse resolution improvement. The K-band imaging capability has been demonstrated with R1 and R2 radars in light precipitation. At decision height (1000 ft. from threshold on a 14,000 ft. runway) and precipitation rates as low as 5 mm/hr., only the highest backscattering backgrounds provide enough return for imaging the entire runway.

Synthetic Imaging Capability -- Direct imaging capabilities presented in the previous section have the unfortunate restriction of dependence on high scattering cross-sections for runway edge definition and mapping of range-azimuth data to elevation-azimuth data in a display device. The analytic results previously presented show the returns from runway surroundings (grass) provide minimal returns requiring enhancement such as reflectors if detection at longer ranges or heavy precipitation rates is required. Numerous passive reflectors can provide enhanced edge definition for direct imaging capabilities. When it is acceptable to use synthetic or internally generated runway imagery, it is advantageous to use active repeaters with frequency translation capabilities to effectively eliminate all returns except the repeater signals. Three such repeaters in a known geometric orientation to the runway can provide range and angular reference information to

generate a synthetic image of the runway. The implementation of this system with frequency translation capability in the repeaters allows generation of return signals which are frequency shifted beyond clutter returns. This clutter suppression technique coupled with repeater power gain potential to offset progagation channel attenuation can provide all-weather synthetic imagery capabilities with arbitrarily high signal-to-noise potential to maximize monopulse resolution improvement. The accuracy of this implementation would be similar to a similarly configured beacon system with the additional benefit of direct ranging capability since the propagation path round trip delay is available for ranging by usual pulse radar techniques.

An example of this type of system was built and tested (Reference 25). Flight test results on the system indicated 2 sigma accuracies of 2m elevation and 11m azimuth at 1 Km range, 6m elevation and 19m azimuth at 4 Km, 17m elevation and 40m range at 8 Km range and 10m range. These accuracies are comparable to accuracies achievable with ILS and demonstrate the feasibility of the radar triangulation concept. From the known locations of the reflectors a synthesized runway image was generated. Pilot usage of the display for landings was not reported, however.

MULTILATERATION SENSORS

Basic Principles

Multilateration is the technique of position determination by measurement of range only. By measuring the range from an unknown location to three or more known locations, the position of the unknown is defined (See Figure 62). Although three measurements are theoretically sufficient to determine position, more are generally used. The primary effect of extra measurements is to reduce geometrical dilution of precision (GDOP).

The concept of GDOP is illustrated in Figure 63 for a two dimensional situation employing two range measurements. If the range vectors are nearly orthogonal (position 1), the error in range measurement transforms into a fairly small position error. However, as the angle between range vectors decreases (position 3), the range error is magnified when transformed to position error.

A second effect of multiple measurements is that, if a least squares type estimator is used to determine position, the accuracy generally increases as the square root of the number of measurements.

There are various methods for obtaining range measurements. Among them are:

- o Multiple Radar Skin Return
- o Side Tone Ranging
- o Pulse Ranging

Skin return with radar is generally very inaccurate, due to the range spread of the target. Side tone ranging can be made extremely accurate in the absence of multipath interference, but it has limited multipath rejection capability. It

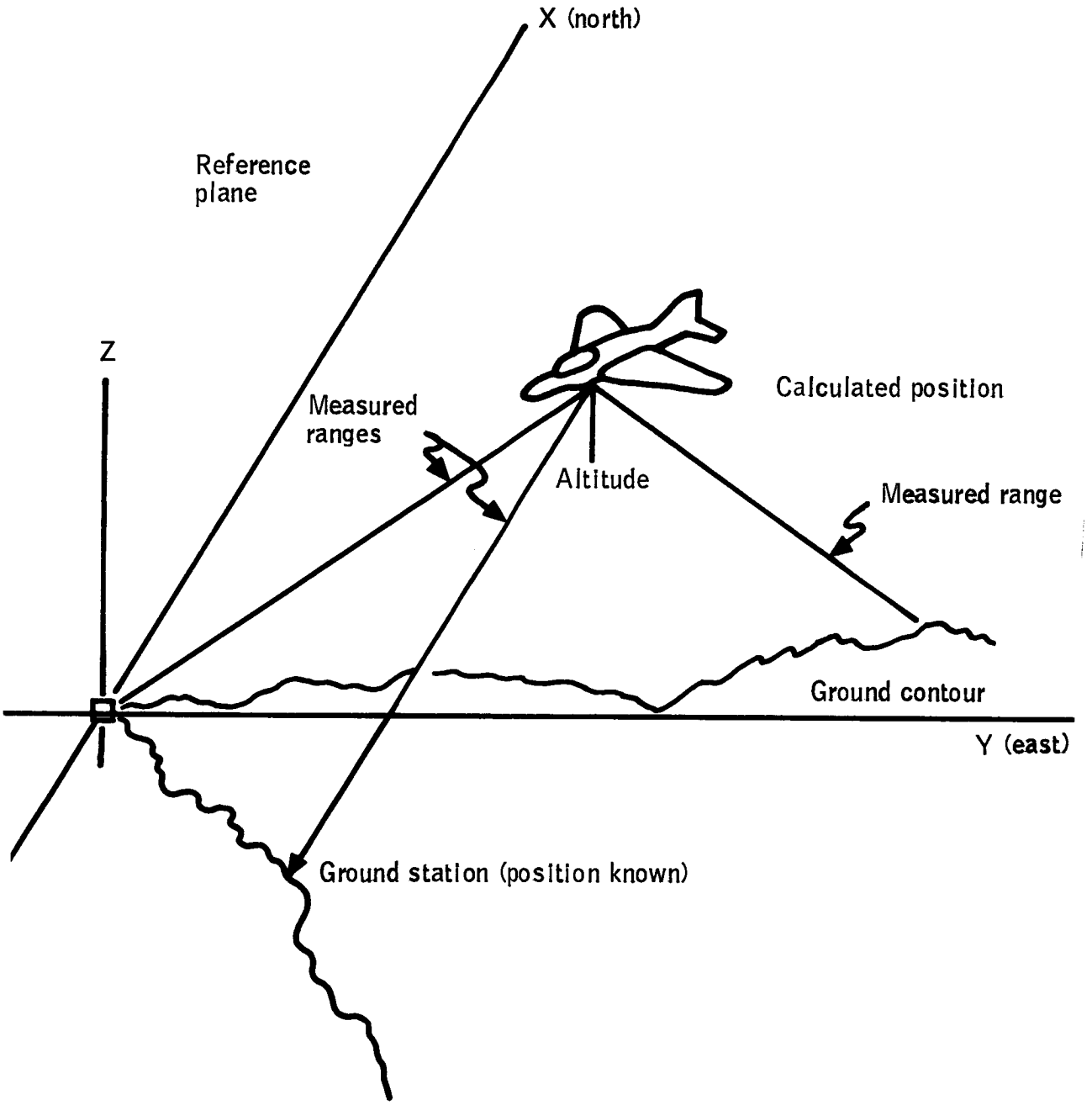

Figure 62 -- The Trilateration Concept

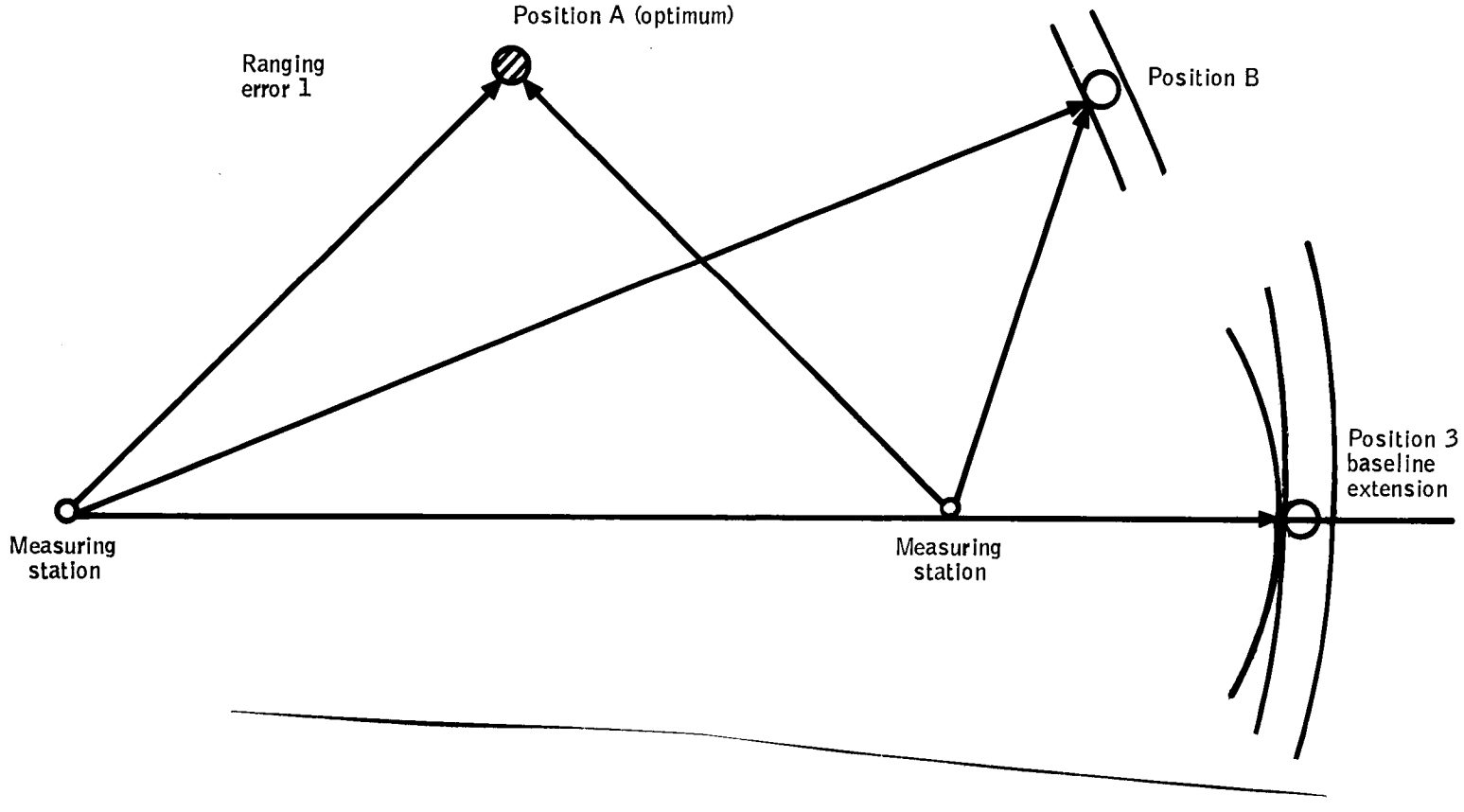

Figure 63 -- Illustration of GDOP

is also very difficult to time share r-f channels with side tone ranging, due to the basically cw nature of the ranging process.

This analysis will therefore be concerned only with pulse ranging wherein an interrogator broadcasts a pulse and starts a clock. Upon reception of the interrogation, a transponder replies with a pulse message. When the interrogator receives the reply, it stops its clock with the round trip time in the clock. A multitude of variations on this basic theme exist; however, the exact nature of interrogation and response does not affect the precision capabilities of the system.

Within this framework, various beacon geometries, pulse bandwidths, bias compensation schemes, etc. exist. In general, a wide bandwidth implies high accuracy and expense. However, it will be shown in the following analysis that even the most inexpensive system consisting of three beacons and using ATCRBS transponders is more than sufficient to provide azimuth and range accuracy, whereas even the most expensive system using satellites, large numbers of beacons and wide bandwidths cannot achieve the specified altitude accuracy.

A multilateration system is a position measuring system, and hence has no imaging capability. It therefore can be considered only for the Basic and Case I ILM capability. It will be shown that accuracy depends on bandwidth. Carrier frequency can be selected such that atmospheric attenuation need not be considered.

Adaptive Threshold Detection

Any pulse transmitted through a physical system has a non-zero rise time during which the amplitude of the pulse is increasing. It is convenient to model the

pulse as a trapezoidal pulse, such that during the rise time the pulse amplitude is increasing linearly with time, and the amplitude is constant at its peak value for some time thereafter.

Because the system is assumed to time share a single rf channel, feedback AGC would be too slow to control the pulse amplitude at the detector. Therefore, if a fixed voltage threshold crossing of the video were used to determine time of pulse arrival, errors on the order of the rise time would be probable.

To allow the use of narrow bandwidth pulses without the accuracy penalty of a fixed threshold system, adaptive threshold detectors are used. An adaptive threshold detector (Figure 64) consists of a peak estimator and amplifier of gain 1/2, the output of which is compared to a delayed version of the signal. When the leading edge of the pulse rises to 1/2 the peak value, the comparison is successful in declaring the arrival of the pulse. In the absence of corrupting factors such as noise or multipath, the adaptive threshold allows time of arrival decisions to be made accurately on pulses of any rise time.

The effect of noise on an adaptive threshold has been analysed in the literature (References 30 and 31). For high signal to noise ratio and a relatively large class of noise probability densities, the variance of the error in threshold crossing time is given by:

$$E(\tilde{t}^2) \cong \frac{t_r^2}{2\ SNR} \tag{75}$$

where t_r is the pulse rise time

SNR is the normal power signal to noise ratio in linear units

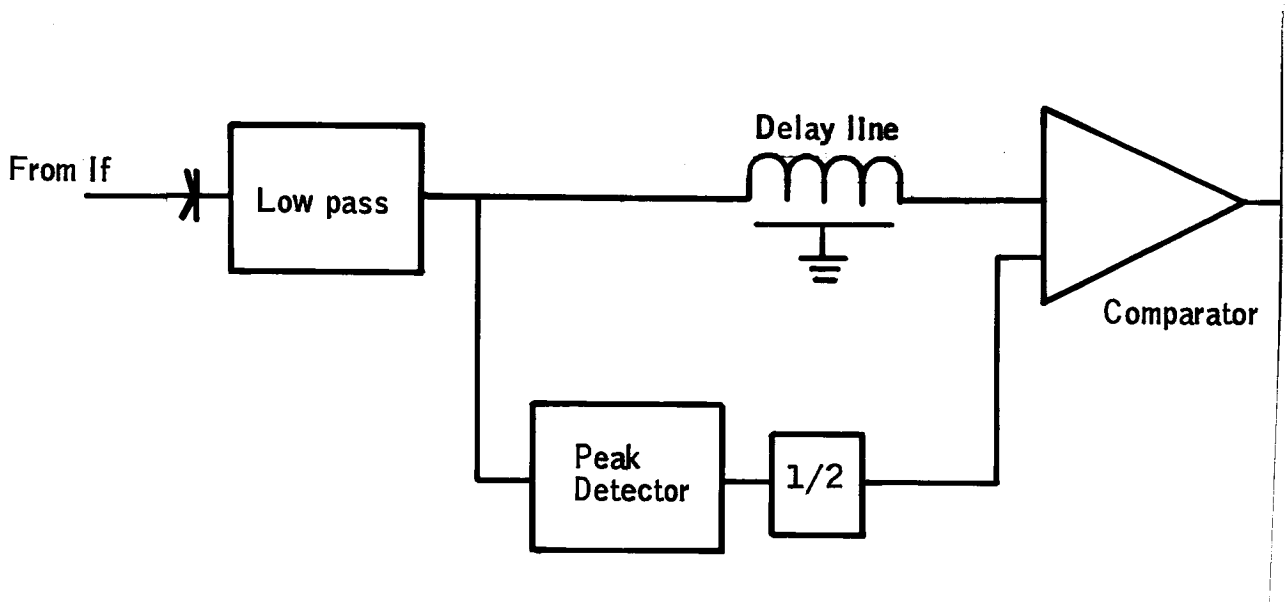

Figure 64 -- Classical Adaptive Threshold Detection

The detector has been found to be a biased estimator (Reference 31) in the presence of noise; however, for signal to noise ratios greater than 20 dB the bias is less than .5% t_r, and the estimator becomes unbiased for high signal-to-noise ratios.

If the rise time of the pulse is the inverse of the system noise bandwidth, which is a reasonable design criterion, the variance of threshold crossing time error asymptotically approaches the Cramer-Rao bound as signal-to-noise ratio increases. It can be concluded that adaptive threshold detection is an appropriate technique for estimation of pulse arrival time, and becomes an optimum estimator with high signal-to-noise ratios.

Effect of Multipath

Although an adaptive threshold detector has good performance in a noise environment, some authors question its validity when corrupted by specular multipath.

It is intuitively obvious that if the multipath arrives after the threshold decision is made, it will have no effect. If the threshold is set at 1/2, the delay line length will be 1/2 $t_r + \varepsilon$. The decision will be made at about,

$$t = t_r + \varepsilon \tag{76}$$

where t_r is the pulse rise time

ε is the extra delay to insure detection on the pulse peak

Consider a system in which the rise time is 100ns. Allowing a 10ns epsilon (ε) gives 110ns. Therefore any multipath with a path difference greater than 33m (108 ft) will not affect the system.

However, short term multipath can have an effect. It is therefore necessary to examine the sources of specular multipath. If the ground station antennas are mounted at a height, z, on flat ground, the reflection from the surface of the earth will have a path distance (Figure 65) of:

$$\Delta R = 2\, z \sin \phi \tag{77}$$

where ϕ is the elevation angle to the aircraft

Reasonable antenna tower heights would be 30m (98 ft) and less, predicated on a compromise between antenna cable loss and obstacle clearance. Then aircraft at elevation angles less than 0.524 rad (30°) will have multipath from the ground arriving during the pulse rise time.

For ILM application, the normal situation is for the aircraft to be at less than 1000m (3281 ft) altitude and at ranges on the order of 20m (11 nm) from any given ground station. This implies elevation angles less than 0.05 rad (2.86°), with sin ϕ about .05 or less. The ground multipath can thus be expected to arrive within 10ns of the direct path, decreasing with altitude to zero delay at touchdown.

The other major source of specular multipath is obstructions. Since an obstruction can exist with any path difference, it is valuable to examine the effect of multipath at various multipath times and phases. Assuming a trapezoidal pulse, the free path pulse can be described by

$$V(t) = \begin{cases} t/t_r & 0 < t < t_r \\ 1 & t > t_r \end{cases} \tag{78}$$

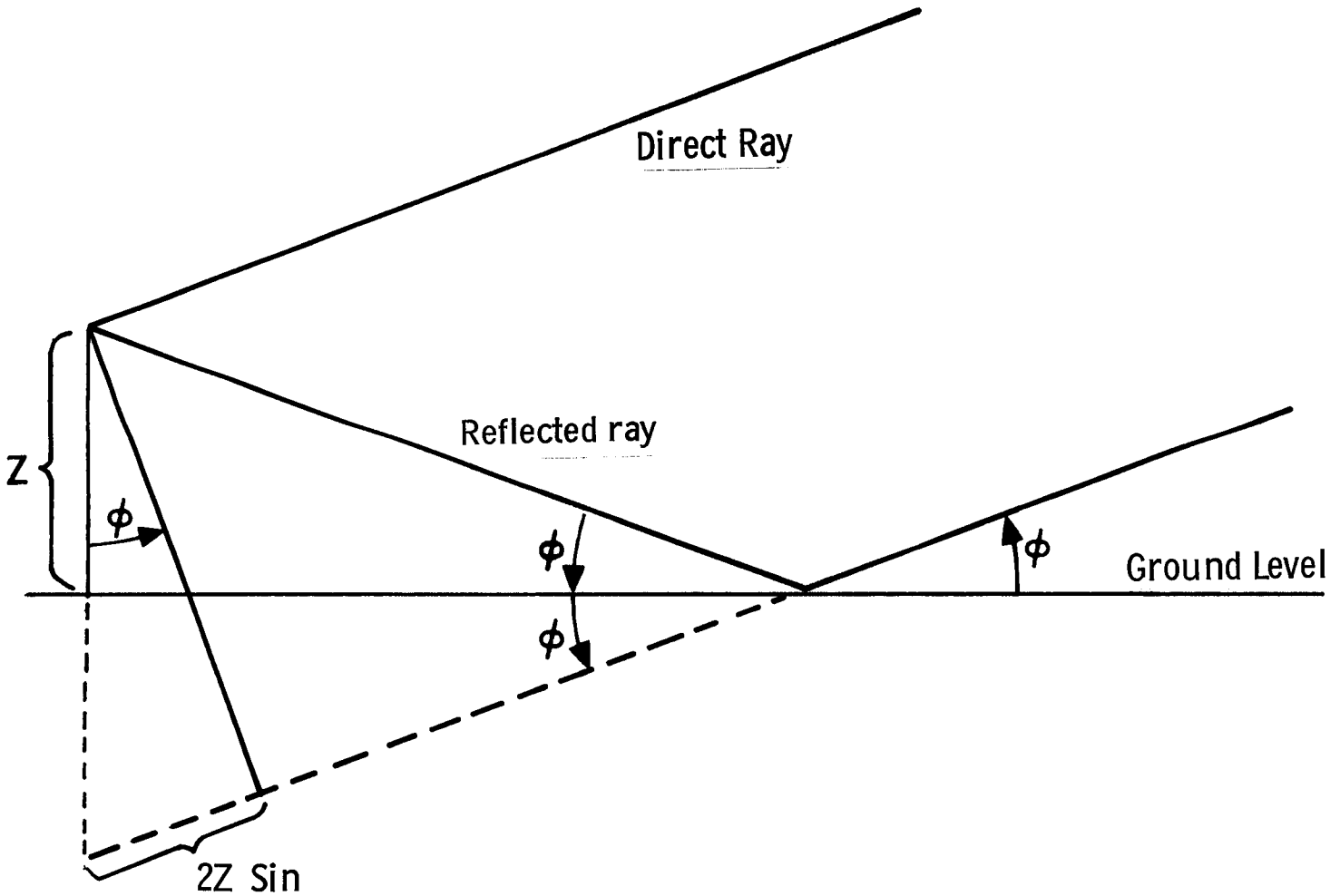

Figure 65 -- Multipath Geometry

The multipath pulse is described by

$$V(t) = \begin{cases} 0 & 0 < t < t_m \\ R\,\dfrac{(t-t_m)}{t_r} & t_m < t < t_r + t_m \\ R & t_r + t_m < t \end{cases}$$

where $R = \rho e^{j\phi}$ is the effective reflection coefficient

t_m is the multipath time

The phase of the effective reflection coefficient is determined by the phase shift on reflection from the surface and the path difference multiplied by the propagation constant. The total pulse can then be described by

$$V(t) = \begin{cases} t/t_r & 0 < t < t_m \\ t/t_r + R\,\dfrac{(t-t_m)}{t_r} & t_m < t < t_r \\ 1 + R\dfrac{(t-t_m)}{t_r} & t_r < t < t_r + t_m \\ 1 + R & t_r + t_m < t \end{cases}$$

Since R is a complex number, and the only observable quantity is the modulus of V, it is not analytically straightforward to solve for the error in threshold crossing time. The equation for V can be iteratively solved for the modulus of V to determine at what time the threshold is crossed. The threshold crossing error is given by

$$T_{CE} = \left\{ T \mid |V(t)| > 1/2 \right\} - T_{r/2} \qquad (81)$$

Figure 66 shows the error in crossing time assuming the detector of Figure 64 with a delay line length equal to .6 t_r, and assuming the amplitude of the multipath to be .75 times the direct amplitude. This amplitude is reasonable for reflections off the earth with no antenna pattern shaping, but is more severe than would be expected at such short delay times from obstructions.

It can be seen from Figure 66 that, depending on the phase of the multipath, the error can be either positive or negative but is almost always less than the multipath delay time. The relationship between threshold error and multipath delay time is highly nonlinear, as can be seen by comparing the plots for a .2 t_r delay time and a .9 t_r delay time.

If the dominant multipath source is known, the value of the delay line time can be adjusted to minimize its error contribution. For example, Figure 67 shows the relationship between multipath error and multipath phase, for a .1 t_r delayed pulse with reflection coefficient .75. Various curves are obtainable by varying the length of the delay line, as shown.

Since the phase of the multipath will be rapidly varying, 2π radians for every wavelength of differential range, due to changing range, and the error as a function of phase is bounded, the specular multipath can be considered as a noise source. Its effect on the system can be examined by performing averaging over phase angle and delay time. Performing this manipulation of the graphs on Figure 66 yields a bias error of .0082 t_r and a standard deviation of .112 t_r. For a 100 nsec rise time system, these errors correspond to range errors of .27m (.9 ft) bias and a standard deviation of 3.67m (12 ft).

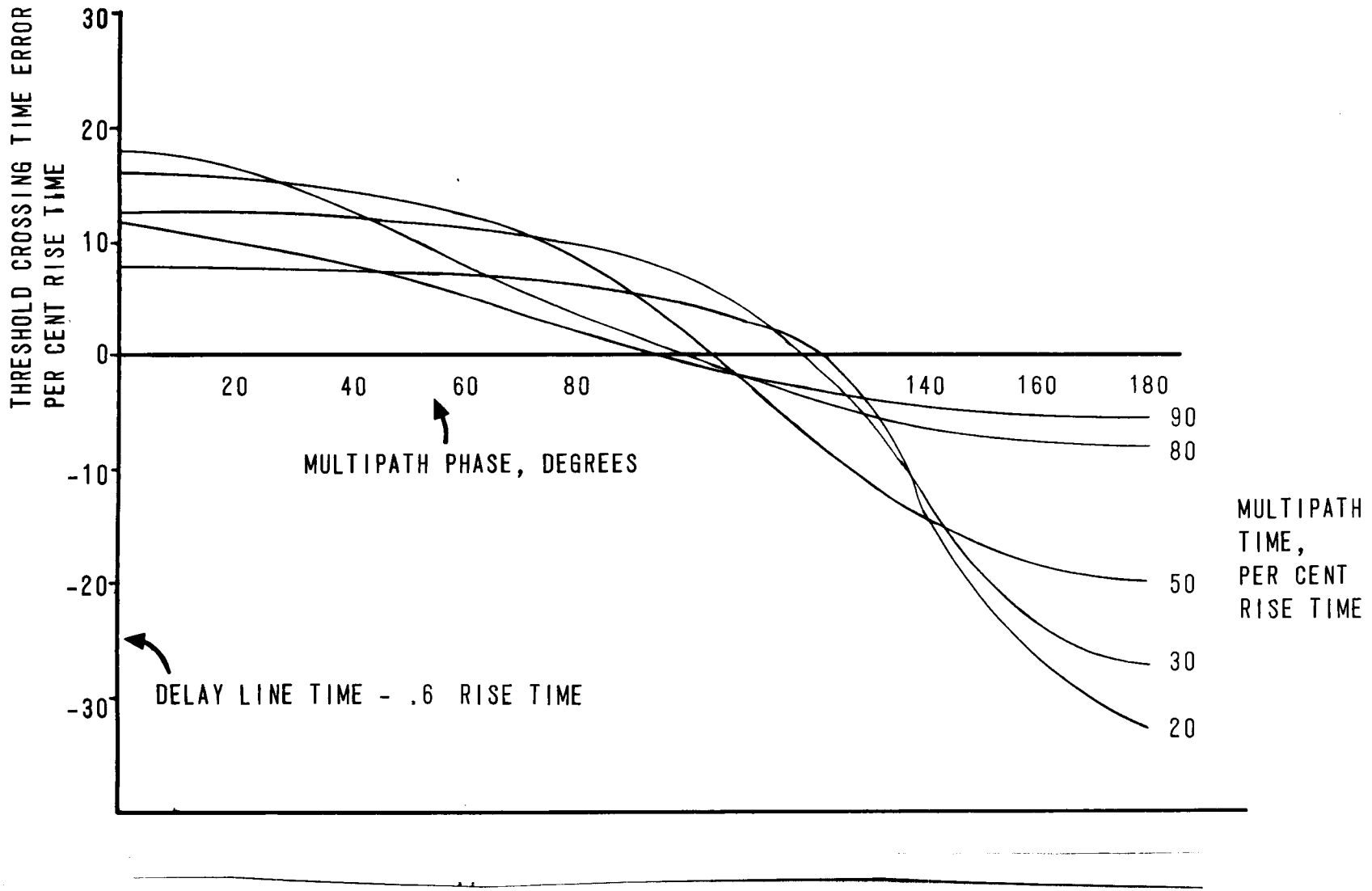

Figure 66 -- Threshold Crossing Time Error

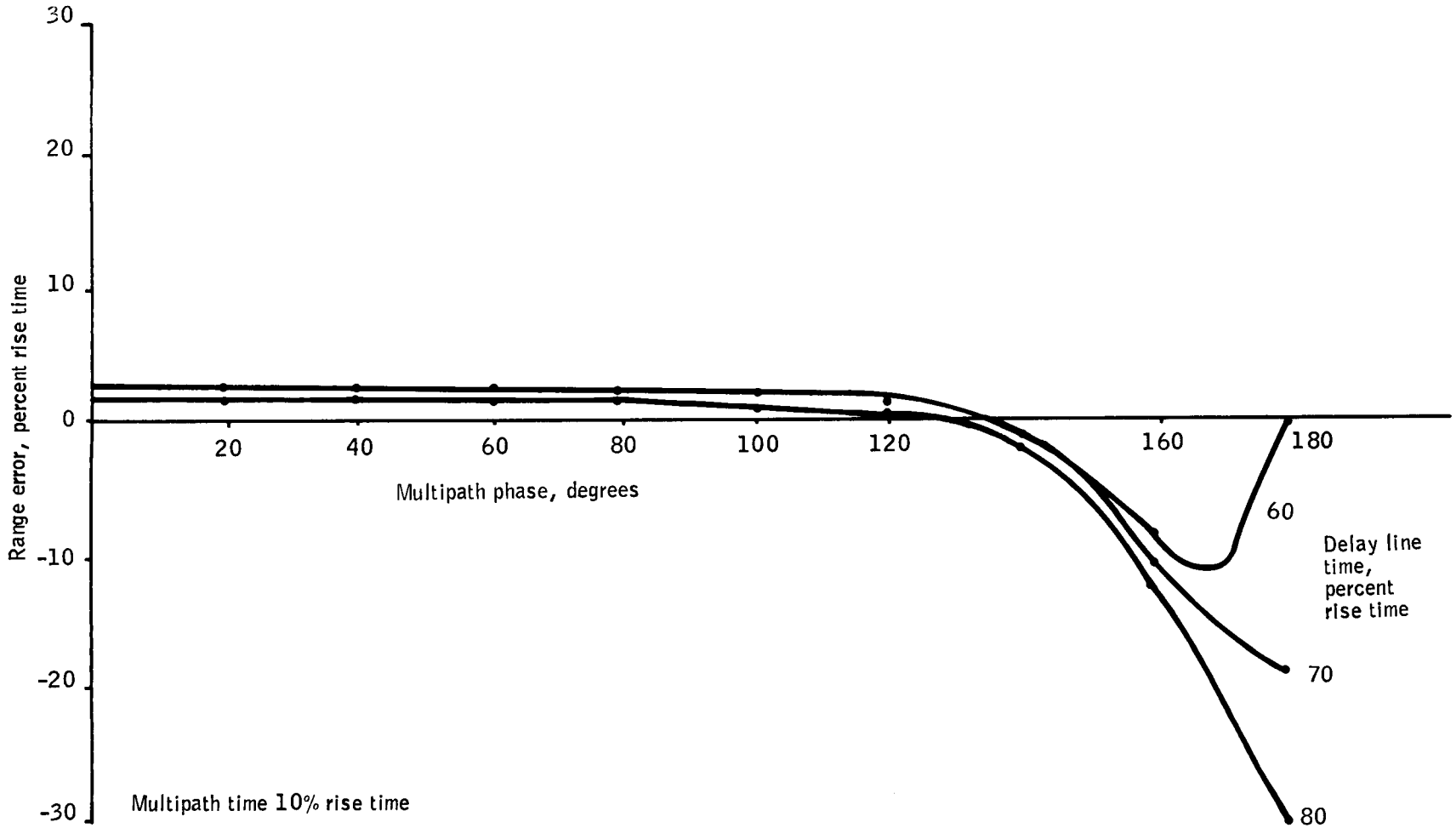

Figure 67 -- Multipath Error vs Phase

Hardware Considerations

A typical transponder block diagram is shown in Figure 68. If the transponder is acting in a response mode, the control section determines when a valid interrogation has been received and immediately replies by transmitting a valid response sequence. If the transponder is an interrogator-timer, a typical operation would be to initiate an interrogation from some external stimulus. During transmission, the receiver is only partially blanked and the interrogation is detected. At this point, the clock is started. When a response message is detected, the clock is stopped with a time value representing range. This range value is not corrupted by delays through the interrogator, so slowly varying changes in that delay are not error sources.

When used as a responder, the "wrap-around" of a response (duplexer leakage) can be used to reduce transponder bias error in various ways. One way is to detect the response wrap around and transmit a second reply. The time between replies can then be measured at the interrogator-timer and used as a measure of transponder delay. Another technique is to maintain a timer in the responder which compares the time between transmission and detection of wrap around, and adjusts a time delay network to keep the total transponder delay constant.

With either technique, the use of high level wrap around to measure bias provides less than optimum bias compensation, because the delay through the receiver for the wrap around may not vary the same way as the delay for low level receptions as time and temperature change.

An alternate mechanism for obtaining a measure of transponder delay is shown in Figure 69. A sample of the transmit energy is tapped off the transmission line and enters a stabilized delay line. When the transmitted pulse gets to the end

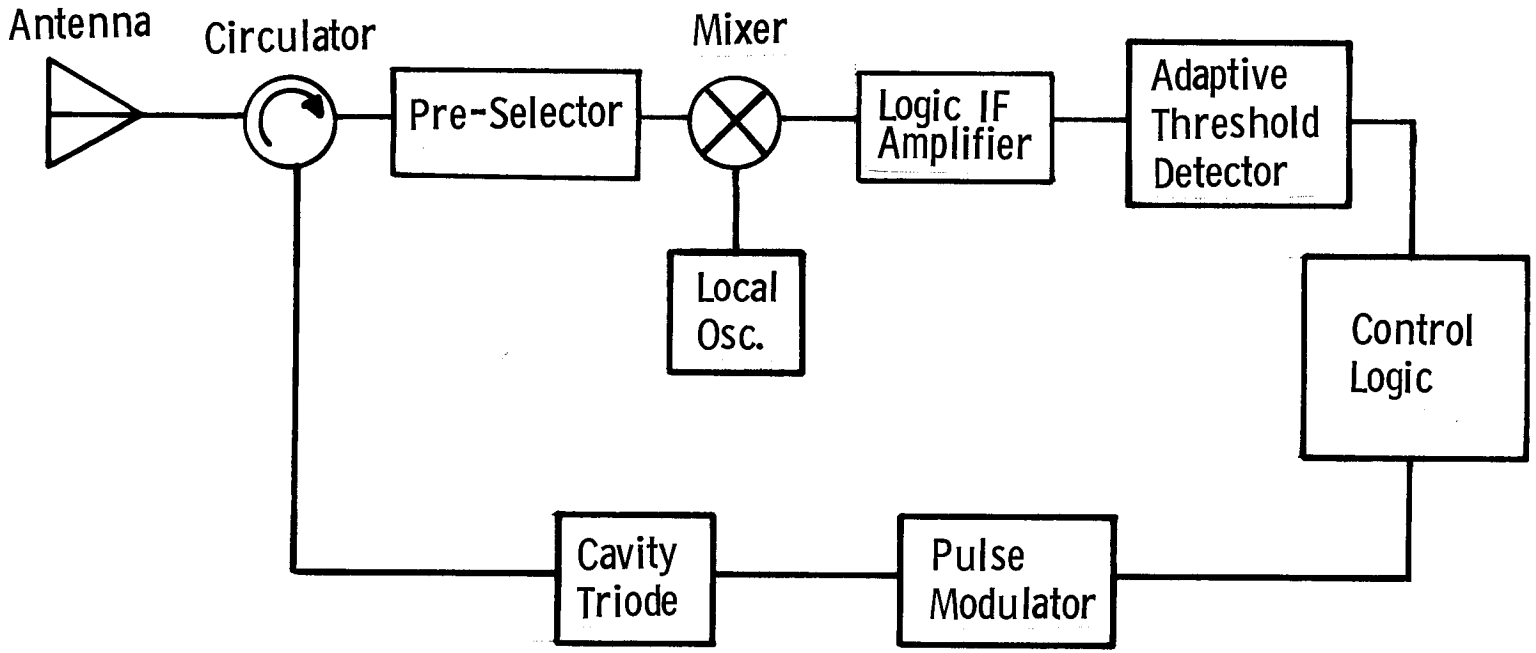

Figure 68 -- Transponder Block Diagram

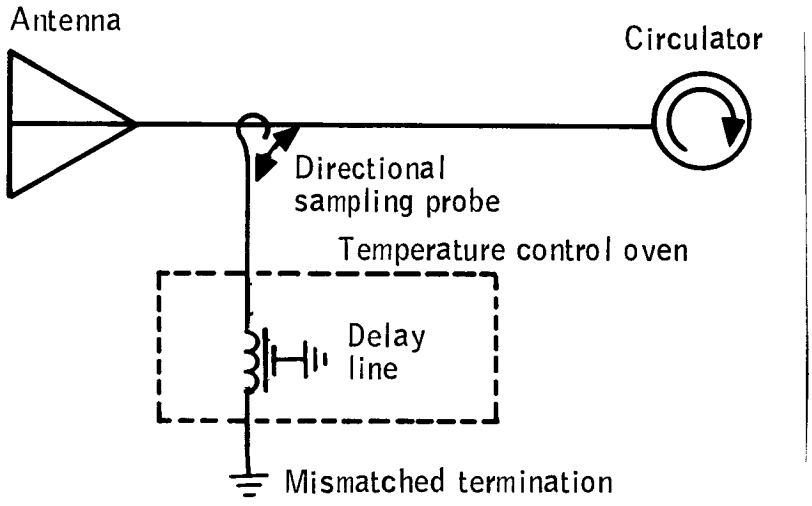

Figure 69 -- Alternate Mechanism for Measuring Transponder Delay

of the line it is reflected by the mismatched termination and returned through the sampler to the transmission line. During transmission, data wrapping around through the duplexer is ignored. When the delayed transmission re-enters the transmission line it is attenuated by twice the sampling probe loss, and can thus be made of an appropriate level for a received message. Either bias compensation technique can then be applied.

By applying appropriate filtering to the bias compensation, transponder bias can be reduced to a fraction of the internal noise type errors.

A second error source fits neither the bias nor the noise category. Since AGC cannot be used due to timing problems and a wide dynamic range is required, log IF strips are normally employed. If the pulses were truly trapezoidal and the transfer characteristic of the IF truly logarithmic, no error would result. However, neither of these approximations is very precise. It has been found (Reference 32) that a typical compensated amplitude dependent error is as depicted in Figure 70. At very low amplitudes, the time estimator is biased, and responds slightly earlier as amplitude increases. In the medium signal level range, the offset in the log function causes arrival estimation to occur later as amplitude increases. Finally, as the IF starts to enter saturation type phenomenon, the arrival time estimation rapidly becomes earlier as amplitude increases and more of the top of the pulse is clipped.

The dominant error source in a well designed system is the quantization of the clock. Time of arrival is noted at the next tick of the clock after the threshold decision is made. Since the threshold can be crossed at any time with equal probability, clock quantization introduces a uniformly distributed noise into

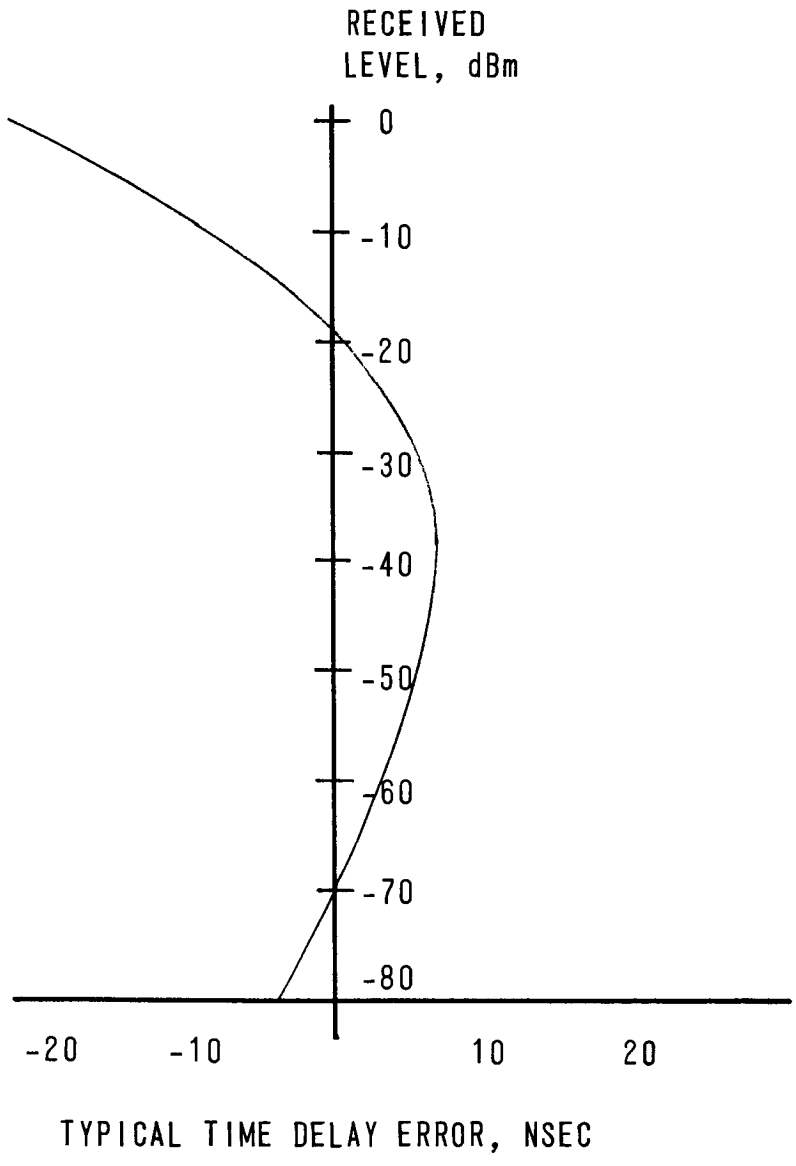
RECEIVED
LEVEL, dBm
0
-10
-20
-30
-40
-50
-60
-70
-80
-20
-10
10
20
TYPICAL TIME DELAY ERROR, NSEC

Figure 70

the ranging at each system node. In a simple two node ranging system, there would be two such independent range errors; one at the interrogator, and one at the responder. The net result is a triangularly distributed range noise. Assuming logic operating at the same speed in both nodes, the variance of such noise is (Reference 33)

$$\sigma_Q^2 = 1/6 \ (f_{clock})^2 \tag{82}$$

Geometrical Dilution of Precision (GDOP)

The selection of the number and location of beacon stations in a multilateration system involves trading off several conflicting factors. Among them are:

- o System accuracy
- o System cost
- o Availability of real estate
- o Line of sight requirements
- o Sampling rate requirements

Reference 34 performs an analysis of the effect of changing the number and location of beacon stations on the accuracy of a multilateration system. It shows that for a system with N beacons:

- o Accuracy is approximately proportional to $\sqrt{N}$
- o Accuracy is much more dependent on the direction to the beacons than on the number of beacons.

It can be concluded from this that the primary reason for introducing more beacons into a multilateration system is to obtain a better geometrical relationship between the aircraft and the beacons. The effect of this geometrical relationship on accuracy is called geometrical dilution of precision (GDOP). Several

GDOP measures have been used, however the common factor is that the GDOP measure is a number associated with a position which when multiplied by the basic system range measuring capability yields a measure of position measuring error. GDOP can be defined for a particular coordinate of an arbitrary coordinate system, or as a root sum square of two or three coordinate's individual GDOP's.

In a typical multilateration system, some sort of least squares position solution would be used to estimate the position from the multiple range measurements. In this case, it can be shown that (Reference 37) the covariance of the position estimate for a single measurement set is

$$V_{\underset{x}{N}} = (H\, V_r^{-1}\, H^T)^{-1} \tag{83}$$

where V_r is the covariance of the measurements

H is the linear sensitivity matrix for the measurements

To use this equation, the non-linear multilateration equations must be linearized about some estimated position.

Reference 33 shows that in cartesian coordinates, the sensitivity matrix is

$$H = \begin{bmatrix} \frac{\Delta x_1}{R_1} & \frac{\Delta x_2}{R_2} & \cdots & \frac{\Delta x_N}{R_N} \\ \frac{\Delta y_1}{R_1} & \frac{\Delta y_2}{R_2} & \cdots & \frac{\Delta y_N}{R_N} \\ \frac{\Delta z_1}{R_1} & \frac{\Delta z_2}{R_2} & \cdots & \frac{\Delta z_N}{R_N} \end{bmatrix} \tag{84}$$

Where $\Delta x(y)\ (z)_i$ is the distance in the x(y)(z) direction between the aircraft and the ith beacon

R_i is the range from the aircraft to the ith beacon

If all the beacons are identical and their measurements are independent, then

$$V_r^{-1} = \begin{bmatrix} \frac{1}{\sigma^2} & & & \\ & 1/\sigma^2 & & \\ & & 1/\sigma^2 & \\ & & & \ddots \; 1/\sigma^2 \end{bmatrix} \tag{85}$$

where σ^2 is the variance of range measurement.

In this case, the position variance is approximately

$$\frac{V_{\tilde{x}}}{\sigma^2} \cong (HH^T)^{-1}$$

Since HH^T is a positive definite symmetric matrix, the main diagonal elements of its inverse take on their minimum values if HH^T is diagonal. Therefore, the reciprocals of the main diagonal elements of HH^T are a lower bound on the variance of position estimation error.

Based on these approximations, computations of GDOP for some representative systems have been made. The first layout is a minimal three dimensional system composed of three beacons arranged in an equilateral triangle 40km (21.6 nm) on a side. Figures 71 and 72 show the equal GDOP curves, in terms of main diagonal variance multipliers. Standard deviation GDOP contours can be obtained by taking the square root of the values shown.

A six beacon symmetric system layout, which would give better altitude data, is shown in Figure 73. The diagonal variance GDOP contours are shown in Figures 74 and 75.

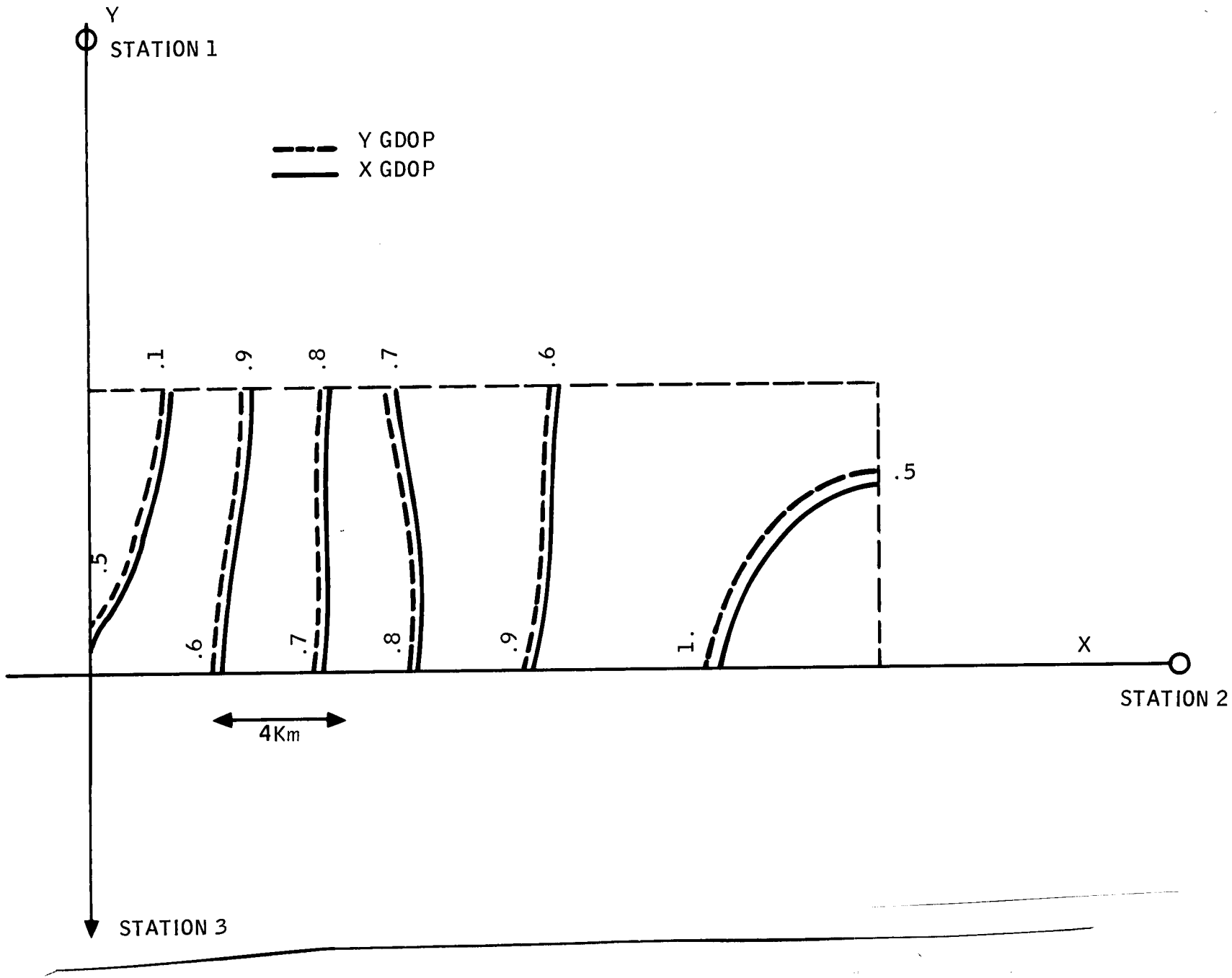

Figure 71 -- Horizontal Plane 6 DOF Near the Center of an Equilateral Triangle

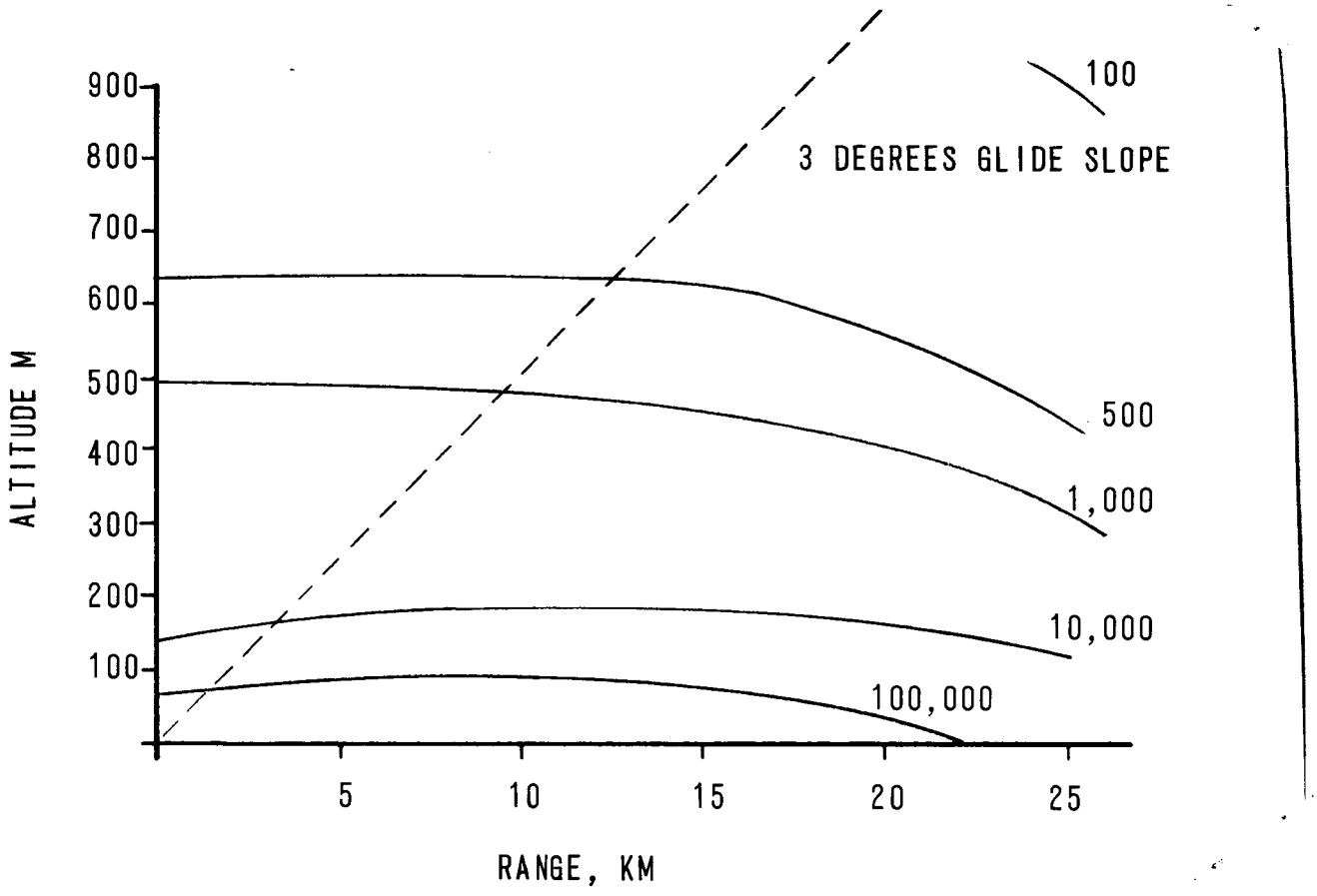

Figure 72 -- Equilateral Triangle Altitude GDOP

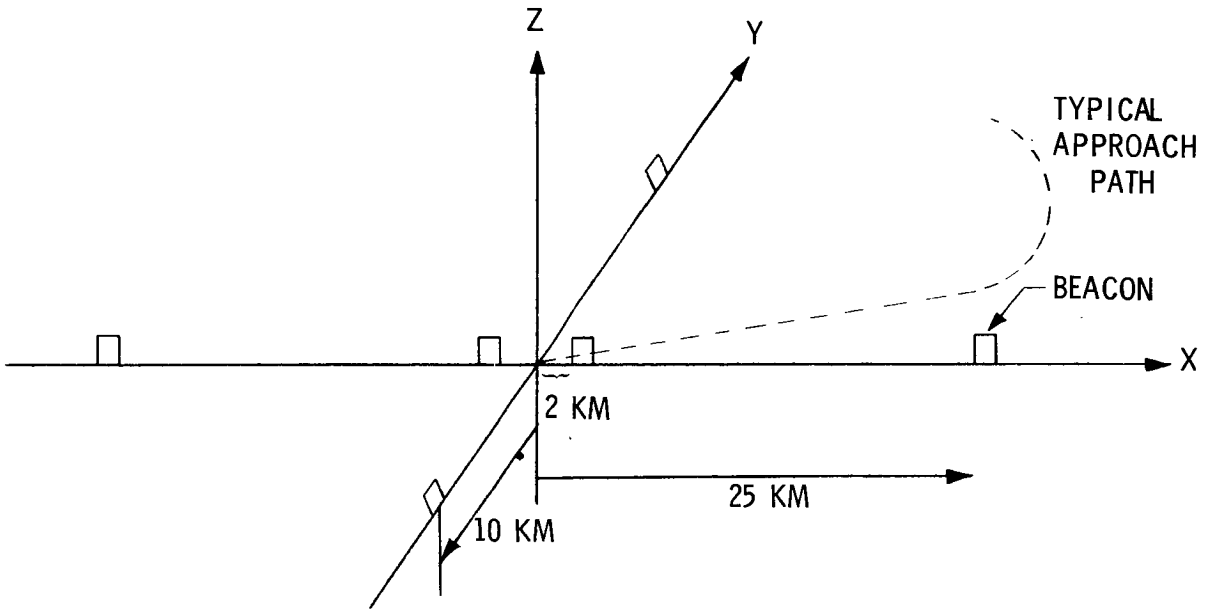

Figure 73 -- Proposed Six Beacon System Layout

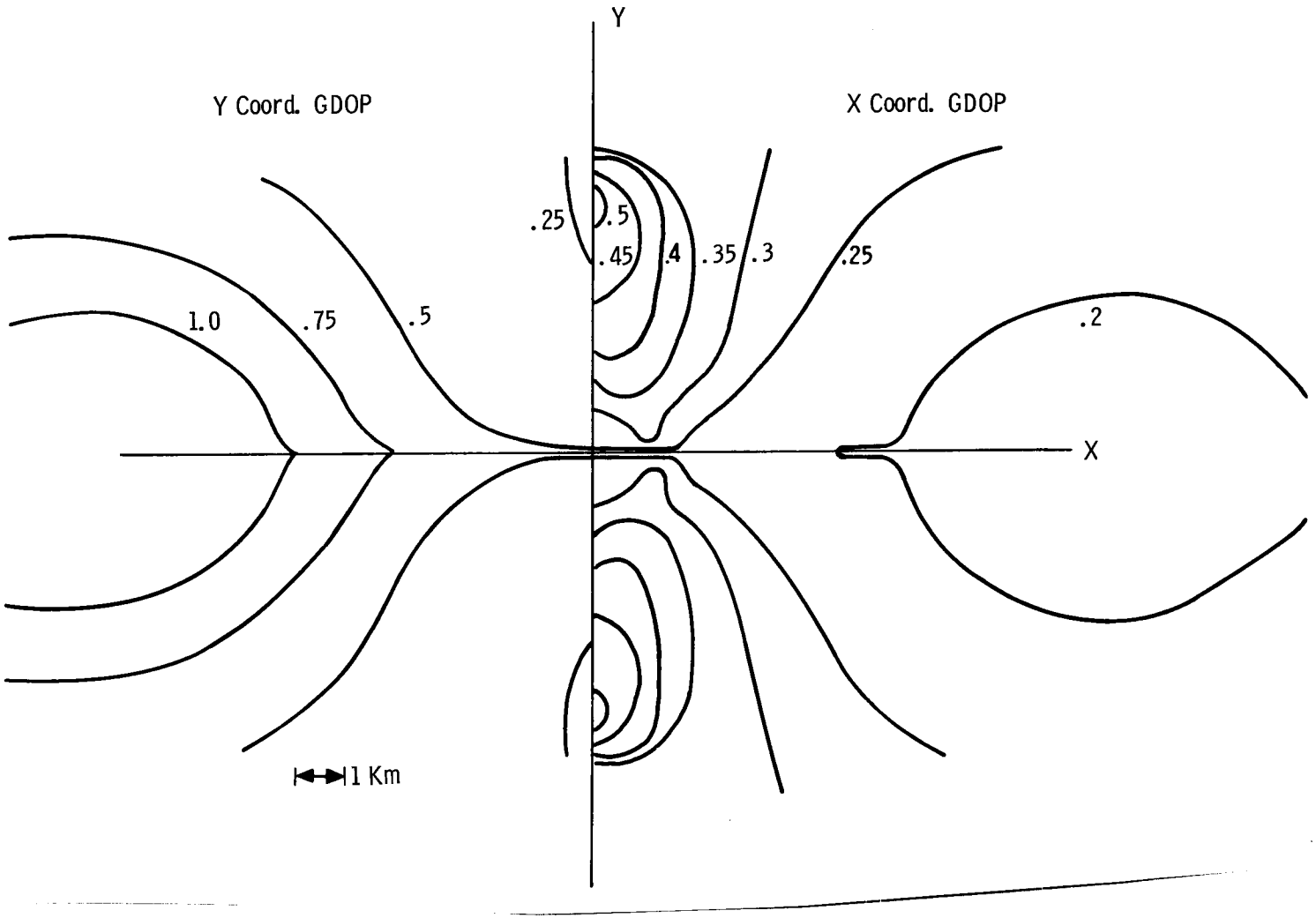

Figure 74 -- Horizontal Plane GDOP for Proposed Six-Beacon System

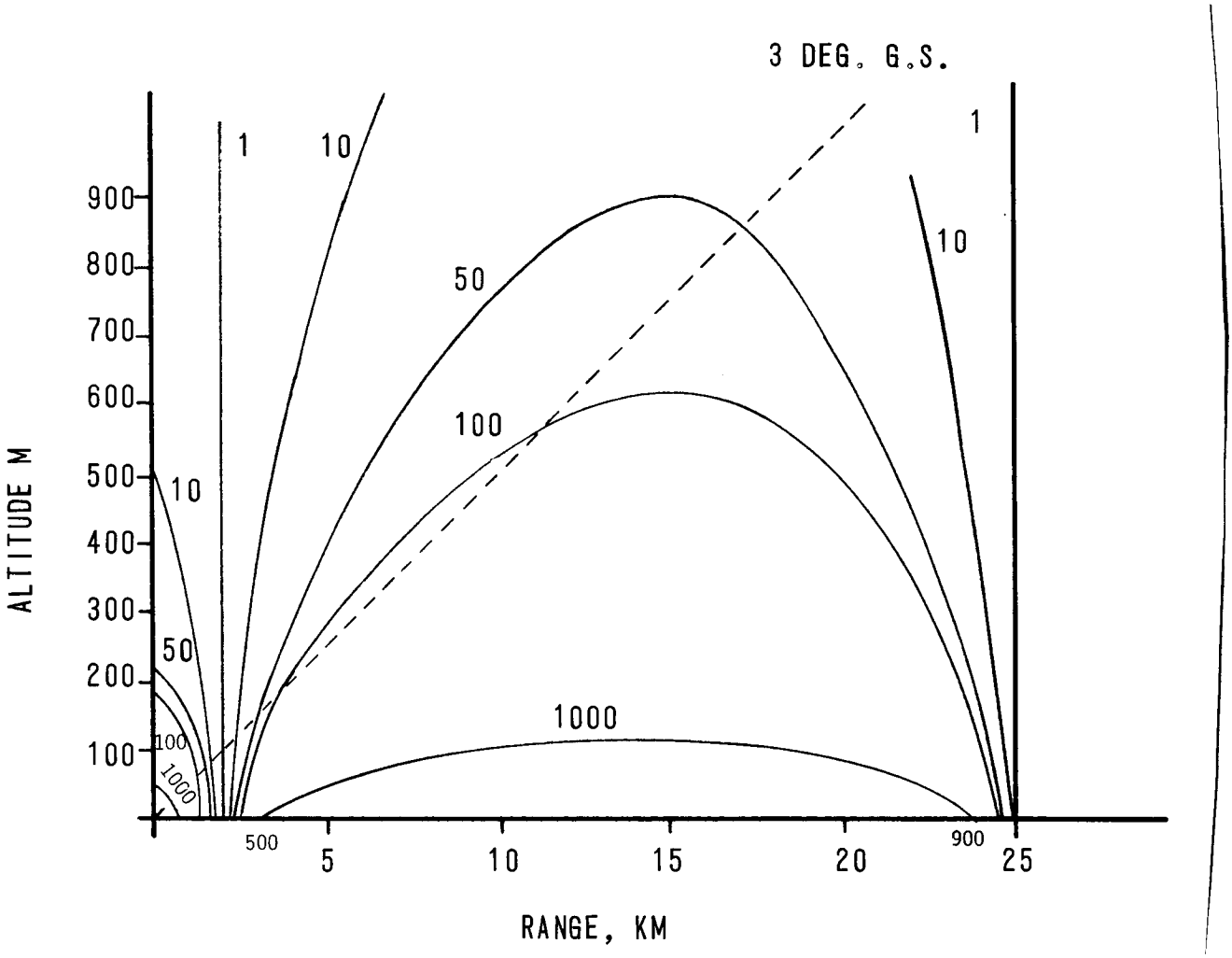

Figure 75. -- Altitude GDOP Proposed Six Beacon Layout

It can be seen from the figures that in the horizontal directions, GDOP values of less than one are easily obtainable with almost any beacon configuration, as long as the area of interest is contained inside the perimeter of the beacons. However, the altitude GDOP for even the six station system is significant. A three degree glide slope is drawn on Figure 75, showing that the standard deviation in ranging error will be multiplied by numbers up to about 10, with no GDOP values less than one appearing. Filtering and/or inertial aiding will reduce the impact of large altitude GDOP, however, the altitude accuracy is still the major problem area.

There are various techniques available to improve the altitude accuracy, including:

- o Barometric altimeters
- o Inertially aided barometric rate of climb sensors (IVSI)
- o Radar altimeters
- o Satellite beacons
- o Aircraft mounted beacons

Barometric altitude sensors are available with varying accuracy as a function of dollars up to the accuracy required at the threshold point (for example, the Honeywell DADS altimeter). Since a data link between the ground and the aircraft is implicit in any ground based multilateration system, compensation for local barometric pressure can be easily accomplished.

Altitude is measured essentially along one coordinate of a cartesian coordinate system tangent to the earth at the runway, such that the vector of the H matrix for the altimeter is

$$H_{alt} = \begin{bmatrix} 0 \\ 0 \\ 1 \end{bmatrix} \tag{87}$$

The system altitude accuracy is then a weighted average of the barometric altimeter accuracy and the multilateration altitude accuracy. If the barometric sensor accuracy is significantly greater than the multilateration accuracy, the overall system accuracy is essentially the accuracy of the barometric sensor in altitude. The accuracy in the horizontal plane is unaffected by the use of an external altitude reference according to this analysis. This is not true in practice, as the estimate of altitude is used to compute the horizontal position estimate. This crosscoupling of coordinates is a second order nonlinear effect, beyond the scope of the approximate techniques used here.

Instantaneous Vertical Speed Indicators (IVSI) are relatively inexpensive sensors which combined with an optimally filtered multilateration system could possibly yield adequate altitude accuracy. Analysis of this combination is extremely complex, and could easily be the subject of a study by itself.

The accuracy of radar altimeters relative to the ground is widely known. A recent U.S. Army requirement calls for a low cost altimeter with a 1m (3.3 ft) accuracy which is expected to be accomplished. If the control and computation for the system is ground based, a ground altitude map can easily be stored for compensation of radar altitude data to the reference coordinate system. As with the barometric sensor, the system altitude accuracy becomes essentially the altimeter accuracy and horizontal accuracy is unaffected to a first order approximation.

If one of the beacons is a satellite effectively directly overhead (or a series

of satellites such that the average effect is the same as a single satellite at the zenith), the altitude accuracy can become essentially the ranging accuracy of the satellite (GDOP approximately 1). Due to the effects of transmission through the ionosphere and the path loss along the extremely long transmission paths, it is unlikely that the ILM altitude accuracy requirements can be met by a single satellite using a simple modulation structure.

When an aircraft is being tracked by a multilateration system, its position becomes known to the system. The definition of a beacon is that it is a station in the multilateration system whose position is known. Therefore, once an aircraft is being tracked by the system, it can be used as a beacon for the location of other aircraft. Other aircraft can then be used for the location of the first, etc., and the system can bootstrap itself toward greater accuracy. This is the principle of the PLRACTRA system (Reference 38), built for the USAF by the Mitre Corporation. It has been demonstrated by flight test and extensive simulation that the concept is workable. The effect is to add a large number of beacons in random locations which smooths the GDOP contours, and improves the overall accuracy. Obviously, analysis of such a system is extremely complex, requiring detailed consideration of beacon location errors, statistics of aircraft availability, etc. A simple approximation is to ignore the effects of beacon aircraft position errors. Consider the 40km (21.6 nm) equilateral triangle system with the addition of three aircraft:

- An aircraft in cruise at 12km (39,370 ft) altitude, with x and y coordinates equal to 40km (21.6 nm).
- An aircraft making a go-around or DME circle approach at 2km (6562 ft) altitude, off to the side of the airport at 20km (10.8 nm).

- An aircraft on the glide slope, directly over the ground beacon at 26km (14 nm) from the airport.

The situation is depicted in Figure 76. The GDOP in the altitude direction along the glide slope is shown in Figure 77. Comparing Figure 77 with Figure 72, it can be seen that the addition of a small number of aircraft in less than optimum locations (optimum would be a high altitude aircraft directly above the runway) provides an immense increase in altitude accuracy. All of this increase is not realizable, since the beacon positions were assumed known and the aircraft beacons have position errors. The effect of bootstrapped tracking can be seen as a great improvement in the uniformity of accuracy.

GDOP Summary

For about any system configuration, the accuracy in any horizontal direction is about equal to and slightly greater than the basic ranging accuracy. A basic system of three stations arranged in an equilateral triangle multiplies ranging errors by numbers from 1/2 to 1, whereas a six beacon system can provide range error multipliers as low as 1/2 depending on the relative position of the aircraft and beacons.

At the low altitudes of ILM usage, the altitude range multipliers are on the order of 30 near the center of the equilateral triangle system, and multipliers on the order of 10 are common even in a six beacon system whose layout is optimized for altitude measuring. Bootstrapped tracking techniques can reduce the range multipliers for altitude to numbers on the order of 4 for an equilateral triangle beacon system if other aircraft are available to bootstrap against.

Satellite stations provide altitude accuracy on the order of the ranging error to the satellite, but this accuracy is not expected to be sufficient for ILM requirements.

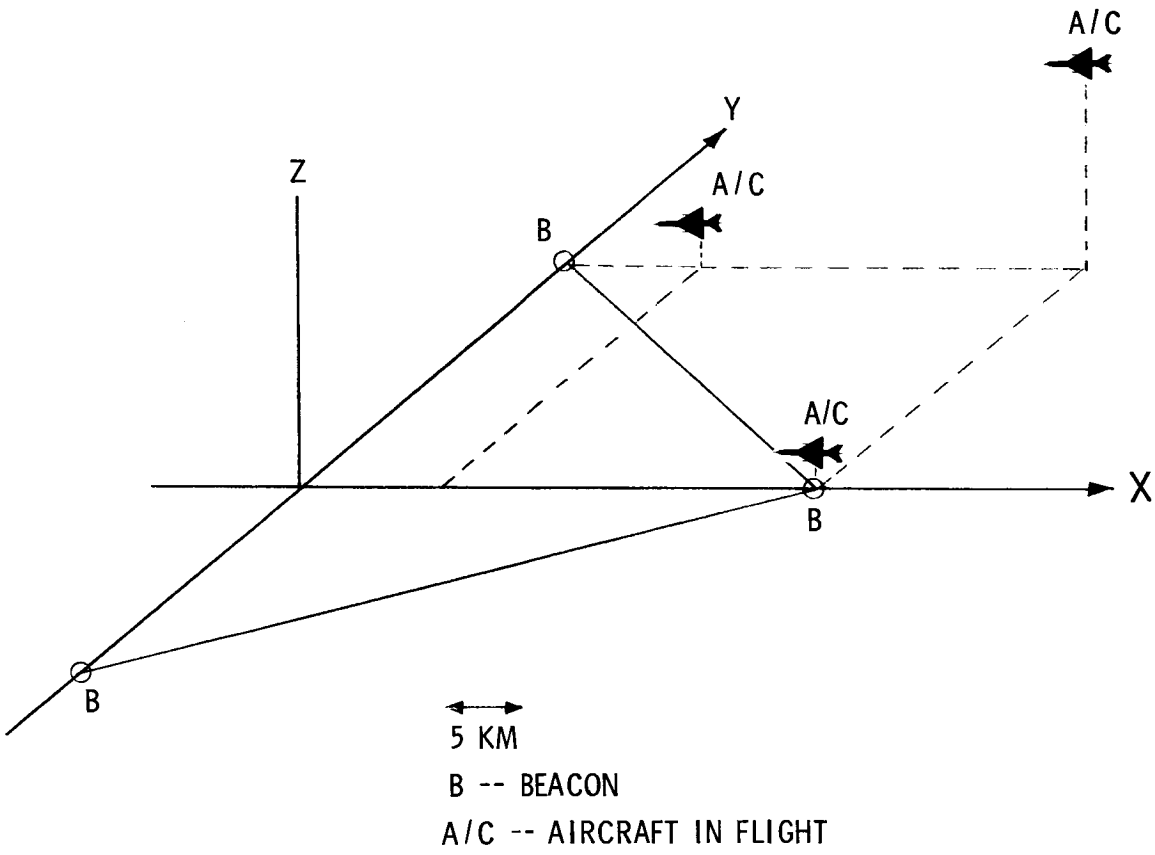

Figure 76 -- PLRACTA Beacon Layout

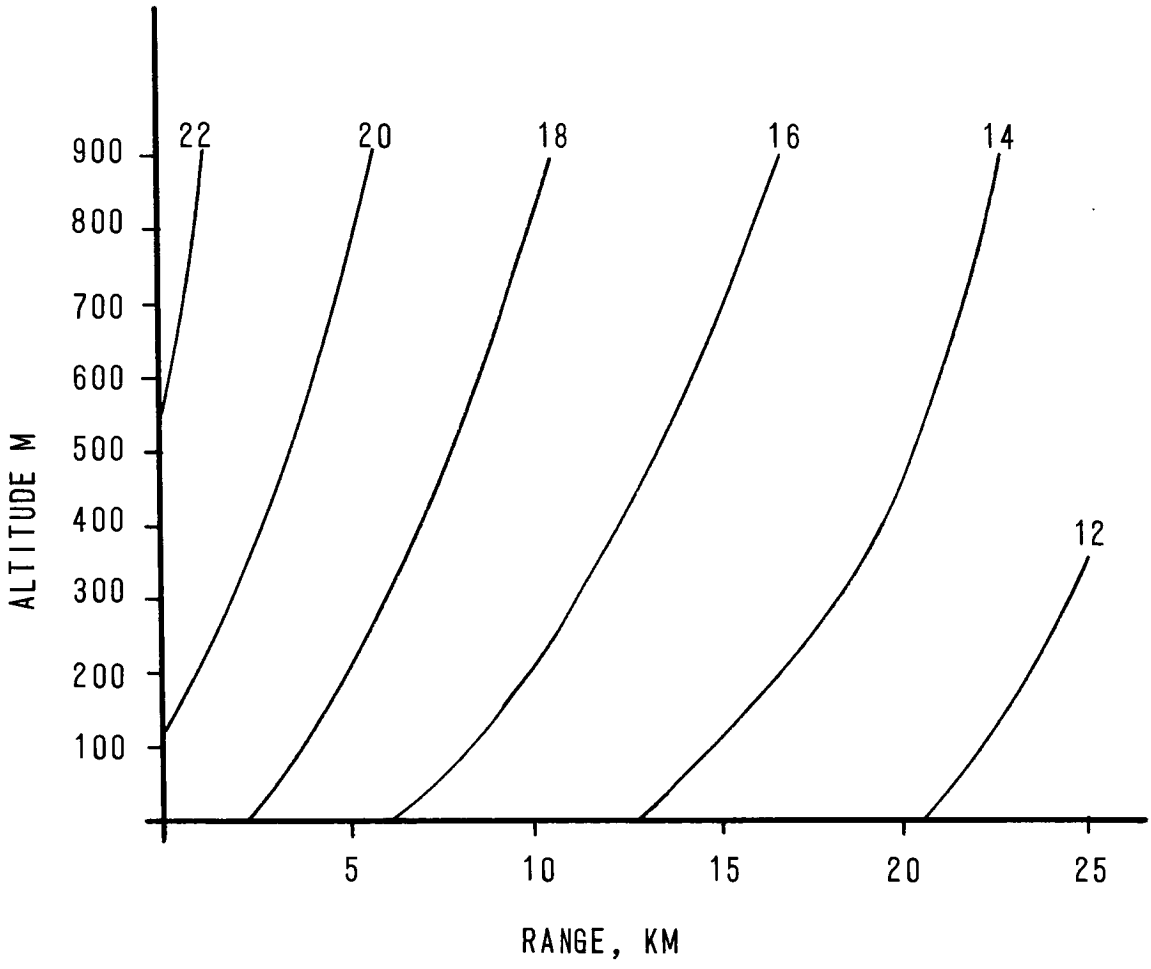

Figure 77 -- PLRACTA Altitude GDOP

It is therefore concluded that multilateration systems require some sort of external altitude reference to obtain ILM threshold accuracy. At 2km (1.1 nm) range, a 5m (16.4 ft) altitude accuracy is required. Using either satellites or bootstrapped tracking techniques with a 1.2m (3.9 ft) basic range accuracy can meet this requirement. However, external reference could provide the required 5m (16.4 ft) altitude accuracy more easily, reliably, and with less cost.

Appropriate external altitude references could be:

- o Radar altimeters, compensated by terrain maps stored on the ground
- o Barometric sensors
- o Combined barometric-inertial sensors (IVSI)

Since altitude is presumed to be externally supplied, the problem reduced to providing adequate horizontal accuracy. Extrapolating the results of Reference 34 and the equilateral triangle system, it can be estimated that horizontal coordinate single shot accuracy for a ground beacon system at the centroid of the beacons is approximately

$$\text{GDOP} \simeq \frac{1.5}{\sqrt{N}}$$

From this estimate, the requirements for ranging accuracy can be obtained.

Bootstrapped navigation provides an increase in the average system accuracy, but the possibility that only the landing aircraft is in the system prevents its use as a solution in all cases.

Filtering

Most of the significant errors in multilateration - quantization, multipath timing errors, etc. - are wide band noise type errors. Each range measurement error

is effectively independent of all the other range measurement errors and the magnitude of the errors is bounded. It can therefore be expected that filtering the multilateration data can provide a significant improvement in overall system accuracy.

Various filtering algorithms are available, which have accuracy somewhat dependent on their complexity (Reference 35). One of the algorithms for which a large amount of analysis has been performed is the Kalman filter. In general, a Kalman filtering algorithm utilizes a model of system dynamics to weight new measurements in a more optimal manner and to take advantage of the previous estimates in forming a new estimate, where the system is the aircraft.

For a ground based multilateration system, the direction of the aircraft axes is, in general, unknown. Therefore, the only dynamical equation which is of use is

$$\ddot{x} = a \tag{88}$$

Where x is the aircraft position

a is the aircraft acceleration

It is assumed that the intention of the pilot is to keep the acceleration zero, and simply fly down the glide path at constant velocity. The acceleration is then a noise disturbance, whose spectrum is determined by the pilot-aircraft response time and variance determined by the characteristics of the atmosphere. To a first approximation, the filter response can be determined by assuming the acceleration to be zero mean white noise. Assuming also the motion in each coordinate to be independent, a difference equation can be written for the aircraft motion in any single coordinate:

$$x_{n+1} = x_n + V_n T + 1/2\ a_n T^2 \tag{89}$$

$$V_{n+1} = V_n + a_n T \tag{90}$$

$$E(a_n) = E(a_n a_m) = 0 \tag{91}$$

$$E(a_n^2) = \sigma_a^2 \tag{92}$$

where x_{n+1} is the aircraft x coordinate at sample time n+1

v_n is the aircraft velocity in the x direction at time n

a_n is the acceleration in the x direction at time n

σ_a^2 is the variance of a

T is the time between samples

Assuming that measurements of that position coordinate are obtained, also corrupted by zero mean white noise, the performance of a Kalman filter has been fully analyzed (Reference 36). The results of the analysis are shown in Figure 78, where T and σ_a are as defined above and σ_x is the standard deviation of the position measurement.

Assuming that the sampling rate, position measuring accuracy, and expected levels of acceleration are matched, the improvement due to filtering can be computed. The system output sampling rate is required to be .1 second, so only sampling rates higher than this need be considered.

Figures 79 and 80 show the position accuracy as a function of sampling rate with acceleration level as a parameter, for various single shot position accuracy measurements. The figures show that even with an RMS acceleration rate of over 1g and a sampling rate as low as 10 samples/second, significant improvement in accuracy can be made via filtering. The accuracy can be seen to be approximately proportional to sampling rate. The variances shown in the figure are the apriori variances, or the variance of position estimation immediately before taking a

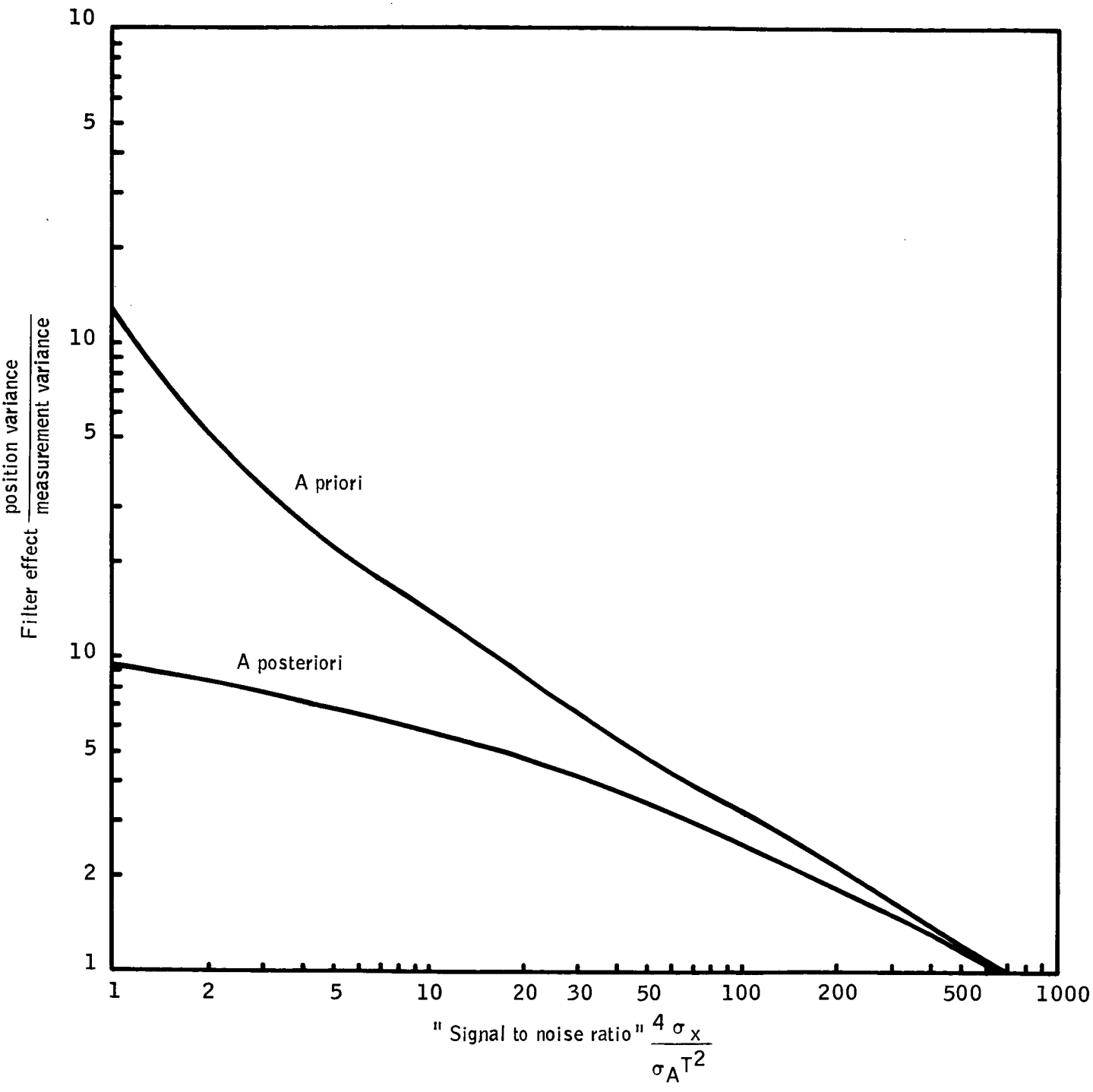

Figure 78-- Effect of Kalman Filter

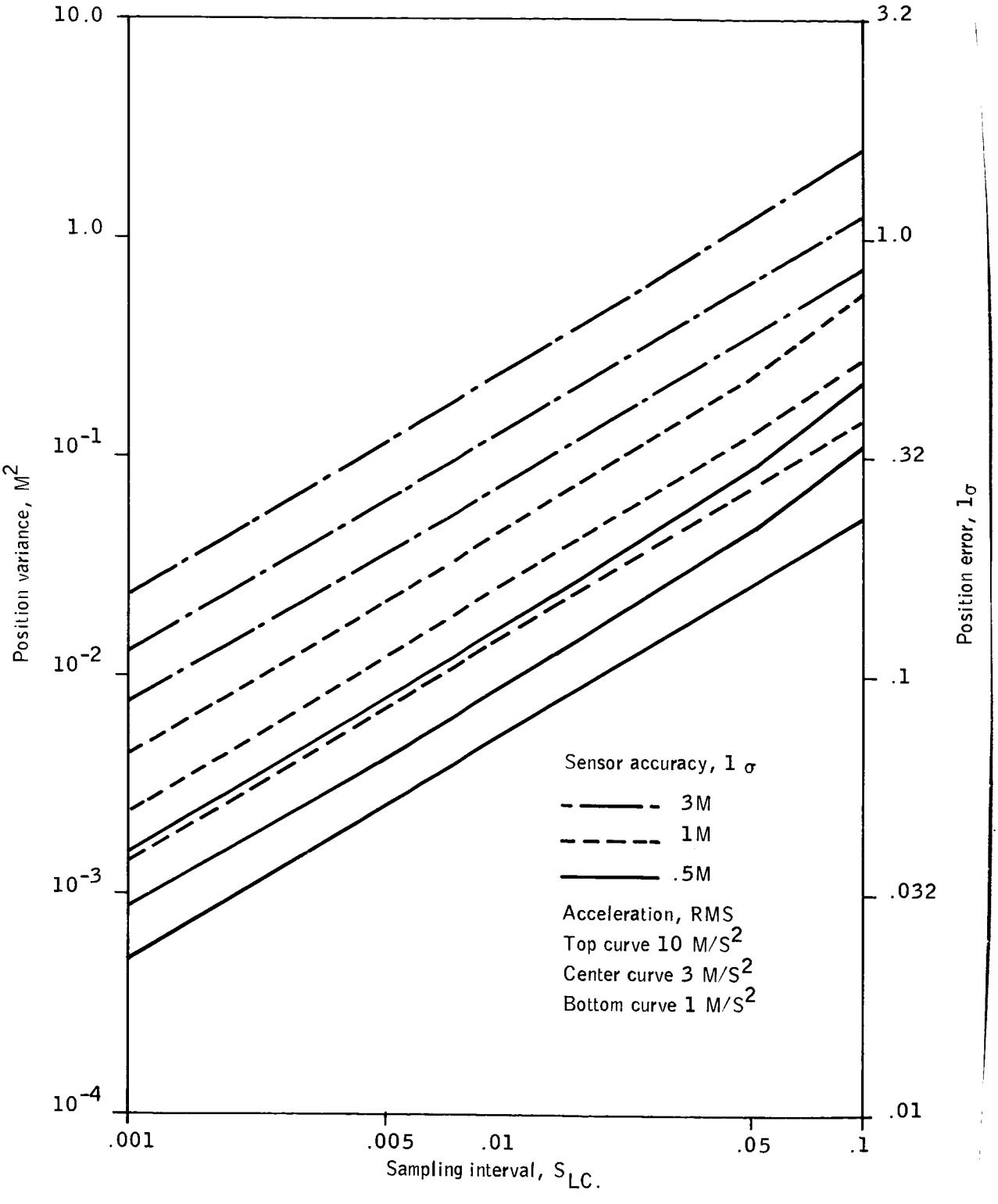

Figure 79 -- Effect of Optimum Filtering

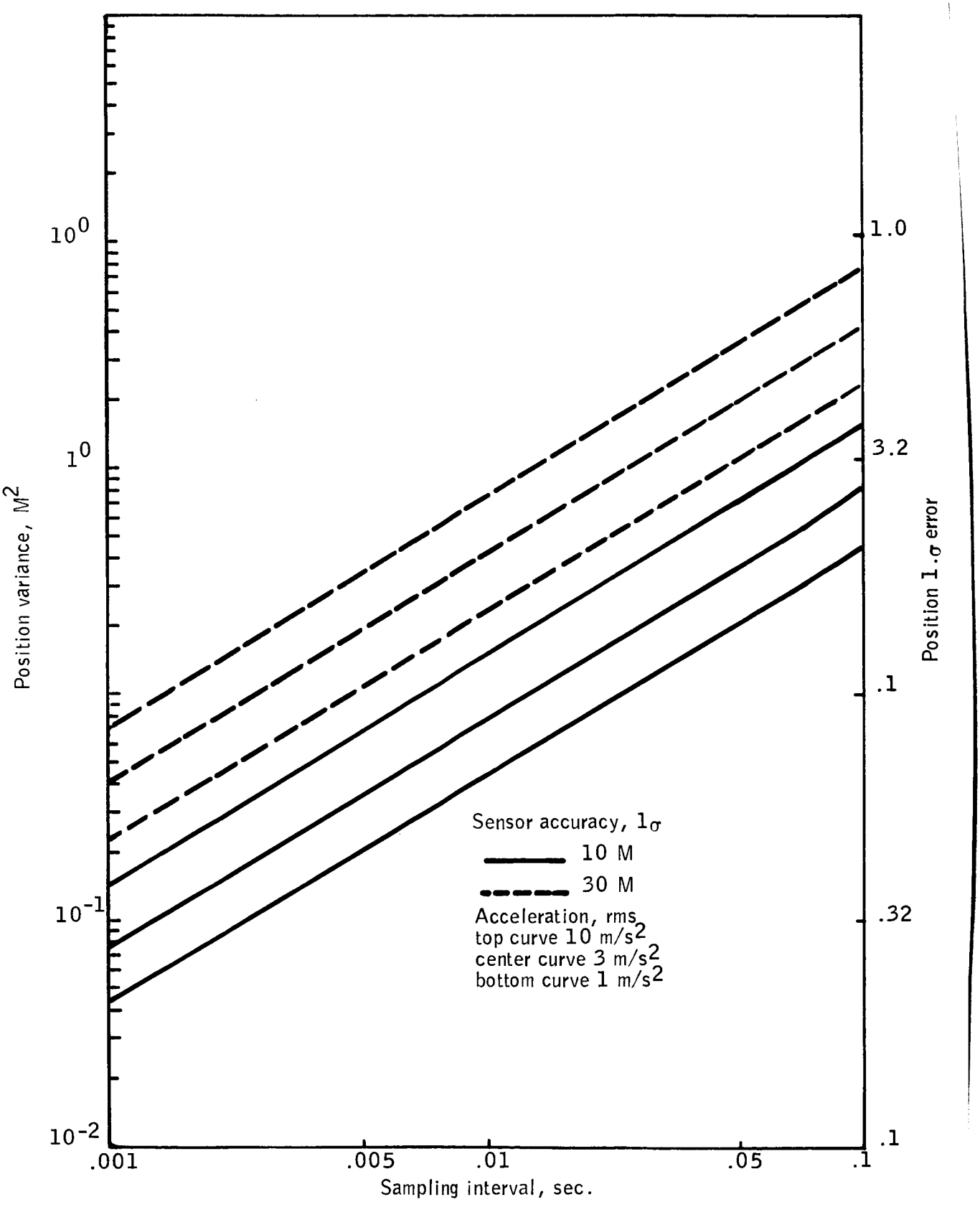

Figure 80 -- Effect of Optimal Filtering (Contd)

new measurement. Immediately after taking a measurement the accuracy would be better, but only slightly so at the sample rates investigated.

The various assumptions of the simplified analysis of Reference 36 prevent a real system from obtaining the improvement shown here. The assumptions are:

- o Acceleration noise is white
- o The system knows what the variances of measurement and acceleration are
- o There are no biases of either measurement or acceleration
- o The system coordinates are independent
- o The sampling rate is matched to the sensor accuracy and acceleration level.

The last assumption is easily met with any of the sampling rates used here, as significant improvement due to filtering is obtained. None of the other assumptions can be satisfied. The effect of non-white noise is to reduce the improvement of accuracy at the higher sampling rates. At very high sampling rates, the accelerations present appear as time varying biases. The system cannot know what the true variances of the disturbances are, but adaptive techniques are available which can estimate them. In any case, the filter variance values must be set for slightly greater disturbance than actually exists to prevent filter divergence and the accuracy depends more heavily on the assumed value than the actual value. Measurement biases are not affected by filtering, and they feed through the filter directly to appear as position errors. Acceleration biases cause a build-up of position error, the asymptotic value of which is approximated by (Reference 33)

$$\bar{x} \cong \frac{T}{H K_v} \bar{a} \tag{93}$$

Where $\bar{x}$ is the position bias error

$\bar{a}$ is the acceleration bias

T is the sample interval

H is the measurement sensitivity

K_v is a filter gain depending on the assumed disturbance variances

There is an apparent design trade-off between position variance and asymptotic bias values, since position variance is somewhat proportional to filter gains. From the figures on variance and the bias equation, it can be seen that filter performance is proportional to sample rate, regardless of the characteristics of the disturbances.

Summary

Position filtering is an effective technique to reduce the effect of noise type errors in a multilateration system. Accuracy improvement on the order of two to one can be expected with a 10 sample per second sampling rate, or on the order of 10 to one with a 100 sample per second rate. Faster sampling directly yields higher accuracy in both variance reduction and filter lag due to acceleration.

The maximum ILM accuracy requirement is for 4.25m (13.7 ft) in azimuth, .55m (1.8 ft) in altitude, and 12.2m (40 ft) in ILM range at the GPIP degrading out along the glide path. The GPIP altitude requirement cannot be met with any multilateration system. The best geometrical relationship investigated was the PLRACTRA concept in which the availability of beacons was a statistical function. Even in this concept, GDOP values on the order of 4 were found, yielding a range

requirement (after filtering) of .15m (.5 ft). Bias errors alone can be expected to be larger than this. Other multilateration concepts had larger GDOP values, and therefore would require more accurate ranging.

Except for altitude, the accuracy requirements are easily met. For example, consider a system with the following parameters:

- o Pulse rise time - 100 ns
- o Clock frequency - 50 MHz
- o Uncompensated bias errors - .5 m (1.6 ft)
- o Beacons in 40 km (21.6 nm) equilateral triangle

With the runway set on one of the beacon baselines as shown in Figure 81, the azimuth GDOP is .5 and the ILM range GDOP is 1. Thus, if azimuth accuracy of 4.25m (13.9 ft) is obtained, 8.5m (27.9 ft) ILM range accuracy follows. Also, the system range accuracy must be 8.5m or better.

The variance in range due to thermal noise, from equation 93 is

$$\sigma_N^2 = \frac{100^2}{2 \times 1000} = 5 \text{ nsec}^2 \tag{94}$$

The variance due to multipath has been previously shown to be $(3.67\text{m})^2$ or $\sigma_M^2 = 121 \text{ nsec}^2$. The quantization noise from equation 92 is

$$\sigma_Q^2 = \frac{1}{6(f_{clock})^2} = 66.7 \text{ nsec}^2 \tag{95}$$

The total variance is then

$$\sigma_R^2 = \sigma_N^2 + \sigma_M^2 + \sigma_Q^2 = 192.7 \text{ nsec}^2 \tag{96}$$

which yields a standard deviation of 13.9 nsec. This corresponds to a range

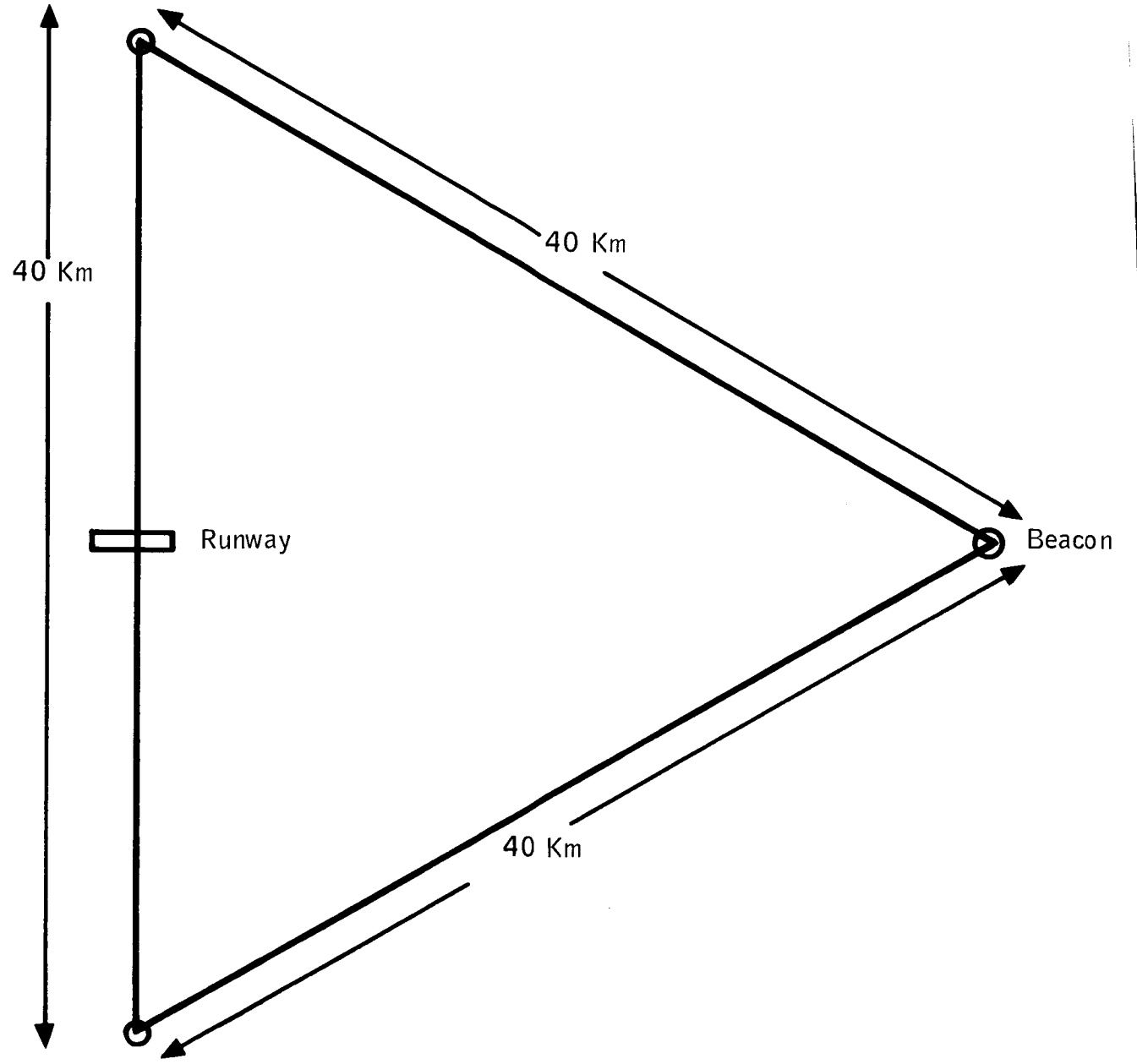

Figure 81 -- ILM Multilateration Layout

standard deviation of 4.65m (15.3 ft). A two sigma range noise of 9.3m (30.5 ft) is obtained without any filtering. Sampling at 10 samples per second, the minimum rate considered, results in approximately a two to one accuracy increase, yielding a filtered two sigma range accuracy of 4.65m (15.3 ft). Root sum squaring with the bias error yields an overall accuracy of 4.68m (15.4 ft), well within the required value of 8.5m (27.9 ft) overall accuracy.

Examining the noise components, it can be seen that the dominant error source by far is the multipath error. Since this error is essentially uncontrollable, it forms a basis for system accuracy. Thermal noise is obviously completely insignificant, such that the signal-to-noise specification could be relaxed if necessary; however, 30 dB at close range is not difficult to obtain. The clock quantization is significant but not dominant. Relaxing the clock specification to a 30 MHz clock results in a range variance on the order of 320 $nsec^2$, or an unfiltered standard deviation of 5.95m (19.5 ft), which still meets the requirements with a 10 sample per second filter.

The system parameters were specifically chosen to be extremely simple to mechanize. The standard ATCRBS transponder has a pulse rise time of 100 nsec. A modification to fit into a multilateration interrogation discipline and to provide real time bias correction could be easily accomplished. Ground interrogators could also use modified transponders with simple omnidirectional antennas, and 50 MHz logic is easily obtainable.

The only failing of a multilateration system is its inability to meet the altitude specification. Satellite systems can provide altitude GDOP values on the order of 1, but down link signal to noise ratio and ionospheric propagation

problems seem to limit ranging accuracy to the order of 6m (19.7 ft) (Reference 34).

The detailed effect of filtering and crosscoupling between coordinates has not been studied. Since the accuracy in the horizontal plane is much greater than the vertical accuracy, the crosscoupling would transfer some of the horizontal accuracy into the vertical plane. In system layouts such as the six beacon altitude optimized system described where some beacons exist primarily to obtain altitude fixes, filtering would prevent accuracy degradation from occurring at the rate of GDOP increase. Both of these effects tend to predict more accuracy than this analysis shows; however, .55m (1.8 ft) altitude accuracy is not obtainable.

External altitude sensors, operating in conjunction with a multilateration system, can provide much greater altitude accuracy than can the multilateration system alone, regardless of beacon geometry. Further study is required to determine the detailed requirements for such altitude sensors.

NUCLEAR SENSOR CAPABILITIES

Currently, efforts are being conducted by several organizations to evaluate the potential of nuclear landing guidance systems. These systems use an airborne radiation detector (gamma rays) and a ground based nuclear radiation source. The potential capabilities of these systems arise out of the accuracies of using high frequency radiation and the insensitivity of the propagation to weather conditions.

Three possible nuclear landing guidance systems are described in this subsection.

The Hermes system (Reference 39) uses a large number of nuclear sources located along the approach to the runway. An airborne digital processor is required to process the coded data received by the detector. The NILS (Reference 40) uses four sources placed near the runway and a mechanical shutter mechanism to modulate the radiation. A NASA program (Reference 41) investigated the feasibility of using very weak radiation sources to determine aircraft position on the runway.

Hermes

This concept was conceived and developed by the Norweigian Defense Research Establishment (NDRE). It is based upon the establishment and detection of a coded pattern of gamma radiation from radioactive sources. A flight corridor is defined by a stationary pattern of low intensity gamma radiation. The pattern is formed by shielding the sources with accurately slitted collimators so that the beams escaping through the slits form V-shaped wedges of different thickness, separation and orientation.

No moving parts are required in these ground emplacements. The radiation pattern is oriented essentially vertically and across the flight direction so that an approaching aircraft will fly through the planes defined by the radiation. Typically the corridor will extend to 4000 to 6000 meters from the runway threshold.

The airborne equipment consists of one or two plastic scintillator detectors (a dome of scintillation material and photomultipliers to count the flashes), an analog-to-digital converter and a small data processor. Thus, as the aircraft flies through the planes of radiation, the detector measures the energy levels (with respect to time) and the computer decodes the information and determines the aircraft location.

The system data rate is 0.2 Hz at 6000 meters and 90 knots and 5 Hz near the runway at 90 knots. Higher aircraft speeds result in higher data rates. Typical accuracies (Reference 39) are quoted as two sigma and include systematic random errors,

Errors	At Runway	At 3 nm (5.5 km)
X (longitudinal)	4 m (13 ft)	10 m (32.8 ft)
Y (lateral)	0.2 m (.66 ft)	10 m (32.8 ft)
Z (height)	0.2 m (.66 ft)	10 m (32.8 ft)

A major disadvantage of the Hermes system described in Reference 39, is that a large number of radioactive sources (approximately 50) must be used and some must be placed along the extension of the runway centerline out to 6 km from the runway. Thus, in the case of most commercial airports, these facilities would have to be located outside the airport boundaries and probably in residential areas.

Reference 39 states that the radiation sources should have source strengths of 100-400 curies depending upon location. In addition, detections are claimed to occur at ranges of over 610 meters (2000 feet).

The recommended radioactive sources are C_o^{60}. It can be manufactured at relatively low cost, it has a half-life of 5 years permitting low maintenance costs, and it has good mechanical properties with a high melting point with good corrosion resistance. Source dimension constraints and handling requirements limit the source activity to approximately 400 curies. The C_o^{60} radiates gamma rays with energies of 1.17 and 1.33 MeV.

The effect of weather on the nuclear landing system is primarily due to variations in the water molecule content in the line-of-sight path between signal source and sensor. The gamma radiation is attenuated exponentially in passing through matter as expressed by the following beam intensity equation:

$$I = I_o e^{-ax} \tag{97}$$

For 1 MeV gamma rays (Cobalt 60 radiates gammas of 1.17 and 1.33 MeV) the thickness of water necessary to reduce the intensity by 0.5 is 11.4 cm (4.5 inches). If we consider 100°F and 100% relative humidity as a worst case weather condition, we have approximately 5 precipitable centimeters of water per km. This corresponds to a maximum intensity variation in one km due to weather of I/Io = 0.74. Due to nuclear source size constraints one km is approximately the maximum operational range for source to sensor distance. Thus, as can be seen, design of the system to cover the full range of weather environments is a minor task.

Nuclear Instrument Landing System (NILS)

This concept was developed and evaluated by R. A. Kaminskas of TRW. It is based on the establishment of a glideslope and localizer by using four gamma ray sources (C_o^{60}) located near the runway. The radiation from these sources is modulated by a mechanical shutter apparatus so that each source radiates energy pulses with a different frequency.

The NILS concept establishes a fixed glideslope/localizer beam in the approach pattern. The approaching aircraft derives its guidance information by comparing signal amplitudes of the beacons and driving toward a zero difference in amplitude to be on the beam. The concept does not include any capability for range to touchdown or stop end of runway measurements.

The radiation detector consists of a scintillation dome and photomultiplier tube. The electronics separate the four frequencies from the four sources and the signal levels are compared. The error signal is then displayed on the standard ILS indicator or flight director.

Reference 40 states that the prototype system tested provided accurate guidance from 926m (1/2 nm) out to touchdown, and for rollout for 1390m (3/4 nm) of runway. These ranges are realized using a 115 curie source strength. Detection at the middle marker (1056m or 3500 feet) was a system requirement that apparently was not achieved since a 350 curie source strength is recommended to meet that requirement.

Several serious problems did arise in the test program. The construction of absorber-shutter-slit combinations to give the desired location-energy relationship to meet the specified system accuracy requirements proved to be impossible within the scope of the study. It may be feasible to correct this with a more elaborate design. However, the use of amplitude comparisons between sources puts requirements on alignment and balancing of signal strength that are extremely difficult to meet. Large initial errors in location caused inverted response in the display (wrong direction for correction). This condition was corrected during the flight test through logic on the processed signals. An operational system will require a more complex set of logic to assure that an aircraft on approach has acquired the localizer and glideslope.

In-Runway Radiation Sources

In a project to determine the feasibility of using very weak radiation sources to determine aircraft runway position, radiation sources of 10 millicurie source

strength were implanted in a runway. As described in Reference 41, these sources were detected reliably at altitudes of up to 15 meters (50 feet). Reliable detection in this case represented a signal/background ratio of 2.5/1.

Conclusions

The data available on the use of nuclear radiation sources and detectors as an Independent Landing Monitor is summarized in the following way. Using the NASA test results as a baseline, a relationship between source strength and detection range is developed based on the $1/R^2$ radiation law. That is, if detection at 15 meters (50 feet) requires 10 millicuries, detection at 152 meters (500 feet) (10x) requires 1 curie (100x). In Figure 82 the heavy curved line is a plot of this relationship. The data from the other two papers is then superimposed on this curve. Reference 39 (NDRE) implies that 400 curies are required for altitudes over 610 meters (2000 feet). Although data is plotted only to 427 meters (1400 feet), Reference 40 (TRW) implies that 115 curies give 795 meter (2600 foot) ranges and 350 curies would give 1070 meter (3500 foot) ranges.

Thus, this data indicates that for radiation source strengths on the order of 400 curies, detection would occur at ranges beyond the 1000 meter minimum effective range (MER). Dependent on the signal processing efficiency, location of the sensors in the aircraft and background radiation levels (both from A/C cargo and natural) ranges to 3000 meters should be achievable.

The effects of weather on the nuclear sensing systems are near negligible. Worst case attenuation is approximately 2.85 db/km.

Although not repeated here, analysis in each of References 39, 40 and 41 show that radiation hazards to landing aircraft, crew and passengers are orders of

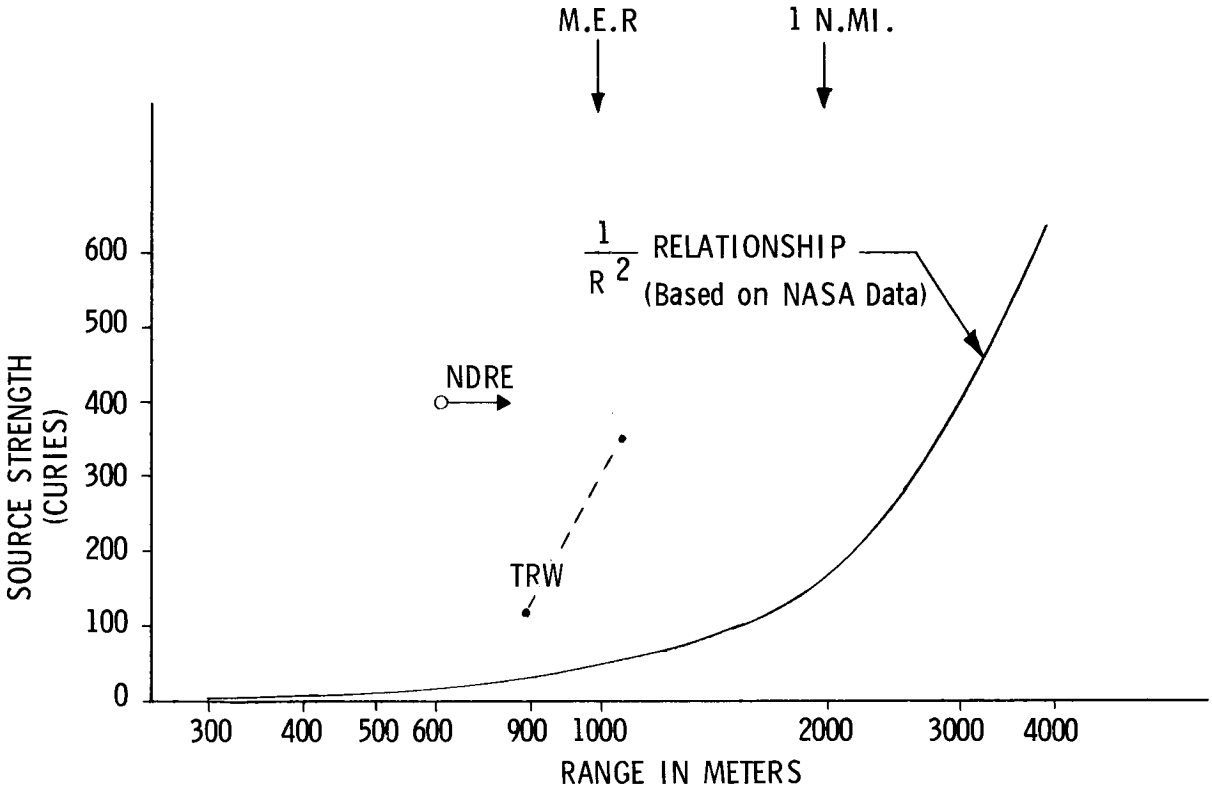

Figure 82 -- Gamma Ray Source Strength vs Range

magnitude less than normal yearly exposures to natural gamma radiation. Precautions must be taken to limit access around the sources on the ground and to assure proper handling of the radioactive materials. This type of constraint tends to limit location of the nuclear sources to controlled access airport property.

Each of the three nuclear landing aids reviewed have potential feasibility for meeting parts of the ILM requirements. The Hermes system, designed as a primary landing aide using more than 50 radiating sources, can probably be simplified significantly and still meet the functional requirements for ILM. More development and testing is required on the NILS to prove beam amplitude shaping can be adequately achieved to balance the beacon signals through the required range of operation. In addition, more sources will be required to cover the minimum range for ILM from prior to decision height to the stop end of the runway (nominally 14,000 feet range).

ILM SENSING CAPABILITIES - REDUNDANT MLS

The Microwave Landing System (MLS) currently in development under FAA sponsorship is expected to be the primary automatic guidance system for aircraft landings in the next decade. Four contracting teams have developed competing systems to meet the MLS requirements defined in Reference 42.

Extensive documentation is available on the characteristics of the four competing systems. Thus, detailed descriptions of the MLS will not be repeated here. Each of the competing concepts have demonstrated through their feasibility studies and flight tests that they approximately meet the requirements as defined in Reference 42.

The K configuration of the MLS is being designed to provide Category III landing capability for commercial transport systems. This configuration includes a high level of redundancy to provide a fail safe, fail operational system for Category III landings. Thus, it will fulfill some of the functions required of an Independent Landing Monitor.

Block diagrams for the ground and airborne configuration K Category III system are shown in Figures 83 and 85. Pictorials of the equipment are shown in Figure 84 and 86. As can be noted in Figure 83 the ground system uses dual redundancy on essentially all of the electronics with extensive monitoring of the outputs. Single highly reliable antennas are used for each function. The airborne configuration is a dual redundant system with additional redundancy internal to each of the channels. Through comparison of the outputs, the remaining operational channel can be selected on single failures in the system. The fail operational MLS can provide guidance to touchdown and through rollout without the need for an additional Independent Landing Monitor. It will, to a high degree of reliability, still provide guidance to the pilot after single point failures.

The MLS as presently configured does not include provision for obstacle detection on the runway nor does it provide for real world image displays.

The sensor requirements for the ILM concepts were based on the MLS requirements for accuracy, data rate, effective range and coverage. Therefore, by definition the MLS meets the requirements in these areas. It should be noted that the range of the MLS is to 30 nm. Feasibility flight tests and analyses on these systems (Reference 43) have shown they are capable of this range under degraded weather conditions. The major meteorological condition, affecting the MLS operating at

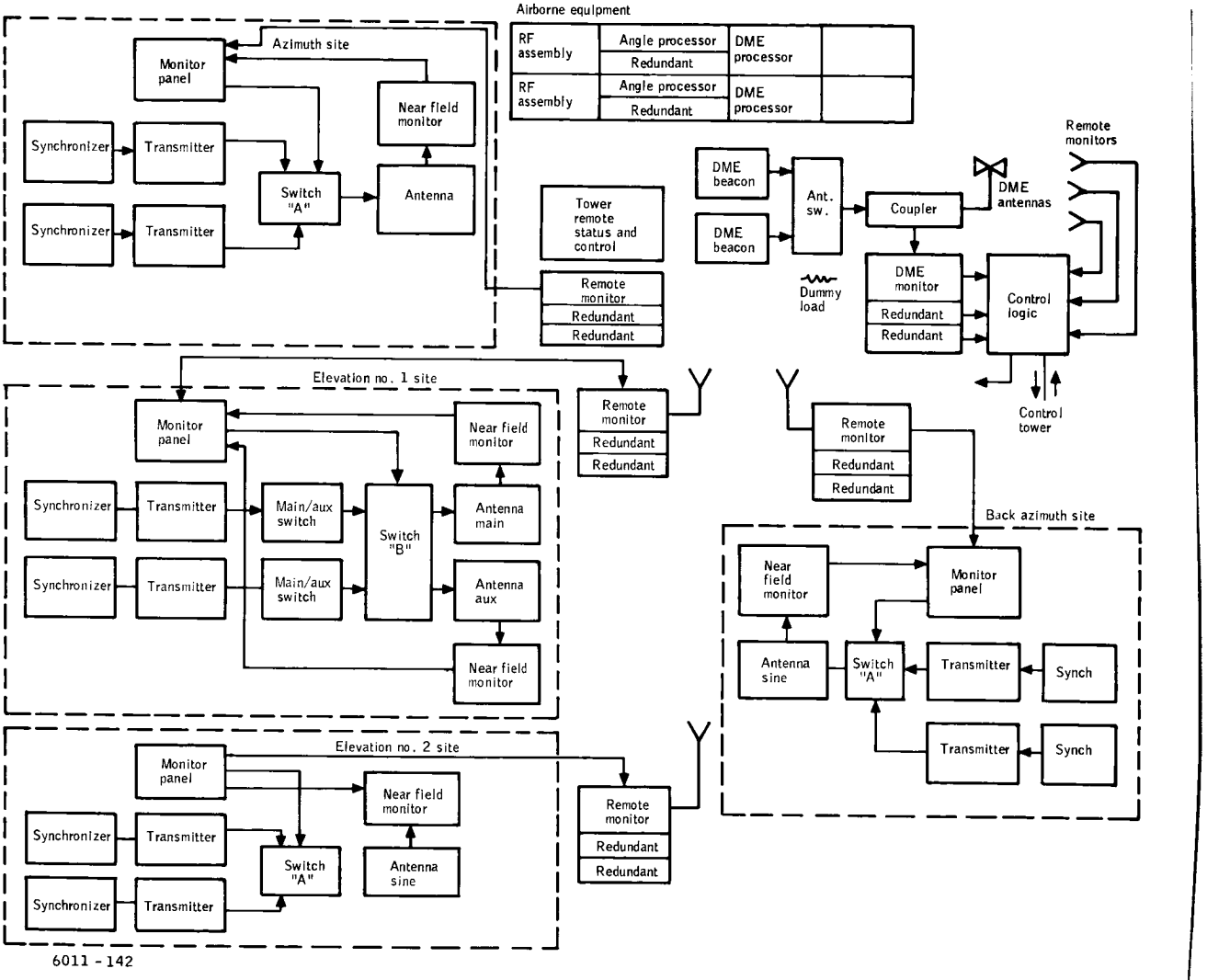

Figure 83 -- System Block Diagram Category III

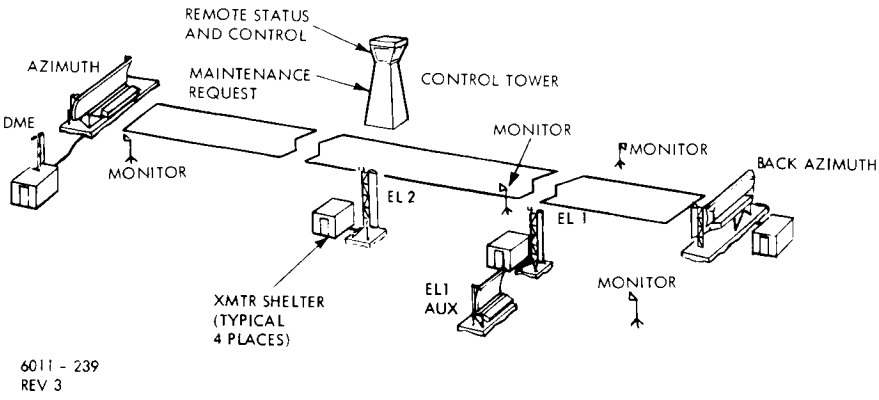

4-1

Figure 84 -- Siting Diagram, Category III

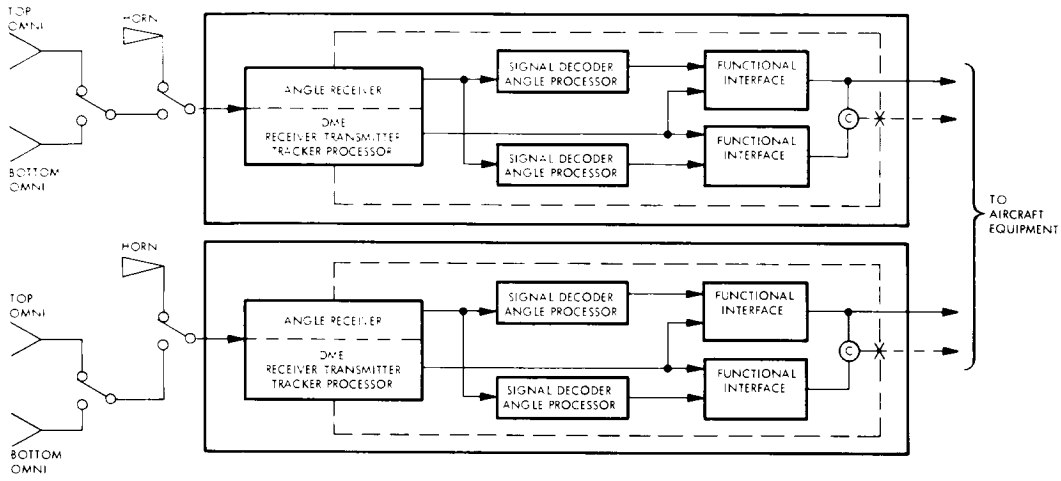

5-1

Figure 85 -- Block Diagram of Airborne Equipment, Category III

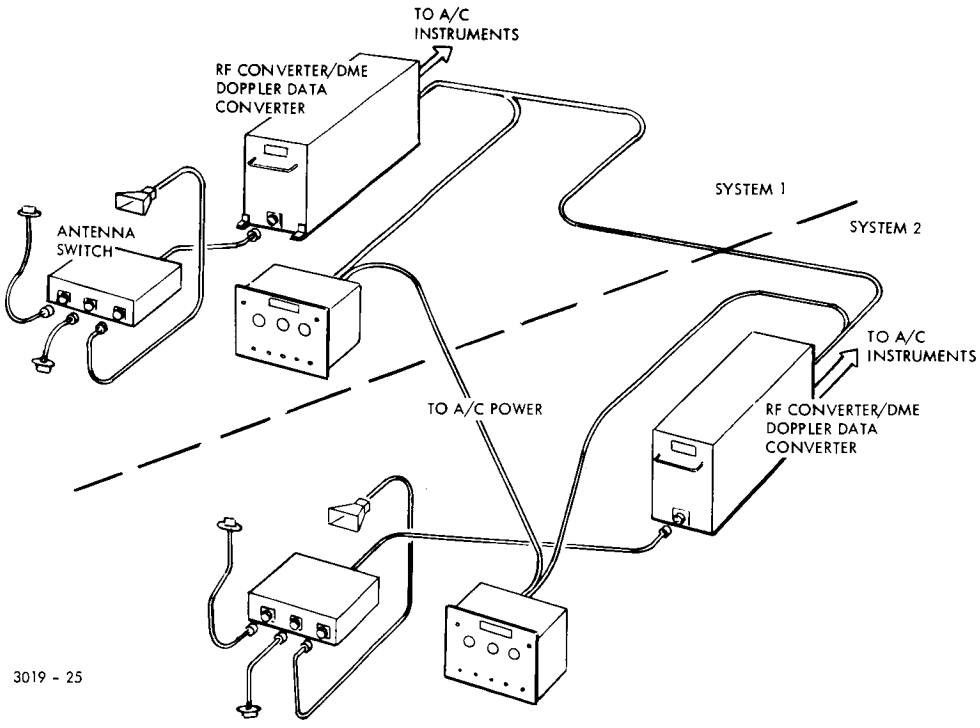

Figure 86-- Pictorial of Airborne Equipment, Category III

C-Band, is rain. The Category III K configuration of the MLS must supply coverage to 30 nm (46 kilometers) in up to 50 mm per hour of rain. Thus, the effective range of 8 nautical miles for the ILM functions can be considered to be fully met with the MLS.

The current studies for MLS design are considering the sensing concept only and do not cover the displays and controls required for the system. The MLS provides outputs which could be compatible with current flight directors or could be used to generate synthetic perspective image displays or other symbolic types of displays. Typical interfacing circuits and outputs (necessary addition for curved and segmented path following) from one of the MLS concepts (Reference 44) are shown in Figures 87 and 88.

The MLS system consists of air derived azimuth/elevation angle equipment and ground derived range equipment. The angle information is a one-way ground-to-air transmission with essentially no limit on the number of aircraft to which it can supply guidance information. The DME equipment has a limit on traffic capacity. The configuration described in References 43 and 44 has provisions to service 83 aircraft with dual transponders which are directly interfering by operating on channel and on code. The traffic model further provides for 400 transponders which are on frequency but off code. This capacity is considered to be adequate through this century.

Feasibility model flight tests and analyses described in Reference 43 have uncovered no significant problems with interference from other airborne equipments or ground radars. Analyses indicate the MLS and ILS can be compatibly sited at the same runways during periods of changeover from one guidance system to another.

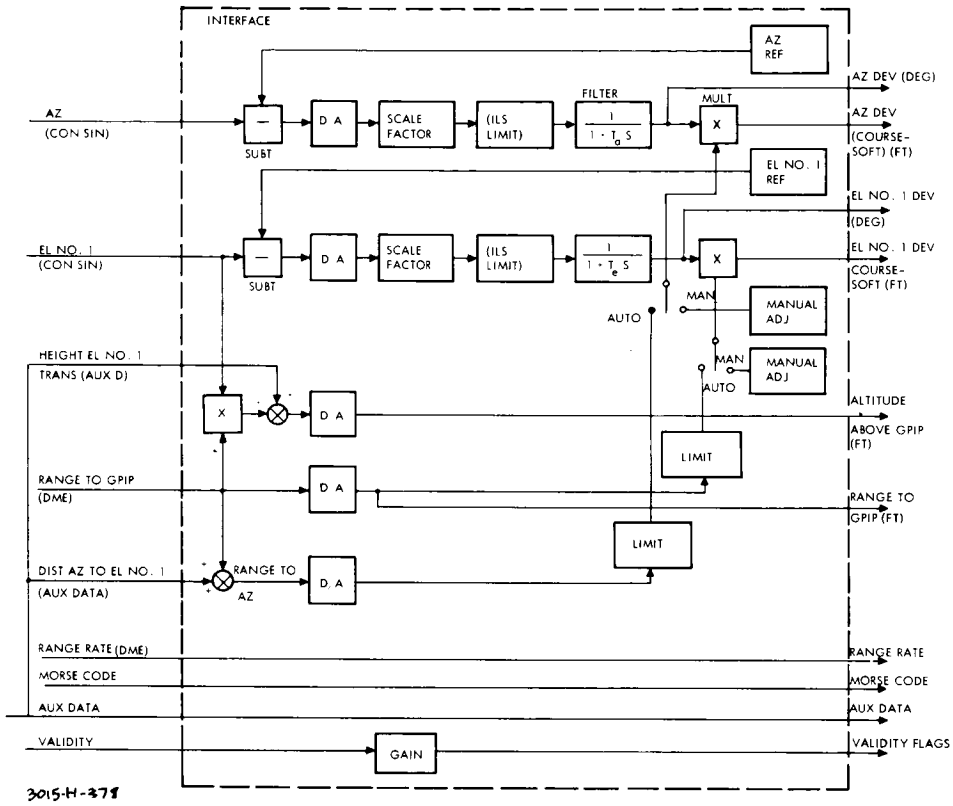

Figure 87 -- Block Diagram of Interface Circuits

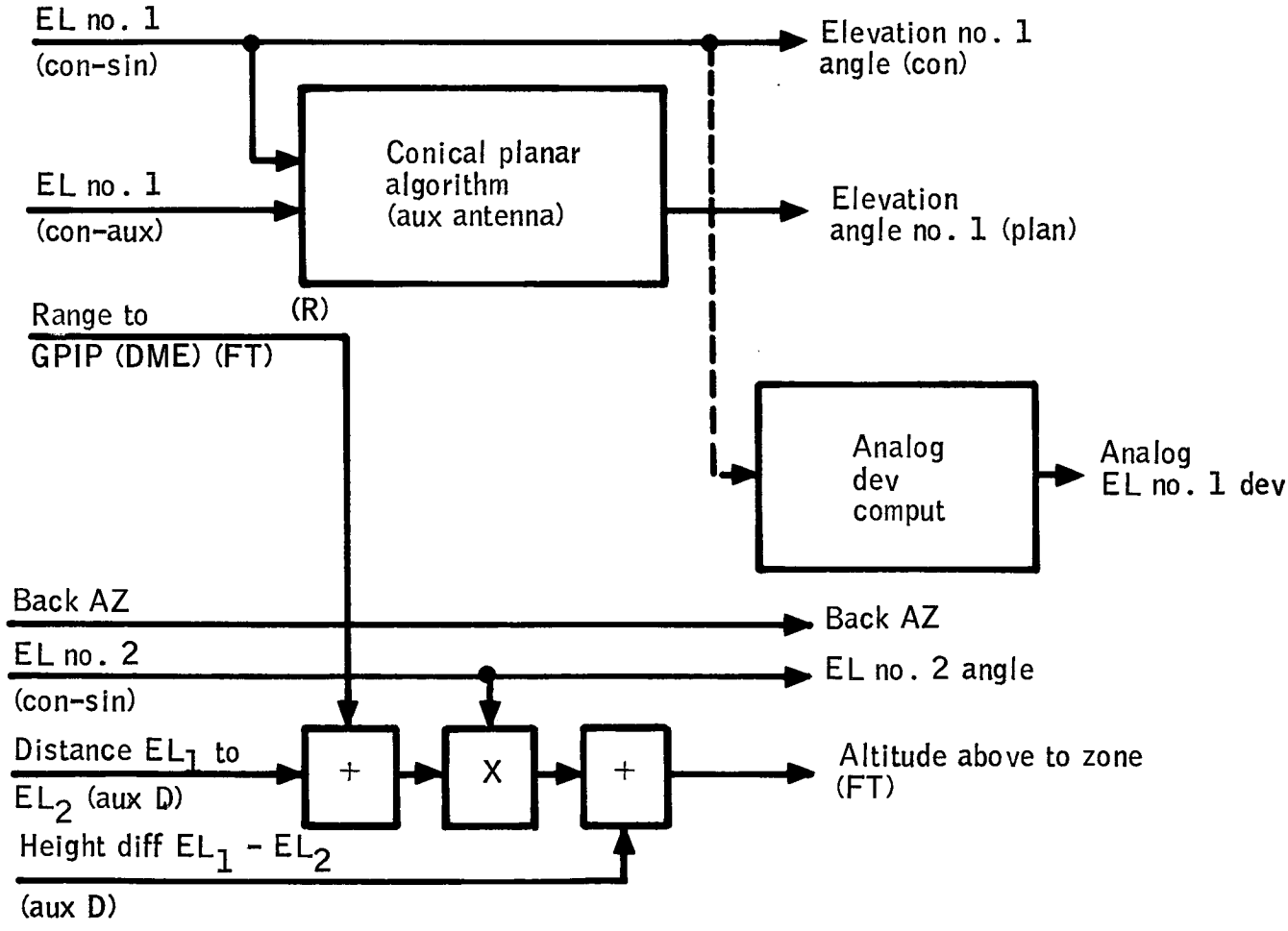

Figure 88-- Block Diagram of Interface Circuits

Cost figures for the various MLS configurations have been generated by each of the contractors and, according to reports, differ by negligible amounts. Using figures based on 1974 dollars, the acquisition cost of units averaged over the first five years of production and excluding installation and non-recurring costs, the selling price of configuration K, Category III fail-operational airborne receivers is $22,000/system. The selling price of a configuration G, Category II, fail-passive airborne receiver is $8,000/system. The difference between these units represents the approximate cost of redundancy in the airborne MLS equipment to upgrade from fail-passive to fail-operational capability.

The selling price estimate for the configuration K ground system is approximately $488,000/system excluding installation and non-recurring costs. A direct cost estimate for a "fail passive" ground configuration is not available, however, preliminary estimates indicate it would be approximately 3/4 of the full configuration K cost or $366,000.

The above cost figures are based on 1974 values and do not include inflation factors. The figures for the airborne units are for MLS equipment only and do not include new displays, display generators or new flight control interfacing equipment necessary to follow curved and segmented approach paths.

A brief physical description and discussion of the performance characteristics of the airborne equipment for a Configuration K system is given in Appendix F. This description is of one of the four systems which were competing for the MLS design. However, physical and performance parameters were reputed to be nearly identical for all systems.

TV SENSOR CAPABILITIES

A television system is comprised of optics, a camera tube, electronics for signal processing and a display. The optical subsystem images the object scene onto the photocathode of the camera tube. The camera tube converts the image to a temporal electrical signal which is processed and amplified by appropriate electronics. The display, typically a cathode ray tube, reconverts the temporal electrical signal to an optical range.

Advances in television tube state-of-the-art, such as image orthicons with MgO targets and SEC vidicons, provide sufficient sensitivity for operation under low ambient lighting conditions. Additional sensitivity can be achieved by inserting one or more stages of electro-optical image intensification between the optics and the camera tube. The combination of image-intensifiers and camera tubes provides a true low light level television system. However, as discussed in this report, the performance of such systems at extremely low light levels (e.g., starlight at 10^{-4} foot candles) is ultimately limited by photon noise at the photocathode of the first intensifier stage. Therefore, because of this theoretical limit on system performance, artificial illumination may be necessary to provide adequate resolution under certain night conditions.

The addition of artificial illumination to a low light level television system can reduce the illumination problem, but not without penalties in size, weight, power and complexity. Also, the active system has an inherent problem of high backscatter not found in the passive system. The discussion which follows investigates first the passive system, including available natural illumination, weather conditions, and theoretical and practical limits on passive system

performance. Active illuminators and the effect of such illumination on LLLTV system performance are discussed separately.

Passive LLLTV Systems

This investigation of passive LLLTV systems describes the environment within which the sensor must operate and identifies theoretical and practical limits on TV system components.

Operating Environment -- Illumination levels available for LLLTV systems will range from full moonlight, clear sky conditions to no moon and overcast conditions. This subsection provides a discussion and analysis of:

1) the magnitude of illumination available for night operation;
2) the spectral distribution of the available illumination;
3) the atmospheric transmission for a number of weather conditions;
4) the effect of aircraft motion on system resolution.

Illumination Levels -- Natural night illumination is due to three sources; the moon, the stars and planets, and airglow. Illumination levels due to these sources as a function of lunar phase and cloud conditions are given in Figure 89 (Reference 45). Figure 90 shows the percentage of time during an average month for which the illumination level does not exceed a given level for clear (cloudless) weather conditions at 0 degree and at 60 degree latitude. It is worth noting that, even for clear weather, the illumination levels are, on the average, below 1.5×10^{-4} for 21 percent of the time during an average month at 0 degree latitude. Cloud cover degrades these levels considerably as indicated in Figure 89.

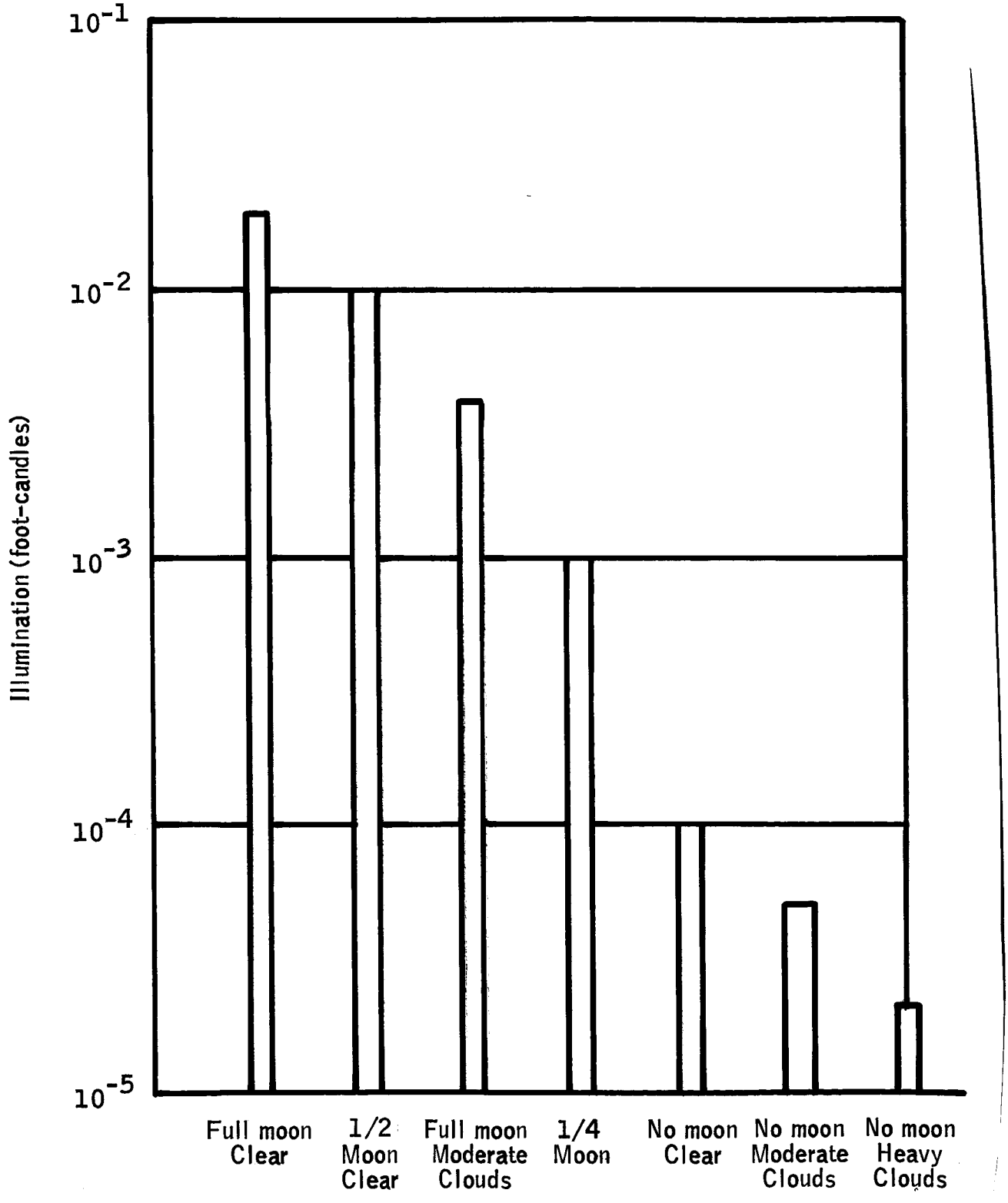

Figure 89 -- Night Scene Illumination for Several Conditions

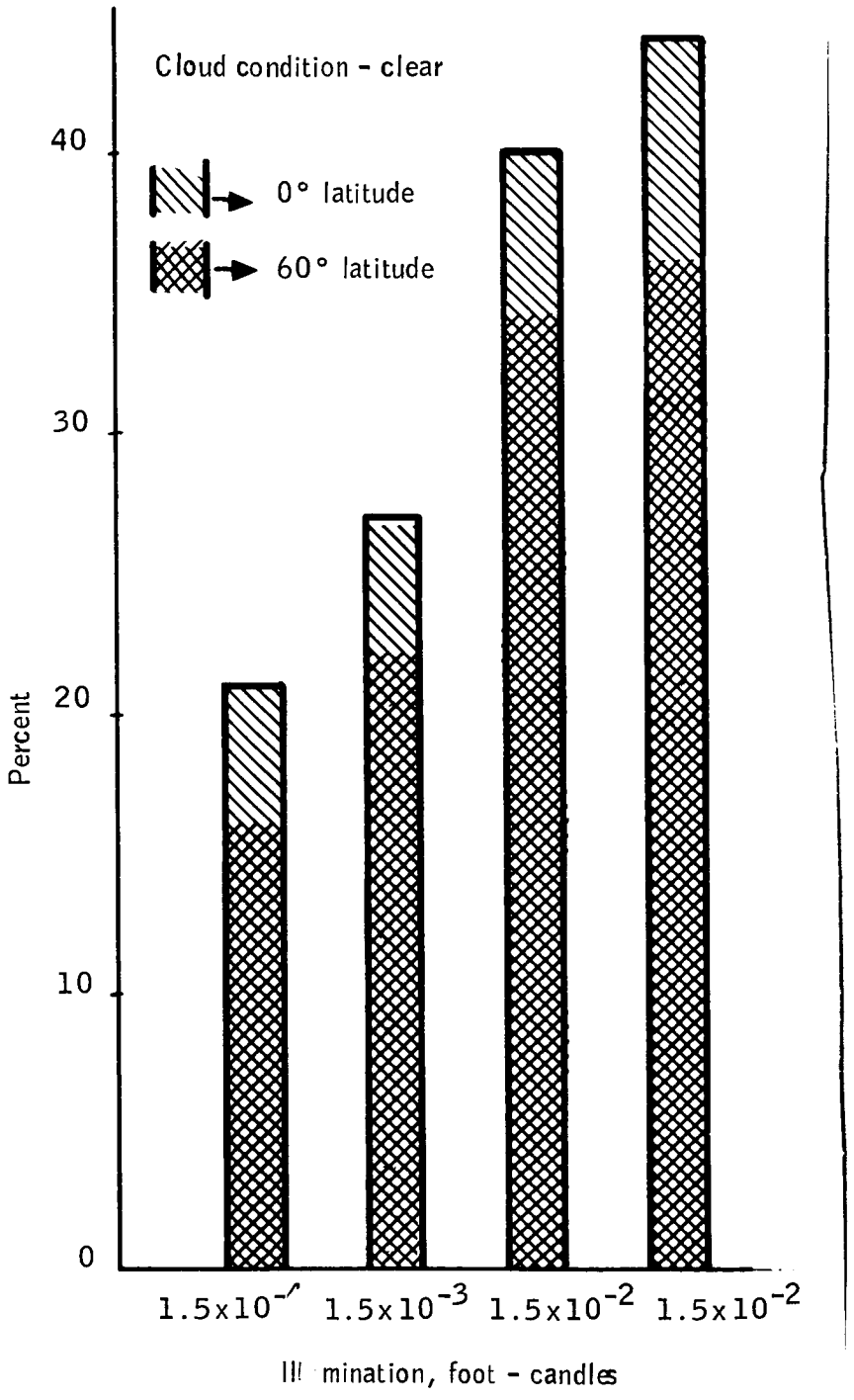

Figure 90 -- Percent of Month for Which Illumination is Less than a Given Level

Spectral Considerations -- The spectral character of daytime illumination is approximately that of a 6000°K blackbody.

The night time spectrum consists of moon light, (that is, solar energy reflected from the moon), starlight, and airglow. Moonlight has approximately the same spectrum as sunlight. The spectrum from the stars is broad because of the large number of sources at different wavelengths; but, the magnitude of illumination is low. Airglow is a phenomenon resulting from ionized particles in the upper atmosphere. It exhibits significant peaks near 1.0 micron. The spectral irradiance due to airglow is larger than that due to stars and, for less than about 1/8 moon, is larger than moonlight. Unfortunately, photosurfaces exhibit extremely low quantum efficiency at 1.0 micron and therefore image intensifiers are not sensitive to airglow.

Atmospheric Attenuation -- Atmospheric attenuation is a result of particle scattering and absorption. The contribution of each effect depends upon the composition of the atmosphere and the wavelength of light under consideration. In the visible and near IR, the primary cause of attenuation is Rayleigh scattering. The attenuation as a function of slant range to the target can be approximated by the following expression for a layered atmosphere (Reference 3) -

$$\tau_a(\lambda) = \exp\left[-\sum_i k\,\beta_i(\lambda)t_i\csc\phi\right] \tag{98}$$

where β_i = extinction coefficient of the i^{th} layer

t_i = thickness of the i^{th} layer

ϕ = depression angle to point of interest

k = constant

Although the extinction coefficient is a function of wavelength, for most purposes an optical extinction coefficient which is not a function of wavelength can be used with small error. Figure 91 shows the atmospheric attenuation as a function of range for the four weather conditions described below. Weather cases I and II are described in the USAF Handbook of Geophysics (Reference 24).

Weather Case	Description
I	U.S. Standard Atmosphere
IA	U.S. Standard Atmosphere with haze layer of 5.56 km (3 nm) visual range extending to 1524.0 m (5000 feet)
II	Maritime Tropical Atmosphere
IIA	Maritime Tropical Atmosphere with haze layer of 3.70 km (2 nm) visual range extending to 1524.0 m (5000 feet)

Particles in the atmosphere will also cause backscattering which has the effect of decreasing contrast at the pickup tube. However, under natural night illumination conditions the backscatter is sufficiently small compared to noise in the system that it can be ignored. (The backscatter cannot be ignored when an artificial source of illumination is used.)

Effect of Image Motion on Resolution -- A TV camera, either vidicon or image orthicon (IO) is basically an integrating device. The image on the photocathode is the integration, over the frame period, of the ground scene. Motion of the aircraft will cause the ground scene to be smeared across the photocathode, with the magnitude of smear depending on the apparent angular velocity of the scene with respect to the aircraft.

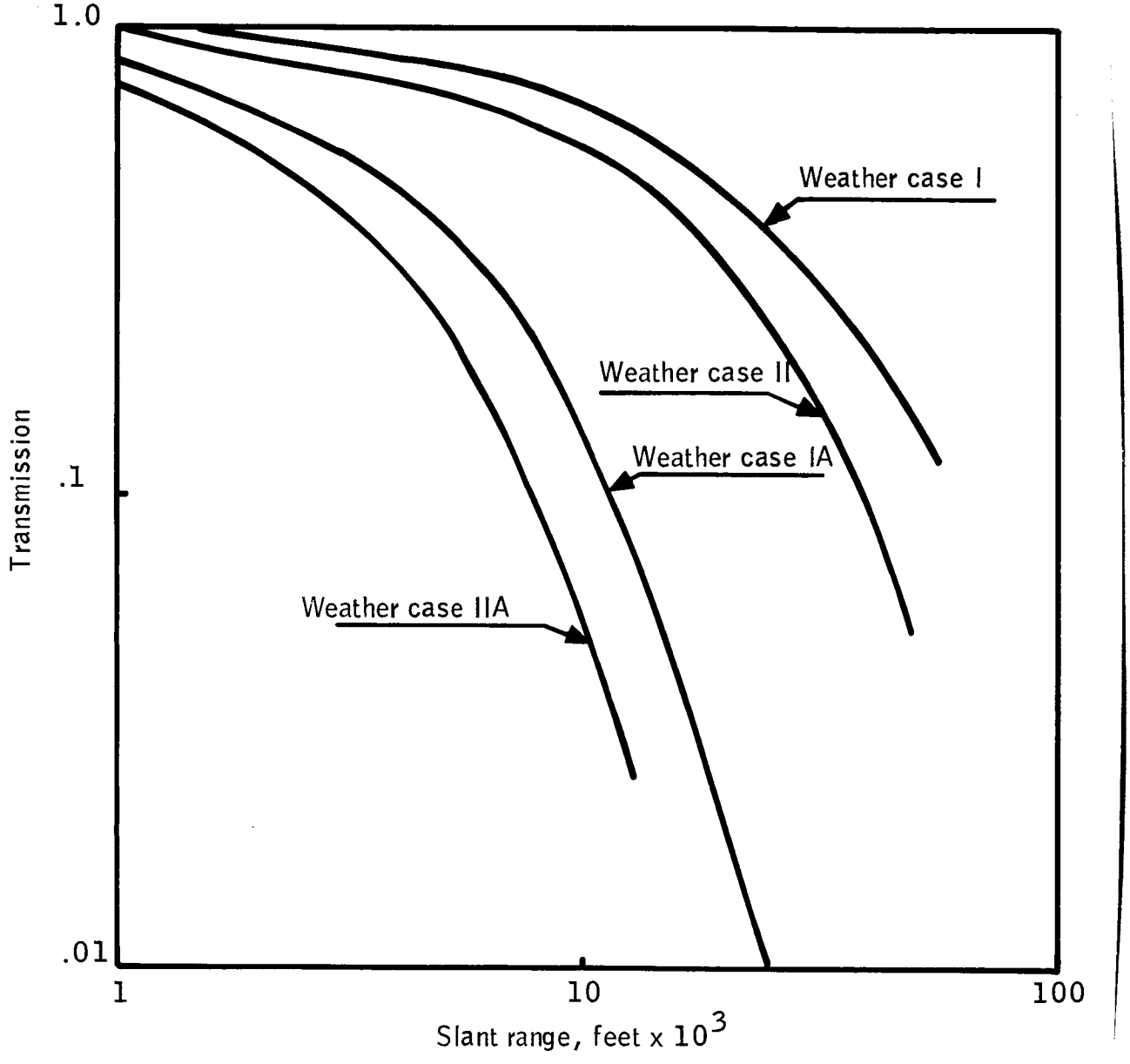

Figure 91 -- Atmospheric Transmission vs Slant Range

For a vertical sensor the apparent angular velocity of the scene due to aircraft forward velocity is simply V/H. However, for a forward-looking sensor the apparent angular velocity with respect to the aircraft is also a function of the depression angle to the scene. Simple geometry shows that the apparent angular velocity of a point at depression angle ϕ is given by

$$\dot{\alpha} = (V/H) \sin^2 \phi \text{ (radians/sec)} \tag{99}$$

Note that the apparent angular velocity varies with depression angle; that is, it varies across the sensor along-track field-of-view. The total angular smear on the photosurface due to aircraft forward velocity is given by

$$\alpha = \dot{\alpha} T \text{ radians} \tag{100}$$

where T is the frame period of the system.

The effective resolution across the total field-of-view (θ) is

$$R_\alpha = \frac{\theta}{\alpha} \text{ (lines)} \tag{101}$$

The total limiting resolution for the system is

$$R_T = \frac{1}{\sqrt{\frac{1}{R^2} + \frac{1}{R_\alpha{}^2}}} \text{ (lines)} \tag{102}$$

Figure 92 shows the limiting resolution as a function of apparent V/H ($\dot{\alpha}$) for a hypothetic 400 line system with 0.349 rad (20°) along track field-of-view. Flight tests of an SEC vidicon system with 0.5 mr static resolution and an image orthicon system with 0.212 mr static resolution showed the resolution of the former degraded to 1.5 mr and the latter to 0.82 mr at a V/H of 0.04 rad/sec

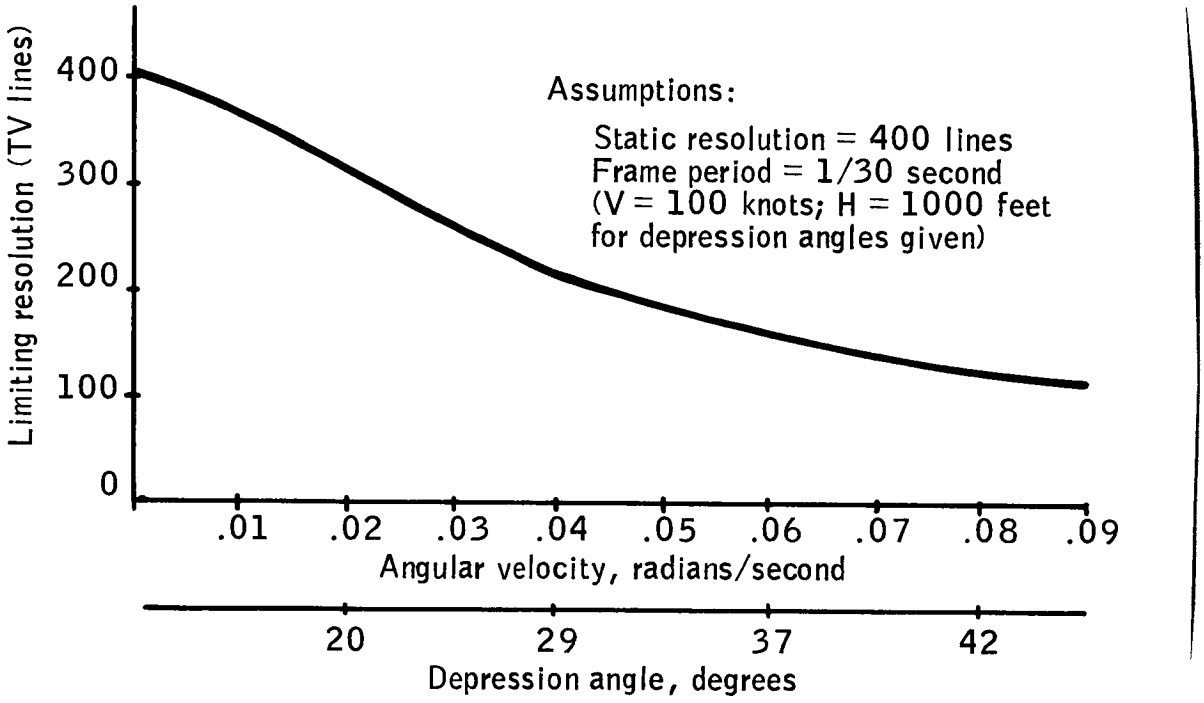

Figure 92 -- Limiting Resolution vs Apparent Angular Velocity

(Reference 47). The degradation factor is about 3 for the SEC vidicon and 4 for the image orthicon system. This difference is attributed to two parameters:

1) the difference between static resolution in the two systems, and

2) the image orthicon tends to exhibit stickiness at low light levels.

A more detailed discussion of image motion effects and compensation for image motion is presented in Reference 46.

Theoretical and Practical Limits to System Performance -- The imaging capability of a low light level television system is influenced by fundamental physical laws and by certain practical limits. The purposes of this subsection are to identify the major factors which limit the imaging capability of the system and to quantify such limitations.

The performance of a TV system (in fact, any imaging system) is usually measured in terms of the following characteristics:

Noise

Resolution

Sensitivity

Dynamic Range

The above characteristics are not necessarily independent as will be demonstrated in the analysis that follows.

Noise Sources -- In an LLLTV system the signal is competing with noise from several sources. Noise generated within the system (internal noise) can be caused by

- o beam noise in an image orthicon
- o thermal noise in the preamplifier of a vidicon (or SEC vidicon)

- o dark current noise in photoemitters (in the image orthicon, SEC vidicon, and image intensifiers)
- o other sources.

Another type of noise, a type not generated in the system, is signal fluctuation noise which is caused by the quasi-random arrival of photons at the photocathode of the pickup device. This noise is inherent in the signal and is a function of the wavelength of incident light and the quantum efficiency of the photocathode.

In well designed low light level television systems, the internal noise can be maintained well below the signal fluctuation noise for extremely low signal levels (on the order of 10^{-8} foot-candles). Such systems use one or more image intensification stages in conjunction with the camera tube to achieve fluctuation-noise limited operation.

Resolution -- The limiting resolution of a system is often described in terms of the maximum resolvable spatial frequency of a 100 percent modulated bar target. The value of resolution obtained corresponds to one point on the modulation transfer curve of the system; namely, the value of modulation at which the bars are just resolvable, typically 3 to 5 percent modulation.

For large signals, the primary sources of degradation in system resolution are:

- o system optics
- o the pickup device
- o the video processor
- o the display

The pickup device is usually the dominant source of degradation, that is, it

usually has a limiting resolution significantly smaller than that of the others. The factors in the pickup device which degrade resolution include:

- o imperfect focus in the image intensifier
- o scanning beam defocus
- o target mesh characteristics

State-of-the-art pickup devices provide limiting resolutions of 500 to 800 TV lines for large signals.

The resolution at low signal levels is limited by signal fluctuation noise as described in the following paragraphs.

Photon Noise Limited Resolution -- The resolution of an electro-optical system at low light levels is limited by statistical fluctuations in the arrival of photons at the photosurface and by the quantum efficiency of the photocathode. The limit, which was first derived by Rose (Reference 48) is developed in Reference 46. The development assumes a checkerboard type pattern on the photocathode with alternating light and dark squares. The derivation then determines the smallest size of the squares such that the dark to light variation in illumination is just detectable above the noise created by quasi-random arrival of photons. For brevity, only the result of the development in Reference 46 is given below.

$$R_1 = \frac{M\sqrt{qmET}}{6k} \quad \text{lines/inch} \tag{103}$$

where M = modulation

q = photocathode quantum efficiency

T = integration time (sec)

E = photocathode illumination (foot-candles)

m = conversion factor (photons/sec/lumen)

k = required signal/noise ratio such that the signal is just discernible

R_1 = photon noise limited resolution of a photosurface

The above expression provides limiting resolution as a function of quantum efficiency, photocathode illumination, exposure time, and modulation. Usually the expression is used as a theoretical limit for a photosurface with q set equal to the quantum efficiency of the photosurface, M=1 and T=1/30 second (or the frame rate of the system). The threshold k is often assumed to be 3.6 (Reference 49) and a value of m for a 2870° tungsten source, usually used as a standard, is $m = 1.06 \times 10^{16}$. Then, grouping the constants

$$R_1 = K\sqrt{qE} \text{ lines/inch} \tag{104}$$

$$\text{where } K = \frac{M\sqrt{mT}}{6k} \tag{105}$$

$$= 1.88 \times 10^7$$

which is the theoretical limit on system resolution at low light levels.

Sensitivity -- The expression in the preceding section shows that limiting resolution is proportional to the square root of photocathode illumination for signal fluctuation noise limited operation. Therefore it is desirable to maximize photocathode illumination. The expression for photocathode illumination is

$$E = \frac{I \cdot r \cdot \tau_a \cdot \pi}{4(T\#)^2} \text{ foot-candles} \tag{106}$$

where I = scene illumination (foot-candles)

r = scene reflectance

τ_a = atmospheric transmission

T# = system T-number

The system T# is defined as

$$T\# = \frac{f\#}{\sqrt{T_o}} \tag{107}$$

or

$$T\# = \frac{\text{(focal length)}}{\text{(clear aperture diameter)}\ (\sqrt{T_o})} \tag{108}$$

where T_o = transmission of the optics

In the above equation the designer has control over the f# and, to some extent, the transmission of the optics, which would be maximized. For a particular set of conditions then, the photocathode illumination can be represented by

$$E = \frac{K_1}{(T\#)^2} \tag{109}$$

and the limiting resolution by

$$R_1 = K\sqrt{qE} = K\sqrt{\frac{qK_1}{(T\#)^2}} = \frac{K_2}{T\#} \tag{110}$$

The total limiting resolution, in terms of TV lines/picture height is given by

$$R_1 = \frac{K_2 S}{T\#} \text{ lines/picture height} \tag{111}$$

where S is the useful photocathode size in inches

From the above equation it can be seen that the photon noise limited resolution can be improved by increasing photocathode size, decreasing T#, or both.

Optical Relationships -- In an optical subsystem the f# is given by

$$f\# = \frac{F}{d} \tag{112}$$

Where d = diameter of entrance aperture

F = system focal length

The field of view (θ) of the system is given by

$$\theta = \frac{S}{F} \tag{113}$$

where S is the size of the photocathode

Combining the two equations to eliminate F yields

$$d \cdot \theta = \frac{S}{f\#} \tag{114}$$

Then, substituting the above in the expression for R_1 gives

$$R_1 = K_2 \cdot d \cdot \theta \sqrt{T_o} \tag{115}$$

It can be seen that the photon noise limited resolution is a function of aperture diameter. It should be pointed out, however, that as the aperture is increased, a greater number of corrective lenses for aberrations are required, hence the transmission of the optics, T_o, decreases. Therefore R_1 is not directly proportional to d, the entrance aperture diameter.

Dynamic Range -- Dynamic range of a system is usually defined in terms of the maximum number of distinct brightness levels the system is capable of reproducing where the commonly accepted increment for brightness levels is $\sqrt{2}$. Then, defining B_d as the brightness of the darkest level obtained on a display, the next

level has a brightness $B = \sqrt{2}\, B_d$. In general the brightness at the nth level is $B = \sqrt{2^n}\, B_d$. The dynamic range of the system is determined by the dynamic range of the pickup device, the electronics and the display.

The display and the image pickup device are the two system components most likely to limit the system dynamic range. Typically, CRT displays can provide up to 14 shades of gray provided that gamma correction (i.e., linearization of the transfer characteristic) is implemented.

The dynamic range of typical television camera tubes ranges from about 30 to 36 dB corresponding to 10 to 12 shades of gray. These figures represent the peak (highlight) signal to RMS noise obtainable with the tube, assuming that the tube is internal noise limited. When image intensification stages are added to increase the sensitivity, the signal fluctuation noise predominates over tube noise. This occurs because the high gain of the intensifier stages amplifies noise as well as signal. The increased magnitude of noise results in decreased dynamic range, at low light levels, when the intensifier stage gain is high.

Critical Components -- The fluctuation noise limited resolution is a theoretical limit which can be approached only if other sources of system noise are sufficiently small. If such conditions do exist, the limiting resolution is a function of optics T# and of photocathode size. The latter is true because the previously developed expression for limiting resolution (R_l) is given in lines per unit length (per inch) of photosensitive surface. This section discusses the performance and limitations of camera tubes, image intensifiers, and system optics, followed by a discussion of tradeoffs for optics T# and photocathode size.

Camera Tube Descriptions -- Television camera tubes are broadly classified as return beam or non-return beam types. The image orthicon and image isocon are return beam tubes and the vidicon, SEC vidicon and Plumbicon are non-return beam tubes. In general the return beam tubes are more sensitive and more complicated than the non-return beam types. The principles of operation of each of the camera tube types is presented below.

- Image Orthicon -- The image orthicon (IO) is comprised of image, target, scanning, and photomultiplier sections as shown in Figure 93, item (a). The scene is imaged on the photocathode which is comprised of a photoemissive surface (e.g., S-1 or S-20 photosurface) from which photoelectrons are emitted in proportion to the number of photons arriving. The emitted photoelectrons are accelerated toward and focussed on the target which is a transparent material; glass in conventional IO's and MgO in very sensitive IO's. The target produces secondary electrons, proportional to the number of impinging photoelectrons, which are collected by the target mesh. Thus a pattern of charge is retained on the target which represents the image. The target is scanned with a low velocity electron beam which deposits sufficient electrons to neutralize the target at any point, with the remaining electrons returned to the photomultiplier section as signal.

- Image Isocon -- The image isocon is fundamentally an image orthicon with a change in the scanning section (Reference 50). The change consists of the addition of a transverse magnetic field and an aperture to the scanning section so that scanning beam electronics reflected from the target

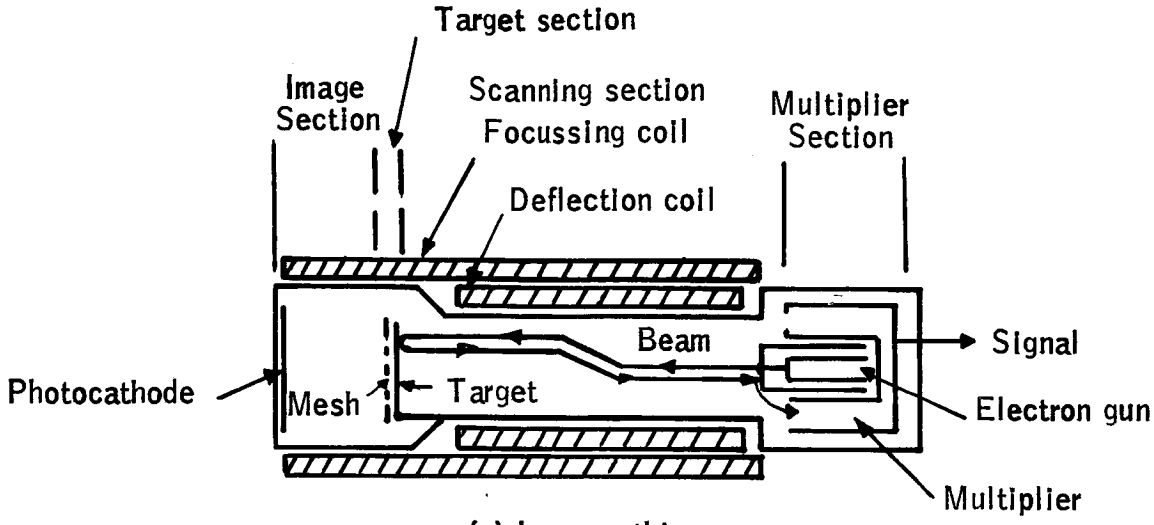

(a) Image orthicon

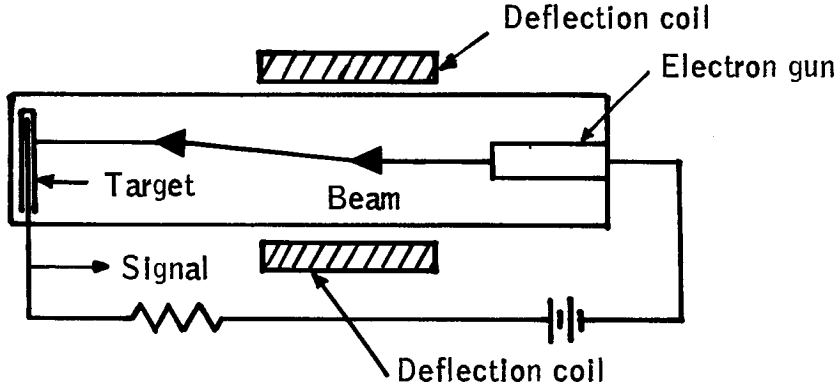

(b) vidicon

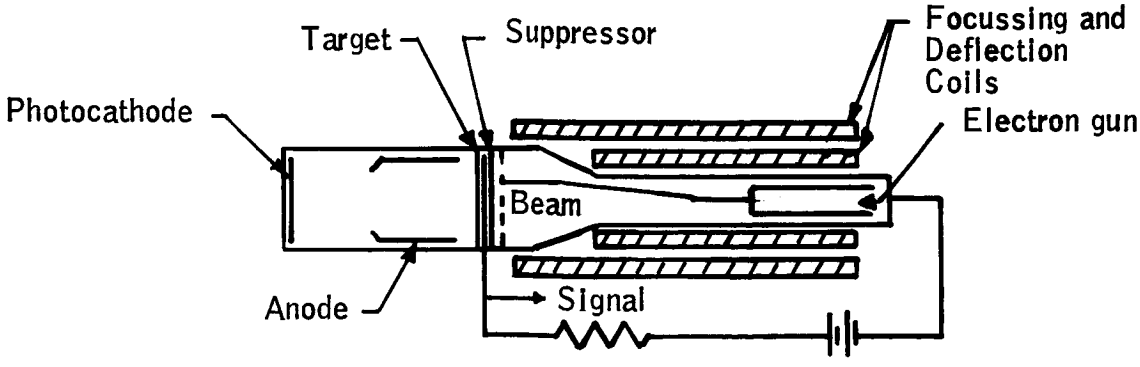

(c) SEC vidicon

Figure 93 -- Camera Tubes

are separated from electrons scattered at the target. Only the scattered electrons, which are proportional to the charge on the target, are allowed to enter the photomultiplier. A resulting improvement in dark current noise is claimed for the image isocon with respect to the image orthicon.

- Vidicon -- The vidicon is comprised of a target section and a scanning beam section as shown in Figure 93, item (b). The target consists of a transparent conductive layer and a photoconductive (PC) layer of material deposited on a glass faceplate. The conductivity of the PC layer is proportional to the number of photons imaged on the surface so that conductivity in the target area varies with the illumination from the scene. The target is scanned with a low velocity electron beam. A positive potential, applied through the load resistor, establishes a voltage drop across the PC layer so that the signal output is proportional to the conductivity of the section of target being scanned.

  Modifications have been incorporated in some vidicons to improve resolution as is the case in the General Electric FPS (focus projection scanning) vidicon and field mesh vidicons.

- SEC Vidicon -- The secondary conduction (SEC) vidicon, shown schematically in Figure 93, item (c), is quite different from the vidicon. The scene is imaged on a photoemissive cathode with the resulting photoelectrons accelerated to focus on the target. The target consists of a supporting membrane of Al_2O_3 on which a layer of aluminum and a layer of KCl are deposited. Photoelectrons penetrate the first two layers

and create secondary electrons in the KCl layer. The secondary electrons migrate to the aluminum signal electrode, thus creating a charge pattern representing the scene. The low velocity scanning beam restores the charge in the KCl layer, with the signal capacitively coupled to the aluminum signal electrode. A suppressor mesh is positioned very close to the target to limit the maximum potential to which the target can rise.

- o Plumbicon -- The plumbicon is essentially a vidicon with a photoconductive layer of lead-monoxide (PbO) with doping instead of the usual photoconductive layers used in vidicons (Reference 51). The doping creates, in principle, a pn diode at the PbO layer. The results are higher sensitivity and lower lag than obtained with conventional vidicons.

Camera Tube Performance Characteristics -- Examining the transfer characteristics of typical examples of each of the five types discussed previously, the image orthicon provides the highest sensitivity of the five, and the plumbicon the lowest. A more useful measure of camera tube performance for low-light-level applications is limiting resolution as a function of photocathode illumination. The criteria for illumination levels chosen earlier in this report was that the system should provide useful imagery at 10^{-4} foot-candles of scene illumination. Under clear atmospheric conditions and for an f/1.0 optical system, the photocathode illumination will be a maximum of about 10^{-5} foot-candles. Under these conditions the SEC vidicon is inadequate while performance of the IO is marginal; therefore image intensifiers will be required for either tube type.

Additional characteristics of the various tube types, such as image lag and blooming/halation, are also extremely important factors for the LLLTV. The image lag or retention effectively lowers the resolution of the device when image motion exists, as in a TV sensor used for airborne search. The blooming/halation problems which occur in image orthicons cause large portions of the picture to be "washed out" when bright light sources exist within the camera field-of-view. This problem can be reduced using a technique developed by General Electric called "automatic beam control". However, it should be pointed out that the problem does not exist in the SEC vidicon.

Examination of available data reveals that the SEC vidicon and the image orthicon are the two tubes most suitable for use in airborne LLLTV applications. However, an image intensifier should be used in conjunction with either tube although for different reasons. An intensifier stage is desirable for the image orthicon to reduce the image stickiness effect and for the SEC vidicon to increase the sensitivity.

Image Intensifiers -- An image intensifier is an optical amplifier in the sense that a scene imaged on the input surface will appear intensified (amplified) on the output surface. Several types of intensifiers are described briefly below.

The most common image intensifier is comprised of a photoemissive surface and a phosphor surface. The scene imaged on the photoemissive surface will produce photoelectrons which are accelerated to the phosphor. Amplification of brightness is controlled by controlling the energy of electrons striking the phosphor

(i.e., by controlling the accelerating voltage). Focussing can be accomplished by electrostatic or magnetic fields, or by placing the two surfaces in close proximity, a technique called proximity focussing. The latter technique is extremely simple but, in general, focus is poor and the magnitude of accelerating voltage, hence the gain, are necessarily low because of the close spacing of the surfaces.

A second means of image intensification uses two surfaces, a photoemitter and a phosphor, but accomplishes amplification by secondary electron emission. Emitted photoelectrons are focussed on a plate comprised of small, electrically hollow tubes coated with a secondary electron emitting material (the plate is sometimes called a microchannel multiplier plate). Image intensification occurs because the number of electrons striking the phosphor is much greater than the number emitted from the photoemitter due to secondary emission ratios much greater than unity in the microchannels. The expected advantage of the microchannel plate intensifier compared to other intensifiers is smaller size. The size can be smaller because less spacing is required between photoemitter and phosphor and because very small accelerating voltages are required so that smaller power supplies can be used.

The modulation transfer functions for an image intensifier and for an SEC vidicon which has a 40 mm photocathode are plotted in Figure 94 to illustrate that image intensifiers provide spatial frequency responses which are significantly higher than those achieved in the camera tube. Therefore, the camera tube resolution is the limiting resolution in the system.

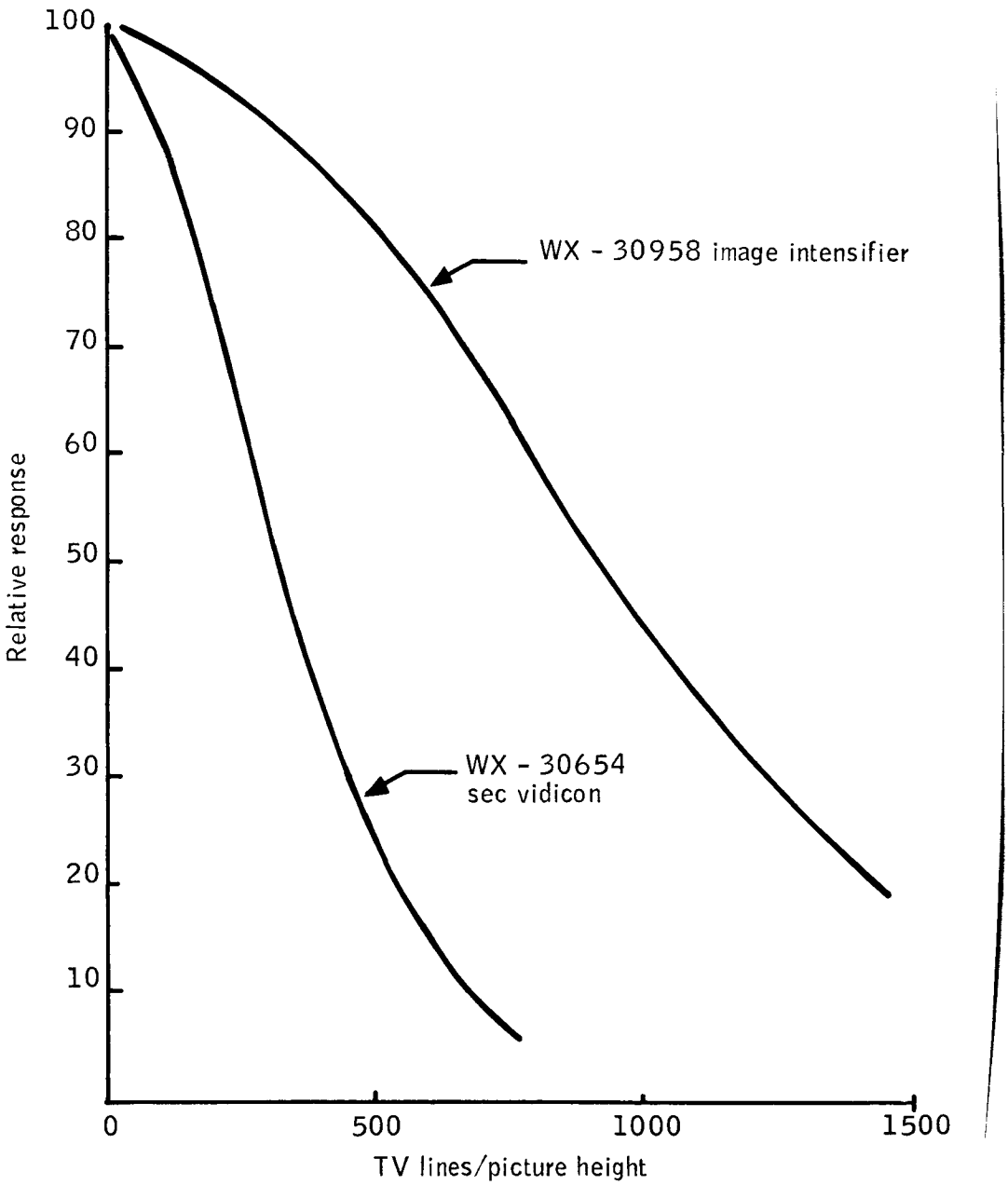

Figure 94-- Comparison of MTF for an Image Intensifier and SEC Vidicon

Camera Tubes in Combination with Image Intensifiers -- Published measured data for a 3-inch image orthicon combined with a 40 mm image intensifier (Reference 53) and for a 1-inch SEC vidicon combined with a 40 mm image intensifier (Reference 54) shows that the image intensifier/image orthicon (I^2O) combination approaches the photon noise limit for a 40 mm photocathode. The image intensifier/SEC vidicon (I-SEC) combination, however, is a factor of 40 less than the theoretical noise limit at the closest point (at about 200 TV lines). Two reasons explain the relatively low sensitivity of the I-SEC compared to the I^2O:1) the sensitivity of the SEC vidicon is lower than that of the image orthicon, and 2) the intensifier used for the I-SEC has a gain of only 200 as compared to 400 for newer intensifiers. The sensitivity of a double stage intensifier coupled to the SEC, estimated by multiplying the data for the I-SEC curve by 400 (the brightness gain of the intensifier), shows performance better than the I^2O for low illumination levels.

Estimated performance curves for two SEC/intensifier combinations verifies that operation near the photon noise limit is presently feasible. One combination is a double stage intensifier (I^2-SEC) with a 25 mm photocathode coupled to a one-inch SEC vidicon. The other combination is a double stage intensifier with a 76 mm photocathode coupled to a one-inch SEC vidicon (Reference 52) and the measured performance of an I^2O with a 50 mm image intensifier.

Optics -- Optics technology has evolved over a period of several centuries to a sophisticated science. Advancements in the technology include development of new optical materials and fabrication techniques such that lenses can be fabricated to great precision with relatively high optical transmission.

Computerized ray tracing and aberration analysis aid in the design so that in many cases, on-axis aberrations are almost eliminated. Because the technology is comparatively mature, it seems reasonable to assume that few major breakthroughs will occur in optics.

Fairchild builds a 9.87 inch T/1.5 objective specifically color corrected for use with the extended red S-20 (S-25) photosurface. The size is approximately 11 inches in diameter by 20 inches in length. The modulation transfer function for the lens is given in Figure 95.

It is estimated that lenses as large as 0.5 meter in diameter can be constructed for television systems. Obviously, the size and weight of such lens systems can become prohibitive.

Combined MTF -- The modulation transfer function (MTF) of a typical state-of-the-art LLLTV front end including optics, image intensifier and camera can be calculated using the MTF's given in Figure 94 and the on-axis curve of Figure 95. The separate MTF's and resultant MTF shown in Figure 96, shows that the SEC vicicon limits resolution at high illumination levels. However, as the ambient illumination falls off, the system becomes photon noise limited at the image intensifier photosurface.

Active Television

An active TV system is one which contains an illumination source. The source can increase the scene illumination and, therefore, the operating resolution of the system at low ambient light levels. Use of an active illuminator does, however, introduce several problems. Backscatter of the source illumination

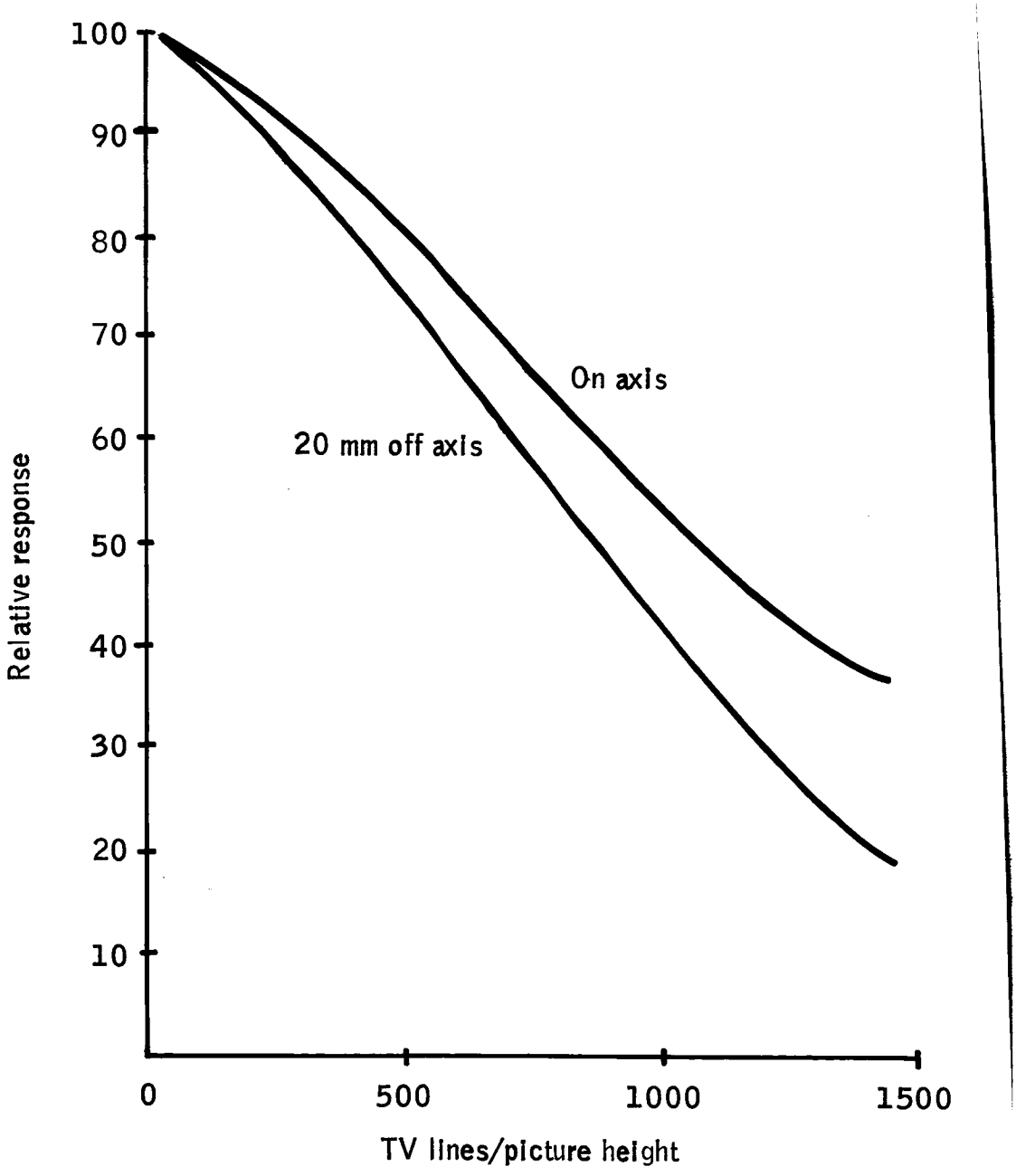

Figure 95 -- MTF of 9.87 Inch, T/1.5 Objective

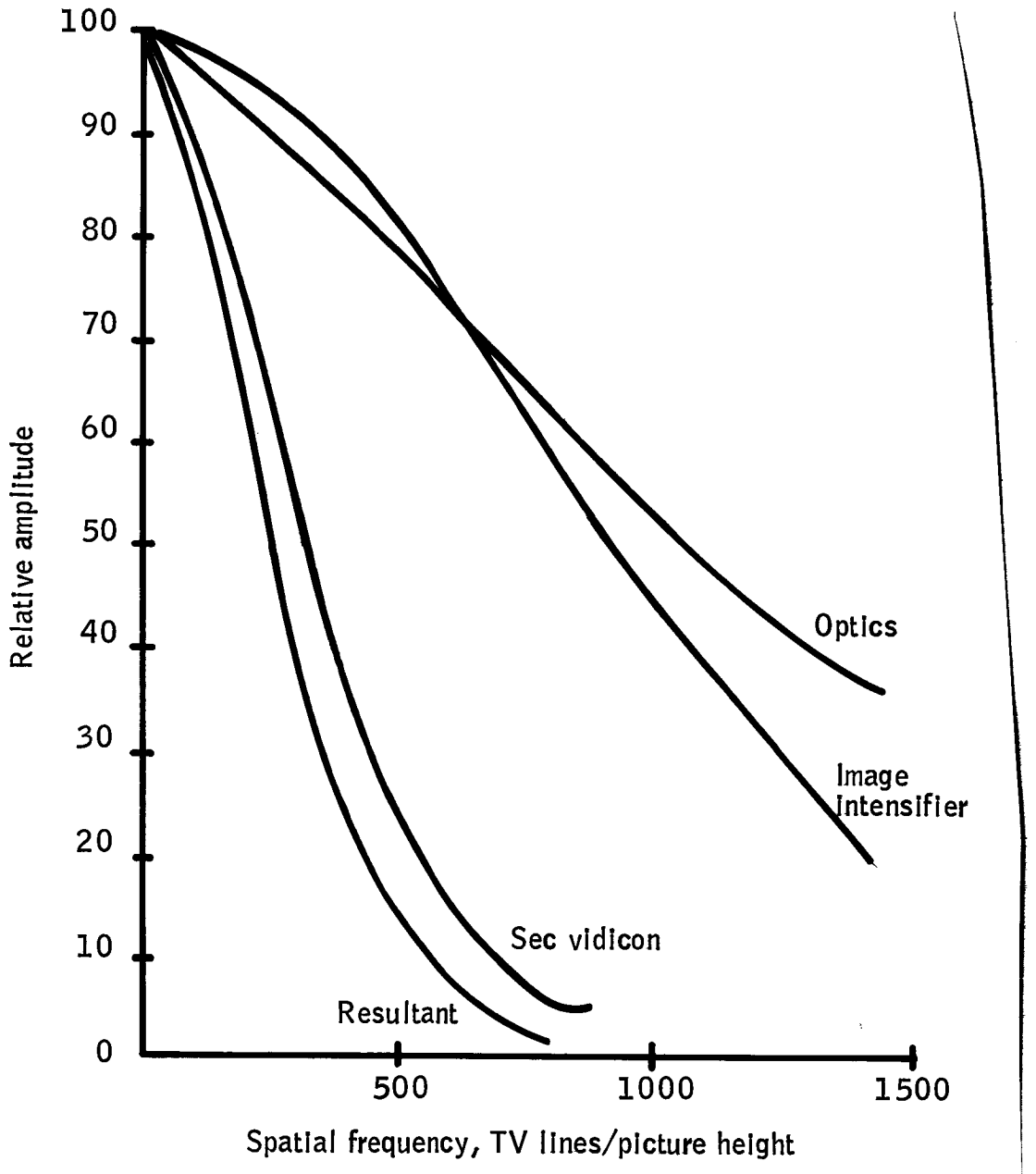

Figure 96 -- Combined MTF for TV System

can reduce effective contrast. Other penalties incurred by including an active source are the additional weight, size, and power requirements which can be very high for significant quantities of active illumination.

Theoretical considerations for selecting illumination sources and camera tubes are discussed below. A survey of existing illumination sources and their applicability to the nighttime TV problem is also presented.

Spectral Considerations -- The two major spectral considerations for active TV systems are matching of the illuminator spectral character to that of the TV tube, and reducing backscatter.

Matching -- One of the more important considerations in selecting a source and sensor is the matching of the emitted spectrum of the illuminator to the spectral response of the sensor. Figure 97 shows the spectral response of three photosurfaces and several illumination sources. The 5000°K curve is typical of a xenon arc lamp. From the figure it is evident that xenon matches well with the S-20 and S-25 surfaces. On the other hand, the S-1 surface is the only one of the three which provides any sensitivity to the 1.06 μ output of a Nd:YAG laser.

Atmospheric Backscatter -- Energy in the visible and near IR is attenuated by scattering and absorption as it propagates through the atmosphere. These effects are described in detail in the passive TV section. In the active system the light from the illuminator is attenuated by scattering and absorption so that only a portion of the emitted energy reaches the ground. In addition to the attenuation, however, another more serious degradation occurs in the active system; the backscattering of energy from the illuminator into the sensor.

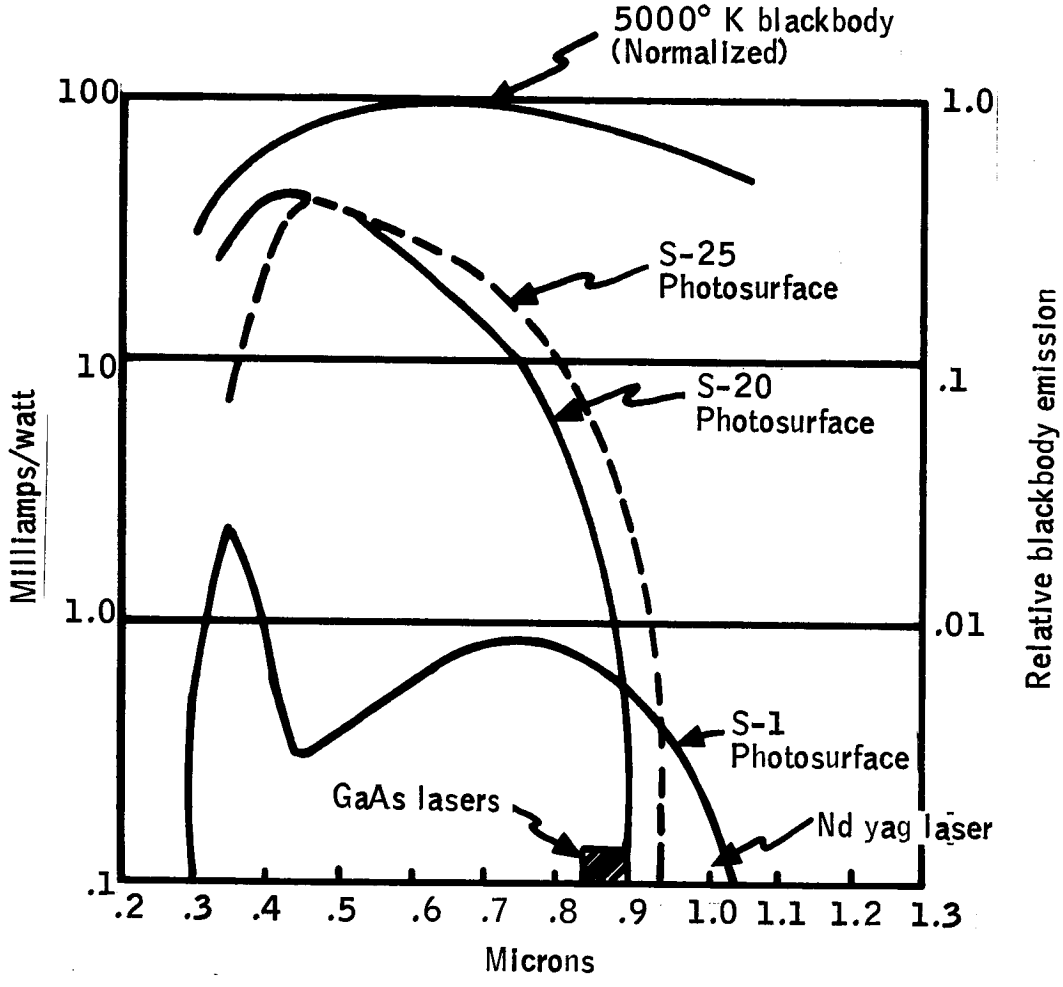

Figure 97 - Spectral Response of Photosurfaces and Emission of Illuminators

Backscatter will reduce the apparent contrast in the system. This can be seen by looking at the expression for contrast at the scene

$$C = \frac{E_T - E_B}{E_B} \tag{116}$$

Where E_T = illumination from the target at the scene

E_B = illumination from the background at the scene

The effect of energy backscattered from the atmosphere is to reduce the contrast at the sensor to

$$C' = \frac{E'_T - E'_B}{E'_B + B} \tag{117}$$

where B = illumination at the sensor due to backscattered energy.

E'_T, E'_B = the illuminations after propagation through an atmosphere having attenuation.

The backscatter which occurs in the active system is, of course, the same effect as that described for the passive system. The difference is that a concentrated source of illumination is located very near the receiver. Suppose an active system has the configuration shown in Figure 98. Then, according to Reference 55, the fraction of emitted energy seen at the receiver due to backscatter is approximated by:

$$B(r) = \int_o^r \frac{Y_1^2}{4s^2} f(s)\, a e^{-2as}\, ds \tag{118}$$

where f(s) = fraction of scattered energy from the illuminator which is in the sensor field-of-view at range s

e^{-2as} = attenuation due to atmospheric scattering

NOTES:

1. Scene to be imaged should be at range between R_2 and R_3
2. Backscatter into sensor begins at range equal to R_1 (For source and sensor continually on)

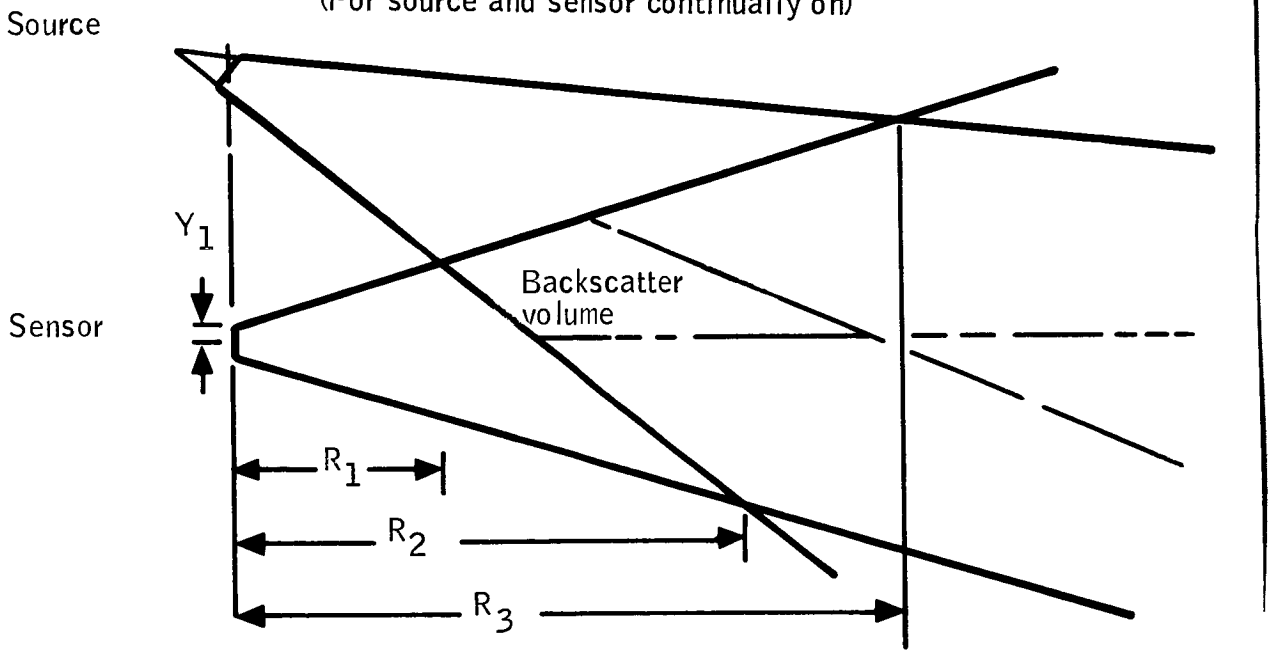

Figure 98 -- Backscatter in an Active System

a = scattering coefficient

Y_1 = sensor aperture radius

The fraction of emitted energy reflected from a Lambertian target scene with reflectivity = 1.0 at range r is given by

$$S(r) = \frac{Y_1^2}{r^2} f(r) e^{-2ar} \tag{119}$$

The attenuation coefficient is a sensitive function of wavelength, as previously demonstrated. Therefore, the visible and near IR wavelengths are preferred for most systems to reduce the backscatter problem which is quite severe in the ultraviolet. The effect of wavelength upon scattering has been verified in many photographic system experiments. In addition to operating systems in the near IR, the effects of backscatter can also be reduced by several techniques described in the following paragraphs.

Backscatter Reduction -- The effect of backscatter can be reduced by two methods in addition to operating at longer wavelengths. One method is to increase the separation between source and sensor as shown in Figure 99. Notice from Figure 98 that f(s) is 0 for $r \leq R_1$; that is, there is no backscatter into the sensor except when sensor and source fields-of-view overlap. Thus, the effective backscatter with the illumination source at D1 is greater than the backscatter with the source at D2. The distance by which the source and sensor can be separated is, in practice, limited by practical considerations. For example, the sensor might be pod mounted under one wing and the source under the other, in which case the separation would be limited by the maximum distance from the fuselage at which the pods could be mounted as limited by structural and aerodynamic considerations.

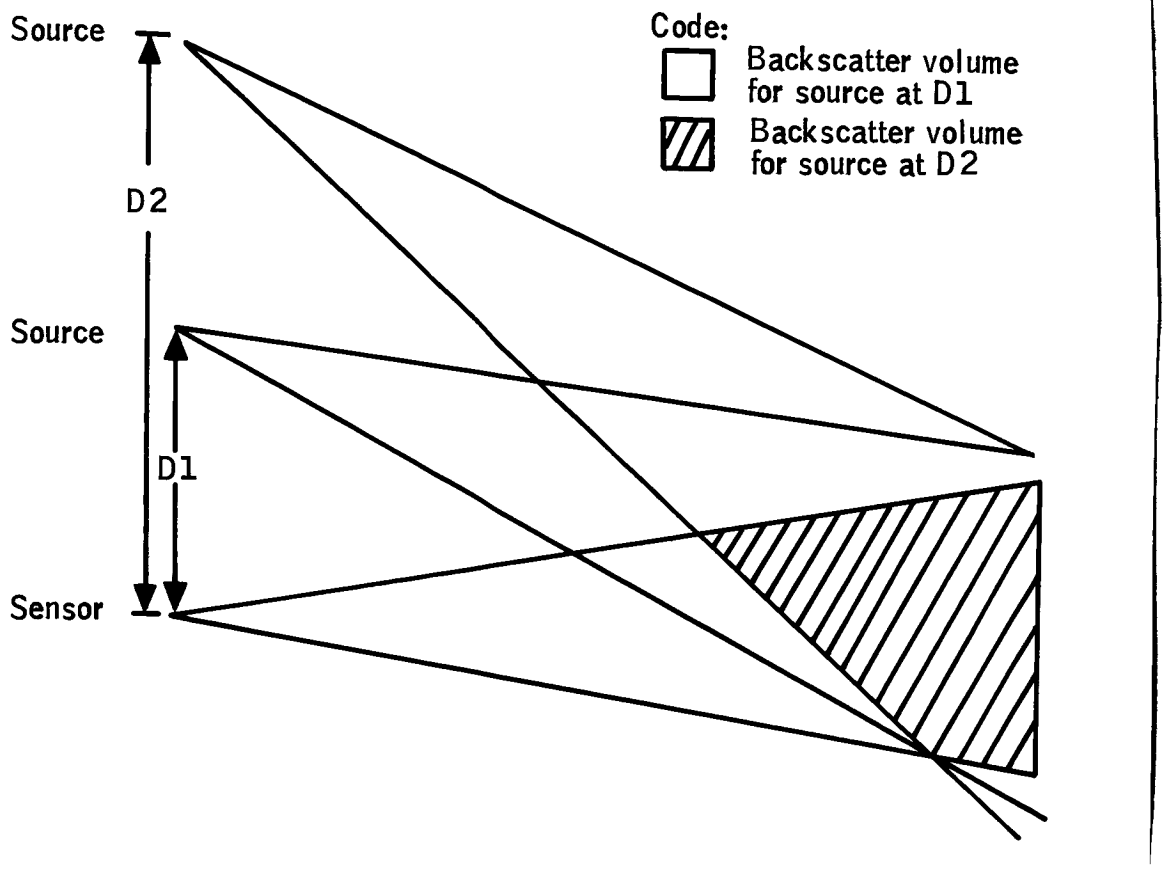

Figure 99 -- Backscatter Reduction

A second method for reducing the effect of backscatter uses a pulsed source with a gated sensor. The timing of the source pulse and sensor gate is ideally such that the sensor is off during the time that the light pulse is traveling from the illuminator to the ground. In such a system the sensor would see no backscatter.

To completely eliminate backscatter effects the illuminator pulse length should be equal to the time required to travel from source to target while the delay between source pulse and sensor gate should be twice that time. As an example, to look at targets at 304.8 m (1000 feet) range, the illuminator pulse should be about 1 μ sec in length and the sensor should be gated on 1 μ sec after the illuminator is turned off. The 1 μ sec exposure time can, however, cause problems depending upon the sensitivity of the sensor. Therefore, it may be desirable to pulse the light source and gate the sensor a number of times for each frame. The net effect is to increase the exposure time by the factor N_p, the number of pulses integrated.

Illumination Requirements -- The passive TV section described the limiting resolution as

$$R_1 = \frac{M\sqrt{\eta mET}}{6k} \tag{120}$$

Therefore, for a given resolution, the relationship between exposure time (T) and photocathode illumination (E) is reciprocal. Notice also that required exposure varies as the square of modulation. Therefore, to achieve a given limiting resolution at modulation less than unity, the exposure must be increased according to the square of modulation. Suppose, for example, that it is

desirable to operate an SEC vidicon with 25 mm photocathode at maximum resolution (i.e., above the photon noise limited resolution). This operation is achieved at about 10^{-4} foot-candles photocathode illumination. For T=1/30 second and M=1, the required exposure in the general case is

$$E_T = \frac{(1/30)\ E}{T} \tag{121}$$

where T = exposure time for a particular system

E = photocathode illumination for 1/30 second exposure time

If N_P pulses are integrated then the required illumination is

$$E'_T = N_P E_T \tag{122}$$

For modulation less than 1

$$E'_T = \frac{N_P E_T}{M^2} \tag{123}$$

Scene Illumination -- The required illumination at the scene is given by

$$E_s = \frac{4 \cdot E'_T \cdot (T^{\#})^2}{r \cdot Ta} \text{ foot-candles} \tag{124}$$

Where r = scene reflectance

Ta = transmission of the atmosphere

$T^{\#}$ = optics T number

The required photocathode illumination is usually given in terms of foot-candles from a 2870°K tungsten source. Therefore, if some other source of illumination is used, a conversion factor must be used. This spectral conversion factor is described below.

Spectral Conversion Factor -- The spectral conversion factor converts from required lumens for a 2870°K source to required lumens from some other source, S. In general, for a specific photocathode (e.g., the S-25 surface), spectral response, $R(\lambda)$, is given in terms of milliamps/watt. Also, for an image intensifier, (or TV camera tube) limiting resolution is given in foot-candles, assuming illumination from a tungsten 2870°K source with the spectral distribution, $W(\lambda)$, given in terms of watts/cm^2/micron. Finally, let the luminosity curve for scotopic vision be called $Y(\lambda)$ lumens/watt. Then, as shown in Reference 46, the conversion factor is

$$K_i = \frac{\int_0^\infty W(\lambda)\, Y(\lambda)\, d\lambda \int_0^\infty S(\lambda)\, R(\lambda)\, d\lambda}{\int_0^\infty S(\lambda)\, Y(\lambda)\, d\lambda \int_0^\infty W(\lambda)\, R(\lambda)\, d\lambda} \quad \frac{\text{lumens 2870°K}}{\text{lumens of source}} \tag{125}$$

Unfortunately, the above expressions must usually be graphically integrated.

In the event that the source of illumination is filtered, then the second integral in the numerator becomes

$$\int_{\lambda 1}^{\lambda 2} S(\lambda)\, R(\lambda)\, d\lambda$$

where λ_1 and λ_2 are lower and upper cutoff frequencies (sharp cutoff is assumed).

The factor K_i is used to determine the illumination required from the source. The required scene illumination E_s is given in terms of candles/foot^2 with a 2870°K source. To find the required illumination from source S, simply divide

$$E'_s = \frac{E_s}{K_i} \text{ (foot-candles)} \tag{126}$$

Available Illuminators -- The available illuminators can be broadly categorized as either wide-band sources or narrow-band sources according to the width of the spectral emission from the sources. Narrow-band sources are the lasers such as gallium-arsenide diodes. Wide-band sources include incandescent lamps and arc discharge tubes as well as some less well known types.

Narrow-Band Sources -- The majority of energy emitted from a laser is contained in one or several very narrow bands. Because of the reduced backscatter, the near infrared is the spectral region offering the most promise for active illumination of TV systems. Although a number of lasers emit in the near IR, the most useful, from the standpoint of size, efficiency and cost, is the gallium arsenide (GaAs) injection laser. Arrays of such lasers can be used to illuminate large areas on the ground. Performance characteristics of typical GaAs lasers are as follows:

Frequency of emitted energy - variable with operating temperature between about 0.83 and 0.95 micron.

Line Width	10-100 Å (depending on power out, etc.)
Pulse Width	Typically 0.1-0.5 μsec
Repetition Rate	Typically 1 KHz
Power Out	2-10 watts typical
Efficiency	0.1 to 10.0%
Operating Temperature	-273°C to 25°C

Wide-Band Sources -- The major categories of wide-band sources of illumination which have possible application for the TV problem are; incandescent glowing wire, arc lamps, and flash lamps.

- Incandescent Lamps -- Incandescent lamps of the glowing wire (typically tungsten) type are characterized by very low conversion efficiencies. Therefore, such lamps require extremely high input power to provide sufficient illumination for nighttime TV.

- Xenon and Krypton Arc Lamps -- Xenon arc lamps can provide extremely high output illumination. For example, the following characteristics are currently available in a water cooled xenon arc lamp (see Reference 56).

Input Power	6,000 watts
Output Light	150,000 lumens
Approx. Color Temperature	5000°K
Life	100 hours

The above lamp is water cooled, requiring 3/4 gallon per minute at 35 to 40 pounds per square inch. The lamp provides continuous operation. Krypton arc tubes will provide more light in the near IR than will the xenon tubes.

- Xenon Flash Lamps -- Xenon flash lamps are of interest for the gated application because they are pulsed. However, at the high power required, the typical pulse durations of such lamps are about 1 millisecond. Pulsed sources must have pulse widths on the order of several microseconds in a gated system. The characteristics of a typical xenon flash lamp are included below because of the possibility that shorter pulse widths may be obtained in the future.

Flash tube envelope o.d.	15 mm (.6 inches)
Arc length	16.5 cm (6.5 inches)
Ave. power input (max.)	10,000 watts
Typical pulse width	1 millisecond
Typical flash rate	5 pulses/second

Example of Illumination Required from a Xenon Arc Source -- An example, considered representative of available equipment and requirements, is given here to indicate the approximate magnitude of the artificial illuminator requirements. For this example, assume:

- Pickup tube is an I-SEC with S-25 photocathode
- Xenon arc source with 5000°K spectrum is used as the illuminator (steady state source)
- Atmospheric transmission = 0.5
- Sensor-scene distance = 914.4m (3000 feet)
- Field-of-view = 0.349 rad (20°) x 0.175 rad (10°)
- Lens T# = 1.5
- Scene reflectance = 0.2
- Scene modulation = 0.2 = M
- Backscatter ignored

For the problem defined above, the required photocathode illumination is 10^{-4} foot-candles to achieve operation not limited by photon noise at 100 percent modulation. For M=0.2

$$E_T' = \frac{10^{-4}}{(.2)^2} = 2.5 \times 10^{-3} \text{ foot-candles} \qquad (127)$$

Required scene illumination is

$$E_s = \frac{4E'_T(T\#)^2}{rta} = 0.225 \text{ foot-candles} \quad (128)$$

The conversion factor K_i, by graphical integration is

$$K_i = 0.285$$

Therefore,

$$E'_s = \frac{E_s}{K_i} = 0.8 \text{ foot-candles} \quad (129)$$

For 914.4 m (3000 ft) range and 0.349 rad (20°) x 0.175 rad (10°) field-of-view, the area on the ground which must be illuminated is approximately 5×10^5 feet^2. The required luminous intensity at the scene is, therefore

$$I_s = F'_s \times \text{area} = 4.0 \times 10^5 \text{ candles} \quad (130)$$

Assuming the reflector is about 80 percent effective in directing energy into the field-of-view, and accounting for the 0.5 atmospheric transmission from scene to source, the total luminous intensity from the lamp must be

$$I'_L = 1.6 \times 10^6 \text{ lumens}$$

Xenon arc lamps have a conversion efficiency of about 30 lumens/watt. Therefore, the required lamp input power would be about 50 kw. In addition, water cooling for the lamp and some sort of cooling for the reflector would also be necessary.

Potential for Active TV -- As shown in the example above, the active system using xenon requires high power and therefore will be large and heavy. Other

extended sources can be expected to exhibit similar power requirements. Lasers will become more efficient in the coming years and gallium arsenide array illuminators may eventually be practical for TV illumination. By 1980 gallium arsenide arrays may be used for illumination. However, size may well be a problem even in that time period.

ILM TV Concept Evaluation

Passive TV -- The MARSAM II computer model (Reference 3) was used to evaluate the potential of a TV sensor to meet the ILM requirements. A brief description of the MARSAM program is given in Appendix B. Three MARSAM weather cases were used to provide data that can be extrapolated to the conditions defined as Category I, II and III. Table 45 summarizes the MARSAM weather cases and includes comparative data for the ILM weather cases.

Representative characteristics for the TV camera tube, lens and display define the TV sensor. A sensitive Vidicon tube is used as the camera. Table 46 and Figures 100 and 101 show the characteristics of this camera tube. Table 47 shows the characteristics of the three lenses used in the three TV systems evaluated. These characteristics represent wide field-of-view (WFOV), narrow field-of-view (NFOV), and tracking field-of-view.

The display characteristics are shown in Table 48 and Figure 102. Three display sizes for a viewing distance of 71 cm (28 inches), as defined in the requirements, are shown in Table 49, one for each field-of-view. As can be readily noted, the display sizes for the WFOV and NFOV are not practical sizes for cockpit installation. Shorter CRT viewing distances would be required to accommodate the large fields-of-view.

Table 45 -- ILM TV Weather Cases

MARSAM Code or Category	VR (nm)	RVR m(ft)	β_i	Habs (g/m^3)	Hrel (%)	Air Mass	Model Homogenous Layer	Precipitation
2A	3.70 km (2)	3706.4 m (12,160)	1.812	12.0	61.6	Maritime Tropical	0-1524.0 m (0-5000 ft)	None
W3	0.93 km (1/2)	926.6 m	7.25	8.1	98.3	---	0-152.4 m (0-500 ft)	Drizzle or Rain
		(3,040)	36.25	8.1	98.3	---	152.4-1524.0m (500-5000 ft)	(5mm/hr)
Cat. I		731.5 m (2,400)						
Cat. II		387.7 m (1,600) 365.8 m (1,200)						
4	0.23 km (1/8)	231.6 m (760)	29.0	2.0	60.0	Maritime Polar	0-1524.0 m (0-5000 ft)	Snow (5mm/hr)
Cat. IIIa		213.4 m (700)						

Table 46 -- VID1 Performance Characteristics

Symbol	Value	Symbol Description
Tube Type	Vidicon	
t	1/30 sec	Frame time
e	0.02	Motion compensation error
d_x	1 inch	Photocathode size in along-track direction
d_y	1 inch	Photocathode size in cross-track direction
K_i	1.21	Illumination conversion factor for pick-up tube
E_o	0.5 ft-cd	Optimum illumination for pick-up tube
Δ_f	10×10^6 cps	Bandwidth of pickup tube
NF	3.14	Amplifier noise figure
R	50 ohms	Amplifier input resistance
I_o vs E	See Figure 100	Signal current characteristics versus illumination for pickup tube
R_{tv} vs C_a, E	See Figure 101	Pickup tube resolution characteristics versus contrast and illumination

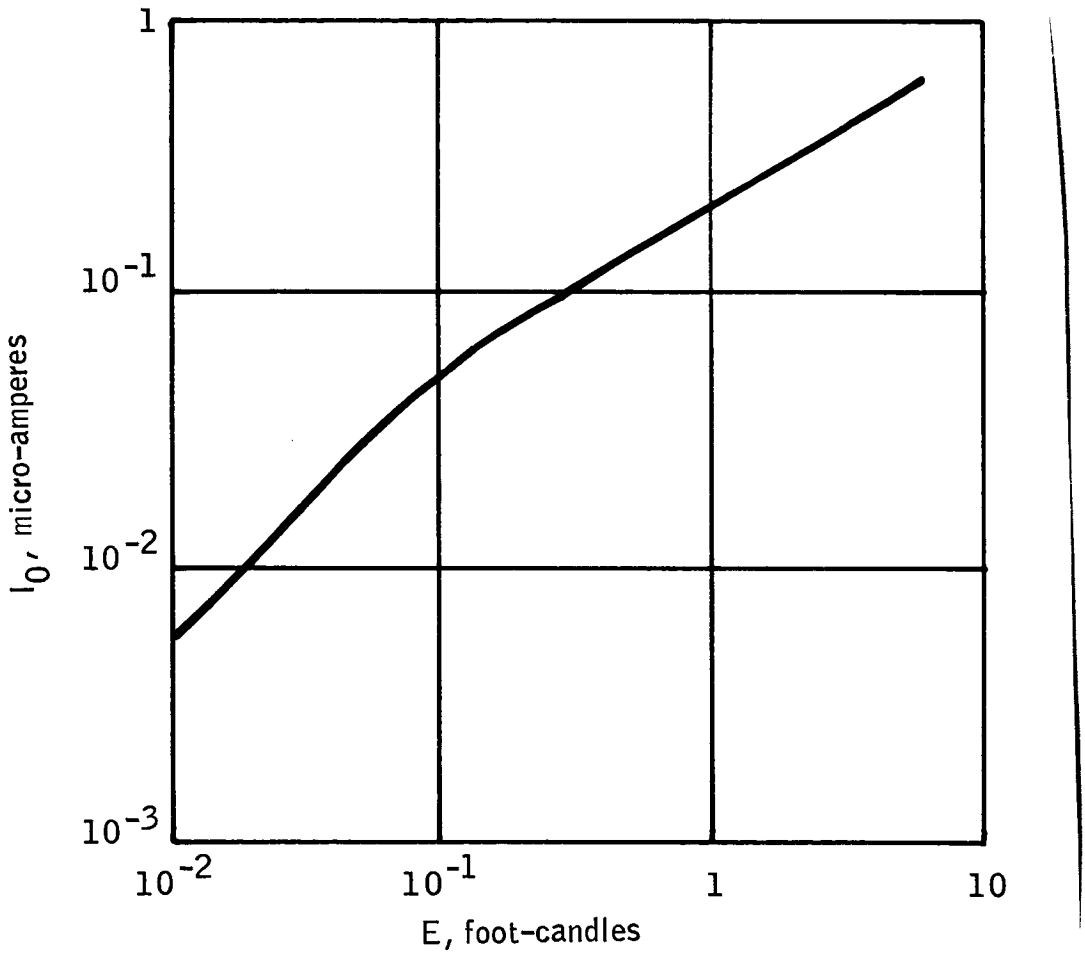

Figure 100 -- VID1 Output Current (I_o) vs Photocathode Illumination (E)

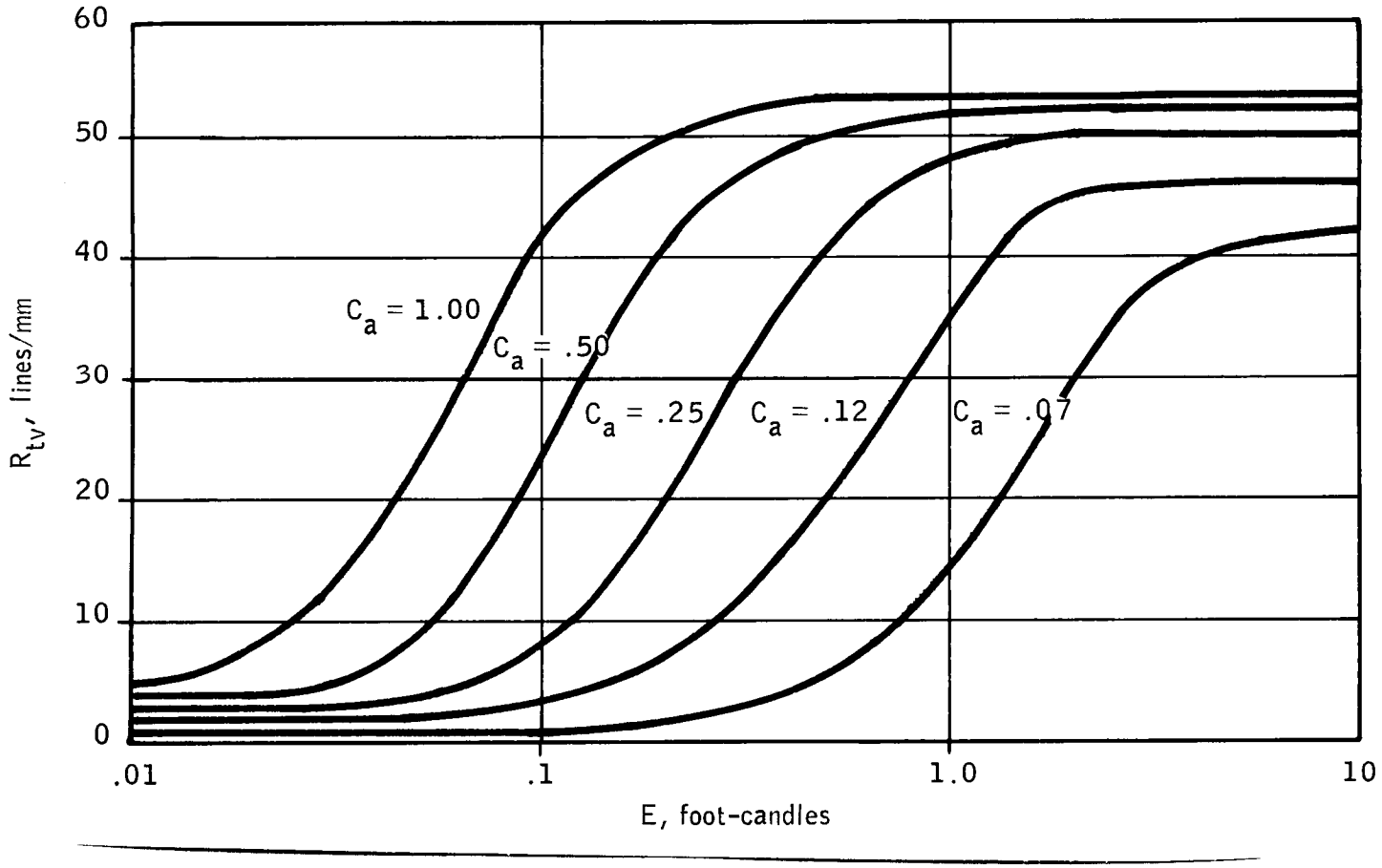

Figure 101 -- VID1 Limiting Resolution (R_{tv}) vs Contrast (C_a) and Photocathode Illumination (E)

Table 47 -- Three TV Lenses

Symbol	Symbol Description	Value WFOV	NFOV	TRACKING
F	Focal Length (in)	1.135	2.04	7.17
T_l	Lens Transmittance	0.8	0.8	0.8
Rawar	Lens Resolution (L/mm)	80.	80.	80.
A_e	Lens F Number	1.37	1.37	3.0
θ_v	Vertical Field-of-View (deg)	21.0	21.0	8.0
θ_h	Horizontal Field-of-View (deg)	47.5	27.5	8.0

Table 48 -- CRT1 Performance Characteristics

Symbol	Value	Symbol Description
N_d	700 lines	Display resolution
V_{mid}	21.0 volts or 10.0 volts	Display input voltage corresponding to display brightness midpoint
V_{max}	27.5 volts	Display input voltage corresponding to display spot defocus
K_m	1.0	Constant which varies display operating point about midpoint
B_{da}	0.0 ft-lamberts	Display ambient brightness
B_d vs V	See Figure 97	Display brightness as a function of input voltage

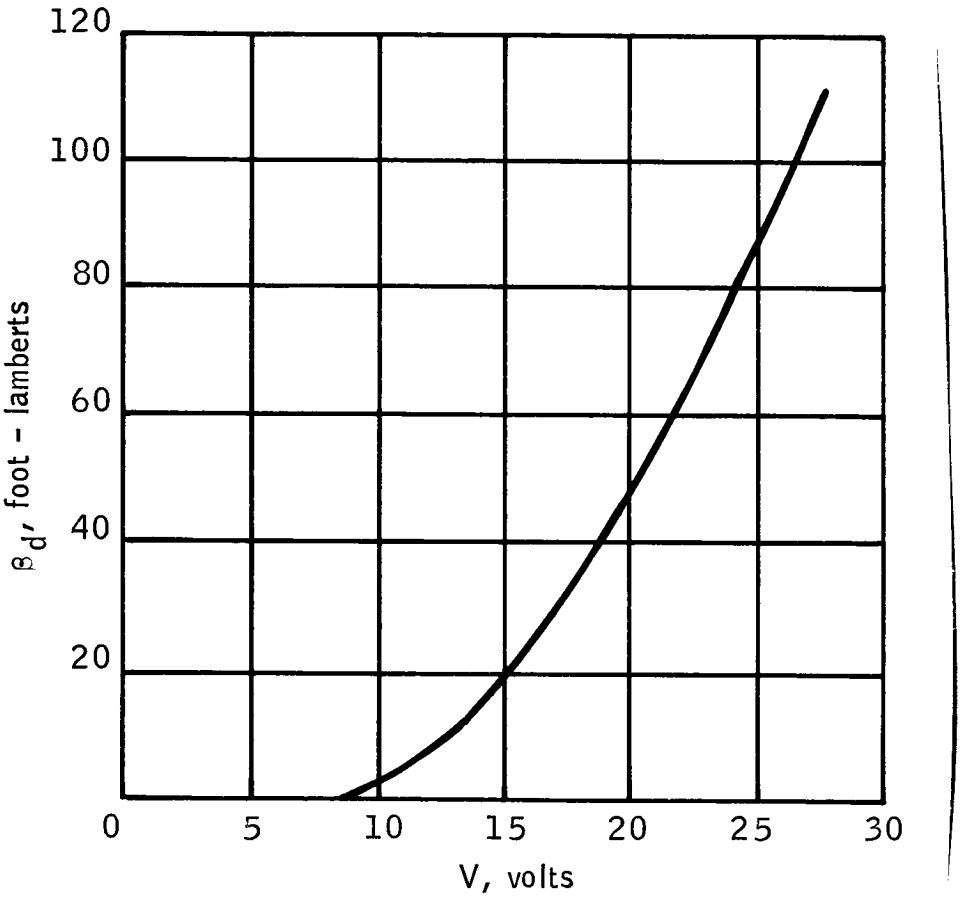

Figure 102-- CRT1 Brightness (B_d) vs Grid Voltage (V)

Table 49 -- TV Display Size

Symbol	Symbol Description	Value		
		WFOV	NFOV	TRACKING
D_{dx}	Display dimension in along track (cm)	26.4	26.4	15.2
D_{dy}	Display dimension in cross track (cm)	62.0	34.8	15.2

Sensor performance was evaluated as a function of slant range by specifying a 0.052 rad (3 degree) glideslope and a wide range of altitudes. Platform velocity was varied from 90 knots to 145 knots with no change in performance. Target and background characteristics used in both the TV and FLIR analyses are summarized in Table 50.

Runway Target -- The ILM runway target is represented by a 23 meter by 1520 meter rectangle of asphalt or concrete. This target is located within a brown grass or snow background. Figures 103 and 104 show the results of this evaluation. The asphalt runway on a snow background provides the highest contrast and, therefore, the best performance as shown by the right edge of the envelope. The concrete runway against snow or grass was slightly more difficult to detect. The asphalt runway on brown grass was significantly worse than the other combinations and is shown as the left edge of the envelopes.

Although detection and recognition capability beyond 1.8 km (1 nm) exist for the better weather condition, Category I conditions (slightly worse than weather W3), degrade performance to less than the minimum effective range (MER) of 1000 m (3280 ft) defined in the requirements.

Runway Lights Target -- Runway lights and approach lights were considered as potential landing aids. For the purpose of evaluation they were located against a brown grass background and were considered both at night and during daylight (reduced illumination in degraded weather). Figures 105 and 106 show the detection ranges for the various conditions. The envelopes represent probabilities greater than zero but less than 1. Although some potential does exist, the TV sensor does not provide detection beyond the MER for all weather conditions examined.

Table 50 -- ILM Targets and Backgrounds (TV and FLIR)

Targets	Dimensions In Meters Length	Width	Height	Reflectivity	Emissivity	Temperature (°K)
Asphalt Runway	1520	23	0	.08	.91	305
Concrete Runway	1520	23	0	.35	.99	305
Obstacle	3	3	3	.12	.9	305
Approach Lights	.1016	.1016	.0508	*	--	---
Runway Lights	.0508	.0508	.0508	*	--	---
IR Heaters	.305	.305	.305	--	.98	400 to 700
Backgrounds						
Brown Grass	--	--	--	.05	.98	300
Snow	--	--	--	.75	.25	300

*Active Target, 7800 Candle Power

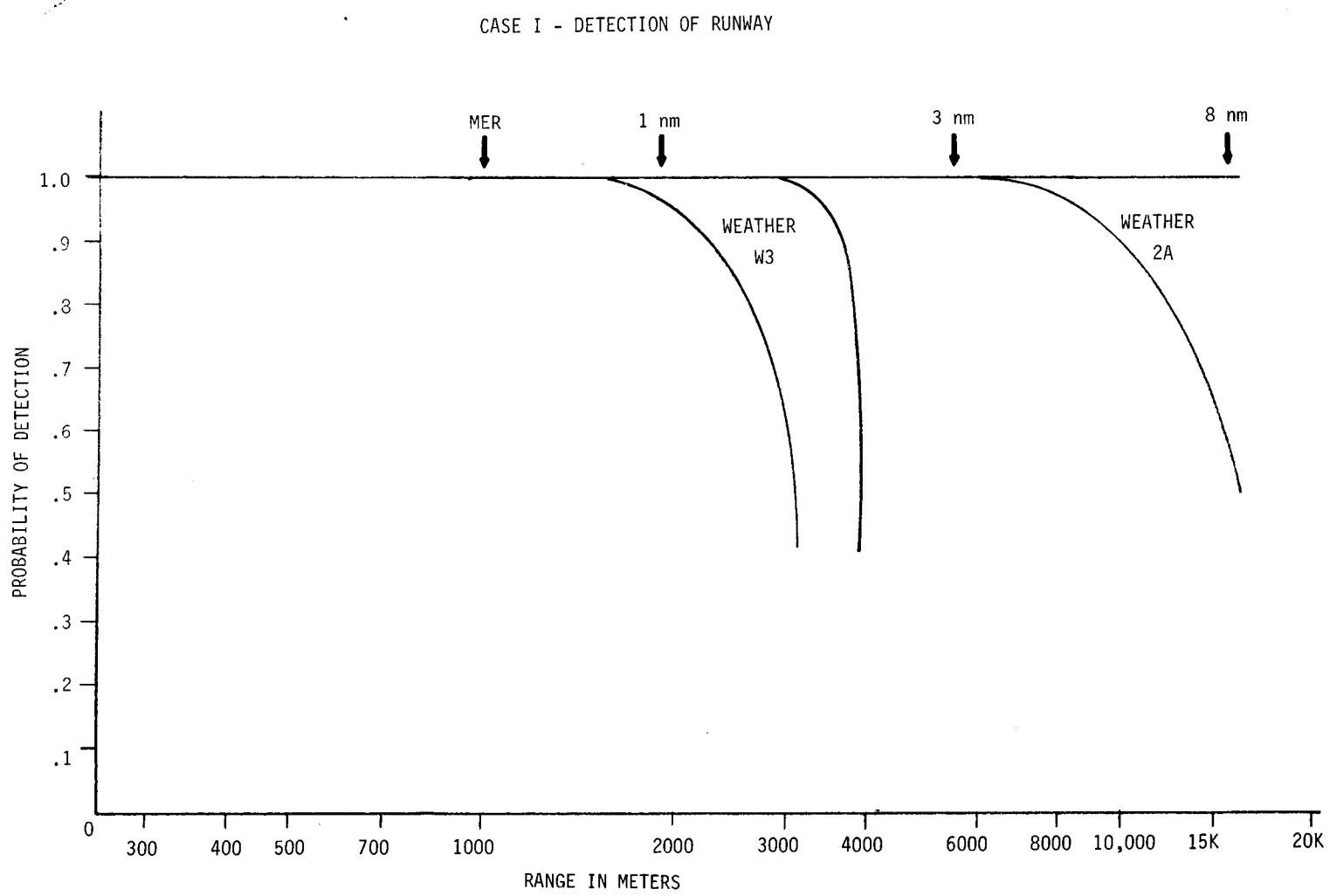

Figure 103 -- TV Performance, Probability of Detection vs Range

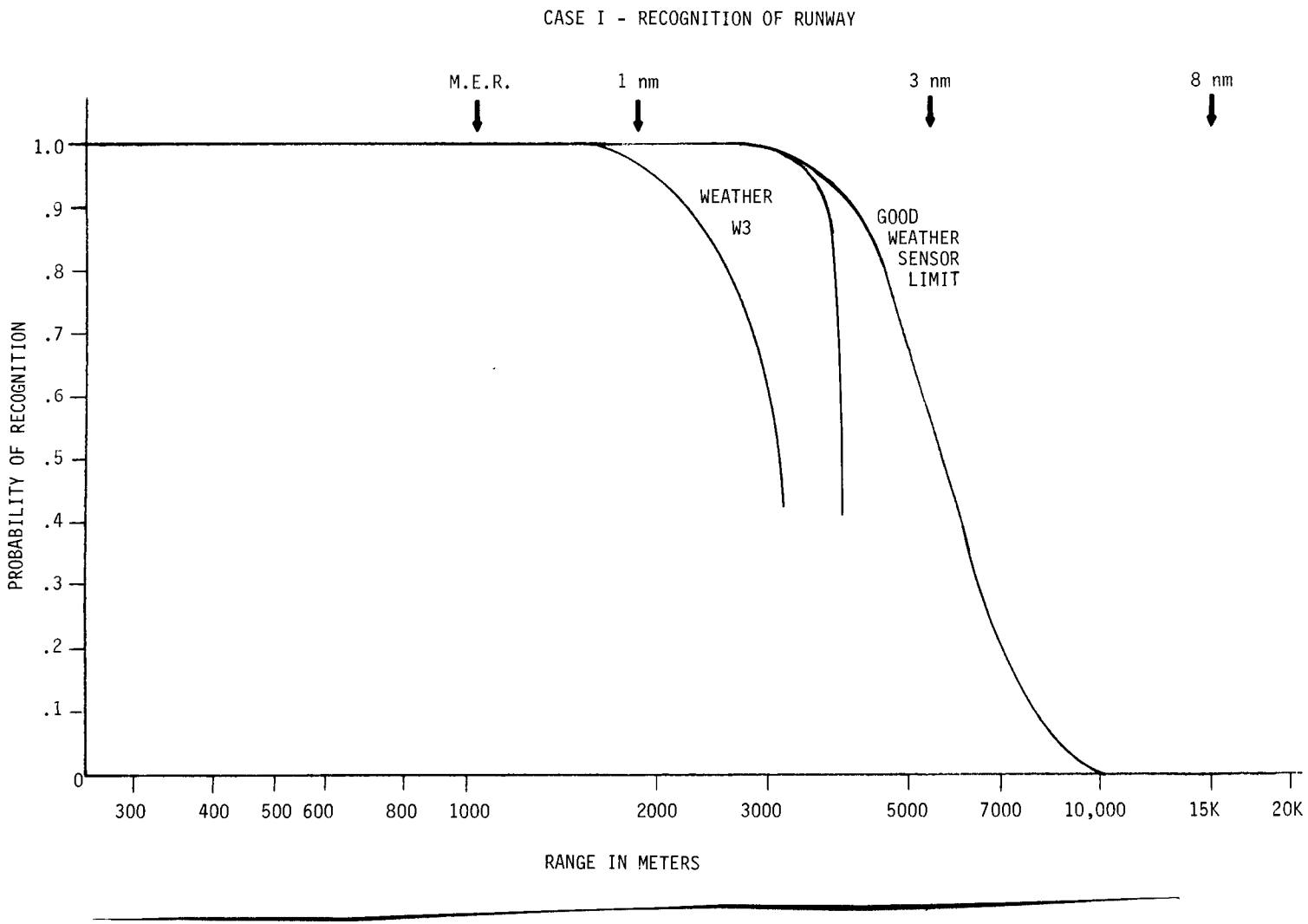

Figure 104-- TV Performance, Probability of Recognition vs Range

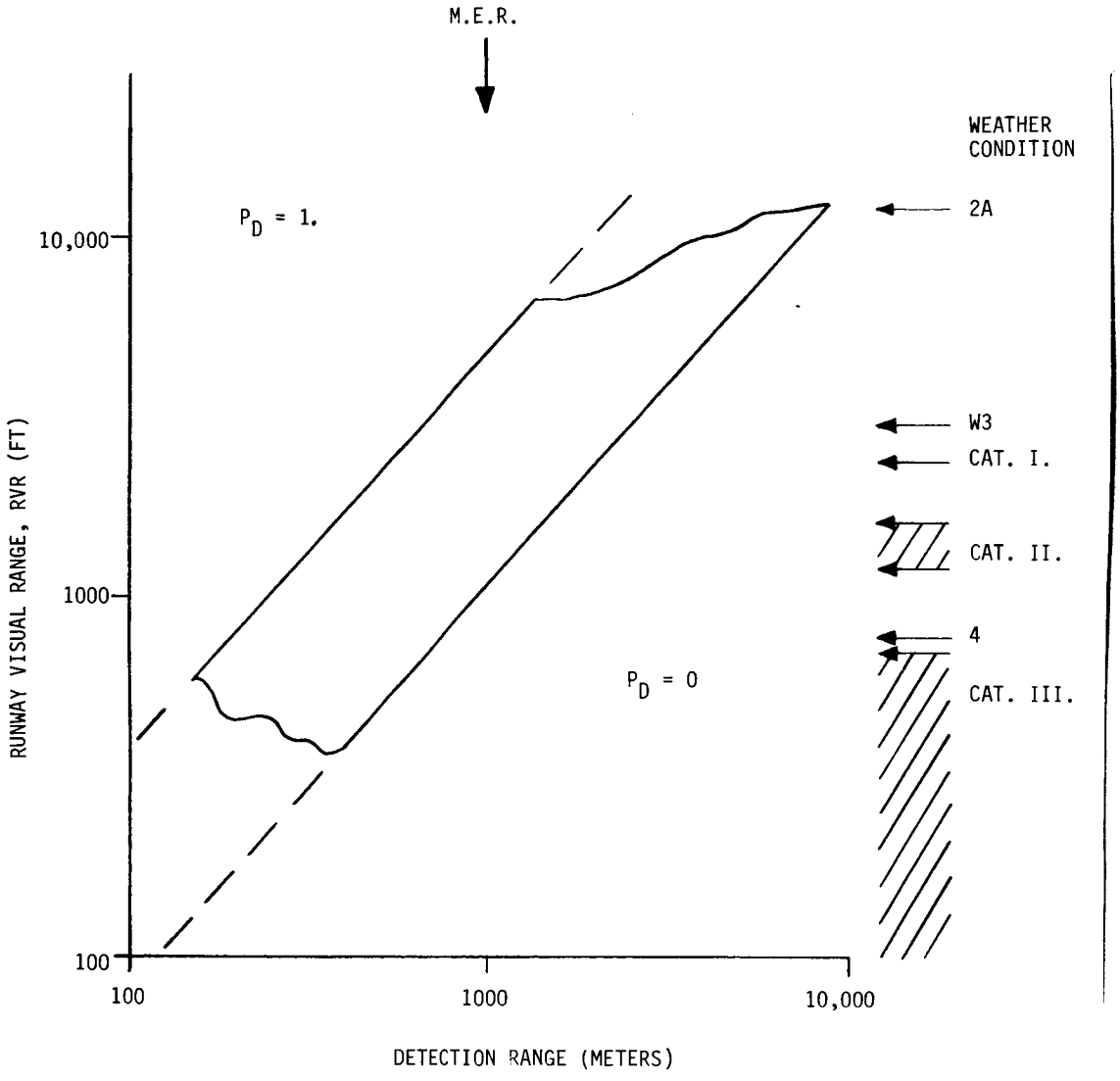

Figure 105 -- TV Performance Against Runway Lights

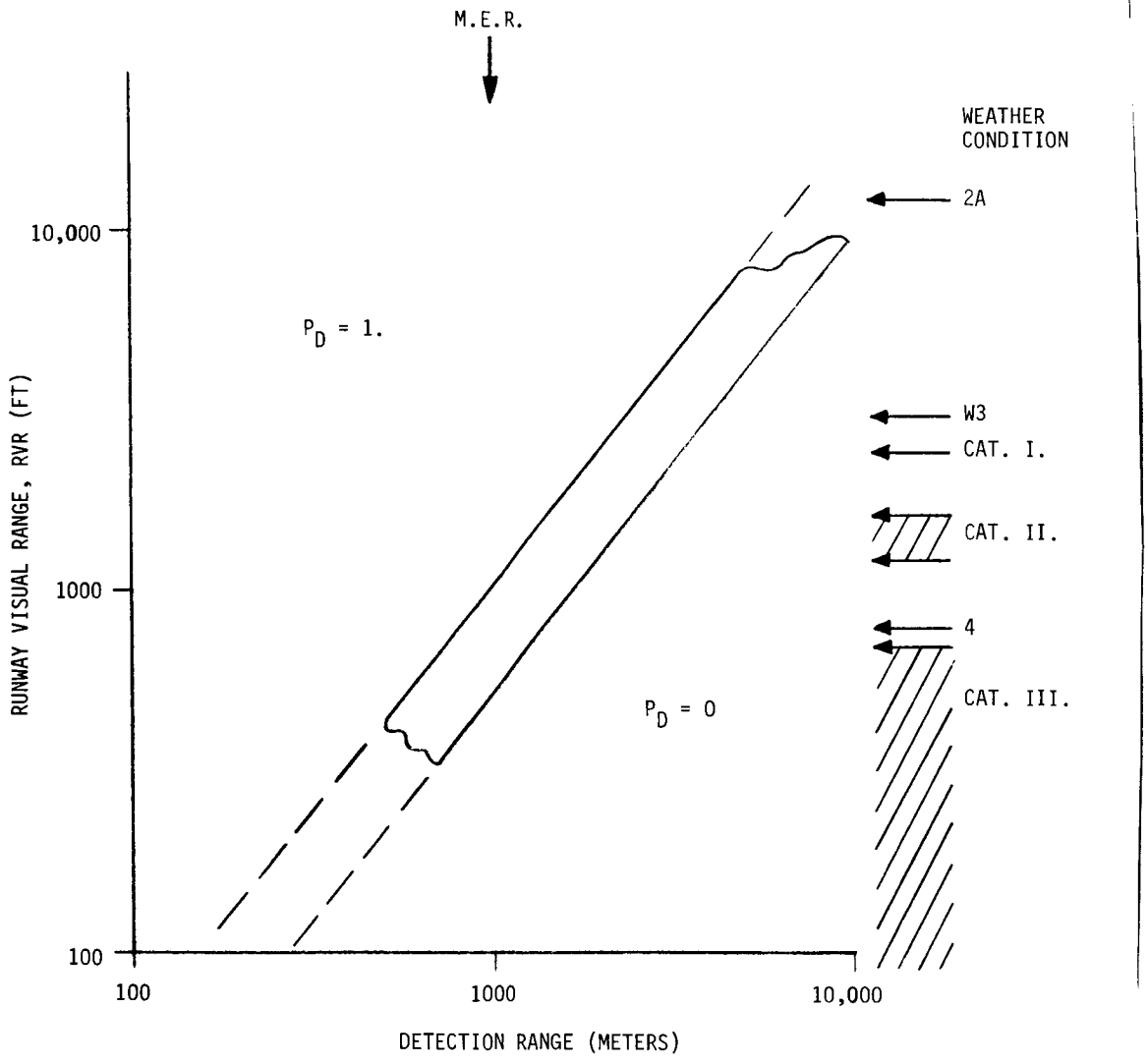

Figure 106 -- TV Performance Against Approach Lights

Obstacle Target -- A 3m by 3m by 3m box was used to represent an obstacle on the runway. Figure 107 shows the detection ranges and Figure 108 shows the recognition ranges for this target. The better performance is for the concrete background; the poorer performance is for the asphalt background.

Active TV -- The active TV sensor has the characteristics of the passive TV with the addition of a laser illuminator and image intensifier. Two stages of intensification were evaluated by assuming a 100 times increase in camera tube sensitivity. The illuminator is a 30 watt laser (average power) spectrally matched to the TV tube. The illuminator is pulsed and the TV tube gated to eliminate most of the backscatter at night.

Detection ranges of 2000 meters were achieved for only the better weather condition. In other cases, detection occurred only at ranges of less than the minimum effective range.

Tracking TV -- The tracking TV has passive TV characteristics as described earlier. System performance is measured not by the observer related probability of detection and recognition but rather by the system signal-to-noise ratio.

Approach Light Target -- In the better weather conditions, the S/N is adequate for tracking at ranges out beyond 8 nautical miles. However, in Category I conditions, tracking is unlikely at ranges over 3000 to 4000 meters (depending upon lighting conditions) and the worse weather conditions result in shorter ranges.

TV Summary

The TV sensor provides only limited operating capability as an ILM system.

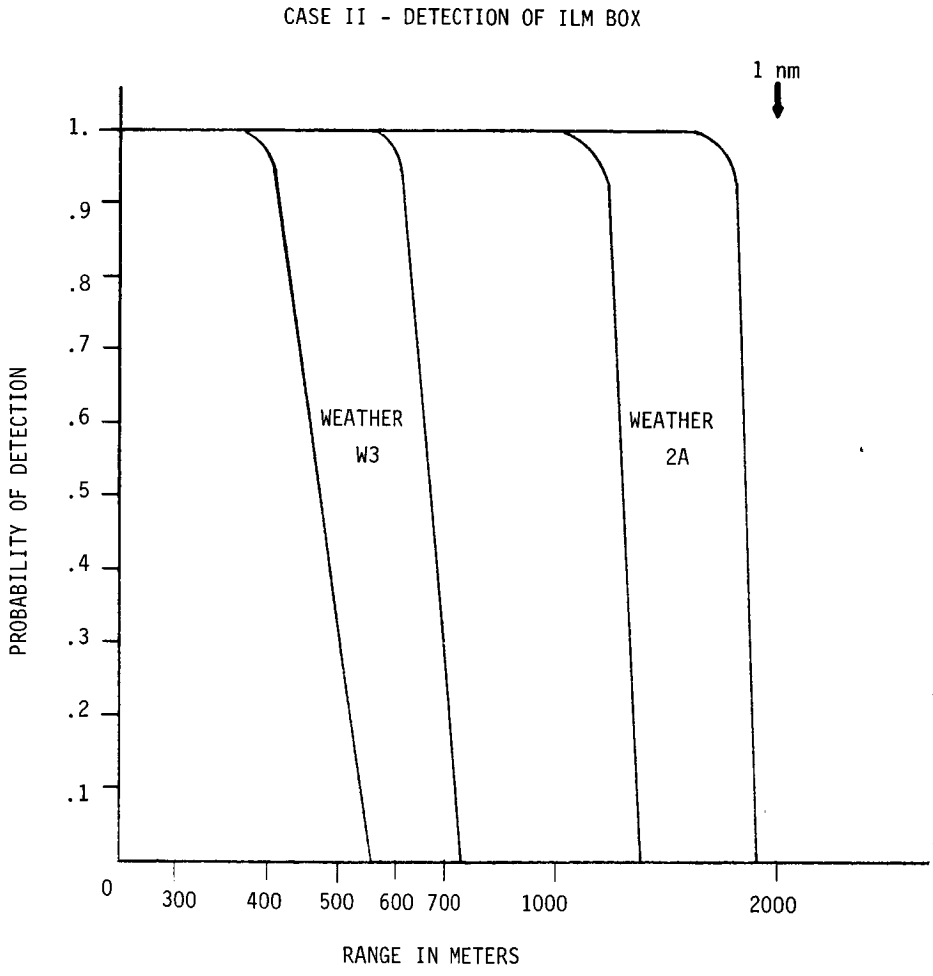

Figure 107 -- TV Performance, Detection of Obstacle

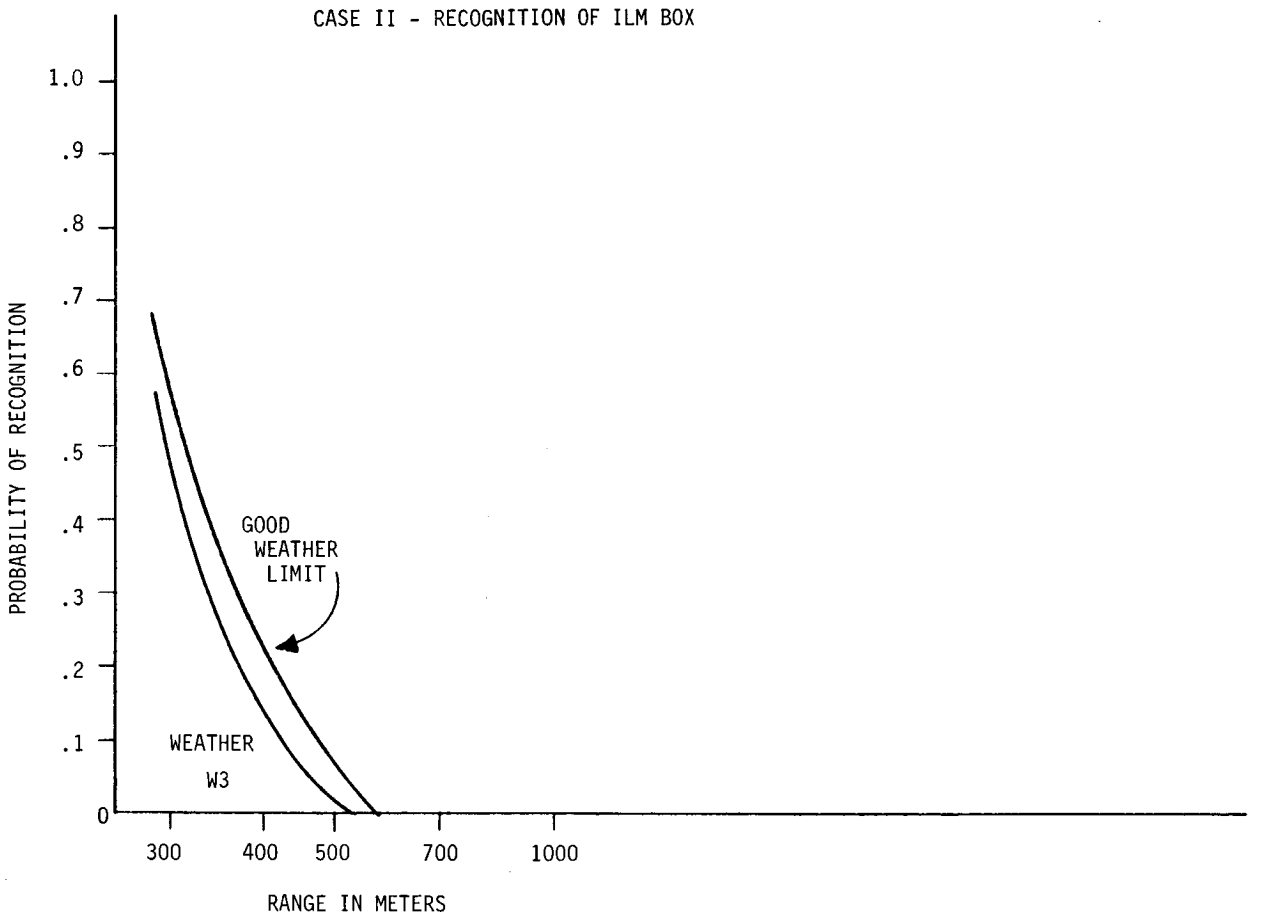

Figure 108 -- TV Performance, Recognition of ILM Box

Adequate detection/recognition ranges are possible only under the better weather conditions. These ranges are summarized below:

	(detection)	(recognition)
o Runway Target		
Weather 2A	2000 - 5000 m,	1200 - 3500 m
Weather W3	500 - 1300 m,	500 - 1100 m
Category I*	400 - 1000 m,	400 - 1000 m
Category II*	300 - 800 m,	300 - 800 m
Weather 4	<1000 m,	<1000 m
Category III*	<1000 m,	<1000 m
o Runway Lights	(detection)	
Weather 2A	7000 - 8000 m	
Weather W3	700 - 2500 m	
Category I*	600 - 2000 m	
Category II*	500 - 1500 m	
Weather 4	<1000 m	
Category III*	<1000 m	
o Approach Lights	(detection)	
Weather 2A	15,000 m	
Weather W3	2600 - 3500 m	
Category I*	2000 - 3000 m	
Category II*	1200 - 2000 m	
Weather 4	800 - 1300 m	
Category III*	<1000 m	

*Results inferred from results of MARSAM weather cases.

- Obstacle Target (detection) (recognition)
  - Weather 2A 1200 - 1800 m, 250 - 400 m
  - Weather W3 400 - 650 m, 250 - 350 m
  - Category I* 300 - 500 m, 200 - 300 m
- Active TV and Tracking TV

  No significant improvement over ranges achieved with passive TV.

In all cases, performance was limited by the contrast relationship in the model. The severe environmental conditions resulted in very low contrast at the sensor. Therefore, sensor improvements in terms of resolution or signal-to-noise ratio will not improve the results since the sensor's inability to provide adequate contrast is the limiting factor. The transmission of visible light is extremely sensitive to weather conditions and those conditions characterized by Categories I, II and III make detection and recognition unlikely at the ranges required of an ILM.

FLIR SENSOR CAPABILITIES

A forward looking infrared (FLIR) system detects and displays infrared energy emitted and/or reflected from the ground ahead of the aircraft. It provides a raster scan frame of the image scene, repeating the frame at periodic intervals to provide imagery in a TV-type format; that is, frame-by-frame so that targets or potential targets appear larger and better resolved in successive frames as the aircraft flies toward the target. Raster scanning is accomplished either by rotating mirrors, prisms, etc., in two axes or by scanning a linear array of detectors.

*Results inferred from results of MARSAM weather cases.

Infrared energy is generally considered to be that energy which lies in the spectral interval from 0.7 micron to approximately 1000 microns, although the part of the spectrum most often used is between 1 and 14 microns.

Environment

This subsection describes the characteristics of the energy received from targets and background; i.e., signatures, and the characteristics of the atmosphere through which the energy is transmitted.

Signatures -- The temperature of the earth and most objects on the earth is usually near 300°K. The spectral emittance for a 300°K blackbody (i.e., with an emissivity of 1), as shown in Figure 109 peaks at a wavelength near 10 microns. It is four orders of magnitude below the peak at 2 microns on the lower end and at 300 microns on the upper end.

For an emissivity less than one, the emitted energy is decreased in proportion to the emissivity. Table 51 shows emissivity averaged over several spectral regions for a number of materials. A characteristic common to most of the materials is that, for the longer wavelengths, the emissivity is typically above 0.9 (exceptions are, for the most part, highly reflective metals such as aluminum, stainless steel, and chrome-plate and highly reflective paints such as aluminum paint). Therefore, signatures at wavelengths longer than 8 microns will be primarily due to thermal differences while at shorter wavelengths the signatures will be functions of both emissivity and temperature.

The energy received from an object in the infrared is a result of radiant and reflected energy. The spectral radiant flux of an object as given by Planck's Law is:

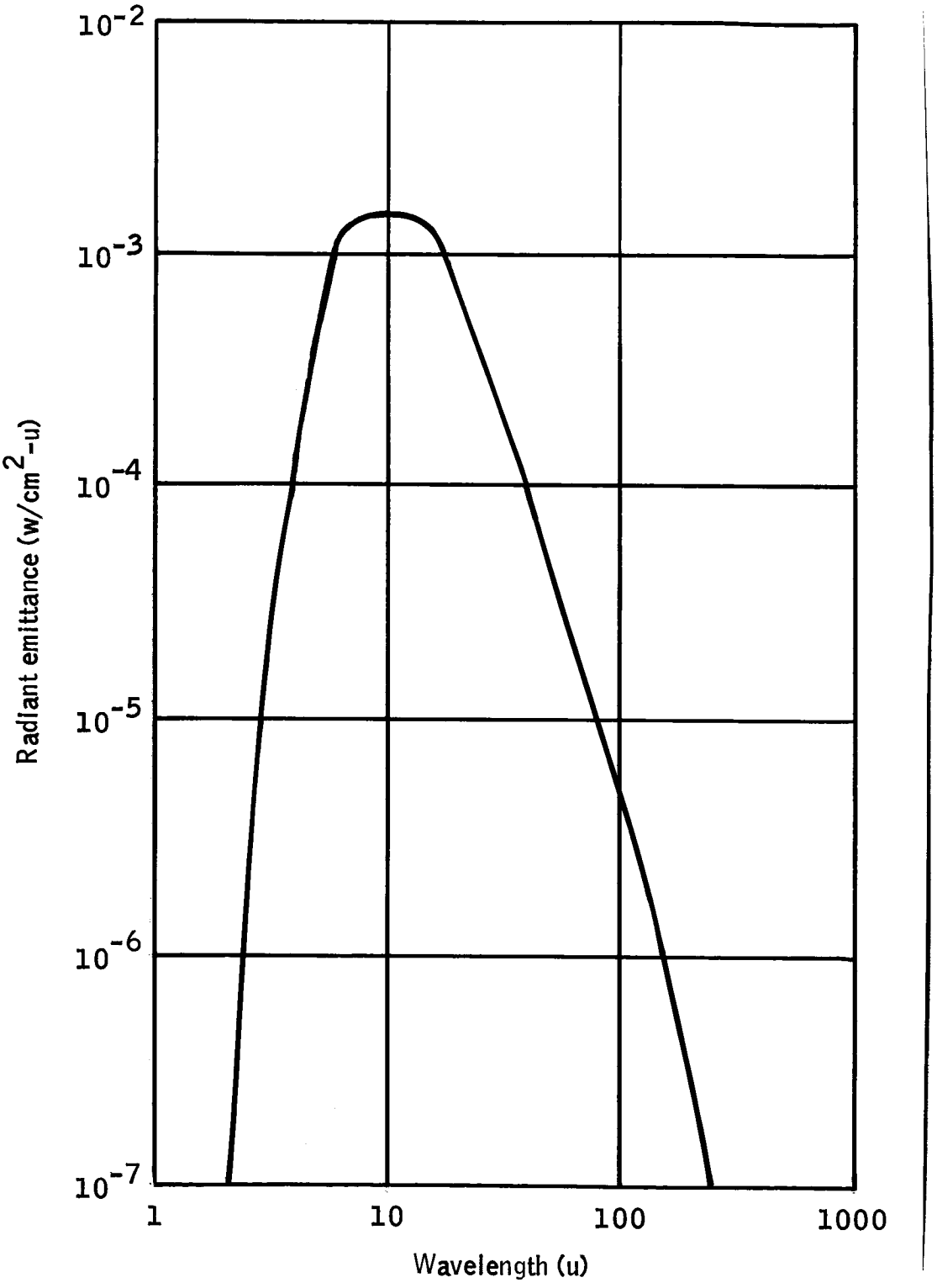

Figure 109 -- Radiant Emittance versus Wavelength
300°K Blackbody

Table 51 -- Emissivity of Materials

Type of Material	Average Emissivity 1-3 Microns	3-5 Microns	8-10 Microns
Fescue, meadow, dry grass	0.61	0.80	0.89
Oak leaf, winter color, top, dry	0.69	0.89	0.91
Laurel, mountain, green leaf	0.72	0.89	0.92
Red pine - needles	0.77	0.97	0.98
Bark, red northern oak	0.79	0.90	0.95
Soil, pullman loam, New Mexico	0.65	0.78	0.93
Soil, Hainanamu silt loam, Hawaii	0.84	0.84	0.94
Sand, Atlantic City, New Jersey	0.35	0.65	---
Paint, pigment No. 6, chrome green 1	0.65	0.85	0.99
Paint, aluminum, chromaton	0.79	0.30	0.37
Cement	0.60	0.88	0.99
Asphaltic road material	0.75	0.79	0.91
Chrome plate on stainless steel	0.35	0.20	0.10

$$W = 2\pi c^2 h \varepsilon(\lambda) \lambda^{-5} (e^{hc/\lambda kt} 1)^{-1} \quad (\text{watts/cm}^2/\text{cm } \lambda) \tag{131}$$

where c = speed of light = 3×10^{10} cm/sec

h = Planck's constant = 6.625×10^{-34} watt sec^2

λ = wavelength of energy (cm)

T = temperature of the object (°K)

k = Boltzmann's constant = 1.38×10^{-23} watt sec/°K

$\varepsilon(\lambda)$ = spectral emissivity of the object

The total radiant flux (power) per unit area over a specific spectral interval is:

$$W = 2\pi c^2 h \int_{\lambda^1}^{\lambda^2} \varepsilon(\lambda) \lambda^{-5} (e^{hc/\lambda kt} - 1)^{-1} \, d\lambda \quad (\text{watts/cm}^2) \tag{132}$$

where λ_1 and λ_2 are endpoints of the spectral interval and emissivity is assumed independent of temperature.

The spectral reflected flux per unit area is given by:

$$X_\lambda = 2\pi r(\lambda) \cdot I(\lambda) \quad (\text{watts/cm}^2/\text{cm } \lambda) \tag{133}$$

where $r(\lambda)$ = spectral reflectivity of the object

$I(\lambda)$ = spectral irradiance due to some illumination source

The primary daytime illumination source is the sun. At night the moon, stars and airglow are the major sources. The total reflected flux over a wavelength interval is

$$X = \pi \int_{\lambda_1}^{\lambda_2} r(\lambda)\, I(\lambda)\, d\lambda \quad (\text{watts/cm}^2) \tag{134}$$

The total energy per unit area available at an object is the sum of W and X.

For opaque bodies, the relationship between emissivity and reflectivity is

$$\varepsilon(\lambda) = 1 - r(\lambda) \tag{135}$$

In a blackbody

$$\varepsilon(\lambda) = 1 \tag{136}$$

and

$$r(\lambda) = 0 \tag{137}$$

Most materials in the real world are nearly opaque to infrared energy so that the above relationships hold in general.

During daylight hours, the irradiance from sunlight may be sufficiently high so that the reflected energy is larger than the emitted energy. At night, the irradiance due to moonlight and starlight is small so that radiant energy predominates. At dawn and dusk, the two terms are of comparable magnitude and because of the relationships between reflectivity and emissivity, the contrast between target and background is very low so that a phenomenon called "wash-out" may occur.

Although IR sensors can be used either during daylight or at night, their primary application is for low light operation where most sensors operating in the visible tend to lose effectiveness. Therefore, the effectiveness of IR sensors will be considered primarily under low light operating conditions where the contribution of reflected energy can be neglected.

Atmospheric Considerations -- Attenuation of infrared energy in the atmosphere is caused mainly by absorption and scattering. Absorption is primarily due to CO_2 and H_2O in the gaseous state in the atmosphere. Figure 110 is a coarse sketch of atmospheric transmission for a typical day, in the spectral region between 1 and 14 microns (see Reference 57). The three intervals 1-2.5, 3-5 and 8-14 microns are often called atmospheric windows because transmission is relatively high within these intervals. The windows dictate the part of the spectrum in which an IR system must operate. At present, most systems operate in the 8-14 micron window although some use the 3-5 micron region.

The transmissivity due to absorption for a particular weather condition can be approximated using calculations described in Reference 11. Determination of H_2O transmissivity is accomplished by entering the precipitable water value into empirical tables (from Reference 11) which give transmissivity as a function of precipitable water and wavelength. The transmissivity, averaged over the spectral interval of interest, is obtained from the table.

Calculation of CO_2 transmissivity requires calculation of an equivalent sea level range from the slant range by a method also described in Reference 11. Empirical tables, providing transmissivity as a function of sea level range and wavelength, are used to determine transmissivity due to CO_2 absorption averaged over the spectral interval of interest.

Attenuation due to scattering is a result of particles having sizes approaching and exceeding the wavelength of the energy of interest. A model for approximating the magnitude of transmissivity due to scattering, using visibility coefficients, is described in Reference 3. The model assumes a layered atmosphere with

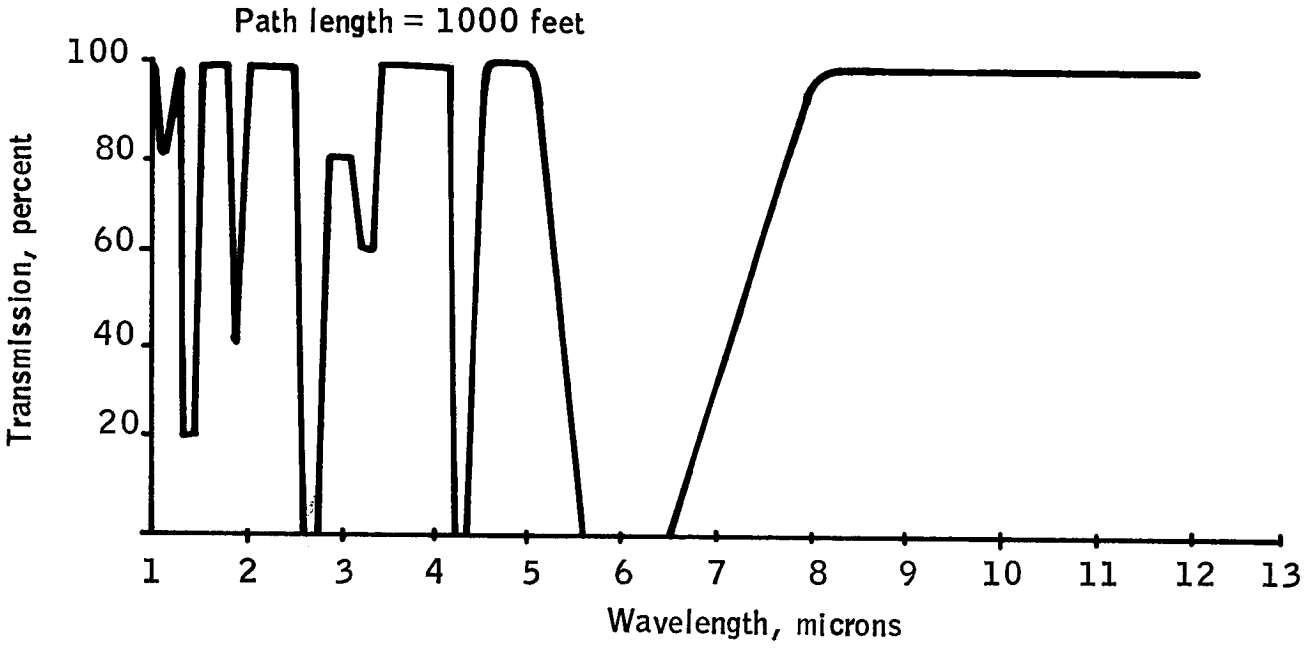

Figure 110 -- Atmospheric Transmission versus Wavelength

a visibility coefficient given for each layer for several weather conditions.

The product of the three transmissivities described above, i.e., due to H_2O absorption, CO_2 absorption, and particle scattering, represents the total one way transmissivity of the atmosphere. Figure 111 shows transmissivity as a function of range for several weather conditions over the 8-14 micron spectral interval.

Spectral Interval -- The performance of an IR system is a function of the following spectrally dependent factors:

1) Emissivity
2) Detector detectivity
3) Atmospheric transmission
4) Blackbody spectral irradiance

Infrared systems are usually designed to operate in one of the three aforementioned atmospheric windows. Most current systems are designed for operation over some or all of the 8-14 micron region for the following reasons:

1) The 300°K blackbody spectral irradiance peaks at about 10 microns with almost 40 percent of the total energy contained in the 8-14 micron interval.
2) Atmospheric losses due to scattering decrease as wavelength increases; therefore, larger wavelengths provide better fog and haze penetration.
3) The photon noise limited detectivity (D*) for objects near 300°K increases rapidly between 5 and 15 microns.

This study will consider systems operating in the 8-14 micron window for the above three reasons and because emphasis on current systems is in that spectral region.

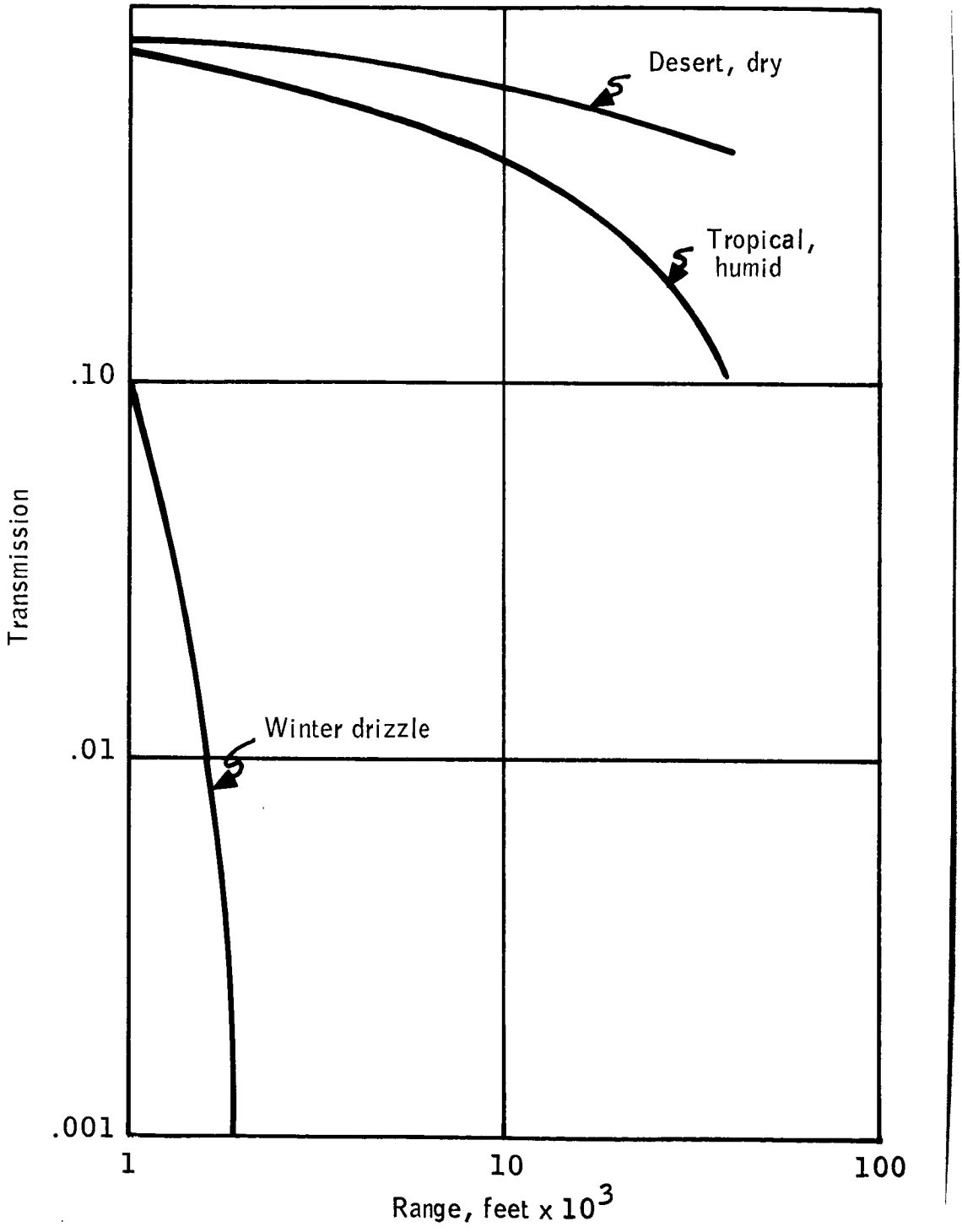

Figure 111-- Atmospheric Transmission vs Range, 8-14 microns

System Performance Characteristics

The performance of an infrared system is measured in terms of the resolution (or spatial frequency response) and available signal to noise ratio of the system. The resolution of the system is a function of the apparent contrast (or modulation) of the signal, of signal power, and of noise as well as characteristics of the detector and optics. This subsection briefly presents the relationships between the parameters and identifies performance limits.

Received Power -- Assuming a square detector such that the area at the target viewed by the detector is square, then the area of the target is

$$A_c = S_r^2 \Delta\theta^2 \tag{138}$$

where S_r = slant range to target

$\Delta\theta$ = instantaneous FOV of the IR system

Assuming that the surface is Lambertian, the radiant intensity from the body is

$$I = \frac{WA_c}{\pi} = \frac{WS_r^2\Delta\theta^2}{\pi} \text{ watts/steradian} \tag{139}$$

where W = radiated power per unit area

Assuming a square aperture, D meters on a side, at the receiver gives a solid angle

$$\Omega = \frac{D^2}{S_r^2} \text{ steradians} \tag{140}$$

subtended by the receiver aperture.

Therefore, the power at the detector is

$$P_d = \frac{\tau_a \tau_o \Delta\theta^2 D^2 W}{\pi} \text{ watts} \qquad (141)$$

where τ_a = atmospheric transmission

τ_o = optics transmission

Spatial Frequency Response -- System spatial frequency response or modulation transfer function (MTF) is a function of:

1) MTF of the ideal scanning cell
2) MTF of the optics
3) MTF due to random effects in the atmosphere and lens
4) MTF due to image motion
5) Frequency response of the detector
6) Frequency response of the video processor
7) MTF of the display
8) MTF of the storage device (if one is used)

Reference 58 shows that for a 0.5mr instantaneous field-of-view, it is possible to make effects 2, 3 and 4 small with respect to the first. However, for a 0.1mr instantaneous field-of-view, image motion and random effects can be significant. For such small fields-of-view, the sensor must be isolated from the aircraft and stabilized to minimize short term motion. Atmospheric random effects will probably be small at night but random effects in the optics must be closely controlled in the manufacturing process and also designed to minimize distortion in the airborne environment.

The frequency response of the video processor can, in general, be made sufficiently high so that very little degradation occurs in existing systems. However, storage

and display media currently exhibit low MTF and tend to seriously degrade the system MTF, although improvements are being made in such devices.

Assuming that the degradation in MTF due to other factors is small compared to the MTF of the instantaneous field-of-view, the analysis is very simple. The MTF of a square aperture is given by:

$$T(k) = \frac{\sin \pi k/\Delta\theta}{\pi k/\Delta\theta} \tag{142}$$

where k = spatial frequency (cycles/scan line)

$\Delta\theta$ = instantaneous field-of-view (radians)

$\frac{1}{\Delta\theta}$ = the first zero of $T(k)$

If contiguous scanning is assumed (that is, the scan lines touch but do not overlap) and if the number of scan lines in each frame is assumed to be equal to $\frac{\theta}{\Delta\theta}$, then the along-track resolution is 1/2 of the cross-track resolution. The truth of this statement is verified by the sampling theorem which essentially states that a sampling rate of S samples per second can be used to quantize frequencies as high as S/2 cycles/second with no ambiguities.

Because the resolution is different in the two orthogonal directions (along-track and cross-track) and because the target being viewed can have any orientation relative to the sensor, the system resolution can be approximated by a $\frac{\sin X}{X}$ type response but with the variables adjusted so that the first zero occurs between $\frac{1}{2\Delta\theta}$ and $\frac{1}{\Delta\theta}$.

Noise -- The signal in an IR system is competing with noise from two sources:

1) Background photon noise, emanating from any object with temperature above 0°K.

2) System noise; that is, noise generated within the system.

Background noise is photon-noise produced by surfaces to which the detector is exposed which have temperatures above 0°K. Sources of such noise include the earth, atmosphere, and that part of the FLIR system near the detector. The background photon noise provides a theoretical limit on the detectivity of detectors which is discussed later.

System noise is an important consideration at the "front end" of the system, prior to signal amplification, where the signal is very small. The most important sources of noise in the front end are the detector and the first amplifier stage. Usually, the amplifier noise can be made sufficiently small so that detector noise dominates as the primary cause for system noise.

Noise equivalent power (NEP) is defined as "that value of incident rms signal power required to produce a rms signal voltage to rms noise voltage ratio of unity" (see Reference 59). Spectral NEP refers to the above definition when the signal is monochromatic and blackbody NEP when the signal has blackbody spectral character. The noise equivalent power of a detector can be expressed in terms of its detectivity, D*, as follows:

$$NEP = \frac{\sqrt{A \quad \Delta f}}{D^*} \tag{143}$$

Where A = detector area

Δf = detector bandwidth

Noise equivalent temperature (NET) is another measure of system performance in the presence of noise. NET is defined as the temperature differential necessary to produce an rms signal equal to the rms noise. Reference 60 derives the following expression for NET:

$$NET = \frac{\pi}{4\sigma} \frac{NEP}{\varepsilon(T)\ F(T\ ,\ \lambda)\ T^3 \Omega A_o} \quad (°K) \tag{144}$$

where σ = Stefan-Boltzmann constant (watts/cm^2-°K^4)

$\varepsilon(T)$ = emissivity as a function of temperature

$F(T,\lambda)$ = fraction of total energy of a blackbody at temperature T contained in wavelength interval λ_1 to λ_2 to which the detector is sensitive

T = temperature of body being observed (°K)

Ω = solid angle which detector sees (instantaneous FOV solid angle)

A_o = area of optics entrance aperture (cm^2)

NEP = noise equivalent power (watts)

System Bandwidth -- The required bandwidth for each detector in an IR scanner is given approximately by

$$\Delta f = \frac{\theta}{\Delta\theta}\ N_S \ (Hz) \tag{145}$$

where θ = total cross-track field-of-view

$\Delta\theta$ = instantaneous field-of-view

N_S = number of times detector is scanned/second

In a FLIR with a linear array of detectors,

$$N_S = I_n \cdot F \tag{146}$$

where I_n = interlace ratio

F = frame rate

Limiting Resolution -- In an infrared system, the limiting resolution is given by the modulation transfer function only if the system is noiseless. In the

presence of noise, the resolution limit depends on the signal-to-noise ratio as well as the MTF. Suppose that the system is scanning a bar pattern (i.e., alternate strips of material with temperature difference ΔT) of frequency k, where k is less than or equal to k_o, the resolution limit determined by the scanning beam. The signal-to-noise ratio for this pattern is given by

$$S/N = \frac{P_H - P_L}{NEP}\sqrt{\frac{k_o}{k}} \tag{147}$$

where P_H = power received from the higher temperature strip

P_L = power received from the lower temperature strip

$\frac{k_o}{k}$ = the improvement factor obtained when the width of the strips exceeds the width of the resolution element

k = spatial frequency, cycles/unit distance

The modulation of the signal is given by:

$$M = \frac{P_H - P_L}{P_H + P_L} \tag{148}$$

which can be rearranged to give

$$P_H - P_L = M(P_H + P_L) \tag{149}$$

Then the signal-to-noise ratio can be rewritten in terms of modulation as:

$$S/N = \frac{M(P_H + P_L)}{NEP}\sqrt{k_o/k} \tag{150}$$

and, solving for modulation yields

$$M = \frac{(S/N) \cdot (NEP)}{P_H + P_L}\sqrt{k/k_o} \tag{151}$$

It is assumed that some minimum value of signal-to-noise ratio (S_{min}) is necessary to just detect the signal. Then, for a particular value of target power

and background power, it is possible to plot the minumum necessary modulation to provide an S/N ratio of k using:

$$M_L = \frac{S_{min}NEP}{P_H + P_L}\sqrt{k/k_o} \tag{152}$$

where M_L = limiting modulation

The graphical procedure for finding the limiting resolution is as follows:

1) The modulation transfer function of the system is plotted.
2) Signal modulation as a function of spatial frequency is plotted for a number of values of input modulation (signal modulation is the product of MTF and input modulation).
3) Limiting modulation (M_L) is plotted for various values of $P_H + P_L$ (in this case, if small temperature differences are assumed, then $P_H \approx P_L$ = received power from a 300°K blackbody and $P_H + P_L$ is a function of atmospheric transmission).
4) The intersection of the limiting modulation curve with the signal modulation curve is the limiting resolution.
5) For a particular weather situation, the atmospheric transmission is a function of range only; therefore, $P_H + P_L$ is a function of range only (for a 300°K target and background) and limiting resolution as a function of range can be plotted.

Optics Relationships -- The diffraction limit of the optics is given by

$$\Delta\theta = \frac{1.22\lambda}{D} \tag{153}$$

where $\Delta\theta$ = instantaneous field-of-view (radians)
λ = middle wavelength of IR being considered (meters)
D = diameter of entrance aperture (meters)

Therefore, to achieve a desired instantaneous field-of-view, it must be true that

$$D \geq \frac{1.22}{\Delta\theta} \tag{154}$$

The effect of the aperture size upon signal and noise power is determined as follows. It was stated previously that

$$NEP = \frac{\sqrt{A \cdot \Delta f}}{D^*} = \frac{d\sqrt{\Delta f}}{D^*} \tag{155}$$

where d = size of detector (m)

Assuming that D* and f are fixed for a given system,

$$NEP = K_1 d \tag{156}$$

$$\text{where} \quad K_1 = \frac{\sqrt{\Delta f}}{D^*}$$

In the expression for received power

$$P_r = \frac{\tau_a \tau_o \Delta\theta^2 D^2 W}{\pi} \tag{157}$$

the transmission factors can be assumed constant for a particular set of conditions. Then,

$$P_r = K_2 (\Delta\theta)^2 \cdot D^2 \tag{158}$$

$$\text{where} \quad K_2 = \tau_o \tau_a \frac{W}{\pi}$$

The signal-to-noise ratio is then

$$S/N = \frac{P_r}{NEP} = \frac{K_2(\Delta\theta)^2 \cdot D^2}{K_1 d} \tag{159}$$

The above expression shows that the signal-to-noise ratio is maximized by minimizing detector size and maximizing entrance aperture.

Mechanization Considerations

Many problems which arise when IR systems are mechanized are basic limitations, such as available size and focal length for optics and physical constraints on the rotational speed of mirrors and prisms. Another important problem is that of scan conversion and display. In some FLIR's, where a linear array of detectors is scanned simultaneously, the outputs must somehow be made compatible with a CRT or other display device. Analog sampling techniques can be used, although high sampling rates are required.

Another technique uses the detector outputs to drive a linear array of photoemissive diodes. The diode outputs are, in turn, scanned across the photocathode of a vidicon. The vidicon is then scanned in conventional TV fashion to provide a raster type output. In either of these techniques, the significant factor which arises is that the dynamic range and resolution of the scan conversion technique will degrade system performance.

The current FLIR designs feature serial scanning techniques which result in a TV display compatible output. These sensors are made possible by new detectors with frequency responses compatible with serial scanning.

Limiting Components

The limiting components in an infrared system are those components which have the predominant effect on signal-to-noise ratio and resolution, primarily the optics and the detector. The theoretical and practical limits on the performance of detectors and optics are discussed below.

Detectors -- Detectors exhibit a number of properties which can limit the performance of IR systems. Among the most important of these properties are:

1) detectivity (D*)

2) frequency response

3) size

The detectivity is a measure of the capability of a detector to see a signal in the presence of noise and is best described in terms of noise equivalent power (NEP). Noise equivalent power is defined as the rms value of sinusoidally modulated radiation power at the detector which will give rise to a rms signal voltage equal to the rms noise voltage from the detector; assuming a 1 Hz bandwidth. The detectivity D* is then defined in terms of NEP as

$$D^* = \frac{\sqrt{A \cdot \Delta f}}{NEP} \tag{160}$$

where A = detector area (cm^2)

Δf = system bandwidth (Hz)

The noise with which the signal competes at the detector output is a result of background photon noise and noise generated in the detector. Assuming that the detector is ideal, with no internal noise and with unit quantum efficiency, the detectivity is a function of background photon noise only and is determined by equating the mean square fluctuation in the rate of photon arrival from the background to that from the target in the spectral range of the detector. Chapter 9 of Reference 57 derives the expression for D* in detail with the results shown in Figure 112. The curve represents the maximum detectivity that can be obtained for a 290°K blackbody source against a 290°K background as a function of cutoff frequency of the detector.

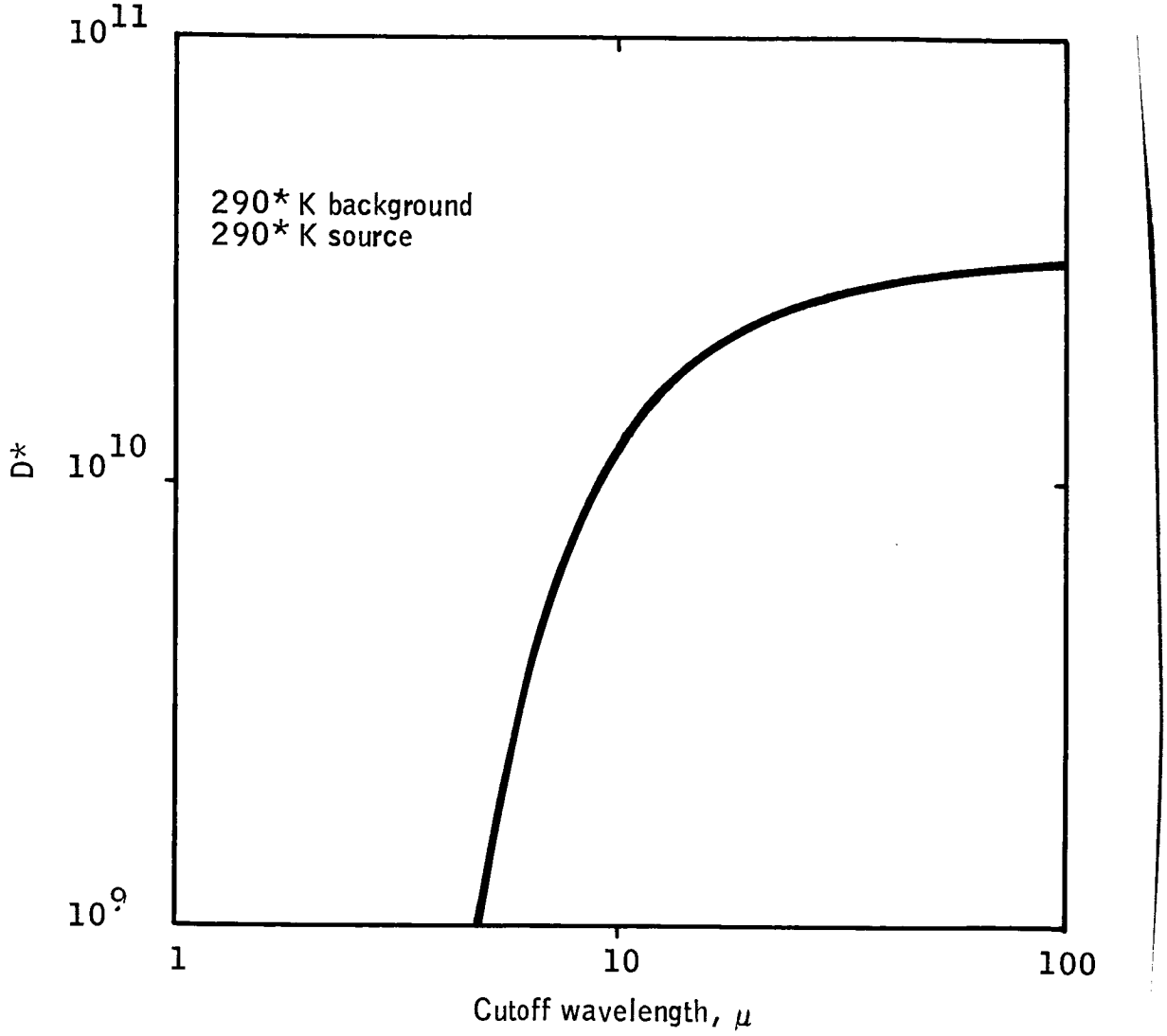

Figure 112-- Photon Noise Limited D*

The detectivity, as defined by Figure 112. is a useful figure of merit because it serves as a limit with which the measured detectivity can be compared. Provided that the detectivity is limited by background photon noise, and not by internal noise, the difference between measured and theoretical detectivity is a function only of the quantum efficiency of the detector.

Noise generated in a semiconductor is a result of current, thermal, and generation-recombination noise (Reference 57). Current noise can be essentially eliminated by technological methods such as improved techniques for preparing ohmic contacts. Thermal noise can be minimized by operating the detector at a low temperature. Generation-recombination noise is minimized by varying the doping in the semiconductor. The above techniques are sufficiently well developed so that, in general, detectors in the 8-14 micron spectral region can be made to operate photon noise limited.

Improvement can be obtained in the detector D* by using cooled apertures. Reference 57 shows that the improvement obtained by limiting an aperture to $\theta°$ is given by

$$D^*(\theta) = \frac{1}{\sin \theta/2} D^*(\pi) \qquad (161)$$

This improvement factor is plotted in Figure 113 as a function of angle and system f number.

Frequency response of the detectors is limited by carrier lifetime in the semiconductors. Decreasing detector temperature to reduce noise increases the carrier lifetime which, in turn, decreases the frequency response of the detector. The parallel scanning FLIRs typically use detectors with a frequency response of approximately 1 MHz at their usual operating temperature of 77°K for (HgCd)Te and

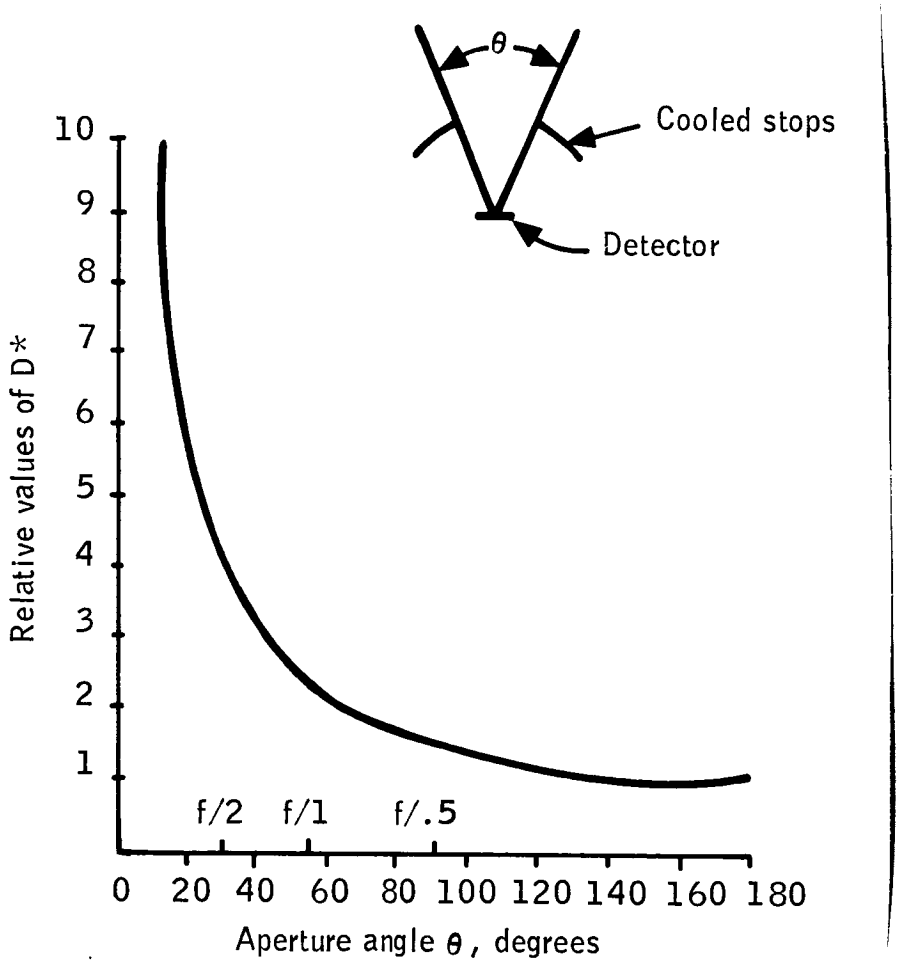

Figure 113-- Improvement in Detectivity With Cooled Aperture Stops

22°K for Ge:Hg. The more recent, serial scanning FLIRS utilize improved detectors with a frequency response of about 5 MHz.

An earlier section of this report showed that the detector size should be minimized to minimize the noise equivalent power. In the past, problems in technology such as packaging and attaching leads, limited the minimum size of detectors to approximately 0.1 x 0.1 mm. Recent improvements in technology now permit sizes down to 0.04 mm. However, edge losses appear as the detector size approaches 4λ, where 4λ = 0.04 mm for a 10 micron system.

Optics -- Optics technology for the relatively long wavelength (8-14 microns) used in the infrared sensor is confronted with two problems not encountered in the visible:

1) the longer wavelengths require greater physical size for equivalent diffraction limits,
2) the 8-14 micron interval represents a comparatively large range in wavelength, which increases the difficulty of correcting for chromatic aberrations.

Current technology can provide refractive optics as large as 0.5 meter in size which perform near the diffraction limits. The large optics require a great deal of correction for aberrations so that total size becomes very large as the optics diameter is increased. The large size and weight of the optics can create the following problems:

- Limited aircraft space and weight provisions may preclude the use of large optics,
- The large optics package is extremely difficult to slew and point,

o Very large diffraction limited optics are extremely costly.

For the above reasons, and because available space and weight in the aircraft are limited, it is likely that the maximum size of the optics in the future will be on the order of 0.2 meters diameter.

Scanning optics currently consist of rotating mirrors or prisms. Scanning of a detector array requires deflection in only one direction so that the rotational speeds are reasonable. For example, in a system with a frame rate of 30 frames/second, a maximum rotation rate of 30 revolutions/second is required. This number is significantly reduced by using many-faceted mirrors or prisms for scanning.

ILM FLIR Concept Evaluation

Imaging FLIR

General -- The MARSAM II computer model (Reference 11) was used to evaluate the potential of a FLIR sensor to meet the ILM requirements. A brief description of the MARSAM program is given in Appendix B. Three MARSAM weather cases were used to provide data that can be extrapolated to the conditions defined as Category I, II and III. Table 52 summarizes the MARSAM weather cases and includes comparative data for the ILM weather cases.

Representative characteristics for the FLIR scanner and display define the FLIR sensor system. Table 53 shows the characteristics of the scanner and Table 54 shows the characteristics of the optics used to define the three FLIR systems. These characteristics represent wide field-of-view (WFOV), narrow field-of-view (NFOV), and tracking field-of-view. The display characteristics are shown in Table 55 and Figure 114. Three display sizes for a viewing distance of 71 cm (28

Table 52 -- ILM FLIR WEATHER CASES

MARSAM Code or Category	VR (nm)	RVR m(ft)	β_i	Habs (g/m^3)	Hrel (%)	Air Mass	Model Homogenous Layer	Precipitation
2A	3.70 km (2)	3706.4 m (12,160)	1.812	12.0	61.6	Maritime Tropical	0-1524.0 m (0-5000 ft)	None
W3	0.93 km ($\frac{1}{2}$)	926.6 m	7.25	8.1	98.3	---	0-152.4 m (0-500 ft)	Drizzle or Rain
		(3,040)	36.25	8.1	98.3	---	152.4-1524.0m (500-5000 ft)	(5mm/hr)
Cat. I		731.5 m (2,400)						
Cat. II		487.7 m (1,600) 365.8 m (1,200)						
4	0.23 km ($\frac{1}{8}$)	231.6 m (760)	29.0	2.0	60.0	Maritime Polar	0-1524.0 m (0-5000 ft)	Snow (5mm/hr)
Cat. III		213.4 m (700)						

Table 53 -- FLIR Characteristics

Symbol	Value	Symbol Description
A_{le}	20.2 cm^2	Effective lens aperture
T	0.3°K	System thermal resolution
θ_x	10^{-3} rad	Angular resolution for in-flight direction
θ_y	10^{-3} rad	Angular resolution for cross-track direction
λ_1	8 microns	Lower wavelength limit of detector
λ_2	14 microns	Upper wavelength limit of detector
D_r	30 dB	Dynamic range of receiver
Receiver Type	Linear	

Table 54 -- FLIR Optics

Sensor Configuration	Field-of-View (VxH)
WFOV	0.367 rad x 0.829 rad (21.0° x 47.5°)
NFOV	0.367 rad x 0.48 rad (21.0° x 27.5°)
Tracking	0.14 rad x 0.14 rad (8.0° x 8.0°)

Table 55 -- CRT1 Performance Characteristics

Symbol	Value	Symbol Description
N_d	700 lines	Display resolution
V_{mid}	21.0 volts or 10.0 volts	Display input voltage corresponding to display brightness midpoint
V_{max}	27.5 volts	Display input voltage corresponding to display spot defocus
K_m	1.0	Constant which varies display operating point about midpoint
B_{da}	0.0 ft-lamberts	Display ambient brightness
B_d vs V	See Figure 114	Display brightness as a function of input voltage

Table 56 -- Display Size

Symbol	Symbol Description	Value		
		WFOV	NFOV	TRACKING
D_{dx}	Display dimension in along track (cm)	26.4	26.4	15.2
D_{dy}	Display dimension in cross track (cm)	62.0	34.8	15.2

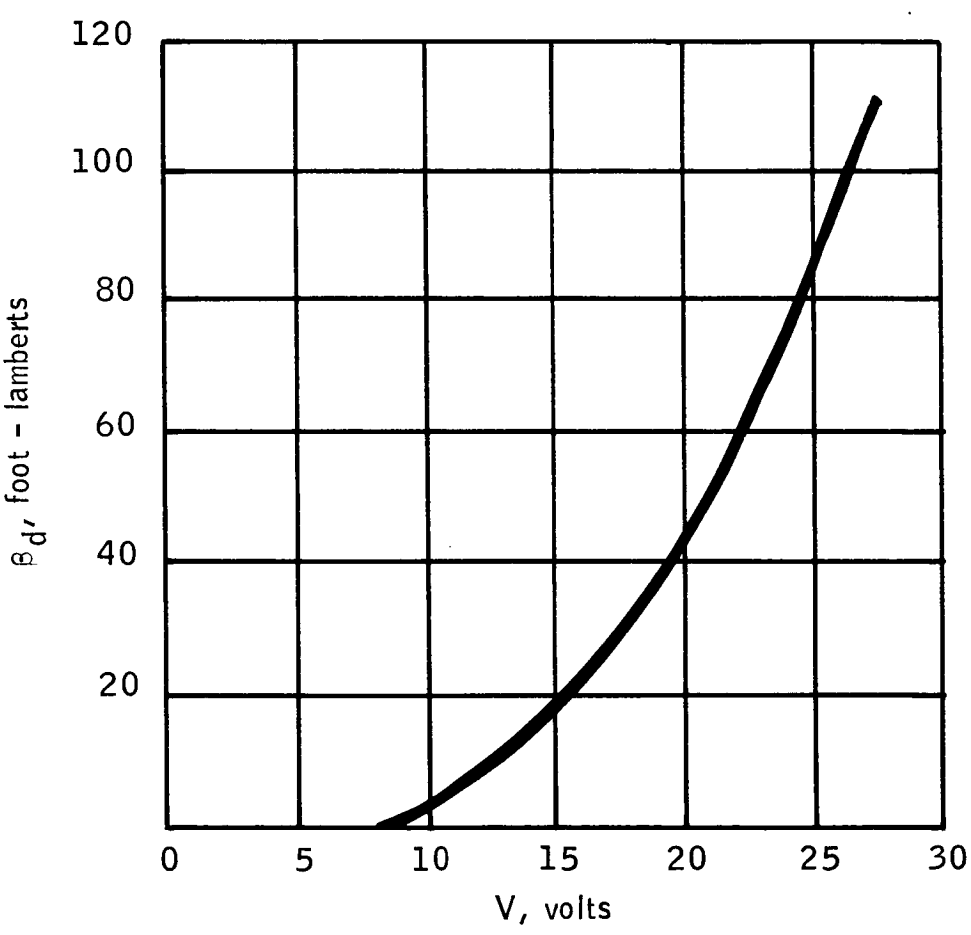

Figure 114 -- CRT1 Brightness (B_d) vs Grid Voltage (V)

in.), as defined in the requirements, are shown in Table 56, one for each field-of-view. As can be noted, the WFOV and NFOV display sizes are too large for practical installation. Shorter display viewing distances are required to accommodate the larger fields-of-view.

Sensor performance was evaluated as a function of slant range by specifying a 3 degree (.052 rad) glideslope and a wide range of altitudes. Platform velocity was varied from 90 knots to 145 knots with no change in performance. The target and background characteristics used in the analysis are summarized in Table 50.

Runway Target -- The ILM runway target is represented by a 23 meter by 1520 meter rectangle of asphalt or concrete. This target is located within a brown grass or snow background. Figures 115 and 116 show the results of this evaluation. Although the detection capability extends to 14.82 km (8 nm) for the better weather condition, target recognition is limited to about 3.70 km (2 nm). In Category I conditions (slightly worse than weather W3), detection and recognition occur at about 1.85 km (1 nm). Category III conditions (worse than weather 4) degrade performance to less than the minimum effective range (MER) of 1000 m defined in the requirements. That is, the probability of detection was zero for all ranges greater than the MER. Worst case targets here are concrete against brown grass and best case targets are concrete against snow (envelope boundaries in Figures 110 and 111).

Heater Target -- Heaters (active IR sources) were considered as potential landing aids. For the purpose of evaluation they were located against a brown grass background. Heater temperatures over the range of 400°K to 700°K (100° to 400°K above ambient) were evaluated. Heater sizes were .305 m x .305 m (1 ft. x 1 ft.) and .076 m x .076 m (3 in. x 3 in.). Because of the small size of the

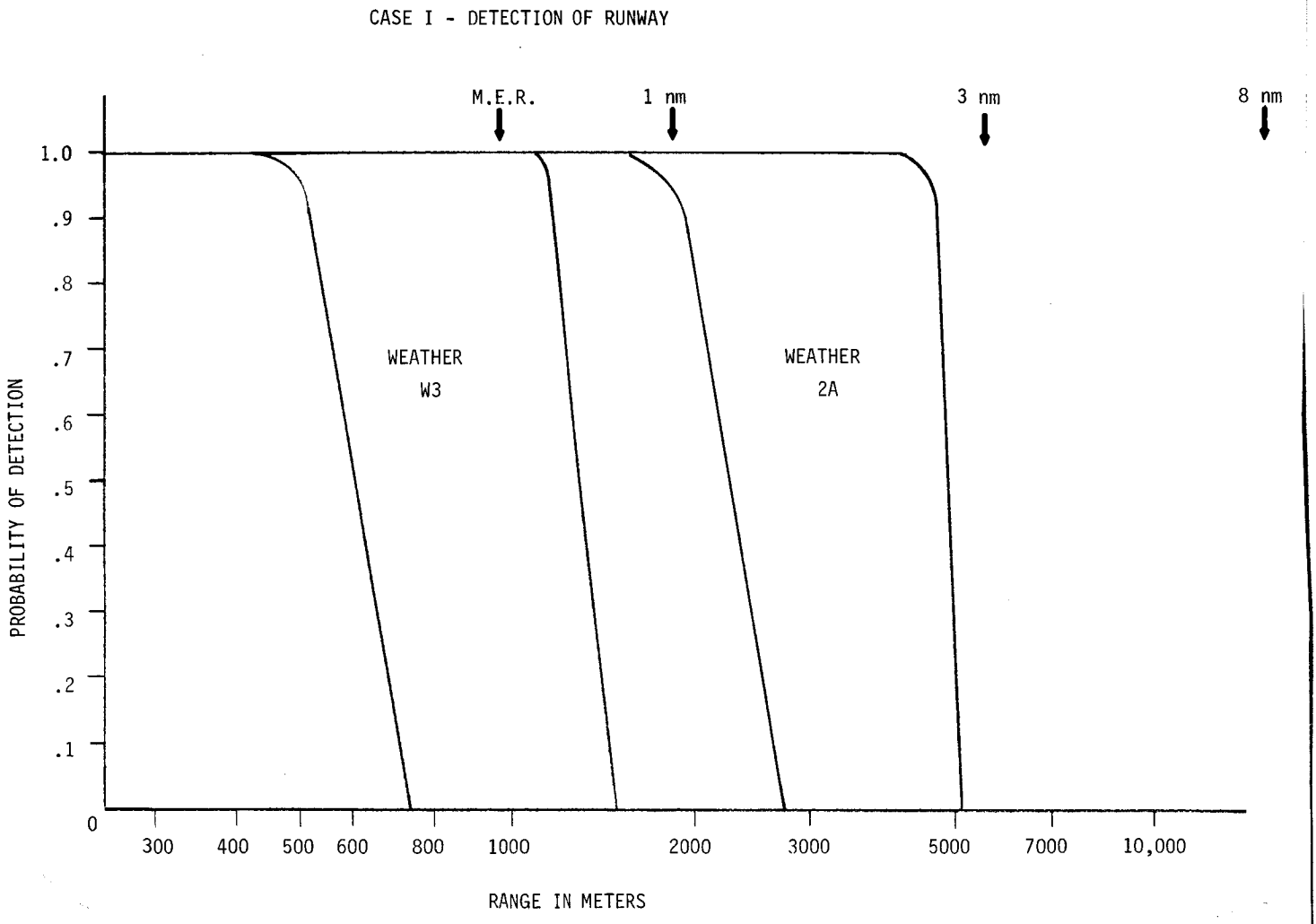

Figure 115 -- FLIR Performance, Probability of Detection vs Range

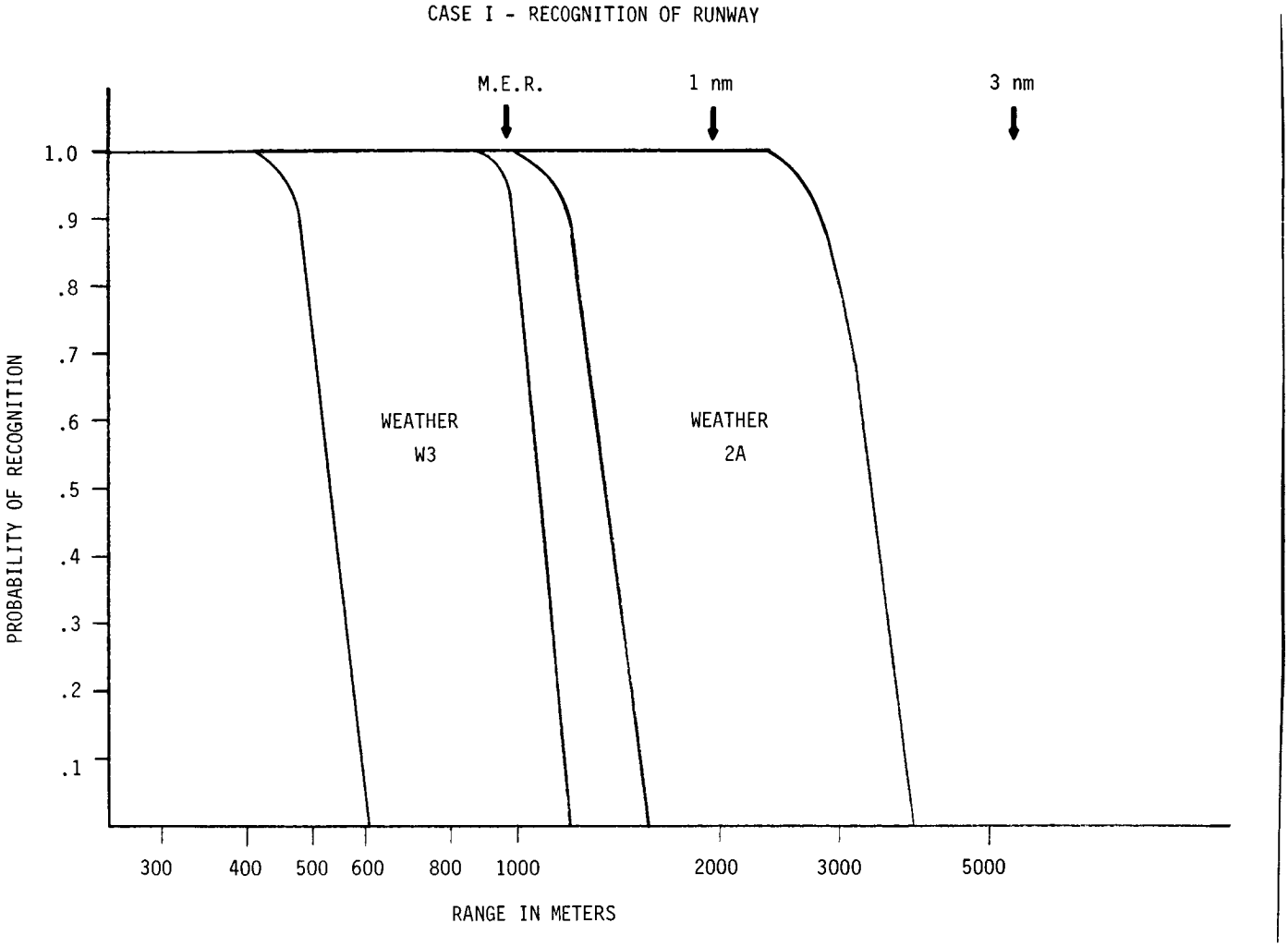

Figure 116 -- FLIR Performance, Probability of Recognition vs Range

heaters (compared to the resolution cell size), performance was worse than for the runways. At ranges greater than the minimum effective range (1000 meters), the probability of detection was low unless the weather was good (better than Category I).

Obstacle Target -- A 3m x by 3m by 3m box was used to represent an obstacle on the runway. Detection occurs at 1.85 km (1 nm) - 3.70 km (2 nm) in the better weather case. Recognition occurs at ranges of less than 600 meters. In the poorer weather cases (Category I and worse), detection occurs at ranges of less than 300 meters.

Tracking FLIR -- The tracking FLIR has characteristics described in the Subsection on tracking optics. System performance is measured, not by the observer-related probability of detection and recognition, but rather by the system signal-to-noise ratio. This FLIR is assumed to track an active IR source as described in an earlier paragraph. Because of the small size of the active target, the signal-to-noise levels were less than 3:1 at ranges over 1.85 km (one nautical mile). Therefore, the tracking system is judged to be poorer in performance than the imaging system with the runway target.

FLIR Summary

The FLIR sensor provides only limited operating capability as an ILM system. Adequate detection/recognition ranges are possible only under the better weather conditions. The results of the analysis are summarized below:

o Runway Target	(detection)	(recognition)
Weather 2A	10,000 m,	4,000 m - 7,000 m
Weather W3	2,000 m - 4,000 m,	2,000 m - 4,000 m
Category I*	1,500 m - 3,000 m,	1,500 m - 3,000 m

	(detection)	(recognition)
Category II*	1,000 m - 2,000 m	1,000 m - 2,000 m
Weather 4	<1,000 m,	<1,000 m
Category III*	<1,000 m,	<1,000 m

- o Heater Target (detection)
  - Weather 2A 5,000 m
  - Weather W3 1,500 m
  - Category I* <1,000 m

o Obstacle Target	(detection)	(recognition)
Weather 2A	2,000 m - 3,500 m,	<600 m
Weather W3	<300 m,	<300 m
Category I*	<300 m,	<300 m

- o Tracking FLIR

  Performance poorer than imaging against runway target. Tracking ranges less than 2,000 m.

*The severity of weather conditions characterized by Categories I, II and III limit the detection and recognition ranges to less than that required of an ILM.

MICROWAVE RADIOMETER ILM

Basic Radiometric Theory

Planck's Law -- Any substance which is at a temperature above absolute zero emits broadband noise energy caused by the thermally excited random movement of atomic particles. For a substance which is a perfect absorber (blackbody) at all frequencies, this energy is described by Planck's law.

Planck's radiation formula is:

$$P(\lambda,T) = \frac{2\,hc^2}{\lambda^5}\left[\exp\left(\frac{hc}{\lambda kt} - 1\right)\right]^{-1} \text{ Watts/m}^2\text{/Hz/Steradian} \qquad (162)$$

where P is the spectral radiance

λ is the wavelength

T is the temperature of the substance

c is the velocity of light

h is Planck's constant = 6.62×10^{-34} joule/sec

k is Boltzmann's constant = 1.38×10^{-23} joule/degree

The radiation formula describes the power available from a source of unit size at a given wavelength by intercepting a unit solid angle. Figure 117 is a plot of Planck's radiation formula for temperatures near normal ambient. It can be seen from Figure 117 that although the peak spectral radiance is in the infrared region, significant energy is still available at microwaves.

Since the region of interest is at a much longer wavelength then the peak energy wavelength, Planck's formula can be accurately represented by the Rayleigh-Jeans approximation. This approximation is derived by replacing the exponential function with a two term Taylor series, resulting in

$$P(\lambda,T) = \frac{2\,ckT}{\lambda^4} \text{ Watts/m}^2\text{/Hz/Steradian} \qquad (163)$$

For frequencies below 100 GHz and temperatures above 50°K, the error in this approximation is less than 3%. Since power and temperature are linearly dependent in this approximation, power may be referenced as a temperature.

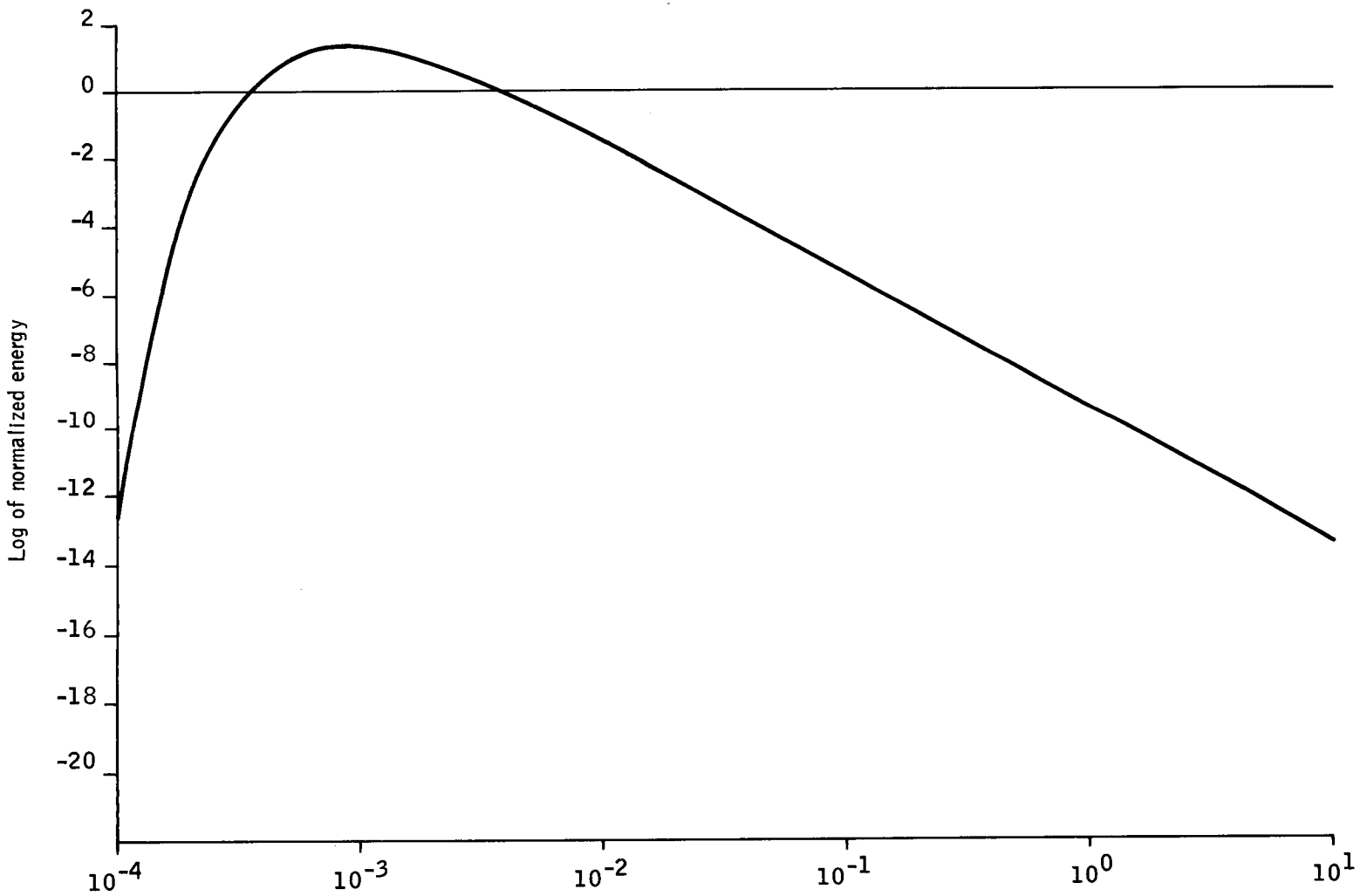

Figure 117 -- Planck's Radiation Function

Grey Body Radiation -- Real substances are not perfect absorbers, but reflect some percentage of incident radiation. For these substances, the emitted energy is related to the "black body" emitted energy through the emissivity ϵ. The emissivity is a function of frequency, incidence angle, surface roughness, etc., because it compensates for all deviations from ideal black body theory.

Conservation of energy requires that, for an opaque substance, the sum of the emissivity and the reflectivity be one. The reflectivity is the percentage of incident energy which is redirected away from the substance.

Atmospheric Emission -- Since the atmosphere absorbs microwave energy, it must also emit microwave energy in accordance with Kirchoff's law. This radiated energy has two effects:

- o It masks the scene
- o It is reflected from the scene

The effective sky temperature reflected from the scene is

$$T_s = \int_o^\infty \alpha_n T(\ell) \exp\left(-\int_o^\ell \alpha_n ds\right) d\ell \qquad (164)$$

where T_s is the sky temperature

α_n is the specific attenuation of the atmosphere in nepers/meter

T is the thermometric temperature of the atmosphere

$ds, d\ell$ are differential path length

Since attenuation decreases rapidly with increasing altitude, the sky temperature is dominated by the lower portions of the atmosphere. For practical purposes, the upper limit of the integral can be set at a path length such that the altitude

is approximately 10 km. The sky temperature is dependent on the integral along a path, and therefore is a function of incidence angle. Since at low incidence angles the path length through the heavily attenuating lower atmosphere is shorter than at grazing angles, the zenith sky will appear cold. The sky temperature will increase with incidence angle until, at 1.571 rad (90°) incidence the sky temperature will be equal to the ground level ambient.

The effect of weather is to change the minimum value of sky temperature. In clear weather, the zenith sky temperature may be less than 100°K. In cloud or fog conditions, the zenith sky temperature will be warmer, and may be only a degree or two different from the ground level ambient.

If a flat earth with a layered atmosphere is assumed, the integral can be approximated by

$$T_s = \sum_{i=1}^{\infty} \left[T_i \left(1-\exp(-\alpha_i \Delta h_i(\cos\theta))\right) \times \exp\left(-\sum_{v=0}^{i-1} \alpha_i \Delta h_i/\cos\theta\right) \right] \quad (165)$$

where T_i is the temperature of the ith layer

α_i is the specific attenuation of the ith layer (nepers/km)

Δh_i is the thickness of the ith layer

θ is the incidence angle

This computation has been performed for the ILM weather cases (see Appendix D), and the results are shown in Figures 118 through 121.

Receivable Power -- If a receiver system is pointed at the ground, the radiometric energy can be detected. Figure 122 shows a generalized scene which is being observed with an antenna.

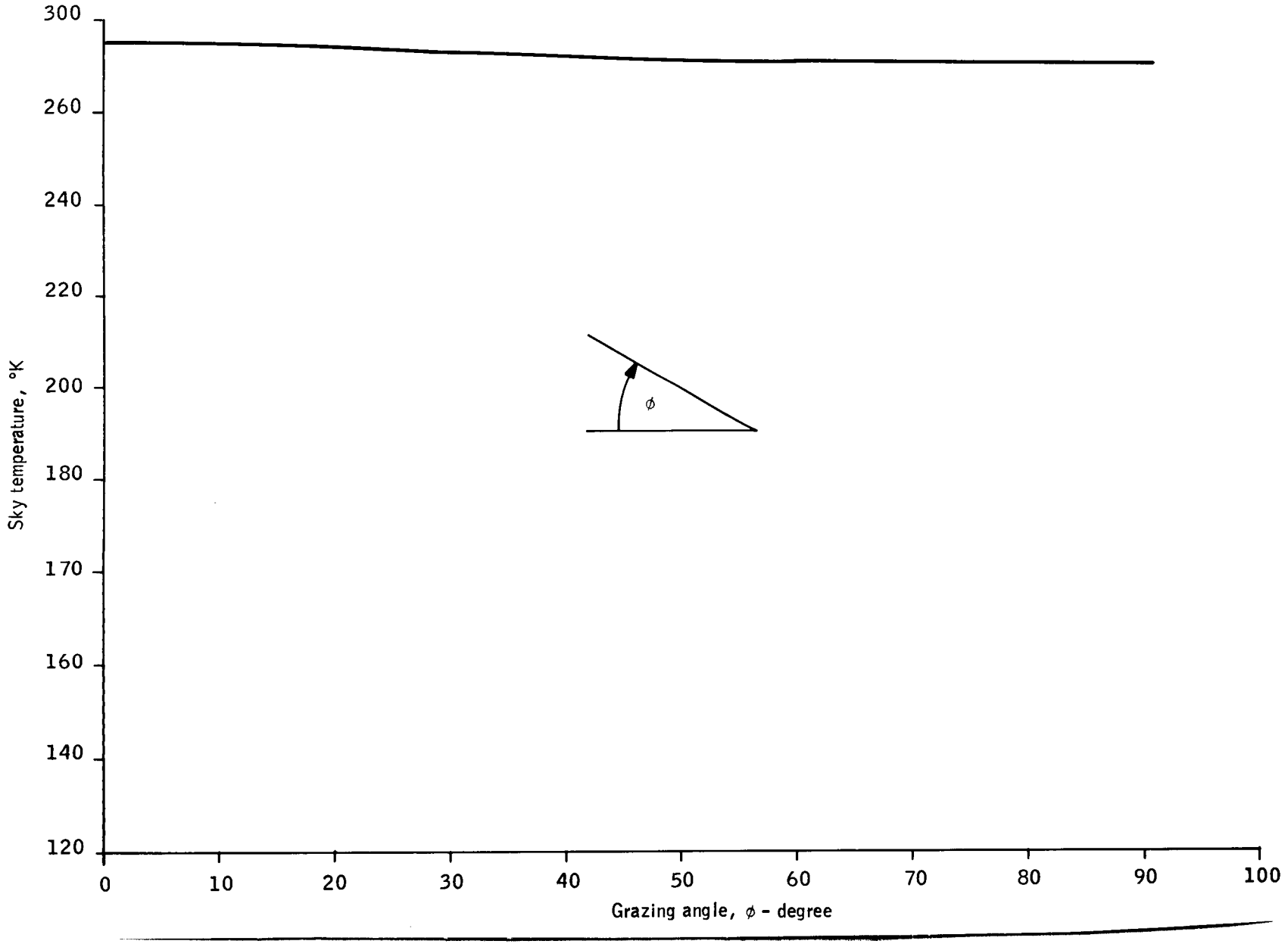

Figure 118- Sky Temperature vs Grazing Angle - ILM Weather Case 1

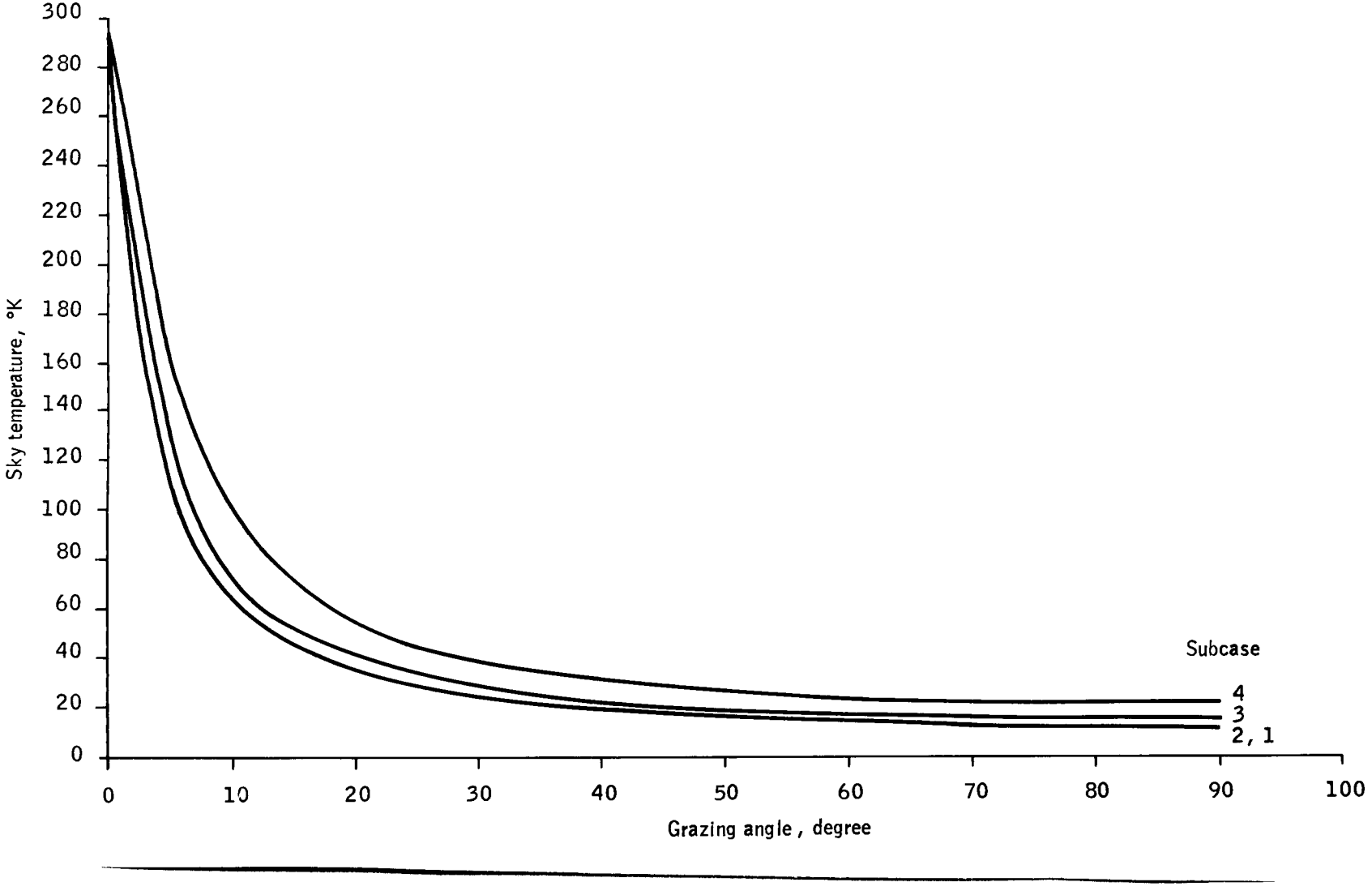

Figure 119 -- Sky Temperature - ILM Weather Case 2

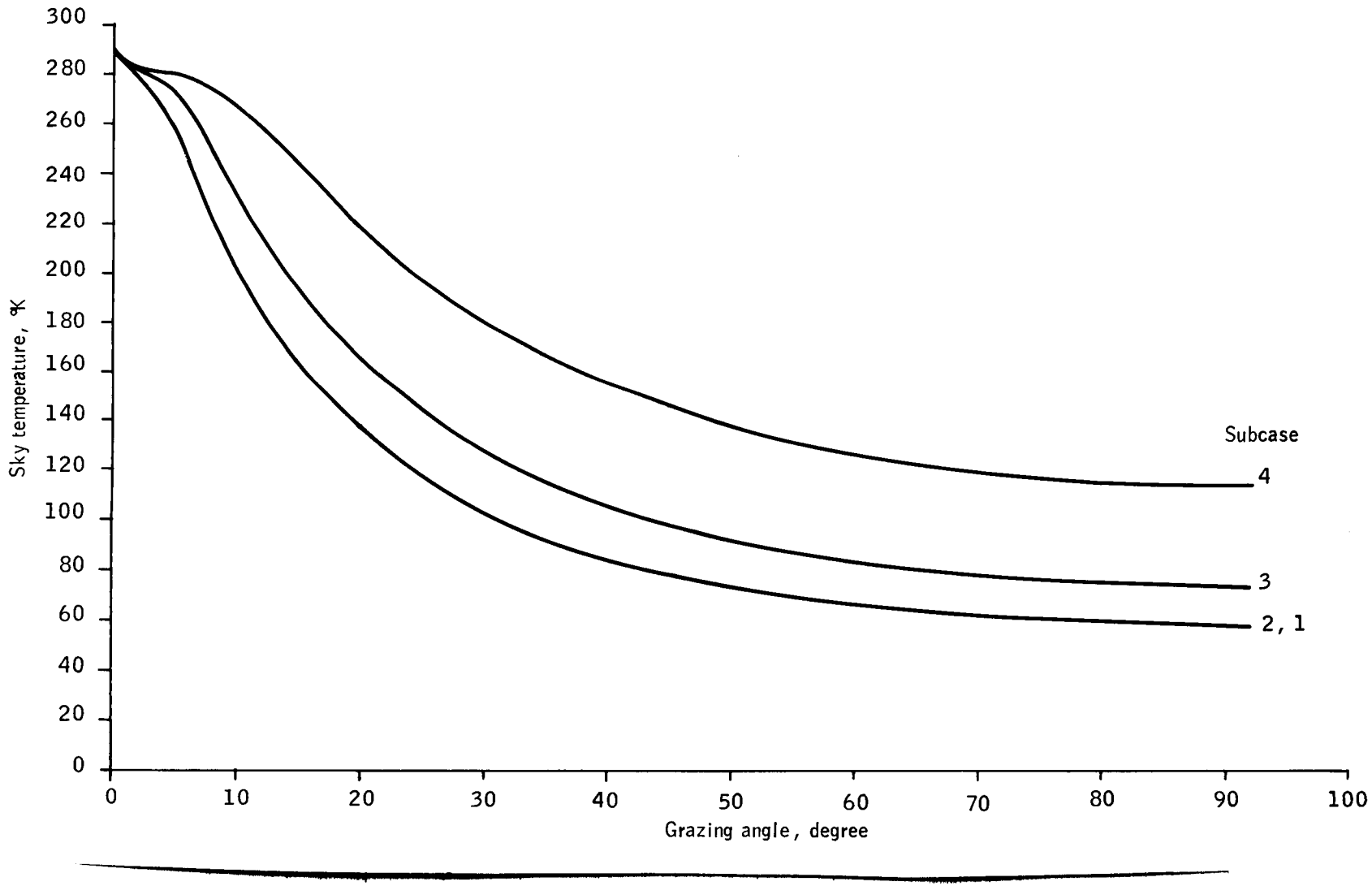

Figure 120 -- Sky Temperature - ILM Weather Case 3

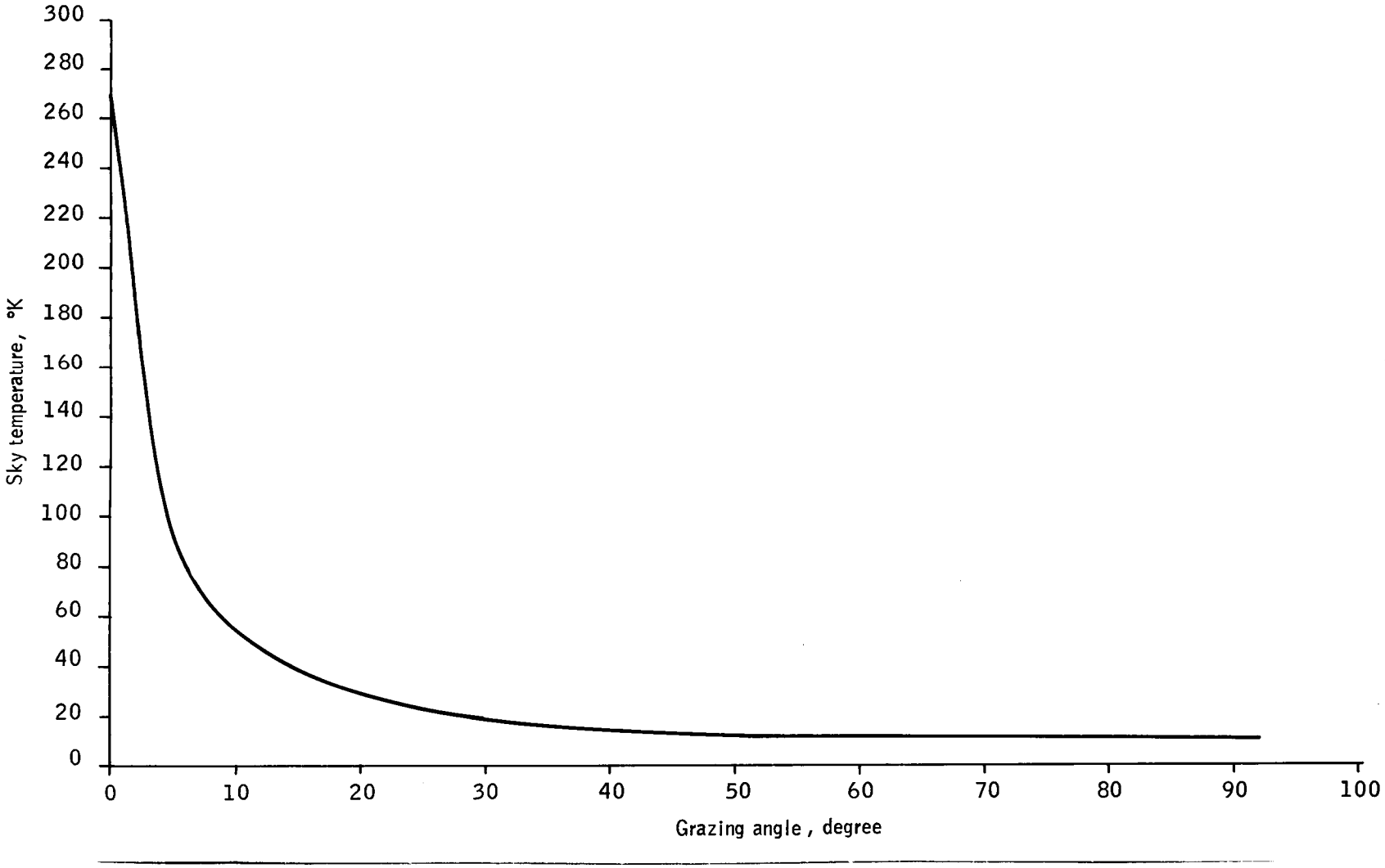

Figure 121 -- Sky Temperature - ILM Weather Case 4

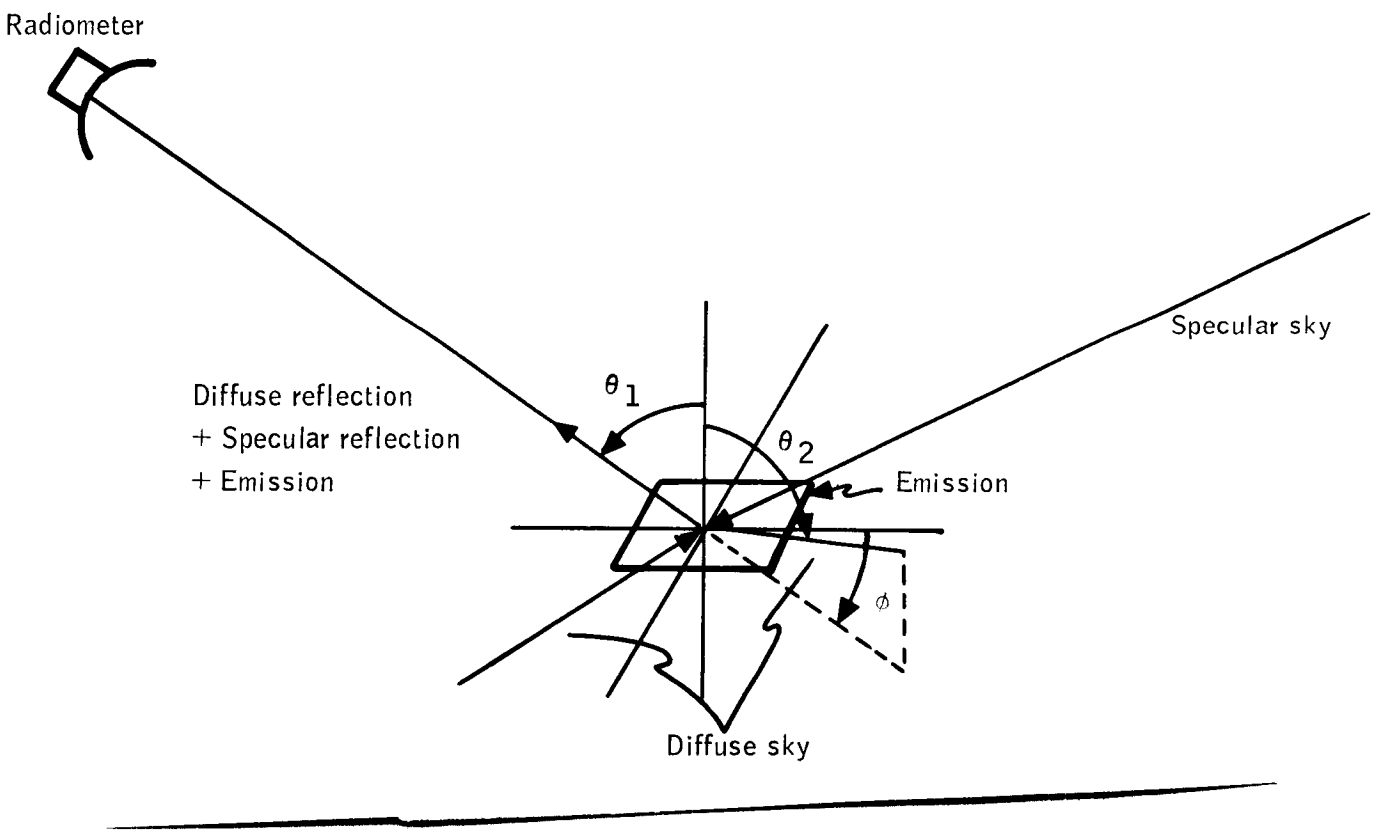

Figure 122 -- Radiometer Scene

In any differential solid angle of antenna coverage, three sources of power are illuminating the antenna:

- o Emission from the scene
- o Reflection of the sky by the scene
- o Emission from the atmosphere between the antenna and the scene

The apparent temperature contribution of a differential area element can be determined by reciprocity. If a source is placed at the receiver aimed at the differential area on the ground, the power will be split into three parts:

- o Specular reflection
- o Diffuse reflection
- o Absorption

The diffuse reflection will be into the entire hemisphere, and can be determined by the differential radar cross section. The specular reflection is in the specular direction, and is determined by the Fresnel reflection coefficient modified by the surface roughness. Any energy which is not reflected specularly or diffusely must be absorbed.

By reciprocity, if the source is replaced by a receiver, the temperature of the sky over the hemisphere must be reflected through the same reflection coefficients, and the absorption coefficient becomes the emissivity of the ground, such that

$$T_{A,P}(\theta_1)\, dA = R^2_{spec} T_s(spec) + \int_{-\pi/2}^{\pi/2}\int (\gamma_{pp}(\theta_1,\theta_2,\phi) + \gamma_{pq}(\theta_1,\theta_2,\phi)) \times T_s(\theta_2) \frac{d\theta_2 d\phi}{4\pi\cos\theta_1} + T_g \left[1-(R^2_{spec} + \int_{-\pi/2}^{\pi/2}\int (\gamma_{pp}(\theta_1,\theta_2,\phi) + \gamma_{pq}(\theta_1,\theta_2,\phi)) \frac{d\theta_2 d\phi}{4\pi\cos\theta_1}\right] \quad (166)$$

where $T_{A,P}(\theta_1)$ is the apparent radiometric temperature for polarization state P at an incidence angle of θ_1

R_{spec} is the rough surface Fresnel reflection coefficient

$T_s(spec)$ is the sky temperature at the specular angle

$\gamma_{pq}(\theta_1,\theta_2,\emptyset)$ is the bistatic differential radar cross section for transmitted polarization P and received polarization q

T_g is the ground temperature

The term multiplying the ground temperature is often referred to as the emissivity of the ground. It can be seen from the equation that it is in general a function of incidence angle. The only exception is a Lambertian surface.

A receiver at some distance r from the surface element will receive this power attenuated by the atmosphere, thus

$$T_{A,P}(\theta_1,r)\ dA = T_{A,P}(\theta_1)dA \times \exp\left(-\int_o^r \alpha(s)ds\right) \tag{167}$$

where $\alpha(s)$ is the specific attenuation of the atmosphere at a distance s from the area element

The emission of the atmosphere over the path from the area element to the receiver is

$$T_{path} = \int_r^o \alpha_n(\ell)\ T\ (\ell)\ \exp\left(-\int_\ell^s \alpha_n(s)ds\right)\ d(-\ell) \tag{168}$$

These integrals are taken in the opposite direction from the integral for sky temperature, since emission near the radiometer is attenuated less than emission near the scene, whereas the opposite is true for sky temperature.

To obtain the radiometic temperature observed by the receiver, it is necessary to integrate the contributions of all the differential areas in the antenna beam, thus

$$T = T_{path} + \frac{\int_{beam} G(x,y)\ T_A(x,y)\ dA}{\int G(x,y)\ dA} \tag{169}$$

where $G(x,y)$ is the antenna gain pointing at position x,y on the ground

The effects of the antenna pattern can be approximated by assuming the beam uniform inside the 3dB beamwidth and zero outside. If it is assumed further that the scene consists of a uniform target on a uniform background, the apparent temperature seen by the antenna is

$$T = T_{path} + F\ T_{AT}(\theta_1,r) + (1-F)\ T_{AB}(\theta_1,r) \tag{170}$$

where F is the beam fill factor, or that percentage of the beam which the target occupies

T_{AT} is the target apparent temperature

T_{AB} is the background apparent temperature

θ_1 is the incidence angle of the radiometer (1.571 rad (90°) grazing angle)

The signal received by the radiometer is the difference between the temperature observed with the target present and the temperature observed with the target absent, or

$$\Delta T = T(F=F_{target}) - T(F=0) \tag{171}$$

Since the received power is a noise field, this temperature appears at the receiver as a change in the variance of the received noise. To sense this change the output of the receiver must be squared and integrated or some other technique appropriate for sensing variance employed.

System Configurations

Imaging Techniques -- In order to convert received microwave energy to an image, the antenna beam must be moved in two dimensions to provide a display of intensity versus position.

Reconnaissance applications typically point the antenna approximately down from the aircraft, scanning the antenna either mechanically or electronically in the cross track direction and allowing the motion of the aircraft to make a scan in the along-track dimension. After the flight, the recorded radiometer data can be converted to an image of the area flown over.

For ILM application, a real time image is required. Thus the antenna must be physically (mechanically or electronically) scanned in two dimensions. There are various scanning techniques available, such as raster scan, conical scan, and pinwheel scan. Selection of a scan pattern depends on the hardware configuration to minimize acceleration of masses, circuit complexity, etc; however, for a limiting system performance analysis the selected pattern is unimportant. The beam must cover the field of view in the amount of time allotted for a frame. This limits the amount of time available for integration of the received microwave energy, and causes a tradeoff between signal to noise ratio and resolution.

Radiometer Receivers -- The simplest form of a radiometer is the total power radiometer, Figure 123. In this radiometer, the amplified noise field is detected with a square law detector and integrated. Two factors limit the sensitivity to less than the theoretical signal fluctuation inaccuracy:

- Receiver self-noise
- Gain variation

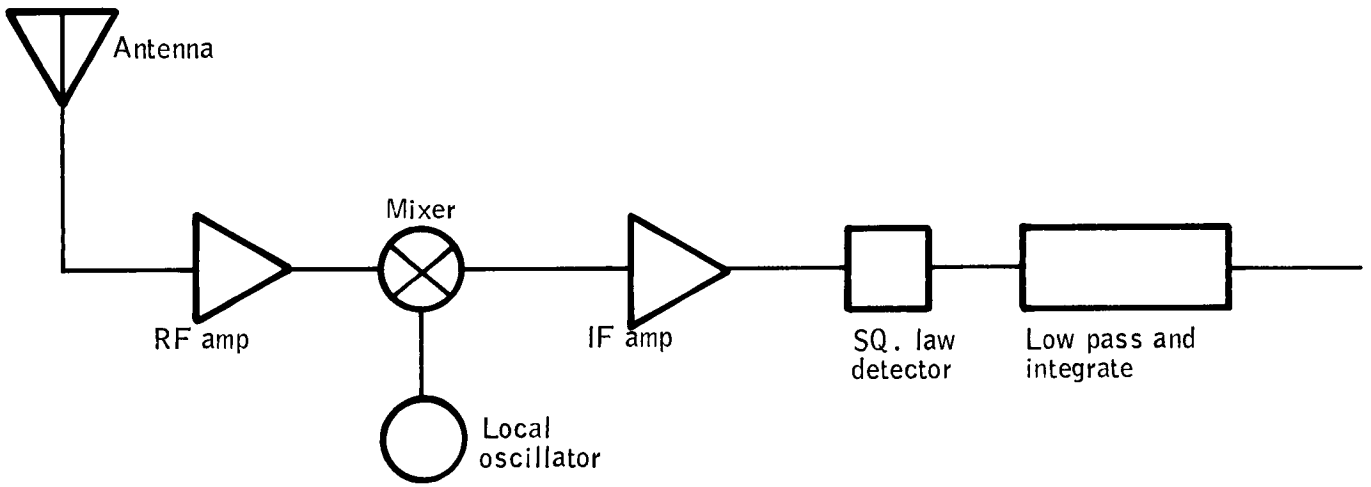

Figure 123 -- Total Power Radiometer

The receiver self-noise is generated by the mixer and amplifiers, and is present regardless of receiver configuration. Gain variation over the integration interval is generally the predominant term, and makes the total power configuration unusable.

Most radiometers in use today are of the Dicke configuration, Figure 124. In this configuration, the RF input is switched between a reference noise source and the antenna. By comparing the output of the receiver when connected to the reference source to the output of the receiver connected to the antenna, the effects of gain variation can be compensated. However, even with perfect switching the energy illuminating the antenna is only observed half the time, reducing the amount of effective integration time.

Many other configurations have been proposed and investigated, but the highest performance is obtainable with a correlation radiometer, Figure 125. Since gain variations are uncorrelated between the two receivers, the gain variation noise is removed. The antenna is continuously connected to the receivers, so that no reduction in sensitivity by switching occurs.

Since the correlation receiver provides the highest practical performance, it is the configuration which will be assumed in the performance analysis.

Any antenna type which provides a pencil beam is usable for radiometry. Traditionally, parabolic dishes or phased array antennas are used. In any case, the beamwidth is inversely proportional to the size of the antenna, and different configurations impact primarily the difficulty of scanning and the complexity of the electronics.

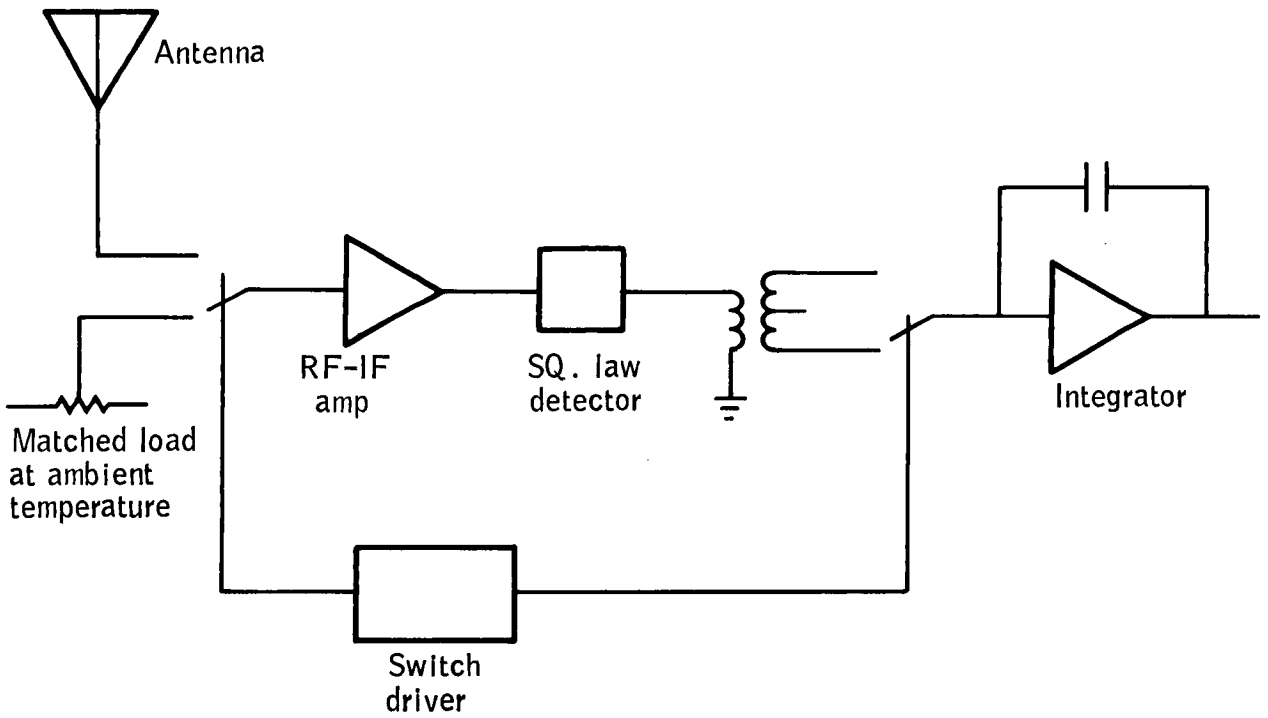

Figure 124 -- DICKE Radiometer

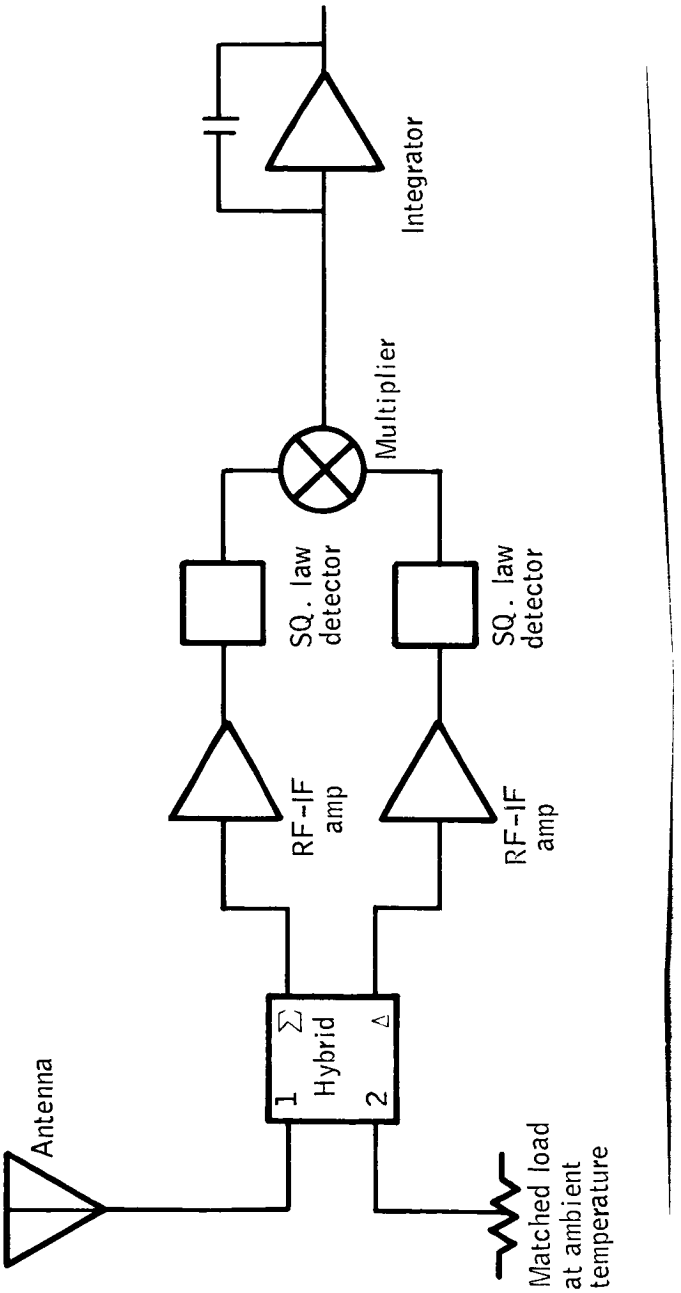

Figure 125 -- Correlation Radiometer

Active Illuminators -- To enhance the performance of radiometers, active microwave illumination may be used. There are basically two different types of illumination:

- o Flood lighting
- o Point sources

In flood lighting, microwave energy from an oscillator, either on the aircraft or on the ground, is broadcast over the area to be imaged. The effect is similar to changing the sky temperature at the particular incidence angle. The effect of sky temperature is to change the apparent temperature of the surface, as demonstrated in equation 170. The second term in equation 170 represents the reflected sky temperature. If a powerful enough source were used, the other terms in equation 170 would become insignificant, as would other directions in the sky temperature integral. Then the apparent temperature integral becomes the normal radar equation, with the runway-background contrast dependent only on the bistatic cross section contrast.

It can be expected that some location for the floodlight, and some level of floodlight power will provide sufficient signal levels in at least some weather. However, even if adequate signal strength and runway-background contrast were always available, a cw floodlight would do nothing for the resolution or scanning rate requirements of the system. Pulsed floodlights could be used, triggering a time scan from initial reception in the range direction. If the floodlight were located at the approach end of the runway, this time scan could be used in lieu of scanning the antenna in elevation and the pulse width could be used to determine the along track resolution. But this is the description of a bistatic imaging radar in that the received signal is purely the reflection of an artificially

pulsed source with range determined by time between transmit and receive. Given this situation, it is unreasonable to use the exotic wide band hardware of a radiometer when a relatively narrowband source can provide the same image.

Point sources could also be observed directly with a radiometer. By outlining the target to be imaged, a very hot border would appear around the target. However, if a point source is the only identifiable image on the display, the signal to noise ratio of that image could be improved by using a narrowband source and narrowband receiver. Further the resolution could be improved by using a monopulse type antenna to split the antenna beam and syncronously pulsed sources could be used to eliminate the necessity for scanning the antenna in two dimensions. What has just been described is not a radiometer, but rather an airborne interferometer. Therefore, it is inappropriate to consider point source illumination for radiometry if radiometry will not meet the requirements in some weather condition without it.

Performance Analysis

Resolution -- The resolution in an image is the distance at which two targets must be spaced for an observer of the image to determine that two objects are present. It is not the dimension of the smallest target which can be detected, since point sources of zero size can be detected if they are isolated.

The primary factors affecting resolution are:

- Antenna beamwidth
- Antenna aperture illumination
- Scanning rate
- Post detection bandwidth

The antenna beamwidth is determined by the physical size of the antenna. Beamwidth versus size is shown in Figure 126 for common radiometer frequencies.

Amplitude or density tapering of the antenna aperture illumination is often used in radar to improve the sidelobe performance of the antenna. However, for an imaging radiometer it can be shown that uniform illumination provides the highest resolution. This corresponds to the statement that uniform illumination provides the highest possible main lobe gain.

The scanning of the antenna converts an image to an electrical signal. For a given size target, the bandwidth of the video signal is proportional to the scanning rate. If the scanning rate is high enough such that the video signal bandwidth from an otherwise resolvable target exceeds the post detection bandwidth of the radiometer, the scanning rate and bandwidth will limit the resolution of the radiometer.

Because of space limitations in the nose of most aircraft, antennas over 1 m diameter are impractical, therefore resolution of the runway to 13 km is not feasible at any frequency under 100 GHz. Below 35 GHz, imaging the runway even at 1.6 km is not practical.

Therefore, only 35 GHz and 94 GHz radiometers will be considered in the remainder of this analysis.

Ignoring the possible effects of scanning rate, bandwidth, and non-uniform illumination, the size of a resolution element without special processing is the 3dB beamwidth of the antenna. Fourier, bootstrap, or other deconvolutional filtering can be used with a large increase in system complexity to increase the

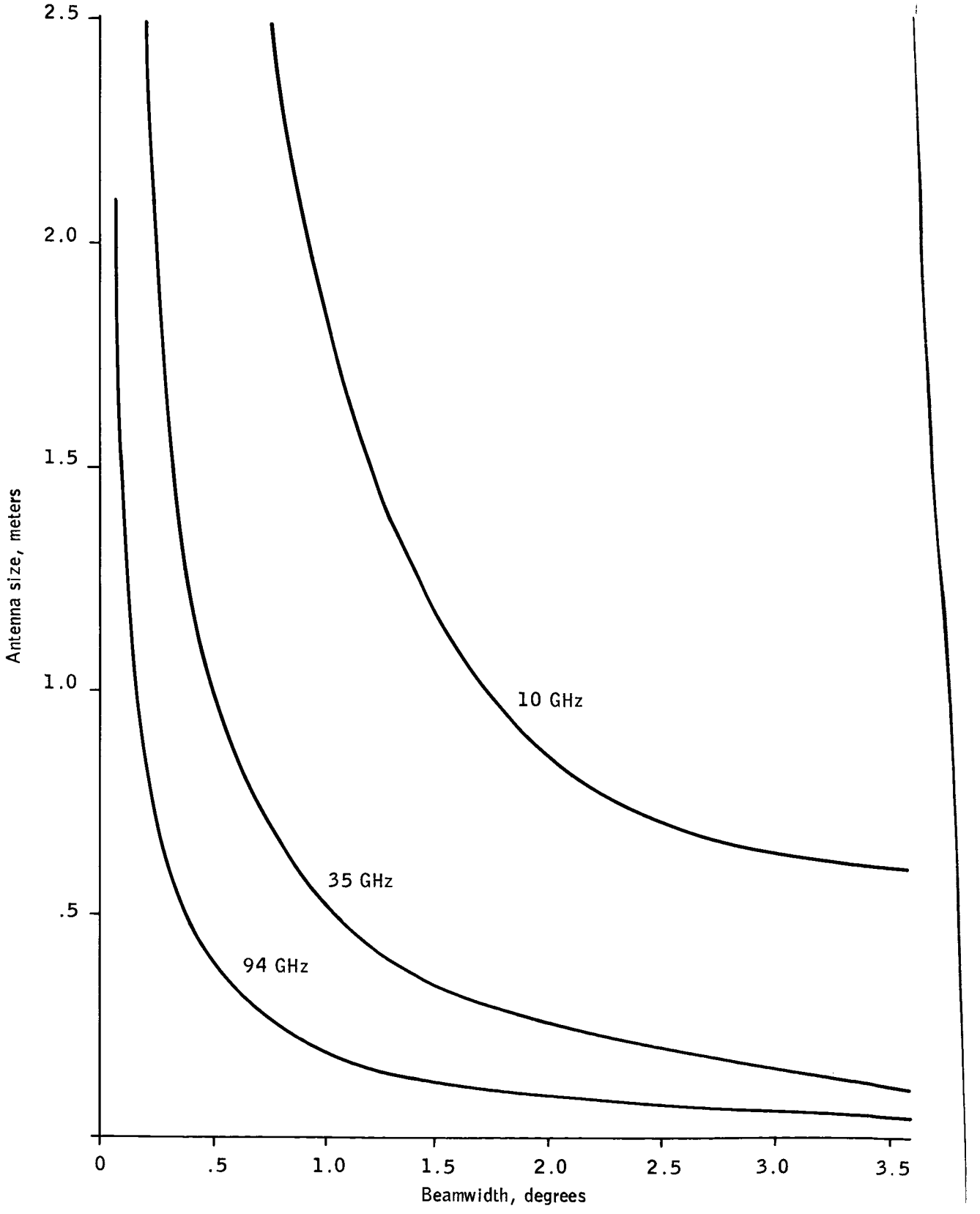

Figure 126-- Antenna Size vs Beamwidth

resolution. If adequate signal to noise ratio is available, the resolution can be increased significantly. However, for a real time system these techniques would require far too much computation. The 3db resolution element is perpendicular to the beam, so that at low grazing angles it is very large in the along track direction. In the cross track or vertical dimension, the resolution cell size is effectively the beamwidth projected to the range. The minimum resolvable dimension for various beamwidths is plotted versus range in Figure 122 for cross track or vertical dimensions. The along track resolution cell size is approximately 20 times this dimension for a 0.052 rad (3°) depression angle.

A possible resolution criterion is that recognition of the runway be assured at the minimum effective range of 1 km. This implies that 8 beamwidths of the antenna must fall within the runway (Reference 3). For the smallest runway, the projected beamwidth must be $\frac{23}{8}$ or about 3 m, and the largest runway requires a 12 m beam.

From Figure 127, beamwidths for recognition can be found. These are summarized in Table 57.

Table 57 -- Beamwidth to Assure Recognition, Degrees

	1km	2km	6km	16km
Small Runway	.17	.08	.03	.01
Large Runway	.68	.34	.11	.04

Another detection criterion requires 2 lines across the runway. Since at these beamwidths, $\tan\phi \cong \phi$, the detection required beamwidth is simply four times the resolution required beamwidth.

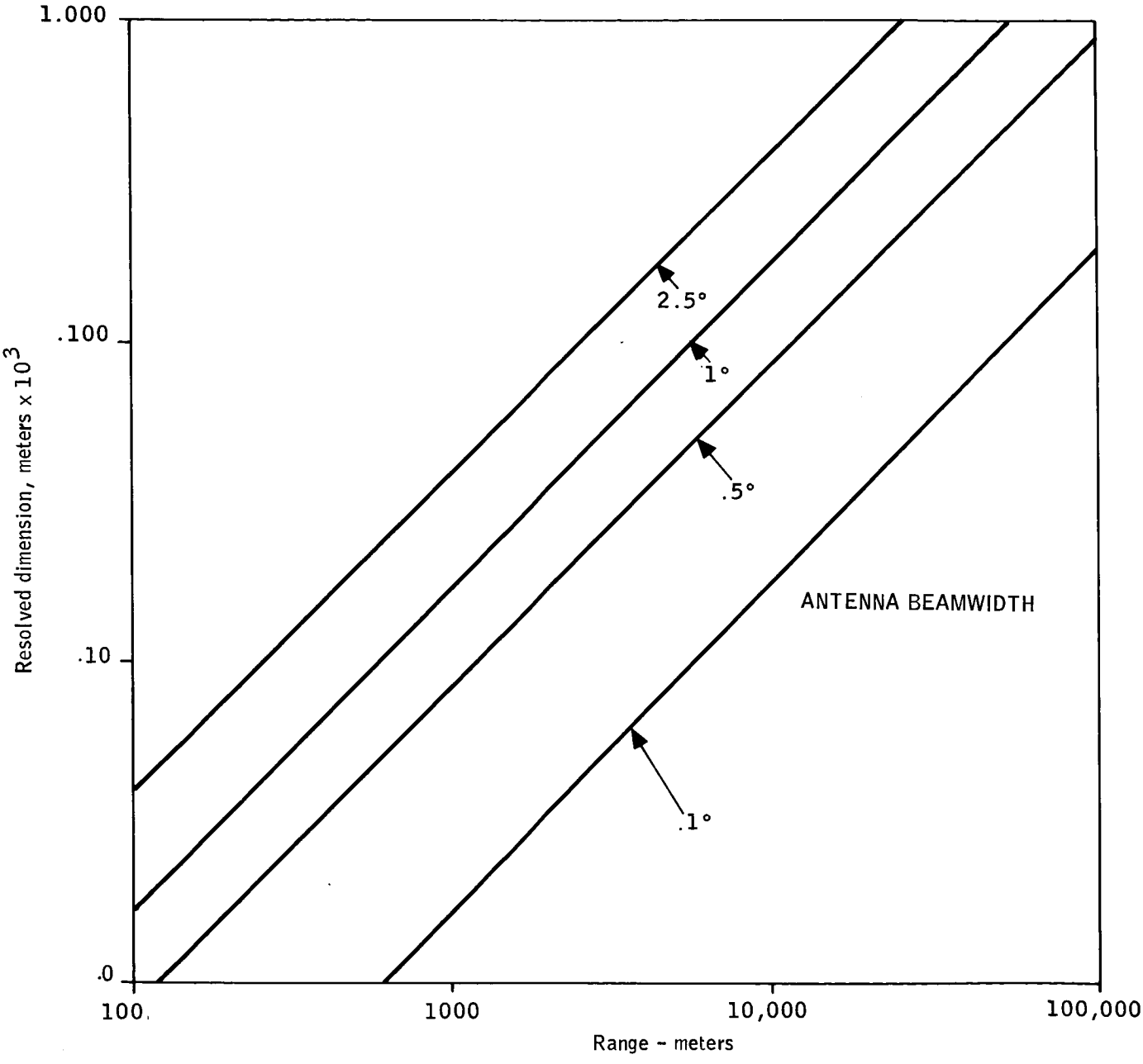

Figure 127 -- Resolution Cell Size vs Range for Various Antenna Beamwidths

From Figure 126, the maximum aperture size of 1 m provides .0087 rad (.5°) at 35 GHz and .0028 rad (.16°) at 94 GHz. Comparing these numbers with Table 57 demonstrates that at 35 GHz, recognition of the largest runway is barely feasible at the minimum effective range, while recognition of the small runway cannot be assured. The large runway would be detected (assuming adequate signal to noise ratio and lack of confusing objects) at about 5 km, while resolution requirements for detection are not obtained for the small runway beyond about 1.5 km. It is highly questionable what value detection-without-recognition has at such short range.

At 94 GHz, recognition of a large runway could occur at about 4 km, with recognition of a small runway occurring at about the minimum effective range. Corresponding detection ranges assuming adequate signal to noise ratio are 16 km for a large runway and 4 km for a small runway.

If a 1 m aperture is the maximum usable size, and the antenna resolution attains its theoretical value, a 35 GHz radiometer is inadequate for all but the largest runways at the minimum effective range. Radiometers at 94 GHz provide resolution barely adequate to recognize smaller runways at minimum range.

Field of View and Scan Rate -- The basic scan rate requirement is that the radiometer cover the field of view in the frame time. If the boresight of the antenna is fixed, then the requirements for crab angles to ±.349 rad (±20°) and pitch from -.052 rad to + .175 rad (-3° to +10°) requires a field of view of approximately .349 rad x .698 rad (20° x 40°). In this case, the field of view requirements do not vary with range to threshold.

If the boresight is made slewable, the basic field of view requirement is that the

vertical coverage of the display must be large enough to encompass the runway at the steepest glide path expected. This provides two options:

- o A fixed field of view could be selected which will display at least the entire runway to some minimum distance.
- o A variable field of view could be selected such that the length of the runway is the vertical extent of the display, with a limiting value of fixed field of view the first option.

The first option is simpler and does not require an external range input. The pilot can use the size of the displayed runway image to estimate range to threshold. The second option would narrow the field of view at longer ranges, allowing a slower scan and a longer integration time. This would improve detection capability at longer ranges, but requires either manual or automatic adjustment of scan rate, field of view, and integration time as a function of range to threshold. A possible compromise is to provide a mode switch, such that the pilot can select whichever field of view provides the most useful information.

The horizontal coverage requirements are not as well defined as the vertical requirements. However, it would be desirable to display the entire runway at bank angles up to .524 rad (30°). This implies a square display. If a slightly narrower horizontal field of view is acceptable, a standard 4:3 aspect ratio can be obtained with the long dimension vertically.

Assuming a .105 rad (6°) maximum glide path, and requiring a 4 km distance along the ground in front of the GPIP, as shown in Figure 128, the portion of the field of view above the glide path is described by

$$\beta_1 = \frac{12.21 + 2.95r}{4 + r} \qquad (172)$$

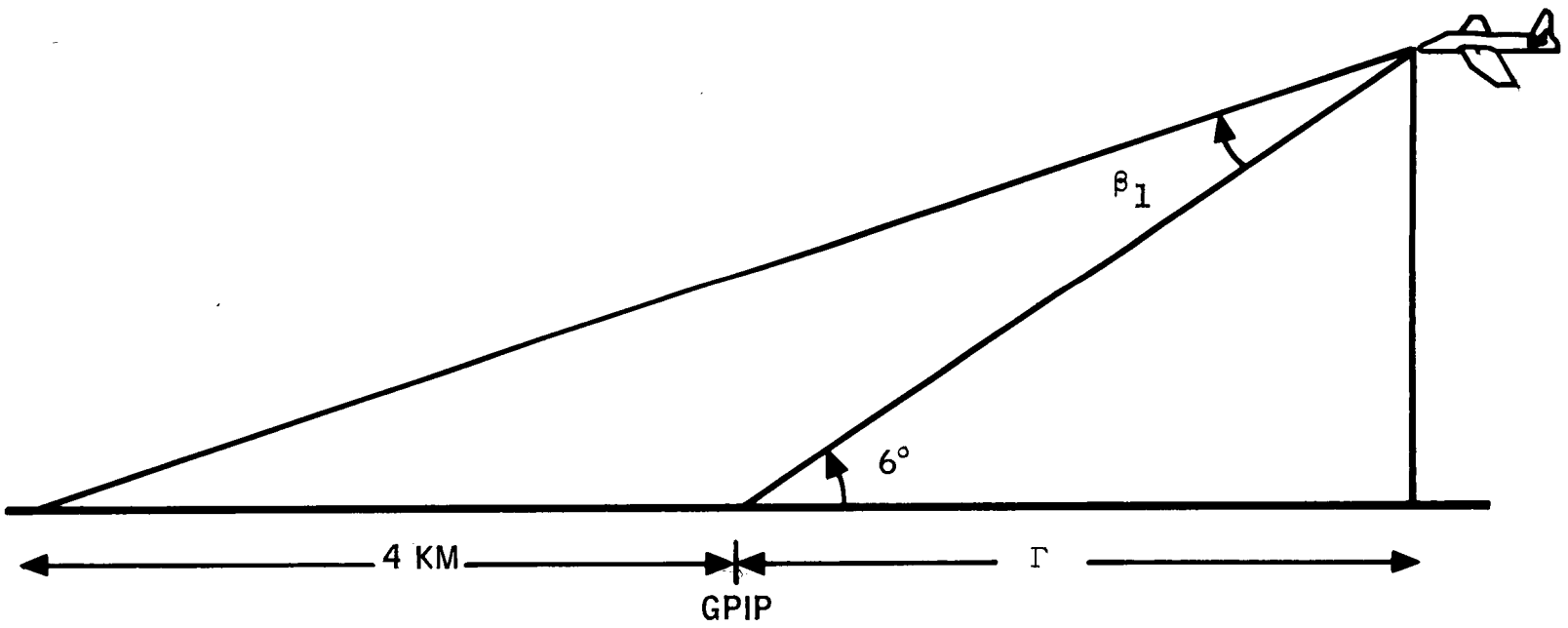

Figure 128 -- Geometry for Field of View Computation

where β_1 is the component of vertical field of view above glide path, in degrees

r is the range to GPIP, in km

Allowing the aiming point to be at 25% of the display from the bottom,

$$\beta = \frac{16.28 + 3.93r}{4 + r} \simeq 4.07 - .035r \tag{173}$$

where β is the vertical field of view

This yields a maximum field of view of .07 rad x .052 rad (4° x 3°), just prior to touch down. At 16 km, the required horizontal field of view is still .069 rad (3.96°). It can be seen that changing the field of view with range does not provide for a significant increase in integration time.

From Section III, it has been determined that the minimum field of view for an ILM is .14 rad (8°). This field of view will be assumed for the remainder of this analysis.

Assuming contiguous non-overlapping scan lines, the number of lines in a frame is

$$N = \frac{\beta}{B} \tag{174}$$

where β is the vertical field of view

B is the beamwidth

The line rate is the frame rate times the number of lines per frame or

$$L = \frac{\beta}{B} F \tag{175}$$

where F is the frame rate (frames/sec)

L is the line rate (lines/sec)

The scanning rate is the line rate times the size of a line, or

$$U = L \left(\frac{\text{lines}}{\text{sec}}\right) \times \alpha \left(\frac{\text{degrees}}{\text{line}}\right) = \frac{\alpha\beta}{B} F \left(\frac{\text{degrees}}{\text{sec}}\right) \quad (176)$$

where U is the scanning rate

α is the horizontal field of view (degrees)

Taking the antenna aperture to be 1 m, the beamwidth at 35 GHz is .009 rad (.5°) and at 94 GHz the beamwidth is .003 rad (.2°). For the maximum .105 rad x .14 rad (6° x 8°) field of view, the 35 GHz scan rate is 16.76 rad/sec (960 degrees per second) and the 94 GHz scan rate is 41.89 rad/sec (2400 degrees per second). For the variable field of view case, the scan rates are shown in Figure 129 as a function of range.

The post detection bandwidth or integration time is selected based on the scan rate and image fidelity requirements. The normal criterion used is (Reference 4, Equation 39-48)

$$T_I = \frac{B}{.4U} \quad (177)$$

where T_I is the integration time

Using this criterion, the minimum integration time for the .009 rad (.5°) beamwidth is 1.3×10^{-3} sec and for the .003 rad (.2°) beamwidth is 2.1×10^{-4} sec.

Antenna Effects

Two types of antennas provide pencil beams as desired for imaging:

- o Arrays
- o Reflectors

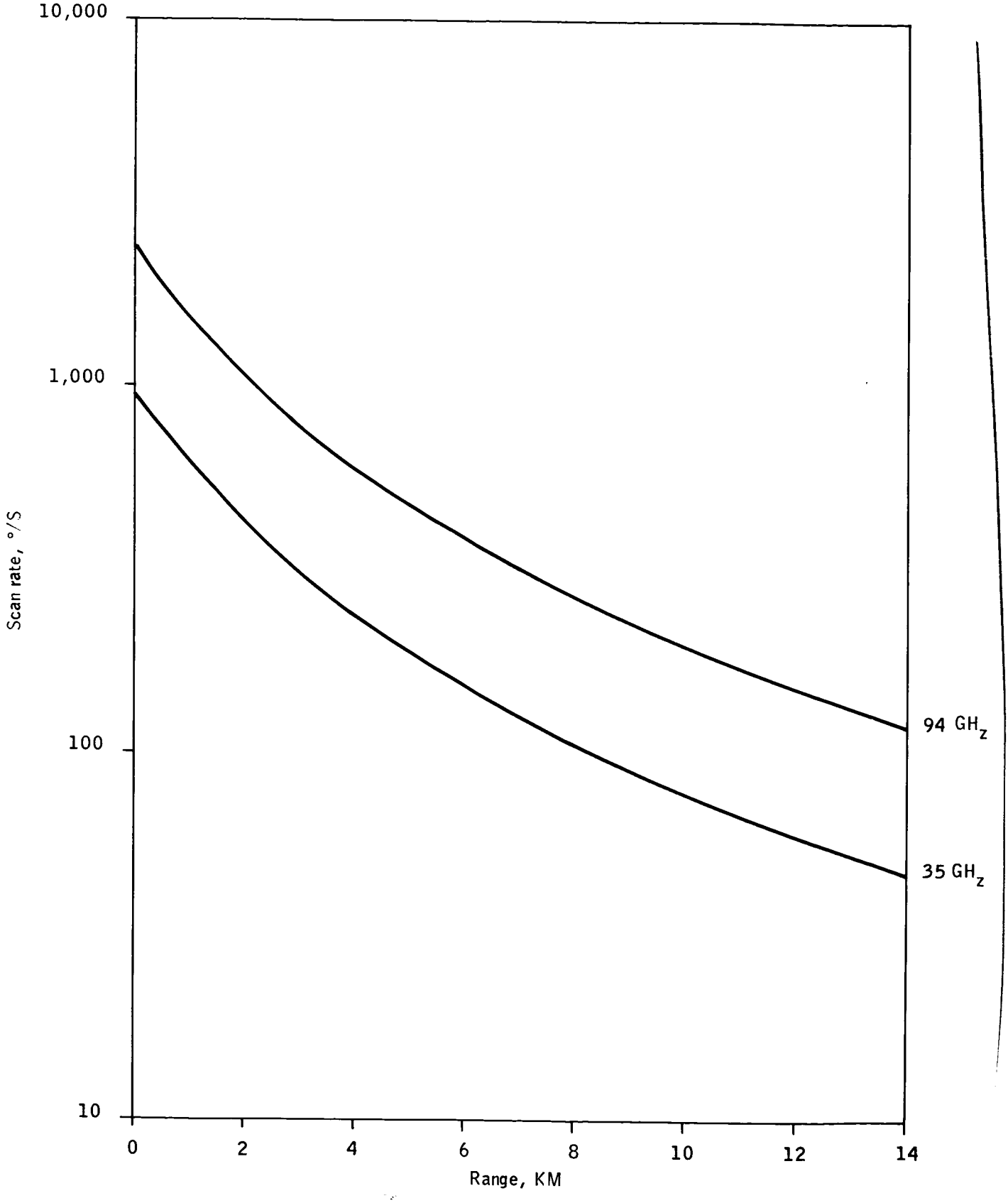

Figure 129 — Scan Rate vs Range

The antenna beamwidth is determined primarily by the physical aperture of the antenna, regardless of which type of antenna is used.

The beam from a phased array antenna is pointed by electronically shifting the relative phase between elements of the array. This allows the antenna to conform to the aircraft rather than vice versa, and permits high speed scanning without large mechanical structures.

The operation of a basic phased array is shown in Figure 130. If a plane wavefront arrives at an angle θ from the normal to the array, all the elements will add in phase if the phase shifters are set to shift the phase by $n\Psi$, where

$$\Psi = \frac{2\pi}{\lambda} s \sin\theta \tag{178}$$

where λ is the wavelength

s is the interelement spacing

With this setting of the phase shifters, waves impinging on the array from any other direction are not summed in phase, but add and subtract in a destructive manner. Thus directionality is obtained by controlling the phase shifters.

If a wave with a different wavelength impinges on the array with the setting of the phase shifters fixed, the angle at which summation in phase occurs is changed. From the basic directionality equation,

$$\Psi = \frac{2\pi}{\lambda 1} s \sin\theta = \frac{2\pi}{c} f_1 \sin\theta = \frac{2\pi}{} f_2 s \sin(\theta + \delta\theta) \tag{179}$$

where λ_1, f_1 are the wavelength and frequency for which the array is adjusted

θ is the angle at which the beam is pointed

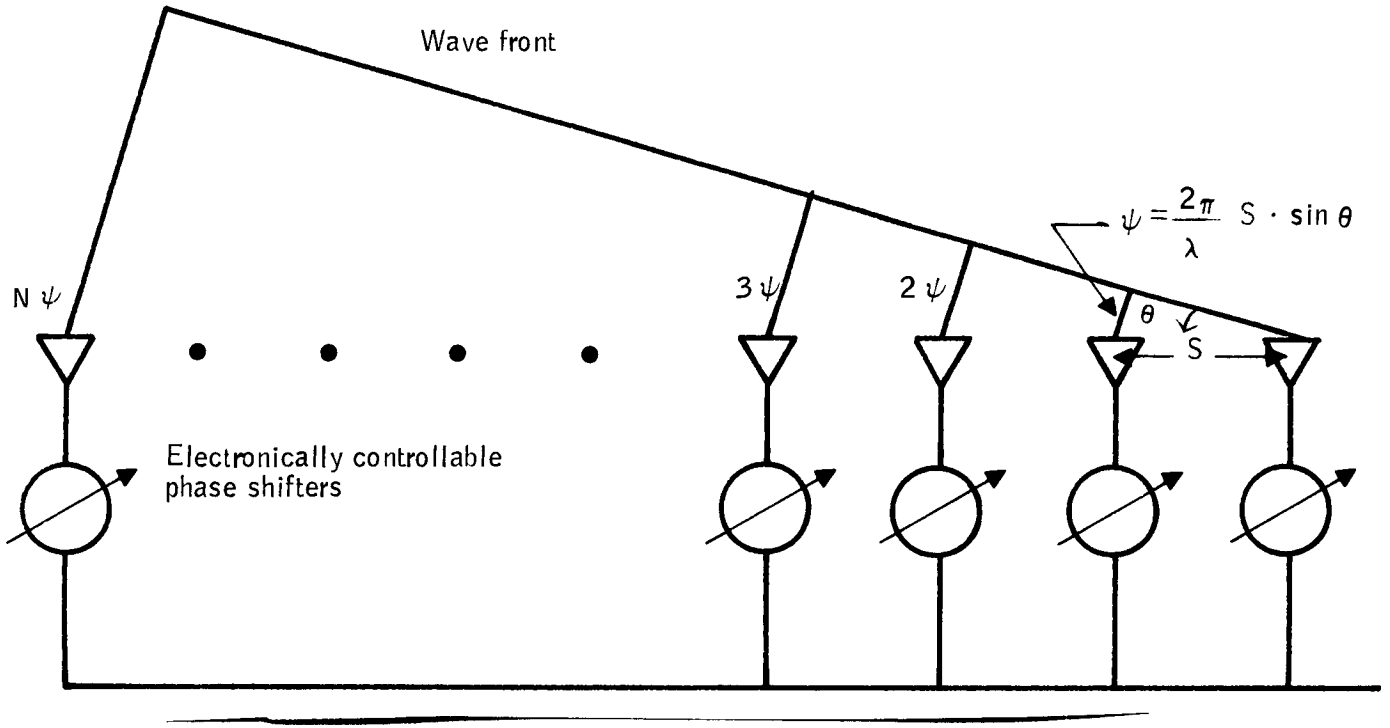

Figure 130 -- Phased Array Antenna

f_2 is a different frequency

$\delta\theta$ is the change in beam pointing angle from f_1 to f_2

As long as $\sin \delta\theta \cong \delta\theta$, this equation can be manipulated to (Reference 4, p. 11-43)

$$\delta\theta \cong .29\ BW_p \tan\theta \tag{180}$$

where BW_p is the percentage bandwidth

$\delta\theta$ is the beam pointing angle change in degrees

This angular change affects a radiometer directly since the radiometer signal is approximately white noise. Thus the beamwidth for a radiometer is the sum of the basic beamwidth plus twice the deviation caused by bandwidth. Figure 131 shows the beamwidth versus scan angle for a 1 m array operating at 35.6 GHz. It is evident from the figure that if slewing to compensate for a .349 rad (20°) crab angle is done electronically, the resolution is significantly degraded. If slewing is performed mechanically and only scanning is performed electronically, resolution degradation is less than 50% for bandwidths under 1 GHz. In this case, the runway area would be approximately on boresight such that it is in the maximum resolution area.

Another type of array antenna is the timed array. If the phase shifters are replaced with time delays, the beamwidth is independent of the bandwidth. Electronic manipulation of time delays is very difficult. A modification to this concept is to use a large number of fixed time delays to form a large number of beams, and switch between them. This type of antenna is called a Blass array, and is exceedingly complex when required to scan in two dimensions electrically. However, it has possible application since all beams are actually accessible.

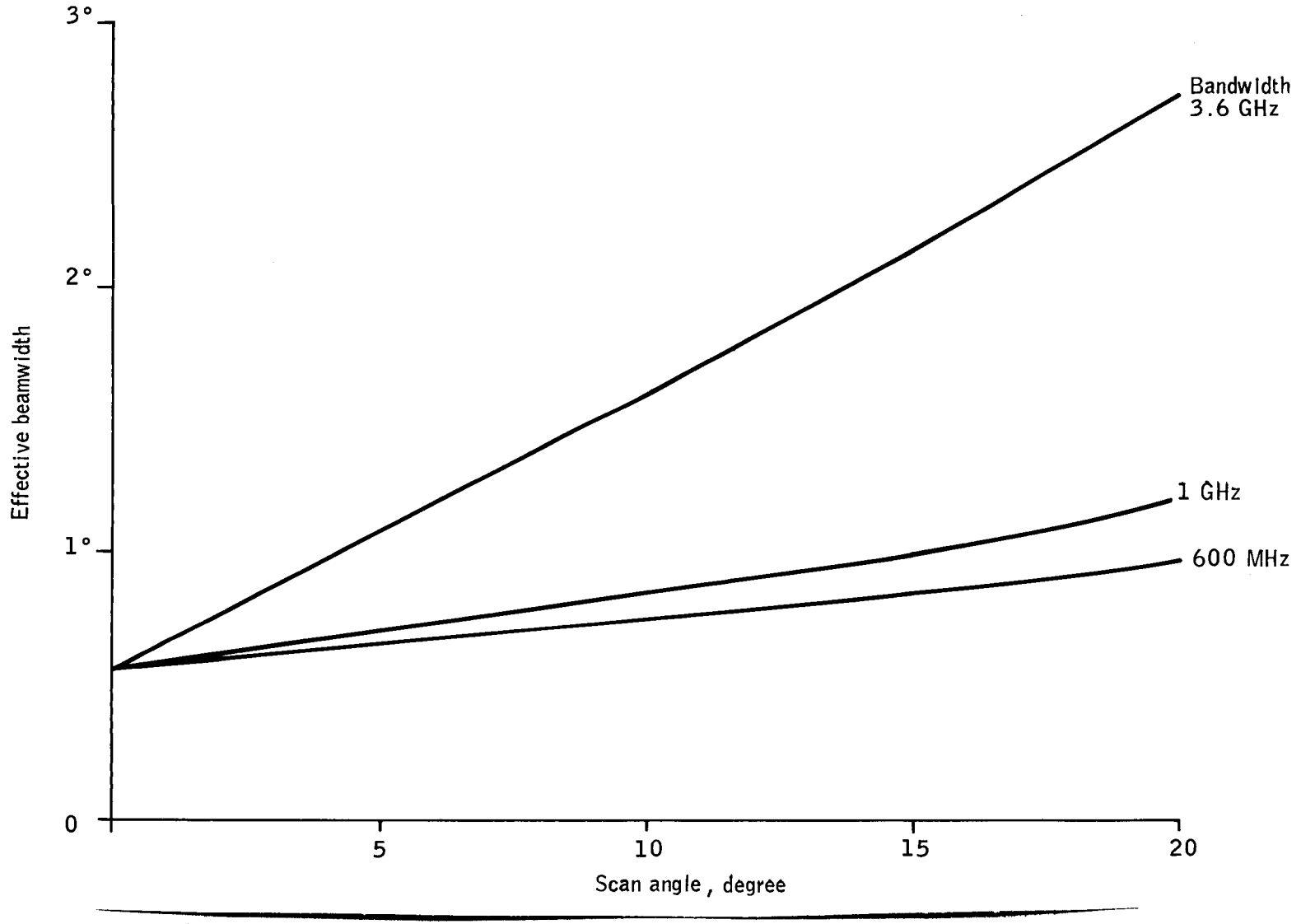

Figure 131 -- Beamwidth vs Scan Angle

If a radiometer receiver is connected to each beam, and the switching performed at the output of the radiometers, a large increase in integration time is obtainable. Such a system illustrated in Figure 132 could be scanned mechanically in one plane, and scanned by receiver switching in the other plane. The number of radiometers required is the number of resolution elements in a given scan line and thus the system requires an immense amount of complex hardware. But it might work.

A parabolic reflector antenna also provides a pencil beam. Scanning of a reflector is accomplished either by moving the entire structure or by moving the antenna feed away from the focus of the reflector.

When scanning by moving the feed, the effective aperture decreases rapidly and side lobes appear such that scanning more than two or three beamwidths is impractical. Therefore the entire antenna assembly must be scanned to cover the field of view required from a radiometer. By moving the entire structure, the aperture remains constant independent of both bandwidth and scan angle, providing uniform resolution normal to the beam.

The problem of moving the structure is that a large mass must be subjected to large accelerations to obtain high scanning rates. Furthermore, with most scanning patterns retrace time must be allowed to return the antenna to its original position at the end of the scan. This decreases the time available to scan and requires a further increase in scanning speed.

A measure of the torque required can be obtained by estimating the moment of inertia of a representative antenna. The moment of inertia of a disk along a diameter is

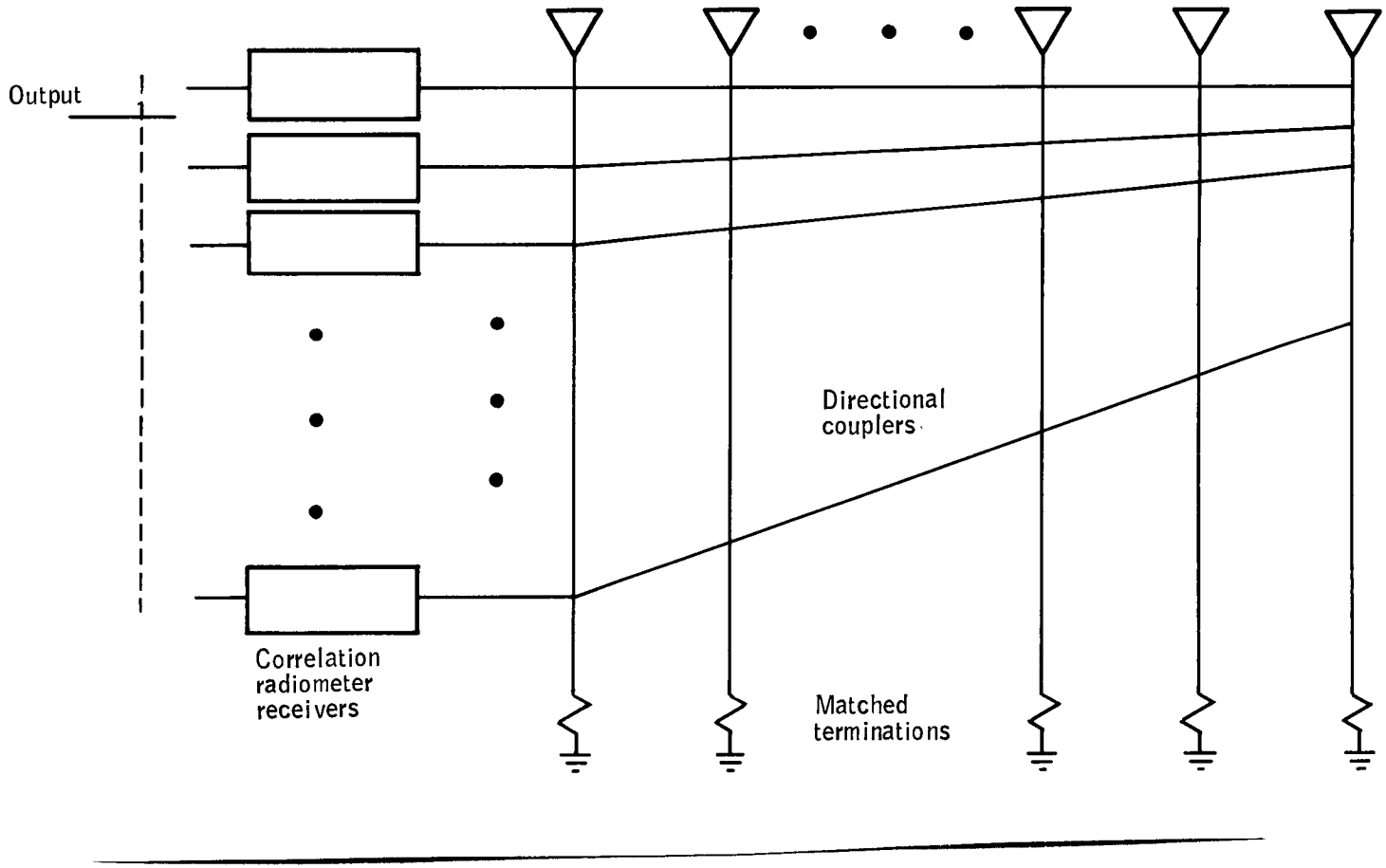

Figure 132 -- Blass Array Radiometer System

$$I = \frac{\pi t\, r^4\, P}{4} \tag{181}$$

where t is the thickness of the disk

r is the radius of the disk

P is the density of the disk material

The thickness of the antenna is determined by the surface irregularities tolerable, the strength of the material, and the expected loads on the antenna structure. Assuming an aluminum antenna 1/3 cm thick, a 1 m parabola would have a moment of inertia of approximately 7.7 $Kg\text{-}m^2$.

If no retrace time is needed, a scan rate of $960^{deg}/sec$ is required. A six degree FOV translates this to

$$\frac{960^{deg/_{sec}}}{6^{deg/_{scan}}} = 160 \text{ scans/sec} \tag{182}$$

If sinusoidal scanning is required, each cycle constitutes two scans, thus the position of the antenna is described by

$$\theta = .05 \sin \left(2\pi \times \frac{160}{2} t\right) \tag{183}$$

(.05 radians $\cong$ 3°, scan goes ±3°)

Diffentiating twice WRT time yields:

$$\ddot{\theta} = .05 \left(2\pi \times \frac{160}{2}\right)^2 \sin \left(2\pi \times \frac{160}{2} t\right) \tag{184}$$

$$= 12{,}633 \sin (160\pi t)$$

Since all units are radians and seconds, 12,633 represents peak acceleration in rad/sec^2.

The required torque is given by

$$T = I\alpha \tag{185}$$

$$= 7.7 \times 12{,}633$$

$$= 97{,}300 \text{ NT-m}$$

$$= 9921 \text{ Kg-m}$$

$$\cong 7174 \text{ ft-lb}$$

By comparison to familiar torque values, it is obvious that this number is not obtainable.

As shown in the section on resolution, even this size antenna must be less than 2.3 km from the runway to allow recognition of the runway image.

In summary, phased array antennas degrade the resolution of the system when reasonable radiometer bandwidths are used and reflector antennas require ridiculous sized motors when a .1 second frame rate is required. Therefore, a beam-switched timed array scanned mechanically in one plane is the only antenna system which could possibly meet the ILM requirements.

Contrast -- The contrast is a measure of the difference in intensity between a target and its background. Several different measures are used in different parts of the literature, but they all define the same quantity.

In radiometry, the factors affecting contrast are:

- Apparent target temperature
- Apparent background temperature
- Scanning rate
- Post detection bandwidth

The scanning rate and post detection bandwidth combine to reduce the otherwise available contrast, since the integrator defining the post detection bandwidth cannot reach its asymptotic target value if the scan rate is too high.

Ignoring for the moment the degradation due to scanning, the asymptotic contrast is dependent on the target and background powers. A contrast definition often used for evaluating the performance of human observers is

$$C = \frac{I_{max} - I_{min}}{I_{max} + I_{min}} \tag{186}$$

where I_{max} is the maximum scene intensity

I_{min} is the minimum scene intensity

Substituting from the section on receivable power and suppressing the subscripts for polarization, incidence angle, and range, the asymptotic contrast becomes

$$C_A = \frac{F\left|T_A(\text{target}) - T_A(\text{background})\right|}{(2-F)(T_A(\text{background})) + F(T_A(\text{target})) + 2\,T_{path}} \tag{187}$$

where T_A is apparent temperature at the appropriate incidence angle, range and polarization

F is the beam fill factor

T_{path} is the path emission

The maximum value of this expression obtainable by changing system configuration is when the target fills the beam entirely, in which case

$$\text{MAX } C_A = \frac{\left|T_A(\text{target}) - T_A(\text{background})\right|}{T_A(\text{target}) + T_A(\text{background}) + 2\,T_{path}} \tag{188}$$

Psycophysical experiments have shown (for example, Reference 3) that a contrast of .02 is required to detect an object on a display. In a large majority of the

runway-background-weather conditions described for this study, this contrast is not available. Even in the best situation, at certain glide slope angles the contrast is inadequate. For example, weather case 4 is the best weather situation for radiometer operation. In this case, the contrast as a function of glide slope is shown in Figures 133 and 134, for a concrete runway and grass or dry snow background. With vertical polarization, there is a contrast reversal between .052 rad (3°) and .07 rad (4°). Since this is the approximate glide slope considered standard, it can be immediately concluded that a vertical polarization radiometer is not acceptable. With horizontal polarization, there is no contrast reversal.

A technique used by FLIR radiometers to improve the contrast is to adaptively control the display bias and gain such that the background is effectively cancelled out. This adaptivity can be either manually controlled by the pilot or automatically controlled by the radiometer display processing circuitry. This technique is not normally used with microwave radiometers, since some targets at high incidence angles appear very cold. With an adaptive controller, any signal with an apparent temperature below the bias level may not provide a signal to the display. Thus, many targets of interest would not appear on the display of a conventional radiometer if such a technique were used. However, in a forward looking microwave radiometer all targets have apparent temperatures near ambient except obstacles. The background (grass, weeds, etc) is cold relative to the runway since the runway is specular and the ground diffuse. Since obstacles, which are microscopically specular but have complex shapes, reflect the zenith sky they will be colder than the background. But their local background is the hot runway, so even with an adaptive bias they will appear on display.

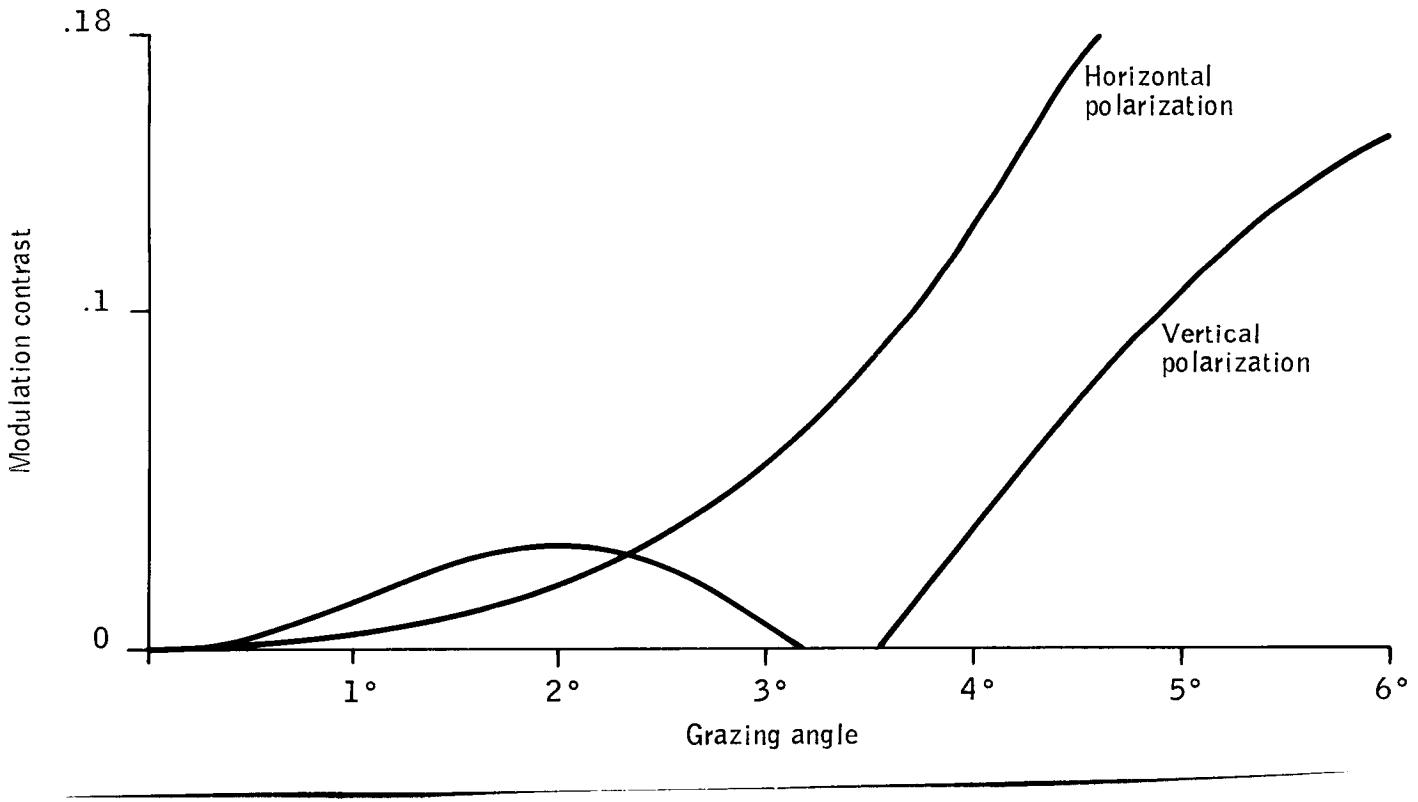

Figure 133-- Contrast of Concrete and Grass at 35 GHz

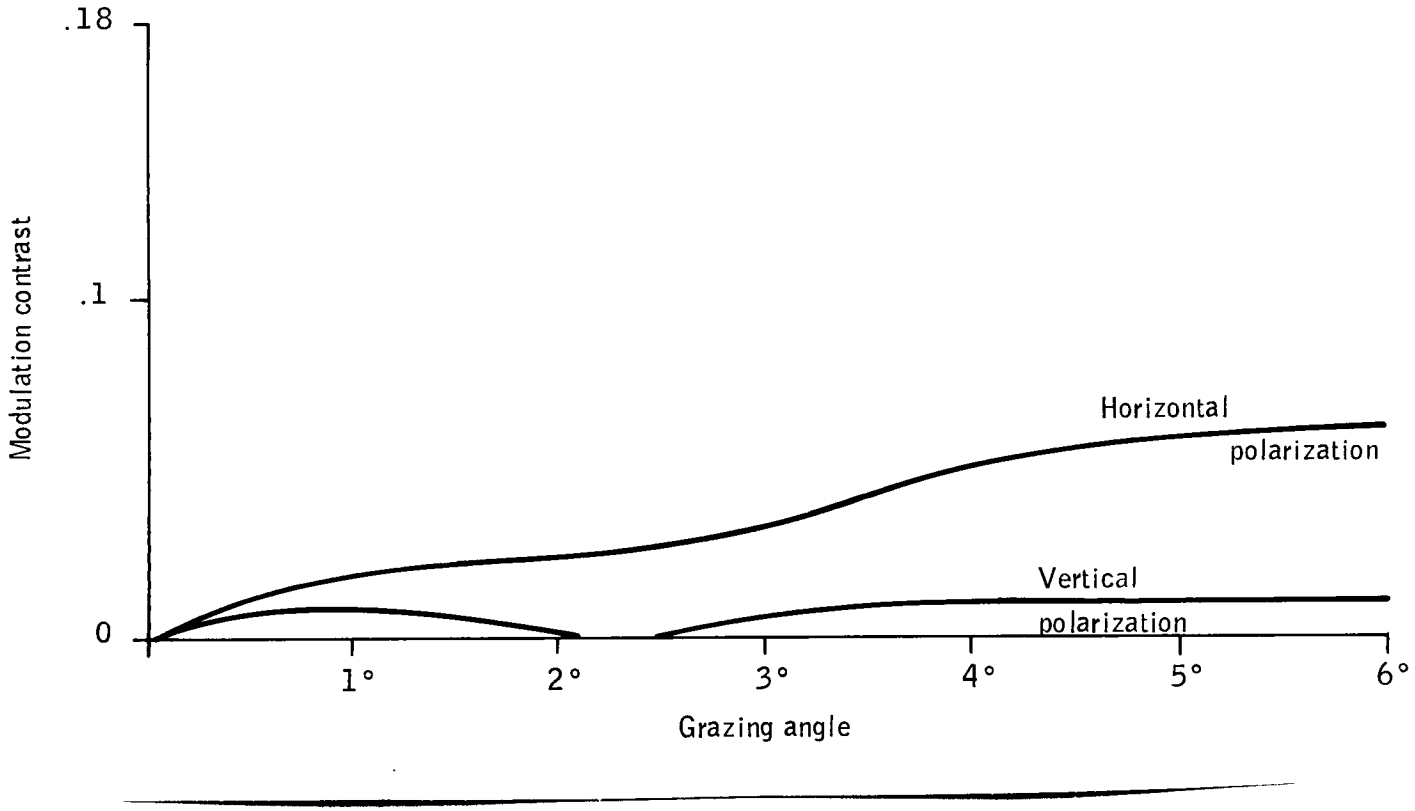

Figure 134 -- Contrast of Concrete and Snow at 35 GHz

With adaptive control, any target which has any temperature difference can appear on the display with any contrast which the display is capable of. Rewriting the contrast equation for the biased case,

$$C = \frac{\left|(I_T-I_A) - (I_B-I_A)\right|}{(I_T-I_A) + (I_B-I_A)} = \frac{\left|I_T-I_B\right|}{I_T+I_B-2I_A} \tag{189}$$

where I_T is the target intensity

I_B is the background intensity

I_A is the adaptive bias intensity

Since the difference terms in parentheses are intensities, the minimum value of any term is zero. Selecting $I_A = \min(I_T, I_B)$, the result is

$$C = \frac{I_T-I_B}{I_T+I_B-2\min(I_T,I_B)} \tag{190}$$

which is identically 1 unless $I_T = I_B$, in which case it is zero. Using this definition of contrast, a contrast of 1 is equivalent to infinite contrast using the definition $C = \Delta T/T$.

Therefore, when using an adaptive control system to display a single target against a uniform background, the contrast is a function of the quality of the adaptivity only. For very small temperature differences, the signal to noise ratio limits the useful gain and hence contrast. It is possible that a lower contrast than the ideal would provide the best detection, since the effect of optimum bias is to make the radiometer signal very small. This allows amplifier noise following the biasing to dominate the radiometer signal. However, it is still true that only noise, and not contrast, limits the detectability of targets.

Signal to Noise Ratio -- The signal to noise ratio with fixed thresholding and gain is the ratio of the mean value of the integrated noise field to the standard deviation of the integrated noise. The signal to noise ratio is dependent on:

- o The RF bandwidth of the radiometer
- o The noise figure of the radiometer
- o The integration time of the radiometer
- o The configuration of the radiometer
- o The apparent temperature of the target
- o The apparent temperature difference between the target and the background.

The RF bandwidth and noise figure are determined by the available state of the art devices. The usable bandwidth is limited by the bandwidth of the antenna, mixer, and amplifiers. Current state of the art at 35 GHz is on the order of 1 GHz. At wider bandwidths all three factors become troublesome. Thus it is unlikely that significantly wider bandwidths will be available in the near future. The noise figure of the radiometer is a measure of the self-noise generated by the receiver. State of the art is about 5 dB, and some progress is being made toward obtaining lower values. A general expression for noise figure of cascaded systems is

$$NF = 1 + \sum_{i=1}^{N} \frac{NF_i - 1}{\sum_{j=1}^{i} G_j} \tag{191}$$

where NF_i is the noise figure of the ith stage

G_j is the gain of the jth stage

It is readily apparent that the noise figure is influenced only by the first few stages. In a typical superheterodyne receiver without preamplifier, the noise

figure is dominated by the mixer noise. RF amplification can reduce this effect, but wideband amplifiers at 35 GHz and above have considerable self-noise. The lowest noise amplifier available has a 3 dB noise figure, but only a .5 GHz bandwidth.

The integration time is determined by the antenna beamwidth and scanning rate requirements. It is generally considered good practice (Reference 63) to allow a 90% voltage buildup of an RC integrator for a step input in the time it takes the antenna to scan one beamwidth.

The configuration of the radiometer affects the signal-to-noise ratio through the percentage of the time the antenna is connected to the receiver.

The apparent temperature of the target and background affect the signal to noise ratio since a noise source with a large variance integrates to give a usable mean value faster, in probability, than a noise source with a low variance.

Reference 63 has derived an expression for signal to noise ratio usable as an approximation for any configuration radiometer. The signal to noise ratio is:

$$S/N = \frac{\Delta T_A \sqrt{BW \times T_I}}{2a^2 \left[T_A + (NF-1)(T_o)\right]} \tag{192}$$

where $\Delta T = (T_A(\text{target}) - T_A(\text{background})) \times \exp - \int_o^r \alpha \, ds$

T_A is the apparent target plus path temperature

a is a configuration constant

NF is the radiometer noise figure

T_o is reference temperature

BW is the predetection bandwidth

T_I is the integration time

The configuration constant for a correlation radiometer is 1, and all targets at low grazing angles have a temperature on the order of 290°K. Assuming a pre-detection bandwidth of 1 GHz and a noise figure of 4 dB, the signal to noise ratio can be simplified to

$$S/N = 21.7\,\Delta T\sqrt{T_1} \tag{193}$$

The required integration time for a switched beam single receiver radiometer was shown to be 1.3×10^{-3} seconds. In this case,

$$S/N \cong .77\,\Delta T \tag{194}$$

With a multi-beam, multi-receiver radiometer, the integration time can be increased proportionally to the number of beams used. If a .14 rad (8°) field of view is covered with .009 rad (.5°) beams, 16 beams are used. For this case, $S/N = 3.1\,\Delta T$.

In logarithmic notation, the signal to noise ratio is

$$S/N = 10 \log \Delta T + L_p + \sqrt{N_{beam}}\ 10 \log .77 \tag{195}$$

where $\Delta T = \left|T_{A,P}(\theta,0)(\text{target}) - T_{A,P}(\theta,0)(\text{background})\right|$

$L_p = -\int_o^r \alpha\, ds$ = path attenuation

N_{beam} is the number of simultaneous beams

Table 58 gives values of 10 log ΔT for a concrete target and grass background, and Table 59 gives summary values of L_p for ranges of interest.

Table 58 -- Radiometer Signal Strength, Concrete Against Grass (dB)

Weather Case	Glide Slope Vertical Polarization 1°	3°	6°	Horizontal Polarization 1°	3°	6°
1	- ∞	-3.9	4.5	- ∞	-3	5.4
2.1	7.4	4.9	18.3	1.5	12.9	19.0
2.2	7.2	4.6	18.3	1.5	12.9	19.0
2.3	6.4	-2.2	18.2	- .4	12.8	19.0
2.4	- .9	6.4	18.2	-5.2	12.4	19.0
3.1	-1.5	9.5	17.6	-10	10.9	18.5
3.2	-2.2	9.6	17.5	-10	10.9	18.5
3.3	- ∞	9.4	17.1	-10	10.3	18.1
3.4	- ∞	8.1	15.9	- ∞	9.0	17.0
4	8.3	6.7	18.0	2.6	12.8	18.7

Table 59 -- Summarized Path Losses (dB)

Weather Case	2km	6km	16km
1	-9.1	-27.3	-74.8
2.1	- .1	- .4	- 1.0
2.2	- .2	- .5	- 1.0
2.3	- .9	- 1.1	- 1.7
2.4	-2.8	- 3.1	- 3.7
3.1	- .2	- .6	- 2.2
3.2	- .3	- .9	- 2.7
3.3	-1.4	- 4.4	- 8.4
3.4	-4.9	-15.0	-25.7
4	- .1	- .3	- .6

It can be seen by examining Table 58 that at glide slope angles of .01745 rad (1°), intrinsic signal levels are too low to provide adequate signal to noise ratio regardless of atmospheric conditions. A 16 beam radiometer has adequate intrinsic signal (S/N ignoring weather attenuation) everywhere else except weather case 1. The lack of signal in weather case 1 is due to the extremely high sky temperature caused by a heavily attenuating atmosphere. Typical intrinsic signal levels are 12-15 dB on a .052 rad (3°) glide slope and 20-22 dB on a (6°) glide slope. From Table 59, this intrinsic signal can be seen to be sufficient except for weather case 1 and case 3.4 at ranges greater than about 4 km.

The primary cause of this degradation is not atmospheric attenuation, as might be expected, but is rather the loss of temperature difference between the target

and the background. This is caused by the increasing zenith sky temperature, which when reflected by the ground is the primary source of signal.

Results for an asphalt runway would be extremely similar. Since grass is the most common background and the radiometer is non-functional for this background, no other backgrounds will be considered.

In conclusion, this study has shown that microwave radiometry is inadequate for even basic ILM use for the following reasons:

- o Resolution is inadequate for recognition at minimum effective range for all but the largest runways.
- o Resolution in the along track direction is 20 times poorer than in the cross track direction so detection of targets which are somewhat symetrical is highly unlikely.
- o Antenna size and scan rate requirements prevent the use of reflector antennas.
- o Phased array antennas when operated at radiometer type bandwidths have an unacceptable resolution degradation.
- o Timed array antennas are extremely complex and require large amounts of external hardware, but are the only possible design.
- o Contrast between target and background is so low that sophisticated contrast enhancement techniques would have to be used.
- o Signal to noise ratios are adequate only on steep glide paths (3° and above), and then only during relatively good weather and with horizontal polarization.

MICROWAVE INTERFEROMETRY

Basic Principles of Interferometry

The basic principle of interferometry is shown in Figure 135. If an electromagnetic wave is traveling in the + x direction, the propagation can be described by

$$E(t,x) = E_o \cos(wt+kx) \tag{196}$$

where E is the field strength of the wave

E_o is the amplitude

w is the radian frequency

$k = \frac{2\pi}{\lambda}$ is the wave number

If this wave is incident on a pair of antennas separated by a distance d, the signals received at antennas are

$$\text{Antenna 1:} \quad E_1(t) = E_o \cos(wt+\emptyset) \tag{197}$$

$$\text{Antenna 2:} \quad E_2(t) = E_o \cos(wt+\emptyset - kd \sin\theta) \tag{198}$$

By comparing the phase of the signal at antenna 1 to the phase at antenna 2, the function

$$\Delta\emptyset = \arg E_1(t) - \arg E_2(t) = kd \sin\theta \tag{199}$$

is obtained. The angle of arrival, θ, is easily obtained since the wave number and antenna spacing are known.

The observation $\Delta\emptyset$ can be made more sensitive to changes in theta by increasing either the wave number or the antenna separation. Writing the antenna separation in terms of the ratio of physical separation to the wavelength yields:

$$\emptyset = 2\pi \left(\frac{d}{\lambda}\right) \sin\theta \tag{200}$$

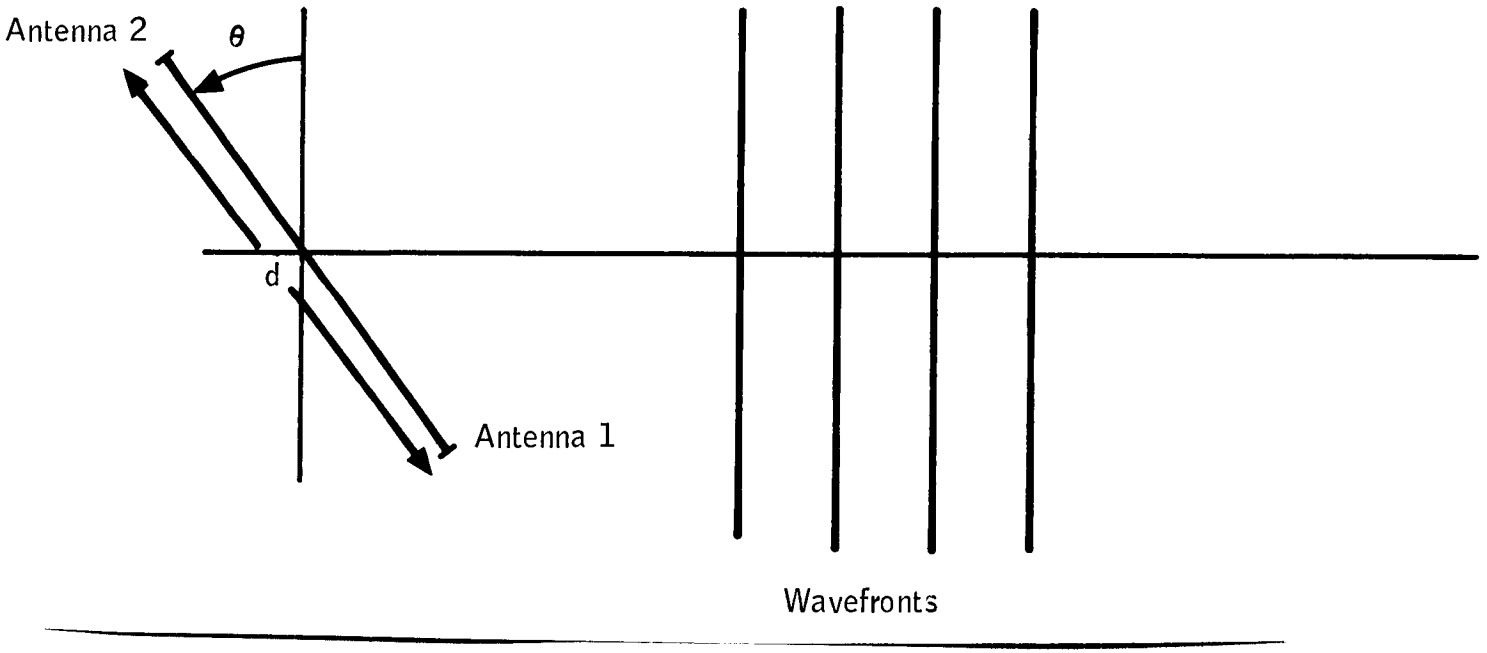

Figure 135 -- Basic Interferometer

The sensitivity of $\Delta\phi$ to changes in theta is

$$\frac{d(\Delta\phi)}{d\theta} = 2\pi \left(\frac{d}{\lambda}\right) \cos\theta \qquad (201)$$

which is directly proportional to the scale separation $n = d/\lambda$. However, since $\Delta\phi$ is a phase difference, it is only measurable modulo 2π. Therefore, when n is greater than one, the measurement of theta has a n-fold ambiguity in each quadrant.

If it is known on which side of the baseline the target lies, the quadrant can be resolved by using pulsed signals, and measuring which antenna receives the signal first. To resolve the n-fold ambiguity, another antenna can be placed on the baseline between the two primary antennas, or multiple frequencies can be used to modify the effective baseline length.

The use of multiple antennas introduces two new problems:

- Some baseline configurations only resolve some of the ambiguities.
- In the presence of noise, a decision error may be made in determining what physical angle corresponds to a pair of phase differences.

The probability of making an error in the resolution of ambiguity places a restriction on the maximum baseline length which is useful in increasing system accuracy. The sources of error in an interferometer are

- Thermal noise
- Diffuse multipath (ground clutter)
- Specular multipath
- Receiver phase stability
- Antenna lead-in phase stability

- o Mutual coupling between antennas
- o Mechanical antenna mounting errors
- o Antenna phase center instability

Since the problem is a short range problem with frequency unconstrained, the frequency and transmitter power levels can be selected such that thermal noise is negligible. Receiver phase stability is a problem in electronics state of the art. Currently, receivers are available which are stable to about .1745 rad (10°). Errors due to lead-in, mutual coupling, antenna mounting and phase center stability are typically .07 rad (4°) total (Reference 66). The dominant limiting factor in either an air-to-ground or ground-to-air interferometer is the multipath environment.

Diffuse Multipath

The effects of diffuse multipath can be analysed using the concept of the glistening surface presented in Reference 64. Assuming that the surface of the earth is described by a random gaussianly distributed deviation from a mean level, and that the reflection of electromagnetic waves is approximated by elemental mirrors, the ground areas which affect the received signal are limited to those areas whose RMS slope redirects transmitted radiation in the direction of the receiver. This area is called the glistening surface and is a function only of the transmit-receive geometry and the RMS slope of the surface.

The most common surface to be considered is a grass surface. By comparing theoretical radar cross section equations developed in Reference 64 with Ohio State measurements of grass backscattering, the effective RMS slope for grass is approximately .30 rad (17°). Thus the glistening surface is described by a trapezoid

whose ends are a distance from the antenna of

$$d_i = 1.44\ h_i \tag{202}$$

where d_i is the distance from the ith antenna to the start of the glistening surface

h_i is the height of the ith antenna

The sides of the surface are described by lines joining the points a distance to the side of the antenna

$$s_i = \pm .312\ h_i \tag{203}$$

The resulting surface is a narrow trapezoidal strip between the transmitter and receiver, shown in Figure 136. The strip is so narrow and so close to the necessary antenna boresight, that antenna beam forming would be ineffective in reducing the diffuse multipath interference.

The total power from the glistening surface is given by the bistatic radar equation

$$P_r = \frac{P_t G_t G_R \lambda^2}{(4\pi)^3} \int_S \frac{\gamma\ dS}{R_1^2 R_2^2} \tag{204}$$

where S is the glistening surface

γ is the bistatic differential cross section at a point on the surface

R_1 is the range from the aircraft to a point on the surface

R_2 is the range from that point on the surface to the receiver

Since this power is approximately Rayleigh distributed, it can be represented as gaussian in amplitude and uniform in phase, the normal white gaussian approximation.

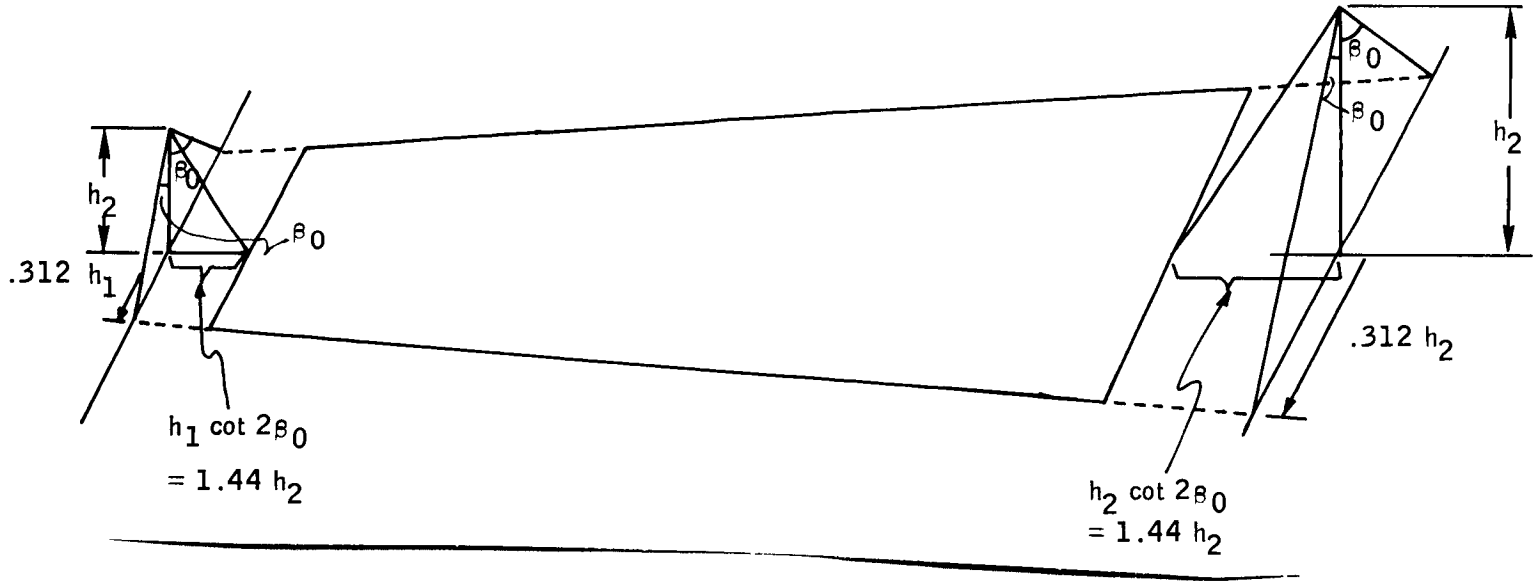

Figure 136 -- The Glistening Surface

The direct power from the transmitter is

$$P_r = \frac{P_t G_t G_R \lambda^2}{(4\pi R)^2} \tag{205}$$

Thus a signal to clutter ratio can be defined as

$$S/C = \frac{4\pi}{R^2 \int_S \frac{\gamma}{R_1^2 R_2^2} dS} \tag{206}$$

A computer program, GLISTEN, has been written to perform the integration in the denominator. The results for an aircraft on a 3° glide slope, operating with an L-band interferometer 3 km from the touchdown point on a flat grass surface is that the clutter limited signal to noise ratio is on the order of 33 dB. Other values are shown in Figure 137. Appendix C shows some of the values of γ used in computing Figure 137.

Specular Multipath

Specular multipath is the mirror-like reflection of electromagnetic waves from surfaces. The characteristics of specular reflections are

- The angle of the center of the reflected beam from the surface normal is equal to the angle of incidence
- The reflected wave front is coherent
- The phase shift on reflection is determined by the Fresnel reflection coefficient
- The width of the reflected beam is determined by the size of the reflecting surface.

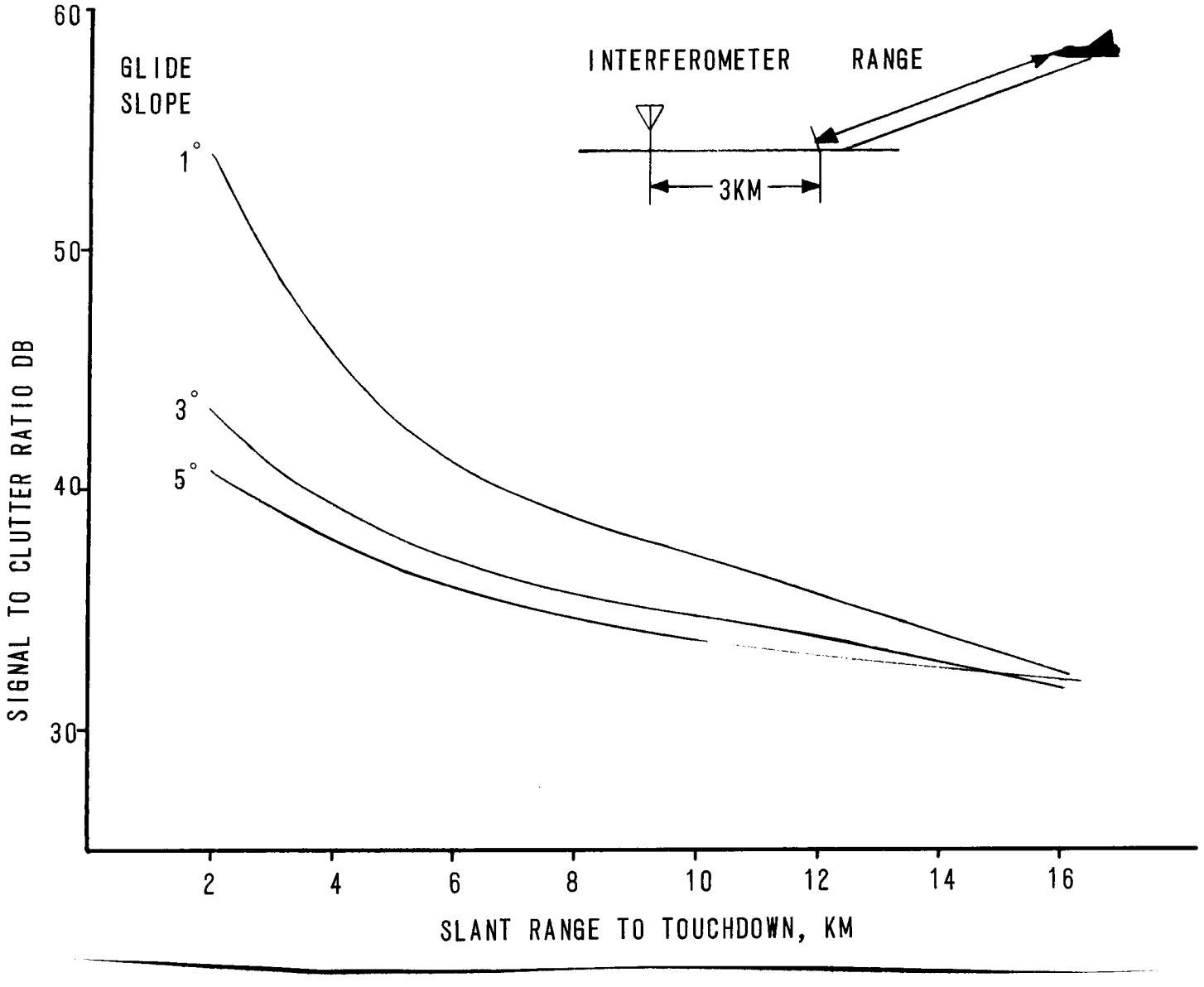

Figure 137 -- Diffuse Multipath S/C Ratios

In the elevation channel of an interferometer system, the primary specular reflection is the reflection from the ground. The ground is effectively an infinite rough surface, so the specular reflection is only in the specular direction, i.e., angle of incidence equals angle of reflection. Thus, if the ground is flat, only the reflection from one point on the ground affects the interferometer. If the ground in front of the interferometer is rising, a second reflection point can influence the interferometer.

In the azimuth channel, the specular ground reflection is not a major problem, since it appears at nearly the same angle as the direct signal. However, reflections from taxiing aircraft, maintenance vehicles, airport buildings and surrounding hills can cause significant errors.

In order to analyse the effects of specular multipath in the azimuth channel, a relatively detailed airdrome scenario must be defined. The effects of a plane earth on the elevation channel are relatively easily analysed.

Elevation Channel Errors -- Consider the scenario of Figure 138. The transmitter is assumed to be far enough away that the direct ray is parallel to the reflected ray before reflection. In this case, the difference in path length between the specular and direct ray is

$$\Delta R = 2z \sin\theta \tag{207}$$

where z is the height of the antenna above the earth

θ is the grazing angle

The field at the antenna due to the multipath is then

$$E_M = \rho E_i \, e^{\,j(\frac{4\pi}{\lambda} z \sin\theta + \phi_r)} \tag{208}$$

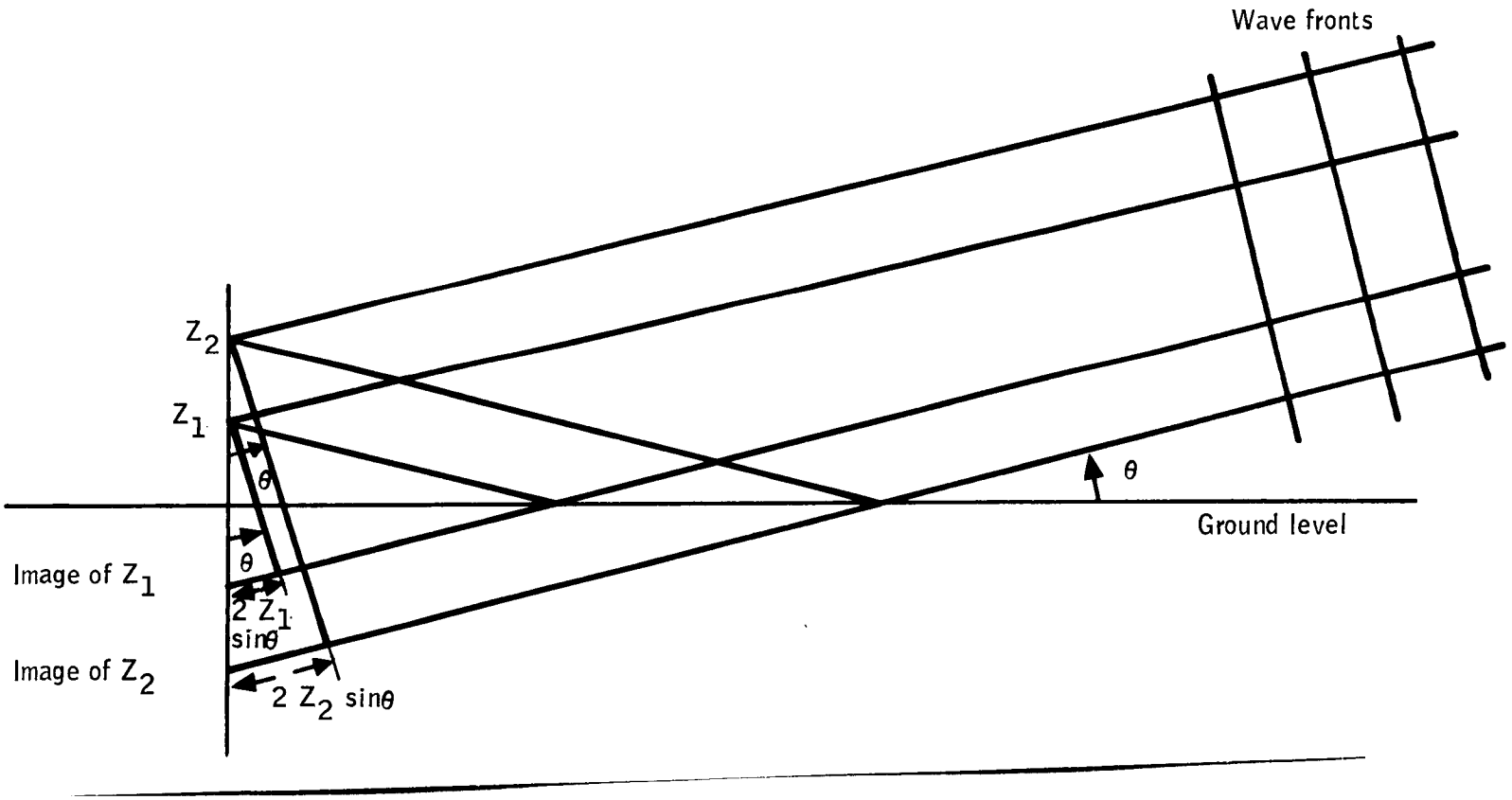

Figure 138 -- Elevation Channel Specular Multipath Scenario

where E_i is the incident field strength

ρ is the magnitude of the reflection coefficient

ϕ_r is the phase of the reflection coefficient

The total field at the antenna is

$$E_1 = E_i \left(1 + \rho\, e^{j\left(\frac{4\pi}{\lambda}\, z \sin\theta + \phi_r\right)}\right) \tag{209}$$

The total field can also be written as

$$E = E_i \left(1 + \rho \cos\left(\frac{4\pi}{\lambda}\, z \sin\theta + \phi_r\right) + j\, \rho \sin\left(\frac{4\pi}{\lambda}\, z \sin\theta + \phi_r\right)\right) \tag{210}$$

The phase angle relative to the phase of the direct wave alone is then

$$\phi_1 = \tan^{-1}\left[\frac{\rho \sin\left(\frac{4\pi}{\lambda}\, z \sin\theta + \phi_r\right)}{1 + \rho \cos\left(\frac{4\pi}{\lambda}\, z \sin\theta + \phi_r\right)}\right] \tag{211}$$

If a second antenna is added a distance $d\lambda$ above the first antenna, its phase relative to its freepath is

$$\phi_2 = \tan^{-1}\left[\frac{\rho \sin\left(\frac{4\pi}{\lambda}\, (z + d\lambda) \sin\theta + \phi_r\right)}{1 + \rho \cos\left(\frac{4\pi}{\lambda}\, (z + d\lambda) + \phi_r\right)}\right] \tag{212}$$

The phase difference assumed by the interferometer system is the difference between the free path phase differences. The error in phase determination caused by specular reflection is then

$$\phi_e = \tan^{-1}\left[\frac{\rho \sin\left(\frac{4\pi}{\lambda}\, z \sin\theta + \phi_r\right)}{1 + \rho \cos\left(\frac{4\pi}{\lambda}\, z \sin\theta + \phi_r\right)}\right] - \tan^{-1}\left[\frac{\rho \sin\left(\frac{4\pi}{\lambda}\, (z + d\lambda) \sin\theta + \phi_r\right)}{1 + \rho \cos\left(\frac{4\pi}{\lambda}\, (z + d\lambda) + \phi_r\right)}\right] \tag{213}$$

Since the error in phase determination is roughly proportional to the magnitude of the reflection coefficient, vertical polarization can be utilized to reduce the phase error. In this case, the reflection coefficient for an infinite rough surface is

$$\rho e^{j\phi} = \left[\exp\ -(4\pi \frac{\sigma}{\lambda} \sin\theta)^2\right] \frac{E_r \sin\theta - \sqrt{E_r - \cos^2\theta}}{E_r \sin\theta + \sqrt{E_r - \cos^2\theta}} \qquad (214)$$

where $\rho e^{j\phi}$ is the reflection coefficient

σ is the rms surface roughness

λ is the wavelength

θ is the grazing angle

E_r is the complex permittivity of the surface

A program to compute the phase error has been written and several cases using a grass surface ($E_r = 80 + j50$, $\sigma = .3$ cm, ref. 74) at L-band have been run. The results are shown in Figure 139 for an interferometer with a 5λ baseline. The results are typical, in that the phase error oscillates, with the period becoming smaller as the height of the interferometer above the surface increases. The amplitude of the error is proportional to the reflection coefficient, being minimum near the pseudo Brewster angle (about 6°).

Azimuth Channel Errors -- The formula for multipath in the elevation channel can be generalized to account for multipath in the azimuth interferometer. There are three major differences between the azimuth and elevation channels:

- o There usually is no single dominant reflection in azimuth
- o The reflecting surfaces in the azimuth case are not infinite

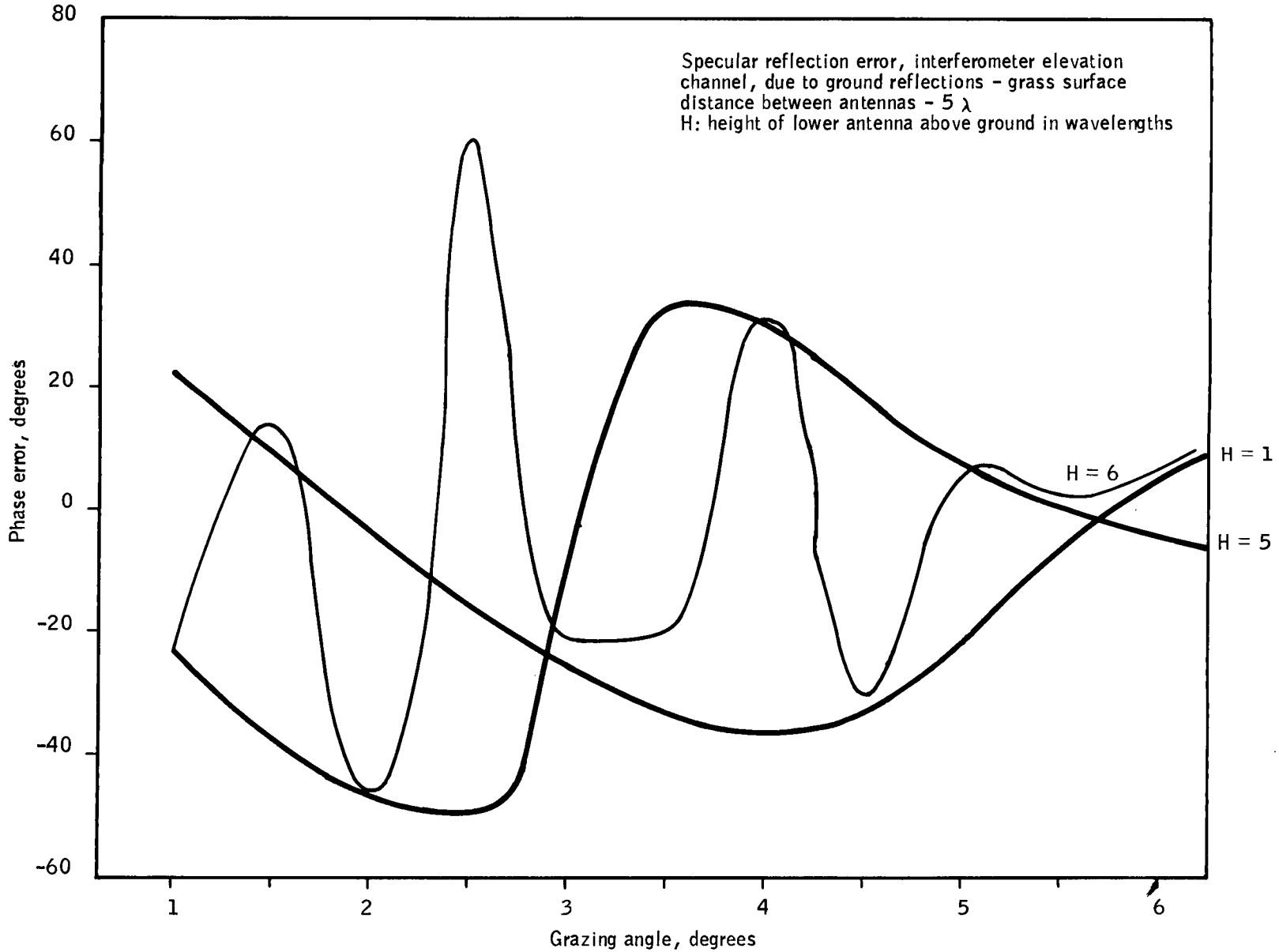

Figure 139 -- Elevation Multipath

- The reflecting surfaces of major concern are vertical, so that the local polarization is orthogonal to the interferometer polarization

To account for multiple reflecting surfaces, the error equation must be extended to the general case. If the jth obstacle is located at a range R_L from the interferometer and the aircraft is at a range R_s, the field at the reference antenna due to this multipath is

$$E_L = E_i \frac{R_s}{R_L} \rho_L e^{j(kR_L+\phi_L)} \tag{215}$$

where E_i is the direct field strength

ρ_L is the magnitude of the coherent reflection coefficient

$K = \frac{2\pi}{\lambda}$ is the propagation constant

ϕ_L is the phase shift of the jth reflection coefficient

The distance from the aircraft on the jth path to a second antenna a distance d separated from the reference antenna is R'_j, which yields a field at the second antenna of

$$E'_L = E_i \frac{R_s}{R'_L} {}_L e^{j(kR'_L + \phi_L)} \tag{216}$$

The total field at the first antenna is

$$E = E_i (e^{jkRs} + R_s \sum_L \frac{\rho_L}{R_L} e^{j(kR_L + \phi_L)} \tag{217}$$

In terms of inphase and quadrature components referenced to the phase of the direct signal, the field is

$$E = E_i (1 + R_S \sum_L \frac{\rho_L}{R_L} \cos(k(R_L-R_s) + \phi_L) + jR_s \sum_L \frac{\rho_L}{R_L} \sin(k(R_L-R_s) + \phi_L) \tag{218}$$

The phase of this total field relative to the direct field alone is

$$\phi = \tan^{-1}\left[\frac{R_s \sum_j \frac{\rho_j}{R_j} \sin\left(k(R_j - R_s) + \phi_j\right)}{1 + R_s \sum_j \frac{\rho_j}{R_j} \cos\left(k(R_j - R_s) + \phi_j\right)}\right] \tag{219}$$

Similarly, the phase at the second antenna relative to the direct field at the second antenna

$$\phi' = \tan^{-1}\left[\frac{R_s \sum_j \frac{\rho_j}{R_j'} \sin\left(k(R_j' - R_s') + \phi_j\right)}{1 + R_s \sum_j \frac{\rho_j}{R_j'} \cos\left(k(R_j' - R_s') + \phi_j\right)}\right] \tag{220}$$

Thus, the phase error due to multiple specular reflections is

$$\Delta\phi = \tan^{-1}\left[\frac{\sum_j \frac{\rho_j}{R_j} \sin\left(k(R_j - R_s) + \phi_j\right)}{\frac{1}{R_s} + \sum_j \frac{\rho_j}{R_j} \cos\left(k(R_j - R_s) + \phi_j\right)}\right] -$$

$$\tan^{-1}\left[\frac{\sum_j \frac{\rho_j}{R_j'} \sin\left(k(R_j' - R_s') + \phi_j\right)}{\frac{1}{R_s} + \sum_j \frac{\rho_j}{R_j'} \cos\left(k(R_j' - R_s') + \phi_j\right)}\right] \tag{221}$$

Since vertical polarization would normally be used to reduce the error due to ground reflection in the elevation channel, the local polarization for reflections affecting the azimuth interferometer is horizontal. Thus, the phase of the reflection coefficient ρ_j can be approximated as π, regardless of permittivity.

The magnitude of the reflection coefficient is not the magnitude of the Fresnel

reflection coefficient, since the scattering objects are not infinite planes. If the object is located in the plane defined by the interferometer baseline and the line from the interferometer and the aircraft, the object can be considered infinite in altitude. Then the reflection coefficient becomes a function of a single object dimension.

If the dimensions of the scattering element are on the order of a few wavelengths, the reflection coefficient is (Reference 64).

$$\rho = \frac{|(1 + R)\cos\theta_2 - (1 - R)\cos\theta_1|}{2\pi(\sin\theta_1 - \sin\theta_2)} \sin\left(\frac{2\pi x}{\lambda}(\sin\theta_1 - \sin\theta_2)\right) \qquad (222)$$

where R is the Fresnel reflection coefficient

θ_1 is the incidence angle

θ_2 is the reflection angle

$2x$ is the size of the surface

If the surface is several wavelengths in dimensions and the incidence and reflection angles are not equal, the lobes caused by the sine function will be so closely spaced that the function $\sin\frac{2\pi x}{\lambda}(\sin\theta_1 - \sin\theta_2)$ can be approximated by its maximum value of 1. This approximation can be applied to buildings and other large structures.

The complexity of the equations is such that no significant conclusions can be made based on the form of the equations. The time alloted did not permit creating a simulation to exercise the equations, so an approximation technique was developed.

The approximate technique is to assume a level of specular multipath interference and compute the maximum error obtainable under that level of interference. The total field at the antenna was

$$E = E_i \left(1 + \sum_j \frac{R_s}{R_j} \rho_j e^{j(k(R_j - R_s) + \phi_j)}\right) \tag{223}$$

The phasor diagram Figure 140 shows this field. The summation has some effective magnitude and phase such that the field can be written

$$E = E_i \left(1 + \rho_e e^{j\phi e}\right) \tag{224}$$

The angle $\Delta\theta_1$ is the phase error at the first antenna, as given by the previous equations. From the diagram, it can be seen that the phase error is maximized when the total normalized field vector is tangent to the circle centered at 1 with a radius equal to ρ_e. In this case,

$$\Delta\theta_{1max} = \sin^{-1} \rho_e \tag{225}$$

To maximize the total error, the phase error on the second antenna must be

$$\Delta\theta_2 = -\Delta\theta_1 \tag{226}$$

in which case

$$\Delta\theta_{max} = 2 \sin^{-1} \rho_e \tag{227}$$

Defining a multipath to signal power ratio as

$$M/S = 20 \log \rho_e \tag{228}$$

the error diagram of Figure 141 can be derived.

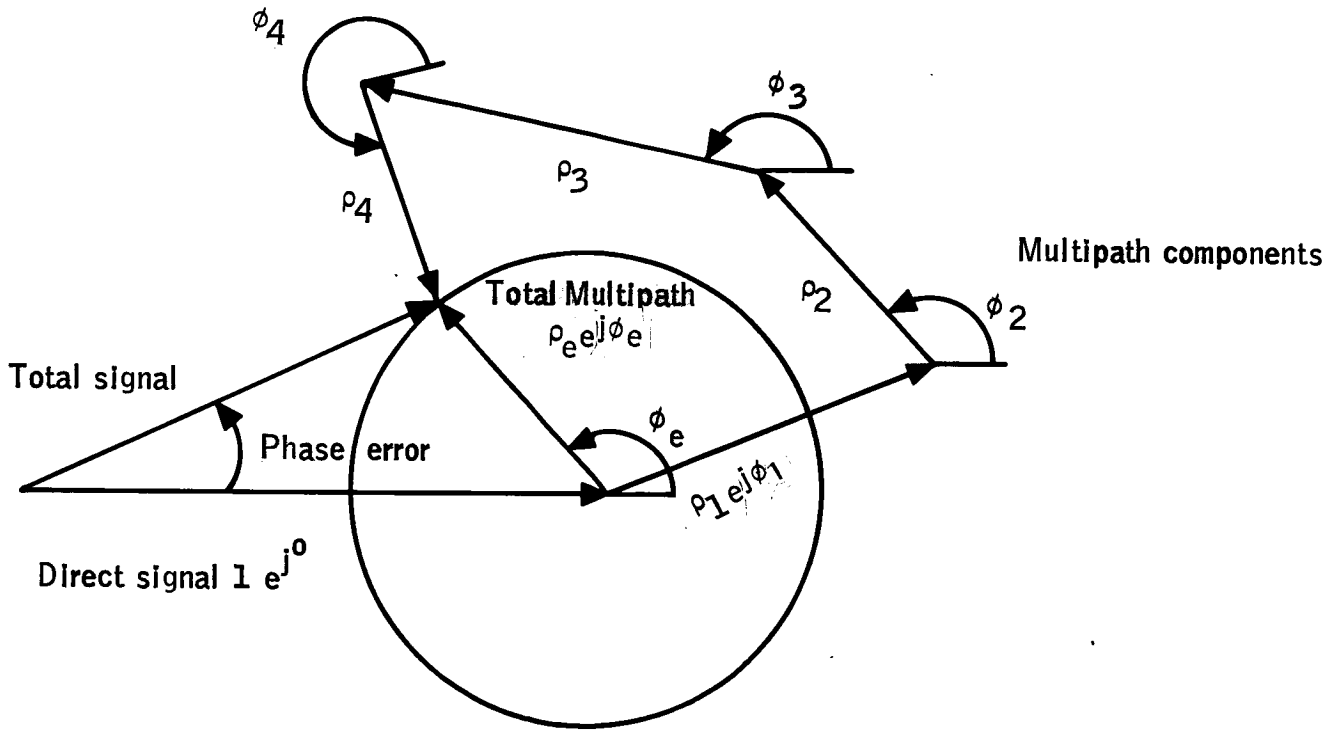

Figure 140 -- Multipath Phasor Diagram

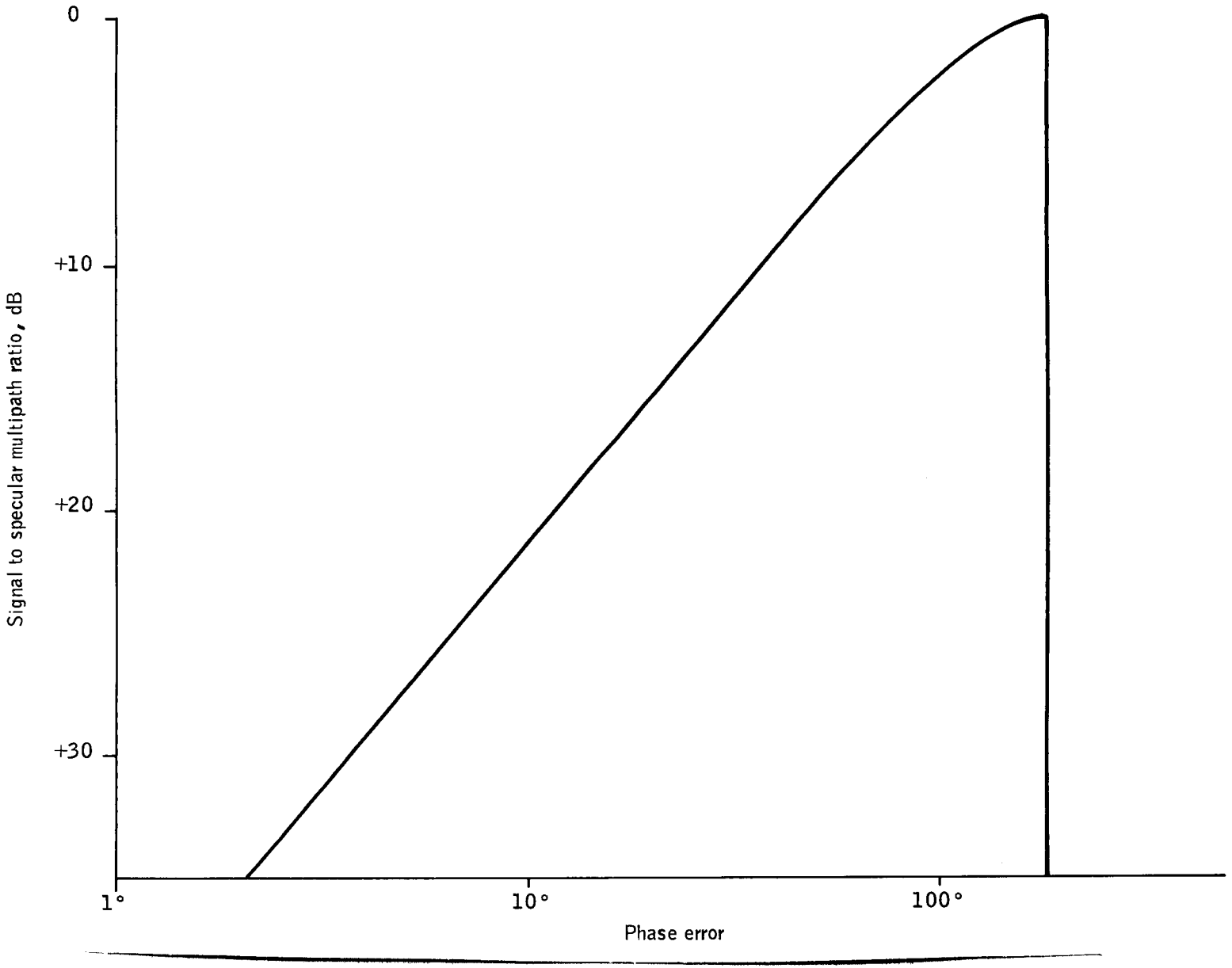

Figure 141-- Maximum Multipath Phase Error

Although it is unlikely that the phase of the summed multipath will take the angles required for the error to be maximized, the possible errors are extremely large. If a single reflector happens to be located such that its specular angle is directed at the interferometer and the reflector is metallic such as a truck or aircraft tail, ρ_e will be approximately 1, and a $^S/_M$ ratio of 0 dB will exist.

Even if no such reflector exists, the specular reflection coefficient is approximately

$$\rho \cong \rho_o \cos \theta \tag{229}$$

where ρ_o is the reflection coefficient at the specular angle

θ is the half angle between the specular angle and the reflection angle

$$\text{when } \frac{2\pi x}{\lambda} (\sin \theta_1 - \sin \theta_2) \cong \sin \left(\frac{2\pi x}{\lambda} (\sin \theta_1 - \sin \theta_2)\right). \tag{230}$$

Therefore it can be expected that a reasonable environment would have $^M/_S$ ratios typically larger than -10 dB, which would allow errors up to 40° in phase. Since the effective phase is varying rapidly as the range changes, the maximum phase error can be expected to be approached quite often during the aircraft's glide path.

Consequences of Specular Reflections -- It has been shown that phase measurement errors on the order of several degrees are to be expected in a ground based interferometer. The dominant error in the elevation channel is the reflection from the ground. If the ground is sufficiently flat, estimation techniques could be used to reduce this error. However, if the terrain characteristics are not fully specified, the estimation would probably increase the error. In addition, the system would become more sensitive to diffuse multipath. Since all the significant

signals are arriving in a very narrow angular region, antenna pattern shaping is probably of little value. In azimuth, the location of significant reflectors cannot be fully defined since often the dominant reflector will be a taxiing aircraft. Antenna pattern shaping can be used to limit the total number of reflectors, however objects on the taxiway cannot be removed.

Since specular reflection obeys reciprocity, the effect of placing the source on the ground and the interferometer in the air would be negligible.

In a fully synchronous pulsed system, range gating could be employed to remove specular reflections. However, the time left for estimating the relative phase of the signals is only the path length difference times the speed of light. The errors in phase comparison caused by thermal noise alone would then deteriorate the system beyond usability.

Clutter Limitation of Baseline Length -- If the signal to clutter ratio is large, it is intuitively obvious that a short baseline of length $d/\lambda = 1$ is optimum for resolving ambiguities, since it has no ambiguities of its own to interfere with the resolution problem. The probability of making a decision error depends on the algorithm used to resolve the ambiguities. If the algorthm is that the angle estimate is the angle corresponding to measured phase value on the long baseline closest in absolute value to the measurement value on the short baseline, the probability of error is

$$P_e = 1-P\left(\frac{I-\frac{1}{2}+\frac{\Delta\phi}{2\pi}}{M} < z < \frac{I+\frac{1}{2}+\frac{\Delta\phi}{2\pi}}{M}\right) \qquad (231)$$

where $\Delta\phi$ is the phase angle on the long baseline
I is the number of full cycles between antenna
M is the long baseline length in wavelengths
z is the phase angle (in circles) on the short baseline

If the measurements are disturbed by Gaussian noise with normalized variance σ^2 the probability of error is

$$P_e = 2 \text{ erfc } \left(\frac{\cos \theta_{max}}{2M \sigma} \right) \tag{232}$$

where θ_{max} is the maximum angle off boresight

If the measurement is made by multiplying to outputs of receivers connected to the antennas together, assuming independent white Gaussian noise in the receivers with a high signal to noise ratio in each receiver, the variance of the measurement is

$$\sigma^2 = \tfrac{1}{2} \left(\frac{1}{S/N_1} + \frac{1}{S/N_2} \right) \tag{233}$$

where S/N_1 is the signal to noise ratio in receiver 1 (linear ratio)

The derivation of these formuli is given in a later paragraph. Figure 142 shows the probability of making an improper ambiguity resolution. Although the figure and the formula are based on a single pulse measurement, it can be seen that extremely high signal to noise ratios are required to adequately resolve ambiguities with long baseline interferometers.

A reasonable design criterion would be to require that, on the average, only one of every ten measurements have an ambiguity resolution error. In this case, a 10 lambda baseline interferometer requires a minimum signal to noise ratio of about 20 dB.

Conclusions

Multipath caused phase errors in a simple ground-air interferometer can be expected to be on the order of several degrees. If the residual specular error after any

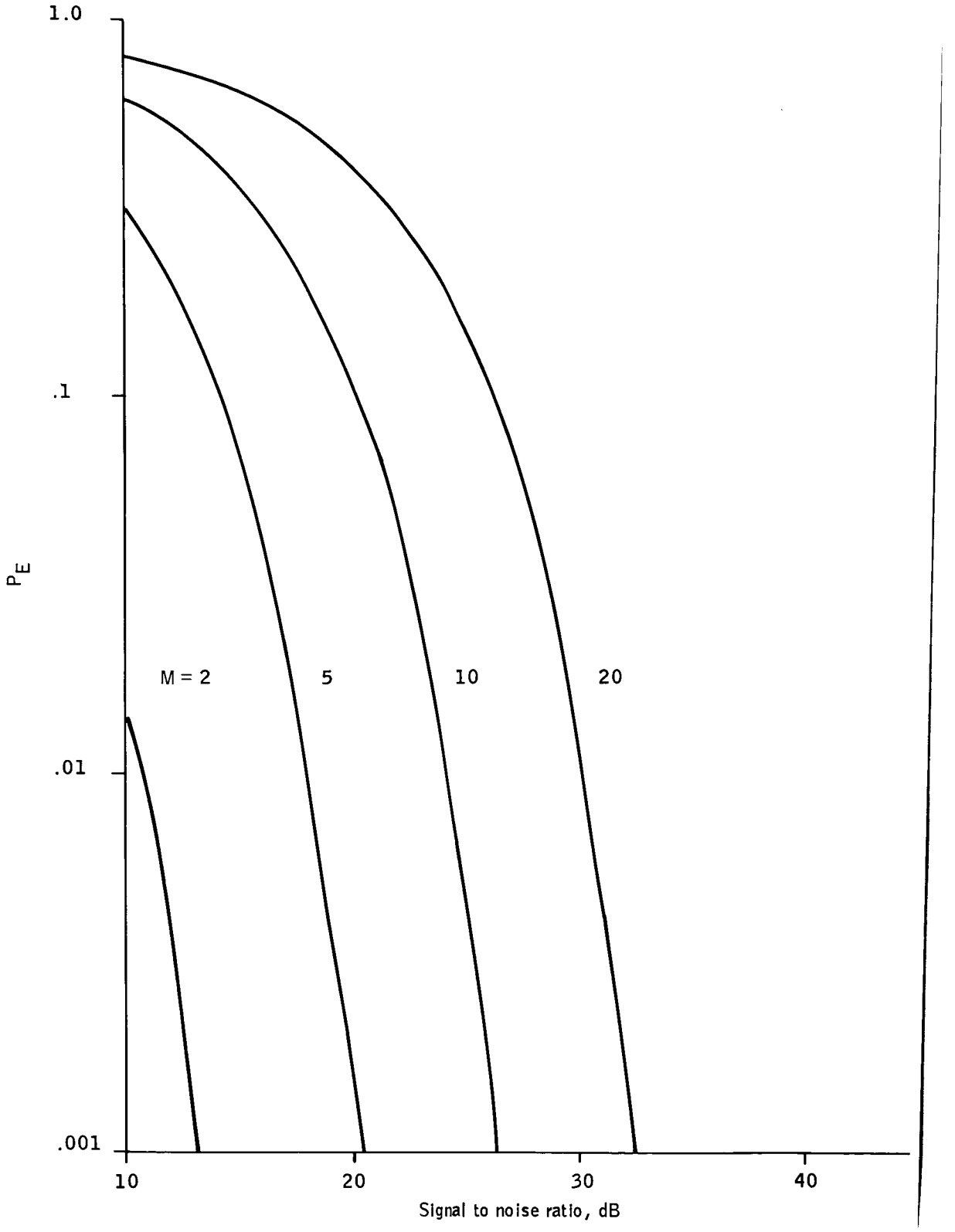

Figure 142 -- Probability of Ambiguity Error

compensation is greater than the size of a grating lobe on the long baseline interferometer, certainly the proper ambiguity resolution cannot be achieved. Because of this, and the probability of ambiguity error due to diffuse multipath, ground-air interferometers are limited to baselines of only a few wavelengths.

The phase measurement errors on the long baseline interferometer cannot be sufficiently reduced to provide angle measurement accuracies similar to MLS.

Therefore, simple interferometers cannot meet even the basic requirements for an ILM.

Derivation of Baseline Limitation Equations

Assume that a 1λ baseline interferometer is being used to resolve the ambiguities on an Mλ baseline interferometer and that the baselines are parallel. If the resolution algorithm is a "closest match" algorithm, the probability of making an ambiguity error is

$$P_e\ (I/\sin\theta = \frac{I}{M} + E) = 1 - P\ \left(\frac{I-\frac{1}{2}}{M} \leq z \leq \frac{I+\frac{1}{2}}{M} \right) \tag{234}$$

where I is the lobe number on the long baseline

E is the phase distance from a lobe edge

θ is the physical angle of the source

z is the phase difference on the short baseline (in circles)

If the phase measurement is corrupted by a Gaussian disturbance with standard deviation σ/cosθ,

$$P_z(x) = \frac{1}{\sqrt{2\pi}\ \sigma/\cos\theta}\ e^{-\left(\frac{(x-\theta)^2}{2(\sigma/\cos\theta)^2}\right)} \tag{235}$$

then

$$1-P_e = \frac{1}{\sqrt{2\pi}\ \sigma/\cos\theta} \int_{\frac{I-\frac{1}{2}}{M}}^{\frac{I+\frac{1}{2}}{M}} e^{-\left(\frac{(x-\frac{I}{M})2}{2(\sigma/\cos\theta)^2}\right)}\ dx \tag{236}$$

$$= \frac{1}{\sqrt{2\pi}\,\sigma/\cos\theta} \int_{-\frac{1}{2M}}^{\frac{1}{2M}} e - \left(\frac{x^2}{2(\sigma/\cos\theta)^2} \right) dx$$

$$P_e = 2\text{erfc} \left(\frac{\cos\theta}{2M\sigma} \right) \tag{237}$$

If the measurement is obtained by multiplying the outputs of two receivers corrupted by white Gaussian noise, the statistics can be directly derived.

Consider two receivers with signals S_1 and S_2.

$$S_1 : A_1 \cos(wt) + n(t) \tag{238}$$

$$S_2 : A_2 \cos(wt + \emptyset) + \hat{n}(t) \tag{239}$$

where n, $\hat{n}$ are independent white Gaussian noise sources

The product of the signals is

$$S_1 x S_2 = \{ [A_1 + n_c(t)] \cos wt + n_s(t) \sin wt \} \{ [A_2 + \hat{n}_c(t)] \cos(wt + \emptyset) + \hat{n}_s(t) \sin(wt + \emptyset) \} \tag{240}$$

where n_c, n_s are the inphase and quadrature noise components of n

Defining $L = A_1A_2 + A_1\hat{n}_c + A_2n_c$ and eliminating all high frequency terms,

$$S_1 x S_2 = \frac{L + n_s\hat{n}_s + n_c\hat{n}_c}{2} \cos\emptyset + \left[\frac{A_1\hat{n}_s - A_2n_s}{2} + \frac{n_c\hat{n}_s - n_s\hat{n}_c}{2} \right] \sin\emptyset \tag{241}$$

Since n and $\hat{n}$ are independent, and $E(n) = E(\hat{n}) = 0$,

$$E(S_1 x S_2) = \frac{A_1A_2}{2} \cos\emptyset \tag{242}$$

The variance of $S_1 x\ S_2$ is found by straight forward computation to be

$$E(S_1 x S_2 - \frac{A_1 A_2}{2} \cos\phi)^2 = \tfrac{1}{4}\left[A_1^2\, E(\hat{n}^2) + A_2 E(n^2) + 2E(n^2)\, E(\hat{n}^2)\right] \tag{243}$$

For noise of spectral density $\frac{n_o}{2}$ of bandwidth B in each channel,

$$\sigma^2(S_1 x S_2) = \frac{n_o B}{4}\left[A_1^2 + A_2^2 + 2n_o B\right] \tag{244}$$

Normalizing the amplitudes such that

$$E(S_1 x S_2) = \cos\phi \tag{245}$$

$$\sigma_n^2 = \left(\frac{2}{A_1 A_2}\right)^2 \sigma^2_{S_1 x S_2} = \frac{n_o B}{A_1^2}\ \frac{n_o B}{A_2^2}\ \frac{2(n_o B)^2}{A_1^2\, A_2^2} \tag{246}$$

If the signal to noise ratio is high, the last term in brackets is negligible and

$$\sigma_n^2 = \frac{N/S_1 + N/S_2}{2} \tag{247}$$

where $N/S_1 = \frac{2n_o B}{A_1^2}$ is the reciprocal of the signal to noise ratio in channel 1

The phase difference is then described by

$$\Delta\phi = \cos^{-1}(x) = \sin^{-1}\left(\frac{\pi}{2} - x\right) = \frac{\pi}{2} - x \text{ for } x \quad \frac{\pi}{2} \tag{248}$$

$$P(x) = \frac{1}{2\pi\,\sigma^2}\ e^{-\left(\frac{(x - \cos\phi)^2}{2\ \sigma^2}\right)} \tag{249}$$

where x is the angle of the source off the baseline.

Since the definition of zero angle is arbitrary, changing origins yields

$$\Delta\phi = x \tag{250}$$

where $\Delta\phi$ is phase difference in radians

This is the formula presented in Reference 66. Since the phase variance is σ_n^2, the physical angle variance is $(\sigma n/\cos\theta)^2$. Substituting into the equations for ambiguity error yields the result presented in the report.

INERTIAL AIDING

Many commercial transports are equipped with Inertial Navigation Systems (INS) for enroute navigation where no radio aids exist. Although current inertial nav systems do not have sufficient accuracy for guidance of the aircraft through the landing phase, they can be used to aid other sensors which are normally noisy or have low data rates.

Inertial information is relatively free from the high frequency noise which plagues RF landing aids; however, low frequency gyro drift induced errors in position, velocity and acceleration occur. For state-of-the-art inertial systems, the error in position increases at approximately 1.85 Km (1 nm) per hour of flight time. The error in velocity is often several knots. Consequently, the inertial information is not directly applicable for precise trajectory control in the landing of the aircraft. The inertial system with it's wideband low noise outputs can be combined with the low frequency accuracies of RF position fixing systems to produce significantly higher guidance accuracies than either system alone will permit.

INS With Low Data Rate Fixes

Some potential ILM sensors could, through time averaging or other techniques, provide accuracies sufficient to meet the ILM functions, but may have resulting data rates too low for adequate aircraft control responses. An inertial reference system could, under these conditions, be used to provide guidance between

fixes from the primary ILM. To determine bounds of the problem, sample analyses were made on two possible conditions.

The accuracy requirements of the MLS system are given in Table 60. For this analysis, we only considered straight-in approaches from 14.82 Km (8 nm) to touchdown.

Table 60 -- Accuracy Requirements, ft. (2σ)

	Distance from Runway Threshold			
	0	1.85 km (1 nm)	5.56 km (3 nm)	14.82 km (8 nm)
Azimuth	14	20	38	103
Elevation	1.8	7.7	33	95
Range	40	58	94	184

For example 1, perfect position fixes were assumed at the outer marker, middle marker and touchdown. Approach velocity of 90 knots was used. The approximate allowable path following error as a function of time or range to threshold is plotted in Figure 143 for both azimuth and elevation. The inertial reference accuracy requirements to maintain accuracy within the allowable errors using these fixes are labeled as INS az and INS el in the figure. Even assuming the perfect fixes, the accuracy requirements on the inertial reference system are in the range of 0.019 km (.01 nm) to 0.519 km (0.28 nm) per hour (2σ). This is much higher accuracy than is available in state-of-the-art inertial reference systems for commercial transports.

The second example analyzed considered the number of position fixes required for an inertial reference system with 1 nautical mile per hour (2σ) accuracy to operate within the allowable errors. Again, for the analysis, perfect fixes and an

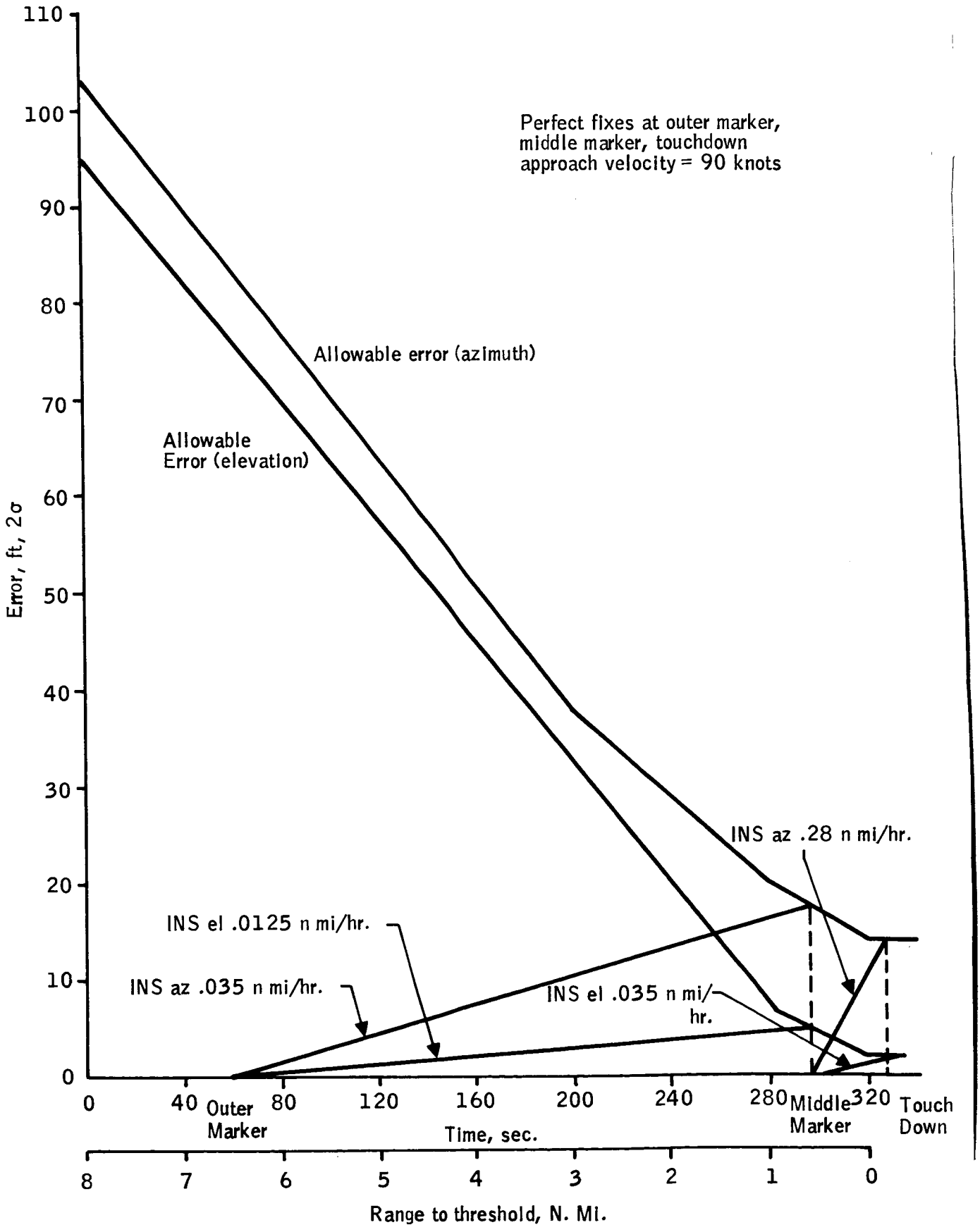

Figure 143 -- Inertial Reference Azimuth and Elevation Accuracy *Requirements*

approach velocity of 90 knots were assumed. The allowable error in azimuth as a function of time or range to threshold is given in Figure 144 and the allowable error in elevation as a function of time or range to threshold is given in Figure 145. As can be noted in the figures, as the aircraft approaches threshold, the allowable error decreases and the corresponding required rate of fixes increases. For azimuth this rate corresponds to .12 fixes per second and for elevation the number is .94 fixes per second.

It should be noted here that these fixes or data rates are significantly less than the basic ILM data rate requirement of 10 samples per second. However, recognizing that perfect fixes cannot be achieved, the data in Table 61 was compiled to show how the data rate varies as a function of the fix errors and as a function of the accuracy of the inertial system at runway threshold. The elevation accuracy requirement dictates extremely high quality fixes and high data rates.

Table 61 -- Position Fix Rate Requirements

		Inertial Reference	
		1 nm/hr (2σ)	3 nm/hr (2σ)
Azimuth	perfect fixes	.12/sec.	.36/sec.
	5 ft. (2σ)	.19/sec.	.57/sec.
	10 ft. (2σ)	.42/sec.	1.3/sec.
Elevation	perfect fixes	.94/sec.	2.8/sec.
	1 ft. (2σ)	2.1/sec.	6.3/sec.

The approach velocity used in the figures was the minimum velocity requirement of 90 knots. Increasing the approach velocity reduces the number of fixes between 14.82 Km (8 nm) and threshold required, but does not reduce the data (fix) rate

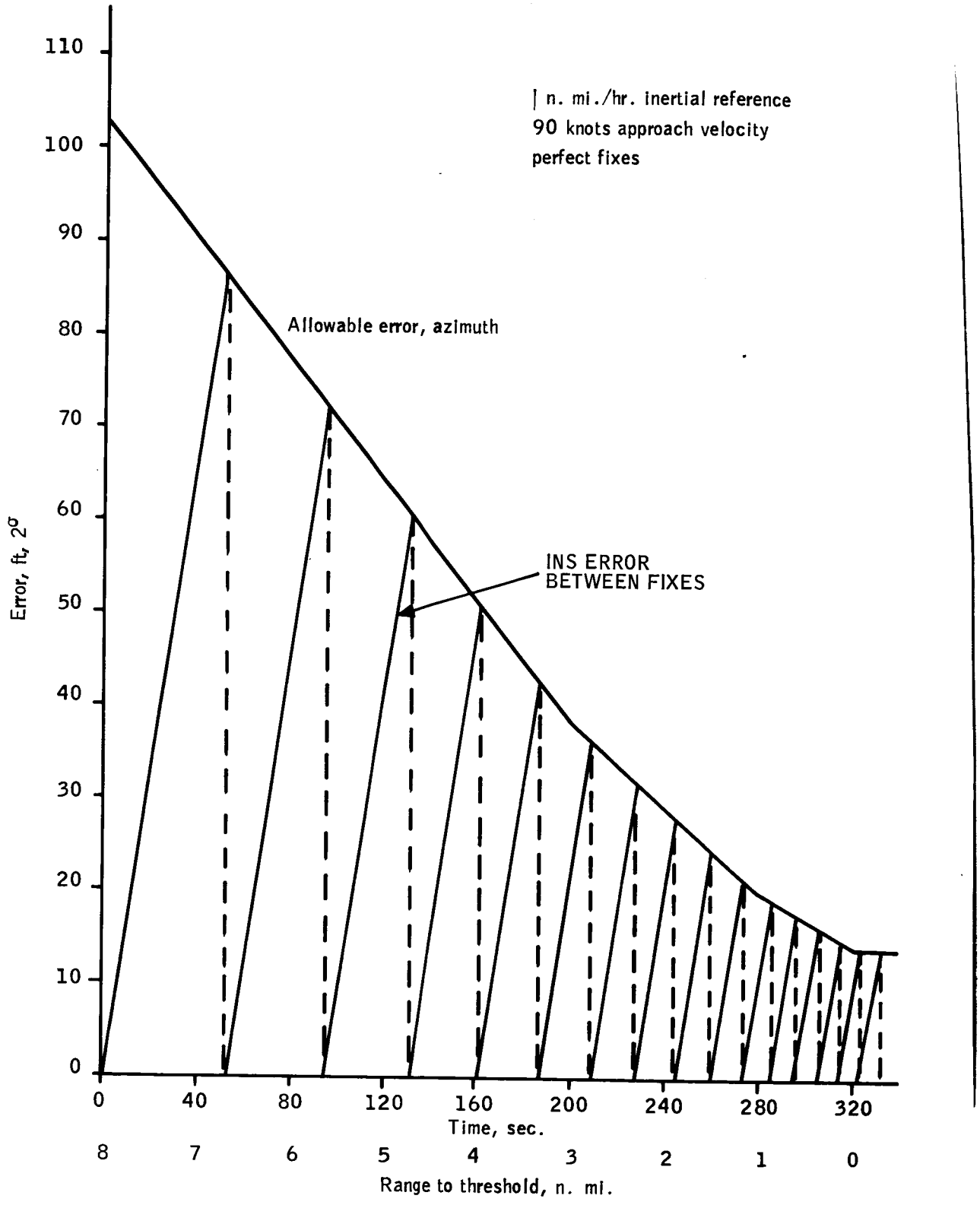

Figure 144 -- Azimuth Fix Inertial Requirements

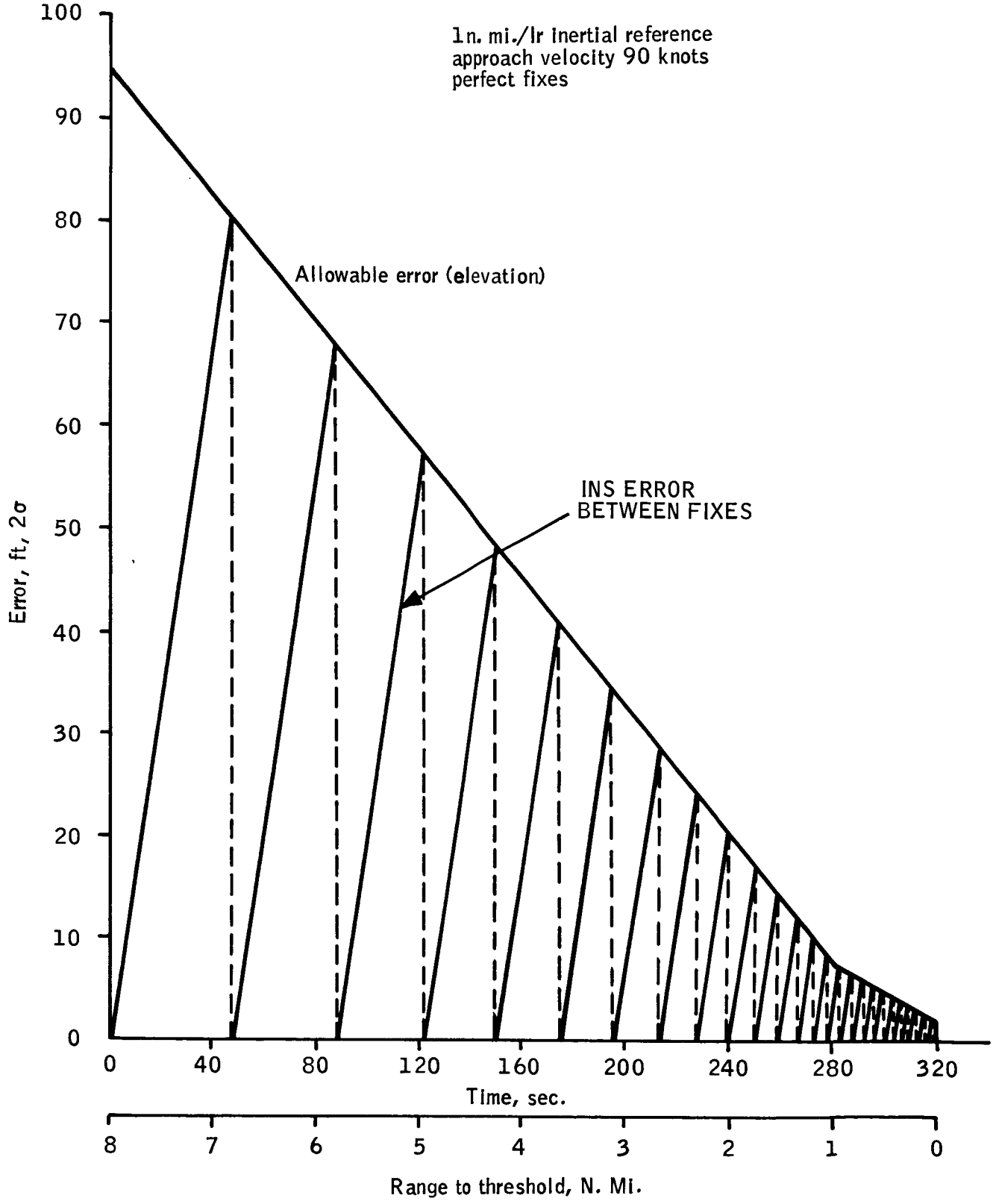

Figure 145 -- Azimuth Fix Inertial Requirements

required at or near the threshold. For sensor errors increasing with time, the slowest aircraft generate the most stringent requirements.

Combination of ILS and Inertial Reference

Automatic landing system designs for commercial transports to date have been based primarily on the utilization of the instrument landing system (ILS) to provide angular deviation data required for acquisition and tracking of the landing glide path. The ILS position accuracy capability results from a combination of bias errors and noise errors. Bias errors are invariant or slowly varying with time generating a relatively constant offset for a given approach. The noise errors occur at a higher frequency and are results of reflections from objects on the ground, noise due to atmospheric interference and other random errors which average to zero error over a period of time.

Combining an inertial system with the ILS guidance permits longer averaging times to significantly reduce the effects of noise errors in the ILS signals. It has no effect on the bias errors. An example of the potential improvement through integrating ILS/inertial is given in Figure 146, as reproduced from Reference 68. Item A shows the integrated sensor output improvement. Items B and C show the aircraft control system response improvements for lateral and vertical positions, respectively. The analysis of Reference 68 showed that the RMS value of path deviation arising from noise errors divided by the distance to the ILS antenna was reduced by a factor of 4.7 in the lateral direction and 3.2 in the vertical direction. The standard deviation of the lateral position was reduced by a factor of 2.25 and the vertical RMS error was divided by 3.14.

For any of the potential ILM sensors which are seriously degraded in accuracy

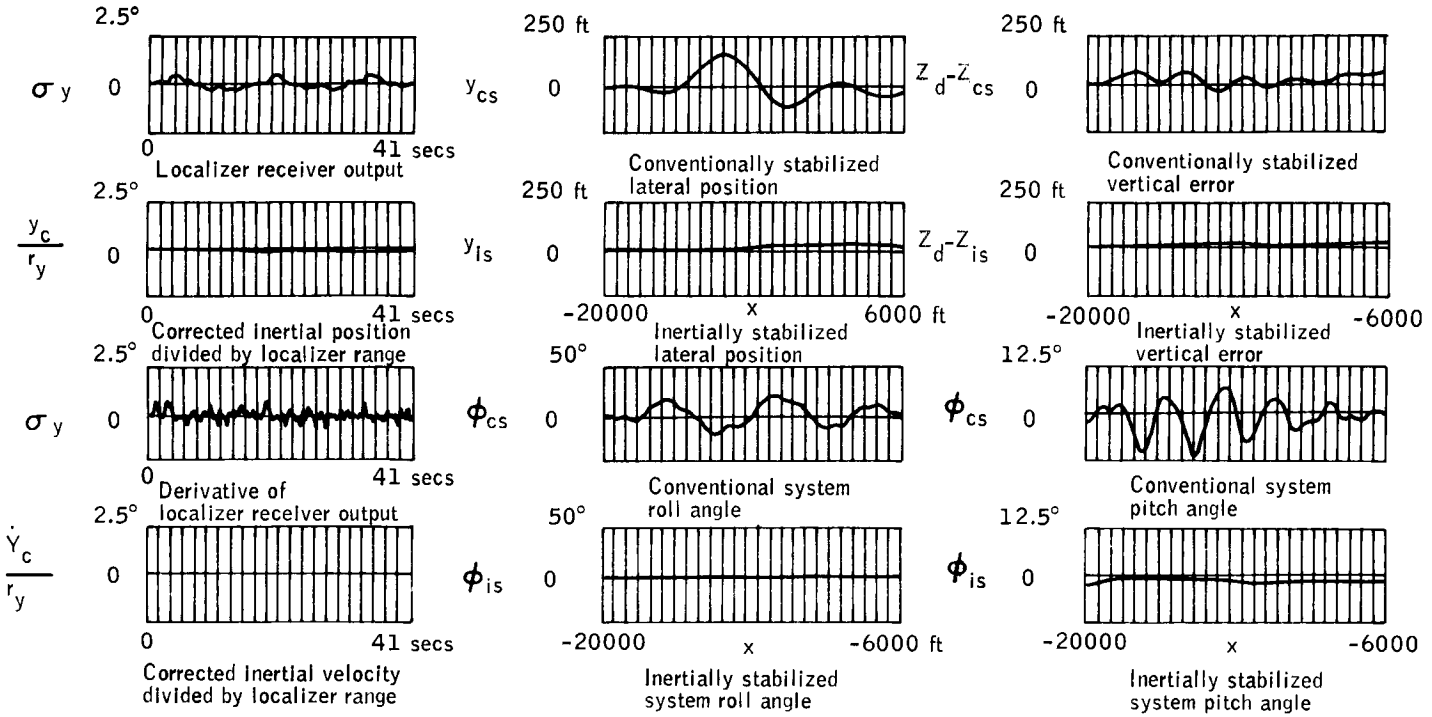

A. Typical localizer receiver and corresponding integrated ILS-inertial sensor outputs illustrating the reduction in noise achieved by sensor integration

B. Lateral position control system responses to localizer beam noise. Root scan square beam noise equal to .114 degrees

C. Vertical position control system responses to glideslope beam noise. Root mean square beam noise equal to .121 degrees

Figure 146 — ILS Inertial Integration Improvements

by high frequency noise, the same or similar improvements should be realizable with integration of an inertial system.

Section VI

SECTION VI
FEASIBLE ILM CONCEPTS

Following the sensor capabilities study, each ILM sensor concept was evaluated against the requirements of the four ILM configurations. Of the 20 sensor concepts evaluated, eight passed as feasible sensor systems for an ILM. Of those, four were selected for further study. These are:

- Imaging Radar
- Radar Triangulation
- Multilateration/Radar Altimetry
- Nuclear

These four feasible ILM sensor configurations are described in this subsection. The description includes concept functional diagram, equipment physical and electrical characteristics, equipment interfaces, and cost estimates. Where possible, variants of the basic ILM concept are discussed.

Redundant MLS and precision approach radar are feasible ILM systems, but to study these systems further was considered beyond the scope of this program. Since MLS development is continuing as the national and international standard for ATC, it was felt that this effort could add nothing to the refinement of MLS.

Precision approach radars have been in use for some time and further study of them was also considered beyond the intent of this program.

All three multilateration concepts were feasible sensor systems. The one selected for the refinement study appeared to be the most accurate and least complex system of the three.

IMAGING RADAR CONCEPT

The use of imaging radar as an Independent Landing Monitor (ILM) has been demonstrated by others during flight testing of prototype systems in moderate precipitation. The imaging radar can penetrate fog but it has visibility limitations under heavy rain and snow conditions. The imaging radar is not independent in the literal sense as its operation requires external altitude information, stabilization inputs, and some form of approach guidance to runway image acquisition at ranges of 1 to 5 kilometers in moderate (5 to 15 mm/hr) rain or (3-9 mm/hr) snow.

The imaging radar configuration is shown in block diagram form in Figure 147. This system has less resolution and accuracy than the baseline MLS configuration in an effort to lessen the cost and complexity required in a monopulse configuration. The specifics of the system are discussed in the following paragraphs.

Fan Beam Antenna

A phased array or slotted waveguide antenna is chosen to minimize spatial requirements in the nose radome. The antenna is envisioned as having a mechanical azimuth skewing capability for offset control (e.g. to compensate large crab angles) and electronic scanning for imaging. A fanbeam pattern is chosen to reduce huge scan rates that would be required for pencil beam systems. The slower scan rate allows reduced scan losses and the potential for precipitation clutter reduction due to decorrelation of the clutter return caused by wind shear. Circular polarization is also used for reduction of precipitation clutter returns.

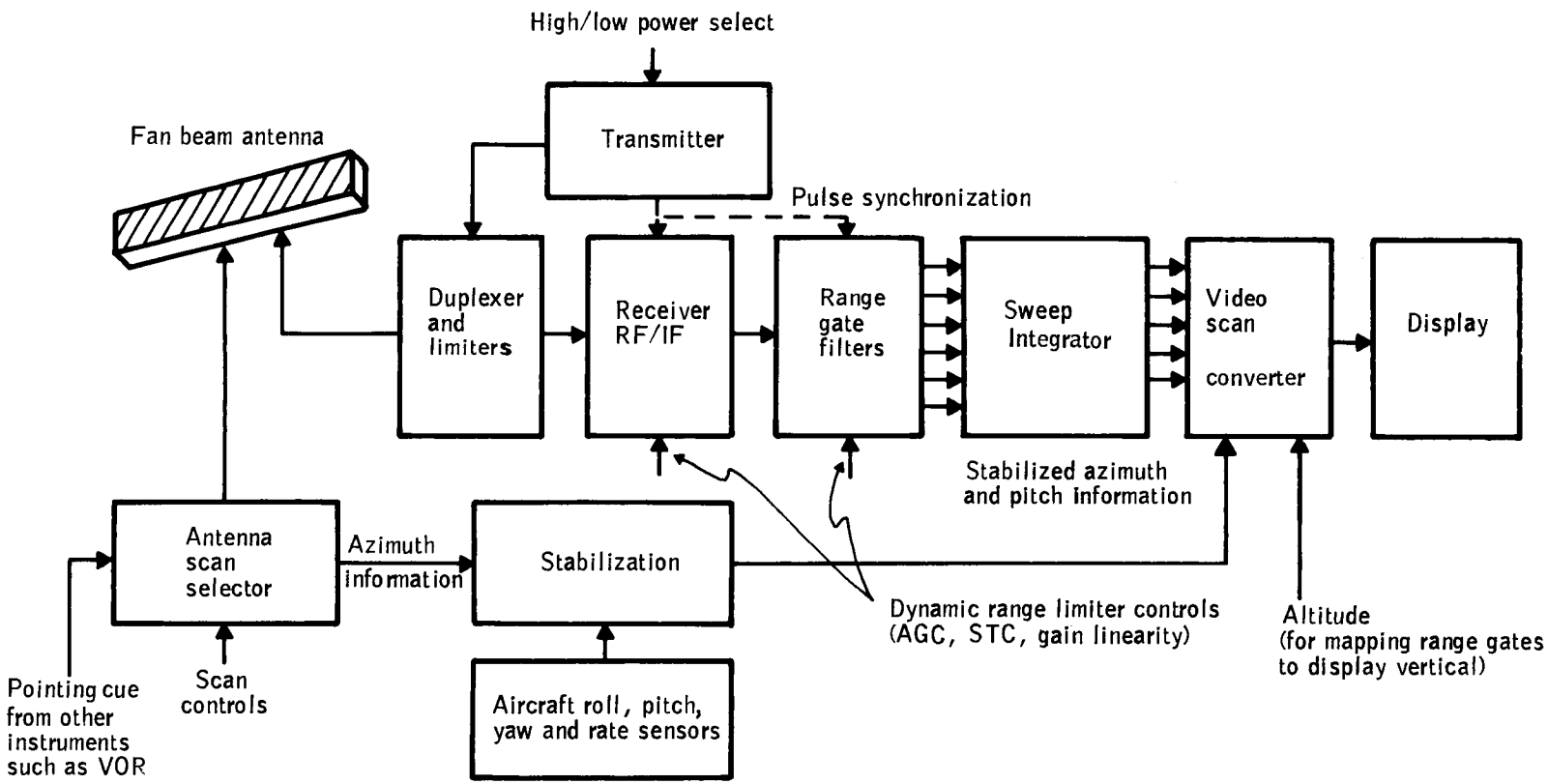

Figure 147 -- ILM Ranging Radar

Stabilization

The stabilization of the imagery will be a function of the required accuracy on the display. The system requirements for an ILM would be relaxed to .009 rad. (.5°) to .016 rad. (.9°), obtainable from the antenna resolutions. This would result in a slight decrease in the detection ranges.

Specified accuracy would require inertial system compensation. The relaxed accuracy requirements can be met with existing aircraft instrument sensors such as a Sperry C-12 gyro compass. (See System Interfaces below)

Transmitter

A K_a-band radar is proposed to eliminate the necessity for monopulse resolution improvement. The proposed transmitter should have a dual power (high/low) capability to minimize duplexer switching time for the shorter range visibility needed for touchdown and rollout imaging. The transmitter could be automatically switched to a lower power for low altitudes. Maximum powers of 65 to 80 kw peak for approximately 40 nanosecond pulse widths would be adequate.

PRF rates are not exactly predictable since return fluctuation rates were not predicted. It is expected that a value of approximately 15,000 pps used by Radar System R2 would be reasonable. Somewhat lower PRF should be acceptable for the proposed slower scan rate of approximately 2.5 Hz over a ±10° sector. Mechanical slewing would be engaged on command from a guidance system such as ILS, MLS or manual. The angular scan rate of approximately 100°/sec provides approximately 4 to 6 msecs to scan a beamwidth and 60 to 90 pulse returns for smoothing fluctuating signals. Although 4 to 6 msec is longer than the predicted correlation time for runway surroundings, correlation times of that order have been observed

(Reference 21). A staggered pulse repetition interval (PRI) is recommended to minimize ambiguous range imaging and mutual ILM interference.

Receiver and Display

The receiver and display subsystem is essentially identical to the existing subsystems of Radars R1 and R2 (see Section V). The operation of the ILM will require receiver tuning as the runway is approached using the dynamic range limiter controls (scan rate control would also be advisable) to optimize the image in adverse weather conditions. This manual control, although undesirable, is necessary until more knowledge is gained on low angle backscattering cross-sections. The controls provide contrast enhancement by nonlinear gain compression and limiting. Variable scan could be used to optimize the signal return correlation characteristics.

Range gate filters are used to subdivide the time domain echo return into range bins based on the dependency of range to target and time delay of the echo. The returns in each range bin are summed by the synchronized sweep integrator. A video scan converter is included to convert the radar range/azimuth output format to azimuth/elevation format for perspective display to the pilot.

System Interfaces

The altitude input for display mapping of range bin to vertical display dimension would be a limiting factor to elevation steering accuracy in that the perspective display may be limited by large altitude variations at low altitudes over uneven terrain. Smoothing of altitude values would have the undesirable effect of lagging the true perspective on the display. Baro altimeter inputs (±20 ft.) at the extended ranges over uneven terrain with a switch to radar

altitude inputs (±2 ft.) below altitudes of 100 ft. in the approach to touchdown may provide adequate accuracy.

The stabilization signal input precision is also a factor in the selection of the system accuracy. Stabilization inputs from gyro instruments are available on most commercial aircraft for roll, pitch, and yaw indications that are adequate for the lower resolution of this potential ILM system. The availability of inertial platforms on larger aircraft such as the Boeing 747 or C-5 would provide more accurate stabilization. ILM requirements, however, would not justify the additional expense of an inertial platform. Typical gyroscopic instruments have synchro errors of the order of 0.25° to 0.75° errors with the higher values resulting from vibrations of .015 g's and 20 to 2,000 cps rates. Inertial platforms, on the other hand, can achieve accuracies of .1° or better (synchro errors) and are typically located for minimum vibration effects. The tracking responses of these systems are sufficiently high (60°/sec) that the ability to follow angular deviations for large aircraft are essentially unlimited. The compensation of the electronics (display stabilization) is thus limited by the synchro accuracy which is a form of quantization accuracy.

The airborne system does not require ground-based electronics although passive reflectors could be used at airports with low runway-to-surroundings contrast to enhance runway outline. Enhancement such as this would be necessary where contrast conditions have been severely degraded by local conditions, such as accumulated snow.

Concept Physical Parameters

The approximate physical parameters of a K_a-band ILM imaging radar are provided

in Table 62. The values are approximate, projected from similar existing systems. The cost values shown are estimated production prices. Installation costs are not included in the estimated prices.

Mutual Interference

Interference between airborne radar equipment, all operating in the same frequency band, could be a major problem in the high density traffic situation. The use of randomly staggered pulse repetition intervals (PRI)'s at the average PRF rate is expected to minimize the interference from other similar ILM's. This procedure also has the additional benefit of minimizing false returns from ambiguous ranges (second-time-around signals). This staggered PRI technique is required due to the low backscattering cross-section of typical runways and smooth terrain.

Table 62 -- Imaging Radar System Physical Parameter Estimates

Component	Size	Weight	Power	Cost
Receiver	45,000 cm^3	10 kg		$10K
Transmitter	45,000 cm^3	25 kg		$24K
Antenna	37,500 cm^3	10 kg		$12K
Hardware, Controls, and Power Supplies	80,000 cm^3	20 kg	1,2 KVA ac, 100 watts dc	$ 8K
Display (6" DVST)	53,000 cm^3	10 kg		$ 8K
TOTAL	260,800 cm^3	75 kg	1.2 KVA ac, 100 watts dc	$62K

Operational procedures, which permit maximum power transmission only during final approach and reduced power transmission for taxiing, take-offs, etc., should be helpful and may be required to minimize interference.

RADAR TRIANGULATION (BEACON OR TRANSPONDER RADAR)

The previously described imaging radar has a weather limitation due to precipitation-induced signal attenuation and clutter levels masking terrain and obstacle returns. The proposed triangulation transponder concept alleviates this problem by retransmitting the signal after frequency translation to eliminate precipitation backscatter effects and, by suitable amplification, to overcome attenuation effects. This application has two principal limitations.

- o The system does not have runway imaging capability since the only information returned are the translator signals for triangulation.
- o Obstacle detection is negated by the frequency translation.

Since detection is made on an amplified, translated return, the detection ranges can be extended almost arbitrarily up to the limits of the S/N at the translator receiver. External stabilization guidance signals similar to that discussed for the imaging radar are still required. The altitude information would not be required if vertically resolving beams and three translators were used. These are feasible under this configuration (assuming suitable radome space available) since a smaller number of targets are available and the excessive scan rates previously described would not be necessary for the limited number (3) of targets. An alternate configuration could use only two translators for azimuth deviations with vertical guidance provided by an external radar altimeter as with the imaging radar concept.

The system capabilities become a function of translator cost tradeoffs for power versus range versus mutual system interference (other ILM systems) and saturation. A detailed tradeoff study was beyond the scope of this project.

This potential ILM, which is an extension of the previously described ILM, will indicate the additional costs involved in this more sophisticated application. The system provides resolutions and accuracies comparable to the imaging radar. Detection is extended to 10 Km and beyond with negligible adverse weather limitations other than S/N limiting at the translator receiver. If the ratio is too low, the ILM could be effectively noise jammed by the translator.

System Description

This system uses the basic K_a-band radar described for the imaging radar. The extension to Ku or X-band would be possible at approximately the same cost. The basic radar systems for X or Ku-band would be cheaper but additional sophistication for monopulsed antennas and parallel receiver channels would tend to equalize the cost. Figure 148 is a representation of the system and demonstrates the similarity of the two concepts for an ILM.

The triangulation concept uses staggered PRI and range gating to minimize interfering signals. It then compares the range gated returns for azimuth deviation information. Figure 149 shows a transponder layout for a typical runway. By staggering the transponders as shown, angular ambiguities are removed to beyond the coarse angular guidance limits provided by the primary guidance system. Return signal comparisons are made on gated signals and not "gates". The smoothed angular accuracies should, therefore, be similar to the smoothed imaging system.

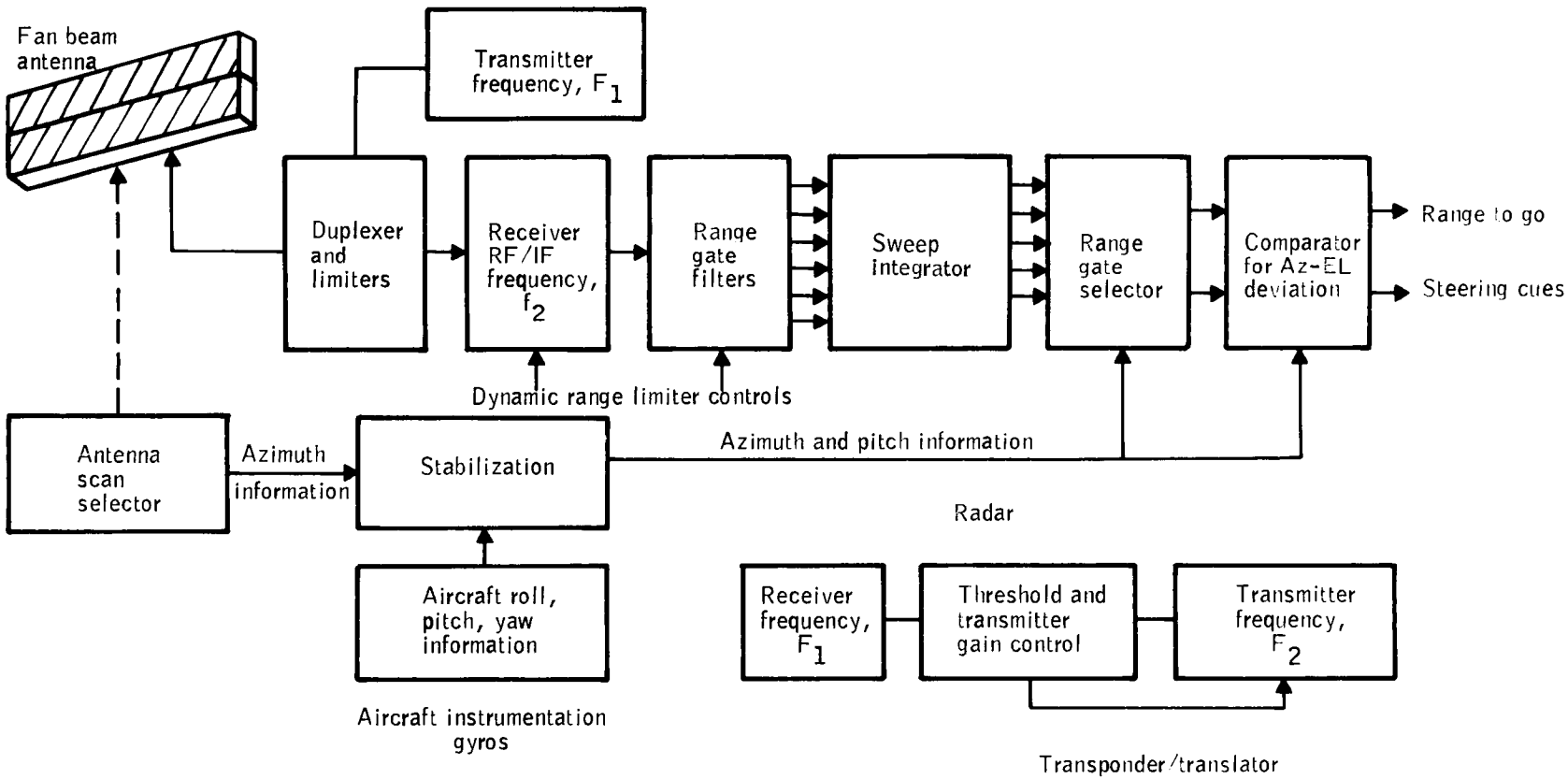

Figure 148 -- ILM Triangulation Radar

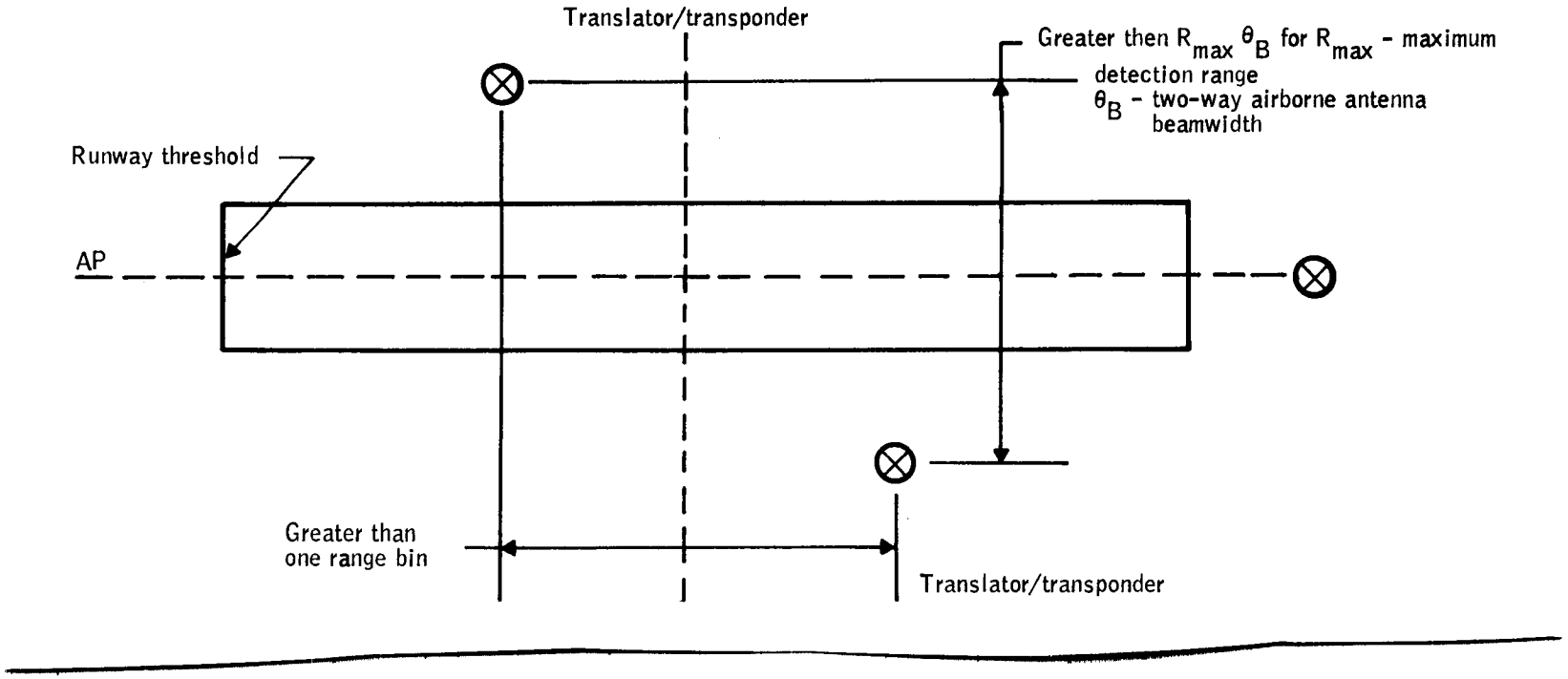

Figure 149 -- Transponder Layout at Runway

However, a quantitative comparison of "real-world perspective" and time-of-arrival signals was not attempted under this study.

An X-band version of this concept was developed and flight tested by Thomson-CSF (Reference 25). Guidance accuracies equivalent to ILS were demonstrated. Use of X-band has the advantage of more immunity to weather variations and can more suitably be used as a dual mode weather/landing aide radar.

System Physical Parameters

The approximate parameters for a K_a-band triangulation system for an ILM are provided in Table 63. The costs are approximate production quantity values for the previous imaging system modified to incorporate frequency translation to achieve precipitation clutter reduction. Installation costs are not included in the estimate.

Mutual Interference

As mentioned under the imaging radar concept, interference generated by radar equipment aboard the various aircraft operating in a terminal area could be a considerable problem since this equipment will be operating in the same frequency band. Mutual interference will be minimized by the range gating, sweep integration, and staggered PRI's. Additionally, the transponder receiver will contain an adaptive threshold to limit the duty cycle of the transponder and to provide gain control on the transmitter.

Table 63 -- Triangulation Radar System

Airborne Physical Parameter Estimates

Component	Size	Weight	Power	Cost
Receiver	45,000 cm^3	15 kg		$15K
Transmitter	45,000 cm^3	22 kg		$20K
Antenna	75,000 cm^3	20 kg		$22K
Computer	25,000 cm^3	5 kg		$10K
Hardware Controls and Power Supplies	80,000 cm^3	25 kg	1.2 KVA ac, 150 watts dc	$10K
TOTAL	270,000 cm^3	87 kg	1.2 KVA ac, 150 watts dc	$77K

Ground-Based Transponder/Translator (3 required)

Component	Size	Weight	Power	Cost
Receiver	45,000 cm^3	10 kg		$ 5K
Transmitter	45,000 cm^3	25 kg		$ 5K
Antenna	60,000 cm^3	15 kg		$ 3K
Hardware, Controls, Power Supplies	100,000 cm^3	30 kg	1 KVA ac, 200 watts dc	$12K
TOTAL	250,000 cm^3 each	80 kg each	1 KVA ac, 200 watts dc each	$25K each

Operating procedures designed to reduce interference problems may be required. These procedures should permit variations in power transmission from the radar equipment dependent upon operational need. Maximum power transmission should be used only during a critical phase such as final approach. Reduced transmission levels should be used during taxi and take-off.

GROUND CONTROLLED MULTILATERATION

Description of Concept

A ground-based multilateration ILM system measures several transmission signal transit times in order to determine the range from ground stations to the aircraft. The transit times are:

- from a command station-to-aircraft-to-command station
- command-remote station No. 1 - aircraft-command
- command-remote station No. 2 - aircraft-command
- command-remote station No. n - aircraft-command

The range from the command site to each remote station is used in the calculations for range to the aircraft from each station. Each target range defines the radius of a spherical surface on which is located the aircraft. Solving for the intersection of the three or more spheres defines the aircraft's position in space.

If the aircraft is at high altitude and/or close to a site, the multilateration techniques provide adequate altitude information. At lower aspect angles, an additional altitude input must be provided in order to minimize the error involved using multilateration only.

Aircraft position is referenced to the approach path localizer and glideslope in order to generate steering commands for a display. These commands are transmitted to the aircraft via the transponder at the command station.

Enhancement of the altitude component of the aircraft's position vector can be provided by airborne equipment or additional ground installations. The airborne equipment will consist of an accurate radar altimeter to measure the aircraft's position above the terrain. Barometric altimeters would be better from an operation's point-of-view but do not have the accuracy required by ILM.

In order to implement the radar altimeter as part of the multilateration complex, a complete terrain map must be stored in the computer at the command station for referencing the altitude measurements to the active runway. For a large air terminal, this will mean a map of terrain under the pre-established approach paths to the runways serviced by MLS. Figure 150 shows a block diagram of this concept. For each horizontal position calculated by the multilateration system, there will be assigned an elevation of that position relative to the runway. Upon receipt of the altitude of the aircraft above the terrain, its altitude relative to the runway will be calculated, referenced to the glideslope, and the resulting difference transmitted to the aircraft for display to the pilot.

A measurement of elevation angles from the GPIP to the aircraft could also be used for computing altitude rather than measuring it as described above. To implement this concept would mean an additional MLS elevation antenna as part of the multilateration system. If complete independence from the MLS is not essential, one of the two MLS elevation angle measuring subsystems could be interfaced with the ILM. See Figure 151.

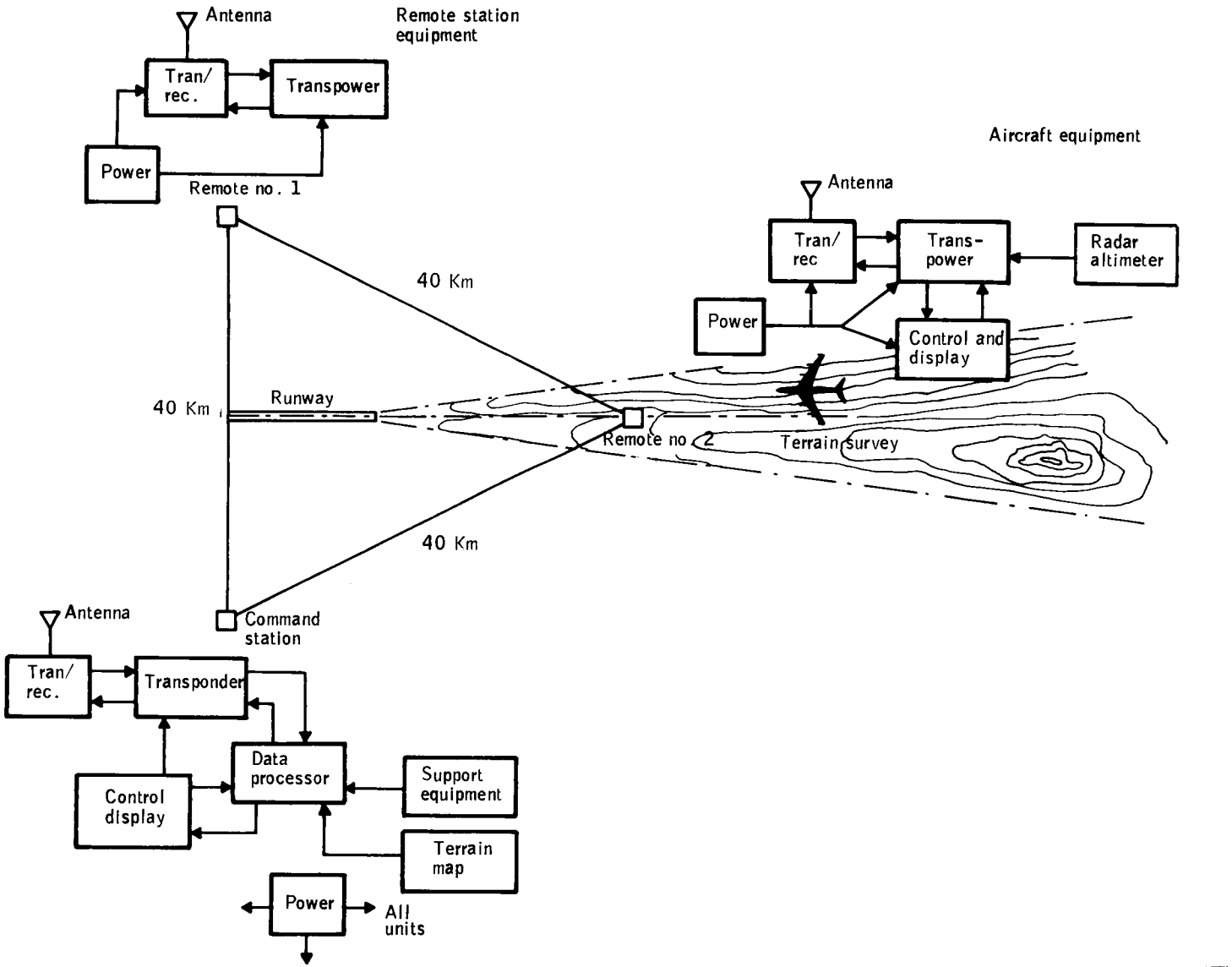

Figure 150 -- Block Diagram for Radar Altimeter Concept

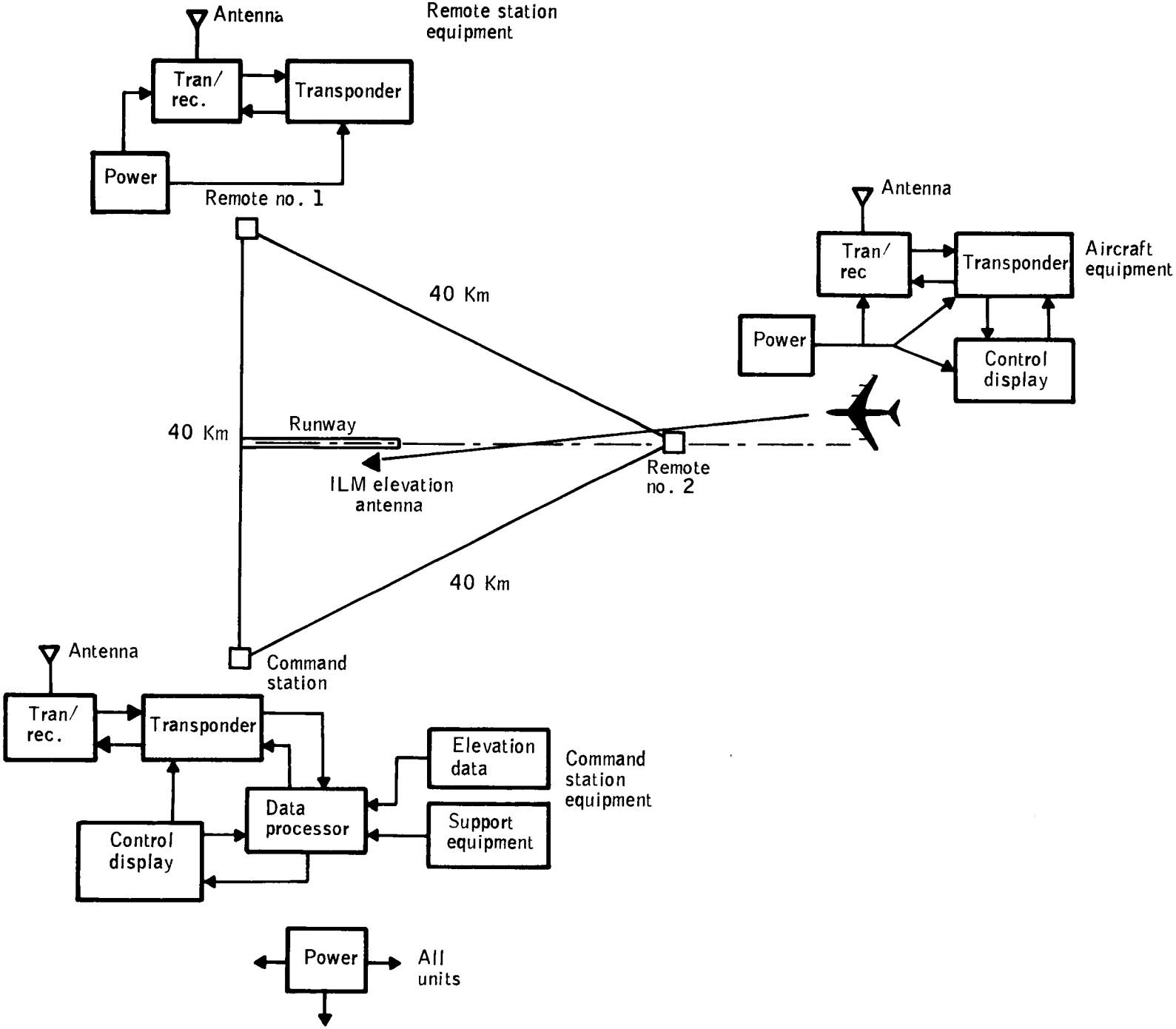

Figure 151 -- Block Diagram of MLS Elevation Antenna System

A ground-based multilateration ILM system, with altitude aiding, consists of three primary equipment complements:

- Command Station Equipment
- Remote Station Equipment
- Aircraft Equipment

The command station provides computations, control, data recording, transmission encoding/decoding, and displays as required for system operating and monitoring.

The remote station responds to interrogation from the command station or from the aircraft, depending on how the system is implemented. In one case, the remote station receives a signal from the command station, responds with a DME pulse to the aircraft, which in turn responds to the command station. Range between stations and the aircraft is determined by measuring signal transit times and knowing the range between command and remote stations.

The system could be implemented in another manner providing the same data. The command station will transmit a pulse to the aircraft and the remote station simultaneously. The remote stations will respond to the command station after receiving a response pulse from the aircraft.

The aircraft encoder/decoder receives the ground station DME signals and responds. It also decodes digital commands for display, and encodes altitude data for transmission to the command station. The radar altimeter measures the aircraft altitude above the terrain which must be combined with terrain elevation, at the aircraft's present position, relative to the runway.

The digital processor at the command station will vary with the multilateration system concept to be implemented. If the processor is to store terrain elevation, considerable memory capacity is visualized. A Kalman filter, to be mechanized for smoothing noisy measurements and generating accurate predictions of future aircraft position, requires a high-speed machine.

Ground support equipment for the computer at the command station consists of computer peripheral devices which allow program loading, verification of operation (simulation), and testing.

The multilateration stations will be installed with about 20 nm between antennas. The arrangement will configure the runway normal to the baseline between two stations. One of these two will probably be the command station. Another station may be located at the outer marker on the approach path.

All stations must maintain line-of-sight (LOS) to each other and to the target aircraft. This requirement may call for the installation of towers on which to mount the antennas.

The delay time between a station (or the aircraft) receiving an interrogation pulse and transmitting a reply must be known precisely. This data will be stored in the computer at the command station for computation of the aircraft's range from the various stations in the complex.

The accuracy of the ground-controlled multilateration ILM system is well within the requirements except for altitude. At present, it is questionable if the MLS altitude accuracy requirement at the threshold can be met by the ILM using an independent altitude measuring source aboard the aircraft. The other altitude

check point (1 nm and 3 nm) accuracies are acceptable assuming that a survey of the terrain is made as accurately as can be conducted with today's electro-transits. The chief altitude errors will come from the altimeter.

One of the radar altimeters on the market today will measure altitude to an accuracy of ± 2 ft. or 2% of altitude if the altimeter can be installed in a temperature-controlled area of an aircraft. If not, the accuracy is ± 3 ft. or 3% of altitude. These values show that altitude will be measured to within the accuracies shown below. These accuracies were calculated at three points along a 3° glideslope and compared to the MLS elevation accuracy (expressed in feet of altitude).

	Error in Feet		
Check Point	± (3 Ft. or 3%)	± (2 Ft. or 2%)	MLS Reqmt.
3 nm (1014' Alt.)	30	20.3	33
1 nm (377' Alt.)	11.3	7.5	11.8
Threshold (58' Alt.)	3	2	1.8

Note that altitude accuracy is a function of altitude and not range from touch-down. If the glideslope is greater than 3°, the accuracy may not be within the MLS standards.

The use of an MLS elevation subsystem as part of the multilateration ILM will provide the same accuracy in altitude as is presently defined for the MLS. This part of the ILM will function together with the existing MLS elevation subsystems but will feed data into the ILM only; it will not be used by the MLS.

The proposed multilateration system consists of ATCRBS transponders at each station and each aircraft modified to:

- Perform bias compensation
- Use adaptive threshold detection
- Reply only to addressed interrogations
- Receive course deviation and range data from the ground
- Drive Analog displays
- Transmit externally-derived altitude data.

It is assumed that some sort of display already exists for aircraft position data. As an example, airport surveillance radar displays could have a symbol added for multilateration data. This symbol would then overlay the radar symbol when both are tracking the aircraft. There is no necessity to present this information to the controller for the system to operate, since system operation (except for address assignment) is totally automatic. Address assignment can be the same assignment as the ATCRBS or DABS beacon assignment.

Physical Description

All of the modifications to ATCRBS, except adaptive threshold detection, consist of adding digital logic to a transponder. Adaptive threshold detection is a trivial cost addition (less than $50) and will not be considered. The required logic is shown in Figure 152. It is assumed that multiple pulse position modulation characters will be used on the link with no attempt to maximize information transfer. Estimates for the number of integrated circuit packages, assuming TTL, MSI, and SSI technology are:

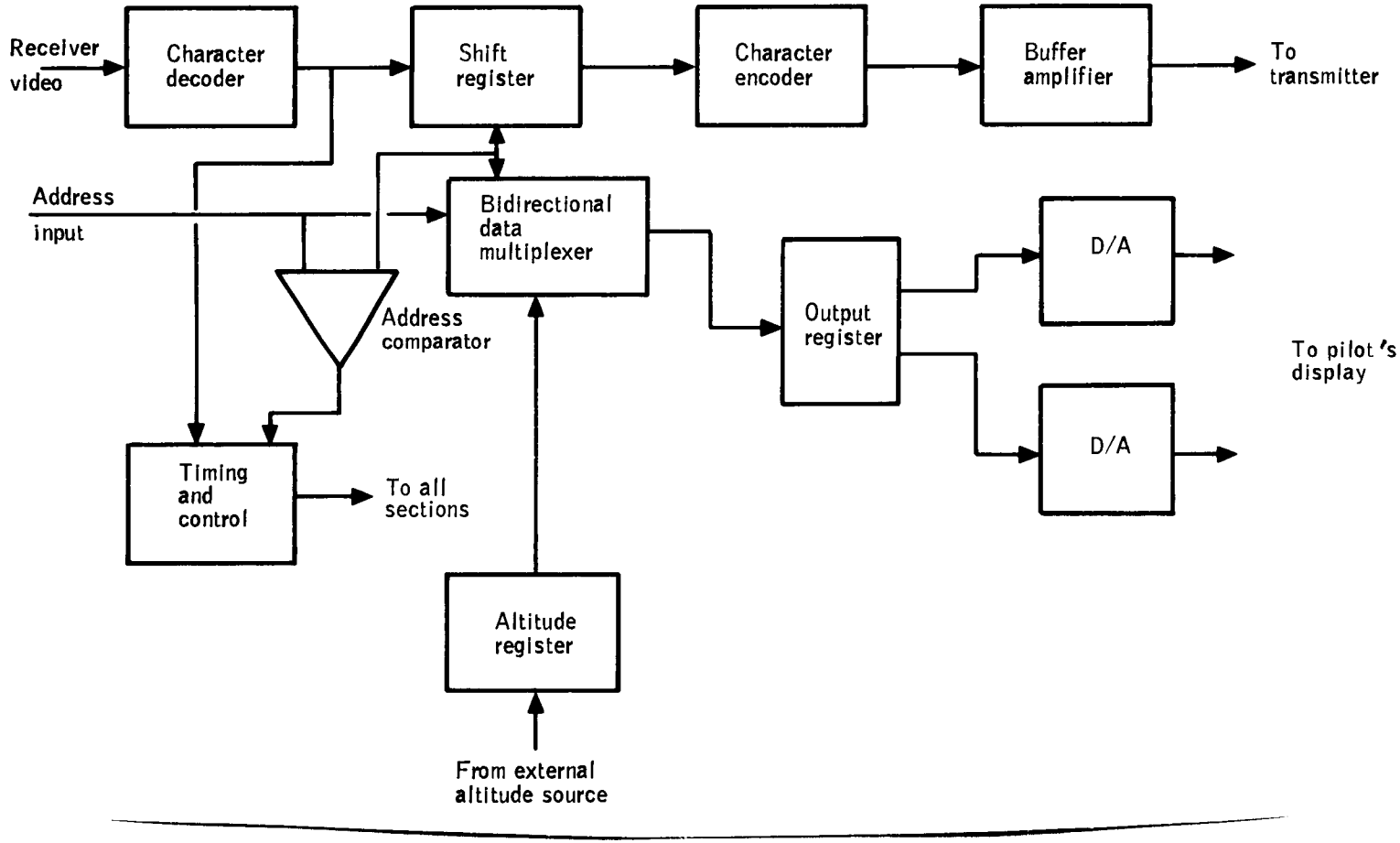

Figure 152 -- Multilateration Transponder Logic Block Diagram

Character decoder	14
Data Shifter	4
Character encoder	4
Buffer/driver amplifier	2
Multiplexer	8
Output Register	2
Altitude Register	2
Address Comparator	1
Control and Timing	19
TOTAL:	60

Also required are packaging, power supplies, a clock oscillator, A/D converters, etc.

For an airline quality unit the cost for transponder modifications becomes:

Logic Circuits	$300
A/D Converters	50
Clock Oscillator	70
Power Supplies	350
Packaging and Cooling	60
Assembly	60
Total Parts:	890
Production Engineering Support:	890
Total Cost:	$1780

Total selling price for this cost is estimated at $2400 for the modification.

For general aviation, commercial grade circuits would be substituted, etc., resulting in the following estimate:

Logic Circuits	$ 60
A/D Converters	50
Clock Oscillator	10
Power Supplies	150
Packaging	25
Assembly	30
Total Parts:	325
Production Engineering:	325
Total Cost:	$ 650

Total price will be about $880 for transponder modification.

To obtain the total system cost, appropriate quality antennas and basic transponder costs must be added. The total airborne station cost is:

	Airline	General Aviation
Transponder	$5000 (Collins)	$595 (Genave, Narco, etc.)
Antenna	30 (blade)	15 (stub)
Additional Logic	2400	880
Total:	$7430	$1490

Ground slave stations are identical to an airborne station, and, therefore, would have the same cost. A minimum of two are required.

The master ground station requires a computer. High-speed computers based on minicomputer technology are available for about $60K, and are capable of performing the function. To obtain satisfactory reliability, a standby redundant

computer should be provided. In addition, logic for initiating data link integrations, counting time until reply, etc., and for interface to ground displays is required. This approximately doubles the complexity of the master station interface logic. The master station cost is:

Logic	$ 5K
Computers	120K
Transponder	5K
Installation dependent software	50K
Antenna (blade) and Mast	2K
	$180K

The software cost is for programming in slave station locations, ground terrain maps, etc. A complete ground system would cost about $200K from these figures.

Size and Weight

Allowing 1.2 square inches/integrated circuit would yield a total circuit board area of 72 sq. in., or two 6 inch square circuit boards. This is relatively sparse packing which could be achieved without the use of multilayer boards. With 1/2" spacing between boards and two 36 cu. in. power supplies, the total volume of the additional logic is 108 cu. in. The weight of the logic is dominated by the power supplies and the package, and would be approximately 6 lbs.

The Collins 621A6 transponder occupies a 3/8 short ATR case (approximately 250 cu. in.) and weighs 14 lbs. Lower performance transponders are smaller and lighter.

The total airborne system would occupy about 360 cu. in. and weigh 20 lbs. Size and weight of the ground system are not significant for a ground installation. Each computer system would occupy about one 72" relay rack, with a third rack for the transponder and additional logic in a sparse layout.

The specified antenna for both the ground and airborne systems is a blade antenna. At L-band, a blade antenna requires about 2cm x 6cm x 6cm. The ground system installations will also require a 1m square ground plane.

Power Requirements

The power requirements for the airborne equipment are:

	Airline	General Aviation
Logic	30w, 115v 400Hz 1Ø	30w, 28VDC
Transponder	54w, 115v 400Hz 1Ø	54w, 28VDC
Total:	84w, 115v 400Hz 1Ø	84w, 28VDC

Frequency Allocation

The system was assumed to operate at L-band such that weather could be ignored, and relatively inexpensive mature technology could be used. Two possible bands offer frequency allocations for a pulsed, airborne radio system. One, at 1.3 to 1.35 GHz is relatively unused at this time. It's second harmonic falls in a radio astronomy band, which might cause reservations in allocating it to a high density pulse system. The other possible band is the collision avoidance band at 1.54 to 1.66 GHz.

If the system were made compatible with the ATCRBS or DABS, it would be allocated 1.03 GHz.

Data Link Protocol

On each transmission, there is a very small amount of data to be transferred. The required transfer on a master to aircraft communication is course deviation and range to go on the uplink, and altitude on the downlink. No other communication requires data transfer except for command and status data to maintain protocol. In order for the data to be meaningful and useful, the link must have a high signal to noise ratio. Therefore, the appropriate modulation is the simplest possible modulation, without regard to information rate or correlation properties.

Since the ranging data is pulse, the obvious choice for data link modulation is pulse position modulation. To simplify the detection/decoding scheme, multiple characters should be used, several of them reserved for use as comma characters. As a specific example, one character might represent the start of an interrogation; another, a range reply; and a third, a calibration reply.

The problem in multilateration is not data rate, detectability, or modulation type, but is the prevention of synchronous garble. Synchronous garble occurs when multiple interrogations or replies arrive at a receiver which needs one or more of those messages at the same time. Since the receiver has no way to separate the messages, it will probably lose the one it needs due to the combination of multiple overlapping messages.

A ground-controlled multilateration system can establish a protocol such that only one message at a time exists by simply making one interrogation at a time, and waiting for the reply before making another interrogation. This protocol absolutely prevents garble, but makes inefficient use of time. If the number of aircraft becomes large, the maximum sample rate decreases resulting in decreased

accuracy from insufficient position filtering. For example, if the system is set up to handle aircraft with a maximum range of 100 Km from the furthest station, the simple protocol would have (500/number of aircraft) samples per second.

Many other protocols are possible to increase the traffic handling capability of the system, such as interrogating an aircraft at long range, then immediately interrogating one at short range. The reply from the short-range aircraft would return before the reply from the long-range aircraft, and two ranges have been taken in the time formerly used for one.

Various other conditions such as line of sight between all the ground stations allow certain efficiencies in data link utilization. Under certain conditions, a small amount of garble may be desirable if it allows an interrogation rate which provides samples more often on the average.

Complex patterns of multiple interrogations can be used if it is computed that this particular pattern will not cause garble. Since the position of all stations is known, this computation can be made.

A general solution to saturation in a multilateration system is far too complex to be attempted here, and is too dependent on specific installation and aircraft distribution to provide meaningful results. However, it can be seen that applying a protocol of sufficient complexity would allow greater than 10 samples per second for several hundred aircraft if a fast enough computer could be employed.

NUCLEAR ILM CONCEPT

Description of Concept

Nuclear instrument landing systems for aircraft have been demonstrated as both safe and feasible in a number of flight test and analyses programs. These programs and their applicability to the ILM problem are discussed in Section V of this report.

Each of the systems identified in Section V have some features desirable to ILM and some features which are not desirable. In this section, we will describe a system concept using features from each of the configurations which potentially can meet ILM requirements at short ranges.

The concept described here is primarily the NILS system developed by TRW as described in Reference 40, with additional variants to provide guidance through rollout and to provide runway range indications. This concept should be able to meet ILM basic and Case I requirements from the middle marker to the stop end of the runway.

The operating principles of the nuclear instrument landing system are similar to those of standard ILS configurations. Instead of radio antennas, four nuclear radiation beams modulated at different frequencies are used; two for the localizer beam, and two for the glideslope beam.

The approximate siting configuration for this concept is as shown in Figure 153. A total of 6 beacons are used; two uprange beacons, two downrange beacons, and two rollout beacons. The uprange beacons provide both glideslope and localizer information from middle marker to the glide path intercept point on the runway.

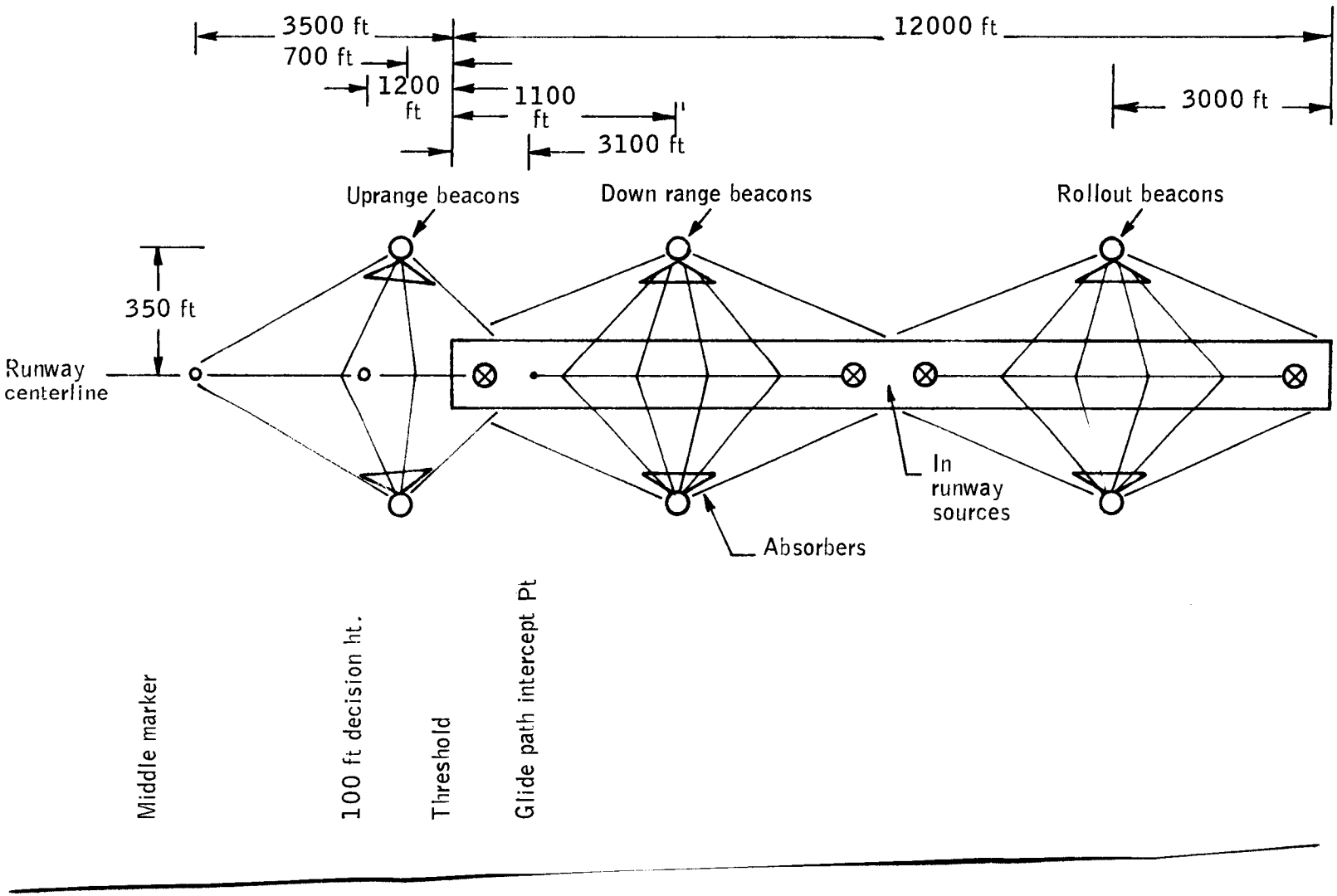

Figure 153 -- Nuclear ILM Siting Configuration

The downrange and rollout beacons provide localizer and range to go information after touchdown on the runway. Four additional runway sources are shown in the figure to provide additional range check points. Range check points are provided every thousand feet along the runway.

The NILS beacons can be used as configured in Reference 40. Cobalt 60 radioactive sources are used. The shutter configuration for the beacons is as shown in Figure 154 and the formation of the guidance beams is as shown in Figure 155. Beacons on the left side of the runway emit overlapping beams of radiations that are modulated at 60 and 90 hertz. The beacons on the right of the runway produce overlapping beams modulated at 24 and 36 hertz.

When the aircraft is on course, it receives equal amplitudes of all four frequencies. Above the glideslope path, the 60 and 25 hertz signals are greater in amplitude than the 90 and 36 hertz signals. When the craft is on the glide path and off to the right, it receives more of the 24 and 36 hertz than the 90 and 60 hertz signals. Position of the aircraft relative to the beam slope and runway centerline is then computed by comparison of the strengths of the four signals.

The NILS uses absorbers with each beacon to provide approximately uniform amplitude signals as the aircraft progresses between the beacons. In this concept, only angular information with no range is derived. To provide course range along runway marks to the landing aircraft, slits could be cut in the absorbers to provide larger amplitude signals at fixed points along the runway as the aircraft proceeds. These could be detected on the aircraft superimposed on the normal localizer/glideslope signals. At longer ranges from the beacon, the absorber is not used. Thus, we have shown in Figure 147 a total of four in-runway sources

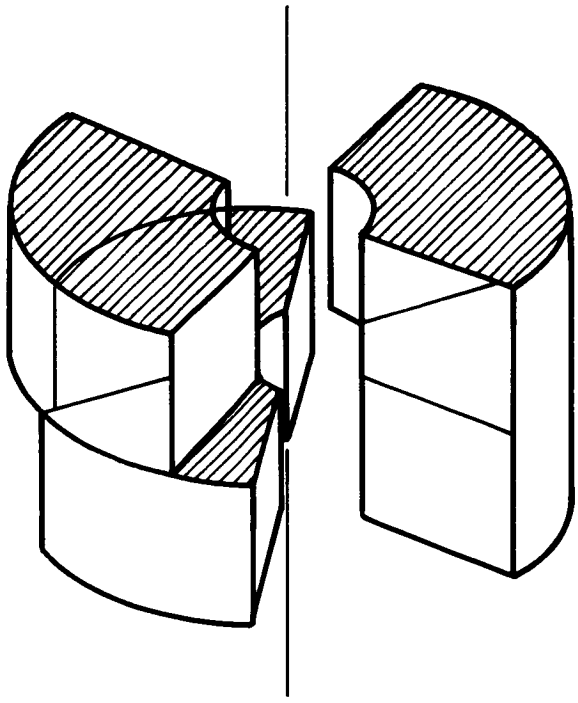

Figure 154 -- NILS Shutter

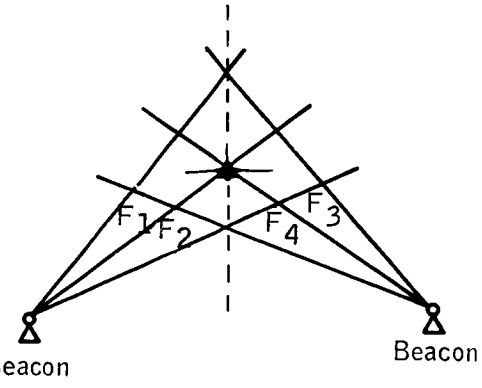

Altitude deviation = $F_1 + F_3 - (F_2 + F_4)$

Cross-range deviation = $F_1 + F_2 - (F_3 + F_4)$

Figure 155 -- Formation of Guidance Beams

similar to those described in Reference 41 as used in flight tests by NASA-AMES. As the aircraft passes over the sources, a higher amplitude radiation signal would be detected.

The airborne detectors are very simple, low-cost configurations. The radiation detector consists of a scintillator and a photomultiplier tube. When gamma rays strike the scintillator, tiny flashes of light are produced with the intensity of flashes proportional to the radiation energy. The flashes are detected by the photomultiplier to produce electrical signals. The glideslope/localizer deviation signals can be processed and displayed on flight directors or ILS indicators. The range mark can be detected and counted to generate a digital range to go indication.

A block diagram of the ground and airborne system is given in Figure 156. The gamma ray emission from the cobalt 60 sources consists of random pulses with rates on the order of 5000 to 10,000 photons per second. The beacon design utilizes a rotating shutter array to modulate these beams at frequencies of 24, 36, 60 and 90 hertz. The photo-multiplier output on the aircraft feeds 4 filters tuned to these frequencies. The outputs of the filters can be amplitude compared to derive deviations from the glideslope or localizer beams.

Several possible variants to this concept could be derived. Additional nuclear beacons could be installed further out along the approach pattern. However, at many airports this is very difficult to achieve since this area is often off airport property, over water, or presents other siting problems.

Depending on the length of the runway, the number of beacons can be varied. For short runways, four beacons may be all that is necessary.

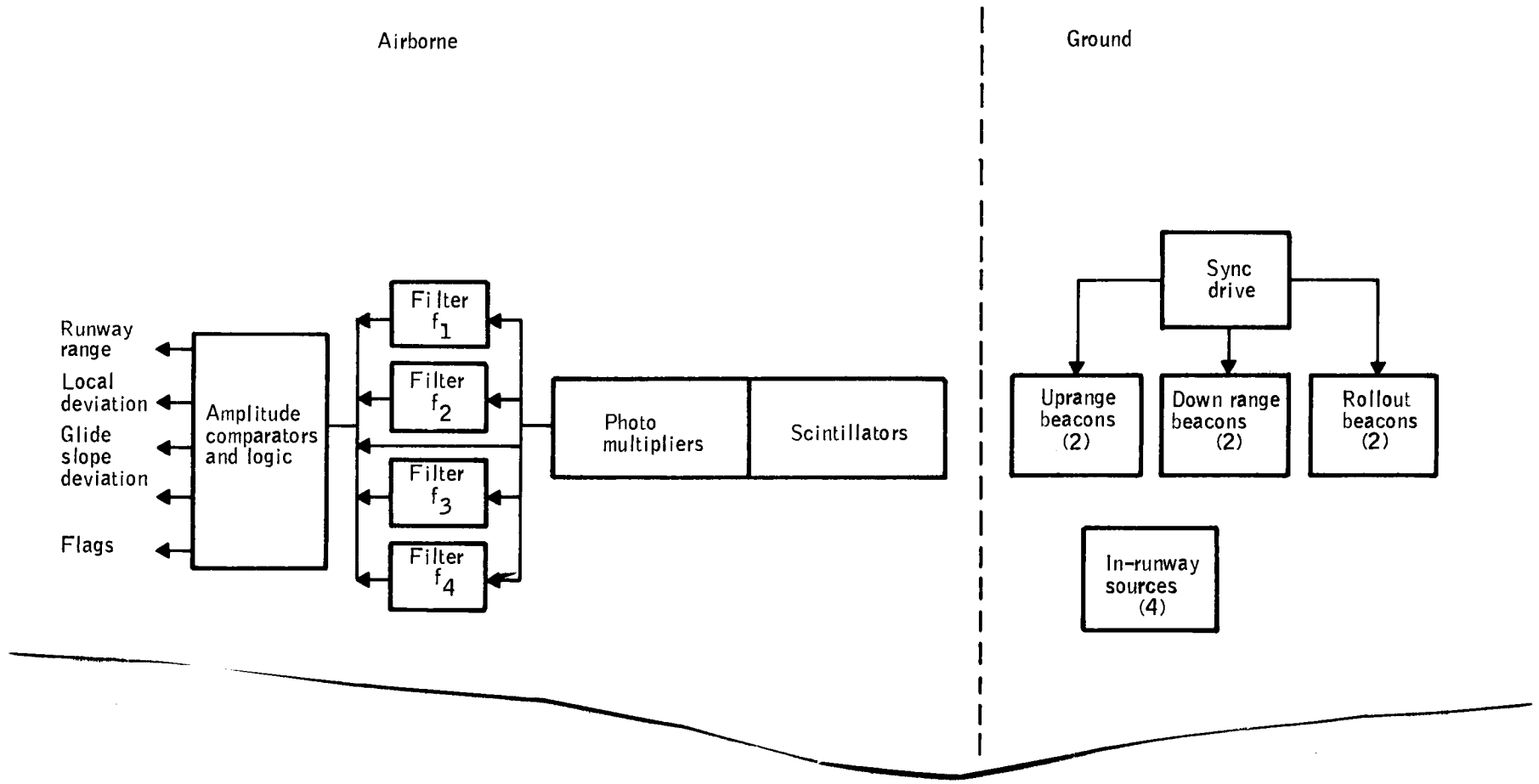

Figure 156 -- Nuclear ILM Block Diagram

The use of gamma radiation makes the system essentially immune to weather conditions. As shown in Section V, worst case weather conditions degrade the signal by less than 2.5 dB/Km.

Nuclear beacons with ranges of 1,000 to 2,000 meters can be used which are, or can be made, safe for passengers, crew and maintenance personnel. Although there may be the usual public concern over nuclear systems, it can be shown the nuclear landing configurations can meet reasonable safety regulations.

The airborne radiation detector system does not require special openings or windows in the aircraft. Thus, it is a very easily installed system. It will work with conventional displays already in the aircraft.

The systems initial cost is low and maintenance costs should also be low.

Flight tests described in References 40 and 41 indicate accuracies equivalent to MLS accuracies are achievable with this concept over the relatively short ranges considered (straight-in approaches from middle marker through rollout).

The concept is capable of handling only fixed glideslope, fixed localizer, straight-in approaches. This may not be a serious constraint at the relatively short approach ranges for which the system is valid.

To provide uniform signals throughout the region, both on and off axes, requires precisely-aligned and shaped beacons and absorbers. Significantly more development work will be required in this area.

System Interfaces

Ideally, this concept should not require any auxiliary data or additional data from other sources. With the beacons located near the runway, it should be possible to utilize a standard configuration for all runways. Thus, siting information would not be required to be supplied at each airport.

One would expect flare maneuvers would still be initiated using the radar altimeter indication of altitude on the runway. However, since guidance is provided with the beacons throughout the flare/touchdown area, it may be possible to derive the flare commands directly from the nuclear system.

Equipment Locations

The approximate equipment locations are shown in Figure 147. The up range beacons ideally should be on pedestals of the same height as the glideslope at that range. However, this is not practical, and lower beacons can be used. The localizer/glideslope error signals are not completely independent when lower altitude beacons are used and a small correction term may be required. The downrange and rollout beacons may be low to the surface and should not cause any significant installation problems. The in-runway sources can be embedded in the runway to leave a smooth runway surface. Several possible configurations are conceivable for these sources. Sources with a slit arrangement, radioactive material painted on the runway, or thin tubes of radioactive material embedded in the runway should all be feasible concepts.

The equipment location for the radiation detectors in the aircraft should be close to the skin of the aircraft with no major structural interference.

Gamma radiation readily penetrates the aircraft skin but could be absorbed by structure or equipment in the beam path. The outputs of the nuclear ILM could be made completely compatible with current flight director glideslope/localizer signal requirements including alarm flags. Runway range or distance to go could be displayed on a digital counter type of display as used for DME range to go displays.

Physical Parameters

A summary of the physical parameters of the nuclear landing system are given in Tables 64 and 65. Table 64 lists the size, weight, power and cost estimates for the airborne components. Table 65 provides size, weight and cost estimates for the ground components of the nuclear landing system.

As can be noted on the tables, the costs of the nuclear system are very low. From private discussions with R. A. Kaminskas of TRW, the cost of the ground beacons was $4,000 each for their test system. This cost could possibly be lowered for production models; however, we assume inflation has balanced out this reduction. The in-runway sources are passive units with much lower strength than the beacons. Thus, the cost would be considerably less. The accumulated cost for 6 beacons and 4 runway sources is estimated at $26,000. These figures do not include airport installation or alignment costs.

The airborne components are very simple for the nuclear landing system. The sensor itself consists of a plastic scintillator block which generates light flashes as gamma rays are absorbed in it. A photomultiplier on one face of the scintillator block is used to detect and measure the quantity of light flashes

Table 64 -- Airborne Component Estimates

	Size	Weight	Power	Cost
Scintillator	4,500 cm^3	10 lbs		$300
Photomultipliers (2)	1,000 cm^3			$150 ea. $300
Electronics	1,000 cm^3	6 lbs	12 watts	$300
Manufacturing Costs				$900
Totals	6,500 cm^3	16 lbs	12 watts	$1800

Table 65 -- Ground Component Estimates

	Size	Weight	Cost
Beacons (6)	.18 m^3 ea.	3000 lbs ea.	$ 4,000 ea. $24,000
In-Runway Sources (4)	.02 m^3 ea.	500 lbs ea.	$ 500 ea. $ 2,000
	Total		$26,000

(scintillations). We assumed the use of two multipliers here to increase reliability of the unit. The electronics consist of four filters and relatively simple logic to compare the amplitude outputs of the filters. The total cost of the airborne unit is estimated at $1800 including manufacturing costs. Special windows in the aircraft or unique installation costs are not required for this system. Outputs would be displayed on a standard flight director or ILS type of cross pointer display. Costs are not included for the displays.

The simplicity and low cost of the components should lead to a relatively high reliability for the configuration. No estimates were made of the reliability of this system; however, it appears completely feasible to incorporate redundant units if necessary to increase reliability of the system.

Mutual Interference

The nuclear landing system is an air derived system. Thus, there are no traffic capacity problems associated with it. Each aircraft within range of the beams derives its own guidance information.

The nuclear landing system using gamma radiation should not generate interference with, or be interfered with by, any of the normal equipments located on the aircraft or in the airport vicinity. The locations of the ground beacons can be shifted to some extent if positioning interference with required locations for other equipment is a problem. The feasibility design was laid out to assure ground equipments would be located on airport property.

The feasibility configuration of the nuclear landing system uses relatively strong radioactive sources (100-400 curies). Thus, proper safety procedures

will have to be developed to assure normal airport ground personnel safety in the general vicinity of the sources. It is clear from the feasibility studies done on the nuclear system that adequate safety procedures can be achieved.

SECTION VII

REFERENCES

1. ITT Gilfillan, Honeywell, and Douglas Aircraft Co.: Prototype Development Program; Microwave Landing System Five Year MLS Development Program Plan (Updated); Volume II. Contract No. DOT-FA72WA-2805 Item 3 Phase II (Task E); April 15, 1974.

2. ITT Gilfillan, Honeywell, and Douglas Aircraft Co.: Appendices; Microwave Landing System Five Year MLS Development Program Plan (Updated); Volume III. Contract No. DOT-FA72WA-2805 Item 3 Phase II (Task E); April 15, 1974.

3. Schaefer, R. W.; Aksamit, E. M. and Heitzmann, R. K.; et.al.: Multiple Airborne Reconnaissance Sensor Assessment Model (MARSAM II), Part I; Description and Summary. ASD-TR-68-3, February 1968.

4. Skolnik, M. J.: Radar Handbook, McGraw-Hill, 1970.

5. FAA: Advisory Circular, No. 120-28A; Criteria for Approval of Category III a Landing Weather Minima. January 18, 1973.

6. Brown, A. D.: Category II - A Simulation Study of Approaches and Landings at Night. Tech. Memo Avionics 59 (BLEU), N71-37606, June 1970.

7. White, J. S.: Landing Rates for Mixed STOL and CTOL Traffic. NASA TN-D 7666, April 1974.

8. Naugler, A. W.; et. al.: High Performance IR Systems Study. AFAL-TR-71-166, December 1971.

9. Anon.: Aircrew Station Visibility Requirements for Military Aircraft. MIL-STD. 850A, June 8, 1967.

10. Bundick, W.: Parametric Analysis of an Imaging Radar for use as an Independent Landing Monitor. NASA TN D-7652, August 1974.

11. Schaefer, R. W.; et.al.: Multiple Airborne Reconnaissance Sensor Assessment Model (MARSAM II) Part II Sensor Systems Analysis. ASD-TR-68-3, February 1968.

12. Barton, D. K.: Radar Systems Analysis. Prentice-Hall, 1964

13. Reference Data for Radio Engineers, 5th Edition. Howard W. Sams, Inc., 1972.

14. Nathanson, E.: Radar Design Principles. McGraw-Hill, 1969.

15. Berkowitz, R. S. : Modern Radar. John Wiley & Sons, 1965.

16. Clavin, A.; Huebner, D. A.; Kilburg, F.J.: An Improved Element for Use in Array Antennas. Trans. on Antennas and Propagation, Volume AP-22, No. 4, July 1974, pp. 521-525.

17. Rihaczek, A. W.: Principles of High Resolution Radar. McGraw-Hill, 1969.

18. Nathanson, F. E.; Reilly, J. P.: Radar Precipitation Echos. Trans. on AES, Volume AES-4, No. 4, July 1968.

19. Jasik, H.; et.al.: Antenna Engineering Handbook. McGraw-Hill, 1961.

20. Gorham, J.A.; Franco, M.: Use of Airborne Radar as a Monitor of Airplane Landing Operations under Adverse Weather Conditions. Lockheed Aircraft Corp., May 1969.

21. De Loor, G. P.: Radar Ground Returns Part III: Further Measurements on the Radar Backscatter of Vegetation and Soils. Physisch Laboratorium TNO, March 1974.

22. Oliver, T.L.; Peake, W. H.: Radar Backscattering Data for Agricultural Surfaces. Ohio State University, February 1969.

23. Behtel, B.: Radar Independent Landing Monitors. 7th Annual Meeting of AIAA, October 1970.

24. Handbook of Geophysics. USAF, Revised Edition, Macmillan Co., 1961.

25. Anon.: Results of the Experiments Undertaken on the Landing Function of a New Multifunction Radar. Thomson - CSF Corporation Memo, October 1972.

26. Maxson Electronics Div.: Maxson's Independent Landing Monitor. Maxson Electronics Corp., October 1971.

27. Ward, H. R. et.al.: GCA Radars: Their History and State of Development. Proceedings of the IEEE, Vol. 62 No. 6, June 1974.

28. Anon.: Proposal for AN/TPN-22 Precision Approach and Landing Radar, Vol. 1, Technical Proposal. ITT Gilfillan, revised 15 July 1974.

29. Stein, K. J.: Radar Design Offers X- or C- Band Option. Aviation Week and Space Technology, August 14, 1967.

30. Torrieri, D. J.: The Uncertainty of Pulse Position due to Noise. AES-8, p. 661, 1972.

31. Anon.: Arrival Time Estimation by Adaptive Thresholding. AES-10, No. 2, P. 178, March 1974.

32. Danker, P.D.; Witt, C. W.: and Christensen, H. H. : Range Only Multiple Aircraft Navigation System. RADC-TR-72-22, 1972.

33. Doty, D.E.: Kalman Filtering Errors in Time-Frequency Aircraft Trackers. University of Minnesota Dept. Electrical Engineering, March 1974.

34. Lee, H. B.: Accuracy Limitations of Range-Range (Spherical) Multilateration Systems. MIT Lincoln Labs, TN 1973-43, March 1974.

35. Singer, R. A., and Behnke, K.W.: Real Time Tracking Filter Evaluation and Selection for Tactical Applications. AES-7 No. 1 p. 100, January 1971

36. Friedland, B.: Optimum Steady State Position and Velocity Estimation Using Noisy Sampled Position Data. AES-4, No. 6, p.906, Nov. 1973.

37. Sage, A.P., and Melsa, J.L.: Estimation Theory with Applications to Communication and Control. McGraw Hill, 1971.

38. Snodgrass, R.C.: Recursive Navigation: Program Description and Characteristic Performance, As Indicated by Simulation and Analysis. ESD-TR-71-362, AD735262, 1974.

39. Holme, N.: Landing Guidance System-Hermes. Agard Conf. Proc. No. 105, June 26-29, 1972.

40. Kaminskas, R.A.: Nuclear Instrument Landing System Phase II Interim Report. N74-20232, January 1973.

41. Drinkwater III, F. J. and Kibort, B. R.: Use of Very Weak Radiation Sources to Determine Aircraft Runway Position. Conf. on Aircraft Operating Problems, Langley Research Center, May 10-12, 1965.

42. Signal Formal Development Team Report to RTCA Special Committee 117. RTCA Sept. 5, 1970.

43. ITT Gilfillan.: Feasibility Demonstration, Test and Evaluation Program, Microwave Landing System. Contract No. DOT-FA72WA-2805 Item 3 Phase II, 19 August 1974.

44. ITT Gilfillan. : A New Non-Visual Precision Approach and Landing Guidance System for ICAO. FAA Contract No. DOT-FA-72WA-2805, August 1973.

45. Biberman, L.: Worldwide Survey of Night Scene Illumination Conditions. Proceedings of the Seminar on Direct-Viewing Electro-Optical Aids to Night Vision. AD 379678, October 1966.

46. Honeywell, Inc.: Navy Carrier-Based Trail and Road Interdiction Study (U) (TRIM III), Volume II, Acquisition Systems, Final Technical Report (Secret). AD 504350L, August 1969.

47. Athar, W. C.: Design Considerations for Airborne Low Light Level Weapons Delivery System. Proc. NAECON, 1967.

48. Rose, A.: A Unified Approach to the Performance of Photographic Film, Television Pick-Up Tubes, and the Human Eye. J. SMPE, Volume 47, No. 4, 1946.

49. Schade, O. H.: The Resolving Power Function in Quantum Processes of Television Cameras. RCA Review, September 1967.

50. Van Asselt, R.L.: The Image Isocon as a Studio, X-Ray, and Low Light Camera Tube. N.E.C. Proceedings, 1968.

51. DeHaan, E. F. and Van Doorn, A.G.: The Plumbicon: A Camera Tube with a Photoconductive Lead Oxide Layer. J. SMPTE, Volume 73, June 1964.

52. Snyder, H.L.: et.al.: Low Light Level TV Viewfinder Simulation Program, Phase A: Part 1. State-of-theArt Review (U) (Secret Report). AD 386770.

53. Anon.: Westinghouse Data Sheet TD 86-827, WL-32000 Intensifier SEC Camera Tube. September 1968.

54. Anon.: Flight Test Plan/Report C-1 Low-Light-Level Television Evaluation (U) (Secret). AD 385405.

55. Steingold and Strauch,: Backscatter Limitations in Active Night-Vision Systems. Memorandum RF-5442-PR, February 1968,

56. Anon.: EG&G Data Sheet 1008 -- DC Xenon and Krypton ARC Discharge Tubes.

57. Kruse, McGlaughlin, McQuistan,: Elements of Infrared Technology. John Wiley & Sons, Inc., New York.

58. Honeywell Inc.: Advanced Low Altitude Reconnaissance (Confidential). Honeywell Radiation Center, Document No. 5-09-10A.

59. Wolfe, N. L.: Handbook of Military Infrared Technology. Office of Naval Research, Dept. of Navy, Washington D. C., 1965.

60. Buttwiller, T. B.: Infrared Scanning System Survey, Honeywell Document MSC-39, November 1965.

61. Hogg, D. C., and Mumford, W. W.: The Effective Noise Temperature of the Sky. Microwave Journal, Vol. 3, p. 80, March 1960.

62. Peake, W. H., and Oliver, T. L.: The Response of Terrestrial Surfaces at Microwave Frequencies. AFAL-TR-70-301, AD 884106, 1971.

63. McGillem and Seling.: Influence of System Parameters on Airborne Microwave Radiometer Design. IEEE Trans. on Mil. Elec., p. 296, October 1963.

64. Beckman and Spizzichino,: The Scattering of Electromagnetic Waves from Rough Surfaces. MacMillan, 1963.

65. Duncan, J.W.: The Effect of Ground Reflections and Scattering on an Interferometer Direction Finder. AES-3 No. 6, p. 922, Nov. 1966.

66. Bullock, L. G.: Oeh, G.R. and Sparanga, J. J.: An Analysis of Wide Band Microwave Monopulse Direction Finding Techniques. AES-7 No. 1 p. 188, Jan. 1971.

67. MacKinnon, D.: Automatic Landing System Optimization Using Inertial Navigation D ta and Modern Control Theory. Agard Conf. Proc. No. 59 on Aircraft Landing Systems, AD714925, May 20-23, 1969.

SECTION VIII

BIBLIOGRAPHY

1. Bundick, W. T.: Parametric Analysis of an Imaging Radar For Use as an Independent Landing Monitor, NASA TN D-7652, August 1974.

2. Gorham, J. A. and Franco, M.: The Use of Airborne Radar as a Monitor of Airplane Landing Operations Under Adverse Weather Conditions. ATA Symposium on Visibility Enhancement in Poor Weather, May 1969.

3. Schmitt, B.: The Independent Landing Monitor System (Forward Looking Radar) for Civil Aircraft. Society of Experimental Test Pilots - Fifth Annual Symposium, 29-31 March 1973.

4. Hunter, I. M.: Properties of Air-Derived and Ground Derived Aircraft Landing Guidance Concepts. Journal of Navigation, Vol. 26, p.431-449, October 1973.

5. Edgar, A. K.: Civil Applications of 3-D Radar. Flight International April 25, 1974.

6. DeCelles, L., Burke, E. and Burroughs, K.: Head-up Display: A Safety Concept. Flight, July 1973.

7. Anon.: Radar Landing System. Flight, January 1971

8. Cowin, H.: Vorloc II - A Simple Directional Aid. Flight International March 1, 1973.

9. Anon.: Cause and Circumstance - The Miracle Mile. Business and Commercial Aviation, August 1972.

10. Glaves, B.: Microwave Landing System. Business and Commercial Aviation, October 1972.

11. Herbert, J. W.: Cockpit Traffic. Flight, May 1972.

12. Anon.: Instrument Letdown with Contact Approach. Flight, Nov. 1973.

13. Smedley, J. W.: Let's Eliminate This Hazard to Pilots and Controllers. Flight, Dec. 1973.

14. McGarty, T.P.: Azimuth-Elevation Estimation Performance of a Spatially Dispersive Channel. ESD-TR-73-344, March 1974.

15. Kocher, D. G.: Prediction of Optical Landing Guidance System Performance in CAT. III-A Minimum Weather. MIT Lincoln Labs Tech Note 1973-47, March 1974.

16. Lee, H. B.: Accuracy Limitations of Range - Range (Spherical) Multilateration Systems. DOT/TSC-RA-3-8-(1), March 1974.

17. Merriam, R. H. and Rosh, J. W.: Microwave Doppler Sensors. Microwave Journal, July 1974.

18. Steigerwald, L.: A Review of Air Traffic Control. University of Toronto, AD893146, July 1971.

19. Marino, D. J.: A Survey of Instrument Landing Systems. Mitre Corp. AD863605, Dec. 1969.

20. Fehlner, L. F. and McCarty, T.A.: A Precision Position and Time Service for the Support of Air Traffic of the Future. Nineteenth Technical Conference of the IATA Dublin, Ireland, 23-28 October 1972.

21. Douvillier, Jr., J. G.: Simulator Evaluation of a Display for Manual Zero-Zero Landings. NASA SP-83 Conference on Aircraft Operating Problems, May 10-12, 1965.

22. Crane, H. L., Yenni, K. and Fisher, B.D.: Flight Investigation of the VFR and IFR Landing Approach Characteristics and Terminal Area Airspace Requirements for a Light STOL Airplane. NASA TM X-3008, June 1974.

23. Anon.: Results of the Experiments Undertaken on the Landing Function of a New Multifunction Radar. Thomson - CSF DT. RCM N 72/955, Oct. 1972.

24. Casserly, G. W., et.al.: Commercial Air Transport Hazard Warning and Avoidance System, Vol. I - Summary, Vol II - Requirement Studies, Volume III - Radar Performance Studies. Polhemus Navigation Sciences, Inc., PNSI-TR-70-0414, May 1970.

25. Maxson Electronics Div.: Maxson's Independent Landing Monitor. Maxson Electronics Corp., Oct. 1971.

26. Item, A., Didisheim, J. and Schmitt, B.: Swissair Evaluation of an Independent Landing Monitor. OFT Report No. 271, Dec. 1973.

27. Bundick, W. T.: A Review of Some Past Landing Display and ILM Work and it's Application to the Terminal Configured Vehicles Program. LWP-1159, April 1974.

28. DeCelles, J. L., Burke, E. J. and Burroughs, K. L.: The Fail-Safe Landing, ALPA 17th Air Safety Forum, 1970.

29. Young, D. W. and Suzansky, J. W.: Research Study of an Aircraft-Contained Zero-Zero Landing System. N68-16635, Dec. 1967.

30. Maeda, H. and Umeda, Y.: An Ultrasonic Altitude-Velocity Sensor for Airplanes in the Vicinity of the Ground. Journal of Aircraft Vol. 9, No. 4, April 1972.

31. Smith, J., Schoonmaker, P.B., Pyron, E. E. and Benbow, R.L.: Principles of Performance Monitoring with Application to Automatic Landing. Journal of Aircraft, Vol. 9, No. 5, pp 339-346, May 1972.

32. Rosell, F. and Willson, R.: Performance Synthesis of Electro-Optical Sensors. AFAL-TR-73-260, August 1973.

33. Sendall, R. and Rosell, F.: E/O Sensor Performance Analysis and Synthesis (TV/IR Comparison Study). AFAL-TR-72-374, April 1973.

34. Klass, P. J.: New Blind Landing Aid in Demonstrated. Aviation Week, Sept. 10, 1962.

35. Klass, P. J.: ILS Monitor Techniques Show Promise. Aviation Week, August 13, 1973.

36. Ebersol, E.T.: Microwave Mapper Brings Them in Safely. Microwaves, Dec. 1972.

37. Bechtel, B.: Radar Independent Landing Monitors. AIAA Paper No. 70-1336, October 1970.

38. Mendez, J. A., Freitag, M., Zinn, W.: Human Factors Analysis of Forward Looking Infrared (FLIR) Imagery in Air-To-Ground Target Detection/Recognition. Proc. 16th Annual Meeting of the Human Factors Society, Oct. 17-19, 1972.

39. Moll, J. D. and Scanlan, L. A.: Visual Time Compression: II. Detecting Moving Targets in Dense Radar Ground Clutter. Proc. 16th Annual Meeting of the Human Factors Society, Oct. 17-19, 1972.

40. Greening, C. P. and Wyman, M. J.: Display Dynamic Range and Radar Target Recognition. Proc. 16th Annual Meeting of the Human Factors Society, Oct. 17-19, 1972.

41. Holliday, G. and Gorham, J. A.: Development Testing of the L-1011 Independent Landing Monitor. SAE National Air Transportation Meeting, May 10-13, 1971.

42. Gold, T.: Visual Perception of Pilots in Carrier Landing. AIAA Paper No. 73-917, September 1973.

43. Leary, F.: All Weather Landing - When? Space/Aeronautics, Feb. 1966.

44. Parks, D. L. and Tubb, D. G.: Simulator Development and Flight Validation of a Perspective Display as an Independent Landing Monitor. AIAA Paper No. 70-924, July, 1970.

45. Duggan, Jr., R. S.: Salt-Self Contained All Weather Landing and Taxiing. AIAA Paper No. 69-1053, Oct. 1969.

46. Drinkwater III, F. J. and Kibort, B.R.: Use of Very Weak Radiation Sources to Determine Aircraft Runway Position. Conference on Aircraft Operating Problems, Langley Research Center, May 10-12, 1965.

47. Gold, T. and Workman, J. D.: Research in the Application of Windshield Projection Displays to the All-Weather Landing Task. J. Aircraft, Vol. 2, No. 4, pg. 328-336, July - Aug. 1965.

48. Samson, C. A., et.al.: Weather Effects on Approach and Landing Systems. FAA-RD-70-47, July 1970.

49. Johnson, E. W., Carmack, D. L. and Hadley, L. M.: Psychological and Procedural Aspects Related to ILS Approach and Landings in Visibilities Less than 1200 Feet. AGARD Conf. Proc. No. 59, May 20 - 23, 1969.

50. MacKinnon, D.: Automatic Landing System Optimization Using Inertial Navigation Data and Modern Control Theory. AGARD Conf. Proc. No. 59, May 20-23, 1969.

51. Loeb, J. L. : Automatic Landing Systems Are Here. AGARD Conf. Proc. No. 59, May 20-23, 1969.

52. ITT Gilfillan: A New Non-Visual Precision Approach and Landing Guidance System for ICAO. DOT-FA-72WA-2805, Aug. 1973.

53. Noll, R. B. and Zvara, J.: Analysis of Terminal ATC System Operations. AGARD Conf. Proc. No. 105, June 26-29, 1972.

54. Holme, N.: Landing Guidance System-Hermes. AGARD Conf. Proc. No. 105, June 26-29, 1972.

55. Bearse, S.V: Air Force to Get Improved Approach Radar. Microwave, Aug. 1974.

56. RTCA Special Committee 117: Microwave Scanning Landing Guidance Systems (LGS). Paper 189-70/SC117FDT-27, September 1970.

57. Kaminskas, R. A.: Nuclear Instrument Landing System Phase II Interim Report. N74-20232, January 1973.

58. Vikan, D.: Tactical Approach Landing Radar. A72-31694 (USAF Edwards AFB), March 1972.

59. Armstrong, B.D. et.al,: Warning Monitors for Automatic Landing: A Feasibility Study. Royal Aircraft Establishment N69-14847, April 1968.

60. Wilckens, V.: Improvements in Pilot/Aircraft Integration by Advanced Contact Analog Displays. 9th Annual Conf. on Manual Control, MIT, May 1973.

61. Brown, A.D.: Category II - A Simulation Study of Approaches and Landings at Night. N71-37606, June 1970.

62. Danker, P. D.,et.al.: Range-Only Multiple Aircraft Navigation System (ROMANS). RADC-TR-72-22, Feb. 1972.

63. McTee, A. C. Utility of DME Information for Final Approach and Throttle Rollout. IPIS-TS-70-3, AD-872823, July 1970.

64. Sherman, N. L. and Winfrey, S. W.: Preliminary Study of a Possible Automatic Landing System. NASA LRC TN-D-7611, July, 1974.

65. Semple, Jr., C.A., et.al.: Analysis of Human Factors Data for Electronic Flight Display Systems. AFFDL-TR-70-174, April 1971.

66. Denery, D. G. et. al.: Preliminary Results on Two-Segment Noise Abatement Studies. NASA ARC TM X-62, 098, Sept. 1971.

67. Warner, J. D. and Fadden, D. M.: Computer Generated Map Displays. FAA Symposium on Area Navigation, January 1972.

68. Bush, R. W., et.al.: A Cockpit Situation Display of Selected NAS/ARTS Data. MIT, AD716425, Dec. 1970.

69. Edwards, J.: Future Landing System Requirements. BALPA 1971 Technical Symposium (Systems in Aviation), Nov. 1971.

70. Kosowsky, L. H. and Koester, K. L.: Millimeter Radar for Landing Applications. 26th Annual National Forum of the American Helicopter Society, June 1970.

71. White, J. S.: Landing Rates for Mixed STOL and CTOL Traffic. NASA ARC TN D-7666, April 1974.

72. Chisholm, D. A. and Kruse, H.: The Variability of Airfield Visibility: A Preliminary Assessment. AFCRL-TR-74-0027, January 1974.

73. FAA Systems Research and Development Service: Engineering and Development Program Plan All Weather Landing. AD 754264, October 1972.

74. Peake, W. H. and Oliver, T. L. : The Response of Terrestrial Surfaces at Microwave Frequencies. AFAL-TR-70-301, May 1971.

75. Roscoe, S. N., Scott, S. G. and Dougherty, D. J.: Flight by Periscope: Making Takeoffs and Landings; the Influence of Image Magnification, Practice, and Various Conditions of Flight. Human Factors Vol. 8, No. 1., Feb. 1966.

76. Talbot, P. D. and Stinet, Jr., G.W.: Landing Approach Evaluation of an Integrated CRT Display for General Aviation Aircraft. NASA TM X-3096, July 1974.

77. Klass, P. J.: Collision Warning/Landing Aid Tested. Aviation Week, Nov. 18, 1974.

78. Anon.: Nuclear ILS for Aircraft Proves Safe and Sound in Feasibility Tests. Electronics Design, Aug. 2, 1974.

79. Park, D.L., et.al.: Control-Display Testing Requirements Study, AFFDL-TR-72-121-Vol I and II, Jan. 1973.

80. Sullivan, N. and Ames, R. W.: Multilateration/Multipath Study for Air Traffic Control. RADC-TR-74-173, July 1974.

81. Morton, G. W.: Feasibility Model of Landing Performance Monitor. FAA-RD-74-79, April 1974.

82. ITT Gilfillan, Honeywell and Douglas Aircraft Co.: Microwave Landing System Five Year MLS Development Program, Vol. I, II and III. Contract Report No. DOT-FA-72WA-2805 Item 3, April 1974.

83. Schaefer, R. W., et.al.: Multiple Airborne Reconnaissance Sensor Assessment Model (Marsam II), Park I, Description and Summary, Part II Sensor System Analysis. ASD-TR-68-3, Feb. 1968.

84. Anon.: Criteria for Approval of Category III a Landing Weather Minima. FAA AC No. 120-28A, January 1973.

85. Naugler, A. W., et. al.: High Performance IR System Study. AFAL-TR-71-166, Dec. 1971.

86. Anon.: Aircrew Station Visibility Requirements for Military Aircraft. MIL-STD. 850A, June 1967.

87. Skolnik, I., et.al.: Radar Handbook, McGraw Hill, 1970.

88. Barton, K.: Radar System Analysis. Prentice-Hall, Inc., 1964.

89. Anon.: Reference Data for Radio Engineeers, 5th Edition, Howard W. Sams, Inc., 1972.

90. Nathanson, E.: Radar Design Principles. McGraw-Hill, 1969.

91. Berkowitz, S. : Modern Radar. John Wiley & Sons, 1965.

92. Clavin, A., Huebner, D. A. and Kilburg, F. J.: An Improved Element for Use in Array Antennas. Trans. on Antennas and Propagation, Volume AP-22, No. 4, pp. 521-525, July 1974.

93. Rihaczek, W.: Principles of High Resolution Radar. McGraw-Hill, 1969

94. Nathanson, F.E.: Reilly, J. P.: Radar Precipitation Echos: Trans. on AES, Volume AES-4, July 1968.

95. Jasik, et.al.: Antenna Engineering Handbook. McGraw-Hill, 1961.

96. DeLoor, G. P.: Radar Ground Returns Part III: Further Measurements on the Radar Backscatter of Vegetation and Soils, Physic Laboratorium TNO, March 1974.

97. Oliver, T. L., Peake,W. H.: Radar Backscattering Data for Agricultural Surfaces February 1969.

98. Ward, H. R.,et.al: GCA Radars: Their History and State of Development. Proceedings of the IEEE, Vol. 62, No. 6, June 1974.

99. Stein, K. J.: Radar Design Offers X-or C-Band Option. Aviation Week, Aug.1967.

100. Torrieri, D. J.: The Uncertainty of Pulse Position due to Noise AES-8, p. 661, 1972.

101. Anon.: Arrival Time Estimation by Adaptive Thresholding. AES-10, No. 2, P. 178, March 1974.

102. Singer, R. A., and Behnke, K.W.: Real Time Tracking Filter Evaluation and Selection for Tactical Applications. AES-7 No. 1 p. 100, January 1971.

103. Friedland, B.: Optimum Steady State Position and Velocity Estimation Using Noisy Sampled Position Data. AES-4, No. 6., p. 906, Nov. 1973.

104. Sage, A.P., and Melsa, J. L.: Estimation Theory with Applications to Communication and Control. McGraw Hill, 1971.

105. Snodgrass, R.C.: Recursive Navigation: Program Description and Characteristic Performance, As Indicated by Simulation and Analysis, ESD-TR-71-362, AD735262.

106. Biberman, L.: Worldwide Survey of Night Scene Illumination Conditions. Proceedings of the Seminar on Direct-Viewing Electro-Optical Aids to Night Vision (U) (Secret). AD 379678, October 1966.

107. Honeywell, Inc.: Navy Carrier-Based Trail and Road Interdiction Study (U) (TRIM III), Volume II, Acquisition Systems, Final Technical Report. AD 504350L, Aug. 1969.

108. Athar, W. C.: Design Considerations for Airborne Low Light Level Weapon Delivery System. Proc. NAECON. 1967.

109. Rose, A.: A Unified Approach to the Performance of Photographic Film, Television Pick-up Tubes, and the Human Eye, J.SMPE, Volume 47, No. 4, 1946.

110. Schade, O. H.: The Resolving Power Function in Quantum Processes of Television Cameras. RCA Review, September 1967.

111. VanAsselt, R.L.: The Image Isocon as a Studio, X-Ray, and Low Light Camera Tube. N.E.C. Proceedings, 1968.

112. DeHaan, E. F. and Van Doorn, A. G.: The Plumbicon: A Camera Tube with a Photoconductive Lead Oxide Layer. J. SMPTE, Volume 73, June 1964, pp 473-476.

113. Kruse, McGlaughlin, McQuistan.:Elements of Infrared Technology. John Wiley & Sons, Inc., New York.

114. Wolfe, W. L.: Handbook of Military Infrared Technology, Office of Naval Research, Dept. of Navy, Washington. D. C., 1965.

115. Hogg, D. C., and Mumford, W. W.: The Effective Noise Temperature of the Sky. Microwave Journal, Vol. 3, March 1960.

116. McGillem and Seling.: Influence of System Parameters on Airborne Microwave Radiometer Design, IEEE Trans. on Mil. Elec., Oct. 63, P. 296.

117. Beckman and Spizzichino: The Scattering of Electromagnetic Waves from Rough Surfaces. MacMillan, 1963.

118. Duncan, J. W.: The Effect of Ground Reflections and Scattering on an Interferometer Direction Finder. AES-3 No. 6, Nov. 1966.

119. Bullock, L. G., Oeh, G. R. and Sparanga, J. J.: An Analysis of Wide Band Microwave Monopulse Direction Finding Techniques. AES-7 No. 1, Jan. 71.

SECTION IX

APPENDICES

APPENDIX A. TENTATIVE MLS ACCURACY REQUIREMENTS

APPENDIX B. MARSAM II COMPUTER PROGRAM SUMMARY

APPENDIX C. SCATTERING OF ELECTROMAGNETIC WAVES

APPENDIX D. ATMOSPHERIC ATTENUATION OF MICROWAVES

APPENDIX E. RADIOMETRY COMPUTER PROGRAMS

APPENDIX F. MLS CONFIGURATION K AIRBORNE EQUIPMENT

REFERENCES

1. Beckmann and Spizzichino, The Scattering of Electro Magnetic Waves from Rough Surfaces, MacMillan, 1963.

2. Semenov, Scattering of Electromagnetic Waves from Restricted Portions of Rough Surfaces with Finite Conductivity, Radiotekhnika i Electronica V, 110, 1965, p. 1952.

3. Barrick, D. E., Rough Surface Scattering Based on the Specular Point Theory, AP16 1968, P449.

4. Beckmann, Scattering by Composite Rough Surfaces, Proc. IEEE, Vol. 53 No. 8, August 1965, p. 1012.

5. Beckmann, Shadowing by Random Rough Surfaces, AP13, May 1965, p. 384.

6. Ruck, Barrick, Stuart, and Krichbaum, Radar Cross Section Handbook, Vol. 2, Plenum Press, 1970.

7. Mitzner, K.: Change in Polarization on Reflection from a Tilted Plane, Radio Science, Vol. 1, 1966, pg. 27.

PATH TEMPERATURES

RANGE= 2 KM.

WEATHER CASE	GLIDE SLOPE=1 DEG.	2 DEG.	3 DEG.	4 DEG.	5 DEG.	6 DEG.	7 DEG.	8 DEG.	9 DEG.
1.0	102.725	195.691	256.728	249.288	252.112	257.123	254.932	256.017	257.161
2.1	11.260	11.601	11.560	10.795	10.349	10.038	9.777	9.585	9.422
2.2	14.251	14.806	14.689	13.152	12.240	11.618	11.133	10.774	10.481
2.3	44.588	51.238	51.665	41.563	35.307	31.036	27.906	25.538	23.670
2.4	84.661	122.958	135.410	110.676	93.903	81.819	72.691	65.583	59.883
3.1	13.062	13.526	13.649	13.576	13.568	13.557	13.512	13.491	13.465
3.2	17.941	18.840	19.095	19.026	19.054	19.074	19.048	19.051	19.049
3.3	60.574	74.714	79.513	78.811	79.623	80.314	80.266	80.664	80.973
3.4	94.740	157.891	189.072	184.270	187.385	190.862	189.727	191.069	192.161
4.0	5.540	5.624	5.640	5.596	5.576	5.555	5.521	5.497	5.471

RANGE= 6

WEATHER CASE	GLIDE SLOPE=1 DEG.	2 DEG.	3 DEG.	4 DEG.	5 DEG.	6 DEG.	7 DEG.	8 DEG.	9 DEG.
1.0	294.274	293.660	293.074	292.499	291.928	291.372	290.809	290.243	289.674
2.1	33.250	29.035	27.308	26.215	25.381	24.682	24.064	23.499	22.972
2.2	41.783	33.411	30.254	28.438	27.168	26.176	25.349	24.627	23.978
2.3	129.343	83.160	65.073	55.228	49.951	44.542	41.233	38.629	36.503
2.4	242.680	181.093	143.934	120.399	104.288	92.571	83.648	76.607	70.894
3.1	38.932	38.714	38.471	38.223	39.255	43.767	46.983	49.407	51.311
3.2	53.374	53.377	53.327	53.264	53.732	55.669	57.088	58.184	59.069
3.3	176.709	178.256	179.358	180.313	177.893	164.402	153.723	145.105	138.029
3.4	271.883	272.104	272.186	272.185	271.224	264.792	257.640	250.234	242.874
4.0	16.554	16.315	16.073	15.834	15.599	15.367	15.137	14.909	14.685

RANGE=16

WEATHER CASE	GLIDE SLOPE=1 DEG.	2 DEG.	3 DEG.	4 DEG.	5 DEG.	6 DEG.	7 DEG.	8 DEG.	9 DEG.
1.0	293.836	292.050	290.272	288.514	286.783	285.067	283.496	283.043	282.785
2.1	68.005	62.079	58.316	55.178	52.340	49.702	47.360	45.234	43.549
2.2	75.343	65.879	60.899	57.145	53.935	51.047	48.525	46.264	44.472
2.3	149.794	109.086	91.430	80.851	73.380	67.579	62.929	59.046	55.962
2.4	248.136	194.143	160.576	138.519	122.777	110.813	101.392	93.715	87.511
3.1	91.203	96.161	113.083	121.289	126.271	129.717	132.240	132.768	133.977
3.2	120.352	122.562	129.436	133.064	135.433	137.192	138.543	138.269	138.829
3.3	261.107	258.745	239.881	225.165	214.014	205.476	198.824	192.740	188.216
3.4	281.513	280.240	279.265	276.821	273.082	268.521	263.645	258.622	253.793
4.0	40.876	39.380	37.900	36.457	35.063	33.729	32.563	31.530	30.740

pushbutton and MLS subsystem status lights which are activated by the self-monitoring circuitry in the MLS equipment. The HN-400 control panel further provides access to the HN-700 microprocessor programming, wherein certain operational options may be implemented. For example, although normal Elevation 1 output is conical, both deviation and total angle may be converted to a planar equivalent through keyboard entry of proper coding to implement an appropriate DME conversion algorithm.

The HL-362 and HL-363 omnidirectional antennas are provided to assure full MLS airborne antenna coverage during the diverse aircraft maneuvers associated with curved approach paths, missed approach, and departures. The HL-181 sector horn antenna provides effective gain enhancement of the guidance signals, as well as assuring adequate coverage for the critical final approach phase of the terminal area mission.